

PHYSIOLOGICALLY BASED PHARMACOKINETIC  
MODELING PROVIDING INSIGHTS INTO THE PHARMACOKINETICS  
OF BUPRENORPHINE, FENTANYL AND NICOTINE  
IN ADULT AND PEDIATRIC PATIENTS

DISSERTATION

zur Erlangung des Grades des Doktors der Naturwissenschaften  
der Naturwissenschaftlich-Technischen Fakultät  
der Universität des Saarlandes

von  
Lukas Georg Kovar  
Apotheker

Saarbrücken

2022

Tag des Kolloquiums: 21.10.2022  
Dekan: Prof. Dr. Jörn Erik Walter  
Berichterstatter: Prof. Dr. Thorsten Lehr  
Prof. Dr. Claus-Michael Lehr  
Prof. Dr. Charlotte Kloft  
Vorsitz: Prof. Dr. Andriy Luzhetskyy  
Akad. Mitarbeiter: Dr. Agnes-Valencia Weiß

Die vorliegende Arbeit wurde von Januar 2019 bis Dezember 2021 unter Anleitung von Herrn Prof. Dr. Thorsten Lehr in der Fachrichtung Klinische Pharmazie der Naturwissenschaftlich-Technischen Fakultät der Universität des Saarlandes angefertigt.



## PUBLICATIONS INCLUDED IN THIS THESIS

---

PUBLICATION I – PBPK MODELING OF BUPRENORPHINE IN ADULT AND PEDIATRIC PATIENTS:

**Physiologically-Based Pharmacokinetic (PBPK) Modeling of Buprenorphine in Adults, Children and Preterm Neonates.**

Lukas Kovar, Christina Schräpel, Dominik Selzer, Yvonne Kohl, Robert Bals, Matthias Schwab and Thorsten Lehr.

*Pharmaceutics* 2020;12(6):578. DOI: 10.3390/pharmaceutics12060578 [1].

PUBLICATION II – PBPK MODELING OF FENTANYL IN ADULT AND PEDIATRIC PATIENTS:

**Physiologically-Based Pharmacokinetic (PBPK) Modeling Providing Insights into Fentanyl Pharmacokinetics in Adults and Pediatric Patients.**

Lukas Kovar, Andreas Weber, Michael Zemlin, Yvonne Kohl, Robert Bals, Bernd Meibohm, Dominik Selzer and Thorsten Lehr.

*Pharmaceutics* 2020;12(10):908. DOI: 10.3390/pharmaceutics12100908 [2].

PUBLICATION III – PBPK MODELING OF NICOTINE BRAIN TISSUE CONCENTRATIONS:

**Comprehensive Parent-Metabolite PBPK/PD Modeling Insights into Nicotine Replacement Therapy Strategies.**

Lukas Kovar, Dominik Selzer, Hannah Britz, Neal Benowitz, Gideon St. Helen, Yvonne Kohl, Robert Bals and Thorsten Lehr.

*Clin Pharmacokinet* 2020;59(9):1119-1134. DOI: 10.1007/s40262-020-00880-4 [3].



## CONTRIBUTION REPORT

---

The author wishes to clarify his contributions to the publications included in this thesis, complemented by the contributor roles taxonomy (CRediT) [4, 5].

### PUBLICATION I – PBPK MODELING OF BUPRENORPHINE IN ADULT AND PEDIATRIC PATIENTS:

The author performed all major working steps that resulted in the publication of Project I. The author planned the work, gathered the information from literature, analyzed the available data, performed the pharmacometric work including adult PBPK modeling and simulation, model extrapolation to pediatric populations, pediatric PBPK modeling and allometric scaling and analyzed the modeling and simulation results. Moreover, he prepared the graphics, the supplementary material and conceived and wrote the manuscript. Conceptualization, Investigation, Methodology, Visualization, Writing – original draft, Writing – review & editing.

### PUBLICATION II – PBPK MODELING OF FENTANYL IN ADULT AND PEDIATRIC PATIENTS:

The author performed all major working steps that resulted in the publication of Project II. The author planned the work, assisted in gathering and reviewed the information from literature, analyzed the available data, performed pharmacometric PBPK modeling work in adult patients, extrapolated the adult PBPK model to pediatric patients, performed the pharmacometric PBPK modeling work in pediatric patients and analyzed the modeling and simulation results. Furthermore, he prepared the graphics, the supplementary material and conceived and wrote the manuscript. Conceptualization, Investigation, Methodology, Visualization, Writing – original draft, Writing – review & editing.

### PUBLICATION III – PBPK MODELING OF NICOTINE BRAIN TISSUE CONCENTRATIONS:

The author performed all major working steps that resulted in the publication of Project III. The author was involved in planning the work, gathered all information from literature, analyzed the available data, performed the pharmacometric PBPK modeling work, expanded the PBPK model with a pharmacodynamic (PD) tolerance heart rate model (PBPK/PD modeling), performed the PBPK/PD model simulations and analyzed the modeling and simulation results. Furthermore, he prepared the graphics, the supplementary material and conceived and wrote the manuscript. Conceptualization, Investigation, Methodology, Visualization, Writing – original draft, Writing – review & editing.



## ABSTRACT

---

The drugs buprenorphine, fentanyl and nicotine are frequently applied for the treatment of pain and smoking cessation, respectively. However, several pharmacokinetic (PK) characteristics are still unclear in both adult and particularly pediatric patients, calling for more research in this field. Here, physiologically based pharmacokinetic (PBPK) modeling represents a valuable tool to enhance the understanding of a drug's PK which may lead to optimization in dosing regimens and pharmacotherapy.

Thus, this work aimed to gain insights into the PK of buprenorphine and fentanyl as well as to investigate nicotine brain tissue concentrations by leveraging PBPK modeling. Additionally, the ability of PBPK modeling to predict plasma concentrations and PK parameters in pediatric populations of different age groups was studied.

For this purpose, PBPK models of the three drugs were built and evaluated with clinical data from adult patients. Buprenorphine and fentanyl models were extrapolated to successfully predict mean and individual plasma concentration-time profiles and PK parameters in children, full-term neonates and preterm neonates. Furthermore, the nicotine PBPK model was applied to simulate and evaluate brain tissue concentrations and was extended to model the positive chronotropic effect of nicotine.

In conclusion, the work provides new insights into the PK of buprenorphine, fentanyl and nicotine and supports the use of PBPK modeling to predict a drug's PK in pediatric patients.

## ZUSAMMENFASSUNG

---

Die Arzneistoffe Buprenorphin, Fentanyl und Nikotin werden häufig in der Schmerztherapie bzw. zur Raucherentwöhnung eingesetzt, während einige ihrer pharmakokinetischen (PK) Eigenschaften weiterhin unerforscht sind. Ein besseres Verständnis der PK dieser Arzneistoffe könnte Anreize zur Therapieoptimierung in erwachsenen und pädiatrischen Patienten geben. Die Physiologie-basierte pharmakokinetische (PBPK) Modellierung besitzt das Potential, hierbei entscheidend zu helfen und offene Fragestellungen zu beantworten.

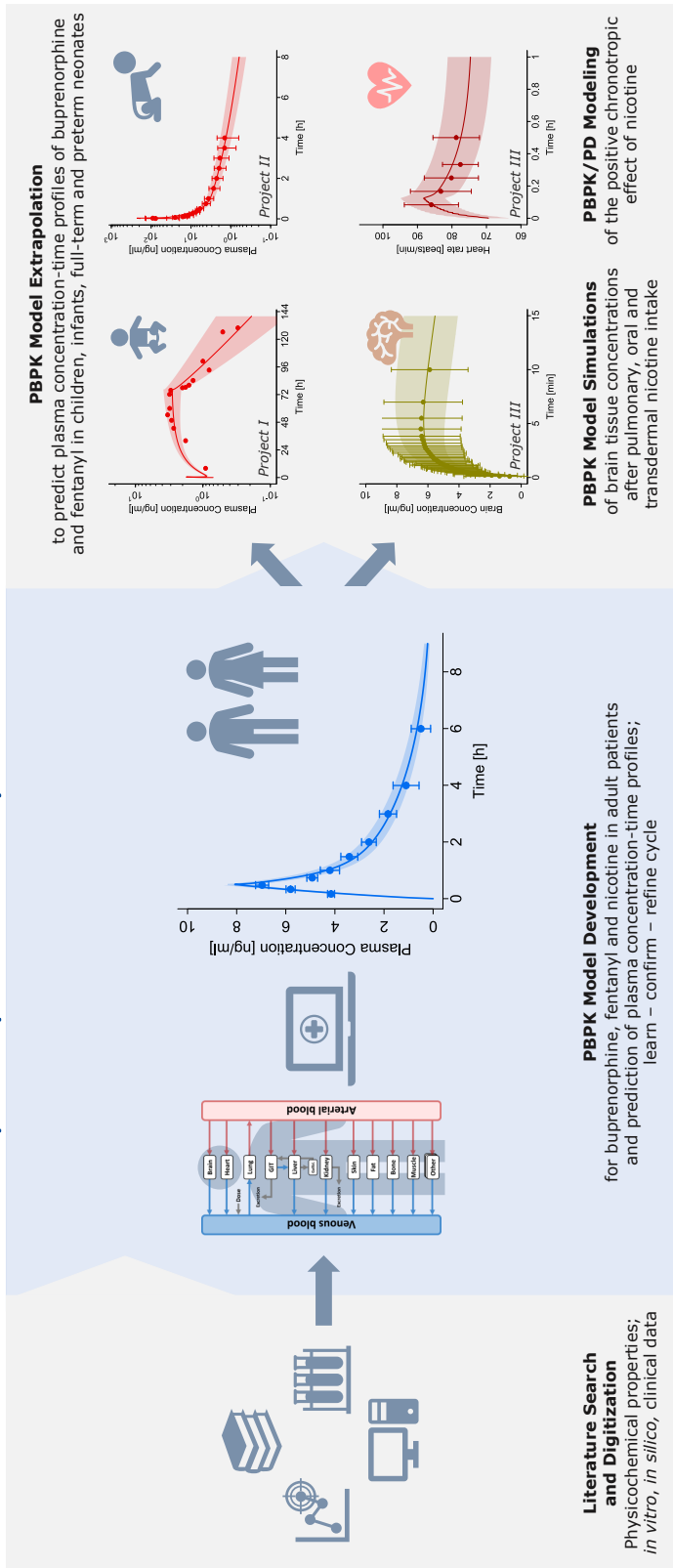
Ziel dieser Arbeit war es, neue Erkenntnisse über die PK von Buprenorphin und Fentanyl sowie über Nikotinhirnkonzentrationen zu erlangen. Zudem wurden die prädiktiven Eigenschaften der PBPK Modellierung für pädiatrische Patientengruppen untersucht.

Hierfür wurden PBPK Modelle für Buprenorphin, Fentanyl und Nikotin mit Daten von erwachsenen Patienten entwickelt und evaluiert. Anschließend wurden die Modelle für Buprenorphin und Fentanyl auf pädiatrische Patientengruppen extrapoliert und Plasmakonzentrations-Zeit-Profile sowie PK Parameter von Kindern, Neu- und Frühgeborenen erfolgreich vorhergesagt. Das Nikotin PBPK Modell wurde für Simulationen von Hirnkonzentrationen verwendet und um den positiv chronotropen Effekt von Nikotin erweitert.

Schlussfolgernd liefert die Arbeit neue Erkenntnisse über die PK von Buprenorphin, Fentanyl und Nikotin und bekräftigt die Verwendbarkeit der PBPK Modellierung, die PK eines Arzneistoffs in pädiatrischen Patienten vorherzusagen.

# GRAPHICAL ABSTRACT

## Physiologically Based Pharmacokinetic Modeling Providing Insights into the Pharmacokinetics of Buprenorphine, Fentanyl and Nicotine in Adult and Pediatric Patients



Graphics adapted from Kovar, L. et al. *Pharmaceutics* 2020;12(6):578 [1], Kovar, L. et al. *Pharmaceutics* 2020;12(10):908 [2] and Kovar, L. et al. *Clin Pharmacokinet* 2020;59(9):1119–1134 [3].



## DANKSAGUNG

---

Ich möchte mich von Herzen bei allen bedanken, die mich während meiner Promotion immer wieder unterstützt haben. Dabei gilt mein Dank allen voran meinem betreuenden Professor Thorsten Lehr für die Möglichkeit, in dem spannenden Themengebiet der Pharmakometrie zu forschen, sowie für all die Anregungen und Ideen, die unsere gemeinsamen Vorhaben und Arbeiten vorangetrieben haben. Ebenfalls möchte ich mich sehr bei Professor Claus-Michael Lehr für seine Unterstützung als wissenschaftlicher Begleiter und Zweitgutachter dieser Arbeit bedanken.

Vielen herzlichen Dank an meine Kolleginnen und Kollegen im Arbeitskreis, die mir immer wieder fachlich unterstützend zur Seite gestanden und sehr zur abwechslungsreichen Zeit während meiner Promotion beigetragen haben. Ein besonderer Dank gilt Dominik Selzer und Andreas Weber für ihre Unterstützung bei der Umsetzung der Arbeit.

Des Weiteren möchte ich Professor Hartmut Derendorf posthum dafür danken, meine Begeisterung für das Feld der Pharmakometrie geweckt zu haben. Ein großes Dankeschön gilt zudem Professor Charlotte Kloft und Professor Wilhelm Huisinga, die es mir ermöglicht haben, am Graduate Research Training Program „PharMetrX – Pharmacometrics and computational disease modeling“ teilzunehmen, sowie allen Co-Autoren, die an meinen wissenschaftlichen Publikationen mitgewirkt haben. Einen großen Dank für die unermüdliche Unterstützung in den vergangenen Jahren möchte ich außerdem an all meine Freunde richten. Abschließend danke ich von ganzem Herzen meiner Familie, insbesondere meiner Verlobten Christina, meiner Mutter Andrea, meinem Vater Andreas, meinem Bruder Johannes und meiner Schwester Anna-Katharina, sowie meinen Großeltern, die mir sehr viel auf meinen Lebensweg mitgegeben haben und die mir immer mit grenzenloser Unterstützung zur Seite stehen.



# CONTENTS

---

## I INTRODUCTION AND AIMS

1	INTRODUCTION	3
1.1	Physiologically Based Pharmacokinetic Modeling . . . . .	3
1.2	Challenges in Pediatric Drug Development and Drug Therapy . .	6
1.3	Model-Informed Drug Discovery and Development in Pediatrics .	7
1.4	Challenges in Pharmacokinetic Predictions for Pediatric Patients .	8
1.5	Physiologically Based Pharmacokinetic Modeling in Pediatric Patients	10
1.6	Investigated Drugs: Buprenorphine, Fentanyl and Nicotine . . . .	13
2	AIMS	17

## II INCLUDED PUBLICATIONS

3	RESULTS	21
3.1	Publication I – PBPK Modeling of Buprenorphine in Adult and Pediatric Patients . . . . .	21
3.1.1	Reference . . . . .	21
3.1.2	Author Contributions . . . . .	21
3.1.3	Copyright . . . . .	21
3.2	Publication II – PBPK Modeling of Fentanyl in Adult and Pediatric Patients . . . . .	45
3.2.1	Reference . . . . .	45
3.2.2	Author Contributions . . . . .	45
3.2.3	Copyright . . . . .	45
3.3	Publication III – PBPK Modeling of Nicotine Brain Tissue Concentrations . . . . .	66
3.3.1	Reference . . . . .	66
3.3.2	Author Contributions . . . . .	66
3.3.3	Copyright . . . . .	66

## III DISCUSSION, OUTLOOK AND CONCLUSIONS

4	DISCUSSION AND OUTLOOK	85
4.1	PBPK Modeling of Buprenorphine in Adult and Pediatric Patients	85
4.2	PBPK Modeling of Fentanyl in Adult and Pediatric Patients . . . .	88
4.3	PBPK Modeling of Nicotine Brain Tissue Concentrations . . . . .	91
5	CONCLUSIONS	93

	BIBLIOGRAPHY	95
--	--------------	----

## IV APPENDIX

A	SUPPLEMENTARY DOCUMENTS	117
A.1	Supplementary Document to Publication I . . . . .	117
A.2	Supplementary Document to Publication II . . . . .	154
A.3	Supplementary Document to Publication III . . . . .	184

<b>B</b>	<b>PUBLICATION HISTORY</b>	<b>259</b>
B.1	Research Articles . . . . .	259
B.2	Review Articles . . . . .	260
B.3	Conference Abstracts . . . . .	260
B.4	Oral Presentations . . . . .	261
B.5	Others . . . . .	261

## LIST OF FIGURES

---

Figure 1.1	Overview of PBPK model components . . . . .	5
Figure 1.2	Ontogeny profiles of CYP <sub>3A4</sub> , CYP <sub>3A5</sub> and CYP <sub>3A7</sub> . . . . .	9
Figure 1.3	Overview of a pediatric PBPK model development workflow	11

## ACRONYMS

---

NOTATION	DESCRIPTION
ADEs	Age-dependent exponents
ADR	Adverse drug reaction
AUC	Area under the concentration-time curve
BPCA	Best Pharmaceuticals for Children Act
CL	Clearance
CNS	Central nervous system
CYP	Cytochrome P <sub>450</sub>
DDI	Drug-drug interaction
EMA	European Medicines Agency
FDA	Food and Drug Administration
$f_m$	Fraction metabolized
GIT	Gastrointestinal tract
MID <sub>3</sub>	Model-informed drug discovery and development
MIDD	Model-informed drug development
MIPD	Model-informed precision dosing
NDA	New drug application
NRT	Nicotine replacement therapy
P-gp	P-glycoprotein
PBPK	Physiologically based pharmacokinetic
PD	Pharmacodynamic(s)
PK	Pharmacokinetic(s)
PREA	Pediatric Research Equity Act
R&D	Research and development
RBC	Red blood cells
SULT	Sulfotransferase
UGT	Uridine 5'-diphospho-glucuronosyltransferase
US	United States of America
WHO	World Health Organization

---



## Part I

### INTRODUCTION AND AIMS

This part introduces the concept and applications of physiologically based pharmacokinetic (PBPK) modeling and elaborates on the challenges in pediatric drug development and pharmacotherapy. Subsequently, an overview of model-informed drug discovery and development (MID<sub>3</sub>) in pediatrics and the prospects of PBPK modeling in this field is provided. Finally, this part depicts the workflow for pediatric PBPK modeling, introduces the three investigated drug compounds, buprenorphine, fentanyl and nicotine, and presents the aims of this work.



## INTRODUCTION

---

### 1.1 PHYSIOLOGICALLY BASED PHARMACOKINETIC MODELING

The field of PBPK modeling has emerged over the past decades with applications ranging from drug-drug interaction (DDI) assessments, study design optimization and dose selection to predictions of pharmacokinetics (PK) in special populations (e.g., pediatrics), thereby reducing the need for animal studies, justifying clinical trial designs and obviating specific clinical investigations [6–10].

PBPK modeling is also leveraged to generate knowledge and hypotheses on PK properties including liberation, absorption, distribution, metabolism and excretion (LADME) mechanisms [6, 11] as well as to simulate tissue-specific concentrations, increasing the understanding of the behavior of drugs [6, 10, 12, 13]. Moreover, PBPK models can be expanded to physiologically based pharmacokinetic/pharmacodynamic (PBPK/PD) models, allowing the investigation not only of drug exposure but also drug effects [10, 12, 13].

These applications are of great interest in drug research and development (R&D) since efficiency in R&D has declined over the past decades due to numerous challenges that impede the approval of new drug therapies [14–16]. Hence, supportive tools to enhance decision-making in R&D, to facilitate productivity and ultimately to improve drug therapy in both adult and pediatric patients are required [11, 16, 17]. Here, pharmacometric approaches have been established to support model-informed drug development (MIDD) and their use has been encouraged by regulatory agencies [8, 17–19]. Pharmacometrics can be defined as the science of developing and applying “mathematical models of biology, pharmacology, disease, and physiology used to describe and quantify interactions between xenobiotics and patients, including beneficial effects and side effects resultant from such interfaces” [20] and comprises various approaches including PBPK modeling [20, 21].

In general, PBPK models are based on three major components: (a) system-specific properties (e.g., organ sizes, organ-specific blood flow rates and tissue compositions), (b) drug-specific properties (e.g., lipophilicity, plasma-protein binding affinity and enzymatic stability) and (c) the structural model that consists of compartments and subcompartments, representing the anatomic arrangement of tissues and organs [12, 22, 23]. In addition, system- and drug-specific properties are combined to drug-biological properties such as tissue partition coefficients or fraction unbound, which are dependent on both organism and drug compound characteristics [23].

These PBPK model components are used for parametrization of an ordinary differential equation system to describe the LADME mechanisms of drug compounds [12]. With that, PBPK models build a mathematical mechanistic framework for the characterization and prediction of drug concentrations and the respective PK [24].

Detailed knowledge on drug properties is key for successful PBPK simulations [12]. Therefore, available data of various sources including information from *in vitro* assays (e.g., microsomal or recombinant enzyme assays), *in silico* methods (e.g., estimation of membrane permeability and tissue distribution) and *in vivo* studies (e.g., plasma concentration data) combined with *in vitro-in vivo* extrapolation techniques are integrated [10, 12, 25]. Additionally, information on the drug product (e.g., formulation properties) and clinical trial conditions (e.g., dose and dosing regimen) are required for PBPK model simulations [23].

System-dependent properties of PBPK models are parameterized based on physiologic and anatomic knowledge such as information on organ sizes and blood flow rates [12]. These properties can be informed by research results and large databases (e.g., from the International Commission on Radiological Protection [26]) and are generally separated from the drug-specific properties [12, 27–30]. This separation enables the assessment of covariates (e.g., organ impairment or enzyme abundance) as well as the extrapolation from adult to pediatric patient populations based on changes of system-specific parameters and LADME characteristics, provided that the relevant anatomic and physiologic information is available [10, 12, 24, 30–32]. In addition, the setup allows the investigation of intrinsic (e.g., age, disease and genetics) as well as extrinsic (e.g., diet and co-medication) factors that may influence system- and drug-specific components and, thus, the LADME processes of a drug [27]. Figure 1.1 depicts a schematic overview of the PBPK model components.

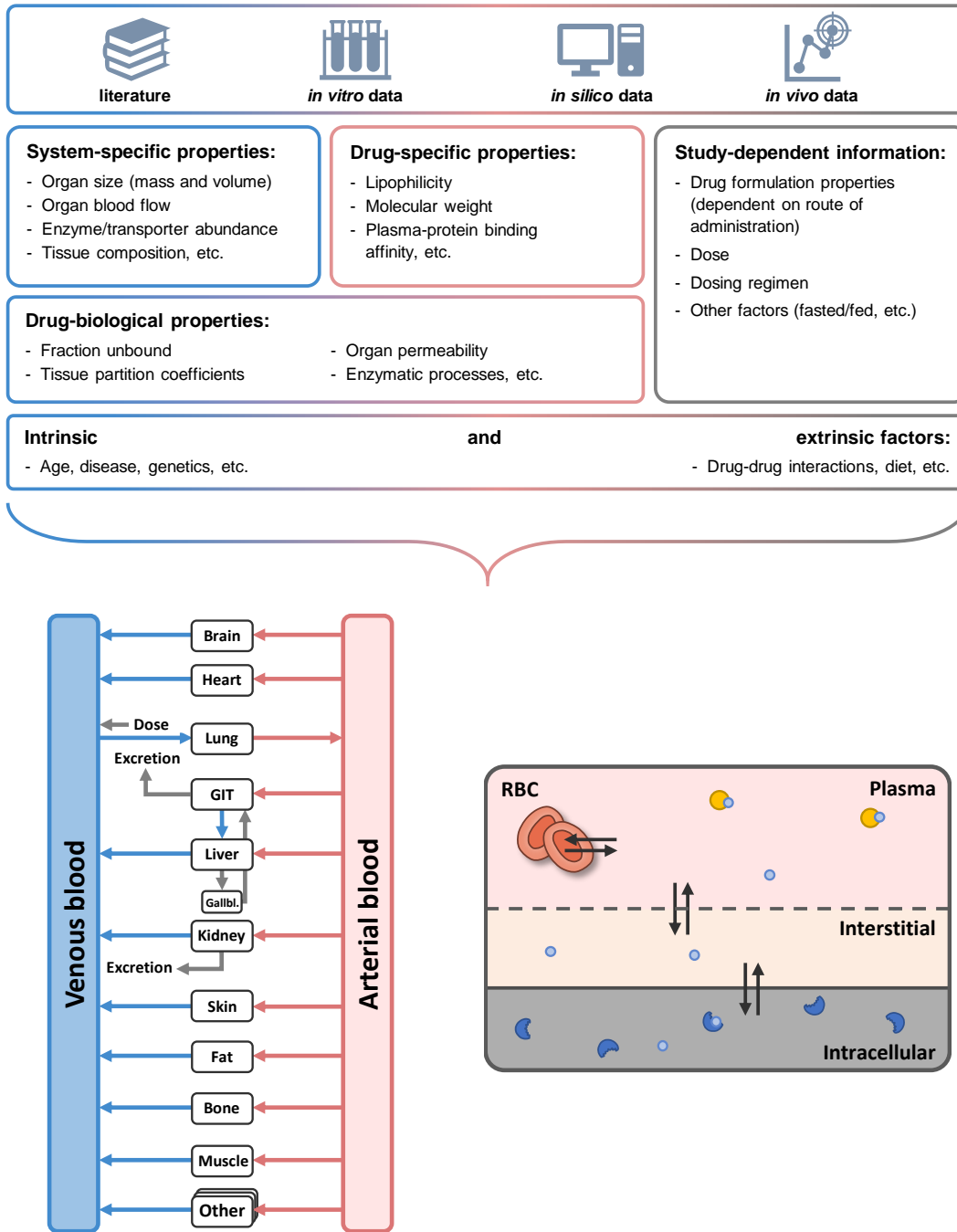


Figure 1.1: Overview of the PBPK model components. The upper part shows data sources, system-specific, drug-specific and drug-biological components, information on formulation properties and study protocol as well as intrinsic and extrinsic factors influencing model components. The lower left part depicts an exemplary PBPK model structure including organs/tissues and blood flows. Organs and tissues can be further subdivided into vascular (plasma and RBC), interstitial and intracellular space (lower right part). Information and data from [2, 12, 22, 23, 27]. The structural model and subcompartmental structures were adapted from Kovar et al. [2], distributed under the terms and conditions of the Creative Commons Attribution (CC BY 4.0) license (<http://creativecommons.org/licenses/by/4.0/>). Here, rectangles represent compartments, arrows denote in-/outflows, blue circles depict drug compounds, orange circles represent plasma proteins and blue crescents represent enzymes. GIT: gastrointestinal tract, RBC: red blood cells.

The development of mechanistic *in silico* models to predict tissue partition coefficients based on drug compound and organism properties has been a key factor to facilitate the development of whole-body PBPK models [6, 12]. The *in silico* models enable the estimation of drug tissue distribution without conducting sophisticated preclinical tissue distribution studies [6, 12, 33–35]. However, it should be noted that partition coefficients in PBPK models that were developed without measured tissue concentration data might not necessarily reflect reality [12]. Thus, PBPK model predictions of specific tissue concentrations may require *in vivo* tissue data to inform and refine the models [12, 36, 37].

Knowledge gaps on physiologic properties such as enzyme and transporter abundances as well as uncertainties regarding model input parameters, among others, can lead to erroneous PK characterization of a drug [38, 39]. In turn, inaccurate PBPK model predictions can indicate model misspecifications such as wrong model assumptions or missing model components and should be investigated [12]. Hence, besides model building, PBPK model development comprises thorough model evaluation in an iterative “learn, confirm, and refine” approach [12]. Here, the complementation of *in vitro* and *in silico* data with observed *in vivo* data (e.g., plasma concentrations and renal excretion data) from clinical studies can help to optimize PBPK models [12, 40]. The evaluated and refined PBPK model can then be used for the intended purpose such as dosing simulations or the assessment of DDI scenarios [12].

In regulatory submissions, PBPK modeling has primarily been used for DDI assessments (period 2008–2017) [9]. However, the highest growth rate in recent publications on PBPK modeling could be observed in the field of special populations that includes the application in pediatrics [7]. This interest may be due to the fact that many drugs are scarcely studied in children, particularly in full-term and preterm neonates [41–47]. In addition, ethical and logistic challenges, that are often unique to pediatric populations especially newborns, [48–53] impede the conduct of clinical trials, resulting in difficulties in drug development and pharmacotherapy in pediatrics [44].

These difficulties in pediatric drug development and drug therapy, the prospect of MID3 to streamline new drug product approvals as well as the potential of PBPK modeling to mechanistically investigate and predict the PK of drugs in both adult and pediatric patients are outlined in the following sections. Moreover, the three drugs investigated in this work, buprenorphine, fentanyl and nicotine, as well as corresponding treatment issues and ambiguities in PK characteristics are introduced.

## 1.2 CHALLENGES IN PEDIATRIC DRUG DEVELOPMENT AND DRUG THERAPY

Drug therapy in pediatric patients poses a huge challenge since many drugs approved for the treatment of adults are hardly investigated in pediatric patient populations and consequently, off-label use is a prevalent phenomenon [41–47]. In a recent study, over 95% of patients in neonatal intensive care units received at least one off-label drug [46].

A triggering factor for the difficulties traces back to the 1960s, when the thalidomide tragedy occurred, leading to increased regulatory requirements for new

medications [44]. Regulatory interventions comprised extended investigations of drug candidates including well-controlled, scientific clinical trials as prerequisite for drug approvals and were introduced to protect patients from ineffective and unsafe medications [44]. However, in the sequel, children were rarely included in clinical studies, resulting in a lack of information on safety, effectiveness and labeling for pediatric populations [44, 54]. As a consequence, the pediatric pharmacologist Harry Shirkey noted that pediatric patients were becoming “therapeutic orphans” [55, 56], which was supported by later reviews of Wilson [54, 57] and Gilman [58].

Subsequently, various efforts were pursued to enhance pediatric clinical pharmacology and to support pediatric clinical trials including preparation of reports and guidances on the evaluation of medications in pediatric patients [44, 59, 60]. While these approaches did not directly lead to an increased fraction of approved drugs for pediatric use [44, 54, 58], they set the scene for several regulatory acts in the United States (US) and Europe including the Best Pharmaceuticals for Children Act (BPCA), the Pediatric Research Equity Act (PREA) and the Paediatric Regulation [44, 61–63]. As a result, the Committee on Drugs of the American Academy of Pediatrics noted over 800 pediatric labeling changes in the US until 2014 [64].

However, as indicated, despite these advances, major challenges in pediatric drug development, drug therapy and off-label use remain in various therapeutic areas such as pain management and antibiotic therapy [41, 45, 64–69]. Ethical, logistic and financial hurdles including enrollment and dosing difficulties impede the conduct of pediatric clinical studies, particularly in neonates [11, 49–53]. Hence, many drugs have not been studied properly, adequate drug formulations may not exist and reliable information on therapeutic decision-making is scarce in pediatrics [49, 51, 52]. This calls for innovative approaches to close knowledge gaps and to support the investigation, development and approval of medicines for pediatric patients [11, 49, 50, 70]. Here, pharmacometric modeling approaches can be leveraged to enhance decision-making, optimize clinical trial design and ultimately improve drug therapy [11, 32, 49, 70–72].

### 1.3 MODEL-INFORMED DRUG DISCOVERY AND DEVELOPMENT IN PEDIATRICS

Clinical pharmacology studies in pediatric patients that aim to investigate the PK, PD and safety of a drug are often difficult to conduct [11, 49–53]. Here, MIDD offers a valuable tool to increase success rates of pediatric clinical trials, informing study design and assisting in various areas of pediatric drug development [9, 11, 50, 53, 70].

The term MIDD describes “the application of a wide range of quantitative models in drug development to facilitate the decision-making process” [19]. In general, these applications build upon existing knowledge and comprise dose selection based on the “exposure-matching” principle, providing supportive evidence for efficacy, model-based dosing, bridging between populations and label recommendations, among others [8, 11, 17–19, 71]. With that, MIDD can help to reduce the number of study participants or even obviate the need for specific clinical trials,

decreasing time and costs in the drug development process and thus holds the potential to address various challenges in a wide range of phases [8, 11, 17–19, 71]. Over time, both the term “MIDD” and the concept have evolved [14, 16, 19, 73, 74]. MIDD, which focuses on the drug development process, has been extended to the drug discovery phase in MID<sub>3</sub> [17, 75].

The US Food and Drug Administration (FDA) guidance for industry on “Clinical Investigation of Medicinal Products in the Pediatric Population” from 2018 suggests the use of MID<sub>3</sub> in the design of pediatric clinical studies, optimization of dosing strategies, maximizing knowledge generation from clinical trials and leveraging available information to bridge knowledge gaps and avoid unnecessary studies [70]. These applications include the extrapolation of existing information from other populations (adults and/or pediatric populations) to the pediatric patient population of interest in order to propose initial dosing recommendations [9, 11, 70]. Moreover, Bi and colleagues have recently demanded the use of MIDD in every stage of all pediatric drug development programs [11]. Here, different pharmacometric approaches such as population pharmacokinetic modeling, allometric scaling as well as PBPK modeling can be leveraged [9, 11].

#### 1.4 CHALLENGES IN PHARMACOKINETIC PREDICTIONS FOR PEDIATRIC PATIENTS

Pediatric populations including adolescents, children, infants, full-term and preterm neonates differ enormously both in obvious categories such as size and age but also in the maturation of various processes affecting the disposition of drug compounds (e.g., enzymatic metabolism) [9, 42]. These anatomic and physiologic differences result in higher body-weight corrected clearances (CL) in infants and young children compared to adults for many drugs [76, 77]. In contrast, the PK and thus dosing in adolescents is often similar to that of adult patients [78, 79], while CL in neonates is often immature [76, 80]. This matter has led to summarizing statements of Oostenbrink and de Wildt stating that “Kids are no little adults and not all kids are the same” [81] or Anderson and Holford who concluded “children are small adults, neonates are immature children” [80]. In adolescents and older children, allometric scaling [25, 82] has been shown to provide accurate CL predictions and can be a useful pharmacometric tool to predict and investigate drug PK [11, 79, 83]. However, for infants and neonates, when rapid maturational changes occur, that affect drug metabolism, distribution and excretion processes, standard allometric scaling with the commonly applied exponent of 0.75 reaches its limits, calling for more mechanistic approaches [79, 83–85]. Mahmood and colleagues introduced body weight-dependent exponents and age-dependent exponents (ADEs) in allometric scaling, that were superior to a fixed exponent of 0.75 [86, 87]. Yet, predictions with body weight-dependent allometric exponents require substantial amount of data in pediatric patients [86, 87] and assessments of ADEs revealed decisive limitations for CL predictions of certain drugs such as ibuprofen (9.5-fold overprediction of CL) or morphine (3.6-fold overprediction of CL) in preterm neonates [86, 87].

One reason for such mispredictions might be the complex nature of enzyme maturation: Although admittedly oversimplified, a review by Hines concluded

that drug metabolizing enzymes can be categorized into three different groups [88]: One group of enzymes – containing the largest clinically relevant cohort of Cytochrome P450 (CYP) enzymes including CYP1A2, CYP2C9, CYP2D6 and CYP3A4 [89] – is barely expressed in the fetus while showing rising expression levels in the first one to two years after birth [88]. The second group of enzymes shows fairly constant levels of expression throughout gestation (e.g., CYP3A5 and Sulfotransferase (SULT) 1A1) [88]. Finally, the third group of metabolizing enzymes, which includes CYP3A7, the major fetal form of CYP3A [90], exhibits its highest expression levels in the fetus but is silenced within the first two years after birth [88]. Figure 1.2 exemplarily depicts three enzyme ontogeny profiles of the described groups as implemented in the PBPK modeling software PK-Sim® [28, 91].

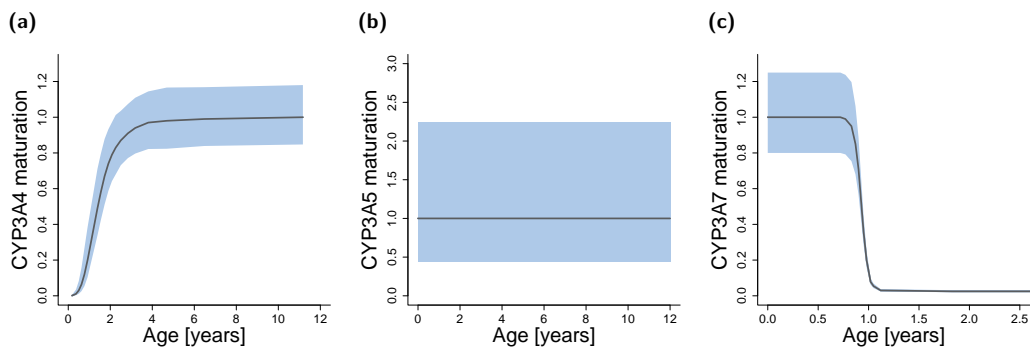


Figure 1.2: Ontogeny profiles of (a) CYP3A4, (b) CYP3A5 and (c) CYP3A7 in the liver as implemented in the PBPK modeling software PK-Sim® [28, 91]. Black lines depict population geometric mean ontogeny, blue areas depict the geometric population standard deviation. Age represents postmenstrual age in years.

As a result, depending on which metabolizing enzymes, transporters and other disposition mechanisms are involved in a drug's PK, elimination of different drugs changes at different rates and, hence, CL predictions in infants and neonates become complex [77]. For instance, significant changes in CL may even occur within a single week after birth (approximately 3-fold increase for sildenafil), requiring immediate dose adaptations [92]. The complexity is aggravated by the matter, that not only developmental changes but also various internal and external factors can impact drug CL, for example, disease state or co-medication [93, 94]. Additionally, PK predictions of solely the parent compound might represent an oversimplification: Some drugs are prodrugs that require bioactivation (e.g., omeprazole [95]), some drugs have active metabolites with similar pharmacological activity (e.g., morphine [96, 97]) and others are metabolized to toxic side-products (e.g., acetaminophen [98]) – all potentially impacted by the maturation of metabolizing enzymes as well as internal and external factors [77].

Thus, there is a clear need for advanced and thoroughly evaluated mechanistic approaches to predict and investigate the PK of drugs and their metabolites in infants, full-term and preterm neonates [99]. Here, PBPK modeling allows the integration of enzyme and transporter ontogeny as well as of other anatomic and physiologic changes and represents a helpful tool for investigation of internal and external factors, optimization of dosing regimens and assistance with the

development of new drug products, helping to avoid insufficient exposure or toxicity [32, 81].

#### 1.5 PHYSIOLOGICALLY BASED PHARMACOKINETIC MODELING IN PEDIATRIC PATIENTS

As outlined in Section 1.4, drug metabolism in pediatric patients may be affected by the complex maturation of different drug metabolizing enzymes, but it can also be influenced by other processes such as age-dependent hepatic blood flow [100, 101]. In addition, physiologic and anatomic differences between pediatric and adult patients can impact absorption, distribution and excretion mechanisms [39, 100, 101]. For example, the composition of gastric fluid in pediatric populations particularly in neonates differ from the one in adults, affecting absorption processes of drug compounds [102]. Drug distribution can be altered due to changes in plasma protein abundance and hence differences in fraction unbound [103]. Finally, excretion mechanisms in pediatric patients such as renal excretion via glomerular filtration are subject to age-dependent maturation [101], which can be integrated in PBPK models [13, 25].

In general, developed PBPK models for drug exposure in adult populations can be extrapolated to a new target population, scaling all relevant model parameters to the anatomy and physiology of the population of interest [12, 30]. Hence, PBPK modeling is prone to be used in pediatric modeling, extrapolating adult PBPK models, that were built and evaluated with available clinical data, to the pediatric target population for guidance on dose selection, optimization of study designs or investigation of a drug's PK [8, 13, 32, 38]. A modeling workflow to develop a pediatric PBPK model has been established and presented in several case studies and reviews [25, 31, 37, 104]. Figure 1.3 exemplifies such a pediatric PBPK modeling workflow from gathering necessary information and data to performing model simulations in the pediatric populations of interest.

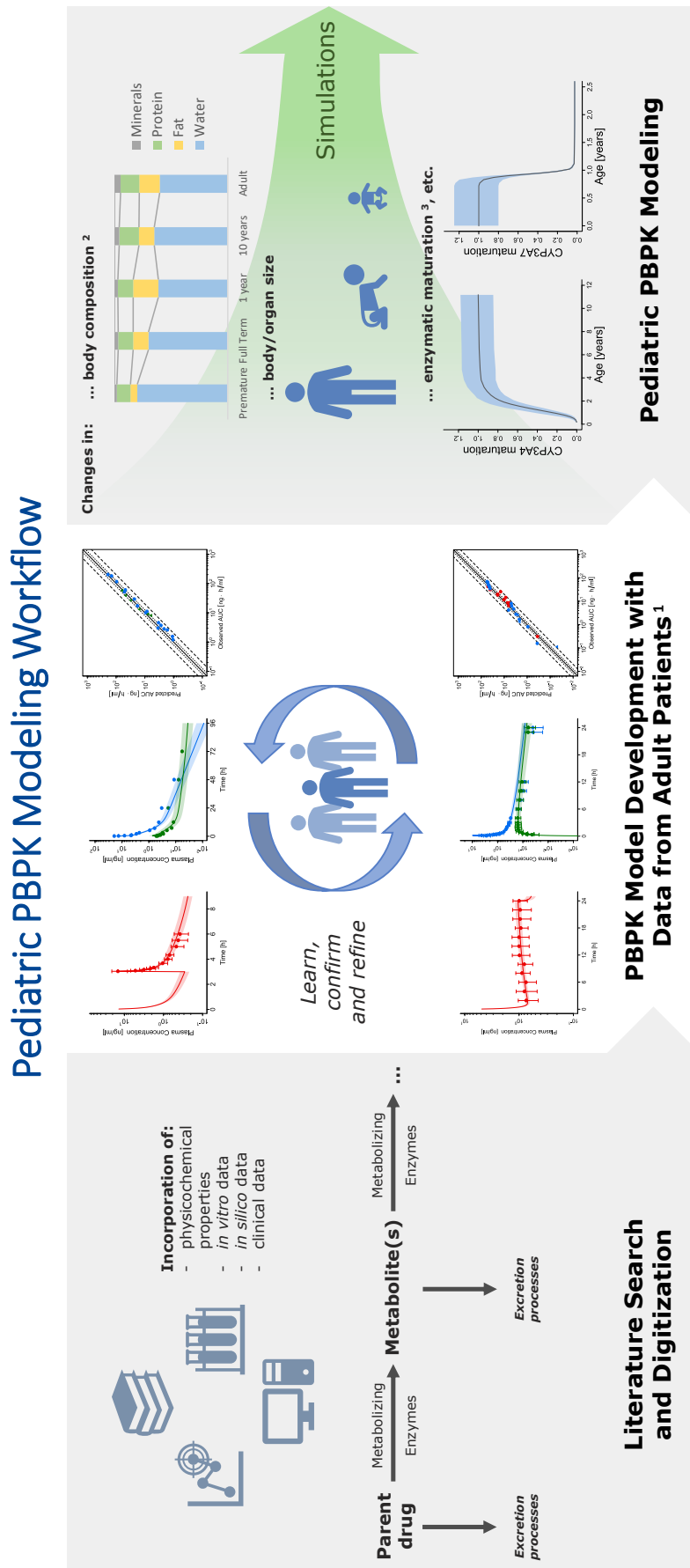


Figure 1.3: Overview of a pediatric PBPK model development workflow. <sup>1</sup> Graphics from [1, 2]. <sup>2</sup> Adapted from [105]. <sup>3</sup> Ontogeny profiles of CYP<sub>3</sub>A<sub>4</sub> and CYP<sub>3</sub>A<sub>7</sub> in the liver as implemented in the PBPK modeling software PK-Sim<sup>®</sup> [28, 91].

The first step of this workflow represents a thorough examination of the available information and data [25]. This comprises the collection and evaluation of *in vitro*, *in silico* and *in vivo* data on drug- and system-specific parameters including physicochemical properties, anatomic and physiologic parameters, LADME data as well as PK data accessible from own data bases or via collection and digitization of published studies [32, 106].

Subsequently, an adult PBPK model is developed provided that adult PK data for the drug of interest is available [25, 31, 32]. Extrapolation of an evaluated adult PBPK model to pediatric populations offers the advantage to establish a thorough understanding of LADME processes in a relatively homogenous population, before performing exposure predictions in pediatrics [25, 32]. On the contrary, naïve predictions based on a pediatric PBPK model that has not been extrapolated from an adult PBPK model feature lower confidence [25, 32].

Hence, if applicable, after gathering and assessing the available data, an adult PBPK model is built and thoroughly evaluated, a step that is crucial for later pediatric PBPK model predictions [25, 31, 32]. System- and drug-specific input parameters required for model building are driven by the model structure, drug substance, intended model application and route of administration [25]. The model building process is followed by an iterative process of model evaluation and model refinement with available clinical PK data according to the learn, confirm and refine paradigm in a “top-down/bottom-up” also called “middle-out” approach [12, 25, 32, 40, 52, 70, 73].

After adult PBPK model development, system-specific model parameters are scaled to the pediatric population of interest and ontogeny information are applied [25]. While drug-specific parameters remain unchanged, some drug-biological properties might need adaptation (e.g., fraction unbound due to the aforementioned ontogeny of plasma protein abundance throughout maturation) [25, 103]. The pediatric PBPK model can then be used to predict drug concentrations and PK parameters in pediatric populations [25]. Here, already available PK data in pediatrics offer the advantage to evaluate model predictions [25].

The use of PBPK modeling in the field of pediatrics has shown a sharp incline in the past decade: El-Khateeb and coworkers pointed out that the number of publications on pediatric PBPK modeling rose 5.5-fold in the investigated time period (2010–2019) [7]. Pediatric PBPK modeling has also gained notable popularity in regulatory new drug application (NDA) submissions, in which the second most common application of PBPK modeling was in pediatrics (15% of applications) [9].

In pediatric drug development, PBPK modeling has been used for planning “first-in-pediatric” PK studies, optimization of study designs, dose selection and optimization as well as DDI assessment, among others [31, 32, 38, 39, 99]. In an update from the FDA on PBPK modeling in regulatory science, Grimstein et al. outlined that the main use of pediatric PBPK modeling in investigational NDA submissions was to propose initial dosing recommendations for clinical studies [9]. To propose a first-in-pediatric PK study dose with modeling and simulation, the dose can be selected in a way to match the same exposure achieved in the adult patient population (“exposure-matching” strategy) [11, 25, 107–109]. It

should be noted, that this strategy yet relies on the assumption of a similar safety and efficacy exposure-response relationship for pediatric and adult patients [11, 110, 111].

Besides its use in drug discovery and development within the MID<sub>3</sub> framework, PBPK modeling can also be applied to investigate and improve pharmacotherapies with drugs that are already established on the market [32, 38, 112]. The integration of increasing physiologic knowledge in PBPK models (e.g., on organ maturation and ontogeny of metabolizing enzymes) allows investigators to generate hypotheses, for example on potential mechanisms causing LADME differences between pediatric and adult patients, and to simulate “what if” scenarios to determine causes for the altered PK [11, 38, 113]. The development of novel pediatric PBPK models that are made publicly available can further promote research activities on the investigated drugs, facilitate model applications in future drug development programs and thereby support efforts to optimize pharmacotherapy [11, 30].

However, to achieve a broader and solidified application of pediatric PBPK modeling and to make pediatric PBPK modeling a more integral part of drug discovery and development, further investigations and evaluations of PBPK model prediction performances, particularly for drugs with complex elimination mechanisms, are needed [13, 32]. Concurrently, many knowledge gaps and ambiguities in drug therapy of pediatric patients especially in infants and neonates still exist, optimal dosing regimens remain unclear and adverse drug reactions (ADRs) impede drug therapy. Here, the development of new PBPK models can help to close knowledge gaps, support the design of clinical studies and ultimately contribute to a better drug therapy in pediatric patients [52, 70, 99, 114].

#### 1.6 INVESTIGATED DRUGS: BUPRENORPHINE, FENTANYL AND NICOTINE

Buprenorphine and fentanyl are opioid analgesic drugs widely used in the treatment of moderate to severe pain in populations of different ages [115–120]. While fentanyl acts as a full agonist on the  $\mu$ -opioid receptor and buprenorphine as a partial agonist, both show a significantly higher receptor potency compared to morphine [115, 119, 121]. As such, both drugs are listed in the World Health Organization (WHO) guideline on cancer pain management from 2018 as potential opioids for the treatment of pain in adults and adolescents [115].

However, buprenorphine and fentanyl also play a crucial role in the treatment of various pediatric populations including full-term and even preterm neonates [47, 117–120]. Depending on indication and patient population, fentanyl is used intravenously, in rapid-acting sublingual and intranasal formulations as well as via transdermal patches and represents the opioid drug most often applied in neonatal intensive care units [119, 120]. The application of buprenorphine in pediatrics has also become widespread with administration routes ranging from intravenous and sublingual to transdermal for the treatment of chronic pain as well as postoperative analgesia [117].

Because pain – caused, for instance, by intubation or mechanical ventilation – can act as a major stressor, that potentially increases morbidity and mortality in critically ill newborns, analgesic treatment is commonly introduced in young pe-

diatric patients [119, 122]. Here, opioids such as fentanyl and buprenorphine play an essential role [119, 123]. Yet, while fentanyl administration typically results in an improved dynamic total respiratory system compliance [124], even low doses of fentanyl can lead to ADRs, in some cases chest wall rigidity, a potentially fatal ADR, hampering fentanyl pharmacotherapy [125, 126].

Moreover, a review on anesthetic use in newborn infants noted that no definitive safety has been established for fentanyl in young children [47], while missing information on PK and PD have been linked to undertreatment of pain in preterm neonates [127]. Völler et al. just recently found out, that fentanyl CL in preterm neonates does not only depend on postnatal but also on gestational age [127].

The CYP<sub>3A4</sub> metabolic pathway depicts the major route of norfentanyl formation from the parent compound fentanyl and was also assumed to represent the main route of fentanyl elimination [116, 128]. Yet, recent studies suggested the presence of unknown metabolites and metabolizing pathways, which remains under debate [129, 130].

Buprenorphine was identified to be a substrate of various CYP and uridine 5'-diphospho-glucuronosyltransferase (UGT) enzymes including CYP<sub>3A4</sub>, CYP<sub>3A7</sub>, CYP<sub>2C8</sub>, UGT<sub>1A1</sub>, UGT<sub>1A3</sub> and UGT<sub>2B7</sub> [131, 132]. As a result, the disposition of the two opioids buprenorphine and fentanyl is affected by the abundances and activity of various CYP and UGT enzymes, that in turn are heavily impacted by maturation processes [91] and potential DDIs [133, 134], many of which have not yet been investigated.

Hence, despite their routine application for sedation and pain control, treatment issues and lack of knowledge in the PK of buprenorphine and fentanyl – especially regarding metabolic and excretion processes – exist, particularly in pediatrics, and a need for further research to close knowledge gaps has been identified [117, 120, 123, 129, 130, 135].

However, conducting investigational clinical studies are cost- and time-intensive and accompanied by ethical and logistic challenges, that are often unique to pediatric populations, especially newborns [48–52, 136]. Here, as described, PBPK modeling can be a valuable tool to study LADME processes in both adult and pediatric populations, support and optimize the design of clinical trials and its use in drug discovery and development is endorsed by the FDA and the European Medicines Agency (EMA) [9, 13, 22, 31, 52, 137, 138]. As both buprenorphine and fentanyl are subject to extensive enzymatic metabolism [129, 131, 139–142], mechanistic modeling offers the potential to integrate prior knowledge on enzyme maturation, enzymatic activity and other disposition processes to investigate untested DDI scenarios and provide new insights into the drug exposure in adult and pediatric patient populations [6, 9, 12, 22, 23, 30, 38].

Since most of the metabolic enzymes involved in the opioids' elimination are barely expressed in neonates [91], an unadjusted allometric scaling approach could lead to biased buprenorphine and fentanyl CL predictions, overestimating degradation processes and thus underestimating exposure [83, 84]. PBPK modeling can incorporate ontogeny information on enzymes and transporters and has been shown to be suited for extrapolations of the PK from adults to pediatric patients including full-term and preterm neonates [9, 23, 30, 52].

Additionally, some PK data from pediatric patients of different age groups has been published for both buprenorphine and fentanyl [143–149]. Hence, besides the aim to close knowledge gaps with regard to buprenorphine and fentanyl PK and therapy, the general performance of the selected PBPK modeling approach to predict plasma concentrations and individual PK parameters of various pediatric age groups can be further evaluated in this work. This assessment could represent a key component for future research activities as difficulties in pediatric drug development impede pharmacotherapy especially for young infants and neonates, calling for innovative approaches to reduce lack of knowledge and to improve pharmacotherapy.

In general, drug concentrations at the site of action are crucial and determine drug effects [150]. However, experimental determination of tissue concentrations can be extremely difficult or not feasible at all [23, 151]. Hence, for pragmatic reasons, drug concentrations are usually measured from venous blood draws, although this central compartment does often not represent the site of action, for example, in case of drugs acting in the central nervous system (CNS) [151]. This matter also applies for the stimulating effects of nicotine in the CNS [152, 153]. Here, PBPK modeling can be applied for simulation and investigation of drug tissue concentrations [6, 27, 38, 154].

Nicotine is consumed worldwide primarily through smoking combustible cigarettes [155]. The WHO attributes over eight million deaths per year – caused by cardiovascular disease, cancer and pulmonary disease, among others – to tobacco use [156]. While a majority of smokers intends to quit smoking every year, the addictive nature of smoking, which is mainly ascribed to the pharmacologically active nicotine, results in low quit rates of about 5% [157, 158]. This calls for intensified research in this field to close knowledge gaps and to improve smoking cessation strategies like nicotine replacement therapies (NRTs), in which nicotine itself plays a crucial role [153].

Besides its effects on the CNS, nicotine also leads to an increase in heart rate (positive chronotropic effect), representing a PD marker that is commonly monitored in clinical trials on smoking and NRTs [152, 159–161]. Such NRTs including nicotine gums and nicotine transdermal therapeutic systems aim to mimic nicotine exposure of cigarettes while avoiding exposure to other toxic tobacco ingredients [153]. However, nicotine plasma concentrations might not represent the ideal exposure marker as nicotine's main site of action is the brain tissue [152, 153]. Thus, it would be of particular interest to get further insights into nicotine's PK regarding brain tissue levels resulting from different routes of nicotine administration. This may improve the understanding of nicotine addiction and could lead to the development of more successful NRT treatment strategies. Here, PBPK modeling allows the estimation of drug exposure at the target tissue [6, 23, 27, 154] and can be used in this work to evaluate differences in simulated nicotine brain tissue concentrations after pulmonary, oral and transdermal nicotine multiple dose administrations.



## AIMS

---

This thesis aimed to gain insights into the PK of buprenorphine, fentanyl and nicotine by leveraging PBPK modeling. In addition, a major objective was to further explore and enhance the ability and value of PBPK modeling to predict mean and individual plasma concentration-time profiles as well as PK parameters in pediatric patients including full-term and preterm neonates. Moreover, the development of the three parent-metabolite PBPK models should contribute to a library of publicly available PBPK models that can be further used in future investigations, promoting research activities on the studied drug compounds.

The aims of this thesis were realized within the scope of the following projects:

### PUBLICATION I – PBPK MODELING OF BUPRENORPHINE IN ADULT AND PEDIATRIC PATIENTS:

The aim of Project I was to develop an adult and pediatric parent-metabolite PBPK model of buprenorphine as well as to investigate the performance of PBPK modeling to predict the PK in pediatric patients of different age groups. For this purpose, the objectives were first, to build and evaluate an intravenous PBPK model of buprenorphine and norbuprenorphine with clinical data from adult patients including a DDI scenario with rifampicin and data on renal excretion, second, to extrapolate the model to children and preterm neonates, accounting for age-related differences, and finally, to apply the extrapolated PBPK model to predict individual plasma concentration-time profiles of buprenorphine after short and long-term infusions in children and preterm neonates. Results should be compared to predictions with allometric scaling approaches. In addition, the assessment of buprenorphine and norbuprenorphine DDI scenarios with the frequently used perpetrator drugs clarithromycin and itraconazole, that had not yet been studied clinically, was planned by leveraging the developed adult PBPK model.

### PUBLICATION II – PBPK MODELING OF FENTANYL IN ADULT AND PEDIATRIC PATIENTS:

The purpose of Project II was to develop a parent-metabolite PBPK model of fentanyl and norfentanyl for both adult and pediatric populations to gain new insights into the PK of fentanyl. Hence, the objectives were first, to build an intravenous PBPK model of fentanyl and norfentanyl in adults, second, to evaluate the model using plasma concentration-time profiles including a DDI scenario with voriconazole and data on renal excretion and finally, to extrapolate the model to pediatrics for prediction of mean plasma concentration-time profiles as well as individual and mean CL parameters in pediatric patients of different age groups. Further, the developed PBPK model should serve as a foundation to investigate fentanyl PK in both adult and pediatric patients

including the investigation of fentanyl plasma concentration peaks potentially related to the occurrence of the ADR chest wall rigidity in neonates.

PUBLICATION III – PBPK MODELING OF NICOTINE BRAIN TISSUE CONCENTRATIONS:

The aim of Project III was to simulate and compare nicotine brain tissue concentrations and heart rate profiles after pulmonary, oral and transdermal nicotine intake as well as to demonstrate the applicability of PBPK modeling to integrate various different routes of drug administration in a single model. Hence, the development of a PBPK/PD model of nicotine and its major metabolite cotinine was planned for a non-smoking and a smoking population. The model should be evaluated with plasma and a brain tissue concentration-time as well as heart rate-time profiles. Finally, the objective was to apply the model to evaluate differences in brain tissue concentrations and heart rate profiles between pulmonary nicotine administration and NRT treatments.

## Part II

### INCLUDED PUBLICATIONS

This part presents the published research articles included in this work.



## RESULTS

---

### 3.1 PUBLICATION I – PBPK MODELING OF BUPRENORPHINE IN ADULT AND PEDIATRIC PATIENTS

#### 3.1.1 *Reference*

#### **Physiologically-Based Pharmacokinetic (PBPK) Modeling of Buprenorphine in Adults, Children and Preterm Neonates.**

Lukas Kovar, Christina Schräpel, Dominik Selzer, Yvonne Kohl, Robert Bals, Matthias Schwab and Thorsten Lehr.

*Pharmaceutics* 2020;12(6):578. DOI: 10.3390/pharmaceutics12060578 [1].

#### 3.1.2 *Author Contributions*

Author contributions according to the contributor roles taxonomy (CRediT) [4, 5] were as following:

Lukas Kovar	Refer to <i>Contribution Report</i> (p. vii)
Christina Schräpel	Conceptualization, Investigation, Methodology, Writing – review & editing
Dominik Selzer	Conceptualization, Visualization, Writing – review & editing
Yvonne Kohl	Funding acquisition, Writing – review & editing
Robert Bals	Funding acquisition, Writing – review & editing
Matthias Schwab	Conceptualization, Funding acquisition, Writing – review & editing
Thorsten Lehr	Conceptualization, Funding acquisition, Investigation, Methodology, Writing – original draft, Writing – review & editing

#### 3.1.3 *Copyright*

©2020 by the authors. Licensee MDPI, Basel, Switzerland. This article is an open access article distributed under the terms and conditions of the Creative Commons Attribution (CC BY 4.0) license (<http://creativecommons.org/licenses/by/4.0/>).



Article

# Physiologically-Based Pharmacokinetic (PBPK) Modeling of Buprenorphine in Adults, Children and Preterm Neonates

Lukas Kovar <sup>1</sup>, Christina Schräpel <sup>1,2</sup>, Dominik Selzer <sup>1</sup>, Yvonne Kohl <sup>3</sup>, Robert Bals <sup>4</sup>, Matthias Schwab <sup>2,5</sup> and Thorsten Lehr <sup>1,\*</sup>

<sup>1</sup> Department of Clinical Pharmacy, Saarland University, 66123 Saarbrücken, Germany; lukas.kovar@uni-saarland.de (L.K.); christina.schraepel@uni-saarland.de (C.S.); dominik.selzer@uni-saarland.de (D.S.)

<sup>2</sup> Dr. Margarete Fischer-Bosch-Institute of Clinical Pharmacology, 70376 Stuttgart, Germany; Matthias.Schwab@ikp-stuttgart.de

<sup>3</sup> Fraunhofer Institute for Biomedical Engineering IBMT, 66280 Sulzbach, Germany; yvonne.kohl@ibmt.fraunhofer.de

<sup>4</sup> Department of Internal Medicine V, Saarland University, 66421 Homburg, Germany; robert.bals@uks.eu

<sup>5</sup> Departments of Clinical Pharmacology, and Pharmacy and Biochemistry, University Tübingen, 72076 Tübingen, Germany

\* Correspondence: thorsten.lehr@mx.uni-saarland.de; Tel.: +49-681-302-70255

Received: 5 June 2020; Accepted: 21 June 2020; Published: 23 June 2020



**Abstract:** Buprenorphine plays a crucial role in the therapeutic management of pain in adults, adolescents and pediatric subpopulations. However, only few pharmacokinetic studies of buprenorphine in children, particularly neonates, are available as conducting clinical trials in this population is especially challenging. Physiologically-based pharmacokinetic (PBPK) modeling allows the prediction of drug exposure in pediatrics based on age-related physiological differences. The aim of this study was to predict the pharmacokinetics of buprenorphine in pediatrics with PBPK modeling. Moreover, the drug-drug interaction (DDI) potential of buprenorphine with CYP3A4 and P-glycoprotein perpetrator drugs should be elucidated. A PBPK model of buprenorphine and norbuprenorphine in adults has been developed and scaled to children and preterm neonates, accounting for age-related changes. One-hundred-percent of the predicted  $AUC_{last}$  values in adults (geometric mean fold error (GMFE): 1.22), 90% of individual  $AUC_{last}$  predictions in children (GMFE: 1.54) and 75% in preterm neonates (GMFE: 1.57) met the 2-fold acceptance criterion. Moreover, the adult model was used to simulate DDI scenarios with clarithromycin, itraconazole and rifampicin. We demonstrate the applicability of scaling adult PBPK models to pediatrics for the prediction of individual plasma profiles. The novel PBPK models could be helpful to further investigate buprenorphine pharmacokinetics in various populations, particularly pediatric subgroups.

**Keywords:** physiologically based pharmacokinetic (PBPK) modeling; buprenorphine; drug-drug interaction (DDI); norbuprenorphine; pediatric scaling; pharmacokinetics

## 1. Introduction

Buprenorphine is a partial agonist of the  $\mu$ -opioid receptor with an analgesic potency 25 to 100 times greater compared with that of morphine [1,2]. As such, buprenorphine plays a crucial role in the therapeutic management of pain in adults and adolescents, which is suggested among others in a recent guideline on cancer pain management of the World Health Organization (WHO) [2]. Furthermore, in recent years the use of buprenorphine has become widespread in pediatrics with indications ranging from postoperative analgesia to chronic pain in palliative care [3,4].

Buprenorphine displays a ceiling effect in adults, in which escalating doses do not cause additional respiratory depression [5,6]. However, this effect does not seem to apply to young children [7,8]. As a result, buprenorphine-related serious adverse reactions (ADR) up to fatal events have been reported, especially in young children, as well as single cases of accidental poisoning due to improperly stored buprenorphine drug products [7,9,10].

As a consequence, a recent meta-analysis by Vicencio-Rosas and colleagues pointed out the need of further research activities on buprenorphine in pediatric populations with particular focus on pharmacokinetic and pharmacodynamic issues [3]. Among others, their goals should be to allow researchers to develop dosage schemes and minimize the risk of ADR [3]. However, pediatric studies are difficult to conduct and are accompanied by numerous ethical challenges, many of which are unique to pediatrics, especially newborns [11]. Physiologically-based pharmacokinetic (PBPK) modeling in pediatrics has shown to be useful for the optimization of clinical study designs, the prediction of starting doses for children and the assessment of potential drug-drug interactions (DDIs) [12–16].

Compared to most other opioid receptor agonists, the potential for drug abuse and drug overdose in adults is lower due to buprenorphine's partial agonism and its ceiling effect in the adult population [9,17]. Hence, buprenorphine has successfully been used in the treatment of opioid use disorders (OUD) and is helping combat the current opioid epidemic [18,19]. However, the increase in buprenorphine prescriptions has also been associated with illicit usage, raising concerns about the potential of misuse and diversion [9,20].

A major metabolic route of elimination of buprenorphine represents the metabolism to the active metabolite, norbuprenorphine, mainly through the cytochrome P450 (CYP) 3A4 enzyme, an enzyme with a high DDI potential [21,22]. As a result, buprenorphine and norbuprenorphine plasma levels can be affected by CYP3A4 inhibitors and inducers [21,23]. Recently conducted DDI studies with CYP3A4 perpetrator drugs have shown significant changes in buprenorphine plasma concentrations after specific oral and sublingual administration scenarios [24–26]. Still, the clinical relevance of other DDIs with frequently used perpetrator drugs (e.g., clarithromycin or itraconazole) and the impact of the inhibition and/or induction of the drug transporter P-glycoprotein (P-gp) remain unclear [23]. PBPK modeling has shown to be a powerful tool in predicting and simulating DDI scenarios and drug concentrations at specific target sites. Moreover, PBPK models are useful to elucidate transporter proteins and their contribution to drug disposition [22,27–29].

The objectives of this study were (1) to establish and evaluate a whole-body parent-metabolite intravenous PBPK model of buprenorphine and norbuprenorphine in adults, (2) to scale the adult PBPK model to pediatrics for the assessment of plasma concentration-time profiles, and (3) to use the developed adult PBPK model for the evaluation of DDIs with frequently used CYP3A4 and P-gp perpetrator drugs that have not been investigated yet. The novel PBPK models are publicly available in the Open Systems Pharmacology (OSP) repository as clinical research tools to support the design of clinical trials in specific populations as well as the development of novel drug formulations. The Supplementary Materials serve as a comprehensive reference manual including detailed documentation of the model performance assessment.

## 2. Materials and Methods

### 2.1. Software

The PBPK models were developed with the PK-Sim<sup>®</sup> modeling software (version 8.0, part of the OSP Suite). Model input parameter optimization was accomplished using the Monte Carlo algorithm implemented in PK-Sim<sup>®</sup>. Clinical data in scientific literature were digitized using GetData Graph Digitizer version 2.26.0.20 (S. Fedorov) according to best practices [30]. Allometric scaling was performed in NONMEM<sup>®</sup> (Version 7.4.3), pharmacokinetic (PK) parameter analyses and graphics with the R programming language version 3.6.1 (R Foundation for Statistical Computing, Vienna, Austria) and R Studio<sup>®</sup> version 1.2.5019 (R Studio, Inc., Boston, MA, USA).

## 2.2. PBPK Parent-Metabolite Model Building in Adults

In agreement with pediatric PBPK model development workflows, first, an adult PBPK model was built and subsequently evaluated with observed plasma profiles to promote confidence in the parametrization of the PBPK model, before the model was scaled to pediatric populations [12,31–33]. For the building of the adult parent-metabolite PBPK model of buprenorphine and norbuprenorphine, an extensive literature search was performed to obtain information on (a) physicochemical properties, (b) distribution, metabolism and excretion processes of the two modeled compounds as well as (c) clinical studies of intravenous administration of buprenorphine. The gathered information was used to implement relevant transport proteins and enzymes involved in distribution, metabolism and excretion processes and to inform drug-dependent model input parameters. The plasma profiles of the identified clinical studies were digitized and split into an internal training and an external test dataset. The selection of studies for the internal dataset was guided by the information contained in the different studies (i.e., dosing regimens, frequent as well as early and late sampling, measurements of norbuprenorphine, measurements of arterial plasma concentrations, etc.). To obtain values for model input parameters, which could not be adequately obtained from literature, parameter estimation was performed by fitting the parent-metabolite model to the training dataset. The external test dataset was used for model evaluation.

Distribution and elimination processes including CYP and uridine 5'-diphosphoglucuronosyltransferase (UGT) enzymes as well as drug transporter were implemented according to the literature [21,34,35]. For the buprenorphine model, these are (1) metabolism of buprenorphine to a major active metabolite norbuprenorphine through CYP3A4 and CYP2C8; (2) metabolism pathways metabolizing buprenorphine to other non-specified metabolites through CYP3A4, CYP3A7, UGT1A1, UGT1A3, and UGT2B7; as well as (3) renal excretion through glomerular filtration. For the norbuprenorphine model, metabolism through UGT1A1 and UGT1A3 as well as renal clearance by glomerular filtration and tubular secretion through the transport protein P-gp were implemented [36,37]. Figure 1 shows a structural overview of the PBPK model including the implemented metabolic processes of buprenorphine and norbuprenorphine. Tissue expression distribution of the implemented enzymes was informed by the PK-Sim<sup>®</sup> expression database [38]. For detailed supplementary information on PBPK model building see Section 1 in the Supplementary Materials.

## 2.3. Pediatric Scaling and Model Applications

After the building and evaluation of the adult PBPK model, the model was scaled to the administration of buprenorphine in children and preterm neonates for a priori predictions of the PK in the two pediatric populations. For this, the adult virtual populations were replaced by pediatric populations. These virtual pediatric populations were based on the patient characteristics of two included pediatric clinical trials with children and preterm neonates, respectively. As a result, both anatomic and physiological parameters as well as enzyme tissue concentrations were scaled to values of the respective target population accounting for age-related changes such as size and composition of tissue compartments, protein binding and maturation of elimination processes. Information on the ontogeny functions for enzymes can be found in [39] and in Table S1 of the Supplementary Materials. For scaling the fraction unbound of buprenorphine to children and preterm neonates, the method of McNamara and Alcorn for alpha-1-acid glycoprotein was applied [40,41]. The extrapolated PBPK model was subsequently used to predict 22 individual plasma concentration-time profiles in children and preterm neonates. To compare the outcome of the PK predictions using the pediatric PBPK models, a classical allometric scaling approach, as described by Tod et al., was used [42]. For detailed information on the allometric scaling, see Section 3 in the Supplementary Materials.

Additionally, the adult PBPK model was used to assess the DDI potential of the CYP and UGT substrate buprenorphine with the three perpetrator drugs clarithromycin, itraconazole and rifampicin. While itraconazole and its metabolites inhibit both CYP3A4 and P-gp competitively, clarithromycin is a mechanism-based inhibitor of the CYP3A4 enzyme and also competitively inhibits

P-gp, yet with a much higher inhibition constant ( $K_i$ ) [22]. In contrast, rifampicin both inhibits and induces the CYP2C8, CYP3A4, UGT1A1, and UGT1A3 enzymes as well as the P-gp efflux transporter [22,43–50]. For the simulation of buprenorphine plasma profiles in the DDI scenarios, the buprenorphine model was coupled with recently published PBPK models of clarithromycin, itraconazole and rifampicin [22]. The rifampicin model was further extended with information on the CYP2C8, UGT1A1 and UGT1A3 induction and inhibition processes. Detailed information is provided in Section 2 of the Supplementary Materials.

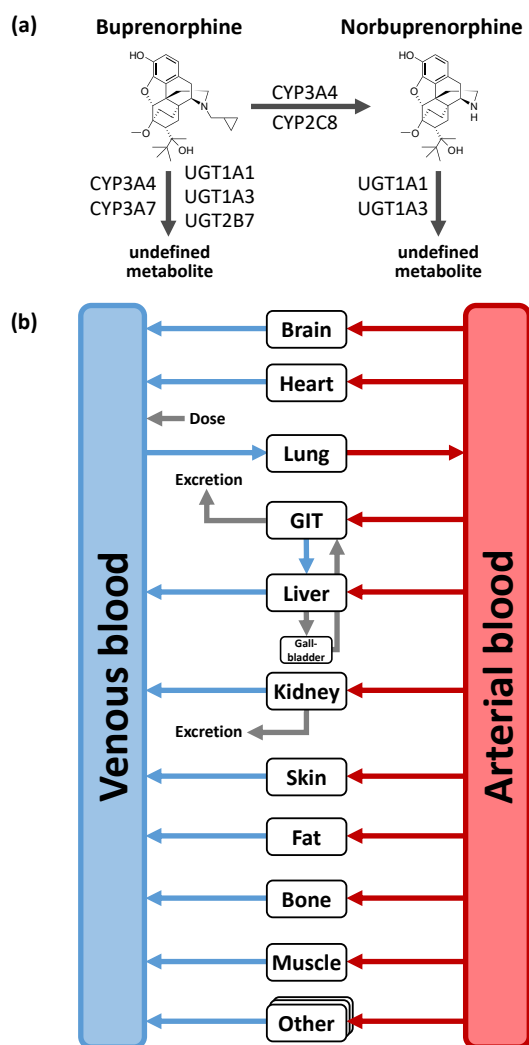


**Figure 1.** Implemented metabolic processes for buprenorphine and norbuprenorphine (a) and structural overview of the physiologically-based pharmacokinetic (PBPK) model (b). Boxes indicate compartments, black lines indicate metabolic processes, blue, grey and red lines denote in-/out-flows. CYP: cytochrome P450, GIT: gastrointestinal tract, UGT: uridine 5'-diphospho-glucuronosyltransferase.

#### 2.4. PBPK Model Evaluation

Adult and pediatric PBPK model performances were evaluated with several methods. Predicted and observed areas under the plasma concentration-time curve from the first to the last data point ( $AUC_{last}$ ) and maximum plasma concentration ( $C_{max}$ ) values as well as the predicted plasma concentrations and their respective values observed were compared in goodness-of-fit plots. Moreover, buprenorphine and norbuprenorphine plasma concentration-time profiles observed both from adult and pediatric studies were visually compared to the plasma profiles predicted with the PBPK models.

To estimate the variability of plasma profiles, virtual populations of 100 individuals were generated representing the corresponding clinical trial population. For detailed information on virtual populations see Section 1.2 in the Supplementary Materials. Individual plasma concentration-time profiles including the corresponding individual demographics were available in one study [51]. Here, populations of 100 individuals with the same demographics were used for simulations only allowing variability in the expression of the implemented enzymes and transporters. Population predictions were plotted as geometric mean with geometric standard deviation. When individual concentration-time datasets were available but demographic values could not be matched to the specific profile, median with 90% population prediction intervals were plotted. The sensitivity of the final PBPK models to single parameter changes (local sensitivity analysis) was investigated with PK-Sim®. Furthermore, two quantitative performance measures were calculated: the mean relative deviation (MRD) of the predicted plasma concentrations for each single plasma profile as well as the geometric mean fold errors (GMFE) of  $AUC_{last}$  and  $C_{max}$  ratios, respectively (for detailed information including equations please refer to Section 4.3 in the Supplementary Materials).  $C_{max}$  values were calculated only for intravenous long-term infusions and norbuprenorphine metabolite. Conclusively, the percentage of model-predicted concentrations falling within 2-fold of the corresponding observed concentrations was examined in addition to the mentioned evaluation measures above.

The DDI effects were evaluated by comparing plasma concentration-time profiles of buprenorphine and norbuprenorphine after buprenorphine administration alone (control) and plasma profiles during concomitant use with the DDI perpetrator (inhibition/induction). Additionally, the corresponding predicted AUC ratios ( $AUC_{inhibition/induction, predicted}/AUC_{control, predicted}$ ) were calculated. Since observed data of a DDI clinical trial with rifampicin was available, the AUC ratio predicted was also compared to the AUC ratio observed in the respective DDI study.

### 3. Results

#### 3.1. PK Data for PBPK Model Development and Pediatric Scaling

After a comprehensive literature search, eight PK studies in adults with 17 different treatment blocks after intravenous administration of buprenorphine were identified. Two of these studies were performed in an elderly population, one was a DDI study with rifampicin as the perpetrator drug. The dataset encompasses wide mean age and dose ranges with 21 to 67.5 years and 0.3 to 16 mg buprenorphine, respectively. In six treatment blocks, norbuprenorphine plasma concentrations were reported. All plasma concentration-time profiles were digitized and split into an internal training ( $n = 7$  profiles) and an external test dataset ( $n = 16$  profiles). The internal training dataset was complemented with information on the fraction of buprenorphine metabolized to norbuprenorphine, fraction of buprenorphine excreted unchanged in urine, and fraction of dose excreted in urine as norbuprenorphine [35,52,53]. For the evaluation of the PBPK model predictions in pediatrics, two clinical trials investigating buprenorphine plasma concentrations in both children (age: 4.6–7.5 years) and preterm neonates (27–34 weeks postmenstrual age) were located and the data digitized. An overview of the included clinical studies, comprising study characteristics and dosing regimens, is shown in Table 1.

Table 1. Overview of clinical studies used for building and evaluation of the PBPK models.

Clinical Study	Dose [mg]	Administration	n	Female [%]	Age [Years]	Weight [kg]	Blood Sample <sup>a</sup>	Norbuprenorphine Measurements	Dataset	Reference
<i>Adults</i>										
Bai et al. 2016	0.3	iv (2 min)	25	24	35.5 (20–53)	76.1 (62.6–93.0)	arterial	no	e	[54]
Bartlett et al. 1980	0.3	iv (1 min) <sup>b</sup>	1	-	-	-	arterial	no	e	[55]
Bullingham et al. 1980 (1)	0.3	iv (1 min)	24	42	64.5 ± 1.6	67.7 ± 2.4	arterial	no	e	[56]
Bullingham et al. 1980 (2)	0.3	iv (1 min, m.d.)	10	40	67.5 ± 6.5	67.5 ± 2.1	arterial	no	e	[56]
Bullingham et al. 1982 (1)	0.3	iv (1 min)	5	60	66.8 ± 2.9	65.0 ± 4.0	arterial	no	e	[57]
Bullingham et al. 1982 (2)	0.3	iv (1 min)	5	60	64.2 ± 2.5	66.4 ± 2.9	arterial	no	i	[57]
Bullingham et al. 1982 (3)	0.3	iv (1 min)	5	60	66.0 ± 3.2	64.8 ± 3.9	arterial	no	e	[57]
Everhart et al. 1999	1	iv (60 min)	6	-	-	-	-	yes	i	[35]
Hagelberg et al. 2016 (1)	1	iv (bolus)	12	42	-(19–23)	-(57–95)	venous	no	e	[26]
Hagelberg et al. 2016 (2) <sup>c</sup>	1	iv (bolus)	12	42	-(19–23)	-(57–95)	venous	no	e	[26]
Harris et al. 2000	4	iv (10 min)	9	11	34 (21–42)	-	venous	no	e	[58]
Huestis et al. 2013 (1)	2	iv (1 min)	5	-	34.6 (32–39)	74.7 (62.1–82.6)	venous	yes	i	[59]
Huestis et al. 2013 (2)	4	iv (1 min)	5	-	34.6 (32–39)	74.7 (62.1–82.6)	venous	yes	e	[59]
Huestis et al. 2013 (3)	8	iv (1 min)	5	-	34.6 (32–39)	74.7 (62.1–82.6)	venous	yes	e	[59]
Huestis et al. 2013 (4)	12	iv (1 min)	5	-	34.6 (32–39)	74.7 (62.1–82.6)	venous	yes	e	[59]
Huestis et al. 2013 (5)	16	iv (1 min)	5	-	34.6 (32–39)	74.7 (62.1–82.6)	venous	yes	i	[59]
Kuhman et al. 1996	1.2	iv (1 min)	5	0	34.4 (27–40)	67.7 (62.6–72.7)	venous	yes	i	[6]
Mendelson et al. 1997	1	iv (30 min)	6	17	29 (21–38)	-	venous	no	e	[60]
<i>Pediatrics</i>										
Barrett et al. 1993 <sup>d</sup>	3 µg/kg + 0.72–2.16 µg/kg/h	iv (30 min + 11–118 h)	12	-	31 weeks (27–34) <sup>e</sup>	1.5 (0.9–2.4)	arterial	no	e	[51]
Olkkola et al. 1989	3 µg/kg	iv (2 min)	10	-	5.9 (4.6–7.5)	21.4 (18.5–25)	venous	no	e	[61]

-: not available, e: external test dataset, i: internal training dataset, iv: intravenous, m.d.: multiple dose, <sup>a</sup> if sample information was not specified, venous blood samples were assumed, <sup>b</sup> administration time not given, based on the observed data and information from other studies, an administration time of 1 min was assumed, <sup>c</sup> with concomitant administration of rifampicin, <sup>d</sup> detailed information on individual patient characteristics and dosing regimens is depicted in Table S2 of the Supplementary Materials, <sup>e</sup> postmenstrual age.

### 3.2. Adult PBPK Model Building and Evaluation

The whole-body PBPK model for adults precisely predicts plasma concentration-time profiles of buprenorphine and norbuprenorphine following intravenous administration of buprenorphine. Visual comparison of predicted to observed plasma profiles are shown in Figure 2 (selection of internal and external dataset) and in detail in Section 4.1 of the Supplementary Materials (all studies, both linear and semilogarithmic plots). Predicted plasma profile trajectories are in close agreement with profiles observed both for buprenorphine venous and arterial blood plasma concentrations as well as for norbuprenorphine plasma concentrations.

All predicted  $AUC_{last}$  and  $C_{max}$  values are within the 2-fold acceptance criterion. The goodness-of-fit plot of predicted versus observed plasma concentrations is shown in Figure 3 together with goodness-of-fit plots of predicted versus observed  $AUC_{last}$  and  $C_{max}$  values. The GMFE values for the adult PBPK model are 1.22 and 1.45 for  $AUC_{last}$  and  $C_{max}$ , respectively. Moreover, 84% of all predicted plasma concentrations fall within 2-fold of the corresponding observed concentration. The overall MRD value for predicted plasma concentrations for the adult PBPK model is 1.70. Detailed results on MRD and GMFE values, calculated for all studies, are provided in Sections 4.4 and 4.5 of the Supplementary Materials, the results of the sensitivity analysis are shown in Section 4.6 of the Supplementary Materials.

Metabolism of buprenorphine to its major active metabolite norbuprenorphine is predominantly mediated through CYP3A4 (~65%) and CYP2C8 (~30%) [21]. In total, this pathway is responsible for about 35% of buprenorphine metabolism [21,35,52]. In contrast, urinary excretion only covers a minor fraction of buprenorphine elimination (0–1%) [26,35,62]. The PBPK model predictions for fraction metabolized to norbuprenorphine of ~37% and for fraction of buprenorphine excreted unchanged in urine of ~0.5% perfectly align with these literature reports (visual comparison of predicted to observed fractions of buprenorphine excreted unchanged in urine are shown in Figure S2 of the Supplementary Materials). Two factors, for the metabolic pathway to norbuprenorphine and the metabolic pathway to other metabolites, were estimated and multiplied with the in vitro literature values for the respective maximum reaction velocities in order to account for the in vivo relation of drug metabolized to norbuprenorphine and to other metabolites, respectively [21,35,52]. Further, the predicted fraction of the dose excreted in urine as norbuprenorphine (~2%) is in concordance with the literature as well (1.3 to 2.1%) [35]. This fraction was achieved by implementing the efflux transporter P-gp in the PBPK model according to the literature [37]. Drug-dependent parameters of the final PBPK model are depicted in Table 2. For detailed information including system-dependent model parameters, see Section 1 of the Supplementary Materials.

### 3.3. Pediatric PBPK Model Building and Evaluation

The adult PBPK model was scaled to two pediatric populations with a mean age of 5.9 years and 31 weeks (postmenstrual age), respectively. The fraction unbound of buprenorphine was calculated with the method of McNamara and Alcorn [40] and resulted in fraction unbound of 5.1% for the child population and 7.2% (mean) for the preterm neonate population. All other drug-dependent parameters were kept fixed to the values of the adult PBPK model. Enzyme concentrations in the respective organs were scaled based on the implemented ontogeny functions [39].

Visual comparison of predicted to observed individual plasma profiles are shown in Figure 4 (selection of plots) and in detail in Section 4.2 of the Supplementary Materials (all plots, both linear and semilogarithmic).

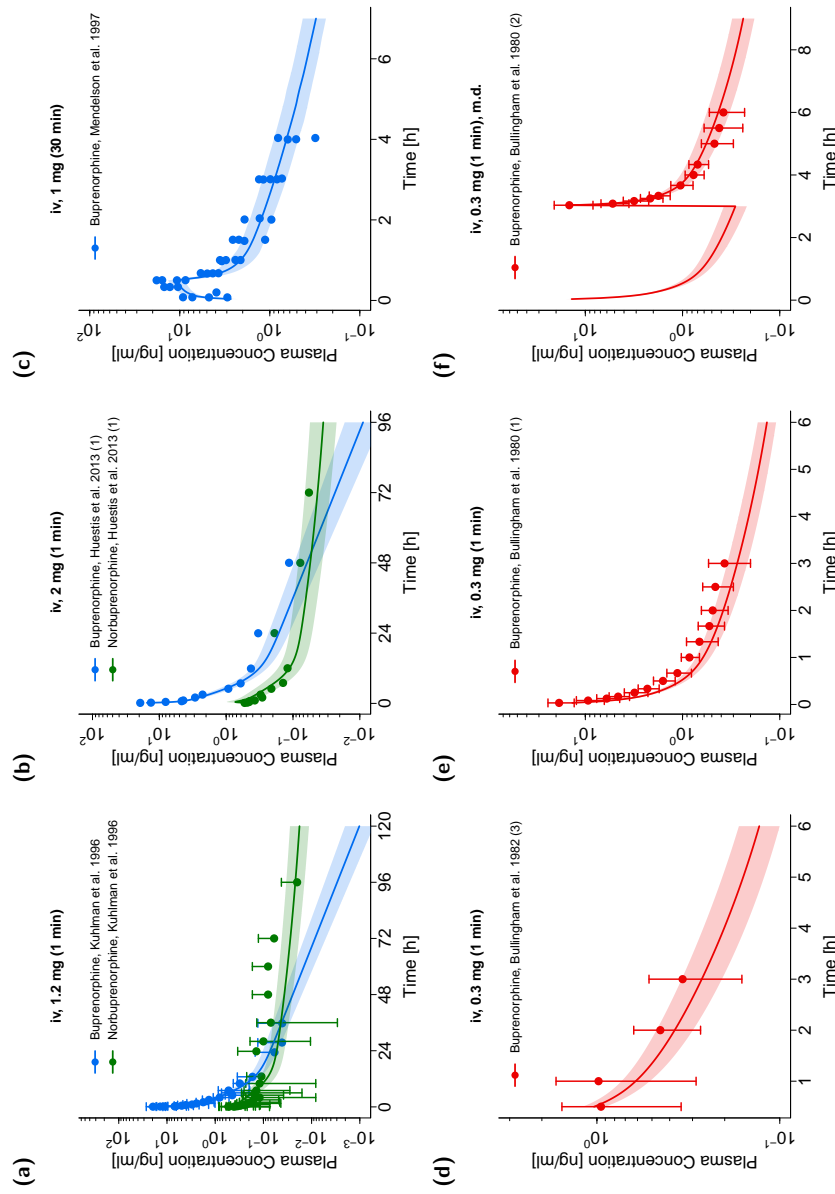


**Figure 2.** Buprenorphine (blue: venous blood, red: arterial blood) and norbuprenorphine (green: venous blood) predicted and observed plasma concentration-time profiles after intravenous administration of buprenorphine in adults. (a,b): selection of internal training dataset, (c–f): selection of external test dataset. Population simulations ( $n = 100$ ) are shown as lines with shaded areas. Observed data are shown as circles  $\pm$  standard deviation if available. References with numbers in parentheses link to a specific observed dataset described in the study table (Table 1). Predicted and observed area under the concentration-time curve from the first to the last data point ( $AUC_{last}$ ) and maximum plasma concentration ( $C_{max}$ ) values are compared in Table S6 of the Supplementary Materials. Predicted and observed plasma concentration-time profiles of all studies in adults are shown in Section 4.1 of the Supplementary Materials both on a linear and a semilogarithmic scale. iv: intravenous, m.d.: multiple dose.

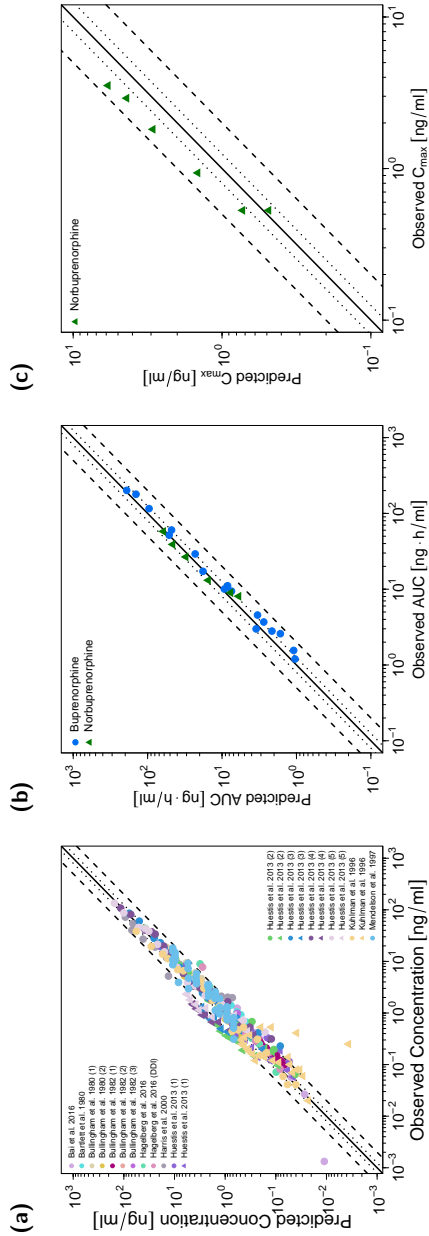


**Figure 3.** Predicted versus observed plasma concentrations (a) as well as predicted versus observed  $AUC_{last}$  (b) and  $C_{max}$  (c) values of buprenorphine and norbuprenorphine for the adult PBPK model. In (a), each symbol represents a single plasma concentration (circles: buprenorphine, triangles: norbuprenorphine). In (b,c), each symbol represents the  $AUC_{last}$  or  $C_{max}$  of a single plasma concentration-time profile (blue circles: buprenorphine, green triangles: norbuprenorphine). As stated in the materials and methods section,  $C_{max}$  values were only calculated for long-term infusions and norbuprenorphine metabolite. The black solid lines mark the lines of identity. Black dotted lines indicate 1.25-fold, black dashed lines indicate 2-fold deviation.  $AUC_{last}$ : area under the plasma concentration-time curve from the first to the last data point,  $C_{max}$ : maximum plasma concentration.

**Table 2.** Buprenorphine and norbuprenorphine drug-dependent parameters.

Parameter	Value	Unit	Source	Literature	Reference	Value	Unit	Source	Literature	Reference	Description
MW	467.64	g/mol	Buprenorphine			413.55	g/mol	Norbuprenorphine			Molecular weight
$pK_{a1}$ (base)	12.54		lit.	[63] <sup>a</sup>	[63] <sup>a</sup>	10.49		lit.	[63] <sup>b</sup>	[63] <sup>b</sup>	Acid dissociation constant
$pK_{a2}$ (acid)	7.50		lit.	[63] <sup>a</sup>	[63] <sup>a</sup>	9.80		lit.	[63] <sup>b</sup>	[63] <sup>b</sup>	Acid dissociation constant
logP	3.40		lit.	[64]	[64]	3.19		lit.	[65] <sup>c</sup>	[65] <sup>c</sup>	Lipophilicity
$f_u$ (adults)	4.0	%	lit.	[66]	[66]	21.7	%	optim.	-	-	Fraction unbound
$f_u$ (children)	5.1	%	calc.	[40,66]	[40,66]						Fraction unbound
$f_u$ (preterm neonates)	7.2	%	calc.	[40,66]	[40,66]						Fraction unbound
CYP2C8 $K_m \rightarrow$ norbup	5.2	$\mu\text{mol/L}$	lit.	[21] <sup>e</sup>	[21] <sup>e</sup>						Michaelis-Menten constant
CYP2C8 $v_{max} \rightarrow$ norbup	$f_1 \cdot 176.3$	$\mu\text{mol}/\text{min}/\text{mg}$ protein	lit.	[21]	[21]						Maximum reaction velocity
CYP3A4 $K_m \rightarrow$ norbup	5.7	$\mu\text{mol/L}$	lit.	[21] <sup>e</sup>	[21] <sup>e</sup>						Michaelis-Menten constant
CYP3A4 $v_{max} \rightarrow$ norbup	$f_1 \cdot 520.0$	$\mu\text{mol}/\text{min}/\text{mg}$ protein	lit.	[21]	[21]						Maximum reaction velocity

Table 2. Cont.

Parameter	Value	Unit	Source	Literature	Reference	Value	Unit	Source	Literature	Reference	Description
CYP3A4 $K_m \rightarrow$ undef	5.7	$\mu\text{mol/L}$	ass.	-	-	-	-	-	-	-	Michaelis-Menten constant
CYP3A4 $v_{\text{max}} \rightarrow$ undef	$f_2 \cdot 1352.1$	$\text{pmol/min/mg protein}$	calc. <sup>d</sup>	-	-	-	-	-	-	-	Maximum reaction velocity
CYP3A7 $K_m \rightarrow$ undef	29.1	$\mu\text{mol/L}$	calc. <sup>d</sup>	-	-	-	-	-	-	-	Michaelis-Menten constant
CYP3A7 $v_{\text{max}} \rightarrow$ undef	$f_2 \cdot 632.6$	$\text{pmol/min/mg protein}$	calc. <sup>d</sup>	-	-	-	-	-	-	-	Maximum reaction velocity
UGT1A1 $K_m \rightarrow$ undef	10.4	$\mu\text{mol/L}$	lit.	10.4	[34] <sup>e</sup>	21.8	$\mu\text{mol/L}$	lit.	21.8	[34] <sup>e</sup>	Michaelis-Menten constant
UGT1A1 $v_{\text{max}} \rightarrow$ undef	$f_2 \cdot 6726.8$	$\text{pmol/min/mg protein}$	lit.	6726.8	[34]	$f_3 \cdot 714.6$	$\text{pmol/min/mg protein}$	lit.	714.6	[34]	Maximum reaction velocity
UGT1A3 $K_m \rightarrow$ undef	1.1	$\mu\text{mol/L}$	lit.	1.1	[34] <sup>e</sup>	14.7	$\mu\text{mol/L}$	lit.	14.7	[34] <sup>e</sup>	Michaelis-Menten constant
UGT1A3 $v_{\text{max}} \rightarrow$ undef	$f_2 \cdot 642.6$	$\text{pmol/min/mg protein}$	lit.	642.6	[34]	$f_3 \cdot 387.0$	$\text{pmol/min/mg protein}$	lit.	387.0	[34]	Maximum reaction velocity
UGT2B7 $K_m \rightarrow$ undef	1.8	$\mu\text{mol/L}$	lit.	1.8	[34] <sup>e</sup>	-	-	-	-	-	Michaelis-Menten constant
UGT2B7 $v_{\text{max}} \rightarrow$ undef	$f_2 \cdot 823.8$	$\text{pmol/min/mg protein}$	lit.	823.8	[34]	-	-	-	-	-	Maximum reaction velocity
P-gp $K_m$	-	-	-	-	-	3.4	$\mu\text{mol/L}$	optim.	-	-	Michaelis-Menten constant
P-gp $k_{\text{cat}}$	-	-	-	-	-	2.14	$1/\text{min}$	optim.	-	-	Transport rate constant
$f_1$	2.80	-	optim.	-	-	-	-	-	-	-	Factor
$f_2$	0.27	-	optim.	-	-	-	-	-	-	-	Factor
$f_3$	-	-	-	-	-	0.43	-	optim.	-	-	Factor
GFR fraction	1.00	-	ass.	-	[34] <sup>e</sup>	1.00	-	ass.	-	-	Filtered drug in the urine
UGT1A1 $K_i$	14.8	$\mu\text{mol/L}$	lit.	14.8	[34] <sup>e</sup>	-	-	-	-	-	Conc. for 50% inhibition
UGT1A3 $K_i$	0.5	$\mu\text{mol/L}$	lit.	0.5	[34] <sup>e</sup>	1.6	$\mu\text{mol/L}$	lit.	1.6	[34] <sup>e</sup>	Conc. for 50% inhibition
Partition coefficients	Diverse	-	calc.	Schmitt	[67]	Diverse	-	calc.	PK-Sim	[38]	Cell to plasma partitioning
Cellular permeability	6.91E-03	$\text{cm/min}$	calc.	PK-Sim	[38]	8.91E-03	$\text{cm/min}$	calc.	PK-Sim	[38]	Perm. into the cellular space

-: not available, ass.: assumed, calc.: calculated, conc.: concentration, CYP: cytochrome P450, GFR: glomerular filtration rate, lit.: literature, norbup: norbuprenorphine, optim.: optimized, perm.: permeability, P-gp: P-glycoprotein, PK-Sim: PK-Sim standard calculation method, Schmitt: Schmitt calculation method, undef: undefined metabolite, UGT: uridine 5'-diphospho-glucuronosyltransferase, <sup>a</sup> DrugBank entry for buprenorphine. <https://www.drugbank.ca/drugs/DB00921>, accessed 21 April 2020, <sup>b</sup> DrugBank entry for norbuprenorphine. <https://www.drugbank.ca/metabolites/DBME100174>, accessed 21 April 2020, <sup>c</sup> HMDB entry for norbuprenorphine. <https://hmdb.ca/metabolites/HMDB0060546>, accessed 21 April 2020, <sup>d</sup> for detailed information please refer to Section 1 in the Supplementary Materials; <sup>e</sup> apparent  $K_i$  and  $K_m$  literature values were corrected according to [68] using the free fractions of buprenorphine and norbuprenorphine in microsomal assays from [36].

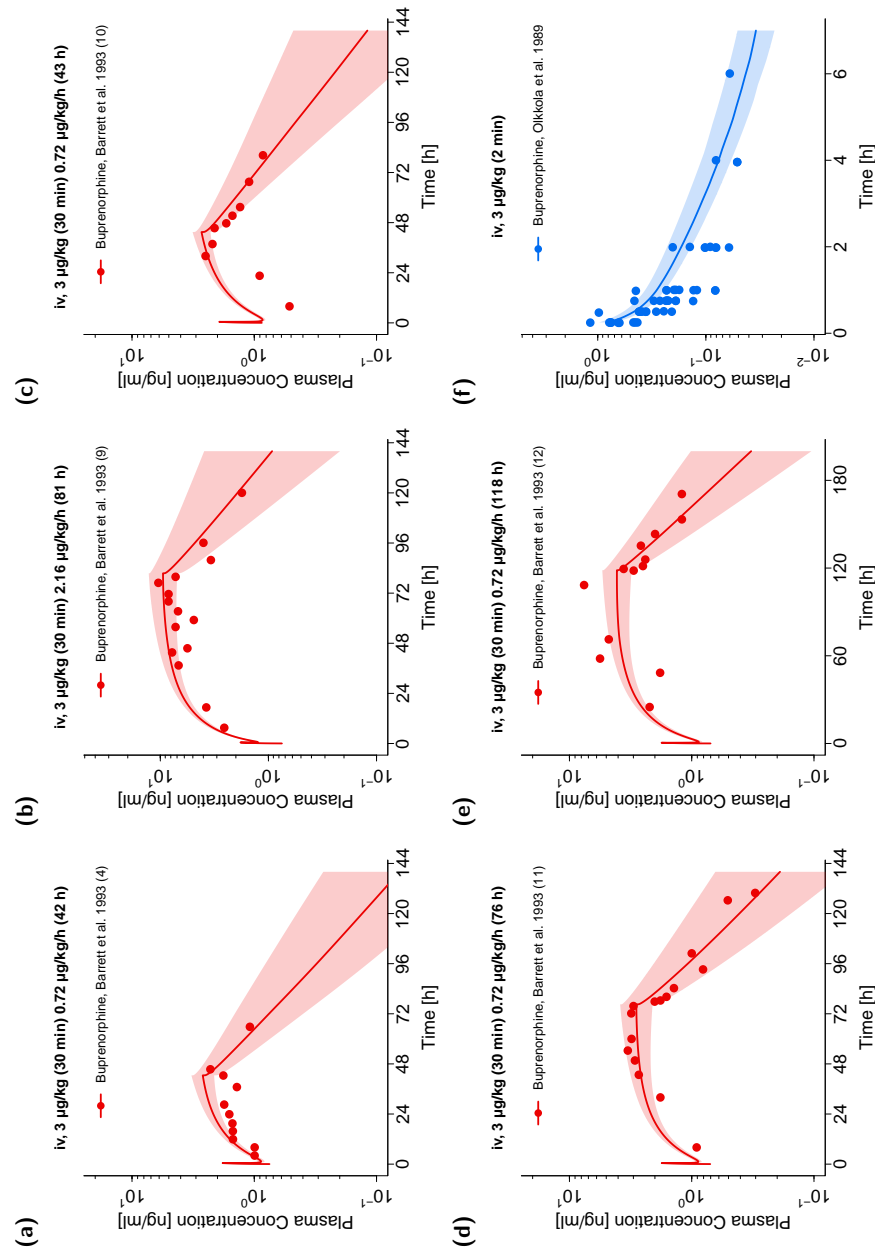


**Figure 4.** Buprenorphine (red: arterial blood, blue: venous blood) predicted and observed plasma concentration-time profiles after intravenous administration of buprenorphine in preterm neonates (a–e) and children (f). Population simulations ( $n = 100$ ) are shown as lines with shaded areas. Observed data are shown as circles. References with numbers in parentheses link to a specific observed dataset described in Table 1 and Table S2 of the Supplementary Materials. Predicted and observed area under the plasma concentration-time curve from the first to the last data point ( $\text{AUC}_{\text{last}}$ ) and maximum plasma concentration ( $C_{\text{max}}$ ) values are compared in Table S6 of the Supplementary Materials. Predicted and observed plasma concentration-time profiles of all studies in pediatrics are shown in Section 4.2 of the Supplementary Materials both on a linear and a semilogarithmic scale. iv: intravenous.

Goodness-of-fit plots of predicted to observed  $AUC_{last}$  and  $C_{max}$  values are shown in Figure 5 accompanied with goodness-of-fit plots of predicted versus observed plasma concentrations. The GMFE values for individual  $AUC_{last}$  predictions were 1.54 for the child and 1.57 for the preterm neonate population, respectively. Ninety percent of individual  $AUC_{last}$  predictions for the child population and 75% of individual  $AUC_{last}$  predictions for the preterm neonate population were within 2-fold of the respective observed values. GMFE of  $C_{max}$  was 1.44 for the long-term infusions in preterm neonates (with 83% of individual  $C_{max}$  predictions within 2-fold range). Moreover, 81% (children) and 80% (preterm neonates) of all predicted plasma concentrations fell within 2-fold of the corresponding observed concentrations (overall MRD values of 1.72 for plasma concentration predictions in children and 1.86 for predictions in preterm neonates). Detailed results for MRD and GMFE values for the pediatric predictions can be found in Sections 4.4 and 4.5 of the Supplementary Materials. The allometric scaling approach led to less precise predictions (see Figure 5c,d) with MRD values of 2.28 (children), 12.46 (preterm neonates without age-dependent exponent) and 2.08 (preterm neonates with age-dependent exponent).

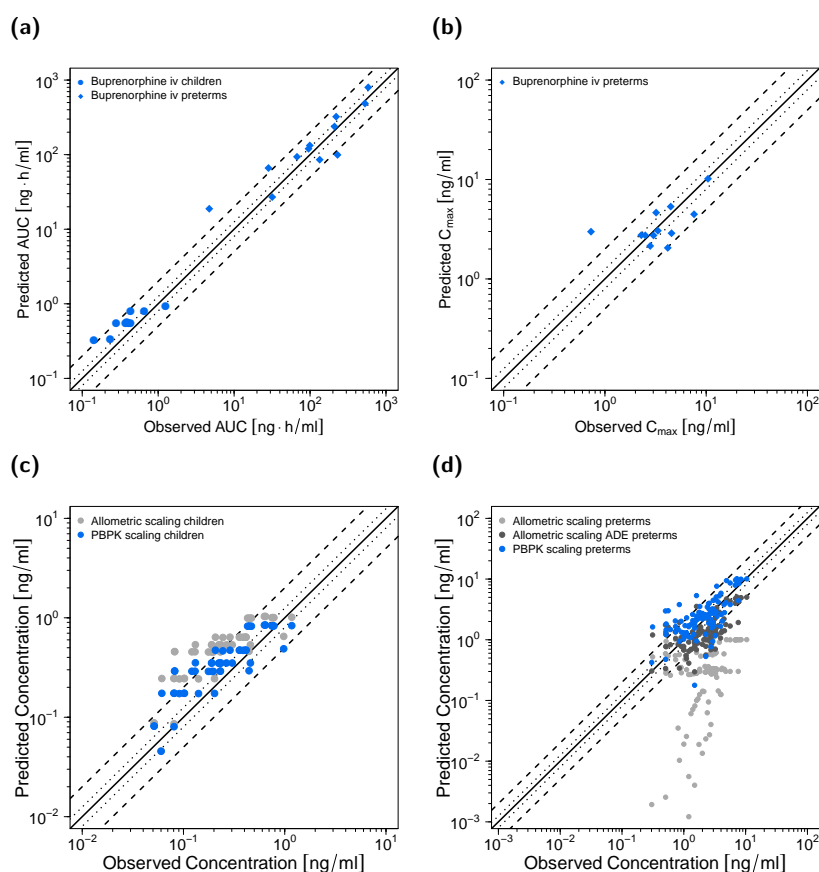


**Figure 5.** Predicted versus observed  $AUC_{last}$  (a) and  $C_{max}$  (b) values of buprenorphine for the pediatric PBPK models as well as predicted versus observed plasma concentrations for children (c) (blue: PBPK modeling, grey: allometric scaling) and preterm neonates (d) (blue: PBPK modeling, grey: allometric scaling, dark grey: allometric scaling with ADE as suggested by Mahmood and Tegenge [69]). In (a,b), each symbol represents the  $AUC_{last}$  or  $C_{max}$  of a single concentration-time profile. In (c,d), each symbol represents a single plasma concentration. As stated in the materials and methods section,  $C_{max}$  values were only calculated for long-term infusions. The black solid lines mark the lines of identity. Black dotted lines indicate 1.25-fold, black dashed lines indicate 2-fold deviation. ADE: age-dependent exponent,  $AUC_{last}$ : area under the plasma concentration-time curve from the first to the last data point,  $C_{max}$ : maximum plasma concentration.

### 3.4. DDI Evaluation with the Adult PBPK Model

The plasma concentration-time profiles of the simulated DDI scenarios are depicted in Figure 6. A slight decrease in buprenorphine AUC could be observed when simulating buprenorphine administration with concomitant rifampicin compared to simulation of buprenorphine administration alone in the setting of the DDI study by Hagelberg et al. [26]. The corresponding ratio of predicted  $AUC_{ratio}$  (0.89) and observed  $AUC_{ratio}$  (0.85) for the DDI was 0.96. The predicted  $AUC_{ratio}$  for norbuprenorphine was 1.13 (see Table 3). For the assessment of DDI potential of buprenorphine with clarithromycin and itraconazole, a dosing regimen of a long-term buprenorphine infusion was selected to achieve similar steady-state plasma concentrations compared with the administration of marketed transdermal patches with 10  $\mu\text{g}/\text{h}$  buprenorphine [70]. The administration of the perpetrator drugs started prior to buprenorphine administration and continued throughout the administration of the buprenorphine infusion. For details regarding the dosing regimens see Table 3. The predicted  $AUC_{ratio}$  of buprenorphine for the DDI with clarithromycin and itraconazole was 1.06 and 1.11, respectively, while the predicted  $AUC_{ratio}$  of norbuprenorphine was calculated to be 0.82 and 0.64.

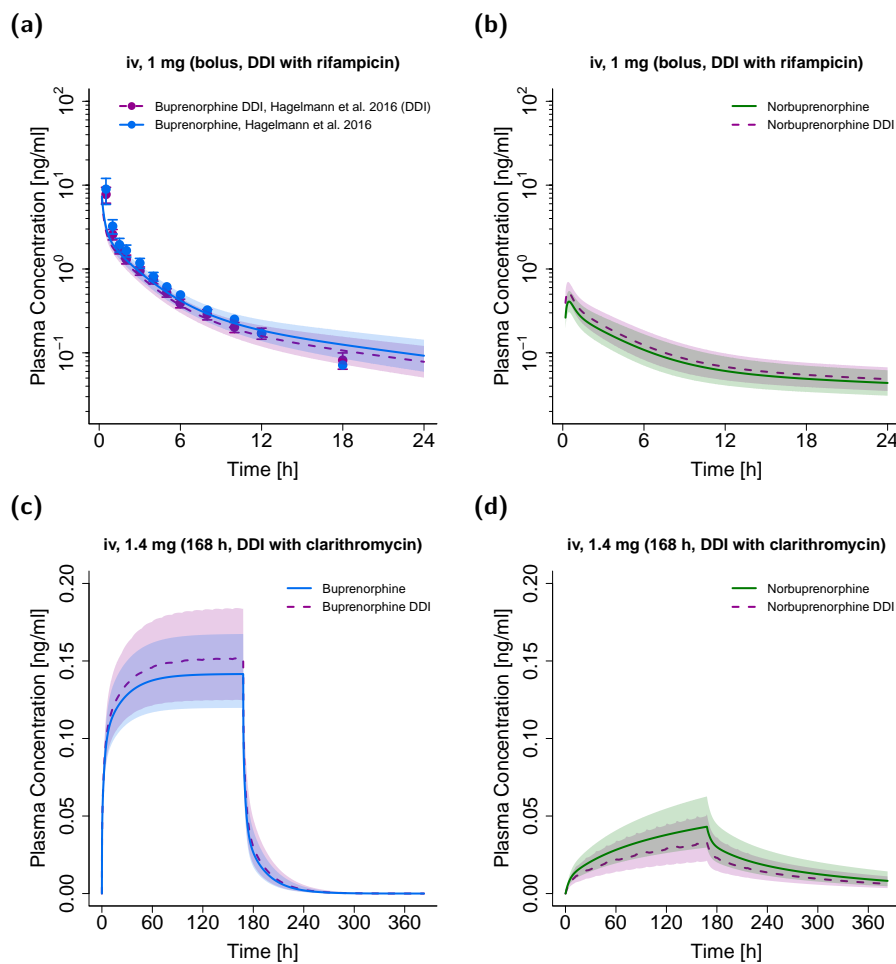
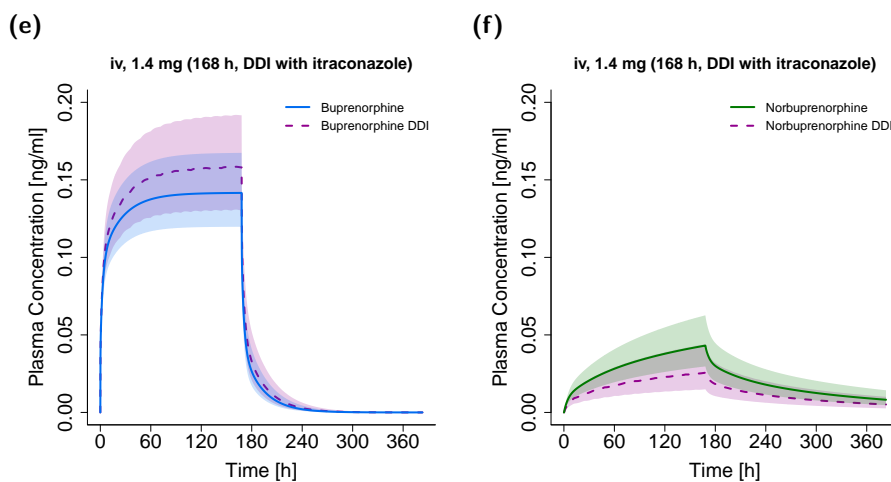


Figure 6. Cont.



**Figure 6.** DDI scenarios for buprenorphine (blue, left panel) and norbuprenorphine (green, right panel) with the perpetrator drugs rifampicin ((a,b), semilogarithmic), clarithromycin ((c,d), linear) and itraconazole ((e,f), linear) in adults. Buprenorphine and norbuprenorphine plasma concentrations during concomitant administration of a DDI perpetrator drug are shown in purple. Population simulations ( $n = 100$ ) are shown as lines with shaded areas. If available, observed data are shown as filled circles  $\pm$  standard deviation (a). References link to a specific observed dataset described in Table 1. Information about dosing regimens as well as observed and predicted AUC ratios for buprenorphine and norbuprenorphine are depicted in Table 3. DDI, drug-drug interaction; iv, intravenous.

Table 3. DDI study dosing regimens with predicted and observed AUC ratios.

Victim Drug [Dose]	Perpetrator Drug [Dose]	Pred. AUC Ratio (Buprenorphine) with/without Perpetrator	Obs. AUC Ratio (Buprenorphine) with/without Perpetrator	Pred. AUC Ratio (Noribuprenorphine) with/without Perpetrator	Obs. AUC Ratio (Noribuprenorphine) with/without Perpetrator	Reference
Buprenorphine [1.4 mg, 168 h iv infusion]	Clarithromycin [250 mg, bid, po]	1.06	-	0.82	-	simulated <sup>a</sup>
Buprenorphine [1.4 mg, 168 h iv infusion]	Itraconazole [100 mg, bid, po] <sup>b</sup>	1.11	-	0.64	-	simulated <sup>a</sup>
Buprenorphine [1 mg, iv bolus]	Rifampicin [600 mg, qd, po]	0.89	0.85	1.11	-	[26]

-: not available, bid: twice daily, iv: intravenous, obs.: observed, po: oral, pred.: predicted, qd: once daily,<sup>a</sup> population simulations were carried out with a virtual population (n = 100) with an age range of 20–50 years and without specific body weight or height restrictions as implemented in PK-Sim<sup>®</sup>,<sup>b</sup> loading dose of 200 mg as first dose.

#### 4. Discussion

In this study, whole-body PBPK models of buprenorphine for an adult and two pediatric populations have been successfully developed. The adult PBPK model provides a consistent representation of the buprenorphine and norbuprenorphine dose–exposure relationship following intravenous administration of a wide dose range (0.3–16 mg) and describes and predicts buprenorphine and norbuprenorphine venous and arterial plasma concentration–time profiles. Thereby, predictions of the fraction of buprenorphine metabolized to norbuprenorphine and fractions of buprenorphine and norbuprenorphine excreted in urine align with literature reports. With the successful scaling of the adult PBPK model to children and preterm neonates, we confirm the potential of PBPK modeling to predict the PK in pediatrics. Moreover, we demonstrate the applicability of scaling an adult PBPK model to preterm neonates in order to predict individual plasma profiles with 75% of AUC ratios falling within 2-fold range. The performance of the PBPK models have been demonstrated by comparison of predicted to observed plasma concentration–time profiles and the respective goodness-of-fit plots, the calculation of MRD values as well as the comparison of predicted to observed  $AUC_{last}$  and  $C_{max}$  values including the calculation of the respective GMFEs.

By defining absorption, distribution, metabolism, and excretion (ADME) as a function of anatomy, physiology and biochemistry, PBPK modeling offers the opportunity of rational scaling between adults and children [31,33]. This study investigated the prediction of individual AUCs and plasma concentrations of 22 individual buprenorphine plasma profiles. In the case of predictions for children at the age of 4.6–7.5 years, 90% of individual AUC predictions were within 2-fold range. In the case of predictions for preterm neonates with 27–34 weeks of postmenstrual age, 75% of individual AUC and 83% of  $C_{max}$  predictions were within 2-fold range, suggesting good predictive model performance. While PK predictions for preterm neonates are particularly challenging [71–73], our results provide evidence that individual predictions of AUC and  $C_{max}$  values can be feasible.

As reported recently in other pediatric PBPK modeling approaches [12], the clearance in children (age range of 1–12 years) was slightly underestimated. This could be partly due to the fact that the implemented ontogeny functions for the CYP and UGT enzymes do not account for partially elevated concentrations in this age group, which has been reported in literature [39,74].

PK predictions with the PBPK modeling approach were superior compared to the allometric approach, especially for the preterm neonate population. The application of the exponent 1.2 for the allometric scaling of clearance in preterm neonates led to an improvement of predictions in this population compared to the exponent of 0.75, supporting the suggested advantages of an age-dependent exponent in allometric scaling by Mahmood and Tegenge [69].

In contrast to the simulated DDI scenario with rifampicin (decrease in buprenorphine AUC of ~11%), concomitant itraconazole administration slightly elevated the AUC of buprenorphine (~11%) due to the inhibition of CYP3A4. Similarly, clarithromycin inhibited the metabolism of buprenorphine to norbuprenorphine through CYP3A4 (AUC elevation of ~6%), while the CYP2C8 and UGT metabolic pathways were not affected by the DDIs with itraconazole and clarithromycin. Recent studies with the perpetrator drugs voriconazole and rifampicin have shown stronger DDI effects after oral and sublingual buprenorphine administration [24–26,75]. This is probably due to the fact that first-pass metabolism in the gut, which can be highly affected by DDIs, is avoided during intravenous buprenorphine administration. As a result, the DDI assessment in this study rather reflects the DDI potential for buprenorphine administrations not affected by first-pass metabolism like intravenous and transdermal applications.

Albeit clarithromycin (mechanism-based inhibition) and itraconazole (competitive inhibition) strongly inhibit CYP3A4 metabolism to norbuprenorphine, AUCs of norbuprenorphine did not vanish (decrease of only ~18% and ~36%, respectively). Firstly, norbuprenorphine can also be produced through CYP2C8. Secondly, the additional inhibition of the efflux transporter P-gp leads to a decreased norbuprenorphine excretion in the model. The simulated DDI scenario with rifampicin led to a less pronounced effect on the AUC of norbuprenorphine (increase of ~11%) despite an effect of comparable

extent on buprenorphine AUC. This can be attributed to a simultaneous induction and inhibition of norbuprenorphine's production (CYP2C8 and CYP3A4) and elimination pathways (UGT1A1 and UGT1A3) by rifampicin.

As plasma concentrations of norbuprenorphine-glucuronide were not available in the included studies, enterohepatic circulation for norbuprenorphine was not implemented in the PBPK model. To account for this missing process, a factor for maximum reaction velocities of UGT1A1 and UGT1A3 norbuprenorphine metabolism was estimated to decrease norbuprenorphine elimination. However, this could still lead to underpredictions of norbuprenorphine plasma levels, especially in terminal phases, multiple-dose regimens and DDI scenarios. Hence, the simulated DDI effects on norbuprenorphine plasma concentrations (increase with coadministration of rifampicin, decrease with coadministration of clarithromycin and itraconazole) have to be interpreted carefully. Moreover, only a limited number of PK studies with reported norbuprenorphine measurements were available for PBPK model building and evaluation [6,59]. Kapil et al. have reported "slightly higher" norbuprenorphine plasma levels after transdermal buprenorphine application during concomitant use of ketoconazole (inhibitor of CYP3A4 and P-gp), which "may be explained by ketoconazole inhibition of the efflux transporter" [3]. The concomitant administration of voriconazole, an inhibitor of CYP3A4 and CYP2C19, with oral buprenorphine led to an increase of norbuprenorphine AUC of ~400% in a recent study [24]. The authors hypothesized that the elevation of norbuprenorphine levels could be due to inhibition of transporters like P-gp among others, which could affect tissue distribution. The inhibition of P-gp did not result in such an increase of norbuprenorphine plasma concentrations in the simulated DDI scenarios. However, if implemented in the model, an enhanced enterohepatic circulation due to inhibition of P-gp might explain the observed increase. Further studies with buprenorphine need to be conducted to investigate the effect of DDIs on norbuprenorphine exposure including distribution and elimination through transport proteins.

Buprenorphine has recently been of interest in mechanistic modeling efforts. Kalluri et al. and Johnson et al. developed two intravenous and sublingual models of buprenorphine with the SimCyp® simulator [53,76]. The model by Kalluri et al. represents an adult PBPK model and was further extended to a pregnant population by Zhang et al. [77]. Ji et al. used the model to assess the influence of benzodiazepines on buprenorphine PK, which was shown to be negligible [78]. While Johnson et al. succeeded in predicting clearance parameters in adults and 6-year-old children, the observed clearance in a younger age group fell "at the bottom end of the predicted results in term newborns" [76]. This could possibly be due to the fact that only CYP3A4 and UGT1A1 were incorporated in the model and considered for ontogeny. The focus of this study was on predictions of clearance values in different populations. Predictions of buprenorphine plasma concentration-time profiles in adults or pediatrics after intravenous administration were not shown.

Moreover, neither of the models included norbuprenorphine, a major active metabolite of buprenorphine [37]. The contribution of norbuprenorphine to the analgesic efficacy seen after buprenorphine administration is still under debate [79]. However, norbuprenorphine showed a higher potency with regard to the induction of dose-related respiratory depression compared to buprenorphine [80], which has recently been confirmed in a clinical trial with sublingual buprenorphine, pointing out the relevance of the metabolite norbuprenorphine [81]. All  $AUC_{last}$  and  $C_{max}$  values of norbuprenorphine plasma concentration-time profiles predicted with the presented PBPK model lie within 2-fold range of the corresponding observed values with an MRD value of 2.27 for the predicted plasma concentrations.

Norbuprenorphine plasma concentration measurements were only available in clinical studies with adults. Hence, PBPK model predictions for norbuprenorphine were only evaluated in this population. Furthermore, the DDI assessment could only be carried out with the adult PBPK model due to the fact that the incorporated perpetrator drug PBPK models were developed for the application in non-pediatric populations [22].

The impact of the inhibition processes of UGT1A1 and UGT1A3 by buprenorphine and norbuprenorphine on the AUC values was negligible as seen in the local sensitivity analysis. This is probably due to the fact that intracellular unbound drug concentrations were far below the respective  $K_i$  values from the literature [34], which is supported by Kress in a recent review [23]. As a result, these inhibitory processes seem to play a minor role in the fate of buprenorphine and norbuprenorphine PK if the in vitro  $K_i$  values can be transferred to the in vivo setting and the range of predicted intracellular concentrations reflects the in vivo scenario.

Transdermal buprenorphine has shown its benefits in the treatment of diverse acute and chronic pain syndromes as well as other difficult-to-treat pain conditions and OUD [18,82]. Sustained-release formulations such as transdermal patches hold the potential to reduce plasma concentration fluctuations and risk for non-adherence. Moreover, recent studies have evaluated the use of transdermal buprenorphine patches in children and its reduced risk of ADR compared to other dosage forms with the need for further investigations [3]. As a result of the good predictive PK performance, the new established intravenous buprenorphine PBPK models could be used to develop transdermal PBPK models for predictions of buprenorphine plasma concentrations after transdermal administration based on patch characteristics and in vitro dissolution data.

## 5. Conclusions

A whole-body parent-metabolite PBPK model of buprenorphine has been developed to predict buprenorphine and norbuprenorphine venous and arterial blood plasma concentration-time profiles as well as buprenorphine and norbuprenorphine urinary excretion after intravenous administration in adults. The model has been used for the assessment of buprenorphine DDIs with clarithromycin, itraconazole as well as rifampicin. Furthermore, the adult PBPK model has been successfully scaled to both a child and a preterm neonate population for predictions of individual plasma concentration-time profiles. The models are thoroughly documented in the Supplementary Materials and publicly available in the OSP repository. With that, the models could support the development of a physiological transdermal buprenorphine model, contribute to a library of PBPK models for predictions in other DDI scenarios, and help with future investigations of buprenorphine and norbuprenorphine pharmacokinetics, including the design of clinical trials and novel formulations both for adults and pediatrics.

**Supplementary Materials:** The following are available online at <http://www.mdpi.com/1999-4923/12/6/578/s1>, Electronic Supplementary Materials: Additional detailed model information and evaluation.

**Author Contributions:** Conceptualization, L.K., C.S., D.S., M.S. and T.L.; Funding acquisition, Y.K., R.B., M.S. and T.L.; Investigation, L.K., C.S. and T.L.; Methodology, L.K., C.S. and T.L.; Visualization, L.K. and D.S.; Writing—original draft, L.K. and T.L.; Writing—review & editing, L.K., C.S., D.S., Y.K., R.B., M.S. and T.L. All authors have read and agreed to the published version of the manuscript.

**Funding:** This research was funded by the German Federal Ministry of Education and Research (BMBF), 031L0153 “Alternativmethoden zum Tierversuch”, 03XP0196 “NanoCare4.0—Anwendungssichere Materialinnovationen” and 031L0188D “Guide-IBD”, the Horizon 2020-PHC-2015 grant U-PGx 668353 and the Robert Bosch Stiftung, Stuttgart, Germany.

**Conflicts of Interest:** Yvonne Kohl, Robert Bals, Matthias Schwab and Thorsten Lehr have received research grants from the German Federal Ministry of Education and Research (BMBF). Lukas Kovar, Christina Schräpel and Dominik Selzer declare no conflicts of interest. The funders had no role in the design of the study; in the collection, analyses, or interpretation of data; in the writing of the manuscript, or in the decision to publish the results.

## References

1. Maunuksela, E.-L.; Korpela, R.; Olkkola, K.T. Double-blind, multiple-dose comparison of buprenorphine and morphine in postoperative pain of children. *Br. J. Anaesth.* **1988**, *60*, 48–55. [CrossRef] [PubMed]
2. WHO. *Guidelines for the Pharmacological and Radiotherapeutic Management of Cancer Pain in Adults and Adolescents*; Licence: CC BY-NC-SA 3.0 IGO; World Health Organization: Geneva, Switzerland, 2018; ISBN 978-92-4-155039-0.

3. Vicencio-Rosas, E.; Pérez-Guillé, M.G.; Flores-Pérez, C.; Flores-Pérez, J.; Trujillo-Jiménez, F.; Chávez-Pacheco, J.L. Buprenorphine and pain treatment in pediatric patients: An update. *J. Pain Res.* **2018**, *11*, 549–559. [[CrossRef](#)] [[PubMed](#)]
4. Michel, E.; Anderson, B.J.; Zernikow, B. Buprenorphine TTS for children—A review of the drug’s clinical pharmacology. *Pediatric Anesth.* **2011**, *21*, 280–290. [[CrossRef](#)] [[PubMed](#)]
5. Dahan, A.; Yassen, A.; Romberg, R.; Sarton, E.; Teppema, L.; Olofsen, E.; Danhof, M. Buprenorphine induces ceiling in respiratory depression but not in analgesia. *Br. J. Anaesth.* **2006**, *96*, 627–632. [[CrossRef](#)] [[PubMed](#)]
6. Kuhlman, J.J.; Lalani, S.; Magluilo, J.; Levine, B.; Darwin, W.D.; Johnson, R.E.; Cone, E.J. Human Pharmacokinetics of Intravenous, Sublingual, and Buccal Buprenorphine. *J. Anal. Toxicol.* **1996**, *20*, 369–378. [[CrossRef](#)]
7. Lo Re, M.; Chaplin, M.; Aronow, B.; Modesto-Lowe, V. Buprenorphine Overdose in Young Children: An Underappreciated Risk. *Clin. Pediatric* **2019**, *58*, 613–617. [[CrossRef](#)]
8. Boyer, E.W. Management of Opioid Analgesic Overdose. *N. Engl. J. Med.* **2012**, *367*, 146–155. [[CrossRef](#)] [[PubMed](#)]
9. Ling, W. Buprenorphine for opioid addiction. *Pain Manag.* **2012**, *2*, 345–350. [[CrossRef](#)] [[PubMed](#)]
10. Post, S.; Spiller, H.A.; Casavant, M.J.; Chounthirath, T.; Smith, G.A. Buprenorphine Exposures Among Children and Adolescents Reported to US Poison Control Centers. *Pediatrics* **2018**, *142*, e20173652. [[CrossRef](#)]
11. Ward, R.M.; Sherwin, C.M.T. Ethics of Drug Studies in the Newborn. *Pediatric Drugs* **2014**, *17*, 37–42. [[CrossRef](#)] [[PubMed](#)]
12. Leong, R.; Vieira, M.L.T.; Zhao, P.; Mulugeta, Y.; Lee, C.S.; Huang, S.-M.; Burckart, G.J. Regulatory experience with physiologically based pharmacokinetic modeling for pediatric drug trials. *Clin. Pharmacol. Ther.* **2012**, *91*, 926–931. [[CrossRef](#)] [[PubMed](#)]
13. Barrett, J.S.; Della Casa Alberighi, O.; Läer, S.; Meibohm, B. Physiologically Based Pharmacokinetic (PBPK) Modeling in Children. *Clin. Pharmacol. Ther.* **2012**, *92*, 40–49. [[CrossRef](#)] [[PubMed](#)]
14. Sager, J.E.; Yu, J.; Ragueneau-Majlessi, I.; Isoherranen, N. Physiologically Based Pharmacokinetic (PBPK) Modeling and Simulation Approaches: A Systematic Review of Published Models, Applications, and Model Verification. *Drug Metab. Dispos.* **2015**, *43*, 1823–1837. [[CrossRef](#)] [[PubMed](#)]
15. Templeton, I.E.; Jones, N.S.; Musib, L. Pediatric Dose Selection and Utility of PBPK in Determining Dose. *AAPS J.* **2018**, *20*, 31. [[CrossRef](#)]
16. Strougo, A.; Yassen, A.; Monnereau, C.; Danhof, M.; Freijer, J. Predicting the “First dose in children” of CYP3A-metabolized drugs: Evaluation of scaling approaches and insights into the CYP3A7-CYP3A4 switch at young ages. *J. Clin. Pharmacol.* **2014**, *54*, 1006–1015. [[CrossRef](#)]
17. Yokell, M.A.; Zaller, N.D.; Green, T.C.; Rich, J.D. Buprenorphine and buprenorphine/naloxone diversion, misuse, and illicit use: An international review. *Curr. Drug Abuse Rev.* **2011**, *4*, 28–41. [[CrossRef](#)]
18. Rosenthal, R.; Goradia, V. Advances in the delivery of buprenorphine for opioid dependence. *Drug Des. Devel. Ther.* **2017**, *11*, 2493–2505. [[CrossRef](#)]
19. Yang, J.C.; Roman-Urrestarazu, A.; Brayne, C. Responses among substance abuse treatment providers to the opioid epidemic in the USA: Variations in buprenorphine and methadone treatment by geography, operational, and payment characteristics, 2007–2016. *PLoS ONE* **2020**, *15*, e0229787. [[CrossRef](#)]
20. Dunlap, B.; Cifu, A.S. Clinical Management of Opioid Use Disorder. *JAMA* **2016**, *316*, 338. [[CrossRef](#)]
21. Picard, N.; Cresteil, T.; Djebli, N.; Marquet, P. In vitro metabolism study of buprenorphine: Evidence for new metabolic pathways. *Drug Metab. Dispos.* **2005**, *33*, 689–695. [[CrossRef](#)]
22. Hanke, N.; Frechen, S.; Moj, D.; Britz, H.; Eissing, T.; Wendl, T.; Lehr, T. PBPK Models for CYP3A4 and P-gp DDI Prediction: A Modeling Network of Rifampicin, Itraconazole, Clarithromycin, Midazolam, Alfentanil, and Digoxin. *CPT Pharmacomet. Syst. Pharmacol.* **2018**, *7*, 647–659. [[CrossRef](#)] [[PubMed](#)]
23. Kress, H.G. Clinical update on the pharmacology, efficacy and safety of transdermal buprenorphine. *Eur. J. Pain* **2009**, *13*, 219–230. [[CrossRef](#)] [[PubMed](#)]
24. Fihlman, M.; Hemmilä, T.; Hagelberg, N.M.; Backman, J.T.; Laitila, J.; Laine, K.; Neuvonen, P.J.; Olkkola, K.T.; Saari, T.I. Voriconazole greatly increases the exposure to oral buprenorphine. *Eur. J. Clin. Pharmacol.* **2018**, *74*, 1615–1622. [[CrossRef](#)] [[PubMed](#)]

25. Fihlman, M.; Hemmilä, T.; Hagelberg, N.M.; Kuusniemi, K.; Backman, J.T.; Laitila, J.; Laine, K.; Neuvonen, P.J.; Olkkola, K.T.; Saari, T.I. Voriconazole more likely than posaconazole increases plasma exposure to sublingual buprenorphine causing a risk of a clinically important interaction. *Eur. J. Clin. Pharmacol.* **2016**, *72*, 1363–1371. [CrossRef]
26. Hagelberg, N.M.; Fihlman, M.; Hemmilä, T.; Backman, J.T.; Laitila, J.; Neuvonen, P.J.; Laine, K.; Olkkola, K.T.; Saari, T.I. Rifampicin decreases exposure to sublingual buprenorphine in healthy subjects. *Pharmacol. Res. Perspect.* **2016**, *4*, e00271. [CrossRef]
27. Kovar, L.; Selzer, D.; Britz, H.; Benowitz, N.; St. Helen, G.; Kohl, Y.; Bals, R.; Lehr, T. Comprehensive Parent–Metabolite PBPK/PD Modeling Insights into Nicotine Replacement Therapy Strategies. *Clin. Pharmacokinet.* **2020**. [CrossRef]
28. Johnson, T.N.; Rostami-Hodjegan, A. Resurgence in the use of physiologically based pharmacokinetic models in pediatric clinical pharmacology: Parallel shift in incorporating the knowledge of biological elements and increased applicability to drug development and clinical practice. *Pediatric Anesth.* **2011**, *21*, 291–301. [CrossRef]
29. Jones, H.M.; Dickins, M.; Youdim, K.; Gosset, J.R.; Attkins, N.J.; Hay, T.L.; Gurrell, I.K.; Logan, Y.R.; Bungay, P.J.; Jones, B.C.; et al. Application of PBPK modelling in drug discovery and development at Pfizer. *Xenobiotica* **2012**, *42*, 94–106. [CrossRef]
30. Wojtyniak, J.-G.; Britz, H.; Selzer, D.; Schwab, M.; Lehr, T. Data Digitizing: Accurate and Precise Data Extraction for Quantitative Systems Pharmacology and Physiologically-Based Pharmacokinetic Modeling. *CPT Pharmacomet. Syst. Pharmacol. Pharmacol.* **2020**. accepted for publication. [CrossRef]
31. Maharaj, A.R.; Barrett, J.S.; Edginton, A.N. A workflow example of PBPK modeling to support pediatric research and development: Case study with lorazepam. *AAPS J.* **2013**, *15*, 455–464. [CrossRef]
32. Maharaj, A.R.; Edginton, A.N. Physiologically Based Pharmacokinetic Modeling and Simulation in Pediatric Drug Development. *CPT Pharmacomet. Syst. Pharmacol.* **2014**, *3*, 1–13. [CrossRef] [PubMed]
33. Ince, I.; Solodenko, J.; Frechen, S.; Dallmann, A.; Niederal, C.; Schlender, J.; Burghaus, R.; Lippert, J.; Willmann, S. Predictive Pediatric Modeling and Simulation Using Ontogeny Information. *J. Clin. Pharmacol.* **2019**, *59*, S95–S103. [CrossRef] [PubMed]
34. Oechsler, S.; Skopp, G. An in vitro approach to estimate putative inhibition of buprenorphine and norbuprenorphine glucuronidation. *Int. J. Legal Med.* **2010**, *124*, 187–194. [CrossRef] [PubMed]
35. Everhart, E.; Cheung, P.; Mendelson, J.; Upton, R.; Jones, R. The mass balance of buprenorphine in humans. *Clin. Pharmacol. Ther.* **1999**, *65*, 152. [CrossRef]
36. Chang, Y.; Moody, D.E. Glucuronidation of buprenorphine and norbuprenorphine by human liver microsomes and UDP-glucuronosyltransferases. *Drug Metab. Lett.* **2009**, *3*, 101–107. [CrossRef]
37. Brown, S.M.; Campbell, S.D.; Crafford, A.; Regina, K.J.; Holtzman, M.J.; Kharasch, E.D. P-glycoprotein is a major determinant of norbuprenorphine brain exposure and antinociception. *J. Pharmacol. Exp. Ther.* **2012**, *343*, 53–61. [CrossRef]
38. Open Systems Pharmacology Suite Community Open Systems Pharmacology Suite Manual, Version 7.4. Available online: <https://github.com/Open-Systems-Pharmacology/OSPSuite.Documentation/blob/master/Open%20Systems%20Pharmacology%20Suite.pdf> (accessed on 25 March 2020).
39. PK-Sim® Ontogeny Database, Version 7.3. Available online: <https://github.com/Open-Systems-Pharmacology/OSPSuite.Documentation/blob/master/PK-SimOntogenyDatabaseVersion7.3.pdf> (accessed on 25 March 2020).
40. McNamara, P.J.; Alcorn, J. Protein binding predictions in infants. *AAPS PharmSci* **2002**, *4*, 19–26. [CrossRef] [PubMed]
41. Takahashi, Y.; Ishii, S.; Arizono, H.; Nishimura, S.; Tsuruda, K.; Saito, N.; Nemoto, H.; Jin, Y.; Esumi, Y. Pharmacokinetics of Buprenorphine Hydrochloride (BN HCl) (1): Absorption, Distribution, Metabolism and Excretion after Percutaneous (TSN-09: BN HCl Containing Tape Application) or Subcutaneous Administration of BN HCl in Rats. *Drug Metab. Pharmacokinet.* **2001**, *16*, 569–583. [CrossRef]
42. Tod, M.; Jullien, V.; Pons, G. Facilitation of Drug Evaluation in Children by Population Methods and Modelling†. *Clin. Pharmacokinet.* **2008**, *47*, 231–243. [CrossRef]
43. Kajosaari, L.I.; Laitila, J.; Neuvonen, P.J.; Backman, J.T. Metabolism of repaglinide by CYP2C8 and CYP3A4 in vitro: Effect of fibrates and rifampicin. *Basic Clin. Pharmacol. Toxicol.* **2005**, *97*, 249–256. [CrossRef]

44. Rajaonarison, J.; Lacarelle, B.; Catalin, J.; Placidi, M.; Rahmani, R. 3'-azido-3'-deoxythymidine drug interactions. Screening for inhibitors in human liver microsomes. *Drug Metab. Dispos.* **1992**, *20*, 578–584. [[PubMed](#)]
45. Chiou, W.J.; de Morais, S.M.; Kikuchi, R.; Voorman, R.L.; Li, X.; Bow, D.A.J. In vitro OATP1B1 and OATP1B3 inhibition is associated with observations of benign clinical unconjugated hyperbilirubinemia. *Xenobiotica* **2014**, *44*, 276–282. [[CrossRef](#)] [[PubMed](#)]
46. Soars, M.G.; Petullo, D.M.; Eckstein, J.A.; Kasper, S.C.; Wrighton, S.A. An assessment of udp-glucuronosyltransferase induction using primary human hepatocytes. *Drug Metab. Dispos.* **2004**, *32*, 140–148. [[CrossRef](#)] [[PubMed](#)]
47. Trottier, J.; El Hussein, D.; Perreault, M.; Pâquet, S.; Caron, P.; Bourassa, S.; Verreault, M.; Inaba, T.T.; Poirier, G.G.; Bélanger, A.; et al. The Human UGT1A3 Enzyme Conjugates Norursodeoxycholic Acid into a C 23 -ester Glucuronide in the Liver. *J. Biol. Chem.* **2010**, *285*, 1113–1121. [[CrossRef](#)] [[PubMed](#)]
48. Reitman, M.L.; Chu, X.; Cai, X.; Yabut, J.; Venkatasubramanian, R.; Zajic, S.; Stone, J.A.; Ding, Y.; Witter, R.; Gibson, C.; et al. Rifampin's Acute Inhibitory and Chronic Inductive Drug Interactions: Experimental and Model-Based Approaches to Drug–Drug Interaction Trial Design. *Clin. Pharmacol. Ther.* **2011**, *89*, 234–242. [[CrossRef](#)] [[PubMed](#)]
49. Greiner, B.; Eichelbaum, M.; Fritz, P.; Kreichgauer, H.-P.; von Richter, O.; Zundler, J.; Kroemer, H.K. The role of intestinal P-glycoprotein in the interaction of digoxin and rifampin. *J. Clin. Investig.* **1999**, *104*, 147–153. [[CrossRef](#)]
50. Buckley, D.B.; Wiegand, C.M.; Prentiss, P.L.; Fahmi, O.A. Time-course of cytochrome P450 (CYP450) induction in cultured human hepatocytes: Evaluation of activity and mRNA expression profiles for six inducible CYP450 enzymes [poster no. P186]. In Proceedings of the 10th International ISSX Meeting, Toronto, ON, Canada, 29 September–3 October 2013.
51. Barrett, D.; Simpson, J.; Rutter, N.; Kurihara-Bergstrom, T.; Shaw, P.; Davis, S. The pharmacokinetics and physiological effects of buprenorphine infusion in premature neonates. *Br. J. Clin. Pharmacol.* **1993**, *36*, 215–219. [[CrossRef](#)]
52. Chiang, C.N.; Hawks, R.L. Pharmacokinetics of the combination tablet of buprenorphine and naloxone. *Drug Alcohol Depend.* **2003**, *70*, S39–S47. [[CrossRef](#)]
53. Kalluri, H.V.; Zhang, H.; Caritis, S.N.; Venkataramanan, R. A physiologically based pharmacokinetic modelling approach to predict buprenorphine pharmacokinetics following intravenous and sublingual administration. *Br. J. Clin. Pharmacol.* **2017**, *83*, 2458–2473. [[CrossRef](#)]
54. Bai, S.A.; Xiang, Q.; Finn, A. Evaluation of the Pharmacokinetics of Single- and Multiple-dose Buprenorphine Buccal Film in Healthy Volunteers. *Clin. Ther.* **2016**, *38*, 358–369. [[CrossRef](#)]
55. Bartlett, A.J.; Lloyd-Jones, J.G.; Rance, M.J.; Flockhart, I.R.; Dockray, G.J.; Bennett, M.R.D.; Moore, R.A. The radioimmunoassay of buprenorphine. *Eur. J. Clin. Pharmacol.* **1980**, *18*, 339–345. [[CrossRef](#)] [[PubMed](#)]
56. Bullingham, R.E.; McQuay, H.J.; Moore, A.; Bennett, M.R. Buprenorphine kinetics. *Clin. Pharmacol. Ther.* **1980**, *28*, 667–672. [[CrossRef](#)] [[PubMed](#)]
57. Bullingham, R.E.; McQuay, H.J.; Porter, E.J.; Allen, M.C.; Moore, R.A. Sublingual buprenorphine used postoperatively: Ten hour plasma drug concentration analysis. *Br. J. Clin. Pharmacol.* **1982**, *13*, 665–673. [[CrossRef](#)] [[PubMed](#)]
58. Harris, D.S.; Jones, R.T.; Welm, S.; Upton, R.A.; Lin, E.; Mendelson, J. Buprenorphine and naloxone co-administration in opiate-dependent patients stabilized on sublingual buprenorphine. *Drug Alcohol Depend.* **2000**, *61*, 85–94. [[CrossRef](#)]
59. Huestis, M.A.; Cone, E.J.; Pirnay, S.O.; Umbricht, A.; Preston, K.L. Intravenous buprenorphine and norbuprenorphine pharmacokinetics in humans. *Drug Alcohol Depend.* **2013**, *131*, 258–262. [[CrossRef](#)]
60. Mendelson, J.; Upton, R.A.; Everhart, E.T.; Jacob, P., III; Jones, R.T. Bioavailability of Sublingual Buprenorphine. *J. Clin. Pharmacol.* **1997**, *37*, 31–37. [[CrossRef](#)]
61. Olkkola, K.; Maunuksela, E.; Korpela, R. Pharmacokinetics of intravenous buprenorphine in children. *Br. J. Clin. Pharmacol.* **1989**, *28*, 202–204. [[CrossRef](#)]
62. Cone, E.J.; Gorodetzky, C.W.; Yousefnejad, D.; Buchwald, W.F.; Johnson, R.E. The metabolism and excretion of buprenorphine in humans. *Drug Metab. Dispos.* **1984**, *12*, 577–581.

63. Wishart, D.S.; Knox, C.; Guo, A.C.; Shrivastava, S.; Hassanali, M.; Stothard, P.; Chang, Z.; Woolsey, J. DrugBank: A comprehensive resource for in silico drug discovery and exploration. *Nucleic Acids Res.* **2006**, *34*, D668–D672. [[CrossRef](#)]
64. Yeola, G.S.; Darandale, S.; Khire, A.; Vavia, P.R. Fabrication and statistical optimization of a polysaccharide-based sublingual film of buprenorphine hydrochloride for breakthrough pain management: In vitro and in vivo performance. *Drug Deliv. Transl. Res.* **2014**, *4*, 116–125. [[CrossRef](#)]
65. Wishart, D.S.; Feunang, Y.D.; Marcu, A.; Guo, A.C.; Liang, K.; Vázquez-Fresno, R.; Sajed, T.; Johnson, D.; Li, C.; Karu, N.; et al. HMDB 4.0: The human metabolome database for 2018. *Nucleic Acids Res.* **2018**, *46*, D608–D617. [[CrossRef](#)]
66. Heel, R.C.; Brogden, R.N.; Speight, T.M.; Avery, G.S. Buprenorphine: A review of its pharmacological properties and therapeutic efficacy. *Drugs* **1979**, *17*, 81–110. [[CrossRef](#)] [[PubMed](#)]
67. Schmitt, W. General approach for the calculation of tissue to plasma partition coefficients. *Toxicol. In Vitro* **2008**, *22*, 457–467. [[CrossRef](#)] [[PubMed](#)]
68. Obach, R.S. Nonspecific binding to microsomes: Impact on scale-up of in vitro intrinsic clearance to hepatic clearance as assessed through examination of warfarin, imipramine, and propranolol. *Drug Metab. Dispos.* **1997**, *25*, 1359–1369. [[PubMed](#)]
69. Mahmood, I.; Tegenge, M.A. A Comparative Study Between Allometric Scaling and Physiologically Based Pharmacokinetic Modeling for the Prediction of Drug Clearance From Neonates to Adolescents. *J. Clin. Pharmacol.* **2019**, *59*, 189–197. [[CrossRef](#)] [[PubMed](#)]
70. Kapil, R.P.; Cipriano, A.; Friedman, K.; Michels, G.; Shet, M.S.; Colucci, S.V.; Apseloff, G.; Kitzmiller, J.; Harris, S.C. Once-Weekly Transdermal Buprenorphine Application Results in Sustained and Consistent Steady-State Plasma Levels. *J. Pain Symptom Manag.* **2013**, *46*, 65–75. [[CrossRef](#)] [[PubMed](#)]
71. Duan, P.; Fisher, J.W.; Yoshida, K.; Zhang, L.; Burckart, G.J.; Wang, J. Physiologically Based Pharmacokinetic Prediction of Linezolid and Emtricitabine in Neonates and Infants. *Clin. Pharmacokinet.* **2017**, *56*, 383–394. [[CrossRef](#)] [[PubMed](#)]
72. Edgington, A.N.; Schmitt, W.; Voith, B.; Willmann, S. A Mechanistic Approach for the Scaling of Clearance in Children. *Clin. Pharmacokinet.* **2006**, *45*, 683–704. [[CrossRef](#)]
73. Edgington, A.N.; Willmann, S. Physiology-based versus allometric scaling of clearance in children; an eliminating process based comparison. *Paediatric Perinat. Drug Ther.* **2006**, *7*, 146–153. [[CrossRef](#)]
74. Kearns, G.L.; Abdel-Rahman, S.M.; Alander, S.W.; Blowey, D.L.; Leeder, J.S.; Kauffman, R.E. Developmental pharmacology–drug disposition, action, and therapy in infants and children. *N. Engl. J. Med.* **2003**, *349*, 1157–1167. [[CrossRef](#)]
75. Kapil, R.P.; Cipriano, A.; Michels, G.H.; Perrino, P.; O’Keefe, S.A.; Shet, M.S.; Colucci, S.V.; Noveck, R.J.; Harris, S.C. Effect of Ketoconazole on the Pharmacokinetic Profile of Buprenorphine following Administration of a Once-Weekly Buprenorphine Transdermal System. *Clin. Drug Investig.* **2012**, *32*, 583–592. [[CrossRef](#)] [[PubMed](#)]
76. Johnson, T.N.; Jamei, M.; Rowland-Yeo, K. How Does In Vivo Biliary Elimination of Drugs Change with Age? Evidence from In Vitro and Clinical Data Using a Systems Pharmacology Approach. *Drug Metab. Dispos.* **2016**, *44*, 1090–1098. [[CrossRef](#)]
77. Zhang, H.; Kalluri, H.V.; Bastian, J.R.; Chen, H.; Alshabi, A.; Caritis, S.N.; Venkataramanan, R. Gestational changes in buprenorphine exposure: A physiologically-based pharmacokinetic analysis. *Br. J. Clin. Pharmacol.* **2018**, *84*, 2075–2087. [[CrossRef](#)] [[PubMed](#)]
78. Ji, B.; Liu, S.; Xue, Y.; He, X.; Man, V.H.; Xie, X.-Q.; Wang, J. Prediction of Drug–Drug Interactions Between Opioids and Overdosed Benzodiazepines Using Physiologically Based Pharmacokinetic (PBPK) Modeling and Simulation. *Drugs R D* **2019**, *19*, 297–305. [[CrossRef](#)]
79. Jensen, M.L.; Foster, D.; Upton, R.; Grant, C.; Martinez, A.; Somogyi, A. Comparison of cerebral pharmacokinetics of buprenorphine and norbuprenorphine in an in vivo sheep model. *Xenobiotica* **2007**, *37*, 441–457. [[CrossRef](#)] [[PubMed](#)]
80. Ohtani, M.; Kotaki, H.; Nishitaten, K.; Sawada, Y.; Iga, T. Kinetics of respiratory depression in rats induced by buprenorphine and its metabolite, norbuprenorphine. *J. Pharmacol. Exp. Ther.* **1997**, *281*, 428–433. [[PubMed](#)]

81. Strang, J.; Knight, A.; Baillie, S.; Reed, K.; Bogdanowicz, K.; Bell, J. Norbuprenorphine and respiratory depression: Exploratory analyses with new lyophilized buprenorphine and sublingual buprenorphine. *Int. J. Clin. Pharmacol. Ther.* **2018**, *56*, 81–85. [[CrossRef](#)]
82. Hans, G.; Robert, D. Transdermal buprenorphine—A critical appraisal of its role in pain management. *J. Pain Res.* **2009**, *2*, 117–134. [[CrossRef](#)]



© 2020 by the authors. Licensee MDPI, Basel, Switzerland. This article is an open access article distributed under the terms and conditions of the Creative Commons Attribution (CC BY) license (<http://creativecommons.org/licenses/by/4.0/>).

### 3.2 PUBLICATION II – PBPK MODELING OF FENTANYL IN ADULT AND PEDIATRIC PATIENTS

#### 3.2.1 Reference

##### **Physiologically-Based Pharmacokinetic (PBPK) Modeling Providing Insights into Fentanyl Pharmacokinetics in Adults and Pediatric Patients.**

Lukas Kovar, Andreas Weber, Michael Zemlin, Yvonne Kohl, Robert Bals, Bernd Meibohm, Dominik Selzer and Thorsten Lehr.

*Pharmaceutics* 2020;12(10):908. DOI: 10.3390/pharmaceutics12100908 [2].

#### 3.2.2 Author Contributions

Author contributions according to the contributor roles taxonomy (CRediT) [4, 5] were as following:

Lukas Kovar	Refer to <i>Contribution Report</i> (p. vii)
Andreas Weber	Conceptualization, Investigation, Methodology, Writing – review & editing
Michael Zemlin	Conceptualization, Writing – original draft, Writing – review & editing
Yvonne Kohl	Funding acquisition, Writing – review & editing
Robert Bals	Funding acquisition, Writing – review & editing
Bernd Meibohm	Conceptualization, Writing – original draft, Writing – review & editing
Dominik Selzer	Investigation, Methodology, Visualization, Writing – original draft, Writing – review & editing
Thorsten Lehr	Conceptualization, Funding acquisition, Investigation, Methodology, Writing – original draft, Writing – review & editing

#### 3.2.3 Copyright

©2020 by the authors. Licensee MDPI, Basel, Switzerland. This article is an open access article distributed under the terms and conditions of the Creative Commons Attribution (CC BY 4.0) license (<http://creativecommons.org/licenses/by/4.0/>).



Article

# Physiologically-Based Pharmacokinetic (PBPK) Modeling Providing Insights into Fentanyl Pharmacokinetics in Adults and Pediatric Patients

Lukas Kovar <sup>1</sup>, Andreas Weber <sup>1</sup>, Michael Zemlin <sup>2</sup>, Yvonne Kohl <sup>3</sup>, Robert Bals <sup>4</sup>, Bernd Meibohm <sup>5</sup>, Dominik Selzer <sup>1</sup> and Thorsten Lehr <sup>1,\*</sup>

<sup>1</sup> Department of Clinical Pharmacy, Saarland University, 66123 Saarbrücken, Germany; lukas.kovar@uni-saarland.de (L.K.); andimattweber@gmail.com (A.W.); dominik.selzer@uni-saarland.de (D.S.)

<sup>2</sup> Department of General Pediatrics and Neonatology, Saarland University Medical Center, 66421 Homburg, Germany; michael.zemlin@uks.eu

<sup>3</sup> Fraunhofer Institute for Biomedical Engineering IBMT, 66280 Sulzbach, Germany; yvonne.kohl@ibmt.fraunhofer.de

<sup>4</sup> Department of Internal Medicine V, Saarland University, 66421 Homburg, Germany; robert.bals@uks.eu

<sup>5</sup> Department of Pharmaceutical Sciences, College of Pharmacy, The University of Tennessee Health Science Center, Memphis, TN 38163, USA; bmeibohm@uthsc.edu

\* Correspondence: thorsten.lehr@mx.uni-saarland.de; Tel.: +49-681-302-70255

Received: 26 August 2020; Accepted: 21 September 2020; Published: 23 September 2020



**Abstract:** Fentanyl is widely used for analgesia, sedation, and anesthesia both in adult and pediatric populations. Yet, only few pharmacokinetic studies of fentanyl in pediatrics exist as conducting clinical trials in this population is especially challenging. Physiologically-based pharmacokinetic (PBPK) modeling is a mechanistic approach to explore drug pharmacokinetics and allows extrapolation from adult to pediatric populations based on age-related physiological differences. The aim of this study was to develop a PBPK model of fentanyl and norfentanyl for both adult and pediatric populations. The adult PBPK model was established in PK-Sim<sup>®</sup> using data from 16 clinical studies and was scaled to several pediatric subpopulations. ~93% of the predicted AUC<sub>last</sub> values in adults and ~88% in pediatrics were within 2-fold of the corresponding value observed. The adult PBPK model predicted a fraction of fentanyl dose metabolized to norfentanyl of ~33% and a fraction excreted in urine of ~7%. In addition, the pediatric PBPK model was used to simulate differences in peak plasma concentrations after bolus injections and short infusions. The novel PBPK models could be helpful to further investigate fentanyl pharmacokinetics in both adult and pediatric populations.

**Keywords:** physiologically-based pharmacokinetic (PBPK) modeling; fentanyl; neonates; norfentanyl; pediatric scaling; drug–drug interaction (DDI); pharmacokinetics

## 1. Introduction

Fentanyl is a strong opioid—approximately 50- to 100-fold more potent compared to morphine—and is extensively used in the therapeutic fields of analgesia, sedation, and anesthesia both in adult and pediatric patients [1–3]. While clinical trials on the pharmacokinetics (PK) of fentanyl suggest several factors such as liver function impacting the dose–exposure relationship, the wide interindividual variability is still not completely understood [3]. As fentanyl is a substrate of the cytochrome P450 (CYP) iso-enzyme 3A4, fentanyl PK can be altered by concomitant administration of CYP3A4 inhibitors and inducers (drug–drug interactions, DDIs) [3].

The major route of metabolic clearance was assumed to be mediated via CYP3A4 metabolizing fentanyl to the inactive metabolite norfentanyl [3,4]. However, recent research activities have suggested a strong involvement of additional metabolic pathways and hypothesized unknown metabolites [5,6].

In critically ill neonates, analgesic therapy is commonly administered, since pain can act as a stressor increasing mortality in this population [1]. Indeed, fentanyl is the opioid analgesic most frequently used in neonatal intensive care units [1], which highlights the importance of fentanyl in pediatrics. Yet, there is still a lack of knowledge regarding fentanyl PK in children [2]. The desired analgesic and sedating effects resulting from administration of fentanyl usually lead to an improvement of respiratory compliance [7,8]. However, adverse drug reactions (ADRs), such as bradycardia, respiratory depression, and, in rare cases, chest wall rigidity, might occur even after low doses of fentanyl administration [1,8]. A recent meta-analysis by Ziesenitz and colleagues concluded the need for further research on fentanyl, especially in larger cohorts and special subpopulations such as preterm neonates and children with hepatic or renal impairment [2]. However, pediatric PK studies are difficult to conduct and are often impeded by ethical and logistic challenges, many of which are unique to pediatrics [9].

Physiologically-based pharmacokinetic (PBPK) modeling can be used for evaluating and extending existing knowledge on drug disposition derived from *in vitro* and *in vivo* investigations into unstudied subpopulations and clinical scenarios [10,11]. An increasing number of drug applications submitted to the US Food and Drug Administration (FDA) and the European Medicines Agency (EMA) have investigated the impact of hepatic disease, pharmacogenomics, and DDIs on drug PK with the help of PBPK modeling [10,12]. Previous PBPK efforts on fentanyl have focused on methodological aspects of simplifying PBPK models [13], on a PBPK approach to support the development of Provisional Advisory Levels (PALs) for hazardous agents [14], and on simulating thyroid and testes tissue concentrations [15], respectively.

In pediatrics, PBPK approaches have also proven its usefulness in designing and optimizing clinical trials and are supported by both the FDA and the EMA [12,16–20]. For a priori PBPK predictions in pediatrics, the PBPK model first needs to be informed and evaluated with published PK data in adults and subsequently extrapolated to pediatric populations—a workflow which has recently been implemented and successfully executed for several drugs [10,21–25].

The aim of the presented work was to develop a whole-body parent-metabolite intravenous PBPK model of fentanyl and norfentanyl in adults as a foundation for further assessment of fentanyl PK and to extrapolate the adult PBPK model for the prediction of plasma concentration–time profiles as well as individual clearance parameters in pediatric patients. The novel PBPK models are publicly available in the Open Systems Pharmacology (OSP) repository as clinical research tools to support the design of clinical trials in specific populations as well as the development of novel drug formulations. The Supplementary Materials serve as an additional reference manual including detailed model performance evaluation.

## 2. Materials and Methods

### 2.1. Software

The PBPK models were developed with the PK-Sim<sup>®</sup> modeling software (version 9.0, 2020, [www.open-systems-pharmacology.org](http://www.open-systems-pharmacology.org)), which is part of the OSP Suite [11]. Clinical plasma data from scientific literature was digitized using GetData Graph Digitizer version 2.26.0.20 (S. Fedorov, 2013) according to best practices [26]. Model input parameters were optimized using the Monte Carlo algorithm implemented in PK-Sim<sup>®</sup>. PK parameter and model performance measure calculation as well as graph plotting were performed with the R programming language version 3.6.1 (R Foundation for Statistical Computing, Vienna, Austria, 2019) and R Studio<sup>®</sup> version 1.2.5019 (R Studio, Inc., Boston, MA, USA, 2019).

## 2.2. PBPK Model Building for Adult Populations

The adult fentanyl parent-metabolite model building was initiated with an extensive literature search to obtain information on physicochemical properties as well as distribution, metabolism and excretion processes of fentanyl and norfentanyl. The gathered information was utilized to implement relevant drug-protein interactions (i.e., for transport proteins and enzymes) and to inform drug-dependent model input parameters. Published clinical studies of intravenous fentanyl administration in single- and multiple-dose regimens were used to extract plasma profiles and measured fractions of fentanyl dose excreted unchanged in urine. The fentanyl and norfentanyl plasma profiles were divided into an internal training and an external test dataset. Studies for the training dataset were selected containing a wide range of profiles (i.e., different dosing regimens, timing and frequency of sampling, measurements of norfentanyl, measurements of arterial and venous plasma concentrations, etc.). The test dataset was used for model evaluation.

Distribution and elimination processes including CYP enzymes as well as drug transporters were implemented according to the literature [5,27,28]. For the fentanyl model, these included (1) metabolism of fentanyl to the inactive metabolite norfentanyl via CYP3A4 and CYP3A7, (2) an unspecific hepatic pathway metabolizing fentanyl to other non-specified metabolites, (3) distribution and excretion via P-glycoprotein (P-gp), and (4) renal excretion through glomerular filtration. It should be noted that the actual role of CYP3A7 in the metabolism of fentanyl is suspected but the true nature of involvement still remains unknown [27,29]. Since CYP3A4 and CYP3A7 exhibit a similar substrate spectrum and CYP3A7 is the major fetal form of CYP3A [30], CYP3A7 might be important for PK predictions of fentanyl in pediatric populations and was therefore incorporated in the model. Considering that norfentanyl is predominantly eliminated via urine, renal clearance was implemented and estimated during the parameter optimization step [5]. Tissue expression distribution of the metabolizing enzymes and P-gp in all model compartments was implemented according to the PK-Sim<sup>®</sup> expression database [31]. Model input parameters, which could not be adequately obtained from literature, were estimated by fitting the parent-metabolite model to the training dataset. For detailed information on PBPK model building see Section 1 in the Supplementary Materials.

## 2.3. PBPK Modeling in Pediatrics

For a priori predictions of plasma concentration-time profiles as well as clearance parameters in pediatrics, the adult PBPK model was scaled to pediatric populations of different age groups. For this, the adult virtual populations were replaced by pediatric virtual populations, changing the physiological and anatomic parameters describing the human body. As a result, anatomic and physiological parameters as well as CYP3A4 and CYP3A7 tissue concentrations were scaled to the particular pediatric target population taking age-related changes such as size of tissue compartments and maturation of enzyme abundances into account. The used ontogeny functions for CYP3A4 and CYP3A7 are depicted in the PK-Sim<sup>®</sup> ontogeny database [32]. Since ontogenetic information regarding the transport protein P-gp were not implemented in PK-Sim<sup>®</sup>, the age-dependent protein abundance was estimated via the published ontogeny function from Prasad et al. [33]. While changes in anatomy and physiology during liver maturation were considered, the rate constant of the implemented unspecific hepatic clearance process was assumed to be independent of age. The unbound fraction of fentanyl was scaled for each particular pediatric population using the method of McNamara and Alcorn for alpha-1-acid glycoprotein [34,35] and compared to a range of published literature values. The remaining drug-dependent parameters were fixed to the values of the adult PBPK model. Next, the extrapolated PBPK model was applied to predict plasma profiles in pediatric populations of different age ranges (i.e., preterm and full-term neonates, infants and children). Additionally, 65 individual clearance values from preterm and full-term neonates were predicted and compared to observed values from three clinical trials [36–38].

#### 2.4. PBPK Model Evaluation and DDI Modeling

Predicted and observed plasma concentrations as well as predicted and observed areas under the plasma concentration–time curve from the first to the last data point ( $AUC_{last}$ ) were compared in goodness-of-fit plots for both the adult and the pediatric PBPK models. Moreover, all simulated fentanyl and norfentanyl plasma concentration–time trajectories were visually compared to the plasma profiles observed from the respective clinical trial. In order to visualize the interindividual variability of the model, virtual populations of 100 individuals were created covering the patient characteristics of the corresponding clinical study population. Detailed information on virtual populations can be found in Section 1.3 in the Supplementary Materials. For plasma profile simulation for individual patients, populations of 100 individuals with the same patient demographics were used, only allowing variability in the expression of the implemented enzymes, transporters and the unspecific hepatic clearance. Furthermore, two quantitative model performance measures were calculated for the adult and pediatric PBPK models: the mean relative deviation (MRD) of the predicted from the observed plasma concentrations for each plasma profile as well as the geometric mean fold error (GMFE) of the computed  $AUC_{last}$  ratios. The sensitivity of the PBPK models to single-parameter changes (local sensitivity analysis) was estimated with PK-Sim<sup>®</sup>. Detailed information on the calculation of MRD, GMFE and sensitivity analysis can be found in Section 3 in the Supplementary Materials.

For further evaluation of the adult PBPK model, a DDI scenario of fentanyl and the CYP3A4 inhibitor voriconazole was predicted and compared with the plasma profiles observed in a clinical trial. For this, the developed fentanyl-norfentanyl PBPK model was coupled with a recently published PBPK model of voriconazole [39]. The mathematical implementation of the competitive and irreversible interaction is described in Section 2 in the Supplementary Materials.

For pediatrics, individual and population mean clearance values extracted from three clinical trials were compared to predictions from the pediatric PBPK model. Finally, for all models, the percentages of model-predicted  $AUC_{last}$  and clearance values falling within 2-fold of the corresponding observed values were calculated.

### 3. Results

#### 3.1. PK Data for PBPK Model Development and Pediatric Scaling

For adult PBPK model development, 16 clinical studies including 24 different treatment arms were utilized, covering a broad dosing range of 0.3–60  $\mu\text{g}/\text{kg}$  body weight intravenous fentanyl in single- and multiple-dosing regimens. Here, three treatment arms also reported plasma concentrations of the metabolite norfentanyl. The dataset included one DDI study with voriconazole as the perpetrator drug as well as 14 study arms with fentanyl administration before or during surgeries. Nine treatment arms measured fentanyl concentrations in arterial blood, 14 in venous blood and one covered both sampling sites. Moreover, three clinical trials provided information on fractions of fentanyl dose excreted unchanged in urine [5,40,41]. All plasma profiles were digitized and split into an internal training ( $n = 9$  profiles) and an external test dataset ( $n = 18$  profiles). An overview of the included clinical studies in adults including study characteristics, dosing regimens, and the assignments to training and test dataset is shown in Table 1.

For predictive performance evaluation of the extrapolated pediatric PBPK model, five clinical trials investigating fentanyl plasma concentrations in preterm neonates, full-term neonates, infants and young children with mean age ranging from 32 weeks of gestational age to approximately three years of chronological age were identified. Moreover, individual clearance values of 65 preterm and full-term neonates were extracted from three published studies. An overview of the clinical studies in pediatrics including study characteristics and dosing regimens is provided in Table 2.

**Table 1.** Overview of clinical studies used for building and evaluation of the adult PBPK model of fentanyl and norfentanyl.

Clinical Study ID	Dose <sup>a</sup> [ $\mu\text{g}/\text{kg}$ ]	Dose <sup>b</sup> [ $\mu\text{g}/\text{h}$ ]	Administration	n	Female [%]	Age [Years]	Weight [kg]	Blood Sample	Surgery	Dataset	Reference
Bentley et al., 1982 (Adult)	10.0		iv (bolus)	5	100	36 $\pm$ 4	64 $\pm$ 3	arterial	yes	e	[42]
Bentley et al., 1982 (Elderly)	10.0		iv (bolus)	4	100	67 $\pm$ 2	68 $\pm$ 7	arterial	yes	e	[42]
Bovill and Sebel 1980	60.0		iv (2 min)	5	40	57 (45–65)	71 (53–87)	venous	yes	e	[41]
Christrup et al., 2008	1.5		iv (-)	7	43	24 (22–28)	68 (52–82)	venous	yes	i	[43]
Duthie et al., 1986 (1)	1.4	100.0	iv (24 h + bolus)	10	-	61 $\pm$ 8	69 $\pm$ 12	venous	yes	e	[44]
Duthie et al., 1986 (2)	1.5	100.0	iv (24 h + bolus)	13	-	49 $\pm$ 14	65 $\pm$ 14	venous	yes	e	[44]
Duthie et al., 1986 (3)	1.4	100.0	iv (24 h + bolus)	10	-	58 $\pm$ 11	69 $\pm$ 11	venous	yes	e	[44]
Duthie et al., 1986 (4)	7.2	100.0	iv (26 h + bolus)	12	-	55 $\pm$ 12	69 $\pm$ 9	venous	yes	i	[44]
Gourlay et al., 1989	1.0		iv (1 min)	6	-	-	70 (40–85)	venous <sup>c</sup>	no	e	[45]
Gupta et al., 1995	50.0		iv (48 h)	6	0	-	-	venous <sup>d</sup>	no	i	[46]
Holley and van Steennis 1988 (1)	1.3	25.0	iv (loading dose + 24 h)	10	0	54 $\pm$ 12	76 $\pm$ 12	arterial	yes	i	[47]
Holley and van Steennis 1988 (2)	2.5	50.0	iv (loading dose + 24 h)	10	0	44 $\pm$ 15	81 $\pm$ 16	arterial	yes	e	[47]
Holley and van Steennis 1988 (3)	5.0	100.0	iv (loading dose + 24 h)	10	0	56 $\pm$ 12	80 $\pm$ 17	arterial	yes	e	[47]
Holley and van Steennis 1988 (4)	6.5	125.0	iv (loading dose + 24 h)	9	0	54 $\pm$ 12	77 $\pm$ 5	arterial	yes	i	[47]
Lim et al., 2012	1.5		iv (5 min)	22	58	23 (19–32)	67 (51–101)	venous	no	e	[48]
MacLeod et al., 2012	0.3		iv (5 sec)	10	51	25 (18–55)	73 $\pm$ 13	arterial	no	i	[49]
McClain and Hug 1980	6.4		iv (1.5 min)	5	0	- (22–29)	75 (65–85)	arterial	no	i	[40]
Saari et al., 2008 <sup>e</sup>	5.0		iv (2 min)	12	42	-	-	venous	no	e	[6]
Saari et al., 2008 (DDI) <sup>e,f</sup>	5.0		iv (2 min)	12	42	-	-	venous	no	e	[6]
Singleton et al., 1987 (1)	20.7		iv (2 min)	7	-	33 (18–41)	-	arterial	yes	e	[50]
Stoeckel et al., 1982	7.6		iv (bolus)	3	33	22 (20–26)	66 (59–77)	venous	no	e	[51]
Streisand et al., 1991	15.0		iv (8 min)	10	0	27 (23–31)	76 (68–85)	arterial	no	e	[52]
Varvel et al., 1989	11.4		iv (5 min)	8	63	45 (33–57)	68 (52–100)	arterial/venous	yes	e	[53]
Ziesentz et al., 2015 <sup>e</sup>	5.0		iv (10 min)	16	25	33 (22–49)	73 (61–85)	venous	no	i	[5]

-: not available, e: external test dataset, i: internal training dataset, iv: intravenous. Age and weight are reported as the mean with standard deviation or range if available. <sup>a</sup> Dose of bolus injection and short infusion, respectively; <sup>b</sup> dose of long-term infusion; <sup>c</sup> venous blood samples from a central venous catheter; <sup>d</sup> sample information was not specified and venous blood samples were assumed; <sup>e</sup> norfentanyl concentrations measured; <sup>f</sup> with concomitant administration of voriconazole.

**Table 2.** Overview of clinical studies used for evaluation of the pediatric PBPK model predictions of fentanyl.

Clinical Study ID	Dose <sup>a</sup> [ $\mu\text{g}/\text{kg}$ ]	Dose <sup>b</sup> [ $\mu\text{g}/\text{kg}/\text{h}$ ]	Administration	n	Female [%]	Chronological Age	Gestational Age	Weight [kg]	Blood Sample	Surgery	Reference
Collins et al., 1985	30.0		iv (1 min)	9	22	-	32 (23–38)	1.1 (0.7–1.6)	arterial	yes	[54]
Gauntlett et al., 1988 (1)	52.5		iv (2 min)	1	-	1 day	38	2.8	arterial	yes	[36]
Gauntlett et al., 1988 (2)	56.5		iv (2 min)	1	-	3 days	40	2.5	arterial	yes	[36]
Gauntlett et al., 1988 (all) <sup>c</sup>	54.1 $\pm$ 2.3		iv (2 min)	14	-	18.0 (1–71) days	38 (32–40)	2.7 (1.9–3.9)	arterial	yes	[36]
Koehnert et al., 1986 (1)	25.0		iv (1–3 min)	1	-	2 days	-	2.0	arterial	yes	[37]
Koehnert et al., 1986 (2)	50.0		iv (1–3 min)	1	-	2 days	-	3.5	arterial	yes	[37]
Koehnert et al., 1986 (all) <sup>c</sup>	10.0–50.0		iv (1–3 min)	14	-	3.0 (0.5–14) days	-	2.9 (1.9–3.8)	arterial	yes	[37]
Saarenmaa et al., 2000 <sup>c</sup>	10.5	1.5	iv (1 h + 58 h)	38	26	0.4 (0–2) days	32 (26–42)	1.8 (0.9–3.6) <sup>d</sup>	arterial	yes	[38]
Singleton et al., 1987 (2)	31.2		iv (2 min)	7	-	6.5 (3–10) months	-	-	arterial	yes	[50]
Singleton et al., 1987 (3)	30.8		iv (2 min)	7	-	2.7 (1–9) years	-	-	venous <sup>e</sup>	yes	[50]

-: not available, iv: intravenous. Age and weight are reported as the mean with range if available. <sup>a</sup> Dose of bolus injection and short infusion, respectively; <sup>b</sup> dose of long-term infusion; <sup>c</sup> studies from which observed individual clearance values were extracted; <sup>d</sup> median and range; <sup>e</sup> venous blood samples from a central venous catheter.

## 3.2. Adult PBPK Model Building and Evaluation

A whole-body adult PBPK model of fentanyl and its metabolite norfentanyl was built and comprehensively evaluated using arterial and venous plasma profiles as well as information on fraction of fentanyl dose excreted unchanged in urine. Model-predicted population profiles are compared to the corresponding study data in Figure 1 (selection of profiles from the training and test dataset) and in detail in Section 3.1 in the Supplementary Materials (all simulated studies, both on a semilogarithmic and linear scale). Simulated plasma profile trajectories of fentanyl for bolus/short-infusion administrations as well as long-term infusions are in close concordance with observed data. This holds true for both fentanyl venous and arterial blood plasma concentrations as well as for venous norfentanyl plasma concentrations.

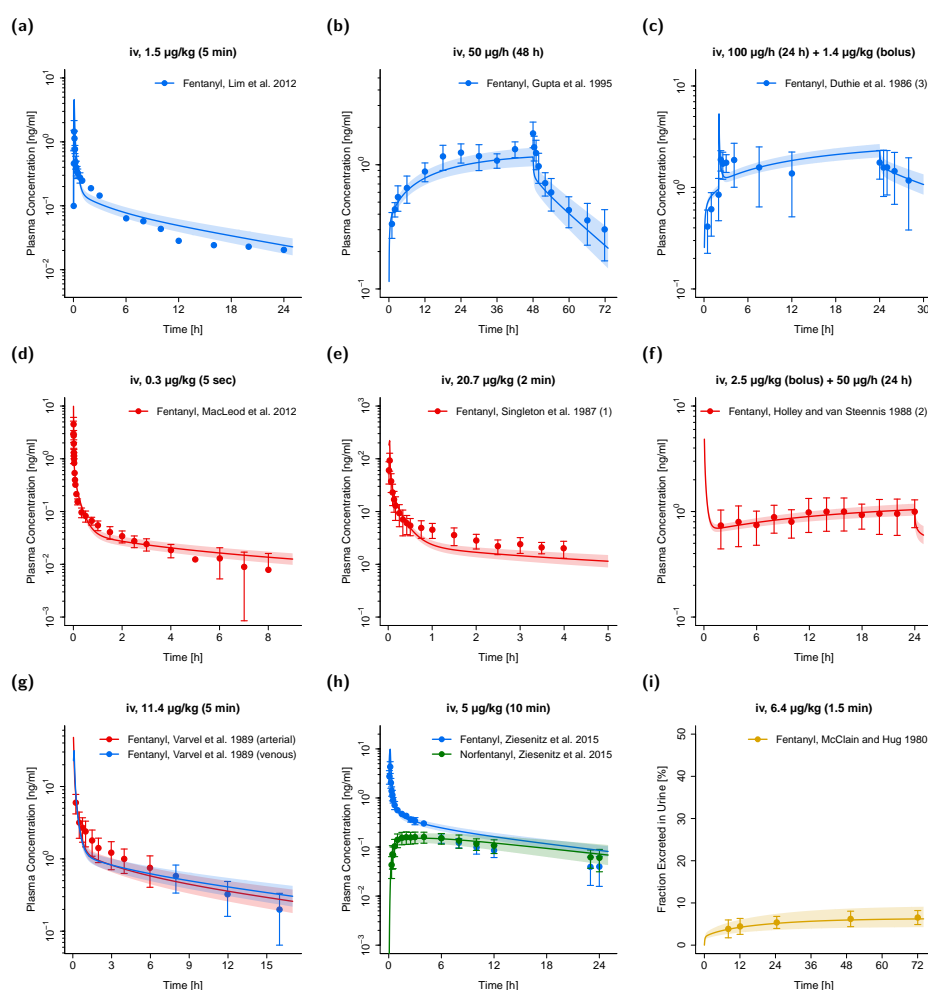


**Figure 1.** Fentanyl (blue: venous blood; red: arterial blood; orange: urine) and norfentanyl (green: venous blood) predicted and observed plasma concentration–time as well as fraction excreted in urine–time profiles after intravenous administration of fentanyl in adults. (a,c,e–g): selection of external test dataset; (b,d,h,i): selection of internal training dataset. Population simulations ( $n = 100$ ) are shown as lines with shaded areas (geometric mean and geometric standard deviation). Observed data is shown as circles  $\pm$  standard deviation if available. References with numbers in parentheses link to a specific observed dataset ID described in the study table (Table 1). Predicted and observed areas under the plasma concentration–time curve from the first to the last data point ( $AUC_{last}$ ) are compared in Table S5 of the Supplementary Materials. Predicted and observed plasma concentration–time profiles of all studies in adults (linear and semilogarithmic) are shown in Section 3.1 in the Supplementary Materials. iv: intravenous.

Goodness-of-fit plots of predicted versus observed  $AUC_{last}$  values and of predicted versus observed plasma concentrations are shown in Figure 2. Twenty-six out of 28 predicted  $AUC_{last}$  values (~93%) fell within the 2-fold acceptance criterion with an overall GMFE of 1.30. One  $AUC_{last}$  outside the 2-fold range was calculated for a venous fentanyl profile, which covered only the first 20 min after a fentanyl bolus administration [45]. The second outlier was calculated for a venous norfentanyl profile with observed norfentanyl concentrations close or below the lower limit of quantification (LLOQ) [6]. The MRD value for all plasma concentration simulations for the adult PBPK model was 1.77 with ~86% of all simulated plasma concentrations falling within 2-fold of the corresponding concentration observed. Detailed results on MRD values and AUC ratios calculated for all studies and results of the sensitivity analysis are presented in Sections 3.4–3.6 of the Supplementary Materials.

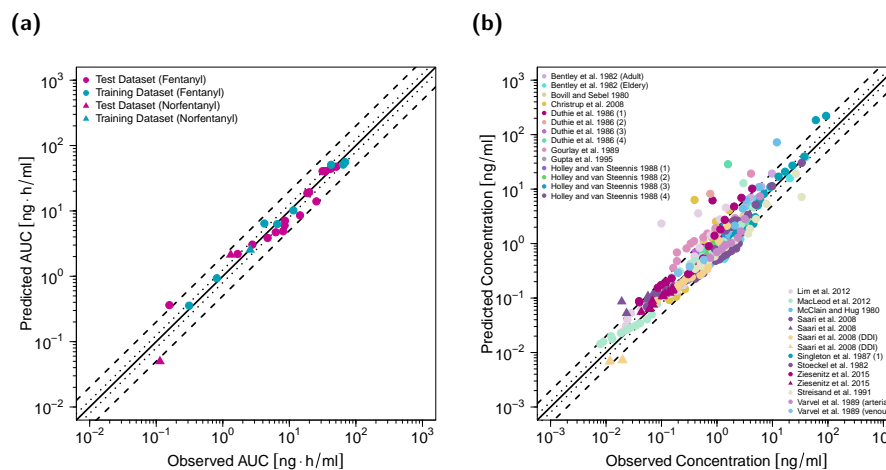


**Figure 2.** Predicted versus observed  $AUC_{last}$  values of fentanyl and norfentanyl grouped by test and training dataset (a) and predicted versus observed plasma concentrations (b) for the adult PBPK model. In (a), each symbol represents the  $AUC_{last}$  of a single plasma concentration–time profile (circles: fentanyl; triangles: norfentanyl). In (b), each symbol represents a single plasma concentration (circles: fentanyl; triangles: norfentanyl). The black solid lines mark the lines of identity. Black dotted lines indicate 1.25-fold, black dashed lines indicate 2-fold deviation.  $AUC_{last}$ : area under the plasma concentration–time curve from the first to the last data point.

While the implemented unspecific hepatic clearance is responsible for approximately 60% of fentanyl elimination, the metabolism of fentanyl to norfentanyl via CYP3A4 and CYP3A7 covers approximately one-third of fentanyl elimination in the PBPK model. The urinary excretion is accountable for only a minor fraction of fentanyl elimination (~7%). Figure 3 shows a structural overview of the implemented elimination processes of fentanyl and norfentanyl as well as a structural overview of the PBPK model. Drug-dependent parameters of the final PBPK model are shown in Table 3. For detailed information including system-dependent model parameters, see Section 1 of the Supplementary Materials.

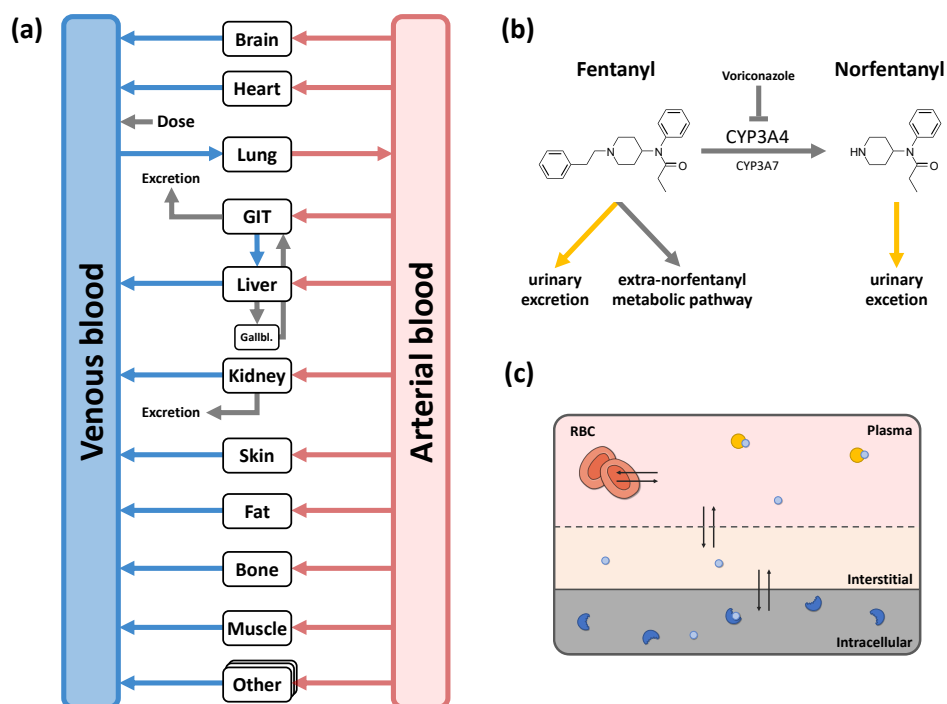


**Figure 3.** Structural overview of the whole-body physiologically-based pharmacokinetic (PBPK) model (a) and implemented elimination processes for fentanyl and norfentanyl (b). Each organ consists of a vascular space (containing plasma and red blood cells), interstitial space, and intracellular space. In (a,c), boxes indicate compartments, arrows denote in-/outflows, blue circles represent molecules, orange circles represent plasma proteins, and blue crescents denote enzymes. In (b), grey arrows indicate metabolic processes and yellow arrows indicate urinary excretion processes. CYP: cytochrome P450; GIT: gastrointestinal tract; Gallbl: gallbladder.

### 3.3. PBPK DDI Modeling

The adult PBPK model was used to predict a DDI scenario of fentanyl with concomitant administration of voriconazole. The simulated plasma concentration–time profiles are compared to the corresponding profiles observed from a clinical DDI study [6] in Figure 4. Here, a slight decrease in fentanyl AUC can be observed when simulating fentanyl administration with concomitant voriconazole compared to simulation of sole fentanyl administration. The corresponding predicted  $AUC_{ratio}$  ( $AUC_{inhibition, predicted}/AUC_{control, predicted} = 1.22$ ) and observed  $AUC_{ratio}$  ( $AUC_{inhibition, observed}/AUC_{control, observed} = 1.33$ ) were very similar. A strong relative decrease in norfentanyl AUC can be observed when simulating fentanyl administration with concomitant voriconazole compared to simulation of sole fentanyl administration. The predicted  $AUC_{ratio}$  for norfentanyl was 0.02 and the observed  $AUC_{ratio}$  0.09. It should be noted that all observed plasma concentrations for norfentanyl during concomitant voriconazole administration were very close to or below the specified LLOQ (black dashed line in Figure 4b) [6].

Table 3. Fentanyl and norfentanyl drug-dependent model parameters.

Parameter	Fentanyl				Norfentanyl				Description		
	Value	Unit	Source	Literature	Reference	Value	Unit	Source		Literature	Reference
MW	336.5	g/mol	lit.	336.5	[55] <sup>a</sup>	232.3	g/mol	lit.	232.3	[55] <sup>b</sup>	Molecular weight
pK <sub>a</sub> (base)	8.99		lit.	8.99	[55] <sup>a</sup>	10.03		lit.	10.03	[55] <sup>b</sup>	Acid dissociation constant
logP	3.49		lit.	3.49	[56]	2.00		lit.	2.00	[55] <sup>b</sup>	Lipophilicity
f <sub>u</sub> (adults)	20.8	%	lit.	20.8	[57]	81.9	%	lit.	81.9	[58]	Unbound fraction
f <sub>u</sub> (pediatrics)	29.0–33.0	%	calc.		[34]						Unbound fraction
CYP3A4 K <sub>m</sub> → norfen	117	μmol/L	lit.	117	[27]						Michaelis–Menten constant
CYP3A4 k <sub>cat</sub> → norfen	20.6	1/min	optim.	-	-						Catalytic rate constant
CYP3A7 K <sub>m</sub> → norfen	596	μmol/L	calc. <sup>c</sup>	-	-						Michaelis–Menten constant
CYP3A7 k <sub>cat</sub> → norfen	5.22	1/min	calc. <sup>c</sup>	-	-						Catalytic rate constant
Unspecific hepatic clearance → undef	1.46	1/min	lit.	-	-						Elimination from plasma (first-order process in the liver)
P-gp K <sub>m</sub>	5.72	μmol/L	optim.	-	-						Michaelis–Menten constant
P-gp k <sub>cat</sub>	1.71	1/min	optim.	-	-						Transport rate constant
B/P ratio	0.87		lit.	0.87	[59]	1.26		calc.	-	-	Blood-to-plasma ratio
GFR fraction	1.00		asm.	-	-	4.30		optim.	-	-	Filtered drug in the urine
Partition coefficients	Diverse <sup>d</sup>		calc.	R&R	[60–62]	Diverse <sup>d</sup>		calc.	Schmitt	[63]	Cell to plasma partitioning
Cellular permeability	Diverse <sup>d</sup>	cm/min	calc.	Ch.-dep. Schmitt	[31]	1.80 × 10 <sup>-2</sup>	cm/min	calc.	PK-Sim	[31]	Perm. into the cellular space
CYP3A4 K <sub>i</sub> of voriconazole	9.33	μmol/L	lit.	9.33	[39]						The inhibitor concentration when reaching half of k <sub>inact</sub>
CYP3A4 k <sub>inact</sub> of voriconazole	0.015	1/min	lit.	0.015	[39]						The maximum inactivation rate constant

-: not available; asm.: assumed; calc.: calculated; Ch.-dep. Schmitt: Charge-dependent Schmitt calculation method; CYP: cytochrome P450; GFR: glomerular filtration rate; lit.: literature; norfen: norfentanyl; optim.: optimized; P-gp: P-glycoprotein; Perm.: permeability; PK-Sim: PK-Sim standard calculation method; Schmitt: Schmitt calculation method; R&R: Rodgers and Rowland calculation method; undef: undefined metabolite; <sup>a</sup> DrugBank entry for fentanyl: <https://www.drugbank.ca/drugs/DB00813>, accessed 30 July 2020; <sup>b</sup> DrugBank entry for norfentanyl: <https://www.drugbank.ca/metabolites/DBMET00341>, accessed 30 July 2020; <sup>c</sup> for detailed information on calculations, please refer to Section 1 in the Supplementary Materials; <sup>d</sup> different values for different organs estimated by the corresponding calculation method.

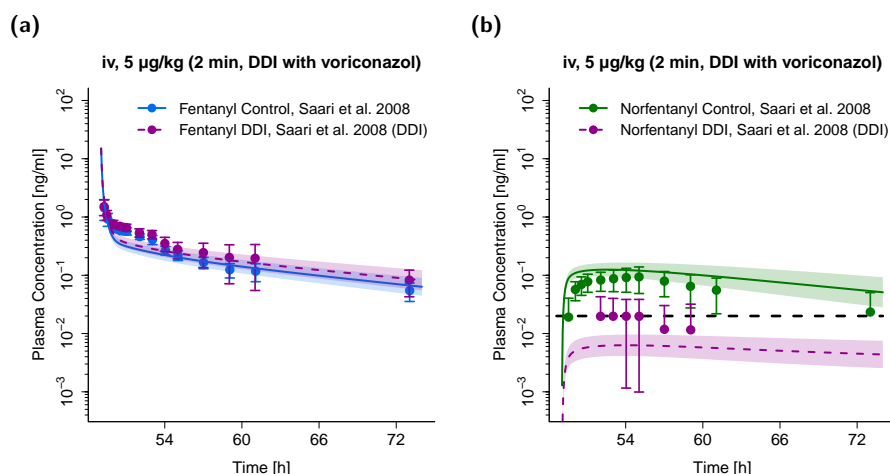


**Figure 4.** DDI scenario for fentanyl (a) and norfentanyl (b) with the perpetrator drug voriconazole in adults. Fentanyl and norfentanyl plasma concentrations during concomitant administration of voriconazole are shown in purple. Plasma concentrations during sole fentanyl administration are shown in blue (fentanyl) and green (norfentanyl), respectively. Population simulations ( $n = 100$ ) are shown as lines with shaded areas (geometric mean and geometric standard deviation). Observed data is shown as filled circles  $\pm$  standard deviation. References link to a specific observed dataset described in Table 1. Black dashed line depicts the specified lower limit of quantification (LLOQ) for norfentanyl [6]. Predicted and observed areas under the plasma concentration–time curve from the first to the last data point ( $AUC_{last}$ ) are compared in Table S5 of the Supplementary Materials. DDI, drug–drug interaction; iv, intravenous.

#### 3.4. Pediatric PBPK Model Building and Evaluation

The adult PBPK model was extrapolated to pediatric populations with mean ages ranging from 32 weeks gestational age in a preterm neonate population up to 2.9 years in a population of young children. In total, plasma concentration–time profiles and clearance values were predicted and compared to observed data for pediatric mean populations and individuals from five different clinical trials.

The scaled unbound fraction of fentanyl resulted in values from 29% for the 2.9-year-old pediatric population to 33% in the preterm neonate populations. This range is in concordance with the measured unbound fentanyl fraction values in pediatrics from the literature (23–38%) [35,64,65]. All other drug-dependent parameters were fixed to the values of the adult PBPK model. Comparison of predicted and observed plasma concentration–time profiles are shown in Figure 5 (semilogarithmic, selection of plots) and in Section 3.2 of the Supplementary Materials (all plots, both linear and semilogarithmic).

The predicted and observed plasma concentrations as well as  $AUC_{last}$  values are compared in goodness-of-fit plots in Figure 6, with 87.5% of  $AUC_{last}$  predictions located within the 2-fold range of the respective observed values and a GMFE of 1.38. Overall, MRD for plasma concentration predictions in pediatrics was calculated to be 2.03. A detailed overview of all MRD and GMFE values for pediatric predictions can be found in Tables S4 and S5 in the Supplementary Materials.

Individual clearance values were predicted and compared to the corresponding values observed from three clinical trials (see Table 2). Here, 72% of the predicted individual values (Figure 7a,b) and 100% of mean values (Figure 7b) are located within the 2-fold range of the corresponding observed values.

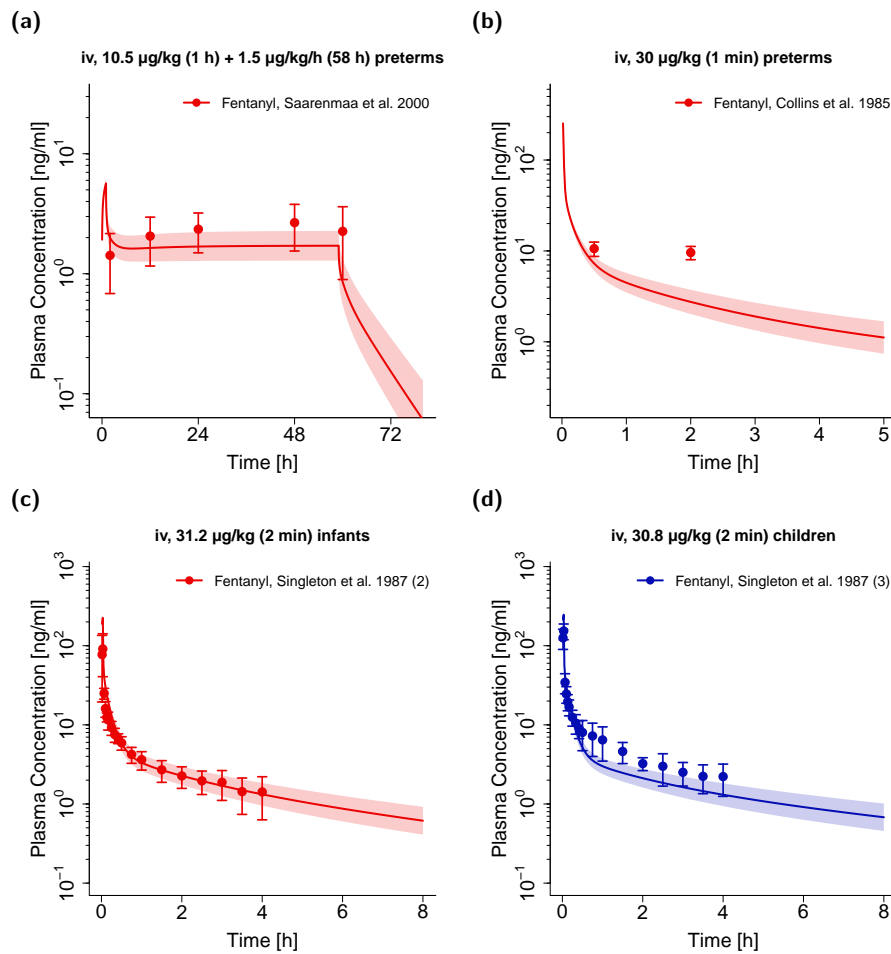


**Figure 5.** Fentanyl (red: arterial blood; blue: venous blood from central venous catheters) predicted and observed plasma concentration–time profiles after intravenous administration in preterm neonates (a,b), infants (c) and young children (d). Population simulations ( $n = 100$ ) are shown as lines with shaded areas (geometric mean and geometric standard deviation). Observed data is shown as circles with standard deviation. References with numbers in parentheses link to a specific observed dataset ID described in Table 2. Predicted and observed area under the plasma concentration–time curve from the first to the last data point ( $AUC_{\text{last}}$ ) values are compared in Table S5 of the Supplementary Materials. Predicted and observed plasma concentration–time profiles of all studies in pediatrics are shown in Section 3.2 of the Supplementary Materials both on a linear and a semilogarithmic scale. iv: intravenous, preterms: preterm neonates.

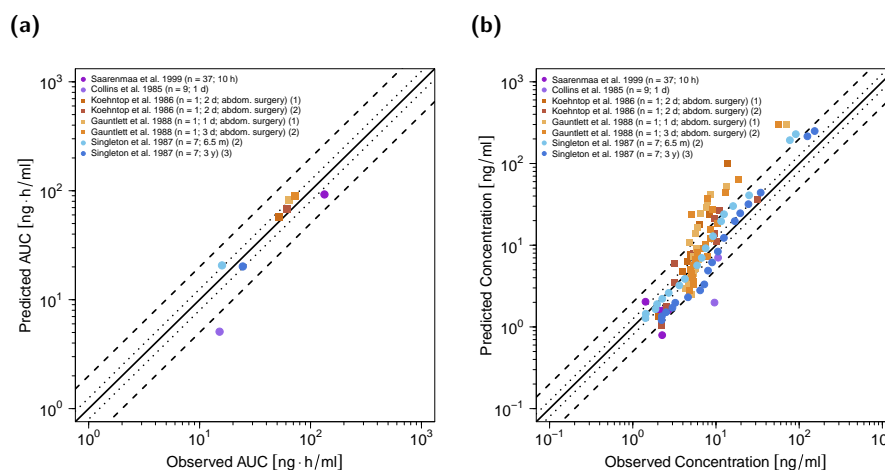


**Figure 6.** Predicted versus observed  $AUC_{last}$  (a) and plasma concentrations (b) of fentanyl for the pediatric PBPK model. Squares depict values for individual patients with adjusted clearances due to increased intraabdominal pressure as explained in Section 3.4; circles depict values for study populations without adjustment of clearances. In (a), each symbol represents the  $AUC_{last}$  of a single plasma concentration–time profile. In (b), each symbol represents a single plasma concentration. The black solid lines mark the lines of identity. Black dotted lines indicate 1.25-fold deviation; black dashed lines indicate 2-fold deviation.  $AUC_{last}$ : area under the plasma concentration–time curve from the first to the last data point; abdom.: abdominal.

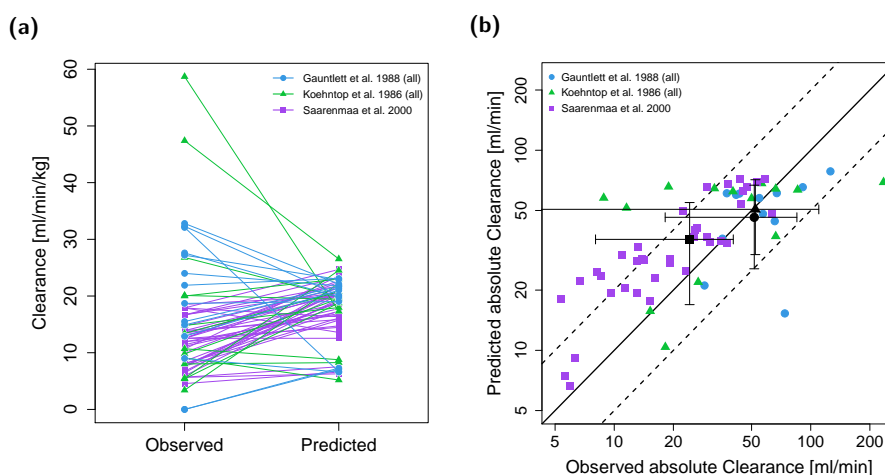


**Figure 7.** Predicted and observed clearance per bodyweight (a) as well as predicted versus observed absolute clearance values for the pediatric PBPK model (b). Each colored symbol represents the individual clearance of a patient; black symbols represent the mean clearances with standard deviations (circles refer to data from Gauntlett et al. [36]; triangles refer to data from Koehntop et al. [37]; squares refer to data from Saarenmaa et al. [38]). In (b), the black solid line marks the line of identity; black dashed lines indicate 2-fold deviation.

### 3.5. Clearance in Neonates with Increased Intraabdominal Pressure

In studies by Gauntlett et al., Koehntop et al. and Saarenmaa et al., several neonates, who had abdominal surgery, showed a significantly reduced fentanyl clearance [36–38] and four corresponding individual plasma profiles were presented in the respective studies [36,37]. The authors hypothesized that the decreased clearance might be due to an increased intraabdominal pressure resulting in a decreased hepatic clearance [36–38]. Hence, the four observed plasma profiles were digitized and

used to estimate decreased clearance values for the CYP3A4, CYP3A7 and unspecific hepatic clearance pathways for each individual. This resulted in a mean reduction in the metabolic clearance of ~83%. For detailed information see Section 1.2 of the Supplementary Materials. The resulting four individual plasma profiles are displayed in Figures S5 and S6 in the Supplementary Materials.

#### 4. Discussion

A whole-body PBPK model of fentanyl for adults has been built and evaluated by describing and predicting arterial (fentanyl) and venous (both fentanyl and norfentanyl) plasma concentration–time profiles as well as fractions of fentanyl dose excreted unchanged in urine following intravenous fentanyl administration. The utilized dataset comprised a wide dose range (0.3–60 µg/kg) including administrations ranging from an intravenous bolus to a 48-h continuous infusion. Following comprehensive evaluation, the adult PBPK model was applied to successfully predict a DDI scenario with voriconazole and was scaled to pediatric populations. Plasma concentration–time profiles and clearance parameters in pediatric patients were predicted with the extrapolated pediatric PBPK model and compared to observed data from five different clinical trials. The descriptive and predictive performance of the PBPK models has been demonstrated by (1) comparison of simulated to observed plasma profiles and clearance parameters, (2) the respective goodness-of-fit plots, (3) the calculation of MRD values as well as (4) the comparison of predicted to observed  $AUC_{last}$  values including the calculation of the respective GMFE.

The adult PBPK model predicts the fraction of fentanyl dose metabolized to norfentanyl of ~33% and the fraction of fentanyl eliminated via an unspecific hepatic clearance of ~60% (hereinafter called “extra-norfentanyl metabolic pathway”). These findings are supported by the prediction results of the DDI study with the CYP3A4 inhibitor voriconazole as a perpetrator drug. Moreover, the fraction of fentanyl dose excreted unchanged in urine was calculated to be ~7%. While fraction excreted in urine is perfectly in accordance with the literature [5,40,41], reports about the fraction of fentanyl metabolized to norfentanyl are divergent. In vitro studies with liver microsomes from the 1990s suggested that metabolism to norfentanyl plays the major role in fentanyl elimination—mainly via CYP3A4 with little contribution of other CYP enzymes [4,27]. Yet, an in vivo DDI crossover study from 2015 showed that concomitant administration of the CYP3A4 and P-gp inhibitor ketoconazole significantly reduced norfentanyl AUC to 24% but increased fentanyl exposure by only ~33% [5]. This strong inhibition of norfentanyl production during ketoconazole treatment supports the assumption of a major involvement of CYP3A in norfentanyl formation [5]. However, Ziesenitz et al. calculated the metabolic clearance of fentanyl to norfentanyl to account only for ~23% of the systemic clearance and concluded that currently unknown metabolites exist [5]. With a fraction of fentanyl metabolized to norfentanyl of approximately one-third, our study supports the theory of an extra-norfentanyl metabolic pathway and currently unknown metabolites. The fact that ritonavir, a drug which interacts with numerous metabolizing enzymes and transporters, had a much more profound effect on fentanyl exposure (AUC increase by ~170%) than ketoconazole provides additional support for the involvement of other elimination pathways in addition to CYP3A4 [66]. It needs to be noted that, in this PBPK model, the extra-norfentanyl metabolic pathway was implemented as an unspecific clearance in the liver, but could also be located at various different sites. Further studies need to be conducted to investigate the characteristics of an extra-norfentanyl elimination pathway.

PBPK modeling permits rational scaling between adult and pediatric patients by defining the PK of a drug as a function of anatomy, physiology and biochemistry and successful applications have recently been shown in different modeling efforts [21–23]. This study demonstrates the applicability of PBPK modeling to predict both clearance values as well as plasma concentration–time profiles and the corresponding AUCs for the analgesic drug fentanyl for preterm neonates to up to 3-year-old children within a whole-body PBPK framework. Here, 87.5% of  $AUC_{last}$  predictions and 100% of predicted population mean clearances were within 2-fold of the respective values observed. The predicted to observed mean clearance ratios ( $CL_{predicted}/CL_{observed}$ ) for the three included clinical trials

were 0.97 and 0.90 for the full-term neonate populations and 1.48 for the preterm neonate population. However, as individual fentanyl PK is highly variable [1,37], prediction of individual plasma profiles and clearance values remains challenging. The model predicted 47 of 65 individual clearance values within 2-fold range based on information on weight and age (chronological and gestational if available). The presented ladder plot (Figure 7a) depicts noticeable mispredictions for some clearance values. This might be attributed to unknown individual CYP3A4, CYP3A7 and P-gp expressions as well as heterogeneity for the unbound fraction, which all exhibit high interindividual variability [32,33,35]. In the model, mean values for enzyme and transporter expressions as well as the unbound fraction were assumed for individual clearance simulations.

As it remains unknown which physiologic elimination pathways the unspecific hepatic clearance covers, no ontogeny information regarding this elimination process was available. Hence, it needs to be noted that the rate constant of this clearance process was not scaled in the model. While the overall reasonable predictive performance of the PBPK scaling supports this approach, the overpredicted clearance values as well as the underprediction of plasma profiles for the preterm neonate population (see Figure 5a,b) could indicate that the unspecific hepatic clearance is less pronounced in preterm neonates. Certainly, these effects could also be mediated by other factors such as the impact of concomitant comedication or the influence of surgery on the PK of fentanyl.

Increased intraabdominal pressure can occur during abdominal surgery [37,67]. This might substantially decrease hepatic blood flow and eventually lead to a reduced fentanyl clearance [36,37,67]. In the PBPK model simulations, the clearance reduction for neonates with abdominal surgery and increased intraabdominal pressure (mean reduction in the metabolic clearance of ~83%) [36–38] showed an overall improvement of predictions. However, it should be noted that not all infants who had abdominal surgery showed a decreased clearance [36,37]. More research is required to further investigate the impact of abdominal surgery and intraabdominal pressure on the PK of fentanyl.

In most clinical scenarios, the administration of fentanyl leads to a desired analgesic and sedating effect, which, among others, usually results in an improvement of respiratory function [7,8]. However, in rare cases, fentanyl might cause a rigidity affecting the respiratory musculature, which can lead to chest wall rigidity—an ADR in pediatric as well as adult populations [1,8]. Albeit commonly assumed that chest wall rigidity occurs with rapid fentanyl administrations of high doses, Dewhirst et al. showed that the ADR may result from doses as low as 1  $\mu\text{g}/\text{kg}$ , mostly from bolus injections lasting less than 15 s (15 of 21) [8]. Simulations with the developed PBPK model in neonates show a large difference in peak arterial plasma concentrations (Figure 8) after bolus injection (1  $\mu\text{g}/\text{kg}$ ,  $C_{\text{max}}$ : 27.1 ng/mL), 2- and 4-min infusions (1  $\mu\text{g}/\text{kg}$ ,  $C_{\text{max}}$ : 6.3 and 3.7 ng/mL, respectively), and even a 3  $\mu\text{g}/\text{kg}$  4 min infusion ( $C_{\text{max}}$ : 11.2 ng/mL).

These large differences of up to 7-fold peak concentrations might partly explain the more frequent occurrence of chest wall rigidity during bolus administration of fentanyl. However, the impact of the high interindividual variability [1,37] should not be disregarded, which might explain the occurrence of the ADR in other case reports with longer infusions [8].

Previous modeling efforts on fentanyl neither included the metabolite norfentanyl nor predicted DDI scenarios [13–15]. Consequently, the fraction of fentanyl metabolized to norfentanyl could not be assessed. Moreover, scaling the PBPK models to pediatric subpopulations in order to predict plasma profiles and clearance values was not part of the scope of the above-mentioned PBPK modeling studies.

Some limitations of the model should be discussed. As no information about the blood-to-plasma ratio in the different pediatric populations was available, the literature value of 0.87 was assumed to be age-independent. However, since the unbound fraction changes age-dependently [34,35,65], the blood-to-plasma ratio could also differ in pediatric compared to adult patients. This could be one of the reasons for some deviations when predicting the plasma concentration–time profiles.

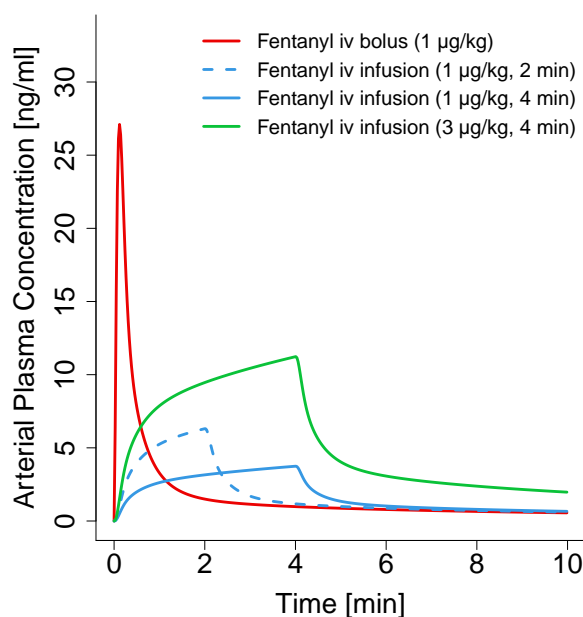


**Figure 8.** Simulations of arterial plasma concentration–time profiles after intravenous fentanyl bolus injection as well as 2- and 4-min infusions of different doses. Lines depict population geometric means ( $n = 100$ ). iv: intravenous.

Moreover, measurements of norfentanyl plasma concentrations were scarce and only available in clinical studies with adults for PBPK model building and evaluation [5,6]. Hence, PBPK model simulations for norfentanyl were only evaluated in this population and should be interpreted with these limitations in mind.

The impact of the metabolic process of CYP3A7 in our PBPK model on fentanyl AUCs was negligible, as shown in the local sensitivity analyses. Solely in PBPK model simulations for neonates, the CYP3A7 elimination process had a small impact. However, as no *in vitro* studies investigating CYP3A7 metabolism of fentanyl with information on the maximum reaction velocity and Michaelis–Menten constant were available, this process needs further investigation.

The ontogeny function for P-gp was adapted from a recent publication [33]. However, the ontogenetic information might need further evaluation since the peptides quantified by the used liquid chromatography–tandem mass spectrometry technique are not only formed from active P-gp but also by splice variants as well as non-glycosylated and truncated proteins [33,68,69].

Many of the PK samples in the analyzed studies were taken during different surgical procedures with largely varying co-medications (e.g., atropine, isoflurane, pancuronium, succinylcholine, and thiopental) possibly affecting fentanyl plasma concentrations. Consequently, some differences in model-predicted and observed plasma concentrations and clearance values could be a result of the varying study conditions.

In addition to intravenous administration, fentanyl is also administered via the transdermal, sublingual and nasal routes [3]. In particular, the continuous administration of fentanyl with transdermal patches is an important analgesic treatment in diseases with chronic pain [70]. Transdermal fentanyl treatment is approved for opioid-tolerant adult patients as well as opioid-tolerant children over two years of age [2,71]. As a sustained-release formulation, transdermal patches can potentially reduce plasma concentration fluctuations, ADRs such as constipation and the risk for non-adherence [70]. Based on the good model performance, the fentanyl PBPK models developed in this analysis could be augmented to mechanistically model and simulate the delivery of fentanyl via more complex formulations, such as transdermal or sublingual vehicles [72].

## 5. Conclusions

A whole-body PBPK model of fentanyl and its metabolite norfentanyl has been developed to predict fentanyl and norfentanyl arterial and venous plasma concentration–time profiles as well as fentanyl urinary excretion after intravenous administration in adults. The model was further evaluated by predicting a DDI scenario with the CYP3A4 inhibitor voriconazole. The fraction of fentanyl metabolized to norfentanyl of ~33% has been predicted, supporting the idea of an extra-norfentanyl metabolic pathway. Subsequently, the adult PBPK model has been successfully scaled to preterm and full-term neonate, infant as well as child subpopulations for predictions of plasma profiles and clearance parameters. With that, we add confidence to the potential of PBPK modeling to predict the PK in pediatric patients. The models are publicly available in the OSP repository. Thereby, the models contribute to a library of PBPK models for predictions in other DDI scenarios, could help to develop models for sustained release from complex formulations, and support future investigations of fentanyl and norfentanyl PK both in adult and pediatric populations.

**Supplementary Materials:** The following are available online at <http://www.mdpi.com/1999-4923/12/10/908/s1>, Electronic Supplementary Materials: Additional model information including detailed model evaluation.

**Author Contributions:** Conceptualization, L.K., A.W., M.Z., B.M. and T.L.; funding acquisition, Y.K., R.B. and T.L.; investigation, L.K., A.W., D.S. and T.L.; methodology, L.K., A.W., D.S. and T.L.; visualization, L.K. and D.S.; writing—original draft, L.K., M.Z., B.M., D.S. and T.L.; writing—review and editing, L.K., A.W., M.Z., Y.K., R.B., B.M., D.S. and T.L. All authors have read and agreed to the published version of the manuscript.

**Funding:** This research was funded by the German Federal Ministry of Education and Research (BMBF), 031L0153 “Alternativmethoden zum Tierversuch” and 03XP0196 “NanoCare4.0—Anwendungssichere Materialinnovationen”. We acknowledge support by the Deutsche Forschungsgemeinschaft (DFG, German Research Foundation) and Saarland University within the funding program Open Access Publishing.

**Acknowledgments:** We thank Sebastian Dahmen for supporting this work during his internship at Saarland University.

**Conflicts of Interest:** Thorsten Lehr, Yvonne Kohl und Robert Bals have received research grants from the German Federal Ministry of Education and Research (BMBF). Lukas Kovar, Andreas Weber, Michael Zemlin, Bernd Meibohm and Dominik Selzer declare no conflicts of interest. The funders had no role in the design of the study; in the collection, analyses, or interpretation of data; in the writing of the manuscript, or in the decision to publish the results.

## References

1. Pacifici, G.M. Clinical Pharmacology of Fentanyl in Preterm Infants. A Review. *Pediatr. Neonatol.* **2015**, *56*, 143–148. [[CrossRef](#)] [[PubMed](#)]
2. Ziesenitz, V.C.; Vaughns, J.D.; Koch, G.; Mikus, G.; van den Anker, J.N. Pharmacokinetics of Fentanyl and Its Derivatives in Children: A Comprehensive Review. *Clin. Pharmacokinet.* **2018**, *57*, 125–149. [[CrossRef](#)] [[PubMed](#)]
3. Kuip, E.J.M.; Zandvliet, M.L.; Koolen, S.L.W.; Mathijssen, R.H.J.; van der Rijt, C.C.D. A review of factors explaining variability in fentanyl pharmacokinetics; focus on implications for cancer patients. *Br. J. Clin. Pharmacol.* **2017**, *83*, 294–313. [[CrossRef](#)] [[PubMed](#)]
4. Guitton, J.; Buronfosse, T.; Désage, M.; Lepape, A.; Brazier, J.L.; Beaune, P. Possible involvement of multiple cytochrome P450s in fentanyl and sufentanil metabolism as opposed to alfentanil. *Biochem. Pharmacol.* **1997**, *53*, 1613–1619. [[CrossRef](#)]
5. Ziesenitz, V.C.; König, S.K.; Mahlke, N.S.; Skopp, G.; Haefeli, W.E.; Mikus, G. Pharmacokinetic interaction of intravenous fentanyl with ketoconazole. *J. Clin. Pharmacol.* **2015**, *55*, 708–717. [[CrossRef](#)]
6. Saari, T.I.; Laine, K.; Neuvonen, M.; Neuvonen, P.J.; Olkkola, K.T. Effect of voriconazole and fluconazole on the pharmacokinetics of intravenous fentanyl. *Eur. J. Clin. Pharmacol.* **2008**, *64*, 25–30. [[CrossRef](#)]
7. Irazuzta, J.; Pascucci, R.; Perlman, N.; Wessel, D. Effects of fentanyl administration on respiratory system compliance in infants. *Crit. Care Med.* **1993**, *21*, 1001–1004. [[CrossRef](#)]
8. Dewhirst, E.; Naguib, A.; Tobias, J.D. Chest wall rigidity in two infants after low-dose fentanyl administration. *Pediatr. Emerg. Care* **2012**, *28*, 465–468. [[CrossRef](#)]

9. Ward, R.M.; Sherwin, C.M.T. Ethics of Drug Studies in the Newborn. *Pediatr. Drugs* **2014**, *17*, 37–42. [[CrossRef](#)]
10. Maharaj, A.R.; Edginton, A.N. Physiologically Based Pharmacokinetic Modeling and Simulation in Pediatric Drug Development. *CPT Pharmacometrics Syst. Pharmacol.* **2014**, *3*, 1–13. [[CrossRef](#)]
11. Lippert, J.; Burghaus, R.; Edginton, A.; Frechen, S.; Karlsson, M.; Kovar, A.; Lehr, T.; Milligan, P.; Nock, V.; Ramusovic, S.; et al. Open Systems Pharmacology Community—An Open Access, Open Source, Open Science Approach to Modeling and Simulation in Pharmaceutical Sciences. *CPT Pharmacometrics Syst. Pharmacol.* **2019**, *8*, 878–882. [[CrossRef](#)] [[PubMed](#)]
12. Yellepeddi, V.; Rower, J.; Liu, X.; Kumar, S.; Rashid, J.; Sherwin, C.M.T. State-of-the-Art Review on Physiologically Based Pharmacokinetic Modeling in Pediatric Drug Development. *Clin. Pharmacokinet.* **2019**, *58*, 1–13. [[CrossRef](#)] [[PubMed](#)]
13. Björkman, S. Reduction and Lumping of Physiologically Based Pharmacokinetic Models: Prediction of the Disposition of Fentanyl and Pethidine in Humans by Successively Simplified Models. *J. Pharmacokinet. Pharmacodyn.* **2003**, *30*, 285–307. [[CrossRef](#)] [[PubMed](#)]
14. Shankaran, H.; Adeshina, F.; Teeguarden, J.G. Physiologically-based pharmacokinetic model for Fentanyl in support of the development of Provisional Advisory Levels. *Toxicol. Appl. Pharmacol.* **2013**, *273*, 464–476. [[CrossRef](#)]
15. Pilari, S.; Gaub, T.; Block, M.; Görlitz, L. Development of physiologically based organ models to evaluate the pharmacokinetics of drugs in the testes and the thyroid gland. *CPT Pharmacomet. Syst. Pharmacol.* **2017**, *6*, 532–542. [[CrossRef](#)]
16. Leong, R.; Vieira, M.L.T.; Zhao, P.; Mulugeta, Y.; Lee, C.S.; Huang, S.-M.; Burckart, G.J. Regulatory experience with physiologically based pharmacokinetic modeling for pediatric drug trials. *Clin. Pharmacol. Ther.* **2012**, *91*, 926–931. [[CrossRef](#)]
17. Barrett, J.S.; Della Casa Alberighi, O.; Läer, S.; Meibohm, B. Physiologically Based Pharmacokinetic (PBPK) Modeling in Children. *Clin. Pharmacol. Ther.* **2012**, *92*, 40–49. [[CrossRef](#)]
18. Templeton, I.E.; Jones, N.S.; Musib, L. Pediatric Dose Selection and Utility of PBPK in Determining Dose. *AAPS J.* **2018**, *20*, 31. [[CrossRef](#)]
19. Michelet, R.; Bocxlaer, J.V.; Vermeulen, A. PBPK in Preterm and Term Neonates: A Review. *Curr. Pharm. Des.* **2018**, *23*, 5943–5954. [[CrossRef](#)]
20. Johnson, T.N.; Rostami-Hodjegan, A. Resurgence in the use of physiologically based pharmacokinetic models in pediatric clinical pharmacology: Parallel shift in incorporating the knowledge of biological elements and increased applicability to drug development and clinical practice. *Pediatr. Anesth.* **2011**, *21*, 291–301. [[CrossRef](#)]
21. Maharaj, A.R.; Barrett, J.S.; Edginton, A.N. A workflow example of PBPK modeling to support pediatric research and development: Case study with lorazepam. *AAPS J.* **2013**, *15*, 455–464. [[CrossRef](#)] [[PubMed](#)]
22. Ince, I.; Solodenko, J.; Frechen, S.; Dallmann, A.; Niederal, C.; Schlender, J.; Burghaus, R.; Lippert, J.; Willmann, S. Predictive Pediatric Modeling and Simulation Using Ontogeny Information. *J. Clin. Pharmacol.* **2019**, *59*, S95–S103. [[CrossRef](#)] [[PubMed](#)]
23. Kovar, L.; Schräpel, C.; Selzer, D.; Kohl, Y.; Bals, R.; Schwab, M.; Lehr, T. Physiologically-Based Pharmacokinetic (PBPK) Modeling of Buprenorphine in Adults, Children and Preterm Neonates. *Pharmaceutics* **2020**, *12*, 578. [[CrossRef](#)] [[PubMed](#)]
24. Hanke, N.; Kunz, C.; Thiemann, M.; Fricke, H.; Lehr, T. Translational PBPK Modeling of the Protein Therapeutic and CD95L Inhibitor Asunercept to Develop Dose Recommendations for Its First Use in Pediatric Glioblastoma Patients. *Pharmaceutics* **2019**, *11*, 152. [[CrossRef](#)]
25. Moj, D.; Britz, H.; Burhenne, J.; Stewart, C.F.; Egerer, G.; Haefeli, W.E.; Lehr, T. A physiologically based pharmacokinetic and pharmacodynamic (PBPK/PD) model of the histone deacetylase (HDAC) inhibitor vorinostat for pediatric and adult patients and its application for dose specification. *Cancer Chemother. Pharmacol.* **2017**, *80*, 1013–1026. [[CrossRef](#)]
26. Wojtyniak, J.-G.; Britz, H.; Selzer, D.; Schwab, M.; Lehr, T. Data Digitizing: Accurate and Precise Data Extraction for Quantitative Systems Pharmacology and Physiologically-Based Pharmacokinetic Modeling. *CPT Pharmacomet. Syst. Pharmacol. Pharmacol.* **2020**. accepted for publication. [[CrossRef](#)]
27. Feierman, D.E.; Lasker, J.M. Metabolism of fentanyl, a synthetic opioid analgesic, by human liver microsomes. Role of CYP3A4. *Drug Metab. Dispos.* **1996**, *24*, 932–939.

28. Yu, C.; Yuan, M.; Yang, H.; Zhuang, X.; Li, H. P-glycoprotein on blood-brain barrier plays a vital role in fentanyl brain exposure and respiratory toxicity in rats. *Toxicol. Sci.* **2018**, *164*, 353–362. [CrossRef]
29. Lötsch, J.; Walter, C.; Parnham, M.J.; Oertel, B.G.; Geisslinger, G. Pharmacokinetics of non-intravenous formulations of fentanyl. *Clin. Pharmacokinet.* **2013**, *52*, 23–36. [CrossRef]
30. Andrew Williams, J.; Ring, B.J.; Cantrell, V.E.; Jones, D.R.; Eckstein, J.; Ruterbories, K.; Hamman, M.A.; Hall, S.D.; Wrighton, S.A. Comparative metabolic capabilities of CYP3A4, CYP3A5, and CYP3A7. *Drug Metab. Dispos.* **2002**, *30*, 883–891. [CrossRef]
31. Open Systems Pharmacology Suite Community Open Systems Pharmacology Suite Manual, Version 7.4. Available online: <https://github.com/Open-Systems-Pharmacology/OSPSuite.Documentation/blob/master/OpenSystemsPharmacologySuite.pdf> (accessed on 25 March 2020).
32. PK-Sim@Ontogeny Database, Version 7.3. Available online: <https://github.com/Open-Systems-Pharmacology/OSPSuite.Documentation/blob/master/PK-Sim> (accessed on 25 March 2020).
33. Prasad, B.; Gaedigk, A.; Vrana, M.; Gaedigk, R.; Leeder, J.; Salphati, L.; Chu, X.; Xiao, G.; Hop, C.; Evers, R.; et al. Ontogeny of Hepatic Drug Transporters as Quantified by LC-MS/MS Proteomics. *Clin. Pharmacol. Ther.* **2016**, *100*, 362–370. [CrossRef] [PubMed]
34. McNamara, P.J.; Alcorn, J. Protein binding predictions in infants. *AAPS PharmSci* **2002**, *4*, 19–26. [CrossRef] [PubMed]
35. Wilson, A.S.; Stiller, R.L.; Davis, P.J.; Fedel, G.; Chakravorti, S.; Israel, B.A.; McGowan, F.X. Fentanyl and Alfentanil Plasma Protein Binding in Preterm and Term Neonates. *Anesth. Analg.* **1997**, *84*, 315–318. [CrossRef] [PubMed]
36. Gauntlett, I.S.; Fisher, D.M.; Hertzka, R.E.; Kuhis, E.; Spellman, M.J.; Rudolph, C. Pharmacokinetics of Fentanyl in Neonatal Humans and Lambs. *Anesthesiology* **1988**, *69*, 683–687. [CrossRef] [PubMed]
37. Koehntop, D.E.; Rodman, J.H.; Brundage, D.M.; Hegland, M.G.; Buckley, J.J. Pharmacokinetics of fentanyl in neonates. *Anesth. Analg.* **1986**, *65*, 227–232. [CrossRef]
38. Saarenmaa, E.; Neuvonen, P.J.; Fellman, V. Gestational age and birth weight effects on plasma clearance of fentanyl in newborn infants. *J. Pediatr.* **2000**, *136*, 767–770. [CrossRef]
39. Li, X.; Frechen, S.; Moj, D.; Lehr, T.; Taubert, M.; Hsin, C.-h.; Mikus, G.; Neuvonen, P.J.; Olkkola, K.T.; Saari, T.I.; et al. A Physiologically Based Pharmacokinetic Model of Voriconazole Integrating Time-Dependent Inhibition of CYP3A4, Genetic Polymorphisms of CYP2C19 and Predictions of Drug–Drug Interactions. *Clin. Pharmacokinet.* **2020**, *59*, 781–808. [CrossRef]
40. McClain, D.A.; Hug, C.C. Intravenous fentanyl kinetics. *Clin. Pharmacol. Ther.* **1980**, *28*, 106–114. [CrossRef]
41. Bovill, J.G.; Sebel, P.S. Pharmacokinetics of high-dose fentanyl. *Br. J. Anaesth.* **1980**, *52*, 795–801. [CrossRef]
42. Bentley, J.B.; Borel, J.D.; Nenad, R.E.; Gillespie, T.J. Age and Fentanyl Pharmacokinetics. *Anesth. Analg.* **1982**, *61*, 968–971. [CrossRef]
43. Christrup, L.; Foster, D.; Popper, L.; Troen, T.; Upton, R. Pharmacokinetics, efficacy, and tolerability of fentanyl following intranasal versus intravenous administration in adults undergoing third-molar extraction: A randomized, double-blind, double-dummy, two-way, crossover study. *Clin. Ther.* **2008**, *30*, 469–481. [CrossRef] [PubMed]
44. Duthie, D.J.R.; McLaren, A.D.; Nimmo, W.S. Pharmacokinetics of fentanyl during constant rate i.v. infusion for the relief of pain after surgery. *Br. J. Anaesth.* **1986**, *58*, 950–956. [CrossRef]
45. Gourlay, G.K.; Murphy, T.M.; Plummer, J.L.; Kowalski, S.R.; Cherry, D.A.; Cousins, M.J. Pharmacokinetics of fentanyl in lumbar and cervical CSF following lumbar epidural and intravenous administration. *Pain* **1989**, *38*, 253–259. [CrossRef]
46. Gupta, S.K.; Southam, M.A.; Hwang, S.S. Evaluation of Diurnal Variation in Fentanyl Clearance. *J. Clin. Pharmacol.* **1995**, *35*, 159–162. [CrossRef] [PubMed]
47. Holley, F.O.; Van Steennis, C. Postoperative analgesia with fentanyl: Pharmacokinetics and pharmacodynamics of constant-rate I.V. and transdermal delivery. *Br. J. Anaesth.* **1988**, *60*, 608–613. [CrossRef] [PubMed]
48. Lim, C.B.S.; Schug, S.A.; Sunderland, V.B.; Paech, M.J.; Liu, Y. A Phase I Pharmacokinetic and Bioavailability Study of a Sublingual Fentanyl Wafer in Healthy Volunteers. *Anesth. Analg.* **2012**, *115*, 1. [CrossRef]
49. MacLeod, D.B.; Habib, A.S.; Ikeda, K.; Spyker, D.A.; Cassella, J.V.; Ho, K.Y.; Gan, T.J. Inhaled Fentanyl Aerosol in Healthy Volunteers. *Anesth. Analg.* **2012**, *115*, 1071–1077. [CrossRef]
50. Singleton, M.A.; Rosen, J.I.; Fisher, D.M. Plasma concentrations of fentanyl in infants, children and adults. *Can. J. Anaesth.* **1987**, *34*, 152–155. [CrossRef]

51. Stoeckel, H.; Schüttler, J.; Magnussen, H.; Hengstmann, J.H. Plasma fentanyl concentrations and the occurrence of respiratory depression in volunteers. *Br. J. Anaesth.* **1982**, *54*, 1087–1095. [CrossRef]
52. Streisand, J.B.; Varvel, J.R.; Stanski, D.R.; Le Maire, L.; Ashburn, M.A.; Hague, B.I.; Tarver, S.D.; Stanley, T.H. Absorption and Bioavailability of Oral Transmucosal Fentanyl Citrate. *Anesthesiology* **1991**, *75*, 223–229. [CrossRef]
53. Varvel, J.R.; Shafer, S.L.; Hwang, S.S.; Coen, P.A.; Stanski, D.R. Absorption Characteristics of Transdermally Administered Fentanyl. *Anesthesiology* **1989**, *70*, 928–934. [CrossRef] [PubMed]
54. Collins, C.; Koren, G.; Crean, P.; Klein, J.; Roy, W.L.; MacLeod, S.M. Fentanyl pharmacokinetics and hemodynamic effects in preterm infants during ligation of patent ductus arteriosus. *Anesth. Analg.* **1985**, *64*, 1078–1080. [CrossRef]
55. Wishart, D.S.; Knox, C.; Guo, A.C.; Shrivastava, S.; Hassanali, M.; Stothard, P.; Chang, Z.; Woolsey, J. DrugBank: A comprehensive resource for in silico drug discovery and exploration. *Nucleic Acids Res.* **2006**, *34*, D668–D672. [CrossRef] [PubMed]
56. Magee, P. Percutaneous absorption: Critical factors in transdermal transport. In *Dermatotoxicology*; Marzulli, F., Maibach, H., Eds.; Hemisphere Publishing Corporation: New York, NY, USA, 1991; pp. 1–35.
57. Bower, S. Plasma protein binding of fentanyl. *J. Pharm. Pharmacol.* **1981**, *33*, 507–514. [CrossRef] [PubMed]
58. Bista, S.R.; Haywood, A.; Hardy, J.; Lobb, M.; Tapuni, A.; Norris, R. Protein binding of fentanyl and its metabolite nor-fentanyl in human plasma, albumin and  $\alpha$ -1 acid glycoprotein. *Xenobiotica* **2015**, *45*, 207–212. [CrossRef]
59. Jantos, R.; Schuhmacher, M.; Veldstra, J.L.; Bosker, W.M.; Klöpping-Ketelaars, I.; Touliou, K.; Sardi, G.M.; Brookhuis, K.A.; Ramaekers, J.G.; Mattern, R.; et al. Determination of blood/serum ratios of different forensically relevant analytes in authentic samples. *Arch. Kriminol.* **2011**, *227*, 188–203.
60. Rodgers, T.; Rowland, M. Physiologically-based Pharmacokinetic Modeling 2: Predicting the tissue distribution of acids, very weak bases, neutrals and zwitterions. *J. Pharm. Sci.* **2006**, *95*, 1238–1257. [CrossRef]
61. Rodgers, T.; Rowland, M. Mechanistic approaches to volume of distribution predictions: Understanding the processes. *Pharm. Res.* **2007**, *24*, 918–933. [CrossRef]
62. Rodgers, T.; Leahy, D.; Rowland, M. Physiologically based pharmacokinetic modeling 1: Predicting the tissue distribution of moderate-to-strong bases. *J. Pharm. Sci.* **2005**, *94*, 1259–1276. [CrossRef]
63. Schmitt, W. General approach for the calculation of tissue to plasma partition coefficients. *Toxicol. In Vitro* **2008**, *22*, 457–467. [CrossRef]
64. Fachinformation Fentanyl HEXAL®Injektionslösung. Available online: [https://www.hexal.biz/praeparate/dokumente/fi/fentanyl\\_hx\\_inj\\_spc-1575534009.pdf](https://www.hexal.biz/praeparate/dokumente/fi/fentanyl_hx_inj_spc-1575534009.pdf) (accessed on 19 August 2020).
65. Rosaeg, O.P.; Kitts, J.B.; Koren, G.; Byford, L.J. Maternal and fetal effects of intravenous patient-controlled fentanyl analgesia during labour in a thrombocytopenic parturient. *Can. J. Anaesth.* **1992**, *39*, 277–281. [CrossRef] [PubMed]
66. Olkkola, K.T.; Palkama, V.J.; Neuvonen, P.J. Ritonavir's role in reducing fentanyl clearance and prolonging its half-life. *Anesthesiology* **1999**, *91*, 681–685. [CrossRef] [PubMed]
67. Diebel, L.N.; Wilson, R.F.; Dulchavsky, S.A.; Saxe, J. Effect of increased intra-abdominal pressure on hepatic arterial, portal venous, and hepatic microcirculatory blood flow. *J. Trauma* **1992**, *33*, 279–282; discussion 282–283. [CrossRef] [PubMed]
68. Thomson, M.M.S.; Hines, R.N.; Schuetz, E.G.; Meibohm, B. Expression patterns of organic anion transporting polypeptides 1B1 and 1B3 protein in human pediatric liver. *Drug Metab. Dispos.* **2016**, *44*, 999–1004. [CrossRef]
69. Wilson, C.; Li, Q.; Gaedigk, R.; Bi, C.; De Wildt, S.N.; Leeder, J.S.; Fridley, B.L. Ontogeny related changes in the pediatric liver metabolome. *Front. Pediatr.* **2020**, in press. [CrossRef]
70. Hadley, G.; Derry, S.; Moore, R.A.; Wiffen, P.J. Transdermal fentanyl for cancer pain. *Cochrane Database Syst. Rev.* **2013**, *28*, 264–265. [CrossRef]

71. DURAGESIC®(Fentanyl Transdermal System) Full Prescribing Information. Available online: [https://www.accessdata.fda.gov/drugsatfda\\_docs/label/2005/19813s0391bl.pdf](https://www.accessdata.fda.gov/drugsatfda_docs/label/2005/19813s0391bl.pdf) (accessed on 14 August 2020).
72. Kovar, L.; Selzer, D.; Britz, H.; Benowitz, N.; St. Helen, G.; Kohl, Y.; Bals, R.; Lehr, T. Comprehensive Parent–Metabolite PBPK/PD Modeling Insights into Nicotine Replacement Therapy Strategies. *Clin. Pharmacokinet.* **2020**. [[CrossRef](#)]



© 2020 by the authors. Licensee MDPI, Basel, Switzerland. This article is an open access article distributed under the terms and conditions of the Creative Commons Attribution (CC BY) license (<http://creativecommons.org/licenses/by/4.0/>).

### 3.3 PUBLICATION III – PBPK MODELING OF NICOTINE BRAIN TISSUE CONCENTRATIONS

#### 3.3.1 Reference

#### **Comprehensive Parent-Metabolite PBPK/PD Modeling Insights into Nicotine Replacement Therapy Strategies.**

Lukas Kovar, Dominik Selzer, Hannah Britz, Neal Benowitz, Gideon St. Helen, Yvonne Kohl, Robert Bals and Thorsten Lehr.

*Clin Pharmacokinet* 2020;59(9):1119-1134. DOI: 10.1007/s40262-020-00880-4 [3].

#### 3.3.2 Author Contributions

Author contributions according to the contributor roles taxonomy (CRediT) [4, 5] were as following:

Lukas Kovar	Refer to <i>Contribution Report</i> (p. vii)
Dominik Selzer	Methodology, Visualization, Writing – original draft, Writing – review & editing
Hannah Britz	Conceptualization, Methodology, Writing – review & editing
Neal Benowitz	Conceptualization, Funding acquisition, Investigation, Writing – review & editing
Gideon St. Helen	Conceptualization, Funding acquisition, Writing – review & editing
Yvonne Kohl	Conceptualization, Funding acquisition, Writing – review & editing
Robert Bals	Conceptualization, Funding acquisition, Writing – review & editing
Thorsten Lehr	Conceptualization, Funding acquisition, Methodology, Writing – original draft, Writing – review & editing

#### 3.3.3 Copyright

This article is licensed under a Creative Commons Attribution-NonCommercial 4.0 International License, which permits any non-commercial use, sharing, adaptation, distribution and reproduction in any medium or format, as long as you give appropriate credit to the original author(s) and the source, provide a link to the Creative Commons licence, and indicate if changes were made. The images or other third party material in this article are included in the article's Creative Commons licence, unless indicated otherwise in a credit line to the material. If material is not included in the article's Creative Commons licence and your intended use is not permitted by statutory regulation or exceeds the permitted use, you will need to obtain permission directly from the copyright holder. To view a copy of this licence, visit <http://creativecommons.org/licenses/by-nc/4.0/>.

Clinical Pharmacokinetics (2020) 59:1119–1134  
<https://doi.org/10.1007/s40262-020-00880-4>

ORIGINAL RESEARCH ARTICLE



## Comprehensive Parent–Metabolite PBPK/PD Modeling Insights into Nicotine Replacement Therapy Strategies

Lukas Kovar<sup>1</sup> · Dominik Selzer<sup>1</sup> · Hannah Britz<sup>1</sup> · Neal Benowitz<sup>2</sup> · Gideon St. Helen<sup>2</sup> · Yvonne Kohl<sup>3</sup> · Robert Bals<sup>4</sup> · Thorsten Lehr<sup>1</sup> 

Published online: 12 March 2020  
© The Author(s) 2020

### Abstract

**Background** Nicotine, the pharmacologically active substance in both tobacco and many electronic cigarette (e-cigarette) liquids, is responsible for the addiction that sustains cigarette smoking. With 8 million deaths worldwide annually, smoking remains one of the major causes of disability and premature death. However, nicotine also plays an important role in smoking cessation strategies.

**Objectives** The aim of this study was to develop a comprehensive, whole-body, physiologically based pharmacokinetic/pharmacodynamic (PBPK/PD) model of nicotine and its major metabolite cotinine, covering various routes of nicotine administration, and to simulate nicotine brain tissue concentrations after the use of combustible cigarettes, e-cigarettes, nicotine gums, and nicotine patches.

**Methods** A parent–metabolite, PBPK/PD model of nicotine for a non-smoking and a smoking population was developed using 91 plasma and brain tissue concentration–time profiles and 11 heart rate profiles. Among others, cytochrome P450 (CYP) 2A6 and 2B6 enzymes were implemented, including kinetics for CYP2A6 poor metabolizers.

**Results** The model is able to precisely describe and predict both nicotine plasma and brain tissue concentrations, cotinine plasma concentrations, and heart rate profiles. 100% of the predicted area under the concentration–time curve (AUC) and maximum concentration ( $C_{\max}$ ) values meet the twofold acceptance criterion with overall geometric mean fold errors of 1.12 and 1.15, respectively. The administration of combustible cigarettes, e-cigarettes, nicotine patches, and nicotine gums was successfully implemented in the model and used to identify differences in steady-state nicotine brain tissue concentration patterns.

**Conclusions** Our PBPK/PD model may be helpful in further investigations of nicotine dependence and smoking cessation strategies. As the model represents the first nicotine PBPK/PD model predicting nicotine concentration and heart rate profiles after the use of e-cigarettes, it could also contribute to a better understanding of the recent increase in youth e-cigarette use.

---

**Electronic supplementary material** The online version of this article (<https://doi.org/10.1007/s40262-020-00880-4>) contains supplementary material, which is available to authorized users.

---

✉ Thorsten Lehr  
[thorsten.lehr@mx.uni-saarland.de](mailto:thorsten.lehr@mx.uni-saarland.de)

<sup>1</sup> Clinical Pharmacy, Saarland University, Campus C2 2, 66123 Saarbrücken, Germany

<sup>2</sup> Department of Medicine, University of California, San Francisco, CA, USA

<sup>3</sup> Fraunhofer Institute for Biomedical Engineering IBMT, Sulzbach, Germany

<sup>4</sup> Department of Internal Medicine V, Saarland University, Homburg, Germany

### Key Points

A whole-body, parent–metabolite, physiologically based pharmacokinetic/pharmacodynamic model of nicotine was built and evaluated for the prediction of nicotine and cotinine plasma concentrations, nicotine brain tissue concentrations, and heart rate profiles after nicotine intake. The model was able to quantify the contribution of the elimination pathways of nicotine being metabolized to cotinine and renally excreted.

The model was applied to simulate nicotine brain tissue concentration patterns after smoking cigarettes, the administration of nicotine gums (2 mg and 4 mg), and a transdermal nicotine patch.

This study demonstrates the applicability of physiologically based pharmacokinetic modeling to investigate brain tissue concentrations and to successfully integrate many different routes of administration in one model: intravenous, pulmonary (combustible cigarettes and electronic cigarettes), oral (solutions, capsules, and nicotine gums), and transdermal (nicotine patches). Moreover, it represents the first nicotine physiologically based pharmacokinetic model that predicts nicotine plasma concentration and heart rate profiles after the use of electronic cigarettes.

## 1 Introduction

Tobacco use is now the leading single preventable cause of death worldwide, causing 8 million deaths per year mainly from cardiovascular disease, cancer, and pulmonary disease, according to the latest World Health Organization (WHO) report on the global tobacco epidemic in 2019 [1]. Moreover, despite more than 70% of smokers wanting to quit and 40% attempting to do so each year, only about 5% are successful [2]. The highly addictive nature of tobacco is caused mainly by the pharmacologically active nicotine and often impedes smoking withdrawal [3]. The low quit rates highlight the tremendous need for more successful smoking cessation strategies. In addition, health risks of electronic cigarettes (e-cigarettes) are currently a topic of considerable debate. Preliminary data from the US National Youth Tobacco Survey indicate a further rise in the rates of e-cigarettes use by youth, where the addictive properties of nicotine also play an important role, and which was recently called an “epidemic of youth use of electronic nicotine delivery system products” by the US Food and Drug Administration [4]. While

e-cigarettes assist smoking cessation for some smokers, the escalating rates raise concerns about addicting a generation of young people to nicotine, with the long-term safety of e-cigarettes still unknown [5]. A better understanding of differences in the pharmacokinetics (PK) of nicotine, including nicotine exposure in the brain after different routes of administration, may enhance the understanding of nicotine addiction with the use of different nicotine delivery products and inform more successful treatment interventions.

While nicotine plays only a minor direct role in causing smoking-induced diseases, addiction to nicotine is the proximate cause of these diseases [3]. When nicotine is inhaled, it is rapidly absorbed into the pulmonary venous circulation, and quickly reaches the brain tissue through arterial circulation. There, it immediately induces pharmacodynamic (PD) effects including the release of dopamine in the mesolimbic area, a key step in causing nicotine addiction [6]. For smokers who intend to quit smoking, nicotine maintenance with nicotine replacement therapies (NRTs) such as nicotine gums or transdermal patches can help reduce smoking rates and facilitate smoking cessation [7, 8]. Although NRTs try to imitate the nicotine exposure of smoking, nicotine appearance in the venous blood is slower and peak concentrations are lower with the use of NRTs, compared with smoking combustible cigarettes [9, 10]. Data on nicotine brain tissue concentrations are scarce and typically complex in nature [11]. Nevertheless, it would be of great interest to also compare differences in nicotine exposure in brain tissue after various routes of nicotine administration.

Genetic factors account for about 30% of the variance in risk for failed smoking cessation [12] and pharmacogenetic testing has shown the potential to optimize smoking cessation therapies [13, 14]. Thus, cytochrome P450 (CYP) enzymes, which are involved in metabolizing nicotine, are of significant interest when investigating nicotine pharmacokinetics. For example, poor metabolizers (PM) of CYP2A6, which is predominantly responsible for nicotine metabolism [15], have a lower risk of developing nicotine dependence and less severe nicotine withdrawal symptoms than normal metabolizers (NM) [16].

In addition to its addictive effects on the brain, nicotine acts as a sympathomimetic drug, releasing catecholamines and thereby inducing peripheral PD effects such as an increase in heart rate [17]. Changes in heart rate represent a surrogate measure for general pharmacological actions of nicotine. Cotinine is widely used as a biomarker for the use of tobacco, as a quantitative marker for exposures to nicotine, and as a measure of compliance with treatments of smoking cessation, owing to its long half-life compared with nicotine (~ 16 h vs ~ 2 h) and consequently, fairly stable cotinine plasma concentrations in regular daily smokers [6, 18].

Physiologically based pharmacokinetic (PBPK) modeling offers a solution to tackle these complexities of nicotine

pharmacokinetics and pharmacodynamics and provides the opportunity to characterize and predict drug exposure in a specific organ or tissue [19]. The aims of this study were (1) to develop a whole-body PBPK/PD model of nicotine and its major metabolite cotinine, covering various routes of administration (i.e., intravenous, oral, transdermal, and pulmonary) including the PK/PD relationship in heart rate changes, (2) to provide a comprehensive publicly available model for further investigations and applications, which may contribute to the WHO's goal of combating the tobacco epidemic and to stop the persistent rise in youth e-cigarette use [1, 4], and finally, (3) to apply the model to investigate differences in brain concentrations between pulmonary administration of nicotine (combustible cigarettes, e-cigarettes) and NRTs.

## 2 Methods

### 2.1 Software

The PBPK/PD modeling and simulation was performed using PK-Sim<sup>®</sup> and MoBi<sup>®</sup> (version 8.0, part of the Open Systems Pharmacology [OSP] suite, <https://www.open-systems-pharmacology.org>). Model input parameter optimization was accomplished using the Monte Carlo algorithm. Clinical data were digitized using GetData Graph Digitizer version 2.26.0.20 (S. Fedorov). PK parameter analyses and graphics were compiled with the R programming language version 3.6.0 (R Foundation for Statistical Computing, Vienna, Austria).

### 2.2 Physiologically Based Pharmacokinetic/Pharmacodynamic (PBPK/PD) Parent–Metabolite Model Building

For PBPK/PD model building, an extensive literature search was performed to collect information on physicochemical properties, liberation, absorption, distribution, metabolism, and excretion (LADME) processes and clinical studies of intravenous, oral, pulmonary, and transdermal administration of nicotine and intravenous administration of cotinine in single- and multiple-dose regimens. Plasma concentration–time profiles, a brain tissue concentration–time profile, fractions of nicotine and cotinine doses excreted unchanged to urine, and heart rate profiles were digitized from 34 clinical studies with 75 different treatment blocks and 891 patients and split into an internal training ( $n = 26$  profiles) and an external test ( $n = 76$  profiles) dataset (for detailed information on clinical studies, see Tables S2.6.1–S2.6.3 of the Electronic Supplementary Material [ESM]). The internal training dataset was used for model building and together with the external test dataset, for model evaluation. The training dataset was selected so as to inform all physiological

processes implemented in the model (e.g., contribution of the CYP2B6 elimination pathway, estimation of urinary excretion).

Hence, for cotinine PBPK model building, three plasma profiles of cotinine administered intravenously were used, which covered a broad dosing range and included information on urinary excretion of cotinine. For the nicotine PBPK model building, plasma profiles of non-smokers and smokers after intravenous administration were included in the training dataset, with a broad dosing range, including studies with cotinine metabolite data, information on the fraction of nicotine excreted unchanged to urine, and the fraction of nicotine metabolized to cotinine. Moreover, a study with plasma concentrations of CYP2A6 poor metabolizers and a study with brain tissue concentrations after nicotine intake were included in the training dataset, to inform model input parameters for CYP2B6 and brain transporters. For the PD heart rate model, three studies with intravenous administration were used for model training, which covered the largest timeframe of heart rate measurements and the highest nicotine peak plasma concentrations. Values for model input parameters that could not be adequately obtained from the literature were estimated by fitting first the cotinine model and subsequently the nicotine model to the training dataset.

The parent–metabolite PBPK/PD model was derived using a stepwise approach. Initially, a cotinine model was developed based on cotinine intravenous training data from healthy non-smoking volunteers. Second, the cotinine model was complemented by a comprehensive PBPK model of the parent compound nicotine, including intravenous, oral, and pulmonary administration of nicotine, using the internal dataset for model training. Third, the oral route of administration for nicotine gums and a transdermal model were established and added to the parent–metabolite PBPK model. Fourth, a modified heart rate-tolerance PD model based on a recently published tolerance model, including circadian rhythm [20] was incorporated into the PBPK model to describe the positive chronotropic effect of nicotine. Finally, the resulting PBPK/PD model was evaluated and used to simulate brain tissue concentration patterns after nicotine administration through different routes.

Distribution and elimination processes including CYP enzymes and transporters were implemented according to the literature [15, 21–23]. For the nicotine model, these are (1) metabolism of nicotine to its major metabolite cotinine through CYP2A6 and CYP2B6, (2) an unspecific hepatic clearance being responsible for the remaining hepatic metabolism of nicotine including metabolism via uridine 5'-diphospho-glucuronosyltransferase 2B10 (UGT2B10) and flavin-containing monooxygenase 3 (FMO3), and (3) two transporters for the influx and efflux of nicotine across the blood–brain barrier (BBB). For cotinine, an unspecific hepatic clearance was implemented. Additionally, renal

excretion through glomerular filtration was implemented as an elimination pathway for both compounds, as they are subject to glomerular filtration under physiological conditions [15, 24]. Reported differences in nicotine clearance between smokers and non-smokers [25] were addressed by estimating different values for the CYP2A6 catalytic rate constant ( $k_{\text{cat}}$ ).

A PD model was added to the PBPK model to describe the positive chronotropic effect of nicotine [9, 26] based on its PK. The model, which best described the heart rate including the drug effect, was a direct-effect  $E_{\text{max}}$  model with absolute effect, including a tolerance development based on a recently published heart rate tolerance model [20]. Figure 1 shows a structural overview of the developed PBPK/PD model. The tolerance compartment was implemented to describe the extent of acute tolerance development of the system and its subsequent reduction in the drug effect on heart rate following the administration of nicotine [27]. The appearance of tolerance was set to depend on the concentration of nicotine, which has been shown in the literature [27]. For detailed information on PBPK/PD model building and virtual populations, see Sect. 2 of the ESM.

### 2.3 PBPK Model of Nicotine Patches, Nicotine Gums, Combustible Cigarettes, and Electronic Cigarettes

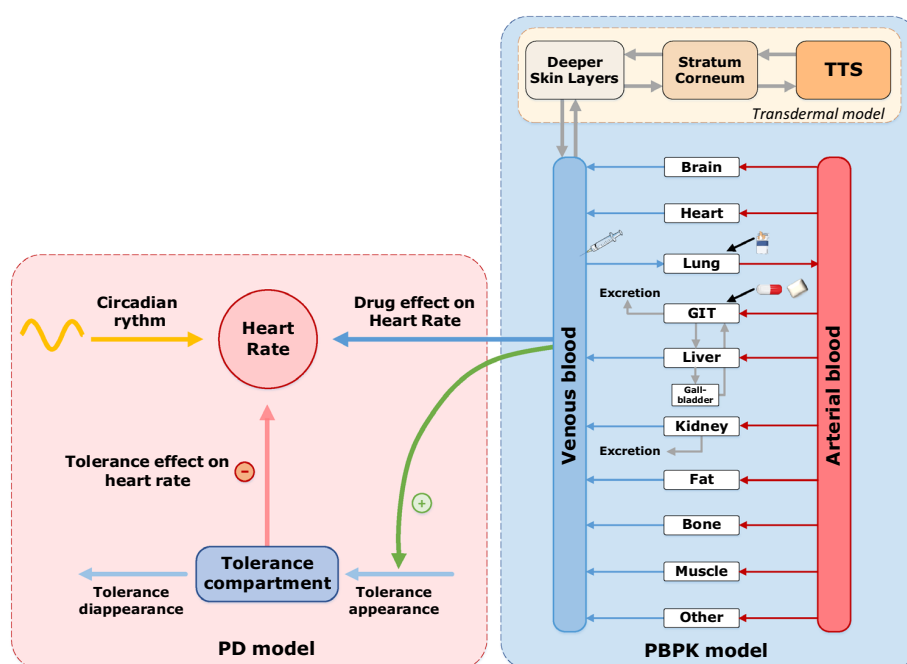
To model and simulate the transdermal application of nicotine with nicotine patches, a transdermal two-compartment skin model was implemented with MoBi<sup>®</sup> and added to the default PBPK model. To model and simulate the

administration of nicotine gums, an oral formulation was used. The corresponding nicotine release was implemented according to a published in vitro release profile of Nicorette<sup>®</sup> chewing gums [28]. A pulmonary route of administration was applied within PK-Sim<sup>®</sup> to model and simulate the inhalation of nicotine with combustible cigarettes and e-cigarettes. Zero-order kinetics were chosen for pulmonary formulations with a duration of the length of smoking, which is supported by the literature [29]. For detailed information see Sects. 2.2–2.4 of the ESM.

### 2.4 PBPK/PD Model Evaluation

All the 102 nicotine and cotinine concentration–time profiles and heart rate profiles observed of the training and test datasets were compared to predicted profiles. Virtual populations of 100 individuals for each study were established according to the population demographics of the respective simulated study. Population predictions were plotted as geometric mean with geometric standard deviation. Visual descriptive (training dataset) and predictive (test dataset) performances of the PBPK/PD model are shown in Sect. 3 and in detail in Sects. 3.1–3.6 and 3.11 of the ESM. Model performance was also evaluated by comparing predicted plasma concentrations with their respective values observed in goodness-of-fit plots. Additionally, the predicted vs observed area under the concentration–time curve from the first to the last data point ( $\text{AUC}_{\text{last}}$ ) and maximum concentration ( $C_{\text{max}}$ ) values were compared in goodness-of-fit plots. The sensitivity of the final PBPK model to single parameter changes (local

**Fig. 1** Structural overview of the developed physiologically based pharmacokinetic/pharmacodynamic (PBPK/PD) model for the intravenous, oral, transdermal, and pulmonary administration of nicotine. Boxes indicate compartments, solid lines denote in-/out-flows, dashed lines indicate relationships. *GIT* gastrointestinal tract, *TTS* transdermal therapeutic system



sensitivity analysis) was investigated with PK-Sim<sup>®</sup>. Further, two quantitative performance measures were calculated: the mean relative deviation (MRD) of the predicted plasma concentrations for each plasma profile and the geometric mean fold errors (GMFE) of  $AUC_{last}$  and  $C_{max}$ , respectively (see Sects. 3.8–3.10 of the ESM).

### 3 Results

#### 3.1 PBPK Model Building and Evaluation

The whole-body PBPK model of nicotine and cotinine precisely describes and predicts plasma concentration–time profiles following intravenous, oral, transdermal, and pulmonary administration and data on brain tissue concentrations (see Figs. 2, 3, 4, 5). For the building and evaluation of the nicotine parent–metabolite PBPK model, 90 plasma concentration–time profiles including 18 cotinine metabolite profiles, a brain tissue concentration–time profile, six

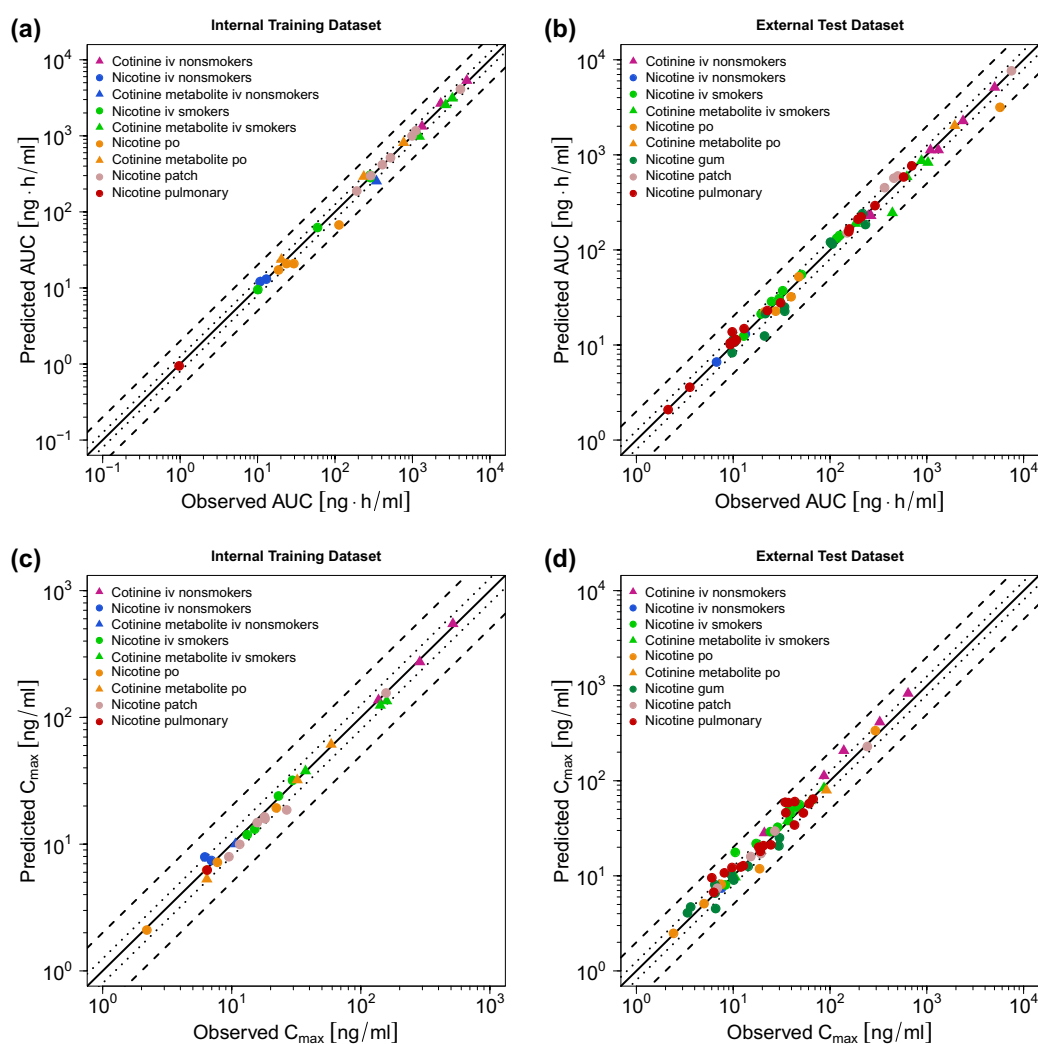


**Fig. 2** Predicted vs observed nicotine and cotinine area under the concentration–time curve from the first to the last data point ( $AUC$ ) [a, b] and maximum concentration ( $C_{max}$ ) [c, d] values of the internal training and the external test dataset. Each symbol represents the  $AUC$  or  $C_{max}$  of a single concentration–time profile (circles: nicotine,

triangles: cotinine metabolite and cotinine intravenous [iv]). The black solid lines mark the lines of identity. Black dotted lines indicate a 1.25-fold deviation, black dashed lines indicate a twofold deviation. *Patch* transdermal therapeutic system (nicotine patch), *po* oral

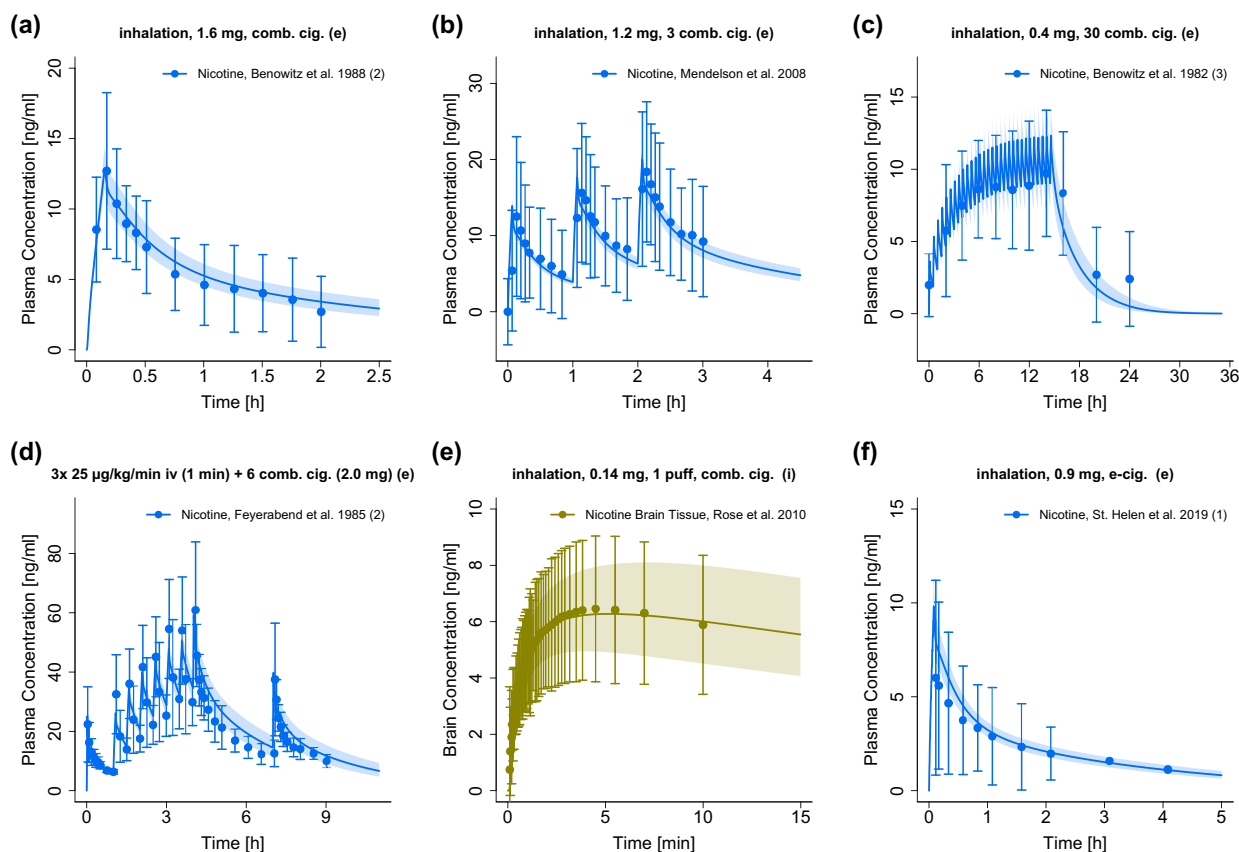


**Fig. 3** Nicotine predicted and observed plasma (blue) and brain tissue (gold) concentration–time profiles after administration of combustible cigarettes (with estimated pulmonary nicotine exposure for plasma simulations) and electronic cigarettes (e-cig.). Population simulation ( $n=100$ ) geometric means are shown as lines; the shaded areas represent the predicted population geometric standard deviations (SDs). Observed data are shown as filled circles  $\pm$  SD. (i): selection of

internal training dataset, (e): selection of external test dataset. References with numbers in parentheses link to a specific observed dataset described in the study table with detailed information about dosing regimens (Tables S2.6.1 and S2.8.2 of the ESM). Predicted and observed area under the concentration–time curve (AUC) and maximum concentration ( $C_{\max}$ ) values are compared in Table S3.8.2 of the ESM. *comb. cig.* combustible cigarette, *iv* intravenous [9, 11, 70–73]

studies on the fraction of nicotine and cotinine excreted unchanged to urine, and one study depicting the fraction of nicotine metabolized to cotinine were used. Drug-dependent parameters of the final parent–metabolite PBPK model are depicted in Table 1. A study overview including key metrics and a detailed description of the PBPK model are listed in Sect. 2 of the ESM.

The good descriptive and predictive model performance is comprehensively demonstrated. Visual comparisons of predicted to observed plasma concentration–time profiles are depicted in Figs. 3, 4, 5 (selection of internal and external datasets for each route of administration) and in detail in Sects. 3.1–3.6 of the ESM (all studies, linear and semilogarithmic plots). The predictions of plasma concentration–time trajectories for all routes of administration are in close agreement with observed plasma concentration data. Moreover, goodness-of-fit plots of predicted to observed  $AUC_{\text{last}}$  and  $C_{\max}$  are shown in Fig. 2 and for each route of administration

separately in Sects. 3.1–3.6 of the ESM together with goodness-of-fit plots of observed vs predicted plasma concentrations. In summary, 100% of both the predicted  $AUC_{\text{last}}$  and  $C_{\max}$  values appear to be within the twofold acceptance criterion. The GMFE values for the nicotine PBPK model are 1.11 and 1.17 for  $AUC_{\text{last}}$  and  $C_{\max}$ , respectively, and 1.14 and 1.11 for the cotinine model. Overall MRD for the nicotine and cotinine PBPK model are 1.44 and 1.77, respectively. Detailed results on GMFE and MRD values calculated for all studies are given in Sect. 3.8 of the ESM and the results of the sensitivity analysis are shown in Sect. 3.10 of the ESM.

Nicotine is mainly metabolized through CYP2A6. However, in CYP2A6 PMs, when people lack CYP2A6 metabolism and cotinine production diminishes (CYP2A6- $k_{\text{cat}}$  of 0), CYP2B6 is responsible for a modest nicotine conversion to cotinine [15, 22]. A CYP2A6 PM plasma concentration–time profile was included in the training dataset to

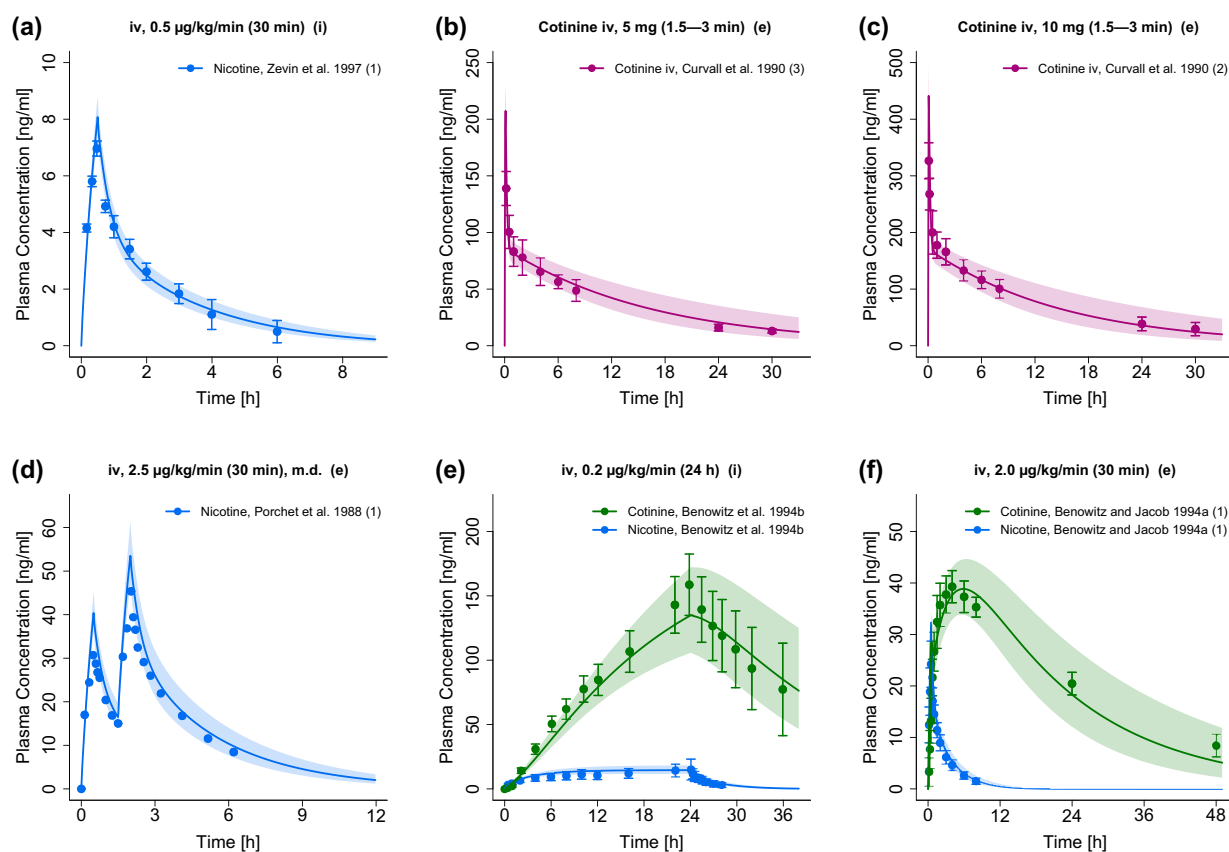


**Fig. 4** Nicotine (blue) and cotinine (purple if administered intravenously, green if metabolite) predicted and observed plasma concentration–time profiles after intravenous administration. **a–c** Non-smokers, **d–f**: smokers. Population simulation ( $n=100$ ) geometric means are shown as lines; the shaded areas represent the predicted population geometric standard deviations (SDs). Observed data are shown as filled circles, if available  $\pm$ SD. (i): selection of internal training

dataset, (e): selection of external test dataset. References with numbers in parentheses link to a specific observed dataset described in the study table with detailed information about dosing regimens (Tables S2.6.1 and S2.6.2 of the ESM). Predicted and observed area under the plasma concentration–time curve (AUC) and maximum plasma concentration ( $C_{\max}$ ) values are compared in Table S3.8.2. of the ESM. *iv* intravenous [22, 27, 74–76]

estimate CYP2B6 metabolism in the model and to describe nicotine plasma concentrations in CYP2A6 PMs (see Fig. 5d) [40]. Additionally, nicotine clearance in smokers appears to be about 15% lower, compared with non-smokers [25]. To account for this difference, CYP2A6- $k_{\text{cat}}$  was estimated separately for the smoker subpopulation, leading to a lower  $k_{\text{cat}}$  in comparison to the non-smoker subpopulation (see Table 1). For detailed information including drug-, system-, and formulation-dependent model parameters, see Sect. 2.1 of the ESM and Tables S2.7.1, S2.8.1–2.8.3, and S2.10.1 of the ESM.

The resulting PBPK model predicts a fraction of nicotine metabolized to cotinine of about 75%, which perfectly aligns with literature reports (70–80%) [15, 22, 23]. Moreover, predicted bioavailabilities after oral (~35%) and pulmonary (~85%) administration of nicotine are in concordance with the literature (20–45% and 80–90%, respectively) [9, 15, 46].

As the published literature suggests, the influx and efflux of nicotine over the BBB play an important role in the characteristics of nicotine brain tissue concentrations [21]. As a result, an influx and an efflux transporter with Michaelis–Menten kinetics were implemented in the BBB, which led to a precise description of experimental nicotine brain tissue concentrations after a puff of a combustible cigarette (see Fig. 3e) [11].

It is known that machine smoking yields of combustible cigarettes are not equivalent to human measures of nicotine uptake [47, 48]. Hence, when machine smoking yields are used as nicotine doses for simulation of plasma concentrations, the model underpredicts observed data for low machine smoking yields and overpredicts observed data for high machine smoking yields (see Fig. S3.6.1 of the ESM). Therefore, pulmonary nicotine exposure for combustible cigarettes was estimated additionally as described in Sect. 2.4 of the ESM (mean deviation to

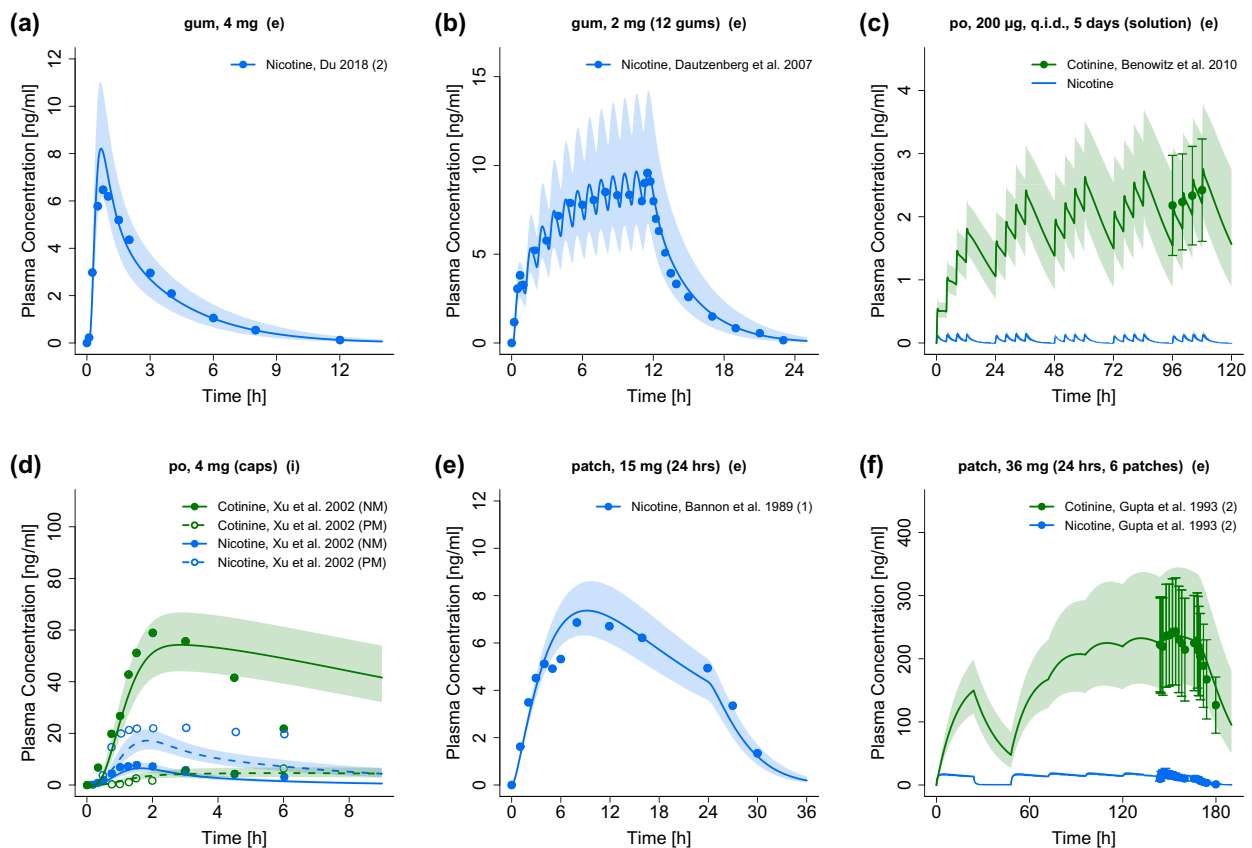


**Fig. 5** Nicotine (blue) and cotinine metabolite (green) predicted and observed plasma concentration–time profiles after oral (gum, solution, capsule) and transdermal administration. Population simulation ( $n=100$ ) geometric means are shown as lines; the shaded areas represent the predicted population geometric standard deviations (SDs). Observed data are shown as circles, if available  $\pm$  SD. (i): selection of internal training dataset, (e): selection of external test dataset. References with numbers in parentheses link to a specific observed data-

set described in the study table with detailed information about dosing regimens (Tables S2.6.1 and S2.8.3 of the ESM). Predicted and observed area under the plasma concentration–time curve (AUC) and maximum plasma concentration ( $C_{\max}$ ) values are compared in Table S3.8.2. of the ESM. *caps* capsule, *NM* normal metabolizer, *patch* transdermal therapeutic system (nicotine patch), *PM* poor metabolizer, *po* oral, *q.i.d.* four times daily [18, 40, 62, 77–79]

machine smoked nicotine yields of 31%), leading to the precise predictions of plasma profiles observed (see Fig. 3 and Fig. S3.5.1 of the ESM).

For the administration of nicotine through transdermal therapeutic systems (TTS), the default PK-Sim<sup>®</sup> PBPK model was expanded with a two-compartment skin model, which consists of the lipophilic stratum corneum and the hydrophilic deeper skin layer routes. The resulting model successfully describes and predicts plasma profiles after single and multiple doses of nicotine patches (see Fig. 5e, f and Sect. 3.4 of the ESM). The model was also able to predict nicotine plasma profiles during the use of nicotine gums in single- and multiple-dose studies (see Fig. 5a, b and Sect. 3.3 of the ESM) and cotinine steady-state plasma concentrations observed in several studies (see Fig. 5c, f and Sect. 3.3 of the ESM) [18].

### 3.2 Brain Concentrations after Different Routes of Administration

The model was used to simulate steady-state brain tissue concentrations throughout a day when smoking combustible cigarettes or e-cigarettes (16 cigarettes during 16 h), administering nicotine gums (16 gums during 16 h), or applying a nicotine patch (for 24 h). Simulations and results of the comparison of area under the brain tissue concentration–time curves, maximum brain tissue concentrations, and peak-trough differences for each type of nicotine administration are depicted in Fig. 6.

**Table 1** Drug-dependent and pharmacodynamic (PD) parameters of the final parent–metabolite physiologically based pharmacokinetic/pharmacodynamic (PBPK/PD) model

Parameter	Unit	Nicotine model		Cotinine model		Description <sup>a</sup>
		Value used in simulation	Literature value [Ref]	Value used in simulation	Literature value [Ref]	
<b>PBPK model</b>						
MW	g/mol	162.2	162.2 [30] <sup>b</sup>	176.2	176.2 [30] <sup>c</sup>	Molecular weight
pK <sub>a1</sub>		8.1 (basic)	8.1 [31]	4.5 (basic)	4.5 [32]	Acid dissociation constant 1
pK <sub>a2</sub>		3.3 (basic)	3.3 [31]			Acid dissociation constant 2
log <i>P</i>		1.6	1.2, 1.4 [31, 33]	−0.1 <sup>f</sup>	0.21 [30] <sup>c</sup>	Lipophilicity
Solubility (pH)	mg/mL	93.3 (7.0)	93.3 (7.0) [30] <sup>b</sup>	117.0 (7.0)	117.0 (7.0) [30] <sup>c</sup>	Solubility
<i>f</i> <sub>u</sub>	%	95.1	80.0–95.1 [34]	97.4	97.4 [35]	Fraction unbound (plasma)
CYP2A6 <i>K</i> <sub>M</sub>	μmol/L	29.4 <sup>f</sup>	11.0, 32.0, 33.0, 144.0 [36–39]			CYP2A6 Michaelis–Menten constant
CYP2A6-NM <i>k</i> <sub>cat</sub> (non-smokers)	1/min	12.0 <sup>f</sup>	–			CYP2A6-NM catalytic rate constant for non-smokers
CYP2A6-NM <i>k</i> <sub>cat</sub> (smokers)	1/min	10.5 <sup>f</sup>	–			CYP2A6-NM catalytic rate constant for smokers
CYP2A6-PM <i>k</i> <sub>cat</sub>	1/min	0.0	0 [40]			CYP2A6-PM catalytic rate constant
CYP2B6 <i>K</i> <sub>M</sub>	μmol/L	820.0	820.0 [41]			CYP2B6 Michaelis–Menten constant
CYP2B6 <i>k</i> <sub>cat</sub>	1/min	16.0 <sup>f</sup>	–			CYP2B6 catalytic rate constant
BBB-transporter <sub>in</sub> <i>K</i> <sub>M</sub>	μmol/L	92.4	92.4 [21]			BBB-transporter <sub>in</sub> Michaelis–Menten constant
BBB-transporter <sub>in</sub> <i>k</i> <sub>cat</sub>	1/s	5.3E + 03 <sup>f</sup>	–			BBB-transporter <sub>in</sub> catalytic rate constant
BBB-transporter <sub>out</sub> <i>K</i> <sub>M</sub>	μmol/L	7.0E − 05 <sup>f</sup>	–			BBB-transporter <sub>out</sub> Michaelis–Menten constant
BBB-transporter <sub>out</sub> <i>k</i> <sub>cat</sub>	1/s	0.4 <sup>f</sup>	–			BBB-transporter <sub>out</sub> catalytic rate constant
GFR fraction		1.0	–	6.0E − 02 <sup>f</sup>	–	Fraction of GFR used for passive elimination by the kidney
Unspecific hepatic clearance	1/min	0.3 <sup>f</sup>	–	2.0E − 02 <sup>f</sup>	–	Elimination from plasma (first-order process in the liver)
Calculation method of partition coefficients		Rodgers and Rowland [42–44]		PK-Sim <sup>®</sup> standard [45] <sup>d</sup>		Organ-plasma partition coefficients
Calculation method of cell permeabilities		PK-Sim <sup>®</sup> standard [45] <sup>d</sup>		PK-Sim <sup>®</sup> standard [45] <sup>d</sup>		Permeation across cell membranes
<b>PD model<sup>e</sup></b>						
<i>E</i> <sub>max</sub>	bpm	111.6 <sup>f</sup>	–			Maximum possible heart rate elevation without tolerance

**Table 1** (continued)

Parameter	Unit	Nicotine model		Cotinine model		Description <sup>a</sup>
		Value used in simulation	Literature value [Ref]	Value used in simulation	Literature value [Ref]	
EC <sub>50</sub>	μmol/L	0.21 <sup>f</sup>	–			Concentration at half-maximum elevation
<i>h</i>		1.3 <sup>f</sup>	–			Hill coefficient
tol <sub>in</sub>	1/h	15.3 <sup>f</sup>	–			Tolerance appearance rate
tol <sub>out</sub>	1/h	0.2 <sup>f</sup>	–			Tolerance disappearance rate
tol <sub>50</sub>	μmol/L	0.07 <sup>f</sup>	–			Scaling parameter for tolerance
amp	%	6.3	6.3 [20]			Circadian amplitude
$\gamma$		0.4 <sup>f</sup>	–			Non-linearity parameter

BBB blood–brain barrier, *bpm* beats/min, *CYP* cytochrome P450, *GFR* glomerular filtration rate, *k<sub>cat</sub>* catalytic rate constant, *NM* normal metabolizer, *PM* poor metabolizer, *Ref* reference, – not available

<sup>a</sup>Descriptions for PD parameters carried over from [20]

<sup>b</sup>DrugBank entry for nicotine. Available from: <https://www.drugbank.ca/drugs/DB00184> [Accessed 21 Oct 2019]

<sup>c</sup>DrugBank entry for cotinine. Available from: <https://www.drugbank.ca/metabolites/DBMET00519>. [Accessed 21 Oct 2019]

<sup>d</sup>Equations and descriptions of calculations can be found in [45]

<sup>e</sup>Individual heart rate baselines and circadian time shift for different study populations are depicted in Sect. 2.9 of the ESM

<sup>f</sup>Model input parameter estimated

### 3.3 PBPK/PD Model Building and Evaluation

The PBPK model has been augmented with a PD nicotine heart rate model (see Fig. 1). The integrated PBPK/PD model is able to capture the effect of nicotine that leads to heart rate peaks rapidly after intravenous and pulmonary nicotine intake. A total of 11 studies evaluating the effect of nicotine on heart rate were used for PD model building and evaluation. Study details and key metrics are listed in Table S2.6.3 of the ESM. Parameters of the final PBPK/PD model are listed in Table 1. PD model performance for both the internal training and the external test dataset is demonstrated by comparing the population predicted to heart rate profiles observed in Fig. 7 (representative studies) and in detail in Sect. 3.11 of the ESM (all studies).

## 4 Discussion

The main outcome of this study is the development of a comprehensive parent–metabolite PBPK/PD model of a drug, which is consumed by over 1.1 billion smokers and which is also used in NRTs as an important smoking cessation strategy [1]. The model provides a consistent representation of the nicotine dose–exposure relationship following intravenous, oral, transdermal, and pulmonary administration in non-smoking and smoking populations. It precisely

describes and predicts nicotine and cotinine plasma and nicotine brain tissue concentrations. Thereby, the model is able to quantify the contribution of the elimination pathways of the fraction of nicotine metabolized to cotinine and urinary excretion of both nicotine and cotinine. Further, the PBPK model has been expanded by a heart rate tolerance model, which includes circadian rhythm, describing the positive chronotropic effect of nicotine. Finally, the model was used to identify differences in brain concentrations between pulmonary administration of nicotine (combustible cigarettes, e-cigarettes) and NRTs.

To reduce smoking dependence, exposure to smoke toxicants, and youth e-cigarette use, all of which are critical public health goals [1, 4], it is crucial to have quantitative tools to better understand both smoking behavior and dependence on nicotine. This model represents an opportunity to simulate concentrations of nicotine in blood plasma and brain tissue with requested dosing regimens after four different routes of administration.

Five other PBPK models of nicotine have been developed so far; however, either important routes of administration, a PD heart rate model, comprehensive predictive performance, and/or the inclusion of a large number of clinical studies are missing [49–53]. The models developed by Plowchalk et al. (for rats), Robinson et al., and Yamazaki et al. (for humans) presented simplified implementations of the nicotine ADME processes [49–51]. While Teeguarden et al. stated that their

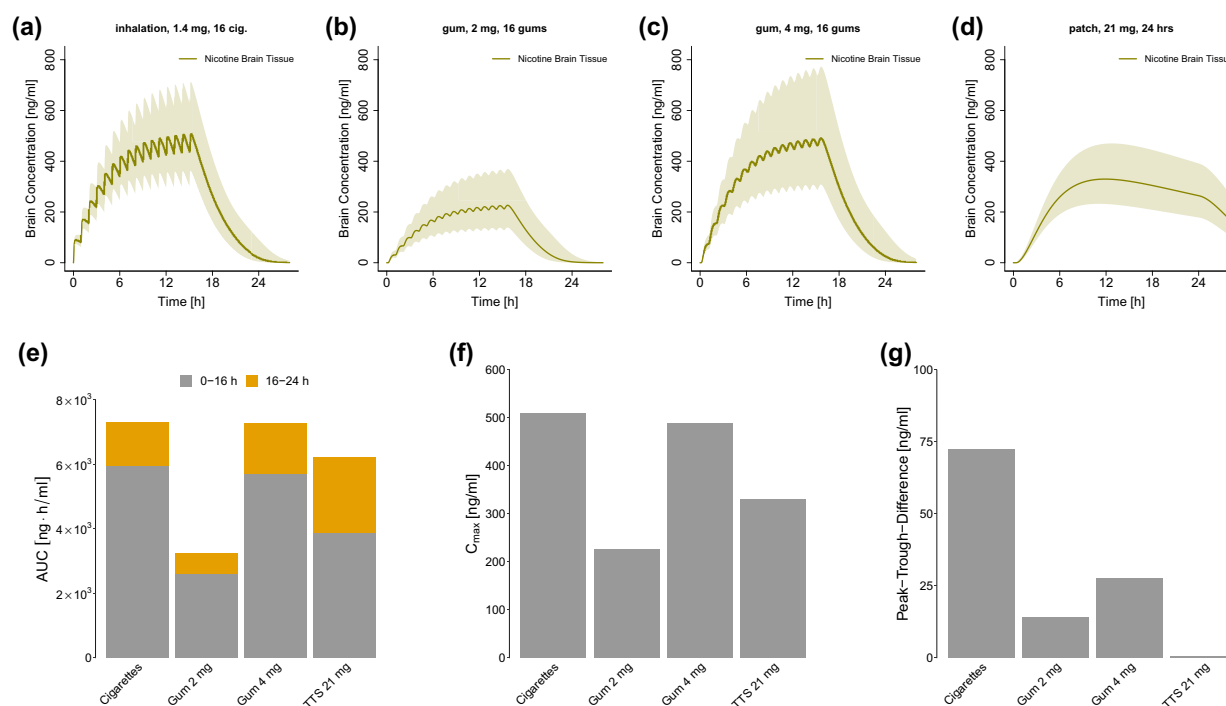


**Fig. 6** Simulations of brain tissue concentration–time profiles after pulmonary (16 h), oral (2 mg and 4 mg gums, 16 h), and transdermal (patch, 24 h) administration (**a–d**) and analysis of the area under the brain tissue concentration–time curve (AUC) of nicotine brain tissue concentrations for the first 16 h (gray) and the last 8 h (orange) (**e**), maximum brain tissue concentrations ( $C_{\max}$ ) (**f**), and peak–trough differences in brain tissue concentrations between minimum brain tissue

concentration ( $C_{\min}$ ) and  $C_{\max}$  in steady state (**g**). Population simulation ( $n=100$ ) geometric means are shown as lines; the shaded areas represent the population geometric standard deviations. Detailed information about dosing regimens, study populations, and parameters used for simulations is given in Tables S2.6.1, S2.7.1, S2.8.1, and S2.8.3 of the ESM. Peak–trough difference is not applicable for the transdermal therapeutic system (nicotine patch). *cig.* cigarettes

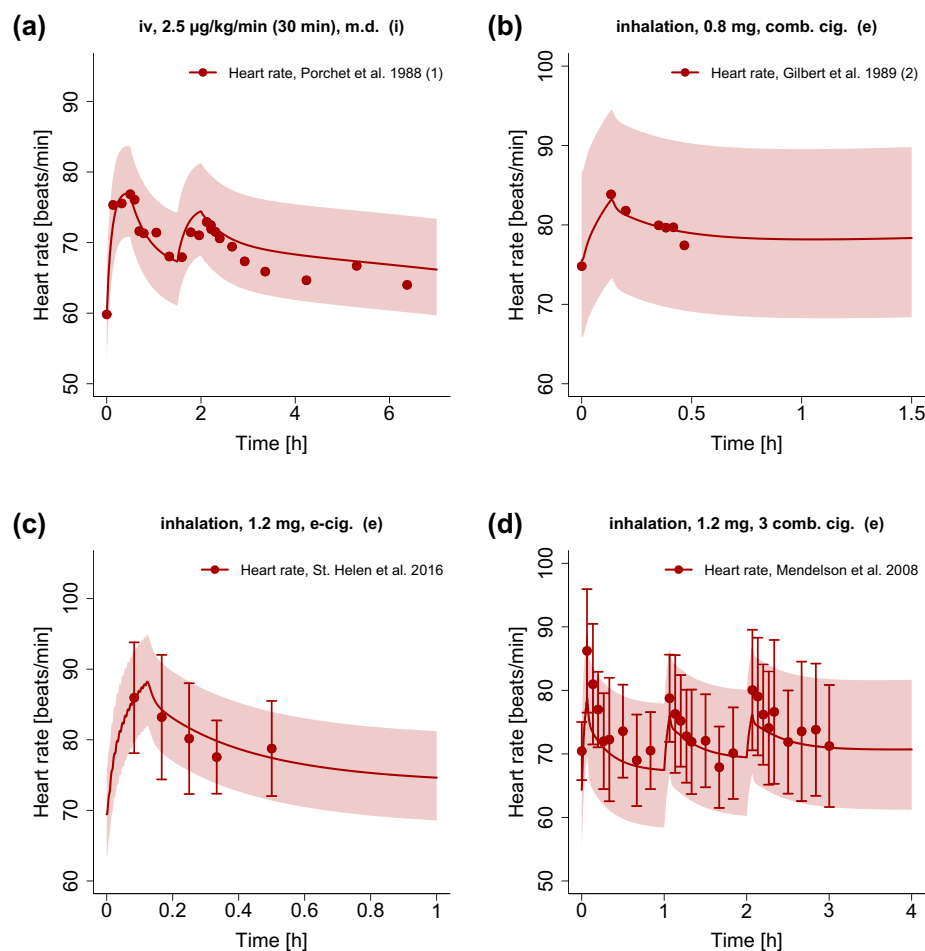
“results should not at this time be considered accurate predictions of outcomes in a population of smokers”, they presented one of the first broad models including several routes of nicotine administration (without a transdermal route) and a PD model [52]. The most current nicotine PBPK/PD model, by Gajewska et al., accurately described heart rate changes after transdermal nicotine intake but struggled to predict heart rate peaks occurring after intravenous nicotine administration and nicotine plasma concentrations after the removal of nicotine patches [53]. While the previously mentioned models provide the information in a condensed form to investigate the models independent of the underlying platform, the presented model relies on the application within the OSP framework. However, all the information can be accessed through the model file, which is publicly available in the OSP repository for application and investigation purposes.

Our PBPK/PD model incorporates comprehensiveness of both the routes of administration (intravenous, transdermal [patches], oral [including gums], and pulmonary [combustible cigarettes and e-cigarettes]) and the number of plasma, brain tissue, and heart rate profiles included

( $n=102$ ) to develop the model. Moreover, this study presents a novel opportunity to simulate nicotine brain tissue concentrations after different routes of administration, based on incorporated information on brain tissue concentrations, in PK-Sim<sup>®</sup> and MoBi<sup>®</sup>.

In contrast with already published nicotine PBPK models, this study includes the two most important CYP enzymes for nicotine metabolism, CYP2A6 and CYP2B6, both highly polymorphic, and incorporated differences between CYP2A6 PMs and NMs [15, 40, 54]. This is crucial for the individualization of NRTs to avoid poor response and adverse drug reactions [55, 56], as pharmacogenetic testing has shown the potential to optimize smoking cessation therapies [13, 14]. Because only one plasma–concentration time profile for PMs was available and concentrations were determined only over 6 h, simulations of plasma concentrations may be less accurate over longer time periods. Hence, additional research on the PK of PMs would be of great interest. The enzymatic pathways responsible for nicotine glucuronidation (UGT2B10) and N-oxidation (FMO3) are subsumed under the unspecific hepatic clearance process.

**Fig. 7** Predicted and observed heart rate profiles after intravenous (iv) and pulmonary (combustible cigarette [comb. cig.] and electronic cigarette [e-cig.]) administration. Population simulation ( $n=100$ ) geometric means are shown as lines; the shaded areas represent the predicted population geometric standard deviations (SDs). Observed data are shown as filled circles, if available  $\pm$  SD. (i): selection of internal training dataset, (e): selection of external test dataset. References with numbers in parentheses link to a specific observed dataset described in the study table with detailed information about dosing regimens (Table S2.6.3 of the ESM). *m.d.* multiple dose [27, 70, 80, 81]



Additionally, we present the first nicotine PBPK model that also includes and predicts nicotine concentration–time and heart rate profiles after e-cigarette use. In light of the ongoing discussions on the health risks of e-cigarettes and the fact that more than a quarter of high school students in the USA are current e-cigarette users with the figures still rising, our data might contribute to a better understanding of the persistent increase in youth e-cigarette use by serving as a basis for future studies on nicotine PK-based addiction models [4, 57].

Being widely used as a quantitative marker for exposures to nicotine and as a measure of compliance with treatments for smoking cessation [6, 18], cotinine was also included in the model. The glomerular filtration rate fraction of 0.06 for cotinine, combined with the description of the fraction of cotinine dose excreted unchanged to urine, indicates high tubular reabsorption of cotinine in the kidney. Accurate cotinine metabolite predictions after intravenous, oral (solutions, capsules), and transdermal administration could allow future investigations to perform reverse calculations to arrive at the amount of nicotine intake from cotinine plasma

concentrations with this model. Because no cotinine metabolite data after pulmonary and nicotine gum intake were available, cotinine formation could not be evaluated for these routes of administration. However, CYP2A6 expression in the lung was implemented according to the PK-Sim<sup>®</sup> expression database, to cover potential differences in cotinine formation [58]. Variability in predictions for most intravenous, oral, and transdermal studies is better covered compared with pulmonary studies, where the variability observed is higher than predicted. This is as expected because variability in model predictions results from physiological differences, while the high variability after smoking results from differences in puffing behavior (such as puff volumes) called smoking topography [59].

As a result, our findings support the assumption that differences in smoking topography also lead to differences in nicotine plasma concentrations [46, 60]. The fact that the model is able to describe nicotine PK after the use of combustible cigarettes and e-cigarettes with the same pulmonary administration model supports recent findings that

differences in plasma PK result from different smoking and vaping patterns, respectively [61].

Although transmucosal absorption was neglected during the administration of nicotine gums, predictions for nicotine plasma profiles show very promising results. The future development of a physiological transmucosal PBPK model could help predict cotinine metabolite concentrations after the administration of nicotine gums. The expansion of our PBPK model with a two-compartment transdermal skin model led to better descriptions of nicotine and cotinine metabolite plasma profiles after transdermal absorption, compared with an existing transdermal nicotine PBPK model [53]. Thereby, it was possible to extrapolate patch parameter sets from the 30-mg single-dose Bannon et al. [62] study to 15-mg and 60-mg patches and to a multiple-dose administration. This indicates that extrapolation from one dose to higher and lower doses as well as from single to multiple doses is possible with the implemented transdermal model. However, more research needs to be conducted to increase the mechanistic component of the transdermal model. As a result of the good predictive PK performance of the intravenous nicotine PBPK model, future studies could use the mechanistic model to de novo predict nicotine and cotinine plasma concentrations based on patch characteristics and in vitro dissolution data.

The simulation study results of nicotine brain concentration patterns show decisive differences: the lower dose nicotine gums (2 mg) yield lower brain concentrations of about half the magnitude ( $C_{\max, \text{brain}}$ ) and extent ( $AUC_{\text{brain}}$ ) as the cigarette study arm does. Brain concentrations during nicotine patch application also do not reach the same magnitude as the simulation with cigarettes does. In contrast, the use of 16 nicotine gums of 4 mg causes similar  $C_{\max, \text{brain}}$  and  $AUC_{\text{brain}}$  values in brain concentrations. However, the fluctuation (peak-trough difference) stays lower, compared with smoking cigarettes. While the  $AUC_{\text{brain}}$  of the nicotine patch trails behind the  $AUC_{\text{brain}}$  of the cigarette study arm after 16 h, the  $AUC_{\text{brain}}$  during the last 8 h is larger, compared with inhalation.

The nicotine brain concentration data used for model building represent nicotine concentrations in the whole brain tissue and do not specifically show concentrations at the nicotine receptor site. Thus, brain concentration simulations were also executed for brain tissue concentrations. To describe the brain tissue concentration profile included in the model development, the implementation of an influx and an efflux transporter in the BBB was necessary and is supported by the literature [21]. As data on nicotine brain tissue concentrations are scarce, only one brain kinetic profile was available to inform the model. Moreover, the brain tissue concentrations were determined only during a time span of 10 min after a single puff of combustible cigarettes [11]. Therefore, extrapolations to brain tissue

simulations, especially of higher doses and longer time-frames, have to be interpreted carefully.

The magnitude of increase in heart rate is a surrogate measure for general pharmacological actions of nicotine. Two PBPK/PD heart rate models from the literature included studies only after intravenous and transdermal administration of nicotine [52, 53]. In contrast, while our PD model was also built based on intravenous administration data, it was expanded and evaluated with heart rate data from study participants consuming combustible cigarettes, e-cigarettes, and nicotine gums. Moreover, we included circadian rhythm for heart rate, as the heart rate undergoes marked fluctuations throughout the day [63]. We succeeded in incorporating acute tolerance development to the heart rate effect, which can not only be observed after the intake of nicotine but also after other substances, such as cocaine or ponesimod [20, 64]. Unfortunately, no heart rate data measured during a whole day of nicotine administration were available. The longest study which is included in the PD model development lasted about 6 h. Hence, extrapolations beyond this time domain should be investigated carefully.

The positive chronotropic effect of nicotine probably results from several effects. First, nicotine stimulates epinephrine and norepinephrine release by the activation of the ligand-gated cation channel nicotine acetylcholine receptors localized mainly on peripheral postganglionic sympathetic nerve endings and the adrenal medulla. Additionally, sympathetic stimulation can occur through the activation of peripheral carotid body chemoreceptors [65–67]. Moreover, a close relationship between plasma concentrations of nicotine and the cardiovascular effects has been observed after acute exposure to nicotine [9, 65]. As a result, the PD effect was linked to the plasma concentrations. Linking the PD effect to concentrations of the heart or the brain compartment led to less precise predictions of heart rate changes.

Simulations of heart rate changes during the administration of four cigarettes, 16 cigarettes (1.4 mg each, smoked within 8 h), 16 nicotine gums (2 mg each), and a transdermal nicotine patch (21 mg in 24 h) have been performed (see Sect. 3.12 of the ESM). The results suggest a persistent increase in the baseline heart rate when smoking one cigarette every 30 min (about 9 beats/min), which is supported by clinical studies [67]. Whereas only a slight increase of heart rate baseline can be observed when simulating the administration of cigarettes smoked 2 h apart, an increased baseline level holds true also for the administration of nicotine gums and the nicotine patch, albeit to a lower extent (about 6 beats/min and 4 beats/min, respectively). These differences are consistent with published work showing a decrease in heart rate when switching from smoking cigarettes to the use of nicotine gums or patches [68, 69].

## 5 Conclusions

A comprehensive whole-body parent–metabolite PBPK/PD model of nicotine and cotinine has been built that can predict (1) nicotine and cotinine plasma concentration–time profiles after various routes of administration, (2) nicotine brain tissue concentrations, and (3) the positive chronotropic effect of nicotine. The physiologically based modeling approach integrated the available *in vitro*, *in vivo*, and *in silico* information on nicotine and could help enhance the understanding of dependence on combustible cigarettes and e-cigarettes. The model was used to simulate and compare nicotine brain concentration patterns during smoking and the application of NRTs. The model is thoroughly documented in the ESM, and the model files are publicly available in the OSP repository (<https://www.open-systems-pharmacology.org>). With that, the model can be used for the development of a detailed physiological transdermal and transmucosal nicotine model, contribute to a library of PBPK models for predictions in special populations, and help with future investigations of nicotine pharmacokinetics and pharmacodynamics, including the design of clinical trials and novel formulations to treat nicotine dependence.

**Acknowledgement** Open Access funding provided by Projekt DEAL.

## Compliance with Ethical Standards

**Funding** This project has received funding from the German Federal Ministry of Education and Research (BMBF), 031L0153, “Alternativmethoden zum Tierversuch” and 03XP0196, “NanoCare4.0 - Anwendungssichere Materialinnovationen”. Data used for model development were collected in part with the support of grants DA039264 and DA012393 from the National Institute on Drug Abuse, USA.

**Conflict of interest** Neal Benowitz has been a consultant to Pfizer and Achieve Life Sciences, companies that market or are developing smoking cessation medications. He has also been a paid witness in litigation against tobacco companies. Lukas Kovar, Dominik Selzer, Hannah Britz, Gideon St.Helen, Yvonne Kohl, Robert Bals, and Thorsten Lehr have no conflicts of interest that are directly relevant to the content of this article.

**Open Access** This article is licensed under a Creative Commons Attribution-NonCommercial 4.0 International License, which permits any non-commercial use, sharing, adaptation, distribution and reproduction in any medium or format, as long as you give appropriate credit to the original author(s) and the source, provide a link to the Creative Commons licence, and indicate if changes were made. The images or other third party material in this article are included in the article’s Creative Commons licence, unless indicated otherwise in a credit line to the material. If material is not included in the article’s Creative Commons licence and your intended use is not permitted by statutory regulation or exceeds the permitted use, you will need to obtain permission directly from the copyright holder. To view a copy of this licence, visit <http://creativecommons.org/licenses/by-nc/4.0/>.

## References

1. World Health Organization. WHO report on the global tobacco epidemic, 2019. Geneva: World Health Organization; 2019. Licence: CC BY-NC-SA 3.0 IGO.
2. World Lung Foundation. The tobacco atlas. 5. Atlanta: American Cancer Society; 2015.
3. Benowitz NL. Nicotine addiction. *N Engl J Med*. 2010;362:2295–303.
4. Remarks prepared for testimony before a U.S. House Energy and Commerce Subcommittee on FDA Regulation of Electronic Nicotine Delivery Systems and Investigation of Vaping Illnesses, Acting Commissioner of Food and Drugs, Norman E. “Ned” Sharpless. 2019. <https://www.fda.gov/news-events/press-announcements/remarks-prepared-testimony-us-house-energy-and-commerce-subcommittee-fda-regulation-electronic>. Accessed 14 Oct 2019.
5. Bhatnagar A, Payne TJ, Robertson RM. Is there a role for electronic cigarettes in tobacco cessation? *J Am Heart Assoc*. 2019;8:e012742.
6. Benowitz NL. Pharmacology of nicotine: addiction, smoking-induced disease, and therapeutics. *Annu Rev Pharmacol Toxicol*. 2009;49:57–71.
7. Batra A, Klingler K, Landfeldt B, Friederich HM, Westin A, Danielsson T. Smoking reduction treatment with 4-mg nicotine gum: a double-blind, randomized, placebo-controlled study. *Clin Pharmacol Ther*. 2005;78:689–96.
8. Hays JT, Croghan IT, Schroeder DR, Offord KP, Hurt RD, Wolter TD, et al. Over-the-counter nicotine patch therapy for smoking cessation: results from randomized, double-blind, placebo-controlled, and open label trials. *Am J Public Health*. 1999;89:1701–7.
9. Benowitz NL, Porchet H, Sheiner L, Jacob P. Nicotine absorption and cardiovascular effects with smokeless tobacco use: comparison with cigarettes and nicotine gum. *Clin Pharmacol Ther*. 1988;44:23–8.
10. Benowitz NL, Chan K, Denaro CP, Jacob P. Stable isotope method for studying transdermal drug absorption: the nicotine patch. *Clin Pharmacol Ther*. 1991;50:286–93.
11. Rose JE, Mukhin AG, Lokitz SJ, Turkington TG, Hershkovic J, Behm FM, et al. Kinetics of brain nicotine accumulation in dependent and nondependent smokers assessed with PET and cigarettes containing <sup>11</sup>C-nicotine. *Proc Natl Acad Sci USA*. 2010;107:5190–5.
12. Xian H, Scherrer JF, Madden PAF, Lyons MJ, Tsuang M, True WR, et al. The heritability of failed smoking cessation and nicotine withdrawal in twins who smoked and attempted to quit. *Nicotine Tob Res*. 2003;5:245–54.
13. Heitjan DF, Asch DA, Ray R, Rukstalis M, Patterson F, Lerman C. Cost-effectiveness of pharmacogenetic testing to tailor smoking-cessation treatment. *Pharmacogenom J*. 2008;8:391–9.
14. Lerman C, Schnoll RA, Hawk LW, Cinciripini P, George TP, Wileyto EP, et al. Use of the nicotine metabolite ratio as a genetically informed biomarker of response to nicotine patch or varenicline for smoking cessation: a randomised, double-blind placebo-controlled trial. *Lancet Respir Med*. 2015;3:131–8.
15. Hukkanen J, Jacob P, Benowitz NL. Metabolism and disposition kinetics of nicotine. *Pharmacol Rev*. 2005;57:79–115.
16. Mroziwicz M, Tyndale RF. Pharmacogenetics: a tool for identifying genetic factors in drug dependence and response to treatment. *Addict Sci Clin Pract*. 2010;5:17–29.
17. Benowitz NL. Cigarette smoking and cardiovascular disease: pathophysiology and implications for treatment. *Prog Cardiovasc Dis*. 2003;46:91–111.

18. Benowitz NL, Dains KM, Dempsey D, Yu L, Jacob P. Estimation of nicotine dose after low-level exposure using plasma and urine nicotine metabolites. *Cancer Epidemiol Biomark Prev.* 2010;19:1160–6.
19. Zhao P, Zhang L, Grillo JA, Liu Q, Bullock JM, Moon YJ, et al. Applications of physiologically based pharmacokinetic (PBPK) modeling and simulation during regulatory review. *Clin Pharmacol Ther.* 2011;89:259–67.
20. Lott D, Lehr T, Dingemans J, Krause A. Modeling tolerance development for the effect on heart rate of the selective  $S1P_1$  receptor modulator ponesimod. *Clin Pharmacol Ther.* 2018;103:1083–92.
21. Tega Y, Yamazaki Y, Akanuma S, Kubo Y, Hosoya K. Impact of nicotine transport across the blood-brain barrier: carrier-mediated transport of nicotine and interaction with central nervous system drugs. *Biol Pharm Bull.* 2018;41:1330–6.
22. Benowitz NL, Jacob P. Metabolism of nicotine to cotinine studied by a dual stable isotope method. *Clin Pharmacol Ther.* 1994;56:483–93.
23. Gubner NR, Kozar-Konieczna A, Szoltysek-Boldys I, Slodczyk-Mankowska E, Goniewicz J, Sobczak A, et al. Cessation of alcohol consumption decreases rate of nicotine metabolism in male alcohol-dependent smokers. *Drug Alcohol Depend.* 2016;163:157–64.
24. De Schepper PJ, Van Hecken A, Daenens P, Van Rossum JM. Kinetics of cotinine after oral and intravenous administration to man. *Eur J Clin Pharmacol.* 1987;31:583–8.
25. Benowitz NL, Jacob P. Nicotine and cotinine elimination pharmacokinetics in smokers and nonsmokers. *Clin Pharmacol Ther.* 1993;53:316–23.
26. Simon DL, Iglauer A. The acute effect of chewing tobacco and smoking in habitual users. *Ann N Y Acad Sci.* 1960;90:119–32.
27. Porchet HC, Benowitz NL, Sheiner LB. Pharmacodynamic model of tolerance: application to nicotine. *J Pharmacol Exp Ther.* 1988;244:231–6.
28. Morjaria Y, Irwin WJ, Barnett PX, Chan RS, Conway BR. In vitro release of nicotine from chewing gum formulations. *Dissolution Technol.* 2004;11:12–5.
29. Houseman TH. Studies of cigarette smoke transfer using radioisotopically labelled tobacco constituents part II: the transference of radioisotopically labelled nicotine to cigarette smoke. *Beitrag zur Tab Int Contrib to Tob Res.* 1973;7:142–7.
30. Wishart DS, Knox C, Guo AC, Shrivastava S, Hassanali M, Stothard P, et al. DrugBank: a comprehensive resource for in silico drug discovery and exploration. *Nucleic Acids Res.* 2006;34:D668–72.
31. Nielsen HM, Rassing MR. Nicotine permeability across the buccal TR146 cell culture model and porcine buccal mucosa in vitro: effect of pH and concentration. *Eur J Pharm Sci.* 2002;16:151–7.
32. Alharbi O, Xu Y, Goodacre R. Simultaneous multiplexed quantification of nicotine and its metabolites using surface enhanced Raman scattering. *Analyst.* 2014;139:4820–7.
33. Zissimos AM, Abraham MH, Barker MC, Box KJ, Tam KY. Calculation of Abraham descriptors from solvent-water partition coefficients in four different systems; evaluation of different methods of calculation. *J Chem Soc Perkin Trans.* 2002;2:470–7.
34. Svensson CK. Clinical pharmacokinetics of nicotine. *Clin Pharmacol Ther.* 1987;12:30–40.
35. Benowitz NL, Kuyt F, Jacob P, Jones RT, Osman AL. Cotinine disposition and effects. *Clin Pharmacol Ther.* 1983;34:604–11.
36. Yamazaki H, Inoue K, Hashimoto M, Shimada T. Roles of CYP2A6 and CYP2B6 in nicotine C-oxidation by human liver microsomes. *Arch Toxicol.* 1999;73:65–70.
37. Fukami T, Nakajima M, Yoshida R, Tsuchiya Y, Fujiki Y, Katoh M, et al. A novel polymorphism of human CYP2A6 gene CYP2A6\*17 has an amino acid substitution (V365M) that decreases enzymatic activity in vitro and in vivo. *Clin Pharmacol Ther.* 2004;76:519–27.
38. Hosono H, Kumondai M, Maekawa M, Yamaguchi H, Mano N, Oda A, et al. Functional characterization of 34 CYP2A6 allelic variants by assessment of nicotine C-oxidation and coumarin 7-hydroxylation activities. *Drug Metab Dispos.* 2017;45:279–85.
39. Murphy SE, Raulinaitis V, Brown KM. Nicotine 5'-oxidation and methyl oxidation by P450 2A enzymes. *Drug Metab Dispos.* 2005;33:1166–73.
40. Xu C, Rao YS, Xu B, Hoffmann E, Jones J, Sellers EM, et al. An in vivo pilot study characterizing the new CYP2A6\*7, \*8, and \*10 alleles. *Biochem Biophys Res Commun.* 2002;290:318–24.
41. Dicke KE, Skrlin SM, Murphy SE. Nicotine and 4-(methylnitrosamino)-1-(3-pyridyl)-butanone metabolism by cytochrome P450 2B6. *Drug Metab Dispos.* 2005;33:1760–4.
42. Rodgers T, Rowland M. Mechanistic approaches to volume of distribution predictions: understanding the processes. *Pharm Res.* 2007;24:918–33.
43. Rodgers T, Leahy D, Rowland M. Physiologically based pharmacokinetic modeling 1: predicting the tissue distribution of moderate-to-strong bases. *J Pharm Sci.* 2005;94:1259–76.
44. Rodgers T, Rowland M. Physiologically-based pharmacokinetic modeling 2: predicting the tissue distribution of acids, very weak bases, neutrals and zwitterions. *J Pharm Sci.* 2006;95:1238–57.
45. Hindmarsh AC, Reynolds DR, Serban R, Woodward CS, Gardner DJ, Cohen SD, et al. Open systems pharmacology suite manual, version 7.4.; 2018.
46. Armitage AK, Dollery CT, George CF, Houseman TH, Lewis PJ, Turner DM. Absorption and metabolism of nicotine from cigarettes. *Br Med J.* 1975;4:313–6.
47. Hammond D, Fong GT, Cummings KM, O'Connor RJ, Giovino GA, McNeill A. Cigarette yields and human exposure: a comparison of alternative testing regimens. *Cancer Epidemiol Biomark Prev.* 2006;15:1495–501.
48. Benowitz NL. Compensatory smoking of low-yield cigarettes. In: Burns DM, Benowitz NL, Amacher RH (eds) *Smok Tob Control Monogr No 13.* 2001: p. 39–64.
49. Robinson DE, Balter NJ, Schwartz SL. A physiologically based pharmacokinetic model for nicotine and cotinine in man. *J Pharmacokinetic Biopharm.* 1992;20:591–609.
50. Plowchalk DR, Andersen ME, DeBethizy JD. A physiologically based pharmacokinetic model for nicotine disposition in the Sprague-Dawley rat. *Toxicol Appl Pharmacol.* 1992;116:177–88.
51. Yamazaki H, Horiuchi K, Takano R, Nagano T, Shimizu M, Kitajima M, et al. Human blood concentrations of cotinine, a bio-monitoring marker for tobacco smoke, extrapolated from nicotine metabolism in rats and humans and physiologically based pharmacokinetic modeling. *Int J Environ Res Public Health.* 2010;7:3406–21.
52. Teeguarden JG, Housand CJ, Smith JN, Hinderliter PM, Gunawan R, Timchalk CA. A multi-route model of nicotine-cotinine pharmacokinetics, pharmacodynamics and brain nicotinic acetylcholine receptor binding in humans. *Regul Toxicol Pharmacol.* 2013;65:12–28.
53. Gajewska M, Worth A, Urani C, Briesen H, Schramm K-W. The acute effects of daily nicotine intake on heart rate—a toxicokinetic and toxicodynamic modelling study. *Regul Toxicol Pharmacol.* 2014;70:312–24.
54. Zanger UM, Klein K, Saussele T, Bliedernicht J, Hofmann MH, Schwab M. Polymorphic CYP2B6: molecular mechanisms and emerging clinical significance. *Pharmacogenomics.* 2007;8:743–59.
55. Eichelbaum M, Ingelman-Sundberg M, Evans WE. Pharmacogenomics and individualized drug therapy. *Annu Rev Med.* 2006;57:119–37.

56. Kovar L, Schmidt S, Derendorf H. Maßgeschneidert: Die Pharmakogenetik ebnet den Weg für erfolgreiche individualisierte Interventionen. *DAZ*. 2018; p. 3000–4.
57. Cullen KA, Ambrose BK, Gentzke AS, Apelberg BJ, Jamal A, King BA. Use of electronic cigarettes and any tobacco product among middle and high school students: United States, 2011–2018. *Am J Public Health*. 2018;67:1277.
58. Meyer M, Schneekener S, Ludewig B, Kuepfer L, Lippert J. Using expression data for quantification of active processes in PBPK modeling. *Drug Metab Dispos*. 2012;40:892–901.
59. Schorp MK. Summary of literature data on smoking topography. In: Pick W, Houlgate P, Schorp MK, et al. (eds) *A Rev Hum Smok Behav Recomm a New ISO Stand Mach Smok Cigarettes*; Rep Ad Hoc WG9 Smok R Beirut, Lebanon Am Univ Beirut. 2005; p. 28–50.
60. Ross KC, Dempsey DA, St. Helen G, Delucchi K, Benowitz NL. The influence of puff characteristics, nicotine dependence, and rate of nicotine metabolism on daily nicotine exposure in African American smokers. *Cancer Epidemiol Biomark Prev*. 2016;25:936–43.
61. St Helen G, Ross KC, Dempsey DA, Havel CM, Jacob P, Benowitz NL. Nicotine delivery and vaping behavior during ad libitum E-cigarette access. *Tob Regul Sci*. 2016;2:363–76.
62. Bannon YB, Corish J, Corrigan OI, Devane JG, Kavanagh M, Mulligan S. Transdermal delivery of nicotine in normal human volunteers: a single dose and multiple dose study. *Eur J Clin Pharmacol*. 1989;37:285–90.
63. Vandewalle G, Middleton B, Rajaratnam SMW, Stone BM, Thorleifsdottir B, Arendt J, et al. Robust circadian rhythm in heart rate and its variability: influence of exogenous melatonin and photoperiod. *J Sleep Res*. 2007;16:148–55.
64. Ambre JJ, Belknap SM, Nelson J, Ruo TI, Shin SG, Atkinson AJ. Acute tolerance to cocaine in humans. *Clin Pharmacol Ther*. 1988;44:1–8.
65. Haass M, Kübler W. Nicotine and sympathetic neurotransmission. *Cardiovasc Drugs Ther*. 1996;10:657–65.
66. Stéphan-Blanchard E, Bach V, Telliez F, Chardon K. Perinatal nicotine/smoking exposure and carotid chemoreceptors during development. *Respir Physiol Neurobiol*. 2013;185:110–9.
67. Benowitz NL, Gourlay SG. Cardiovascular toxicity of nicotine: implications for nicotine replacement therapy. *J Am Coll Cardiol*. 1997;29:1422–31.
68. Fagerström KO, Schneider NG, Lunell E. Effectiveness of nicotine patch and nicotine gum as individual versus combined treatments for tobacco withdrawal symptoms. *Psychopharmacology*. 1993;111:271–7.
69. Stein PK, Rottman JN, Kleiger RE. Effect of 21 mg transdermal nicotine patches and smoking cessation on heart rate variability. *Am J Cardiol*. 1996;77:701–5.
70. Mendelson JH, Goletiani N, Sholar MB, Siegel AJ, Mello NK. Effects of smoking successive low- and high-nicotine cigarettes on hypothalamic-pituitary-adrenal axis hormones and mood in men. *Neuropsychopharmacology*. 2008;33:749–60.
71. Benowitz NL, Kuyt F, Jacob P. Circadian blood nicotine concentrations during cigarette smoking. *Clin Pharmacol Ther*. 1982;32:758–64.
72. Feyerabend C, Ings RM, Russel MA. Nicotine pharmacokinetics and its application to intake from smoking. *Br J Clin Pharmacol*. 1985;19:239–47.
73. St Helen G, Nardone N, Addo N, Dempsey D, Havel C, Jacob P BN. Differences in nicotine intake and effects from electronic and combustible cigarettes among dual users. *Addiction*. 2019. <https://doi.org/10.1111/add.14884>. [Epub ahead of print].
74. Zevin S, Jacob P, Benowitz N. Cotinine effects on nicotine metabolism. *Clin Pharmacol Ther*. 1997;61:649–54.
75. Curvall M, Elwin CE, Kazemi-Vala E, Warholm C, Enzell CR. The pharmacokinetics of cotinine in plasma and saliva from non-smoking healthy volunteers. *Eur J Clin Pharmacol*. 1990;38:281–7.
76. Benowitz NL, Jacob P, Fong I, Gupta S. Nicotine metabolic profile in man: comparison of cigarette smoking and transdermal nicotine. *J Pharmacol Exp Ther*. 1994;268:296–303.
77. Du D. A single-dose, crossover-design bioequivalence study comparing two nicotine gum formulations in healthy subjects. *Adv Ther*. 2018;35:1169–80.
78. Dautzenberg B, Nides M, Kienzler J-L, Callens A. Pharmacokinetics, safety and efficacy from randomized controlled trials of 1 and 2 mg nicotine bitartrate lozenges (Nicotinell). *BMC Clin Pharmacol*. 2007;7:11.
79. Gupta SK, Benowitz NL, Jacob P, Rolf CN, Gorsline J. Bioavailability and absorption kinetics of nicotine following application of a transdermal system. *Br J Clin Pharmacol*. 1993;36:221–7.
80. Gilbert DG, Robinson JH, Chamberlin CL, Spielberger CD. Effects of smoking/nicotine on anxiety, heart rate, and lateralization of EEG during a stressful movie. *Psychophysiology*. 1989;26:311–20.
81. St Helen G, Havel C, Dempsey DA, Jacob P, Benowitz NL. Nicotine delivery, retention and pharmacokinetics from various electronic cigarettes. *Addiction*. 2016;111:535–44.

## Part III

### DISCUSSION, OUTLOOK AND CONCLUSIONS

This part provides a comprehensive discussion of the results presented in this thesis as well as future outlooks and overall conclusions.



## DISCUSSION AND OUTLOOK

---

Buprenorphine, fentanyl and nicotine are frequently applied in the treatment of pain and smoking cessation, respectively [115–119, 156, 158, 162]. Still, treatment issues and ambiguities in PK characteristics exist in both adult and pediatric patients [47, 116, 117, 120, 123, 129, 130, 135, 158, 163]. In addition, pediatric drug therapy in general remains a huge challenge with off-label use in pediatrics as well as medication errors in pediatric and neonatal intensive care units representing significant health care issues [42, 45, 46, 64]. Thus, there is a strong need for advances in pediatric medical care, particularly for young infants and neonates [44]. For this, the PK and PD of drugs need to be further investigated in pediatric populations, which may increase evidence base for pharmacotherapy [44]. However, ethical, cost and time challenges impede the conduct of clinical trials [11, 49, 51–53]. Here, pharmacometric approaches such as PBPK modeling can step in to investigate the PK of drugs, inform study design, predict unexplored exposure scenarios, bridge knowledge gaps and thereby improve decision-making in drug development and optimize drug therapy [6, 9–12, 75, 81].

The presented work had three major objectives: (1) to gain new insights into the PK of the two opioid analgetics buprenorphine and fentanyl in adult and pediatric patients by leveraging PBPK modeling, (2) to further explore and support the value of PBPK modeling to predict individual and mean plasma concentration-time profiles as well as PK parameters of pediatric patients including full-term and preterm neonates and (3) to simulate and evaluate differences in nicotine brain tissue concentrations and heart rate profiles after pulmonary, oral and transdermal nicotine administration.

### 4.1 PBPK MODELING OF BUPRENORPHINE IN ADULT AND PEDIATRIC PATIENTS

In the first publication presented in this thesis, a parent-metabolite PBPK model of buprenorphine was developed for adult and pediatric patients. The adult PBPK model was used to predict buprenorphine and norbuprenorphine plasma concentration-time profiles after intravenous administration and further applied to assess the DDI liability of buprenorphine and its metabolite with the perpetrator drugs clarithromycin and itraconazole. After extrapolation to pediatric populations, the PBPK model was leveraged to investigate the performance of PK predictions for children and preterm neonates which were superior to results from two allometric scaling approaches [1].

The application of PBPK modeling in the field of special populations including pediatrics has been increasing lately [7]. Its use in regulatory NDA submissions has been established [9] and its application in pediatric drug development further suggested, provided its robustness and reliability, calling for additional research in this area [32].

Project I presents a pediatric PBPK modeling case example of a drug that is frequently used to treat pediatric patients and cleared via various different elimination pathways [117, 131, 132]. The developed adult PBPK model was extrapolated to pediatric populations and used to predict plasma concentration-time profiles of buprenorphine in a child population (4.6–7.5 years) and in individual preterm neonates (27–34 weeks postmenstrual age). Model predicted plasma profile trajectories and the corresponding area under the concentration-time curve (AUC) values were in close agreement with observed data for most patients, demonstrating the potential of PBPK modeling to predict plasma profiles and AUC values in individual patients of the vulnerable preterm neonate population [1]. The good model performance (evaluated both visually and with quantitative measures) thus provides further evidence for PK predictions in pediatric patients and supports the use of PBPK modeling in MIDD [1, 11].

Hereby, the option to integrate knowledge on enzyme and transporter maturation in PBPK models [13] offers great advantages for PK predictions especially in young infants and neonates. In these populations, rapid changes in organ maturation and enzyme abundances may result in rapid changes of PK parameters: For instance, Mukherjee et al. and Völler et al. showed that CL parameters can significantly change within the first few days after birth due to maturation processes [92, 127]. Such changes in anatomy and physiology during the 72-hour long-term infusions investigated in Project I could be considered in the performed PBPK simulations for the aging virtual preterm neonate populations as implemented in the applied software [29].

As indicated, allometric scaling has been shown to provide accurate predictions for adolescent patients [11, 79, 83], while uncertainties increase in younger pediatric populations [11]. For infants, full-term neonates and preterm neonates, CL predictions with unadjusted allometric scaling usually exhibit more discrepancies as rapid developmental changes occur and CL mechanisms are yet immature [11, 79, 83]. Here, PBPK modeling presents a mechanistic physiological framework allowing the integration of maturation processes (e.g., enzyme and transporter ontogeny functions; cf., Figure 1.2) and thus, can be favorable if LADME processes of the drug are sufficiently well characterized [11, 25, 83, 164]. The case study in Project I supports this argument as PBPK modeling provided more accurate predictions of buprenorphine plasma concentrations compared to allometric scaling for both the child and particularly the preterm neonate population. ADE allometric scaling was superior to the unadjusted allometric scaling approach albeit less precise than PBPK model predictions.

In a recent work by Wu and Peters on pediatric extrapolation for children less than two years of age, PBPK modeling also showed superior performance to simple allometric scaling and population pharmacokinetic pediatric extrapolation while the performance was comparable to ADE allometric scaling [165]. Additional work on this topic, particularly regarding predictions in neonatal patients and for transporter substrates [137] as well as research on transporter ontogeny profiles [30] is thus of great interest for further evaluations. In addition, PK data for model evaluation is helpful to confirm model predictions and usually still needed to support regulatory decisions [11, 32].

Bi and coworkers have recently suggested the incorporation of MIDD approaches in all phases of pediatric drug development to decrease the required number of enrolled patients and to optimize the success rate of pediatric clinical trials [11]. The FDA MIDD pilot program yielded successful examples in industry where MIDD approaches including pediatric PBPK modeling led to savings in time and resources [8]. Here, it should be kept in mind, that dose predictions in pediatrics based on the “exposure-matching” strategy rely on the assumption of a similar exposure-response relationship for safety and efficacy in pediatric and adult patients [11, 110, 111].

As outlined in Section 1.5, the pediatric PBPK modeling workflow comprises the development of an adult PBPK model that should be thoroughly evaluated with clinical data before extrapolation to pediatric populations [25, 31, 37, 104]. Leong and colleagues described, that one reason for CL mispredictions in pediatric patients may be attributed to inadequacies of the underlying adult PBPK model [31]. Poor model predictions with the adult PBPK model may transition into poor predictions with the scaled pediatric PBPK model [25, 32, 37]. The importance of a thorough adult PBPK model evaluation has also been stressed by Maharaj and Edginton [25], highlighting this step as a key for adequate pediatric PBPK model development [25, 31]. In the presented work, the PBPK model was developed based on available *in vitro*, *in silico* and clinical *in vivo* data (plasma concentrations and fractions of dose excreted in urine), combining the “top-down” and “bottom-up” approaches (“middle-out” approach [12, 24, 40, 52]). The good prediction performance of the adult buprenorphine PBPK model, as shown in Section 3.1, was hence particularly meaningful for the pediatric PBPK model prediction results.

As the output of a PBPK simulation is the composition of various modeled processes, which in turn are simplifications of complex physiologic mechanisms and include several assumptions, many factors (e.g., parameter uncertainties, missing mechanisms, etc.) can impact prediction accuracy [32]. Thus, detailed knowledge on LADME processes of the drug including elimination mechanisms and metabolizing enzymes as well as on age-dependent physiological changes is crucial for extrapolation of PBPK models from adult to pediatric patients [12, 32, 39]. The importance of such detailed knowledge on processes affecting the drug’s disposition to obtain accurate predictions could be observed also within this modeling work. For example, as described in Section 1.6, the PK of buprenorphine is affected by various CYP and UGT enzymes including CYP3A4, CYP3A7, CYP2C8, UGT1A1, UGT1A3 and UGT2B7 [131, 132]. As these enzymes exhibit unique ontogeny profiles during maturation [91], the metabolic pathways were not subsumed to a single CL mechanism but integrated separately in the developed PBPK model to allow successful model extrapolation and model predictions in pediatric patients. Of note, since genetic polymorphisms that can affect drug metabolism have been described for some of the involved enzymes (e.g., CYP2C8 and UGT1A1 [166, 167]), detailed knowledge on a patient’s genotypes could further improve future individual PBPK model predictions.

A published DDI study from buprenorphine with the perpetrator drug rifampicin (inhibitor and inducer of CYP2C8, CYP3A4, UGT1A1, UGT1A3 and the efflux

transporter P-glycoprotein (P-gp), among others [168–171]) was used to additionally evaluate the adult PBPK model. The ratio of the predicted and observed DDI effect of concomitant rifampicin administration on buprenorphine AUC was 0.96, reflecting a good prediction of the *in vivo* DDI scenario.

As described, PBPK models can be leveraged to gain information on a drug's DDI potential [6, 12]. This data can be used to inform the design of DDI studies, obviate specific DDI *in vivo* studies and/or support drug therapy and labeling [8, 172–174]. In this work, the developed adult PBPK model was employed to simulate DDIs of buprenorphine in yet unexplored DDI scenarios with the frequently used strong CYP<sub>3A4</sub> inhibitors clarithromycin and itraconazole to gain further insights into the PK of buprenorphine and its active metabolite norbuprenorphine (see Section 3.1).

Since DDI data are often not available in pediatric populations [39], PBPK model simulations can be particularly helpful in pediatric drug development [11]. In the presented project, DDI simulations were performed only for an adult population as the perpetrator drug models were built and evaluated only for the application in non-pediatric populations [1, 170]. Moreover, due to missing observed data, DDI modeling performance of the developed buprenorphine model could only be evaluated for the adult PBPK model. However, the developed models were made publicly available, allowing its application and evaluation in future investigations of DDI scenarios in various patient populations.

Initial investigations on buprenorphine's exposure-response relationship in the treatment of the neonatal abstinence syndrome have suggested that buprenorphine concentrations were the primary driver of its PD effect [135]. Hence, the PBPK model could prospectively serve as a basis to develop an extended PBPK/PD model to quantify and assess the PD effect of buprenorphine. Furthermore, besides its application in *in silico* investigations of DDI scenarios, the developed buprenorphine PBPK model may be used to support the design of future clinical trials and novel formulations for both adult and pediatric populations [1].

#### 4.2 PBPK MODELING OF FENTANYL IN ADULT AND PEDIATRIC PATIENTS

The second publication presented in this thesis focused on PBPK modeling of fentanyl and norfentanyl in adult and pediatric patients and aimed to gain new insights into the PK of fentanyl. The adult PBPK model was built and evaluated with plasma concentration-time profiles from various clinical settings including intravenous bolus, short infusion and long-term infusion administrations. Fraction of dose excreted in urine data was additionally integrated to inform renal excretion processes. Furthermore, the PBPK model was employed to predict a published DDI study with fentanyl and the CYP<sub>3A4</sub> inhibitor voriconazole for further model evaluation. Here, the moderate increase in fentanyl AUC as well as the strong decrease in norfentanyl exposure was successfully predicted with the PBPK model [2].

After model evaluation, the PBPK model was used to generate knowledge and support hypotheses on the PK of fentanyl and its clinical application regarding a potentially fatal ADR. First, the developed model supports the assumption of an

“extra-norfentanyl metabolic pathway”, suggesting the involvement of additional metabolic mechanisms (besides CYP<sub>3A4</sub>) in the degradation of fentanyl, and the existence of yet unknown metabolites [2, 129]. The fraction metabolized ( $f_m$ ) through CYP<sub>3A4</sub>, which represents a crucial parameter for DDI predictions [12], was estimated to be only about one third, while the extra-norfentanyl metabolic pathway accounted for ~60% of fentanyl elimination in model simulations. About 7% of the administered fentanyl dose was excreted unchanged renally (see Section 3.2), consistent with literature reports [130, 142, 175].

The occurrence of the ADR chest wall rigidity in pediatric populations after fentanyl administration has been observed mostly after bolus injections [125]. To investigate differences in peak arterial plasma concentrations between intravenous bolus injections and short infusions in neonates, an adult PBPK model was built and evaluated before extrapolation to pediatric populations [2]. Similarly as in Project I, the developed adult PBPK model showed good prediction performance. Both arterial and venous fentanyl blood plasma concentration-time profiles as well as fractions of fentanyl dose excreted unchanged in urine were successfully described and predicted, setting the foundation for PBPK modeling in pediatric populations. After model extrapolation, mean plasma concentration-time profiles and CL parameters from child, infant and neonate populations were used to evaluate the pediatric PBPK model predictions. Finally, the model was leveraged to simulate peak arterial plasma concentrations in a neonatal population after fentanyl administration. Model simulations showed large differences in maximum arterial plasma concentrations (up to 7-fold) between intravenous bolus injections and short infusions, which might partly explain the increased occurrence of the ADR after fentanyl bolus administrations.

Of note, ontogeny functions of transporters have not yet been integrated in the modeling software PK-Sim<sup>®</sup> [91]. However, the efflux transporter P-gp was part of the fentanyl PBPK model. Hence, a recently published ontogeny function of P-gp [176] was incorporated for model extrapolation to pediatric populations, accounting for differences in P-gp abundance between adult and pediatric patients. As described by Bi et al., the accumulated experience with MIDD applications may lead to new policy development and refinement [11]. Here, the two case examples of buprenorphine and fentanyl pediatric PBPK modeling could further promote the use of the PBPK modeling approach as a predictive tool in the pharmacometric toolbox [24].

Besides its application in MID<sub>3</sub>, PBPK modeling has been proposed to facilitate personalized medicine within the concept of model-informed precision dosing (MIPD) and could tackle clinical dosing issues in the future, yet requiring accurate predictions at the individual patient level [39, 177, 178].

In Section 3.1, the potential of PBPK modeling to predict plasma concentration-time profiles and AUC values in individual patients (here, preterm neonates) has been successfully demonstrated. Simulation results with the fentanyl PBPK model (see Section 3.2) showed that predictions of mean population CL values in full-term and preterm neonates were accurate while predictions of individual CL values remained very challenging and scattered around the mean. This could have been due to the high inter-individual variability in abundances of involved

enzymes (see [Figure 1.2](#) and [\[91\]](#)). As the specific enzyme (and transporter) expression of an individual patient is usually not known, simulations of drug exposure for individual patients based on population mean enzyme expression levels and individual demographic information can lead to mispredictions. Hence, the application of PBPK modeling in MIPD has been tied to the collection of more detailed physiological information [\[39, 177\]](#). The fact that information on age and weight alone might not be predictive enough for accurate individual PK simulations has also been discussed for ibuprofen in a study by Mahmood on allometric scaling [\[85\]](#).

However, this obstacle could be tackled in the future, combining PBPK modeling with the concept of liquid biopsies [\[178–181\]](#). Plasma-derived exosomes as liquid biopsies can be used to quantify the *in vivo* activity of hepatic enzymes via collection of a diagnostically amenable biofluid [\[178, 179\]](#). Subsequently, the information on protein expressions in individual patients may be leveraged to inform PBPK model predictions [\[178, 180, 181\]](#). This approach could be a highly valuable tool to enhance individual predictions with PBPK modeling and to promote its application in MIPD in the future [\[39, 178–181\]](#).

While the vast majority of predicted fentanyl and norfentanyl plasma concentration-time profiles as well as fraction of fentanyl dose excreted unchanged in urine were in close concordance with observed data, discrepancies could be observed for some studies. These might be partially explained by the design of the included clinical studies since over 70% of the observed mean plasma concentration-time profiles were collected from patients during surgeries or post-surgery (see [Table 1](#) and [2](#) in [Section 3.2](#)). Consequently, many patients received various co-medications (e.g., isoflurane, succinylcholine or thiopental) that could have affected fentanyl and norfentanyl disposition.

The developed fentanyl PBPK model could already be successfully leveraged in subsequent investigations in the working group: After coupling the PBPK model with a skin permeation model, plasma concentrations during transdermal fentanyl administration and effects of dermal heat application on fentanyl exposure were *in situ* predicted based on *in vitro* dissolution and permeation experiments (*in vitro-in vivo* extrapolation). Moreover, as the fentanyl PBPK model is publicly available, it can be further employed in future investigations of fentanyl and norfentanyl PK in both adult and pediatric populations [\[2\]](#).

It is a general paradigm, when generating new PK information such as clinical data (e.g., from DDI studies), this knowledge should be incorporated to refine the PBPK model following the iterative learn, confirm and refine cycle [\[11, 12, 70, 73\]](#). Meaningful simulation results rely on the availability of high-quality data and benefit from experimental clinical studies [\[38\]](#). While PBPK models can already be used to inform study designs, predict exposure in various populations, investigate DDI scenarios and make dosing recommendations for different patient populations, observed clinical data are still required to evaluate and refine models, enhance confidence in model simulations and support regulatory decisions in the drug development process [\[10, 12, 32\]](#).

### 4.3 PBPK MODELING OF NICOTINE BRAIN TISSUE CONCENTRATIONS

In Project III, a parent-metabolite PBPK model of nicotine and its major metabolite cotinine, covering various routes of administration (i.e., intravenous, oral, transdermal and pulmonary), was developed and expanded to study the PK/PD relationship regarding heart rate changes during nicotine intake. The PBPK/PD model was able to describe and predict both nicotine and cotinine plasma concentrations and fractions excreted in urine, nicotine brain tissue concentrations and heart rate profiles. After comprehensive model evaluation with 102 nicotine and cotinine concentration–time and heart rate–time profiles, the model was applied to simulate and evaluate differences in nicotine brain tissue concentration patterns during pulmonary, oral and transdermal nicotine administration (see Figure 6 in Section 3.3). The model also represents the first nicotine PBPK/PD model predicting nicotine plasma concentration–time and heart rate–time profiles after the use of electronic cigarettes. Finally, the feasibility to integrate the intravenous (bolus injections and infusions), pulmonary (cigarettes), oral (nicotine solutions, capsules and gums) and transdermal (nicotine patches) administration routes in a single model was demonstrated [3].

In all three presented projects, the available clinical data were split into an internal training and an external test dataset. This approach can help to detect model misspecifications during the model development process [182]. Clinical data were allocated in a way to inform all physiological processes integrated in the PBPK models (e.g., contribution of metabolic pathways, renal excretion, etc.) and to cover wide dose ranges, as has been recently performed [170, 182–184].

The extensive data availability of nicotine and cotinine plasma concentration–time profiles after various routes of nicotine administration, fractions of nicotine and cotinine dose excreted in urine and cotinine plasma concentration–time profiles after cotinine administration allowed a comprehensive model evaluation that emphasizes the good PBPK model performance (see Section 3.3 and Section A.3). Moreover, the developed parent-metabolite PBPK model showed a fraction of nicotine metabolized to cotinine of ~75% [3], aligning well with literature reports for nicotine to cotinine conversion of 70–80% [185–187].

As described in Section 1.1, the mathematical description of the organism in PBPK modeling enables the simulation of tissue-specific drug concentrations at the target site, which can be particularly useful when drug tissue concentrations are challenging to determine [6, 12, 39]. However, as outlined by Jones and Rowland-Yeo, models developed solely based on *in silico* partition coefficients may describe an “oversimplification” of tissue kinetics [12]. This in turn can result in significant discrepancies between simulated and observed *in vivo* tissue levels even though plasma concentration–time data were included in model building [12, 36, 37]. Thus, the opportunity to integrate available nicotine *in vivo* brain tissue distribution data in the PBPK model development was a valuable step to increase confidence in simulated tissue concentrations [12, 13, 37]. Yet, it should be noted, that the incorporated observed nicotine tissue concentration–time profile only covered measurements during the first ten minutes after a single puff of combustible cigarettes [163]. As a result, extrapolations in brain tissue simulations to multiple dose applications and longer timeframes have to be interpreted with caution [3].

Due to its mechanistic setting, PBPK models also offer the possibility to translate physiological and other sources of variability into PK variability of a drug in a population of interest [12]. With that, the expected variability can be investigated based on prior knowledge on the study population, biochemical variability and other factors that might impact the PK [12].

In this work, observed differences in PK variability between intravenous, oral, transdermal and pulmonary nicotine intake [159, 161, 188, 189] were evaluated with the developed nicotine PBPK model. In the past, high variability in nicotine plasma concentrations observed in studies with combustible cigarettes has been attributed to differences in puffing behavior (called smoking topography) [190]. This hypothesis was evaluated, comparing model predicted and observed variability in nicotine plasma concentrations. The predicted variabilities for plasma concentrations after intravenous, oral and transdermal nicotine administration better aligned with the observed ones as compared to the findings after pulmonary nicotine intake studies (see Section 3.3). Here, the observed variability in plasma concentrations after pulmonary administration was substantially higher than predicted. This was probably because model predicted variability was only allowed to result from anatomic and physiological differences while variability in inhaled nicotine dose (due to smoking topography differences) was set to zero. Consequently, it can be assumed that the higher observed variability in nicotine plasma concentrations after pulmonary nicotine intake resulted from differences in smoking topography. This supports literature reports that suggest differences in smoking topography result in differences in nicotine plasma concentrations [3, 191, 192].

As described in Section 1.6, the positive chronotropic effect of nicotine results in an elevated heart rate, which represents a commonly monitored PD marker in clinical trials [152, 159–161]. To describe and predict the positive chronotropic effect of nicotine, the developed PBPK model was expanded by a direct-link PD model [3]. For this, the PD model was coded and implemented in the MoBi<sup>®</sup> software based on a recently published PD heart rate tolerance model with circadian rhythm [3, 193]. The direct-link model was selected since nicotine peak concentrations and peaks of the positive chronotropic effect occur at about the same time [194, 195]. In addition, the observed decrease in sensitivity towards nicotine intake, that results in a reduction of nicotine's positive chronotropic effect intensity (clockwise hysteresis loop), necessitated the implementation of an acute tolerance mechanism [193, 196]. After PBPK/PD model development, the model was further applied to simulate and evaluate differences in elevated baseline heart rates between two different smoking protocols (cigarettes smoked 30 minutes or 2 hours apart) as well as oral and transdermal nicotine administration (see Section 3.3 and Section A.3). The successful extension of the nicotine PBPK model with the PD heart rate model may further support and encourage the use of PBPK/PD modeling and simulation in future studies.

## CONCLUSIONS

---

The presented work provides new insights into the PK of buprenorphine, fentanyl and nicotine in both adult and pediatric patient populations. Among others, PBPK modeling was leveraged to assess DDI scenarios of buprenorphine and norbuprenorphine, to support the presence of an extra-norfentanyl metabolic pathway in the elimination of fentanyl and to investigate peak arterial plasma concentrations of fentanyl in neonates after intravenous short infusions and bolus administrations. Moreover, the nicotine PBPK/PD model was employed to simulate and evaluate differences in brain tissue concentrations and heart rate levels after various routes of nicotine administration.

In addition, the value of PBPK modeling to predict plasma concentration-time profiles in pediatric patient populations was explored. The developed pediatric PBPK models of buprenorphine and fentanyl were used for successful predictions of plasma profiles and PK parameters (population mean and individual data) of children, infants, full-term neonates and preterm neonates. With that, this thesis adds further knowledge, experience and evidence within the field of pediatric PBPK modeling, an area that has been pointed out for further elaboration [137]. While PBPK model predictions of CL and plasma concentrations in individuals are possible, accurate results without detailed information on the individual patient, including metabolic enzyme and transporter abundances, remain challenging. Hence, further research approaches advancing, evaluating and supporting the use of PBPK modeling in this field are required, could increase the understanding of drug PK and facilitate the application of PBPK modeling in MID<sub>3</sub> and pharmacotherapy [11, 32, 182].

All three developed PBPK models have been made publicly available, contributing to an extended library of thoroughly developed PBPK models of CYP, UGT and transporter substrates that can be used by the research community to further investigate unexplored exposure scenarios, assess novel DDIs and simulate “what if” scenarios [38, 138]. When new PK data becomes available, the developed PBPK models may be evaluated in additional populations within the learn, confirm and refine cycle [12]. Furthermore, the models can be employed in future research efforts to optimize the design and evaluation of studies, thereby supporting drug development and ultimately improving pharmacotherapy for adult and pediatric patients [6, 31, 99].



## BIBLIOGRAPHY

---

- [1] Lukas Kovar, Christina Schräpel, Dominik Selzer, Yvonne Kohl, Robert Bals, Matthias Schwab, and Thorsten Lehr. "Physiologically-Based Pharmacokinetic (PBPK) Modeling of Buprenorphine in Adults, Children and Preterm Neonates." In: *Pharmaceutics* 12.6 (2020), p. 578. ISSN: 1999-4923. DOI: [10.3390/pharmaceutics12060578](https://doi.org/10.3390/pharmaceutics12060578).
- [2] Lukas Kovar, Andreas Weber, Michael Zemlin, Yvonne Kohl, Robert Bals, Bernd Meibohm, Dominik Selzer, and Thorsten Lehr. "Physiologically-Based Pharmacokinetic (PBPK) Modeling Providing Insights into Fentanyl Pharmacokinetics in Adults and Pediatric Patients." In: *Pharmaceutics* 12.10 (2020), p. 908. ISSN: 1999-4923. DOI: [10.3390/pharmaceutics12100908](https://doi.org/10.3390/pharmaceutics12100908).
- [3] Lukas Kovar, Dominik Selzer, Hannah Britz, Neal Benowitz, Gideon St. Helen, Yvonne Kohl, Robert Bals, and Thorsten Lehr. "Comprehensive Parent-Metabolite PBPK/PD Modeling Insights into Nicotine Replacement Therapy Strategies." In: *Clinical pharmacokinetics* 59.9 (2020), pp. 1119–1134. ISSN: 1179-1926. DOI: [10.1007/s40262-020-00880-4](https://doi.org/10.1007/s40262-020-00880-4).
- [4] Alex O. Holcombe. "Contributorship, Not Authorship: Use CRediT to Indicate Who Did What." In: *Publications* 7.3 (2019), p. 48. ISSN: 2304-6775. DOI: [10.3390/publications7030048](https://doi.org/10.3390/publications7030048).
- [5] Amy Brand, Liz Allen, Micah Altman, Marjorie Hlava, and Jo Scott. "Beyond authorship: attribution, contribution, collaboration, and credit." In: *Learned Publishing* 28.2 (2015), pp. 151–155. ISSN: 09531513. DOI: [10.1087/20150211](https://doi.org/10.1087/20150211).
- [6] Hannah M Jones et al. "Application of PBPK modelling in drug discovery and development at Pfizer." In: *Xenobiotica; the fate of foreign compounds in biological systems* 42.1 (2012), pp. 94–106. ISSN: 1366-5928. DOI: [10.3109/00498254.2011.627477](https://doi.org/10.3109/00498254.2011.627477).
- [7] Eman El-Khateeb, Susan Burkhill, Susan Murby, Hamza Amirat, Amin Rostami-Hodjegan, and Amais Ahmad. "Physiological-based pharmacokinetic modeling trends in pharmaceutical drug development over the last 20-years; in-depth analysis of applications, organizations, and platforms." In: *Biopharmaceutics & drug disposition* 42.4 (2021), pp. 107–117. ISSN: 1099-081X. DOI: [10.1002/bdd.2257](https://doi.org/10.1002/bdd.2257).
- [8] Gerald R. Galluppi et al. "Industrial Perspective on the Benefits Realized From the FDA's Model-Informed Drug Development Paired Meeting Pilot Program." In: *Clinical pharmacology and therapeutics* 110.5 (2021), pp. 1172–1175. ISSN: 1532-6535. DOI: [10.1002/cpt.2265](https://doi.org/10.1002/cpt.2265).

- [9] Manuela Grimstein, Yuching Yang, Xinyuan Zhang, Joseph Grillo, Shiew-Mei Huang, Issam Zineh, and Yaning Wang. "Physiologically Based Pharmacokinetic Modeling in Regulatory Science: An Update From the U.S. Food and Drug Administration's Office of Clinical Pharmacology." In: *Journal of pharmaceutical sciences* 108.1 (2019), pp. 21–25. ISSN: 1520-6017. DOI: [10.1016/j.xphs.2018.10.033](https://doi.org/10.1016/j.xphs.2018.10.033).
- [10] C. Wagner, P. Zhao, Y. Pan, V. Hsu, J. Grillo, S. M. Huang, and V. Sinha. "Application of Physiologically Based Pharmacokinetic (PBPK) Modeling to Support Dose Selection: Report of an FDA Public Workshop on PBPK." In: *CPT: pharmacometrics & systems pharmacology* 4.4 (2015), pp. 226–30. ISSN: 2163-8306. DOI: [10.1002/psp4.33](https://doi.org/10.1002/psp4.33).
- [11] Youwei Bi et al. "Role of Model-Informed Drug Development in Pediatric Drug Development, Regulatory Evaluation, and Labeling." In: *Journal of clinical pharmacology* 59 Suppl 1.S1 (2019), S104–S111. ISSN: 1552-4604. DOI: [10.1002/jcph.1478](https://doi.org/10.1002/jcph.1478).
- [12] HM Jones and K Rowland-Yeo. "Basic concepts in physiologically based pharmacokinetic modeling in drug discovery and development." In: *CPT: pharmacometrics & systems pharmacology* 2.8 (2013), e63. ISSN: 2163-8306. DOI: [10.1038/psp.2013.41](https://doi.org/10.1038/psp.2013.41).
- [13] J. S. Barrett, O. Della Casa Alberighi, S. Läer, and B. Meibohm. "Physiologically based pharmacokinetic (PBPK) modeling in children." In: *Clinical pharmacology and therapeutics* 92.1 (2012), pp. 40–9. ISSN: 1532-6535. DOI: [10.1038/clpt.2012.64](https://doi.org/10.1038/clpt.2012.64).
- [14] R. L. Lalonde et al. "Model-based drug development." In: *Clinical pharmacology and therapeutics* 82.1 (2007), pp. 21–32. ISSN: 0009-9236. DOI: [10.1038/sj.clpt.6100235](https://doi.org/10.1038/sj.clpt.6100235).
- [15] Jack W. Scannell, Alex Blanckley, Helen Boldon, and Brian Warrington. "Diagnosing the decline in pharmaceutical R&D efficiency." In: *Nature reviews. Drug discovery* 11.3 (2012), pp. 191–200. ISSN: 1474-1784. DOI: [10.1038/nrd3681](https://doi.org/10.1038/nrd3681).
- [16] P A Milligan et al. "Model-based drug development: a rational approach to efficiently accelerate drug development." In: *Clinical pharmacology and therapeutics* 93.6 (2013), pp. 502–14. ISSN: 1532-6535. DOI: [10.1038/clpt.2013.54](https://doi.org/10.1038/clpt.2013.54).
- [17] EFPIA MID3 Workgroup et al. "Good Practices in Model-Informed Drug Discovery and Development: Practice, Application, and Documentation." In: *CPT: pharmacometrics & systems pharmacology* 5.3 (2016), pp. 93–122. ISSN: 2163-8306. DOI: [10.1002/psp4.12049](https://doi.org/10.1002/psp4.12049).
- [18] Joo Yeon Lee et al. "Impact of pharmacometric analyses on new drug approval and labelling decisions: a review of 198 submissions between 2000 and 2008." In: *Clinical pharmacokinetics* 50.10 (2011), pp. 627–35. ISSN: 1179-1926. DOI: [10.2165/11593210-000000000-00000](https://doi.org/10.2165/11593210-000000000-00000).

- [19] Yaning Wang, Hao Zhu, Rajanikanth Madabushi, Qi Liu, Shiew-Mei Huang, and Issam Zineh. "Model-Informed Drug Development: Current US Regulatory Practice and Future Considerations." In: *Clinical pharmacology and therapeutics* 105.4 (2019), pp. 899–911. ISSN: 1532-6535. DOI: [10.1002/cpt.1363](https://doi.org/10.1002/cpt.1363).
- [20] Jeffrey S Barrett, Michael J Fossler, K David Cadieu, and Marc R Gastonguay. "Pharmacometrics: a multidisciplinary field to facilitate critical thinking in drug development and translational research settings." In: *Journal of clinical pharmacology* 48.5 (2008), pp. 632–49. ISSN: 0091-2700. DOI: [10.1177/0091270008315318](https://doi.org/10.1177/0091270008315318).
- [21] Piet H van der Graaf. "CPT: Pharmacometrics and Systems Pharmacology." In: *CPT: pharmacometrics & systems pharmacology* 1.9 (2012), e8. ISSN: 2163-8306. DOI: [10.1038/psp.2012.8](https://doi.org/10.1038/psp.2012.8).
- [22] Malcolm Rowland, Carl Peck, and Geoffrey Tucker. "Physiologically-based pharmacokinetics in drug development and regulatory science." In: *Annual review of pharmacology and toxicology* 51 (2011), pp. 45–73. ISSN: 1545-4304. DOI: [10.1146/annurev-pharmtox-010510-100540](https://doi.org/10.1146/annurev-pharmtox-010510-100540).
- [23] L Kuepfer, C Niederal, T Wendl, J-F Schlender, S Willmann, J Lippert, M Block, T Eissing, and D Teutonico. "Applied Concepts in PBPK Modeling: How to Build a PBPK/PD Model." In: *CPT: pharmacometrics & systems pharmacology* 5.10 (2016), pp. 516–531. ISSN: 2163-8306. DOI: [10.1002/psp4.12134](https://doi.org/10.1002/psp4.12134).
- [24] H M Jones, Y Chen, C Gibson, T Heimbach, N Parrott, S A Peters, J Snoeys, V V Upreti, M Zheng, and S D Hall. "Physiologically based pharmacokinetic modeling in drug discovery and development: a pharmaceutical industry perspective." In: *Clinical pharmacology and therapeutics* 97.3 (2015), pp. 247–62. ISSN: 1532-6535. DOI: [10.1002/cpt.37](https://doi.org/10.1002/cpt.37).
- [25] A R Maharaj and A N Edginton. "Physiologically based pharmacokinetic modeling and simulation in pediatric drug development." In: *CPT: pharmacometrics & systems pharmacology* 3.11 (2014), e150. ISSN: 2163-8306. DOI: [10.1038/psp.2014.45](https://doi.org/10.1038/psp.2014.45).
- [26] J. Valentin. "Basic anatomical and physiological data for use in radiological protection: reference values: ICRP Publication 89: Approved by the Commission in September 2001." In: *Annals of the ICRP* 32.3-4 (2002), pp. 1–277. ISSN: 0146-6453. DOI: [10.1016/S0146-6453\(03\)00002-2](https://doi.org/10.1016/S0146-6453(03)00002-2).
- [27] P. Zhao et al. "Applications of physiologically based pharmacokinetic (PBPK) modeling and simulation during regulatory review." In: *Clinical pharmacology and therapeutics* 89.2 (2011), pp. 259–67. ISSN: 1532-6535. DOI: [10.1038/clpt.2010.298](https://doi.org/10.1038/clpt.2010.298).
- [28] Jörg Lippert et al. "Open Systems Pharmacology Community-An Open Access, Open Source, Open Science Approach to Modeling and Simulation in Pharmaceutical Sciences." In: *CPT: pharmacometrics & systems pharmacology* 8.12 (2019), pp. 878–882. ISSN: 2163-8306. DOI: [10.1002/psp4.12473](https://doi.org/10.1002/psp4.12473).

- [29] *Open Systems Pharmacology Suite Manual*. 2021. URL: <https://raw.githubusercontent.com/Open-Systems-Pharmacology/OSPSuite.Documentation/master/OpenSystemsPharmacologySuite.pdf> (visited on 08/24/2021).
- [30] Ibrahim Ince, Juri Solodenko, Sebastian Frechen, André Dallmann, Christoph Niederalt, Jan Schlender, Rolf Burghaus, Jörg Lippert, and Stefan Willmann. "Predictive Pediatric Modeling and Simulation Using Ontogeny Information." In: *Journal of clinical pharmacology* 59 Suppl 1.S1 (2019), S95–S103. ISSN: 1552-4604. DOI: [10.1002/jcph.1497](https://doi.org/10.1002/jcph.1497).
- [31] R Leong, M L T Vieira, P Zhao, Y Mulugeta, C S Lee, S-M Huang, and G J Burckart. "Regulatory experience with physiologically based pharmacokinetic modeling for pediatric drug trials." In: *Clinical pharmacology and therapeutics* 91.5 (2012), pp. 926–31. ISSN: 1532-6535. DOI: [10.1038/clpt.2012.19](https://doi.org/10.1038/clpt.2012.19).
- [32] Venkata Yellepeddi, Joseph Rower, Xiaoxi Liu, Shaun Kumar, Jahidur Rashid, and Catherine M. T. Sherwin. "State-of-the-Art Review on Physiologically Based Pharmacokinetic Modeling in Pediatric Drug Development." In: *Clinical pharmacokinetics* 58.1 (2019), pp. 1–13. ISSN: 1179-1926. DOI: [10.1007/s40262-018-0677-y](https://doi.org/10.1007/s40262-018-0677-y).
- [33] Trudy Rodgers, David Leahy, and Malcolm Rowland. "Physiologically based pharmacokinetic modeling 1: predicting the tissue distribution of moderate-to-strong bases." In: *Journal of pharmaceutical sciences* 94.6 (2005), pp. 1259–76. ISSN: 0022-3549. DOI: [10.1002/jps.20322](https://doi.org/10.1002/jps.20322).
- [34] Trudy Rodgers and Malcolm Rowland. "Physiologically based pharmacokinetic modelling 2: predicting the tissue distribution of acids, very weak bases, neutrals and zwitterions." In: *Journal of pharmaceutical sciences* 95.6 (2006), pp. 1238–57. ISSN: 0022-3549. DOI: [10.1002/jps.20502](https://doi.org/10.1002/jps.20502).
- [35] Walter Schmitt. "General approach for the calculation of tissue to plasma partition coefficients." In: *Toxicology in vitro: an international journal published in association with BIBRA* 22.2 (2008), pp. 457–67. ISSN: 0887-2333. DOI: [10.1016/j.tiv.2007.09.010](https://doi.org/10.1016/j.tiv.2007.09.010).
- [36] Samuel L M Arnold and Frederick Buckner. "Hydroxychloroquine for Treatment of SARS-CoV-2 Infection? Improving Our Confidence in a Model-Based Approach to Dose Selection." In: *Clinical and translational science* 13.4 (2020), pp. 642–645. ISSN: 1752-8062. DOI: [10.1111/cts.12797](https://doi.org/10.1111/cts.12797).
- [37] A. R. Maharaj, J. S. Barrett, and A. N. Edginton. "A workflow example of PBPK modeling to support pediatric research and development: case study with lorazepam." In: *The AAPS journal* 15.2 (2013), pp. 455–64. ISSN: 1550-7416. DOI: [10.1208/s12248-013-9451-0](https://doi.org/10.1208/s12248-013-9451-0).
- [38] Feras Khalil and Stephanie Läer. "Physiologically based pharmacokinetic modeling: methodology, applications, and limitations with a focus on its role in pediatric drug development." In: *Journal of biomedicine & biotechnology* 2011 (2011), p. 907461. ISSN: 1110-7251. DOI: [10.1155/2011/907461](https://doi.org/10.1155/2011/907461).

- [39] Kefei Wang, Kun Jiang, Xiaoyi Wei, Yulan Li, Tiejie Wang, and Yang Song. "Physiologically Based Pharmacokinetic Models Are Effective Support for Pediatric Drug Development." In: *AAPS PharmSciTech* 22.6 (2021), p. 208. ISSN: 1530-9932. DOI: [10.1208/s12249-021-02076-w](https://doi.org/10.1208/s12249-021-02076-w).
- [40] Nikolaos Tsamandouras, Amin Rostami-Hodjegan, and Leon Aarons. "Combining the 'bottom up' and 'top down' approaches in pharmacokinetic modelling: fitting PBPK models to observed clinical data." In: *British journal of clinical pharmacology* 79.1 (2015), pp. 48–55. ISSN: 1365-2125. DOI: [10.1111/bcp.12234](https://doi.org/10.1111/bcp.12234).
- [41] Verica Ivanovska, Carin M. A. Rademaker, Liset van Dijk, and Aukje K. Mantel-Teeuwisse. "Pediatric drug formulations: a review of challenges and progress." In: *Pediatrics* 134.2 (2014), pp. 361–72. ISSN: 1098-4275. DOI: [10.1542/peds.2013-3225](https://doi.org/10.1542/peds.2013-3225).
- [42] S Balan, M A Hassali, and V S L Mak. "Challenges in pediatric drug use: A pharmacist point of view." In: *Research in social & administrative pharmacy: RSAP* 13.3 (2017), pp. 653–655. ISSN: 1934-8150. DOI: [10.1016/j.sapharm.2016.06.014](https://doi.org/10.1016/j.sapharm.2016.06.014).
- [43] Marie-Claude Grégoire and G Allen Finley. "Why were we abandoned? Orphan drugs in paediatric pain." In: *Paediatrics & child health* 12.2 (2007), pp. 95–6. ISSN: 1205-7088. DOI: [10.1093/pch/12.2.95](https://doi.org/10.1093/pch/12.2.95).
- [44] Robert M. Ward, Daniel K. Benjamin, Jonathan M. Davis, Richard L. Gorman, Ralph Kauffman, Gregory L. Kearns, Mary Dianne Murphy, and Catherine M. T. Sherwin. "The Need for Pediatric Drug Development." In: *The Journal of pediatrics* 192 (2018), pp. 13–21. ISSN: 1097-6833. DOI: [10.1016/j.jpeds.2017.08.011](https://doi.org/10.1016/j.jpeds.2017.08.011).
- [45] Anwar A. Alghamdi, Richard N. Keers, Adam Sutherland, and Darren M. Ashcroft. "Prevalence and Nature of Medication Errors and Preventable Adverse Drug Events in Paediatric and Neonatal Intensive Care Settings: A Systematic Review." In: *Drug safety* 42.12 (2019), pp. 1423–1436. ISSN: 1179-1942. DOI: [10.1007/s40264-019-00856-9](https://doi.org/10.1007/s40264-019-00856-9).
- [46] Hadar Nir-Neuman, Ibrahim Abu-Kishk, Michal Toledano, Eli Heyman, Tomer Ziv-Baran, and Matitihu Berkovitch. "Unlicensed and Off-Label Medication Use in Pediatric and Neonatal Intensive Care Units: No Change Over a Decade." In: *Advances in therapy* 35.7 (2018), pp. 1122–1132. ISSN: 1865-8652. DOI: [10.1007/s12325-018-0732-y](https://doi.org/10.1007/s12325-018-0732-y).
- [47] Viviane G. Nasr and Jonathan M. Davis. "Anesthetic use in newborn infants: the urgent need for rigorous evaluation." In: *Pediatric research* 78.1 (2015), pp. 2–6. ISSN: 1530-0447. DOI: [10.1038/pr.2015.58](https://doi.org/10.1038/pr.2015.58).
- [48] David B. Fogel. "Factors associated with clinical trials that fail and opportunities for improving the likelihood of success: A review." In: *Contemporary clinical trials communications* 11.July (2018), pp. 156–164. ISSN: 2451-8654. DOI: [10.1016/j.conctc.2018.08.001](https://doi.org/10.1016/j.conctc.2018.08.001).

- [49] Robert M. Ward and Catherine M. T. Sherwin. "Ethics of drug studies in the newborn." In: *Paediatric drugs* 17.1 (2015), pp. 37–42. ISSN: 1179-2019. DOI: [10.1007/s40272-014-0099-8](https://doi.org/10.1007/s40272-014-0099-8).
- [50] Fei Tang, Chee M. Ng, Henrietta S. Bada, and Markos Leggas. "Clinical pharmacology and dosing regimen optimization of neonatal opioid withdrawal syndrome treatments." In: *Clinical and translational science* 14.4 (2021), pp. 1231–1249. ISSN: 1752-8062. DOI: [10.1111/cts.12994](https://doi.org/10.1111/cts.12994).
- [51] Matthew M Laughon, Debbie Avant, Nidhi Tripathi, Christoph P Hornik, Michael Cohen-Wolkowicz, Reese H Clark, P Brian Smith, and William Rodriguez. "Drug labeling and exposure in neonates." In: *JAMA pediatrics* 168.2 (2014), pp. 130–6. ISSN: 2168-6211. DOI: [10.1001/jamapediatrics.2013.4208](https://doi.org/10.1001/jamapediatrics.2013.4208).
- [52] Robin Michelet, Jan Van Bocxlaer, and An Vermeulen. "PBPK in Preterm and Term Neonates: A Review." In: *Current pharmaceutical design* 23.38 (2017), pp. 5943–5954. DOI: [10.2174/1381612823666171009143840](https://doi.org/10.2174/1381612823666171009143840).
- [53] J D Momper, Y Mulugeta, and G J Burckart. "Failed Pediatric Drug Development Trials." In: *Clinical pharmacology and therapeutics* 98.3 (2015), pp. 245–51. ISSN: 1532-6535. DOI: [10.1002/cpt.142](https://doi.org/10.1002/cpt.142).
- [54] John T. Wilson. "Questions and Answers on Labeling of Drugs for Children." In: *Drug Information Journal* 33.2 (1999), pp. 375–383. ISSN: 0092-8615. DOI: [10.1177/009286159903300208](https://doi.org/10.1177/009286159903300208).
- [55] H Shirkey. "Therapeutic orphans." In: *The Journal of pediatrics* 72.1 (1968), pp. 119–20. ISSN: 0022-3476. DOI: [10.1016/s0022-3476\(68\)80414-7](https://doi.org/10.1016/s0022-3476(68)80414-7).
- [56] Lainie Friedman Ross. "50 Years Ago in The Journal of Pediatrics: Editorial Comment: Therapeutic Orphans." In: *The Journal of pediatrics* 192.January (2018), p. 59. ISSN: 1097-6833. DOI: [10.1016/j.jpeds.2017.07.017](https://doi.org/10.1016/j.jpeds.2017.07.017).
- [57] JT Wilson. "Pragmatic assessment of medicines available for young children and pregnant or breast-feeding women." In: *Basic and therapeutic aspects of perinatal pharmacology*. Ed. by PL Morselli, S Garattini, and F Sereni. New York: Raven Press, 1975, pp. 411–21.
- [58] Jamie T. Gilman and Peter Gal. "Pharmacokinetic and pharmacodynamic data collection in children and neonates. A quiet frontier." In: *Clinical pharmacokinetics* 23.1 (1992), pp. 1–9. ISSN: 0312-5963. DOI: [10.2165/00003088-199223010-00001](https://doi.org/10.2165/00003088-199223010-00001).
- [59] American Academy of Pediatrics. Committee on Drugs. "Guidelines for the Ethical Conduct of Studies to Evaluate Drugs in Pediatric Populations." In: *Pediatrics* 60 (1977), pp. 91–101.
- [60] *The Belmont Report. Ethical Principles and Guidelines for the Protection of Human Subjects of Research. The National Commission for the Protection of Human Subjects of Biomedical and Behavioral Research.* 1979. URL: <https://www.hhs.gov/ohrp/sites/default/files/the-belmont-report-508c-FINAL.pdf> (visited on 08/13/2021).

- [61] *Best Pharmaceuticals for Children Act*. 2002. URL: <https://www.congress.gov/107/plaws/publ109/PLAW-107publ109.pdf> (visited on 08/13/2021).
- [62] *Pediatric Research Equity Act of 2003*. 2003. URL: <https://www.congress.gov/108/plaws/publ155/PLAW-108publ155.pdf> (visited on 08/13/2021).
- [63] *REGULATION (EC) No 1901/2006 OF THE EUROPEAN PARLIAMENT AND OF THE COUNCIL of 12 December 2006 on medicinal products for paediatric use and amending Regulation (EEC) No 1768/92, Directive 2001/20/EC, Directive 2001/83/EC and Regulation (EC) No 726/2004*. 2006. URL: <https://eur-lex.europa.eu/legal-content/EN/TXT/PDF/?uri=CELEX:32006R1901&from=EN> (visited on 08/13/2021).
- [64] Kathleen A. Neville, Daniel A.C. Frattarelli, Jeffrey L. Galinkin, Thomas P. Green, Timothy D. Johnson, Ian M. Paul, and John N. Van Den Anker. "Off-Label Use of Drugs in Children." In: *Pediatrics* 133:3 (2014), pp. 563–567. ISSN: 0031-4005. DOI: [10.1542/peds.2013-4060](https://doi.org/10.1542/peds.2013-4060).
- [65] Ahmad Ismail. "The Challenges of Providing Effective Pain Management for Children in the Pediatric Intensive Care Unit." In: *Pain management nursing: official journal of the American Society of Pain Management Nurses* 17:6 (2016), pp. 372–383. ISSN: 1532-8635. DOI: [10.1016/j.pmn.2016.08.005](https://doi.org/10.1016/j.pmn.2016.08.005).
- [66] Soumya Swaminathan and Banu Rekha. "Pediatric tuberculosis: global overview and challenges." In: *Clinical infectious diseases: an official publication of the Infectious Diseases Society of America* 50 Suppl 3:S3 (2010), S184–94. ISSN: 1537-6591. DOI: [10.1086/651490](https://doi.org/10.1086/651490).
- [67] Aaron N Sachs, Debbie Avant, Catherine S Lee, William Rodriguez, and M Dianne Murphy. "Pediatric information in drug product labeling." In: *JAMA* 307:18 (2012), pp. 1914–5. ISSN: 1538-3598. DOI: [10.1001/jama.2012.3435](https://doi.org/10.1001/jama.2012.3435).
- [68] Mariëlle Eerdeken, Christoph Beuter, Claudia Lefeber, and John van den Anker. "The challenge of developing pain medications for children: therapeutic needs and future perspectives." In: *Journal of pain research* 12 (2019), pp. 1649–1664. ISSN: 1178-7090. DOI: [10.2147/JPR.S195788](https://doi.org/10.2147/JPR.S195788).
- [69] *Best Pharmaceuticals for Children Act and Pediatric Research Equity Act. July 2016. Status Report to Congress. Department of Health and Human Services Food and Drug Administration*. 2016. URL: <https://www.fda.gov/media/99184/download> (visited on 08/13/2021).
- [70] *E11(R1) Addendum: Clinical Investigation of Medicinal Products in the Pediatric Population - Guidance for Industry*. U.S. Department of Health and Human Services, Food and Drug Administration, Center for Drug Evaluation and Research (CDER), Center for Biologics Evaluation and Research (CBER). 2018. URL: <https://www.fda.gov/media/101398/download> (visited on 08/13/2021).
- [71] Danna Chan, Vijay Ivaturi, and Janel Long-Boyle. "The time is now: model-based dosing to optimize drug therapy." In: *International Journal of Pharmacokinetics* 2:4 (2017), pp. 213–215. ISSN: 2053-0846. DOI: [10.4155/ipk-2017-0011](https://doi.org/10.4155/ipk-2017-0011).

- [72] Craig R. Rayner et al. "Model-Informed Drug Development for Anti-Infectives: State of the Art and Future." In: *Clinical pharmacology and therapeutics* 109.4 (2021), pp. 867–891. ISSN: 1532-6535. DOI: [10.1002/cpt.2198](https://doi.org/10.1002/cpt.2198).
- [73] L B Sheiner. "Learning versus confirming in clinical drug development." In: *Clinical pharmacology and therapeutics* 61.3 (1997), pp. 275–91. ISSN: 0009-9236. DOI: [10.1016/S0009-9236\(97\)90160-0](https://doi.org/10.1016/S0009-9236(97)90160-0).
- [74] Carl C. Peck, William H. Barr, Leslie Z. Benet, Jerry Collins, Robert E. Desjardins, Daniel E. Furst, John G. Harter, Gerhard Levy, Thomas Ludden, and John H. Rodman. "Opportunities for integration of pharmacokinetics, pharmacodynamics, and toxicokinetics in rational drug development." In: *Journal of clinical pharmacology* 34.2 (1994), pp. 111–9. ISSN: 0091-2700. DOI: [10.1002/j.1552-4604.1994.tb03974.x](https://doi.org/10.1002/j.1552-4604.1994.tb03974.x).
- [75] Sriram Krishnaswami, Daren Austin, Oscar Della Pasqua, Marc R. Gastonguay, Jogarao Gobburu, Piet H. van der Graaf, Daniele Ouellet, Stacey Tannenbaum, and Sandra A. G. Visser. "MID<sub>3</sub>: Mission Impossible or Model-Informed Drug Discovery and Development? Point-Counterpoint Discussions on Key Challenges." In: *Clinical pharmacology and therapeutics* 107.4 (2020), pp. 762–772. ISSN: 1532-6535. DOI: [10.1002/cpt.1788](https://doi.org/10.1002/cpt.1788).
- [76] Saskia N de Wildt. "Profound changes in drug metabolism enzymes and possible effects on drug therapy in neonates and children." In: *Expert opinion on drug metabolism & toxicology* 7.8 (2011), pp. 935–48. ISSN: 1744-7607. DOI: [10.1517/17425255.2011.577739](https://doi.org/10.1517/17425255.2011.577739).
- [77] Saskia N. de Wildt, D. Tibboel, and J. S. Leeder. "Drug metabolism for the paediatrician." In: *Archives of disease in childhood* 99.12 (2014), pp. 1137–42. ISSN: 1468-2044. DOI: [10.1136/archdischild-2013-305212](https://doi.org/10.1136/archdischild-2013-305212).
- [78] European Medicines Agency. *Guideline on the role of pharmacokinetics in the development of medicinal products in the paediatric population*. 2006. URL: [http://www.ema.europa.eu/docs/en\\_GB/document\\_library/Scientific\\_guideline/2009/09/WC500003066.pdf](http://www.ema.europa.eu/docs/en_GB/document_library/Scientific_guideline/2009/09/WC500003066.pdf) (visited on 08/19/2021).
- [79] Jeremiah D Momper, Yeruk Mulugeta, Dionna J Green, Alyson Karesh, Kevin M Krudys, Hari C Sachs, Lynn P Yao, and Gilbert J Burckart. "Adolescent dosing and labeling since the Food and Drug Administration Amendments Act of 2007." In: *JAMA pediatrics* 167.10 (2013), pp. 926–32. ISSN: 2168-6211. DOI: [10.1001/jamapediatrics.2013.465](https://doi.org/10.1001/jamapediatrics.2013.465).
- [80] Brian J. Anderson and Nick H. G. Holford. "Understanding dosing: children are small adults, neonates are immature children." In: *Archives of disease in childhood* 98.9 (2013), pp. 737–44. ISSN: 1468-2044. DOI: [10.1136/archdischild-2013-303720](https://doi.org/10.1136/archdischild-2013-303720).
- [81] Rianne Oostenbrink and Saskia N. de Wildt. "Drug trials: Kids are no little adults and not all kids are the same." In: *Journal of clinical epidemiology* 71 (2016), pp. 111–2. ISSN: 1878-5921. DOI: [10.1016/j.jclinepi.2015.06.020](https://doi.org/10.1016/j.jclinepi.2015.06.020).

- [82] Michel Tod, Vincent Jullien, and Gérard Pons. "Facilitation of drug evaluation in children by population methods and modelling." In: *Clinical pharmacokinetics* 47.4 (2008), pp. 231–43. ISSN: 0312-5963. DOI: [10.2165/00003088-200847040-00002](https://doi.org/10.2165/00003088-200847040-00002).
- [83] Elisa A. M. Calvier, Elke H. J. Krekels, Pyry A. J. Väitalo, Amin Rostami-Hodjegan, Dick Tibboel, Meindert Danhof, and Catherijne A. J. Knibbe. "Allometric Scaling of Clearance in Paediatric Patients: When Does the Magic of 0.75 Fade?" In: *Clinical pharmacokinetics* 56.3 (2017), pp. 273–285. ISSN: 1179-1926. DOI: [10.1007/s40262-016-0436-x](https://doi.org/10.1007/s40262-016-0436-x).
- [84] Iftekhar Mahmood. "Prediction of drug clearance in children from adults: a comparison of several allometric methods." In: *British journal of clinical pharmacology* 61.5 (2006), pp. 545–57. ISSN: 0306-5251. DOI: [10.1111/j.1365-2125.2006.02622.x](https://doi.org/10.1111/j.1365-2125.2006.02622.x).
- [85] Iftekhar Mahmood. "Prediction of drug clearance in children: impact of allometric exponents, body weight, and age." In: *Therapeutic drug monitoring* 29.3 (2007), pp. 271–8. ISSN: 0163-4356. DOI: [10.1097/FTD.0b013e318042d3c4](https://doi.org/10.1097/FTD.0b013e318042d3c4).
- [86] Iftekhar Mahmood, Carl-Michael Staschen, and Kosalaram Goteti. "Prediction of drug clearance in children: an evaluation of the predictive performance of several models." In: *The AAPS journal* 16.6 (2014), pp. 1334–43. ISSN: 1550-7416. DOI: [10.1208/s12248-014-9667-7](https://doi.org/10.1208/s12248-014-9667-7).
- [87] Iftekhar Mahmood. "Prediction of Drug Clearance in Premature and Mature Neonates, Infants, and Children  $\leq 2$  Years of Age: A Comparison of the Predictive Performance of 4 Allometric Models." In: *Journal of clinical pharmacology* 56.6 (2016), pp. 733–9. ISSN: 1552-4604. DOI: [10.1002/jcph.652](https://doi.org/10.1002/jcph.652).
- [88] Ronald N. Hines. "The ontogeny of drug metabolism enzymes and implications for adverse drug events." In: *Pharmacology & therapeutics* 118.2 (2008), pp. 250–67. ISSN: 0163-7258. DOI: [10.1016/j.pharmthera.2008.02.005](https://doi.org/10.1016/j.pharmthera.2008.02.005).
- [89] Ulrich M. Zanger and Matthias Schwab. "Cytochrome P450 enzymes in drug metabolism: regulation of gene expression, enzyme activities, and impact of genetic variation." In: *Pharmacology & therapeutics* 138.1 (2013), pp. 103–41. ISSN: 1879-016X. DOI: [10.1016/j.pharmthera.2012.12.007](https://doi.org/10.1016/j.pharmthera.2012.12.007).
- [90] J. Andrew Williams, Barbara J. Ring, Varon E. Cantrell, David R. Jones, James Eckstein, Kenneth Ruterbories, Mitchell A. Hamman, Stephen D. Hall, and Steven A. Wrighton. "Comparative metabolic capabilities of CYP3A4, CYP3A5, and CYP3A7." In: *Drug metabolism and disposition: the biological fate of chemicals* 30.8 (2002), pp. 883–91. ISSN: 0090-9556. DOI: [10.1124/dmd.30.8.883](https://doi.org/10.1124/dmd.30.8.883).
- [91] *PK-Sim® Ontogeny Database, Version 7.3*. 2018. URL: <https://github.com/Open-Systems-Pharmacology/OSPSuite.Documentation/blob/master/PK-SimOntogenyDatabaseVersion7.3.pdf> (visited on 03/25/2020).

- [92] A. Mukherjee, T. Dombi, B. Wittke, and R. Lalonde. "Population pharmacokinetics of sildenafil in term neonates: evidence of rapid maturation of metabolic clearance in the early postnatal period." In: *Clinical pharmacology and therapeutics* 85.1 (2009), pp. 56–63. ISSN: 1532-6535. DOI: [10.1038/clpt.2008.177](https://doi.org/10.1038/clpt.2008.177).
- [93] Roosmarijn F. W. De Cock, Karel Allegaert, Catherine M. T. Sherwin, Elisabet I. Nielsen, Matthijs de Hoog, Johannes N. van den Anker, Meindert Danhof, and Catherijne A. J. Knibbe. "A neonatal amikacin covariate model can be used to predict ontogeny of other drugs eliminated through glomerular filtration in neonates." In: *Pharmaceutical research* 31.3 (2014), pp. 754–67. ISSN: 1573-904X. DOI: [10.1007/s11095-013-1197-y](https://doi.org/10.1007/s11095-013-1197-y).
- [94] Janneke M. Brussee et al. "Predicting CYP3A-mediated midazolam metabolism in critically ill neonates, infants, children and adults with inflammation and organ failure." In: *British journal of clinical pharmacology* 84.2 (2018), pp. 358–368. ISSN: 1365-2125. DOI: [10.1111/bcp.13459](https://doi.org/10.1111/bcp.13459).
- [95] Troy E. Gibbons and Benjamin D. Gold. "The use of proton pump inhibitors in children: a comprehensive review." In: *Paediatric drugs* 5.1 (2003), pp. 25–40. ISSN: 1174-5878. DOI: [10.2165/00128072-200305010-00003](https://doi.org/10.2165/00128072-200305010-00003).
- [96] Gavril W. Pasternak, Richard J. Bodnar, Janet A. Clark, and Charles E. Inturrisi. "Morphine-6-glucuronide, a potent mu agonist." In: *Life sciences* 41.26 (1987), pp. 2845–9. ISSN: 0024-3205. DOI: [10.1016/0024-3205\(87\)90431-0](https://doi.org/10.1016/0024-3205(87)90431-0).
- [97] R. Klimas and G. Mikus. "Morphine-6-glucuronide is responsible for the analgesic effect after morphine administration: a quantitative review of morphine, morphine-6-glucuronide, and morphine-3-glucuronide." In: *British journal of anaesthesia* 113.6 (2014), pp. 935–44. ISSN: 1471-6771. DOI: [10.1093/bja/aeu186](https://doi.org/10.1093/bja/aeu186).
- [98] Elizabeth M. Lancaster, Jonathan R. Hiatt, and Ali Zarrinpar. "Acetaminophen hepatotoxicity: an updated review." In: *Archives of toxicology* 89.2 (2015), pp. 193–9. ISSN: 1432-0738. DOI: [10.1007/s00204-014-1432-2](https://doi.org/10.1007/s00204-014-1432-2).
- [99] Robert M. Ward, Daniel Benjamin, Jeffrey S. Barrett, Karel Allegaert, Ronald Portman, Jonathan M. Davis, and Mark A. Turner. "Safety, dosing, and pharmaceutical quality for studies that evaluate medicinal products (including biological products) in neonates." In: *Pediatric research* 81.5 (2017), pp. 692–711. ISSN: 1530-0447. DOI: [10.1038/pr.2016.221](https://doi.org/10.1038/pr.2016.221).
- [100] Gail D. Anderson and Anne M. Lynn. "Optimizing pediatric dosing: a developmental pharmacologic approach." In: *Pharmacotherapy* 29.6 (2009), pp. 680–90. ISSN: 1875-9114. DOI: [10.1592/phco.29.6.680](https://doi.org/10.1592/phco.29.6.680).
- [101] Eva Fernandez, Raul Perez, Alfredo Hernandez, Pilar Tejada, Marta Arteta, and Jose T. Ramos. "Factors and Mechanisms for Pharmacokinetic Differences between Pediatric Population and Adults." In: *Pharmaceutics* 3.1 (2011), pp. 53–72. ISSN: 1999-4923. DOI: [10.3390/pharmaceutics3010053](https://doi.org/10.3390/pharmaceutics3010053).

- [102] Jens Van Den Abeele, Maissa Rayyan, Ilse Hoffman, Els Van de Vijver, Wei Zhu, and Patrick Augustijns. "Gastric fluid composition in a paediatric population: Age-dependent changes relevant for gastrointestinal drug disposition." In: *European journal of pharmaceutical sciences: official journal of the European Federation for Pharmaceutical Sciences* 123 (2018), pp. 301–311. ISSN: 1879-0720. DOI: [10.1016/j.ejps.2018.07.022](https://doi.org/10.1016/j.ejps.2018.07.022).
- [103] Patrick J. McNamara and Jane Alcorn. "Protein binding predictions in infants." In: *AAPS pharmSci* 4.1 (2002), E4. ISSN: 1522-1059. DOI: [10.1208/ps040104](https://doi.org/10.1208/ps040104).
- [104] Andrea N. Edginton. "Knowledge-driven approaches for the guidance of first-in-children dosing." In: *Paediatric anaesthesia* 21.3 (2011), pp. 206–13. ISSN: 1460-9592. DOI: [10.1111/j.1460-9592.2010.03473.x](https://doi.org/10.1111/j.1460-9592.2010.03473.x).
- [105] M Puig. "Body composition and growth." In: *Nutrition in Pediatrics*. Ed. by WA Walker and JB Watkins. 2nd ed. Hamilton, Ontario: BC Decker, 1996. ISBN: 155009226X.
- [106] Jan-Georg Wojtyniak, Hannah Britz, Dominik Selzer, Matthias Schwab, and Thorsten Lehr. "Data Digitizing: Accurate and Precise Data Extraction for Quantitative Systems Pharmacology and Physiologically-Based Pharmacokinetic Modeling." In: *CPT: pharmacometrics & systems pharmacology* 9.6 (2020), pp. 322–331. ISSN: 2163-8306. DOI: [10.1002/psp4.12511](https://doi.org/10.1002/psp4.12511).
- [107] Nina Hanke, Claudia Kunz, Meinolf Thiemann, Harald Fricke, and Thorsten Lehr. "Translational PBPK Modeling of the Protein Therapeutic and CD95L Inhibitor Asunercept to Develop Dose Recommendations for Its First Use in Pediatric Glioblastoma Patients." In: *Pharmaceutics* 11.4 (2019), p. 152. ISSN: 1999-4923. DOI: [10.3390/pharmaceutics11040152](https://doi.org/10.3390/pharmaceutics11040152).
- [108] Memoona Rashid, Muhammad Sarfraz, Mosab Arafat, Amjad Hussain, Nasir Abbas, Muhammad Waqas Sadiq, Muhammad Fawad Rasool, and Nadeem Irfan Bukhari. "Prediction of lisinopril pediatric dose from the reference adult dose by employing a physiologically based pharmacokinetic model." In: *BMC pharmacology & toxicology* 21.1 (2020), p. 56. ISSN: 2050-6511. DOI: [10.1186/s40360-020-00429-y](https://doi.org/10.1186/s40360-020-00429-y).
- [109] Laura Oggianu, Alice B. Ke, Manoranjenni Chetty, Rossella Picollo, Vanessa Petrucci, Fabrizio Calisti, Fabio Garofolo, and Serena Tongiani. "Estimation of an Appropriate Dose of Trazodone for Pediatric Insomnia and the Potential for a Trazodone-Atomoxetine Interaction." In: *CPT: pharmacometrics & systems pharmacology* 9.2 (2020), pp. 77–86. ISSN: 2163-8306. DOI: [10.1002/psp4.12480](https://doi.org/10.1002/psp4.12480).
- [110] Yeruk Mulugeta et al. "Exposure Matching for Extrapolation of Efficacy in Pediatric Drug Development." In: *Journal of clinical pharmacology* 56.11 (2016), pp. 1326–1334. ISSN: 1552-4604. DOI: [10.1002/jcph.744](https://doi.org/10.1002/jcph.744).
- [111] A. A. Vinks, C. Emoto, and T. Fukuda. "Modeling and simulation in pediatric drug therapy: Application of pharmacometrics to define the right dose for children." In: *Clinical pharmacology and therapeutics* 98.3 (2015), pp. 298–308. ISSN: 1532-6535. DOI: [10.1002/cpt.169](https://doi.org/10.1002/cpt.169).

- [112] Brian Cicali, Tao Long, Sarah Kim, and Rodrigo Cristofolletti. "Assessing the impact of cystic fibrosis on the antipyretic response of ibuprofen in children: Physiologically-based modeling as a candle in the dark." In: *British journal of clinical pharmacology* 86.11 (2020), pp. 2247–2255. ISSN: 1365-2125. DOI: [10.1111/bcp.14326](https://doi.org/10.1111/bcp.14326).
- [113] Shruthi Vaidhyanathan, Xiaoning Wang, John Crison, Sailesh Varia, Julia Z H Gao, Ajay Saxena, and David Good. "Bioequivalence Comparison of Pediatric Dasatinib Formulations and Elucidation of Absorption Mechanisms Through Integrated PBPK Modeling." In: *Journal of pharmaceutical sciences* 108.1 (2019), pp. 741–749. ISSN: 1520-6017. DOI: [10.1016/j.xphs.2018.11.005](https://doi.org/10.1016/j.xphs.2018.11.005).
- [114] K. Allegaert and J van den Anker. "Neonatal drug therapy: The first frontier of therapeutics for children." In: *Clinical pharmacology and therapeutics* 98.3 (2015), pp. 288–97. ISSN: 1532-6535. DOI: [10.1002/cpt.166](https://doi.org/10.1002/cpt.166).
- [115] World Health Organization. *WHO guidelines for the pharmacological and radiotherapeutic management of cancer pain in adults and adolescents*. Geneva: Licence: CC BY-NC-SA 3.0 IGO, 2018. ISBN: 978-92-4-155039-0.
- [116] Evelien J M Kuip, Maarten L Zandvliet, Stijn L W Koolen, Ron H J Mathijssen, and Carin C D van der Rijt. "A review of factors explaining variability in fentanyl pharmacokinetics; focus on implications for cancer patients." In: *British journal of clinical pharmacology* 83.2 (2017), pp. 294–313. ISSN: 1365-2125. DOI: [10.1111/bcp.13129](https://doi.org/10.1111/bcp.13129).
- [117] Erendira Vicencio-Rosas, María Gabriela Pérez-Guillé, Carmen Flores-Pérez, Janett Flores-Pérez, Francisca Trujillo-Jiménez, and Juan Luis Chávez-Pacheco. "Buprenorphine and pain treatment in pediatric patients: an update." In: *Journal of pain research* 11 (2018), pp. 549–559. ISSN: 1178-7090. DOI: [10.2147/JPR.S153903](https://doi.org/10.2147/JPR.S153903).
- [118] Erik Michel, Brian J. Anderson, and Boris Zernikow. "Buprenorphine TTS for children—a review of the drug's clinical pharmacology." In: *Paediatric anaesthesia* 21.3 (2011), pp. 280–90. ISSN: 1460-9592. DOI: [10.1111/j.1460-9592.2010.03437.x](https://doi.org/10.1111/j.1460-9592.2010.03437.x).
- [119] Gian Maria Pacifici. "Clinical pharmacology of fentanyl in preterm infants. A review." In: *Pediatrics and neonatology* 56.3 (2015), pp. 143–8. ISSN: 2212-1692. DOI: [10.1016/j.pedneo.2014.06.002](https://doi.org/10.1016/j.pedneo.2014.06.002).
- [120] Victoria C. Ziesenitz, Janelle D. Vaughns, Gilbert Koch, Gerd Mikus, and Johannes N. van den Anker. "Pharmacokinetics of Fentanyl and Its Derivatives in Children: A Comprehensive Review." In: *Clinical pharmacokinetics* 57.2 (2018), pp. 125–149. ISSN: 1179-1926. DOI: [10.1007/s40262-017-0569-6](https://doi.org/10.1007/s40262-017-0569-6).
- [121] E L Maunuksela, R Korpela, and K T Olkkola. "Double-blind, multiple-dose comparison of buprenorphine and morphine in postoperative pain of children." In: *British journal of anaesthesia* 60.1 (1988), pp. 48–55. ISSN: 0007-0912. DOI: [10.1093/bja/60.1.48](https://doi.org/10.1093/bja/60.1.48).

- [122] J V Aranda, Waldemar Carlo, Pat Hummel, R. Thomas, Vicki Tutag Lehr, and K J S Anand. "Analgesia and sedation during mechanical ventilation in neonates." In: *Clinical therapeutics* 27.6 (2005), pp. 877–99. ISSN: 0149-2918. DOI: [10.1016/j.clinthera.2005.06.019](https://doi.org/10.1016/j.clinthera.2005.06.019).
- [123] Ricardo Carbajal et al. "Sedation and analgesia practices in neonatal intensive care units (EUROPAIN): results from a prospective cohort study." In: *The Lancet. Respiratory medicine* 3.10 (2015), pp. 796–812. ISSN: 2213-2619. DOI: [10.1016/S2213-2600\(15\)00331-8](https://doi.org/10.1016/S2213-2600(15)00331-8).
- [124] J Irazuzta, R Pascucci, N Perlman, and D Wessel. "Effects of fentanyl administration on respiratory system compliance in infants." In: *Critical care medicine* 21.7 (1993), pp. 1001–4. ISSN: 0090-3493. DOI: [10.1097/00003246-199307000-00013](https://doi.org/10.1097/00003246-199307000-00013).
- [125] Elisabeth Dewhirst, Aymen Naguib, and Joseph D. Tobias. "Chest wall rigidity in two infants after low-dose fentanyl administration." In: *Pediatric emergency care* 28.5 (2012), pp. 465–8. ISSN: 1535-1815. DOI: [10.1097/PEC.0b013e3182535a2a](https://doi.org/10.1097/PEC.0b013e3182535a2a).
- [126] Hubert Fahrenstich, Joanne Steffan, Nikolaus Kau, and Peter Bartmann. "Fentanyl-induced chest wall rigidity and laryngospasm in preterm and term infants." In: *Critical care medicine* 28.3 (2000), pp. 836–9. ISSN: 0090-3493. DOI: [10.1097/00003246-200003000-00037](https://doi.org/10.1097/00003246-200003000-00037).
- [127] Swantje Völler, Robert B Flint, Peter Andriessen, Karel Allegaert, Luc J I Zimmermann, Kian D Liem, Birgit C P Koch, Sinno H P Simons, Catherijne A J Knibbe, and DINO study group. "Rapidly maturing fentanyl clearance in preterm neonates." In: *Archives of disease in childhood. Fetal and neonatal edition* 104.6 (2019), F598–F603. ISSN: 1468-2052. DOI: [10.1136/archdischild-2018-315920](https://doi.org/10.1136/archdischild-2018-315920).
- [128] Jérôme Guitton, Thierry Buronfosse, Michel Désage, Alain Lepape, Jean Louis Brazier, and Philippe Beaune. "Possible involvement of multiple cytochrome P450s in fentanyl and sufentanil metabolism as opposed to alfentanil." In: *Biochemical pharmacology* 53.11 (1997), pp. 1613–9. ISSN: 0006-2952. DOI: [10.1016/s0006-2952\(96\)00893-3](https://doi.org/10.1016/s0006-2952(96)00893-3).
- [129] Victoria C. Ziesenitz, Sonja K. König, Nina S. Mahlke, Gisela Skopp, Walter E. Haefeli, and Gerd Mikus. "Pharmacokinetic interaction of intravenous fentanyl with ketoconazole." In: *Journal of clinical pharmacology* 55.6 (2015), pp. 708–17. ISSN: 1552-4604. DOI: [10.1002/jcph.469](https://doi.org/10.1002/jcph.469).
- [130] Teijo I. Saari, Kari Laine, Mikko Neuvonen, Pertti J. Neuvonen, and Klaus T. Olkkola. "Effect of voriconazole and fluconazole on the pharmacokinetics of intravenous fentanyl." In: *European journal of clinical pharmacology* 64.1 (2008), pp. 25–30. ISSN: 1432-1041. DOI: [10.1007/s00228-007-0398-x](https://doi.org/10.1007/s00228-007-0398-x).
- [131] Nicolas Picard, Thierry Cresteil, Nassim Djebli, and Pierre Marquet. "In vitro metabolism study of buprenorphine: evidence for new metabolic pathways." In: *Drug metabolism and disposition: the biological fate of chemicals* 33.5 (2005), pp. 689–95. ISSN: 0090-9556. DOI: [10.1124/dmd.105.003681](https://doi.org/10.1124/dmd.105.003681).

- [132] Stephanie Oechsler and Gisela Skopp. "An in vitro approach to estimate putative inhibition of buprenorphine and norbuprenorphine glucuronidation." In: *International journal of legal medicine* 124.3 (2010), pp. 187–94. ISSN: 1437-1596. DOI: [10.1007/s00414-010-0418-8](https://doi.org/10.1007/s00414-010-0418-8).
- [133] Thomas M. Polasek, Frank P Y Lin, John O. Miners, and Matthew P. Doogue. "Perpetrators of pharmacokinetic drug-drug interactions arising from altered cytochrome P450 activity: a criteria-based assessment." In: *British journal of clinical pharmacology* 71.5 (2011), pp. 727–36. ISSN: 1365-2125. DOI: [10.1111/j.1365-2125.2011.03903.x](https://doi.org/10.1111/j.1365-2125.2011.03903.x).
- [134] Arthur G. Roberts and Morgan E. Gibbs. "Mechanisms and the clinical relevance of complex drug-drug interactions." In: *Clinical pharmacology: advances and applications* 10 (2018), pp. 123–134. ISSN: 1179-1438. DOI: [10.2147/CPAA.S146115](https://doi.org/10.2147/CPAA.S146115).
- [135] Walter K. Kraft. "Buprenorphine in Neonatal Abstinence Syndrome." In: *Clinical pharmacology and therapeutics* 103.1 (2018), pp. 112–119. ISSN: 1532-6535. DOI: [10.1002/cpt.930](https://doi.org/10.1002/cpt.930).
- [136] Steve Morgan, Paul Grootendorst, Joel Lexchin, Colleen Cunningham, and Devon Greyson. "The cost of drug development: a systematic review." In: *Health policy (Amsterdam, Netherlands)* 100.1 (2011), pp. 4–17. ISSN: 1872-6054. DOI: [10.1016/j.healthpol.2010.12.002](https://doi.org/10.1016/j.healthpol.2010.12.002).
- [137] Ian E. Templeton, Nicholas S. Jones, and Luna Musib. "Pediatric Dose Selection and Utility of PBPK in Determining Dose." In: *The AAPS journal* 20.2 (2018), p. 31. ISSN: 1550-7416. DOI: [10.1208/s12248-018-0187-8](https://doi.org/10.1208/s12248-018-0187-8).
- [138] Trevor N. Johnson and Amin Rostami-Hodjegan. "Resurgence in the use of physiologically based pharmacokinetic models in pediatric clinical pharmacology: parallel shift in incorporating the knowledge of biological elements and increased applicability to drug development and clinical practice." In: *Paediatric anaesthesia* 21.3 (2011), pp. 291–301. ISSN: 1460-9592. DOI: [10.1111/j.1460-9592.2010.03323.x](https://doi.org/10.1111/j.1460-9592.2010.03323.x).
- [139] E Everhart, P Cheung, J Mendelson, R Upton, and R Jones. "The mass balance of buprenorphine in humans." In: *Clinical Pharmacology & Therapeutics* 65.2 (1999), pp. 152–152. ISSN: 00099236. DOI: [10.1016/S0009-9236\(99\)80138-6](https://doi.org/10.1016/S0009-9236(99)80138-6).
- [140] Nora M. Hagelberg, Mari Fihlman, Tuija Hemmilä, Janne T. Backman, Jouko Laitila, Pertti J. Neuvonen, Kari Laine, Klaus T. Olkkola, and Teijo I. Saari. "Rifampicin decreases exposure to sublingual buprenorphine in healthy subjects." In: *Pharmacology research & perspectives* 4.6 (2016), e00271. ISSN: 2052-1707. DOI: [10.1002/prp2.271](https://doi.org/10.1002/prp2.271).
- [141] D E Feierman and J M Lasker. "Metabolism of fentanyl, a synthetic opioid analgesic, by human liver microsomes. Role of CYP<sub>3A4</sub>." In: *Drug metabolism and disposition: the biological fate of chemicals* 24.9 (1996), pp. 932–9. ISSN: 0090-9556.

- [142] Deborah A McClain and Carl C Hug. "Intravenous fentanyl kinetics." In: *Clinical pharmacology and therapeutics* 28.1 (1980), pp. 106–14. ISSN: 0009-9236. DOI: [10.1038/clpt.1980.138](https://doi.org/10.1038/clpt.1980.138).
- [143] D A Barrett, J Simpson, N Rutter, T Kurihara-Bergstrom, P N Shaw, and S S Davis. "The pharmacokinetics and physiological effects of buprenorphine infusion in premature neonates." In: *British journal of clinical pharmacology* 36.3 (1993), pp. 215–9. ISSN: 0306-5251. DOI: [10.1111/j.1365-2125.1993.tb04220.x](https://doi.org/10.1111/j.1365-2125.1993.tb04220.x).
- [144] K T Olkkola, E L Maunuksela, and R Korpela. "Pharmacokinetics of intravenous buprenorphine in children." In: *British journal of clinical pharmacology* 28.2 (1989), pp. 202–4. ISSN: 0306-5251. DOI: [10.1111/j.1365-2125.1989.tb05418.x](https://doi.org/10.1111/j.1365-2125.1989.tb05418.x).
- [145] Mark A. Singleton, Judith I. Rosen, and Dennis M. Fisher. "Plasma concentrations of fentanyl in infants, children and adults." In: *Canadian journal of anaesthesia = Journal canadien d'anesthesie* 34.2 (1987), pp. 152–5. ISSN: 0832-610X. DOI: [10.1007/BF03015333](https://doi.org/10.1007/BF03015333).
- [146] Elina Saarenmaa, Pertti J. Neuvonen, and Vineta Fellman. "Gestational age and birth weight effects on plasma clearance of fentanyl in newborn infants." In: *The Journal of pediatrics* 136.6 (2000), pp. 767–70. ISSN: 0022-3476. DOI: [10.1067/mpd.2000.105366](https://doi.org/10.1067/mpd.2000.105366).
- [147] D. E. Koehntop, J. H. Rodman, D. M. Brundage, M. G. Hegland, and J. J. Buckley. "Pharmacokinetics of fentanyl in neonates." In: *Anesthesia and analgesia* 65.3 (1986), pp. 227–32. ISSN: 0003-2999. DOI: [10.1213/00000539-198603000-00002](https://doi.org/10.1213/00000539-198603000-00002).
- [148] C. Collins, G. Koren, P. Crean, J. Klein, W. L. Roy, and S. M. MacLeod. "Fentanyl pharmacokinetics and hemodynamic effects in preterm infants during ligation of patent ductus arteriosus." In: *Anesthesia and analgesia* 64.11 (1985), pp. 1078–80. ISSN: 0003-2999. DOI: [10.1213/00000539-198511000-00007](https://doi.org/10.1213/00000539-198511000-00007).
- [149] Ian S. Gauntlett, Dennis M. Fisher, Robert E. Hertzka, Eckhard Kuhls, Michael J. Spellman, and Colin Rudolph. "Pharmacokinetics of fentanyl in neonatal humans and lambs: effects of age." In: *Anesthesiology* 69.5 (1988), pp. 683–7. ISSN: 0003-3022. DOI: [10.1097/00000542-198811000-00008](https://doi.org/10.1097/00000542-198811000-00008).
- [150] Daniel Gonzalez, Stephan Schmidt, and Hartmut Derendorf. "Importance of relating efficacy measures to unbound drug concentrations for anti-infective agents." In: *Clinical microbiology reviews* 26.2 (2013), pp. 274–88. ISSN: 1098-6618. DOI: [10.1128/CMR.00092-12](https://doi.org/10.1128/CMR.00092-12).
- [151] Paul Morgan, Piet H. Van Der Graaf, John Arrowsmith, Doug E. Feltner, Kira S. Drummond, Craig D. Wegner, and Steve D. A. Street. "Can the flow of medicines be improved? Fundamental pharmacokinetic and pharmacological principles toward improving Phase II survival." In: *Drug discovery today* 17.9-10 (2012), pp. 419–24. ISSN: 1878-5832. DOI: [10.1016/j.drudis.2011.12.020](https://doi.org/10.1016/j.drudis.2011.12.020).

- [152] Neal L. Benowitz. "Pharmacology of nicotine: addiction, smoking-induced disease, and therapeutics." In: *Annual review of pharmacology and toxicology* 49.1 (2009), pp. 57–71. ISSN: 0362-1642. DOI: [10.1146/annurev.pharmtox.48.113006.094742](https://doi.org/10.1146/annurev.pharmtox.48.113006.094742).
- [153] Judith J Prochaska and Neal L Benowitz. "The Past, Present, and Future of Nicotine Addiction Therapy." In: *Annual review of medicine* 67.3 (2016), pp. 467–86. ISSN: 1545-326X. DOI: [10.1146/annurev-med-111314-033712](https://doi.org/10.1146/annurev-med-111314-033712).
- [154] Nina Hanke, Denise Türk, Dominik Selzer, Naoki Ishiguro, Thomas Ebner, Sabrina Wiebe, Fabian Müller, Peter Stopfer, Valerie Nock, and Thorsten Lehr. "A Comprehensive Whole-Body Physiologically Based Pharmacokinetic Drug-Drug-Gene Interaction Model of Metformin and Cimetidine in Healthy Adults and Renally Impaired Individuals." In: *Clinical pharmacokinetics* 59.11 (2020), pp. 1419–1431. ISSN: 1179-1926. DOI: [10.1007/s40262-020-00896-w](https://doi.org/10.1007/s40262-020-00896-w).
- [155] World Health Organization. *WHO Report on the Global Tobacco Epidemic, 2019*. Geneva: Licence: CC BY-NC-SA 3.0 IGO, 2019. ISBN: 978-92-4-151620-4.
- [156] World Health Organization. *WHO report on the global tobacco epidemic 2021: addressing new and emerging products*. Geneva: Licence: CC BY-NC-SA 3.0 IGO, 2021. ISBN: 978-92-4-003209-5.
- [157] Michael Eriksen, Judith Mackay, Neil Schluger, Farhad Islami, and Jeffrey Drope. *The Tobacco Atlas*. 5th. Atlanta: American Cancer Society, 2015. ISBN: 978-1-60443-235-0.
- [158] Neal L Benowitz. "Nicotine addiction." In: *The New England journal of medicine* 362.24 (2010), pp. 2295–303. ISSN: 1533-4406. DOI: [10.1056/NEJMra0809890](https://doi.org/10.1056/NEJMra0809890).
- [159] Jack H. Mendelson, Nathalie Goletiani, Michelle B. Sholar, Arthur J. Siegel, and Nancy K. Mello. "Effects of smoking successive low- and high-nicotine cigarettes on hypothalamic-pituitary-adrenal axis hormones and mood in men." In: *Neuropsychopharmacology: official publication of the American College of Neuropsychopharmacology* 33.4 (2008), pp. 749–60. ISSN: 0893-133X. DOI: [10.1038/sj.npp.1301455](https://doi.org/10.1038/sj.npp.1301455).
- [160] D G Gilbert, J H Robinson, C L Chamberlin, and C D Spielberger. "Effects of smoking/nicotine on anxiety, heart rate, and lateralization of EEG during a stressful movie." In: *Psychophysiology* 26.3 (1989), pp. 311–20. ISSN: 0048-5772. DOI: [10.1111/j.1469-8986.1989.tb01924.x](https://doi.org/10.1111/j.1469-8986.1989.tb01924.x).
- [161] Neal L. Benowitz, Herve Porchet, Lewis Sheiner, and Peyton Jacob. "Nicotine absorption and cardiovascular effects with smokeless tobacco use: comparison with cigarettes and nicotine gum." In: *Clinical pharmacology and therapeutics* 44.1 (1988), pp. 23–8. ISSN: 0009-9236. DOI: [10.1038/clpt.1988.107](https://doi.org/10.1038/clpt.1988.107).

- [162] Daniel Kotz, Anil Batra, and Sabrina Kastaun. "Smoking Cessation Attempts and Common Strategies Employed." In: *Deutsches Arzteblatt international* 117.1-2 (2020), pp. 7–13. ISSN: 1866-0452. DOI: [10.3238/arztebl.2020.0007](https://doi.org/10.3238/arztebl.2020.0007).
- [163] Jed E. Rose, Alexey G. Mukhin, Stephen J. Lokitz, Timothy G. Turkington, Joseph Herskovic, Frederique M. Behm, Sudha Garg, and Pradeep K. Garg. "Kinetics of brain nicotine accumulation in dependent and nondependent smokers assessed with PET and cigarettes containing  $^{11}\text{C}$ -nicotine." In: *Proceedings of the National Academy of Sciences of the United States of America* 107.11 (2010), pp. 5190–5. ISSN: 1091-6490. DOI: [10.1073/pnas.0909184107](https://doi.org/10.1073/pnas.0909184107).
- [164] Wangda Zhou, Trevor N Johnson, Khanh H Bui, S Y Amy Cheung, Jianguo Li, Hongmei Xu, Nidal Al-Huniti, and Diansong Zhou. "Predictive Performance of Physiologically Based Pharmacokinetic (PBPK) Modeling of Drugs Extensively Metabolized by Major Cytochrome P450s in Children." In: *Clinical pharmacology and therapeutics* 104.1 (2018), pp. 188–200. ISSN: 1532-6535. DOI: [10.1002/cpt.905](https://doi.org/10.1002/cpt.905).
- [165] Qier Wu and Sheila Annie Peters. "A Retrospective Evaluation of Allometry, Population Pharmacokinetics, and Physiologically-Based Pharmacokinetics for Pediatric Dosing Using Clearance as a Surrogate." In: *CPT: pharmacometrics & systems pharmacology* 8.4 (2019), pp. 220–229. ISSN: 2163-8306. DOI: [10.1002/psp4.12385](https://doi.org/10.1002/psp4.12385).
- [166] Elena García-Martín, Carmen Martínez, José M. Ladero, and José A G Agúndez. "Interethnic and intraethnic variability of CYP2C8 and CYP2C9 polymorphisms in healthy individuals." In: *Molecular diagnosis & therapy* 10.1 (2006), pp. 29–40. ISSN: 1177-1062. DOI: [10.1007/BF03256440](https://doi.org/10.1007/BF03256440).
- [167] John O. Miners, Ross A. McKinnon, and Peter I. Mackenzie. "Genetic polymorphisms of UDP-glucuronosyltransferases and their functional significance." In: *Toxicology* 181-182 (2002), pp. 453–6. ISSN: 0300-483X. DOI: [10.1016/s0300-483x\(02\)00449-3](https://doi.org/10.1016/s0300-483x(02)00449-3).
- [168] Lauri I Kajosaari, Jouko Laitila, Pertti J Neuvonen, and Janne T Backman. "Metabolism of repaglinide by CYP2C8 and CYP3A4 in vitro: effect of fibrates and rifampicin." In: *Basic & clinical pharmacology & toxicology* 97.4 (2005), pp. 249–56. ISSN: 1742-7835. DOI: [10.1111/j.1742-7843.2005.pto\\_157.x](https://doi.org/10.1111/j.1742-7843.2005.pto_157.x).
- [169] Jocelyn Trottier et al. "The human UGT1A3 enzyme conjugates norursodeoxycholic acid into a C23-ester glucuronide in the liver." In: *The Journal of biological chemistry* 285.2 (2010), pp. 1113–21. ISSN: 1083-351X. DOI: [10.1074/jbc.M109.073908](https://doi.org/10.1074/jbc.M109.073908).
- [170] Nina Hanke, Sebastian Frechen, Daniel Moj, Hannah Britz, Thomas Eissing, Thomas Wendl, and Thorsten Lehr. "PBPK Models for CYP3A4 and P-gp DDI Prediction: A Modeling Network of Rifampicin, Itraconazole, Clarithromycin, Midazolam, Alfentanil, and Digoxin." In: *CPT: pharmacometrics & systems pharmacology* 7.10 (2018), pp. 647–659. ISSN: 2163-8306. DOI: [10.1002/psp4.12343](https://doi.org/10.1002/psp4.12343).

- [171] William J. Chiou, Sonia M. de Morais, Ryota Kikuchi, Richard L. Voorman, Xiaofeng Li, and Daniel A. J. Bow. "In vitro OATP<sub>1B1</sub> and OATP<sub>1B3</sub> inhibition is associated with observations of benign clinical unconjugated hyperbilirubinemia." In: *Xenobiotica; the fate of foreign compounds in biological systems* 44.3 (2014), pp. 276–82. ISSN: 1366-5928. DOI: [10.3109/00498254.2013.820006](https://doi.org/10.3109/00498254.2013.820006).
- [172] *Clinical Drug Interaction Studies - Cytochrome P<sub>450</sub> Enzyme- and Transporter-Mediated Drug Interactions. Guidance for Industry*. U.S. Department of Health and Human Services Food and Drug Administration Center for Drug Evaluation and Research (CDER). 2020. URL: <https://www.fda.gov/media/134581/download> (visited on 10/04/2021).
- [173] European Medicines Agency. *Guideline on the investigation of drug interactions*. 2012. URL: [https://www.ema.europa.eu/en/documents/scientific-guideline/guideline-guideline-investigation-drug-interactions-revision-1\\_en.pdf](https://www.ema.europa.eu/en/documents/scientific-guideline/guideline-guideline-investigation-drug-interactions-revision-1_en.pdf) (visited on 10/04/2021).
- [174] Sirimas Sudsakorn, Praveen Bahadduri, Jennifer Fretland, and Chuang Lu. "2020 FDA Drug-drug Interaction Guidance: A Comparison Analysis and Action Plan by Pharmaceutical Industrial Scientists." In: *Current drug metabolism* 21.6 (2020), pp. 403–426. ISSN: 1875-5453. DOI: [10.2174/1389200221666200620210522](https://doi.org/10.2174/1389200221666200620210522).
- [175] J G Bovill and P S Sebel. "Pharmacokinetics of high-dose fentanyl. A study in patients undergoing cardiac surgery." In: *British journal of anaesthesia* 52.8 (1980), pp. 795–801. ISSN: 0007-0912. DOI: [10.1093/bja/52.8.795](https://doi.org/10.1093/bja/52.8.795).
- [176] B. Prasad et al. "Ontogeny of Hepatic Drug Transporters as Quantified by LC-MS/MS Proteomics." In: *Clinical pharmacology and therapeutics* 100.4 (2016), pp. 362–70. ISSN: 1532-6535. DOI: [10.1002/cpt.409](https://doi.org/10.1002/cpt.409).
- [177] A. S. Darwich et al. "Why has model-informed precision dosing not yet become common clinical reality? Lessons from the past and a roadmap for the future." In: *Clinical pharmacology and therapeutics* 101.5 (2017), pp. 646–656. ISSN: 1532-6535. DOI: [10.1002/cpt.659](https://doi.org/10.1002/cpt.659).
- [178] A. S. Darwich et al. "Model-Informed Precision Dosing: Background, Requirements, Validation, Implementation, and Forward Trajectory of Individualizing Drug Therapy." In: *Annual review of pharmacology and toxicology* 61.1 (2021), pp. 225–245. ISSN: 1545-4304. DOI: [10.1146/annurev-pharmtox-033020-113257](https://doi.org/10.1146/annurev-pharmtox-033020-113257).
- [179] Andrew Rowland, Warit Ruanglertboon, Madelé van Dyk, Dhilushi Wijayakumara, Linda S. Wood, Robyn Meech, Peter I. Mackenzie, A. David Rodrigues, Jean-Claude Marshall, and Michael J. Sorich. "Plasma extracellular nanovesicle (exosome)-derived biomarkers for drug metabolism pathways: a novel approach to characterize variability in drug exposure." In: *British journal of clinical pharmacology* 85.1 (2019), pp. 216–226. ISSN: 1365-2125. DOI: [10.1111/bcp.13793](https://doi.org/10.1111/bcp.13793).

- [180] Brahim Achour, Zubida M. Al-Majdoub, Agnieszka Grybos-Gajniak, Kristi Lea, Peter Kilford, Mian Zhang, David Knight, Jill Barber, Jeoffrey Schageman, and Amin Rostami-Hodjegan. "Liquid Biopsy Enables Quantification of the Abundance and Interindividual Variability of Hepatic Enzymes and Transporters." In: *Clinical pharmacology and therapeutics* 109.1 (2021), pp. 222–232. ISSN: 1532-6535. DOI: [10.1002/cpt.2102](https://doi.org/10.1002/cpt.2102).
- [181] David Rodrigues and Andrew Rowland. "From Endogenous Compounds as Biomarkers to Plasma-Derived Nanovesicles as Liquid Biopsy; Has the Golden Age of Translational Pharmacokinetics-Absorption, Distribution, Metabolism, Excretion-Drug-Drug Interaction Science Finally Arrived?" In: *Clinical pharmacology and therapeutics* 105.6 (2019), pp. 1407–1420. ISSN: 1532-6535. DOI: [10.1002/cpt.1328](https://doi.org/10.1002/cpt.1328).
- [182] Jan-Georg Wojtyniak. "Model Informed Drug Development and Precision Dosing for Drug-Drug-Gene-Interactions: Application of Physiologically-Based Pharmacokinetic Modeling." PhD thesis. Saarland University, 2021, pp. 1–325. DOI: [10.22028/D291-34276](https://doi.org/10.22028/D291-34276).
- [183] Nadine Schaefer, Daniel Moj, Thorsten Lehr, Peter H. Schmidt, and Frank Ramsthaler. "The feasibility of physiologically based pharmacokinetic modeling in forensic medicine illustrated by the example of morphine." In: *International journal of legal medicine* 132.2 (2018), pp. 415–424. ISSN: 1437-1596. DOI: [10.1007/s00414-017-1754-8](https://doi.org/10.1007/s00414-017-1754-8).
- [184] Daniel Moj, Hannah Britz, Jürgen Burhenne, Clinton F. Stewart, Gerlinde Egerer, Walter E. Haefeli, and Thorsten Lehr. "A physiologically based pharmacokinetic and pharmacodynamic (PBPK/PD) model of the histone deacetylase (HDAC) inhibitor vorinostat for pediatric and adult patients and its application for dose specification." In: *Cancer chemotherapy and pharmacology* 80.5 (2017), pp. 1013–1026. ISSN: 1432-0843. DOI: [10.1007/s00280-017-3447-x](https://doi.org/10.1007/s00280-017-3447-x).
- [185] Janne Hukkanen, Peyton Jacob, and Neal L Benowitz. "Metabolism and disposition kinetics of nicotine." In: *Pharmacological reviews* 57.1 (2005), pp. 79–115. ISSN: 0031-6997. DOI: [10.1124/pr.57.1.3](https://doi.org/10.1124/pr.57.1.3).
- [186] Neal L. Benowitz and Peyton Jacob. "Metabolism of nicotine to cotinine studied by a dual stable isotope method." In: *Clinical pharmacology and therapeutics* 56.5 (1994), pp. 483–93. ISSN: 0009-9236. DOI: [10.1038/clpt.1994.169](https://doi.org/10.1038/clpt.1994.169).
- [187] Neal L Benowitz, Janne Hukkanen, and Peyton Jacob. "Nicotine chemistry, metabolism, kinetics and biomarkers." In: *Handbook of experimental pharmacology* 192 (2009), pp. 29–60. ISSN: 0171-2004. DOI: [10.1007/978-3-540-69248-5\\_2](https://doi.org/10.1007/978-3-540-69248-5_2).
- [188] Shoshana Zevin, Peyton Jacob, and Neal Benowitz. "Cotinine effects on nicotine metabolism." In: *Clinical pharmacology and therapeutics* 61.6 (1997), pp. 649–54. ISSN: 0009-9236. DOI: [10.1016/S0009-9236\(97\)90099-0](https://doi.org/10.1016/S0009-9236(97)90099-0).

- [189] S. K. Gupta, N. L. Benowitz, P. Jacob, C. N. Rolf, and J. Gorsline. "Bioavailability and absorption kinetics of nicotine following application of a transdermal system." In: *British journal of clinical pharmacology* 36.3 (1993), pp. 221–7. ISSN: 0306-5251. DOI: [10.1111/j.1365-2125.1993.tb04221.x](https://doi.org/10.1111/j.1365-2125.1993.tb04221.x).
- [190] Schorp, MK. "Summary of literature data on smoking topography." In: *A Review of Human Smoking Behaviour and Recommendations for a New ISO Standard for the Machine Smoking of Cigarettes; Report of the Ad Hoc WG9 Smoking Behavior Review Team to ISO/TC 126 WG 9*. Ed. by W Pickworth, P Houlgate, MK Schorp, M Dixon, M Borgerding, and G Zaatari. 2005, pp. 28–50.
- [191] Kathryn C. Ross, Delia A. Dempsey, Gideon St. Helen, Kevin Delucchi, and Neal L. Benowitz. "The Influence of Puff Characteristics, Nicotine Dependence, and Rate of Nicotine Metabolism on Daily Nicotine Exposure in African American Smokers." In: *Cancer epidemiology, biomarkers & prevention: a publication of the American Association for Cancer Research, cosponsored by the American Society of Preventive Oncology* 25.6 (2016), pp. 936–43. ISSN: 1538-7755. DOI: [10.1158/1055-9965.EPI-15-1034](https://doi.org/10.1158/1055-9965.EPI-15-1034).
- [192] A K Armitage, C T Dollery, C F George, T H Houseman, P J Lewis, and D M Turner. "Absorption and metabolism of nicotine from cigarettes." In: *British medical journal* 4.5992 (1975), pp. 313–6. ISSN: 0007-1447. DOI: [10.1136/bmj.4.5992.313](https://doi.org/10.1136/bmj.4.5992.313).
- [193] Dominik Lott, Thorsten Lehr, Jasper Dingemanse, and Andreas Krause. "Modeling Tolerance Development for the Effect on Heart Rate of the Selective S1P1 Receptor Modulator Ponesimod." In: *Clinical pharmacology and therapeutics* 103.6 (2018), pp. 1083–1092. ISSN: 1532-6535. DOI: [10.1002/cpt.877](https://doi.org/10.1002/cpt.877).
- [194] H C Porchet, N L Benowitz, and L B Sheiner. "Pharmacodynamic model of tolerance: application to nicotine." In: *The Journal of pharmacology and experimental therapeutics* 244.1 (1988), pp. 231–6. ISSN: 0022-3565.
- [195] B Meibohm and H Derendorf. "Basic concepts of pharmacokinetic/pharmacodynamic (PK/PD) modelling." In: *International journal of clinical pharmacology and therapeutics* 35.10 (1997), pp. 401–13. ISSN: 0946-1965.
- [196] Harmut Derendorf and Bernd Meibohm. "Modeling of pharmacokinetic/pharmacodynamic (PK/PD) relationships: concepts and perspectives." In: *Pharmaceutical research* 16.2 (1999), pp. 176–85. ISSN: 0724-8741. DOI: [10.1023/a:1011907920641](https://doi.org/10.1023/a:1011907920641).

Part IV

APPENDIX





## SUPPLEMENTARY DOCUMENTS

---

### A.1 SUPPLEMENTARY DOCUMENT TO PUBLICATION I – PBPK MODELING OF BUPRENORPHINE IN ADULT AND PEDIATRIC PATIENTS

## Pharmaceutics

# Supplementary Materials: Physiologically-Based Pharmacokinetic (PBPK) Modeling of Buprenorphine in Adults, Children and Preterm Neonates

Lukas Kovar, Christina Schräpel, Dominik Selzer, Yvonne Kohl, Robert Bals, Matthias Schwab and Thorsten Lehr

## Contents

<b>1</b>	<b>PBPK Model Building</b>	<b>2</b>
1.1	PBPK Model Building – General . . . . .	2
1.2	System-dependent Parameters and Virtual Populations . . . . .	3
<b>2</b>	<b>Drug-Drug-Interaction (DDI) Modeling</b>	<b>6</b>
2.1	DDI Modeling – General . . . . .	6
2.2	Mathematical Implementation of DDIs . . . . .	7
2.2.1	Competitive Inhibition . . . . .	7
2.2.2	Mechanism-Based Inhibition (MBI) . . . . .	7
2.2.3	Induction . . . . .	8
<b>3</b>	<b>Allometric Scaling</b>	<b>9</b>
<b>4</b>	<b>PBPK Model Evaluation</b>	<b>11</b>
4.1	Adult PBPK Model Evaluation . . . . .	12
4.2	Pediatric PBPK Model Evaluation . . . . .	20
4.3	Quantitative PBPK Model Evaluation . . . . .	26
4.4	Mean Relative Deviation (MRD) Values of Buprenorphine and Norbuprenorphine Plasma Concentration Predictions . . . . .	26
4.5	Geometric Mean Fold Error (GMFE) of $AUC_{last}$ and $C_{max}$ Predictions . . . . .	28
4.6	Buprenorphine and Norbuprenorphine PBPK Model Sensitivity Analysis . . . . .	30
	<b>References</b>	<b>32</b>

## 1 PBPK Model Building

### 1.1 PBPK Model Building – General

In agreement with pediatric physiologically based pharmacokinetic (PBPK) model development workflows, first, an adult PBPK model was built and evaluated with observed plasma profiles to gain confidence in the parametrization of the PBPK model, before the model was scaled to pediatric populations [1–4]. The general model building process is described in the methods section of the main manuscript. This includes the implementation of important distribution and elimination processes including cytochrome P450 (CYP) and uridine 5'-diphospho-glucuronosyltransferase (UGT) enzymes as well as transporters. For the buprenorphine model these are the metabolism of buprenorphine to norbuprenorphine through CYP3A4 and CYP2C8 [5], the metabolism pathways metabolizing buprenorphine to other non-specified metabolites through CYP3A4, CYP3A7, UGT1A1, UGT1A3 and UGT2B7 as well as renal excretion through glomerular filtration.

For the metabolite norbuprenorphine metabolism through UGT1A1 and UGT1A3 as well as renal clearance by glomerular filtration and tubular secretion through the transport protein P-glycoprotein (P-gp) were implemented in the model [6, 7]. The respective Michaelis-Menten constants ( $K_m$ ) and maximum reaction velocities ( $v_{max}$ ) were obtained from published *in vitro* experiments [5, 8]. As nonspecific binding influences  $K_m$  and  $K_i$  values in *in vitro* assays in microsomes, the values need to be adjusted by multiplication with fraction unbound in the microsomal assay ( $f_{u,mic}$ ) [9]. Hence, the obtained literature values of  $K_m$  and  $K_i$  were multiplied by measured  $f_{u,mic}$  values of buprenorphine (0.42) and norbuprenorphine (0.84), respectively [6]. The enzyme CYP3A4 catalyzes two different metabolic pathways of buprenorphine, the metabolism to norbuprenorphine ( $R_1$ ) and a reaction, in which norbuprenorphine is not the product substance ( $R_2$ ) [5]. For the latter one, no specific  $K_m$  and  $v_{max}$  values were reported. Hence, the  $K_{m,R_2}$  value was assumed to be the same as for  $R_1$  and  $v_{max,R_2}$  was calculated to be a multiple of  $v_{max,R_1}$  using the amount of buprenorphine consumed and the amount of norbuprenorphine produced, respectively, from the *in vitro* study by Picard et al. yielding a  $v_{max,R_2}$  value of 1352.1 pmol/min/mg microsomal protein [5].

Studies have shown that CYP3A7 is involved in buprenorphine metabolism [5, 10]. CYP3A7 is the major fetal form of CYP3A [11]. Hence, CYP3A7 can be important for PK predictions of CYP3A substrates in pediatrics and therefore was incorporated in our model for predictions in pediatrics.  $K_m$  and  $v_{max}$  values for the metabolism of buprenorphine through CYP3A7 have not been reported. However, a study by Williams et al. provides information on the relative metabolic capabilities of CYP3A4 and CYP3A7 to metabolize a structurally diverse set of molecules ( $n=15$ ) by comparing  $K_m$  [ $\mu\text{mol/L}$ ] and  $v_{max}$  [ $\text{nmol/min/nmol P450}$ ] values [11]. The dataset was extended by three more molecules including their respective  $K_m$  and  $v_{max}$  values from a recently published study [12]. On average,  $K_m$  values for CYP3A7 were 5.1 times higher compared to the respective  $K_m$  values of CYP3A4 for the model substances,  $v_{max}$  values were 75% lower. These factors were used and multiplied with the  $K_m$  and  $v_{max}$  values for the metabolism of buprenorphine through CYP3A4 (5.7  $\mu\text{mol/L}$  and 12.5 pmol/min/pmol P450, calculated from 1352.1 pmol/min/mg microsomal protein and the content of CYP3A4 enzyme of 108 pmol P450/mg microsomal protein in liver microsomes [5, 13, 14]) to obtain the values for CYP3A7. This yields a  $K_m$  value of 29.1  $\mu\text{mol/L}$  and a  $v_{max}$  value of 3.17 pmol/min/pmol P450 or 632.6 pmol/min/mg microsomal protein using the protein content of CYP3A7 enzyme of 199.57 pmol P450/mg microsomal protein in fetal liver microsomes [15].

According to the literature, about 35% of buprenorphine is metabolized to norbuprenorphine [5, 16, 17]. In order to achieve this amount, two factors for the metabolism to norbuprenorphine and the metabolism to other metabolites, respectively, were estimated and multiplied with the *in vitro* literature values for the respective maximum reaction velocities (see Table 2 in the main manuscript).

## 1.2 System-dependent Parameters and Virtual Populations

PBPK modeling enables mechanistic representation of drug disposition in virtual individuals. Virtual individuals with all system-dependent physiological parameters such as blood flow rates and organ compositions were generated in PK-Sim<sup>®</sup> based on the demographic characteristics of the respective study population (see Table 1 in the manuscript and Table S2). The applied algorithms for the generation of virtual individuals have been previously reported [18]. If no information on study demographics was available, a standard 30-year-old male was assumed with weight and height values according to the PK-Sim<sup>®</sup> database.

Virtual populations of 100 individuals for each study were set up according to the population demographics of each respective simulated study. If no age range was specified, virtual populations were created with individuals 20 to 50 years of age and without specific body weight or height restrictions as implemented in PK-Sim<sup>®</sup>. In the generated virtual populations, demographics such as age, height, weight and corresponding organ volumes, tissue compositions, blood flow rates, etc. were varied by an implemented algorithm in PK-Sim<sup>®</sup> within the limits of the ICRP (International Commission on Radiological Protection) or NHANES (National Health and Nutrition Examination Survey) databases [19, 20]. Tissue expression distributions of the enzymes and proteins were provided in the PK-Sim<sup>®</sup> expression database according to the literature [21–23].

Additionally, variability of the expression levels of the implemented drug metabolizing enzymes CYP2C8, CYP3A4, CYP3A7, UGT1A1, UGT1A3 and UGT2B7 as well as of the transport protein P-gp was implemented. System-dependent parameters, such as information on reference concentrations and the respective variabilities of metabolizing enzymes and transporters are shown in Table S1. Population predictions were plotted as geometric mean with geometric standard deviation. If all individual concentration-time datasets were available but demographic values could not be matched to the specific profile, median with 90% population prediction intervals were plotted.

**Table S1:** System-dependent parameters and expression of relevant enzymes and transporters.

Enzyme / Transporter	Mean reference concentration [ $\mu\text{mol/L}$ ] <sup>a</sup>	Geometric standard deviation of the reference concentration in adults <sup>b</sup>	Relative expression in the different organs <sup>c</sup>	Ontogeny function	Half-life liver [hours]	Half-life Intestine [hours]
<b>Enzymes</b>						
CYP2C8	2.56 [14]	2.05 [24]	RT-PCR [21]	[24]	23	23
CYP3A4	4.32 [14]	1.18 (liver)[24] 1.45 (intestine)[24]	RT-PCR [21]	[24]	36	23
CYP3A7	7.98 [15]	1.25 [24]	RT-PCR [21]	[24]	36	23
UGT1A1	1.30 [25]	1.37 [24]	RT-PCR [23]	[24]	36	23
UGT1A3	0.40 [25]	1.60 <sup>d</sup>	RT-PCR [23]	[24] <sup>d</sup>	36	23
UGT2B7	2.78 [25]	1.60 [24]	EST [26]	[24]	36	23
<b>Transporters</b>						
P-gp	1.41 [27]	1.60 [28]	RT-PCR [22] <sup>e</sup>	-	36	23

**CYP:** cytochrome P450, **EST:** Expressed Sequence Tags, **P-gp:** P-glycoprotein, **RT-PCR:** reverse transcription polymerase chain reaction, **UGT:** uridine 5'-diphospho-glucuronosyltransferase

<sup>a</sup> [ $\mu\text{mol protein/L}$ ] in the tissue of the highest expression

<sup>b</sup> for information on geometric standard deviation in pediatrics, please refer to [24]

<sup>c</sup> PK-Sim<sup>®</sup> expression database profile

<sup>d</sup> since no specific ontogeny function for UGT1A3 is implemented in PK-Sim<sup>®</sup>, the same ontogeny function as for UGT2B7 was assumed based on ontogeny information in [29]

<sup>e</sup> with the relative expression in intestinal mucosa increased by factor 3.57 according to [27]

**Table S2:** Extension of Table 1 in the main manuscript with detailed information on the demographics and dosing regimens of the study by Barrett et al. [30]

Clinical study	Loading dose <sup>a</sup> (30 min) [µg/kg]	Second Dose <sup>a</sup> [µg/kg/h]	Infusion Time (second dose) [h]	n	Female [%]	Age <sup>b</sup> [weeks]	Weight [kg]	Blood sample	Norbuprenorphine measurements
Barrett et al. 1993 (1)	3.00	0.72	48	1	-	31	1.5	arterial	no
Barrett et al. 1993 (2)	3.00	0.72	24	1	-	30	0.9	arterial	no
Barrett et al. 1993 (3)	3.00	0.72	11	1	-	32	1.3	arterial	no
Barrett et al. 1993 (4)	3.00	0.72	42	1	-	31	1.8	arterial	no
Barrett et al. 1993 (5)	3.00	0.72	42	1	-	30	1.5	arterial	no
Barrett et al. 1993 (6)	3.00	1.44	23	1	-	28	1.2	arterial	no
Barrett et al. 1993 (7)	3.00	1.44	77	1	-	31	1.1	arterial	no
Barrett et al. 1993 (8)	3.00	0.72	42	1	-	34	1.8	arterial	no
Barrett et al. 1993 (9)	3.00	2.16	81	1	-	30	1.6	arterial	no
Barrett et al. 1993 (10)	3.00	0.72	43	1	-	32	2.4	arterial	no
Barrett et al. 1993 (11)	3.00	0.72	76	1	-	31	1.6	arterial	no
Barrett et al. 1993 (12)	3.00	0.72	118	1	-	27	1.0	arterial	no

-: not available

<sup>a</sup> intravenous administration<sup>b</sup> postmenstrual age

## 2 Drug-Drug-Interaction (DDI) Modeling

### 2.1 DDI Modeling – General

Rifampicin is both an inhibitor and inducer of different CYP enzymes. This includes the enzymes CYP2C8, CYP3A4, UGT1A1 and UGT1A3 as well as the transporter P-gp among others [31–39]. A previously developed rifampicin PBPK model [27] was used for the DDI assessment and was extended by interaction constants describing the induction of CYP2C8, UGT1A1 and UGT1A3 as well as the competitive inhibition of CYP2C8, UGT1A1 and UGT1A3 by rifampicin. The parameters of the extended rifampicin model are shown in Table S3.

**Table S3:** Drug-dependent parameters of the rifampicin PBPK model (adopted from [27])

Parameter	Value	Unit	Source	Literature	Reference	Description
MW	822.94	g/mol	Literature	822.94	[40]	Molecular weight
pKa (acid)	1.70	-	Literature	1.70	[41]	First acid dissociation constant
pKa (base)	7.90	-	Literature	7.90	[41]	Second acid dissociation constant
Solubility (pH 7.5)	2.80	g/l	Literature	2.80	[42]	Solubility
logP	2.50	-	Optimized	1.30, 2.70	[40, 43]	Lipophilicity
$f_u$	17.00	%	Literature	17.00	[36]	Fraction unbound
B/P ratio	0.89	-	Calculated	0.90 <sup>a</sup>	[44]	Blood/plasma ratio
OATP1B1 $K_m$	1.50	$\mu\text{mol/l}$	Literature	1.50	[45]	OATP1B1 Michaelis-Menten constant
OATP1B1 $k_{\text{cat}}$	105.41	1/min	Optimized	-	-	OATP1B1 transport rate constant
AADAC $K_m$	195.10	$\mu\text{mol/l}$	Literature	195.10	[46]	AADAC Michaelis-Menten constant
AADAC $k_{\text{cat}}$	9.87	1/min	Optimized	-	-	AADAC catalytic rate constant
P-gp $K_m$	55.00	$\mu\text{mol/l}$	Literature	55.00	[47]	P-gp Michaelis-Menten constant
P-gp $k_{\text{cat}}$	0.61	1/min	Optimized	-	-	P-gp transport rate constant
GFR fraction	1.00	-	Assumed	-	-	Fraction of filtered drug in the urine
EHC continuous fraction	1.00	-	Assumed	-	-	Fraction of bile continually released
Induction $\text{EC}_{50}$	0.34	$\mu\text{mol/l}$	Literature	0.80*0.42	[36, 48]	Conc. for half-maximal induction
$E_{\text{max}}$ OATP1B1	0.38	-	Optimized	-	-	Maximum <i>in vivo</i> induction effect
$E_{\text{max}}$ OATP1B3	0.38	-	Assumed	-	-	Maximum <i>in vivo</i> induction effect
$E_{\text{max}}$ AADAC	0.99	-	Optimized	-	-	Maximum <i>in vivo</i> induction effect
$E_{\text{max}}$ P-gp	2.50	-	Literature	2.50	[38]	Maximum <i>in vivo</i> induction effect
$E_{\text{max}}$ CYP2C8	3.20	-	Literature	3.20	[39]	Maximum <i>in vivo</i> induction effect
$E_{\text{max}}$ CYP3A4	9.00	-	Literature	9.00	[36]	Maximum <i>in vivo</i> induction effect
$E_{\text{max}}$ UGT1A1	1.30	-	Literature	1.30	[34]	Maximum <i>in vivo</i> induction effect
$E_{\text{max}}$ UGT1A3	1.40	-	Literature	1.40	[35]	Maximum <i>in vivo</i> induction effect
OATP1B1 $K_i$	0.48	$\mu\text{mol/l}$	Literature	0.48	[49]	Conc. for half-maximal inhibition
OATP1B3 $K_i$	0.90	$\mu\text{mol/l}$	Literature	0.90	[50]	Conc. for half-maximal inhibition
P-gp $K_i$	169.00	$\mu\text{mol/l}$	Literature	169.00	[37]	Conc. for half-maximal inhibition
CYP2C8 $K_i$	30.20	$\mu\text{mol/l}$	Literature	30.20	[31]	Conc. for half-maximal inhibition
CYP3A4 $K_i$	18.50	$\mu\text{mol/l}$	Literature	18.50	[31]	Conc. for half-maximal inhibition
UGT1A1 $K_i$	33.00	$\mu\text{mol/l}$	Literature	33.00	[33]	Conc. for half-maximal inhibition
UGT1A3 $K_i$	600.00	$\mu\text{mol/l}$	Literature	600.00	[32]	Conc. for half-maximal inhibition
Partition coefficients	Diverse	-	Calculated	R&R	[51, 52]	Cell to plasma partition coefficients
Cellular permeability	2.93E-05	cm/min	Calculated	PK-Sim	[13]	Permeability into the cellular space
Intestinal permeability	1.24E-05	cm/min	Optimized	3.84E-07	Calculated	Transcellular intestinal permeability
Formulation	Solution	-	-	-	-	-

**AADAC:** arylacetamide deacetylase, **conc:** concentration, **CYP:** cytochrome P450, **EHC:** enterohepatic circulation, **GFR:** glomerular filtration rate, **OATP:** organic anion transporting polypeptide, **P-gp:** P-glycoprotein, **PK-Sim:** PK-Sim standard calculation method, **R&R:** Rodgers and Rowland calculation method, **UGT:** uridine 5'-diphospho-glucuronosyltransferase

<sup>a</sup> Blood/serum concentration ratio

For the simulation of the DDI with itraconazole and clarithromycin two previously published PBPK models were used [27]. The parameters of both models can be found in the supplementary material of the respective publication [27].

The DDI simulations presented in the manuscript depict pure predictions. No DDI study was used for model input parameter estimation during buprenorphine and norbuprenorphine PBPK model

development. Interaction parameters necessary for DDI simulation were obtained from literature or from the published DDI perpetrator PBPK models. With that, the adult PBPK model could not only be evaluated by its predictive performance with the test dataset but also by prediction of a DDI study [53].

## 2.2 Mathematical Implementation of DDIs

### 2.2.1 Competitive Inhibition

Competitive inhibition describes the reversible binding of an inhibitor to the active site of an enzyme or transporter and hence, the competition of substrate and inhibitor for binding. This inhibition process can be overcome by high substrate concentrations leading to a concentration-dependency. As a result of competitive inhibition  $v_{max}$  is not affected, while  $K_m$  is increased through the inhibition yielding  $K_{m,app}$  (Equation S1). The reaction velocity ( $v$ ) for the substrate during concomitant administration with a competitive inhibitor is described by Equation S2 [13]:

$$K_{m,app} = K_m \cdot \left(1 + \frac{[I]}{K_i}\right) \quad (S1)$$

$$v = \frac{v_{max} \cdot [S]}{K_{m,app} + [S]} \quad (S2)$$

with  $K_{m,app}$  = Michaelis-Menten constant in the presence of inhibitor,  $K_m$  = Michaelis-Menten constant,  $[I]$  = free inhibitor concentration,  $K_i$  = dissociation constant of the inhibitor-enzyme/transporter complex,  $v$  = reaction velocity,  $v_{max}$  = maximum reaction velocity,  $[S]$  = free substrate concentration.

### 2.2.2 Mechanism-Based Inhibition (MBI)

Mechanism-based inhibition (MBI) is an irreversible type of inhibition. *De novo* synthesis of the inactivated protein and clearance of the mechanism-based inactivator is required to return to baseline activity of the enzyme or transporter (time-dependency). In the case of MBI, the protein degradation rate constant ( $k_{deg}$ ) is increased ( $k_{deg,app}$ , Equation S3), while the synthesis ( $R_{syn}$ ) is not affected by the inhibition process. The protein turnover during MBI is described by Equation S4. As mechanism-based inactivators are also competitive inhibitors, the  $K_m$  in the Michaelis-Menten reaction velocity equation is substituted by  $K_{m,app}$  as in Equation S5 [13]:

$$k_{deg,app} = k_{deg} + \left(\frac{k_{inact} \cdot [I]}{K_I + [I]}\right) \quad (S3)$$

$$\frac{dE(t)}{dt} = R_{syn} - k_{deg,app} \cdot E(t) \quad (S4)$$

$$v = \frac{v_{max} \cdot [S]}{K_{m,app} + [S]} = \frac{k_{cat} \cdot E(t) \cdot [S]}{K_{m,app} + [S]} \quad (S5)$$

with  $k_{deg,app}$  = enzyme or transporter degradation rate constant in the presence of mechanism-based inactivator,  $k_{deg}$  = enzyme or transporter degradation rate constant,  $k_{inact}$  = maximum inactivation rate constant,  $[I]$  = free inactivator concentration,  $K_I$  = concentration for half-maximal inactivation,  $E(t)$  = enzyme or transporter concentration,  $R_{syn}$  = rate of enzyme or transporter synthesis,  $v$  =

reaction velocity,  $v_{max}$  = maximum reaction velocity,  $[S]$  = free substrate concentration,  $K_{m,app}$  = Michaelis-Menten constant in the presence of inactivator,  $k_{cat}$  = catalytic rate constant.

### 2.2.3 Induction

Induction of an enzyme or transporter is often mediated through activation of the transcription factor pregnane X receptor (PXR). Similarly as in the case of an MBI, the return to baseline activity requires the clearance of the inducer and degradation of the induced protein (time-dependency). However, in contrast to the MBI, in this case  $R_{syn}$  is increased ( $R_{syn,app}$ , Equation S6), while  $k_{deg}$  remains unchanged. The protein turnover during induction is described by Equation S7 [13]:

$$R_{syn,app} = R_{syn} \cdot \left( 1 + \frac{E_{max} \cdot [Ind]}{EC_{50} + [Ind]} \right) \quad (S6)$$

$$\frac{dE(t)}{dt} = R_{syn,app} - k_{deg} \cdot E(t) \quad (S7)$$

$$v = \frac{v_{max} \cdot [S]}{K_m + [S]} = \frac{k_{cat} \cdot E(t) \cdot [S]}{K_m + [S]} \quad (S8)$$

with  $R_{syn,app}$  = rate of enzyme or transporter synthesis in the presence of inducer,  $R_{syn}$  = rate of enzyme or transporter synthesis,  $E_{max}$  = maximal induction effect *in vivo*,  $[Ind]$  = free inducer concentration,  $EC_{50}$  = concentration for half-maximal induction *in vivo*,  $E(t)$  = enzyme or transporter concentration,  $k_{deg}$  = enzyme or transporter degradation rate constant,  $v$  = reaction velocity,  $v_{max}$  = maximum reaction velocity,  $[S]$  = free substrate concentration,  $K_m$  = Michaelis-Menten constant,  $k_{cat}$  = catalytic rate constant.

### 3 Allometric Scaling

After the development of the adult PBPK model, the model was scaled to a children and preterm neonate population for *a priori* predictions of the PK in pediatrics as described in the methods section of the main manuscript. In order to compare the PBPK model predictions for plasma concentration-time profiles observed in pediatric patients, a classical allometric scaling approach as described by Tod et al. was used [54]. Here, the parameters of classical compartmental models are scaled by allometry from adults to the pediatric populations with:

$$CL_{pediatrics} = CL_{adults} \cdot \left( \frac{BW_{pediatrics}}{BW_{adults}} \right)^{0.75} \quad (S9)$$

$$Q_{2,pediatrics} = Q_{2,adults} \cdot \left( \frac{BW_{pediatrics}}{BW_{adults}} \right)^{0.75} \quad (S10)$$

$$Q_{3,pediatrics} = Q_{3,adults} \cdot \left( \frac{BW_{pediatrics}}{BW_{adults}} \right)^{0.75} \quad (S11)$$

$$V_{c,pediatrics} = V_{c,adults} \cdot \left( \frac{BW_{pediatrics}}{BW_{adults}} \right) \quad (S12)$$

$$V_{2,pediatrics} = V_{2,adults} \cdot \left( \frac{BW_{pediatrics}}{BW_{adults}} \right) \quad (S13)$$

$$V_{3,pediatrics} = V_{3,adults} \cdot \left( \frac{BW_{pediatrics}}{BW_{adults}} \right) \quad (S14)$$

To obtain the relevant parameters of the elimination clearance, intercompartmental clearances and volume of distributions in adults ( $CL$ ,  $Q_2$ ,  $Q_3$ ,  $V_c$ ,  $V_2$  and  $V_3$  of a classical three compartment model, which best described the observed plasma concentration-time profiles), the parameters were estimated with NONMEM<sup>®</sup> using the internal dataset from the PBPK modeling approach. Body weight values of the adult (71 kg) and pediatric patients (see Table 1 in the main manuscript and Table S2) were extracted from the corresponding study information. In the case of scaling the elimination clearance for preterm neonates ( $CL_{preterm\ neonates}$ ), the calculation was performed both with an exponent of 0.75 and with the age-dependent exponent of 1.2 as suggested by Mahmood and Tegenge [55]:

$$CL_{preterm\ neonates, ADE} = CL_{adults} \cdot \left( \frac{BW_{pediatrics}}{BW_{adults}} \right)^{1.2} \quad (S15)$$

The plasma concentrations were then simulated with the scaled parameters (Table S4) and compared with the corresponding plasma concentrations observed.

**Table S4:** Parameters calculated with the allometric scaling approach

Clinical study	CL [ml/min] <sup>a</sup>	CL [ml/min] <sup>b</sup>	Q <sub>2</sub> [ml/min]	Q <sub>3</sub> [ml/min]	V <sub>c</sub> [L]	V <sub>2</sub> [L]	V <sub>3</sub> [L]
Adults (internal dataset)	982.0	982.0	2980.0	554.0	29.6	105.0	676.0
Barrett et al. 1993 (1)	54.5	9.6	165.0	31.0	0.6	2.2	14.3
Barrett et al. 1993 (2)	37.8	5.3	115.0	21.0	0.4	1.4	8.8
Barrett et al. 1993 (3)	50.1	8.4	152.0	28.0	0.6	2.0	12.8
Barrett et al. 1993 (4)	61.4	12.0	186.0	35.0	0.7	2.6	16.8
Barrett et al. 1993 (5)	54.5	9.6	165.0	31.0	0.6	2.2	14.3
Barrett et al. 1993 (6)	44.9	7.1	136.0	25.0	0.5	1.7	11.1
Barrett et al. 1993 (7)	44.4	6.9	135.0	25.0	0.5	1.7	10.9
Barrett et al. 1993 (8)	61.4	11.6	186.0	35.0	0.7	2.6	16.8
Barrett et al. 1993 (9)	56.9	10.3	173.0	32.0	0.7	2.4	15.2
Barrett et al. 1993 (10)	77.5	16.9	235.0	44.0	1.0	3.6	22.9
Barrett et al. 1993 (11)	56.7	10.2	172.0	32.0	0.7	2.3	15.1
Barrett et al. 1993 (12)	41.4	6.2	126.0	23.0	0.4	1.5	9.9
Olkola et al. 1989	400.0	400.0	1214.0	226.0	8.9	32.0	204.0

CL: elimination clearance, Q<sub>2</sub>: intercompartmental clearance between compartment 2 and the central compartment, Q<sub>3</sub>: intercompartmental clearance between compartment 3 and the central compartment, V<sub>c</sub>: volume of the central compartment, V<sub>2</sub> and V<sub>3</sub>: peripheral compartment volumes

<sup>a</sup> elimination clearance parameter calculated using the allometric scaling approach without an age-dependent exponent

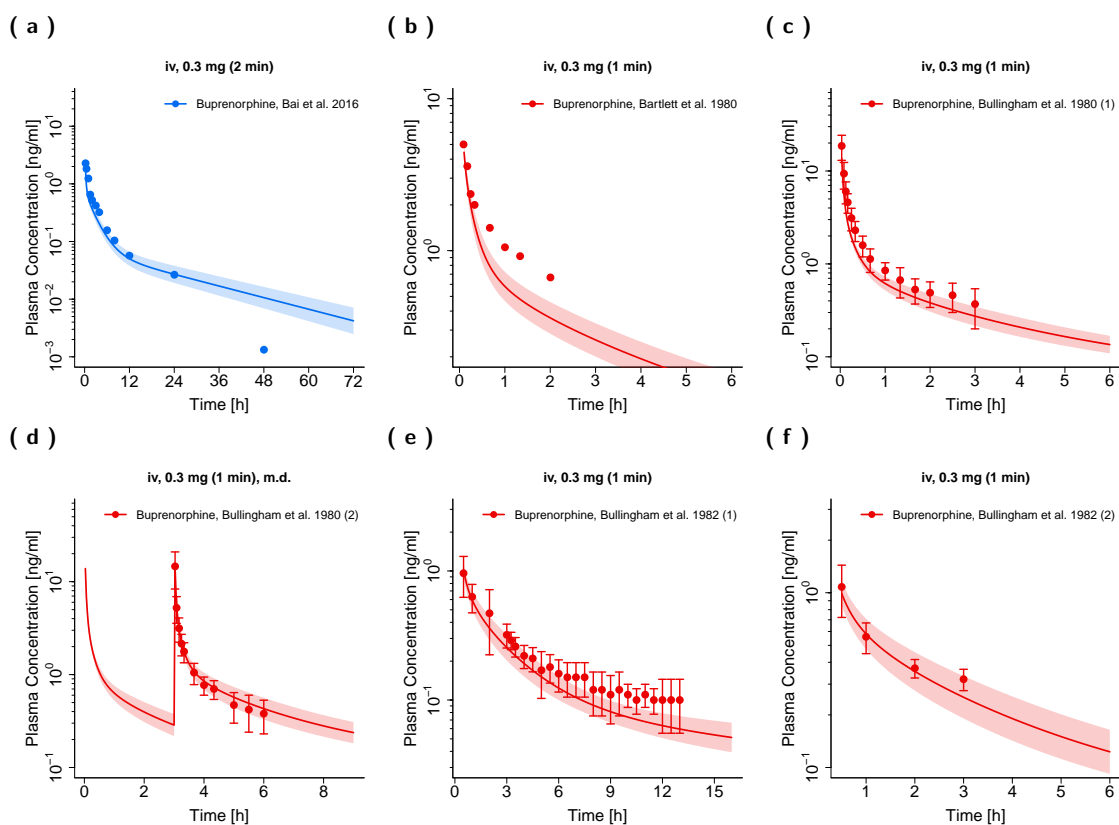
<sup>b</sup> elimination clearance parameter calculated using the allometric scaling approach with an age-dependent exponent as suggested by Mahmood and Tegenge [55]

## 4 PBPK Model Evaluation

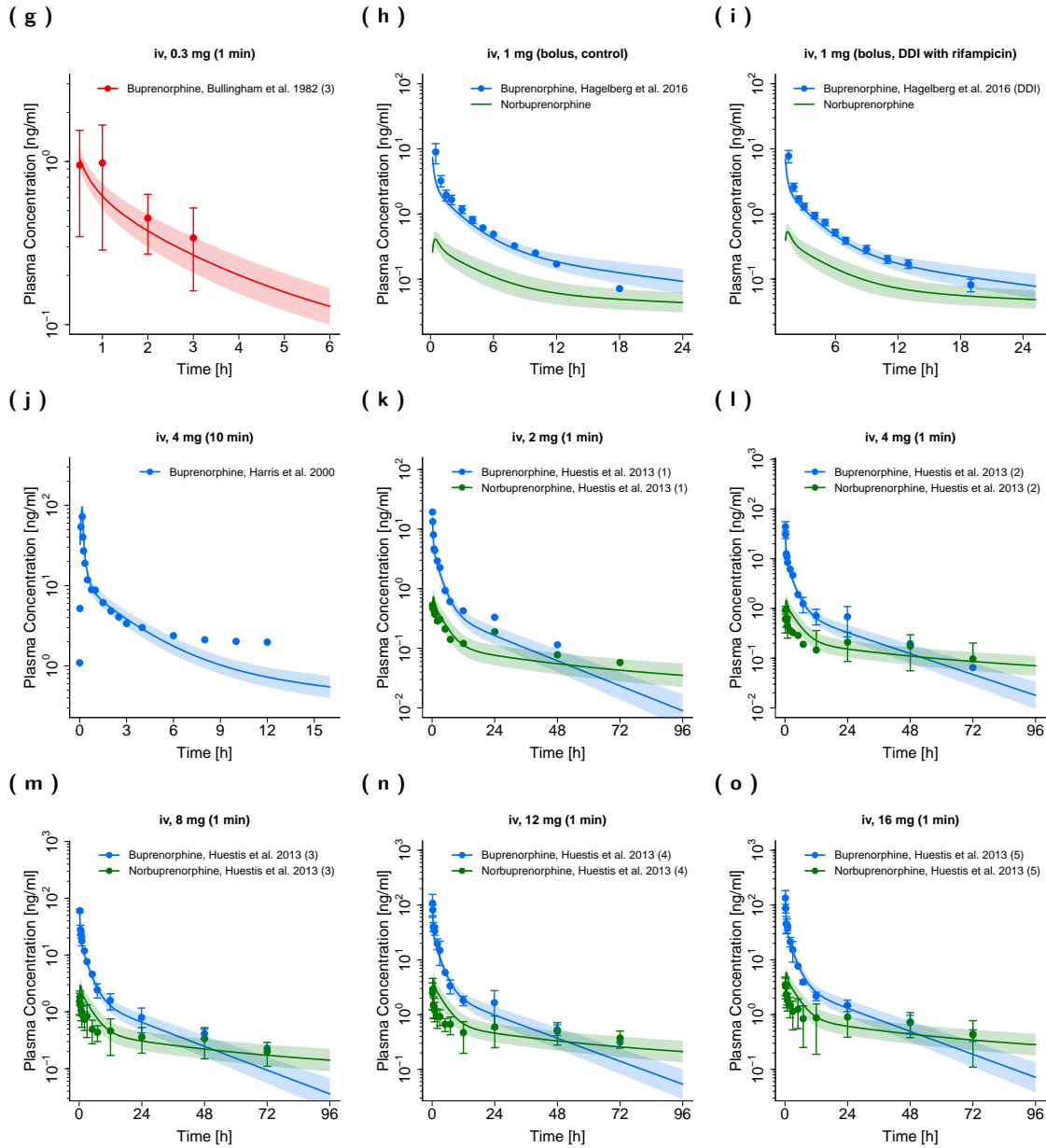
The descriptive (internal training dataset) and predictive (external test dataset) performance of the PBPK model is comprehensively demonstrated in this section: Linear and semilogarithmic plots of population predictions of plasma concentration-time profiles are compared to the observed profiles for both adult and pediatric PBPK models in Figures S1, S2, S5 and S6. Further, linear plots of population predictions of fractions of buprenorphine excreted unchanged in urine as well as fraction of dose excreted in urine as norbuprenorphine are compared to measured values in Figure S2. Moreover, goodness-of-fit plots comparing predicted to observed plasma concentrations are shown in Figures S3 and S7. Predicted compared to observed area under the plasma concentration-time curves from the first to the last data point ( $AUC_{last}$ ) and maximum concentrations ( $C_{max}$ ) values for long-term infusions in preterm neonates and norbuprenorphine metabolite are shown in Figures S4 and S8. The mean relative deviation (MRD) values as well as the predicted and observed  $AUC_{last}$  and  $C_{max}$  values including the geometric mean fold errors (GMFE) are listed in Tables S5 and S6. A local sensitivity analysis was performed in a steady-state scenario (1.4 mg (adults), 0.7 mg (children), 0.009 mg (preterm neonates), 168 hours long-term infusion, mimicking steady-state plasma concentrations of about 0.13 ng/ml, which were achieved with an administration of marketed transdermal buprenorphine patches [56]). A detailed description and the results of the sensitivity analysis can be found in Section 4.6.

## 4.1 Adult PBPK Model Evaluation

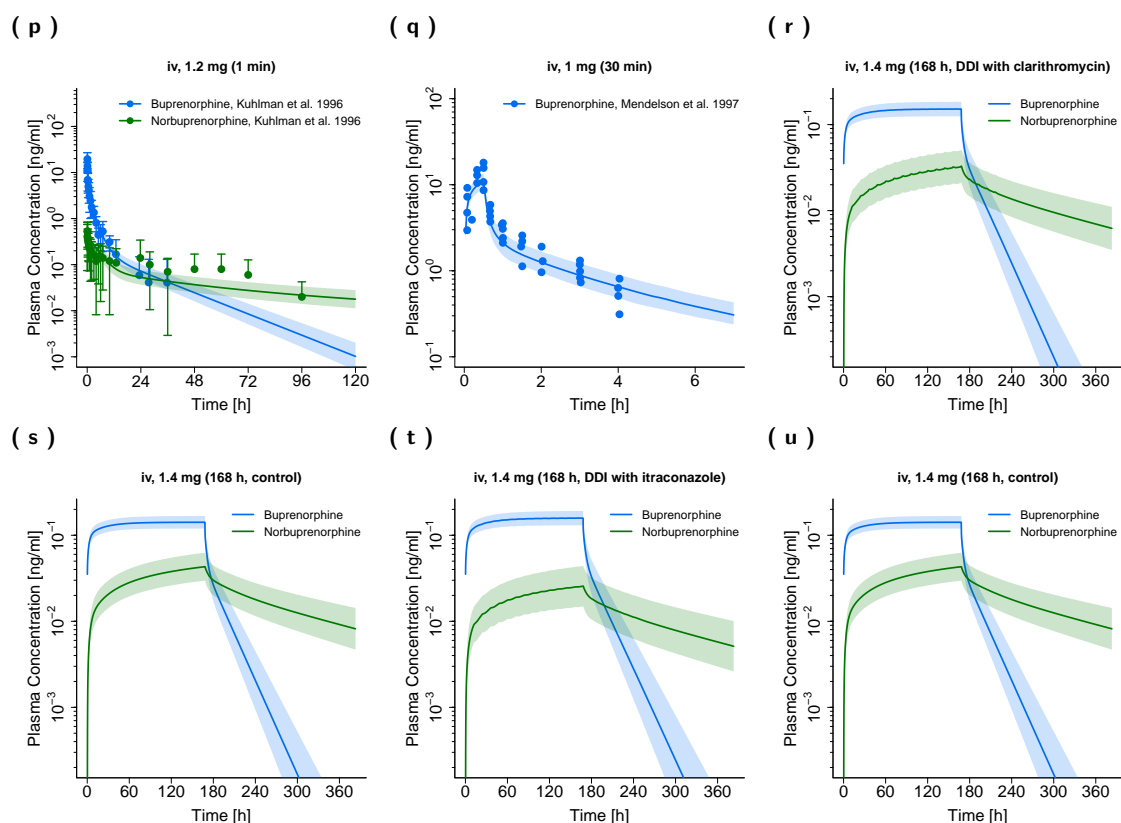
In this section, linear and semilogarithmic plots of plasma concentration-time profiles, linear plots of fractions of buprenorphine dose excreted unchanged in urine and fraction of dose excreted in urine as norbuprenorphine (Figures S1 and S2), a goodness-of-fit plot of predicted compared to observed plasma concentrations (Figure S3) and goodness-of-fit plots of predicted compared to observed  $AUC_{last}$  and  $C_{max}$  values (Figure S4) after intravenous administration of buprenorphine in adults are shown.



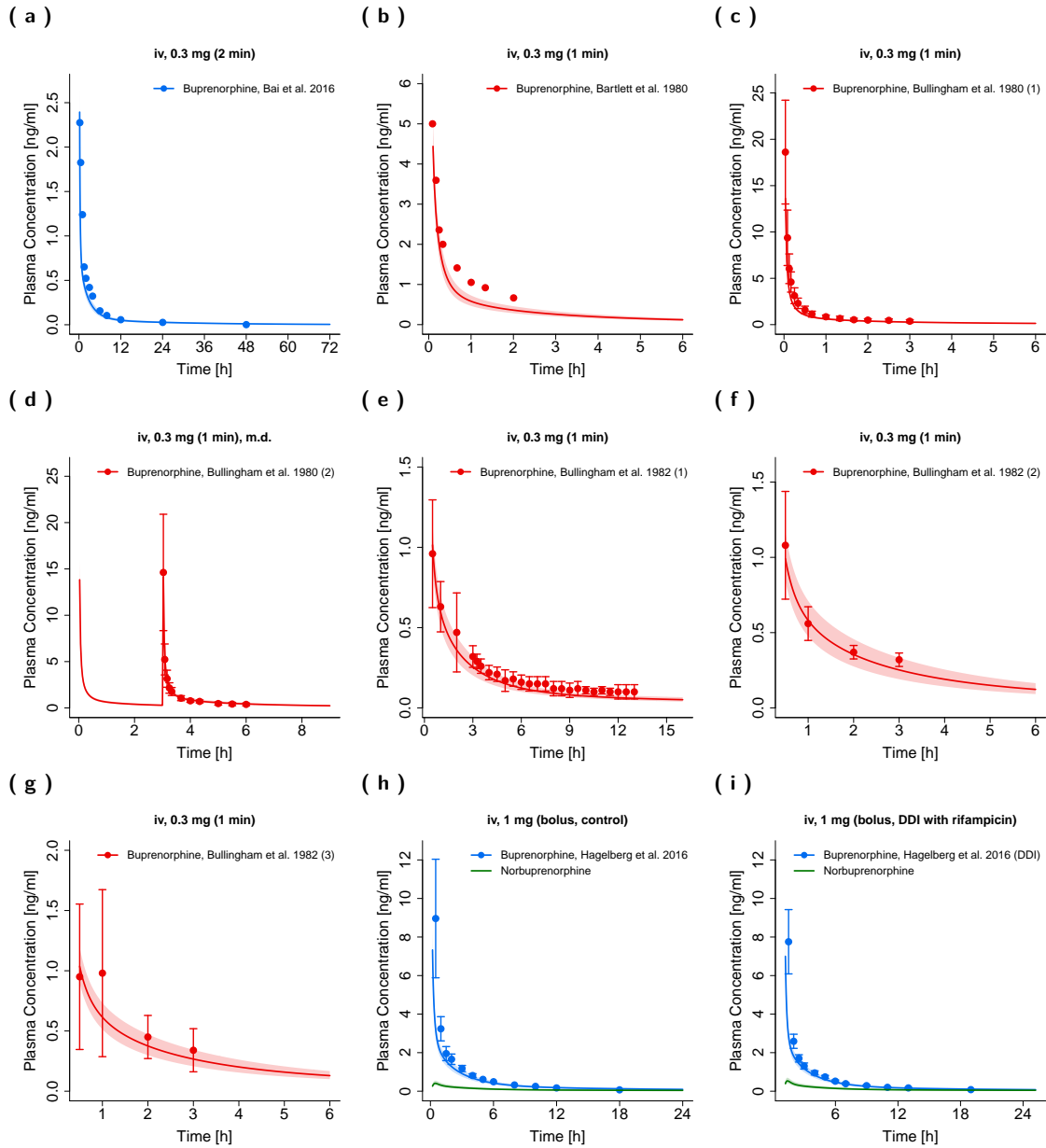
**Figure S1: Buprenorphine (blue: venous blood, red: arterial blood) and norbuprenorphine (green: venous blood) plasma concentration-time profiles (semilogarithmic) after intravenous administration of buprenorphine in adults.** Observed data are shown as circles, if available  $\pm$  standard deviation (SD). Population simulation ( $n=100$ ) geometric means are shown as lines; the shaded areas represent the predicted population geometric SD except for subfigure (q) where the line represents the population median and the shaded area the 90% population prediction interval. References with numbers in parentheses link to a specific observed dataset described in the study table (Table 1 in the main manuscript). Predicted and observed  $AUC_{last}$  and  $C_{max}$  values are compared in Table S6. DDI, drug-drug-interaction; iv, intravenous; m.d., multiple dose.



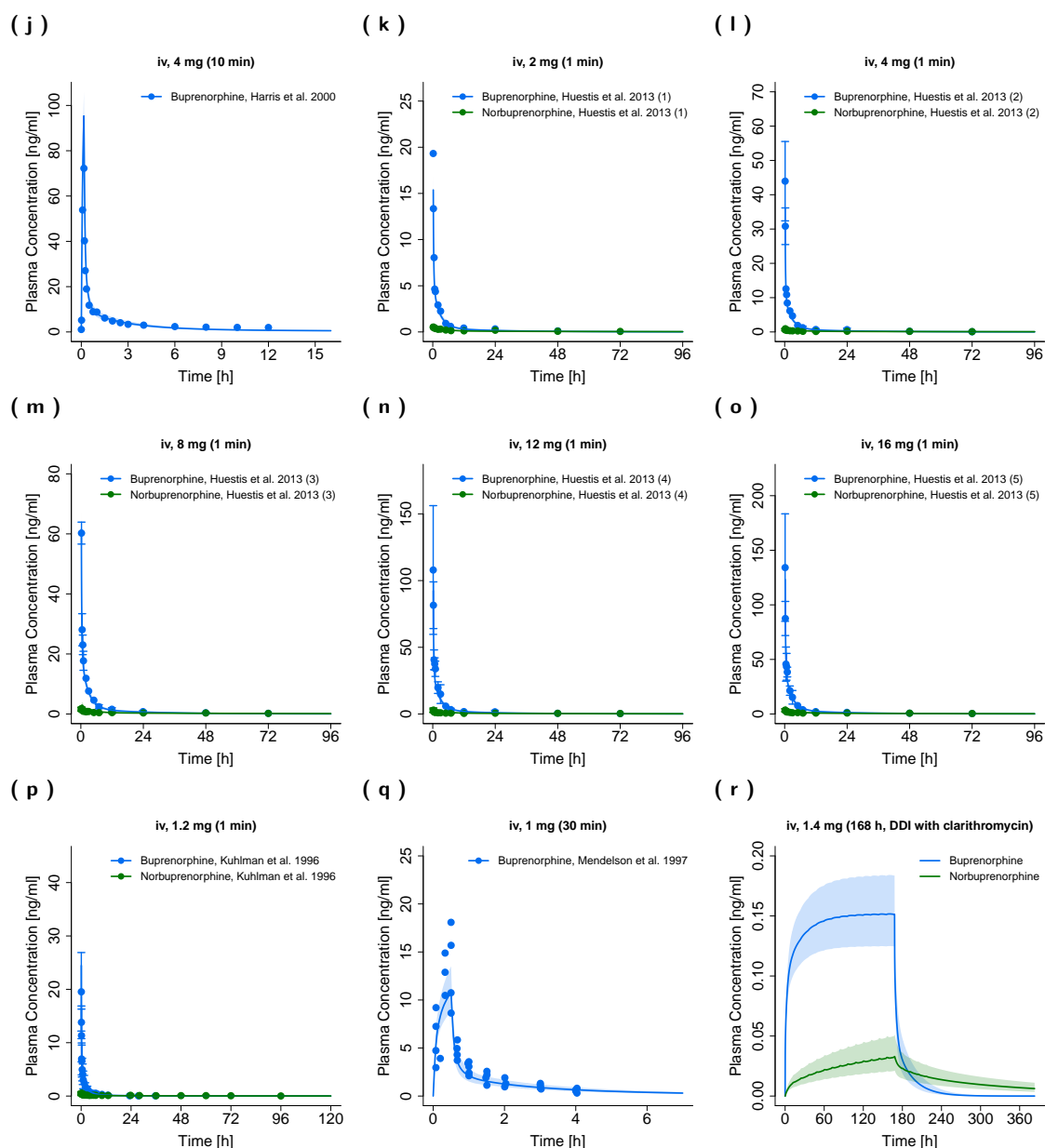
**Figure S1: Buprenorphine (blue: venous blood, red: arterial blood) and norbuprenorphine (green: venous blood) plasma concentration-time profiles (semilogarithmic) after intravenous administration of buprenorphine in adults.** Observed data are shown as circles, if available  $\pm$  standard deviation (SD). Population simulation ( $n=100$ ) geometric means are shown as lines; the shaded areas represent the predicted population geometric SD except for subfigure (q) where the line represents the population median and the shaded area the 90% population prediction interval. References with numbers in parentheses link to a specific observed dataset described in the study table (Table 1 in the main manuscript). Predicted and observed  $AUC_{last}$  and  $C_{max}$  values are compared in Table S6. DDI, drug-drug-interaction; iv, intravenous; m.d., multiple dose. (continued)



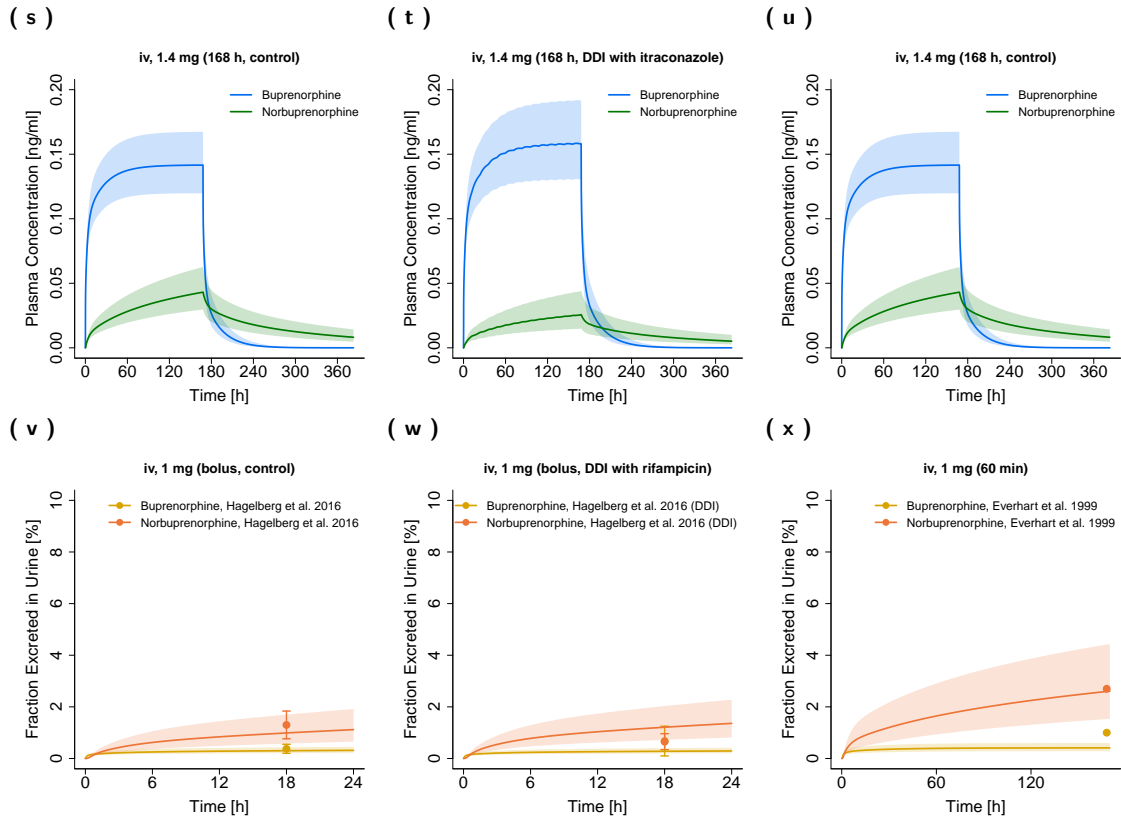
**Figure S1: Buprenorphine (blue: venous blood, red: arterial blood) and norbuprenorphine (green: venous blood) plasma concentration-time profiles (semilogarithmic) after intravenous administration of buprenorphine in adults.** Observed data are shown as circles, if available  $\pm$  standard deviation (SD). Population simulation ( $n=100$ ) geometric means are shown as lines; the shaded areas represent the predicted population geometric SD except for subfigure (q) where the line represents the population median and the shaded area the 90% population prediction interval. References with numbers in parentheses link to a specific observed dataset described in the study table (Table 1 in the main manuscript). Predicted and observed  $AUC_{last}$  and  $C_{max}$  values are compared in Table S6. **DDI**, drug-drug-interaction; **iv**, intravenous; **m.d.**, multiple dose. (continued)



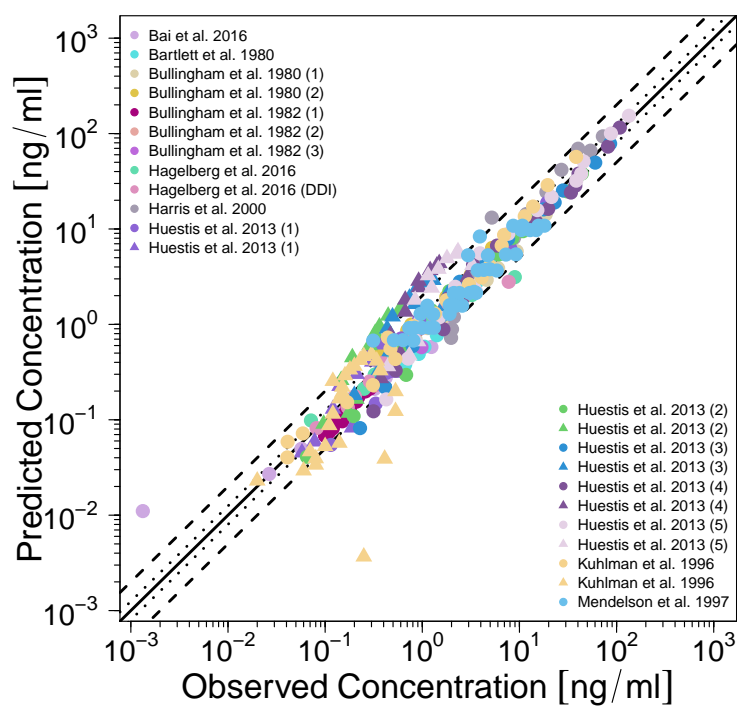
**Figure S2: Buprenorphine (blue: venous blood, red: arterial blood) and norbuprenorphine (green: venous blood) plasma concentration-time profiles (linear) as well as fraction of buprenorphine (yellow) and norbuprenorphine (orange) excreted in urine after intravenous administration of buprenorphine in adults.** Observed data are shown as circles, if available  $\pm$  standard deviation (SD). Population simulation ( $n=100$ ) geometric means are shown as lines; the shaded areas represent the predicted population geometric SD except for subfigure (q) where the line represents the population median and the shaded area the 90% population prediction interval. References with numbers in parentheses link to a specific observed dataset described in the study table (Table 1 in the main manuscript). Predicted and observed  $AUC_{last}$  and  $C_{max}$  values are compared in Table S6. DDI, drug-drug-interaction; iv, intravenous; m.d., multiple dose.



**Figure S2: Buprenorphine (blue: venous blood, red: arterial blood) and norbuprenorphine (green: venous blood) plasma concentration-time profiles (linear) as well as fraction of buprenorphine (yellow) and norbuprenorphine (orange) excreted in urine after intravenous administration of buprenorphine in adults.** Observed data are shown as circles, if available  $\pm$  standard deviation (SD). Population simulation ( $n=100$ ) geometric means are shown as lines; the shaded areas represent the predicted population geometric SD except for subfigure (q) where the line represents the population median and the shaded area the 90% population prediction interval. References with numbers in parentheses link to a specific observed dataset described in the study table (Table 1 in the main manuscript). Predicted and observed  $AUC_{last}$  and  $C_{max}$  values are compared in Table S6. DDI, drug-drug-interaction; iv, intravenous; m.d., multiple dose. (continued)

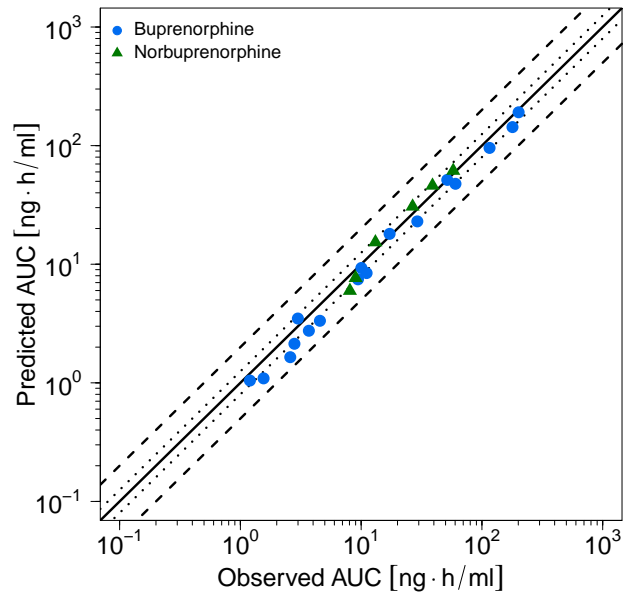
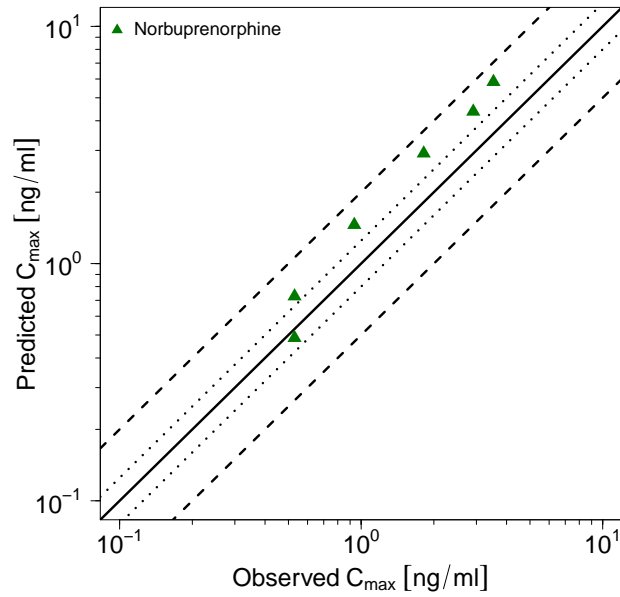


**Figure S2: Buprenorphine (blue: venous blood, red: arterial blood) and norbuprenorphine (green: venous blood) plasma concentration-time profiles (linear) as well as fraction of buprenorphine (yellow) and norbuprenorphine (orange) excreted in urine after intravenous administration of buprenorphine in adults.** Observed data are shown as circles, if available  $\pm$  standard deviation (SD). Population simulation ( $n=100$ ) geometric means are shown as lines; the shaded areas represent the predicted population geometric SD except for subfigure (q) where the line represents the population median and the shaded area the 90% population prediction interval. References with numbers in parentheses link to a specific observed dataset described in the study table (Table 1 in the main manuscript). Predicted and observed  $AUC_{last}$  and  $C_{max}$  values are compared in Table S6. **DDI**, drug-drug-interaction; **iv**, intravenous; **m.d.**, multiple dose. (continued)



**Figure S3: Predicted versus observed plasma concentrations of buprenorphine and norbuprenorphine after intravenous administration of buprenorphine in adults.** The black solid line marks the line of identity. Black dotted lines indicate 1.25-fold, black dashed lines indicate 2-fold deviation.

(a) AUC

(b)  $C_{\max}$ 

**Figure S4: Predicted versus observed buprenorphine and norbuprenorphine AUC (a) and norbuprenorphine  $C_{\max}$  (b) values after intravenous administration of buprenorphine in adults.**  $C_{\max}$  values were only calculated for long-term infusions and norbuprenorphine metabolite. Each symbol represents the  $AUC_{\text{last}}$  or  $C_{\max}$  of a different plasma profile. The black solid lines mark the lines of identity. Black dotted lines indicate 1.25-fold, black dashed lines indicate 2-fold deviation. **AUC**, area under the plasma concentration-time curve from the first to the last data point;  **$C_{\max}$** , maximum plasma concentration.

## 4.2 Pediatric PBPK Model Evaluation

In this section, linear and semilogarithmic plots of plasma concentration-time profiles (Figures S5 and S6), goodness-of-fit plots of predicted compared to observed plasma concentrations including the results of the allometric scaling approach (Figure S7) and goodness-of-fit plots of predicted compared to observed  $AUC_{last}$  and  $C_{max}$  values (Figure S8) after intravenous administration of buprenorphine in pediatrics are shown.

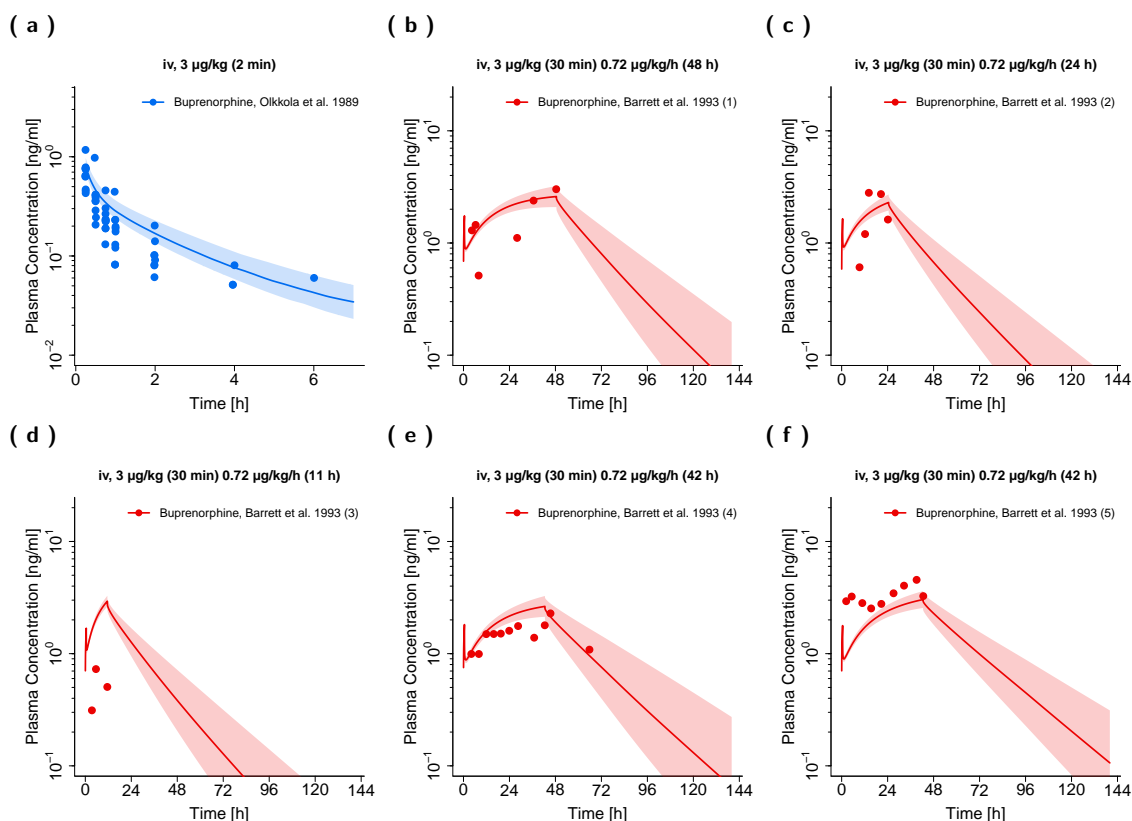


**Figure S5: Buprenorphine (blue: venous blood, red: arterial blood) plasma concentration-time profiles (semilogarithmic) after intravenous administration of buprenorphine in pediatrics.** Observed data are shown as circles. Population simulation ( $n=100$ ) geometric means are shown as lines; the shaded areas represent the predicted population geometric SD except for subfigure (a) where the line represents the population median and the shaded area the 90% population prediction interval. References with numbers in parentheses link to a specific observed dataset described in the study table (Table 1 in the main manuscript and Table S2). Predicted and observed  $AUC_{last}$  and  $C_{max}$  values are compared in Table S6. iv, intravenous.

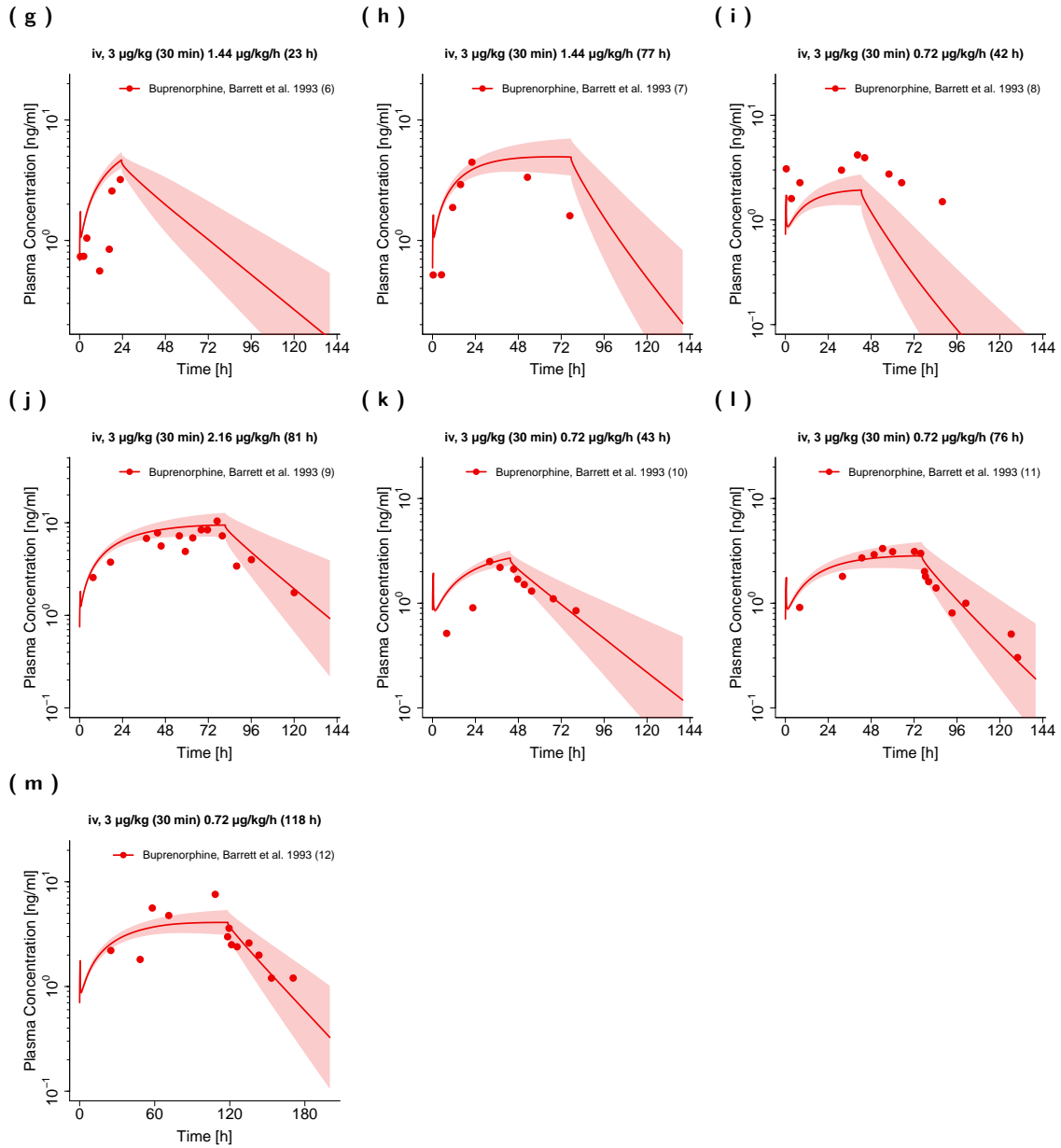


**Figure S5: Buprenorphine (blue: venous blood, red: arterial blood) plasma concentration-time profiles (semilogarithmic) after intravenous administration of buprenorphine in pediatrics.** Observed data are shown as circles. Population simulation ( $n=100$ ) geometric means are shown as lines; the shaded areas represent the predicted population geometric SD except for subfigure (a) where the line represents the population median and the shaded area the 90% population prediction interval. References with numbers in parentheses link to a specific observed dataset described in the study table (Table 1 in the main manuscript and Table S2). Predicted and observed  $AUC_{last}$  and  $C_{max}$  values are compared in Table S6. iv, intravenous. (continued)

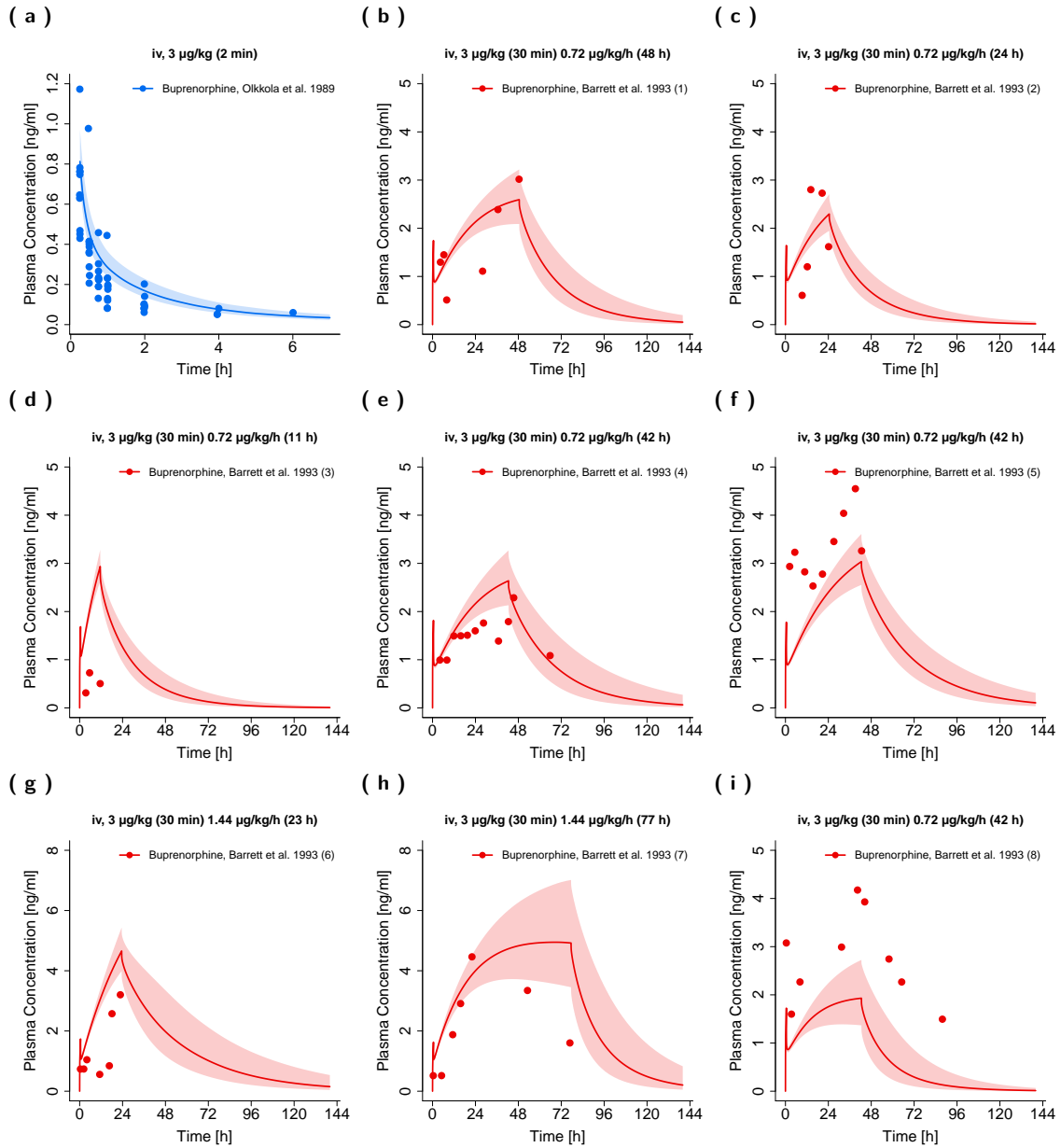


**Figure S6: Buprenorphine (blue: venous blood, red: arterial blood) plasma concentration-time profiles (linear) after intravenous administration of buprenorphine in pediatrics.** Observed data are shown as circles. Population simulation ( $n=100$ ) geometric means are shown as lines; the shaded areas represent the predicted population geometric SD except for subfigure (a) where the line represents the population median and the shaded area the 90% population prediction interval. References with numbers in parentheses link to a specific observed dataset described in the study table (Table 1 in the main manuscript and Table S2). Predicted and observed  $AUC_{last}$  and  $C_{max}$  values are compared in Table S6. **iv**, intravenous.

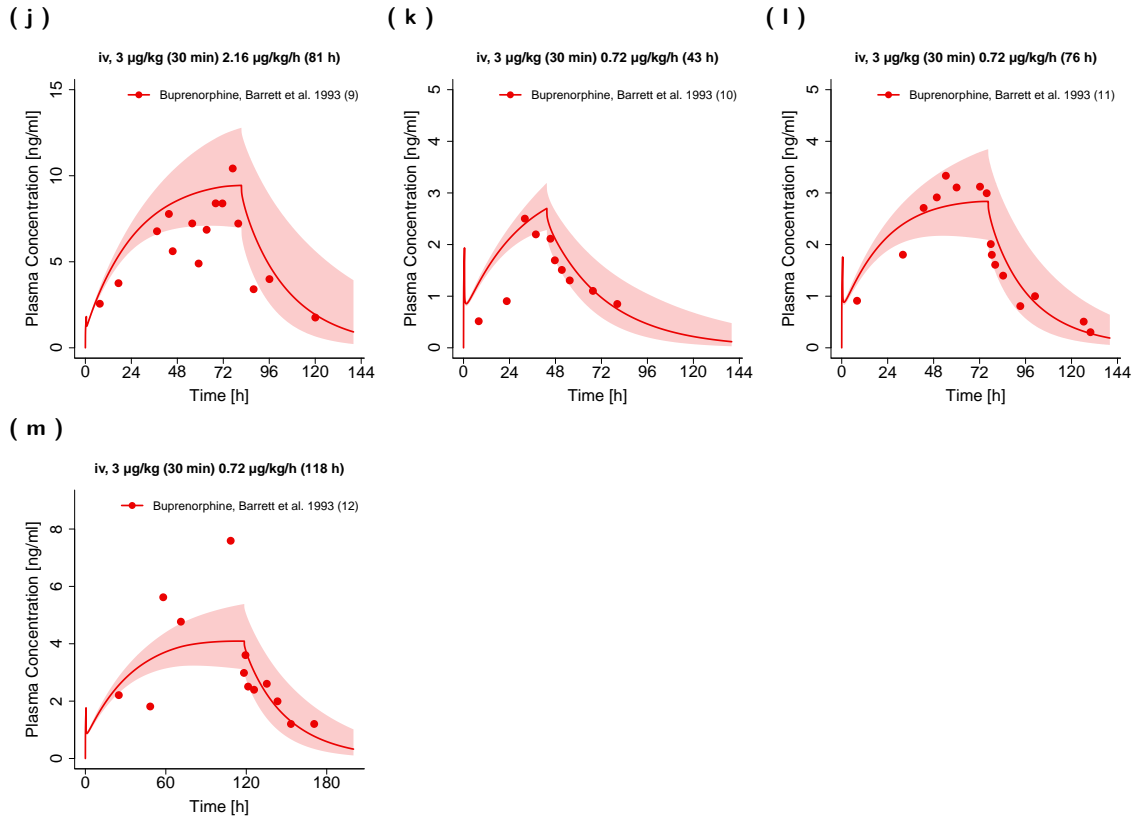
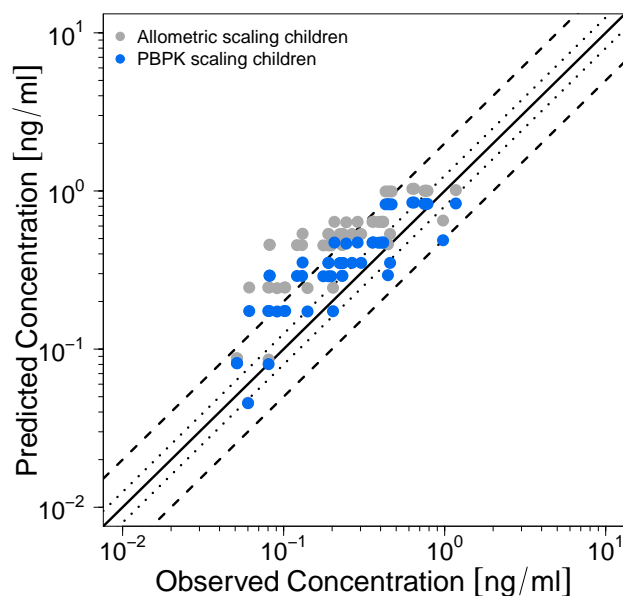
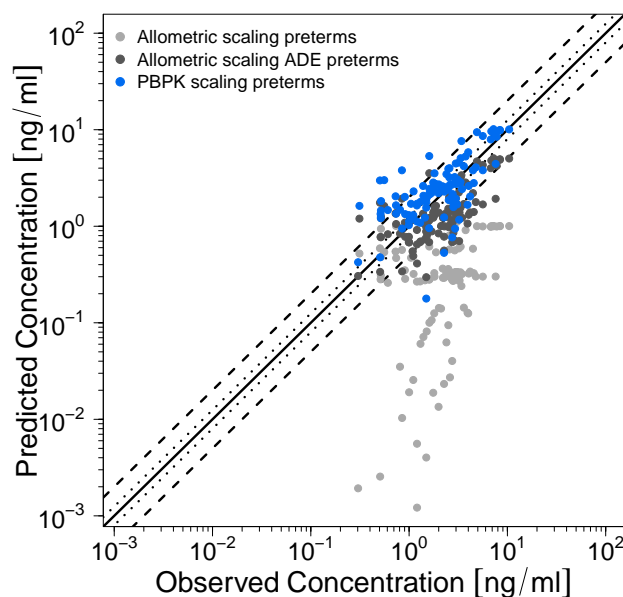


**Figure S6: Buprenorphine (blue: venous blood, red: arterial blood) plasma concentration-time profiles (linear) after intravenous administration of buprenorphine in pediatrics.** Observed data are shown as circles. Population simulation ( $n=100$ ) geometric means are shown as lines; the shaded areas represent the predicted population geometric SD except for subfigure (a) where the line represents the population median and the shaded area the 90% population prediction interval. References with numbers in parentheses link to a specific observed dataset described in the study table (Table 1 in the main manuscript and Table S2). Predicted and observed  $AUC_{last}$  and  $C_{max}$  values are compared in Table S6. iv, intravenous. (continued)

(a) Children

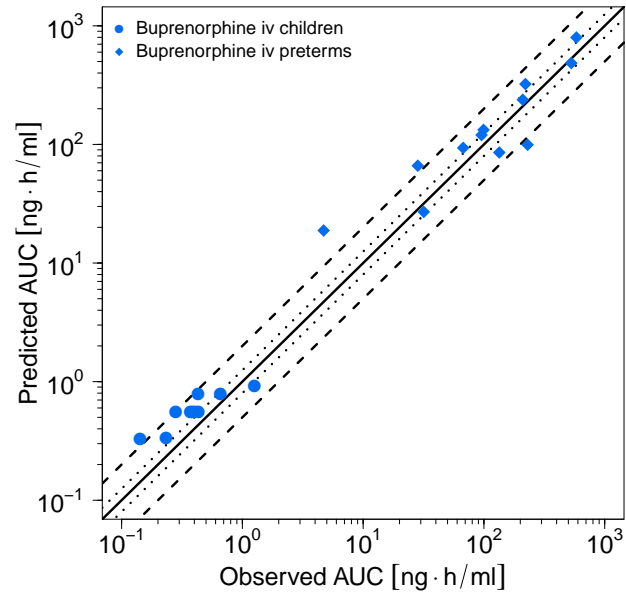
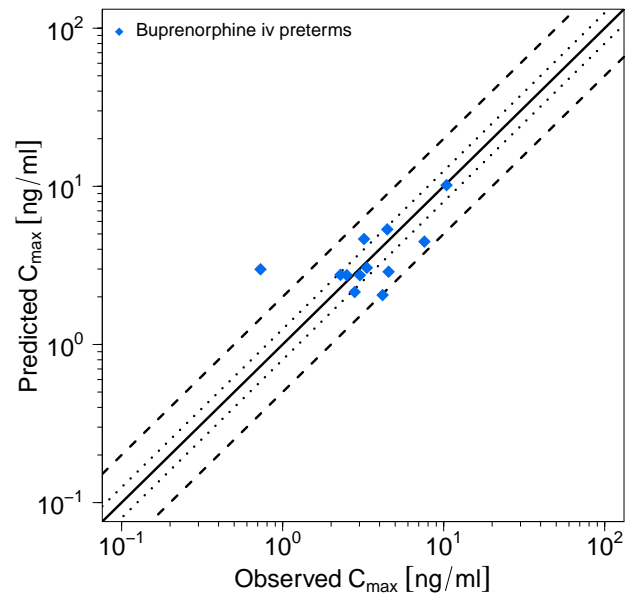


(b) Preterm neonates



**Figure S7: Predicted versus observed plasma concentrations of buprenorphine and norbuprenorphine after intravenous administration of buprenorphine in (a) children and (b) preterm neonates.** Blue circles represent predicted versus observed plasma concentrations derived from the PBPK scaling approach. Light grey circles represent predicted versus observed plasma concentrations derived from the classical allometric scaling approach; dark grey circles represent predicted versus observed plasma concentrations derived from allometric scaling with an age-dependent exponent of 1.2 for preterm neonates as suggested by Mahmood and Tegenge [55] (for detailed information on the allometric scaling approach see Section 3). The black solid lines mark the lines of identity. Black dotted lines indicate 1.25-fold, black dashed lines indicate 2-fold deviation.

(a) AUC

(b)  $C_{\max}$ 

**Figure S8: Predicted versus observed buprenorphine and norbuprenorphine AUC (a) and  $C_{\max}$  (b) values after intravenous administration of buprenorphine in pediatrics.**  $C_{\max}$  values were only calculated for long-term infusions. Each symbol represents the  $AUC_{\text{last}}$  or  $C_{\max}$  of a different plasma profile. The black solid lines mark the lines of identity. Black dotted lines indicate 1.25-fold, black dashed lines indicate 2-fold deviation. **AUC**, area under the plasma concentration-time curve from the first to the last data point;  **$C_{\max}$** , maximum plasma concentration.

### 4.3 Quantitative PBPK Model Evaluation

As quantitative performance measures, mean relative deviations (MRD) of the predicted plasma concentrations for all observed and the respective predicted plasma concentrations as well as the geometric mean fold errors (GMFE) of the predicted versus observed  $AUC_{last}$  and  $C_{max}$  values were calculated according to Equation S16 and Equation S17, respectively.  $C_{max}$  values were only calculated for long-term infusions and norbuprenorphine metabolite since  $C_{max}$  values of a substance administered as intravenous bolus injection or as short-term infusions are very sensitive to the timing of blood sampling.

$$MRD = 10^x \text{ with } x = \sqrt{\frac{1}{n} \sum_{i=1}^n (\log_{10} \hat{c}_i - \log_{10} c_i)^2} \quad (S16)$$

Here,  $c_i$  is the  $i$ th observed plasma concentration,  $\hat{c}_i$  is the respective predicted plasma concentration and  $n$  equals the number of observed values. Overall MRD values of  $\leq 2$  were considered as reasonable predictions [57]. MRD values for all studies are given in Table S5.

$$GMFE = 10^x \text{ with } x = \frac{1}{n} \sum_{i=1}^n \left| \log_{10} \left( \frac{\hat{a}_i}{a_i} \right) \right| \quad (S17)$$

Here,  $a_i$  is the  $i$ th observed  $AUC_{last}$  or  $C_{max}$  value, respectively,  $\hat{a}_i$  is the predicted  $AUC_{last}$  or  $C_{max}$  value, respectively, and  $n$  equals the number of studies. The calculated GMFE values are shown in Table S6.

### 4.4 Mean Relative Deviation (MRD) Values of Buprenorphine and Norbuprenorphine Plasma Concentration Predictions

**Table S5:** Mean relative deviation (MRD) values of buprenorphine and norbuprenorphine plasma concentration predictions.

Route & Dose	Compound	MRD	Reference
<b>Buprenorphine iv adults</b>			
iv, 0.3 mg (2 min)	Buprenorphine	2.06	Bai et al. 2016 [58]
iv, 0.3 mg (1 min)	Buprenorphine	1.58	Bartlett et al. 1980 [59]
iv, 0.3 mg (1 min)	Buprenorphine	1.35	Bullingham et al. 1980 (1) [60]
iv, 0.3 mg (1 min), m.d.	Buprenorphine	1.26	Bullingham et al. 1980 (2) [60]
iv, 0.3 mg (1 min)	Buprenorphine	1.37	Bullingham et al. 1982 (1) [61]
iv, 0.3 mg (1 min)	Buprenorphine	1.21	Bullingham et al. 1982 (2) [61]
iv, 0.3 mg (1 min)	Buprenorphine	1.42	Bullingham et al. 1982 (3) [61]
iv, 1 mg (bolus)	Buprenorphine	1.44	Hagelberg et al. 2016 [53]
iv, 1 mg (bolus, DDI with rifampicin)	Buprenorphine	1.39	Hagelberg et al. 2016 (DDI) [53]
iv, 1 mg (30 min)	Buprenorphine	1.43	Mendelson et al. 1997 [62]
iv, 1.2 mg (1 min)	Buprenorphine	1.27	Kuhlman et al. 1996 [63]
iv, 1.2 mg (1 min)	Norbuprenorphine	3.13	Kuhlman et al. 1996 [63]
iv, 2 mg (1 min)	Buprenorphine	1.42	Huestis et al. 2013 (1) [64]
iv, 2 mg (1 min)	Norbuprenorphine	1.54	Huestis et al. 2013 (1) [64]
iv, 4 mg (10 min)	Buprenorphine	1.58	Harris et al. 2000 [64]
iv, 4 mg (1 min)	Buprenorphine	1.40	Huestis et al. 2013 (2) [64]
iv, 4 mg (1 min)	Norbuprenorphine	1.98	Huestis et al. 2013 (2) [64]
iv, 8 mg (1 min)	Buprenorphine	1.44	Huestis et al. 2013 (3) [64]
iv, 8 mg (1 min)	Norbuprenorphine	1.91	Huestis et al. 2013 (3) [64]
iv, 12 mg (1 min)	Buprenorphine	1.46	Huestis et al. 2013 (4) [64]
iv, 12 mg (1 min)	Norbuprenorphine	2.18	Huestis et al. 2013 (4) [64]
iv, 16 mg (1 min)	Buprenorphine	1.40	Huestis et al. 2013 (5) [64]
<b>Overall MRD</b>		<b>1.74 (1.21–4.58)</b>	
		<b>34/45 with MRD <math>\leq 2</math></b>	

DDI: drug-drug-interaction, iv: intravenous, m.d.: multiple dose, MRD: mean relative deviation

**Table S5:** Mean relative deviation (MRD) values of buprenorphine and norbuprenorphine plasma concentration predictions. (continued)

Route & Dose	Compound	MRD	Reference
iv, 16 mg (1 min)	Norbuprenorphine	1.99	Huestis et al. 2013 (5) [64]
<b>MRD</b>		<b>1.70 (1.21–3.13)</b>	
		<b>20/23 with MRD ≤ 2</b>	
<b>Buprenorphine iv children</b>			
iv, 3 µg/kg (2 min)	Buprenorphine	1.44	Olkkola et al. 1989 (1) [65]
iv, 3 µg/kg (2 min)	Buprenorphine	1.27	Olkkola et al. 1989 (2) [65]
iv, 3 µg/kg (2 min)	Buprenorphine	1.86	Olkkola et al. 1989 (3) [65]
iv, 3 µg/kg (2 min)	Buprenorphine	1.39	Olkkola et al. 1989 (4) [65]
iv, 3 µg/kg (2 min)	Buprenorphine	1.46	Olkkola et al. 1989 (5) [65]
iv, 3 µg/kg (2 min)	Buprenorphine	1.55	Olkkola et al. 1989 (6) [65]
iv, 3 µg/kg (2 min)	Buprenorphine	2.00	Olkkola et al. 1989 (7) [65]
iv, 3 µg/kg (2 min)	Buprenorphine	1.75	Olkkola et al. 1989 (8) [65]
iv, 3 µg/kg (2 min)	Buprenorphine	2.00	Olkkola et al. 1989 (9) [65]
iv, 3 µg/kg (2 min)	Buprenorphine	2.62	Olkkola et al. 1989 (10) [65]
<b>MRD</b>		<b>1.72 (1.27–2.62)</b>	
		<b>8/10 with MRD ≤ 2</b>	
<b>Buprenorphine iv preterms</b>			
iv, 3 µg/kg (30 min) 0.72 µg/kg/h (48 h)	Buprenorphine	1.66	Barrett et al. 1993 (1) [30]
iv, 3 µg/kg (30 min) 0.72 µg/kg/h (24 h)	Buprenorphine	1.66	Barrett et al. 1993 (2) [30]
iv, 3 µg/kg (30 min) 0.72 µg/kg/h (11 h)	Buprenorphine	4.58	Barrett et al. 1993 (3) [30]
iv, 3 µg/kg (30 min) 0.72 µg/kg/h (42 h)	Buprenorphine	1.34	Barrett et al. 1993 (4) [30]
iv, 3 µg/kg (30 min) 0.72 µg/kg/h (42 h)	Buprenorphine	1.85	Barrett et al. 1993 (5) [30]
iv, 3 µg/kg (30 min) 1.44 µg/kg/h (23 h)	Buprenorphine	2.65	Barrett et al. 1993 (6) [30]
iv, 3 µg/kg (30 min) 1.44 µg/kg/h (77 h)	Buprenorphine	2.22	Barrett et al. 1993 (7) [30]
iv, 3 µg/kg (30 min) 0.72 µg/kg/h (42 h)	Buprenorphine	2.98	Barrett et al. 1993 (8) [30]
iv, 3 µg/kg (30 min) 2.16 µg/kg/h (81 h)	Buprenorphine	1.46	Barrett et al. 1993 (9) [30]
iv, 3 µg/kg (30 min) 0.72 µg/kg/h (43 h)	Buprenorphine	1.51	Barrett et al. 1993 (10) [30]
iv, 3 µg/kg (30 min) 0.72 µg/kg/h (76 h)	Buprenorphine	1.33	Barrett et al. 1993 (11) [30]
iv, 3 µg/kg (30 min) 0.72 µg/kg/h (118 h)	Buprenorphine	1.42	Barrett et al. 1993 (12) [30]
<b>MRD</b>		<b>1.86 (1.33–4.58)</b>	
		<b>8/12 with MRD ≤ 2</b>	
<b>Overall MRD</b>		<b>1.74 (1.21–4.58)</b>	
		<b>34/45 with MRD ≤ 2</b>	

DDI: drug-drug-interaction, iv: intravenous, m.d.: multiple dose, MRD: mean relative deviation

### 4.5 Geometric Mean Fold Error (GMFE) of AUC<sub>last</sub> and C<sub>max</sub> Predictions

**Table S6:** Predicted and observed AUC<sub>last</sub> and C<sub>max</sub> values of buprenorphine and norbuprenorphine plasma concentrations

Route	Compound	AUC <sub>last</sub>		C <sub>max</sub>		Pred/Obs	Pred/Obs	Reference
		Pred [ng·h/ml]	Obs [ng·h/ml]	Pred [ng/ml]	Obs [ng/ml]			
<b>Buprenorphine iv adults</b>								
iv, 0.3 mg (2 min)	Buprenorphine	3.34	4.56	0.73	-	-	-	Bai et al. 2016 [58]
iv, 0.3 mg (1 min)	Buprenorphine	1.65	2.59	0.64	-	-	-	Bartlett et al. 1980 [59]
iv, 0.3 mg (1 min)	Buprenorphine	2.75	3.69	0.75	-	-	-	Bullingham et al. 1980 (1) [60]
iv, 0.3 mg (1 min), m.d.	Buprenorphine	3.49	2.99	1.17	-	-	-	Bullingham et al. 1980 (2) [60]
iv, 0.3 mg (1 min)	Buprenorphine	2.14	2.80	0.76	-	-	-	Bullingham et al. 1982 (1) [61]
iv, 0.3 mg (1 min)	Buprenorphine	1.05	1.20	0.87	-	-	-	Bullingham et al. 1982 (2) [61]
iv, 0.3 mg (1 min)	Buprenorphine	1.09	1.56	0.70	-	-	-	Bullingham et al. 1982 (3) [61]
iv, 1 mg (bolus)	Buprenorphine	8.42	11.09	0.76	-	-	-	Hagelberg et al. 2016 [53]
iv, 1 mg (bolus, DDI with rifampicin)	Buprenorphine	7.46	9.41	0.79	-	-	-	Hagelberg et al. 2016 (DDI) [53]
iv, 1 mg (30 min)	Buprenorphine	9.31	10.04	0.93	-	-	-	Mendelson et al. 1997 [62]
iv, 1.2 mg (1 min)	Buprenorphine	18.04	17.20	1.05	-	-	-	Kuhlman et al. 1996 [63]
iv, 1.2 mg (1 min)	Norbuprenorphine	5.98	8.07	0.74	0.49	0.53	0.92	Kuhlman et al. 1996 [63]
iv, 2 mg (1 min)	Buprenorphine	22.97	29.19	0.79	-	-	-	Huestis et al. 2013 (1) [64]
iv, 2 mg (1 min)	Norbuprenorphine	7.67	8.99	0.85	0.73	0.53	1.37	Huestis et al. 2013 (1) [64]
iv, 4 mg (10 min)	Buprenorphine	51.44	51.64	1.00	-	-	-	Harris et al. 2000 [64]
iv, 4 mg (1 min)	Buprenorphine	47.68	60.38	0.79	-	-	-	Huestis et al. 2013 (2) [64]
iv, 4 mg (1 min)	Norbuprenorphine	15.34	13.12	1.17	1.46	0.94	1.56	Huestis et al. 2013 (2) [64]
iv, 8 mg (1 min)	Buprenorphine	95.68	115.63	0.83	-	-	-	Huestis et al. 2013 (3) [64]
iv, 8 mg (1 min)	Norbuprenorphine	30.68	26.68	1.15	2.91	1.82	1.61	Huestis et al. 2013 (3) [64]
iv, 12 mg (1 min)	Buprenorphine	143.30	179.05	0.80	-	-	-	Huestis et al. 2013 (4) [64]
iv, 12 mg (1 min)	Norbuprenorphine	46.05	38.98	1.18	4.37	2.91	1.50	Huestis et al. 2013 (4) [64]
iv, 16 mg (1 min)	Buprenorphine	191.08	201.30	0.95	-	-	-	Huestis et al. 2013 (5) [64]
iv, 16 mg (1 min)	Norbuprenorphine	61.44	57.87	1.06	5.84	3.53	1.65	Huestis et al. 2013 (5) [64]
<b>GMFE</b>		<b>1.22 (1.00–1.57)</b>		<b>1.22 (1.00–1.57)</b>		<b>1.45 (1.09–1.65)</b>		
		<b>23/23 with GMFE ≤ 2</b>		<b>23/23 with GMFE ≤ 2</b>		<b>6/6 with GMFE ≤ 2</b>		
<b>Buprenorphine iv children</b>								
iv, 3 µg/kg (2 min)	Buprenorphine	0.92	1.26	0.73	-	-	-	Oikkola et al. 1989 (1) [65]
iv, 3 µg/kg (2 min)	Buprenorphine	0.79	0.66	1.21	-	-	-	Oikkola et al. 1989 (2) [65]
iv, 3 µg/kg (2 min)	Buprenorphine	0.79	0.43	1.83	-	-	-	Oikkola et al. 1989 (3) [65]
iv, 3 µg/kg (2 min)	Buprenorphine	0.55	0.43	1.28	-	-	-	Oikkola et al. 1989 (4) [65]
iv, 3 µg/kg (2 min)	Buprenorphine	0.55	0.41	1.36	-	-	-	Oikkola et al. 1989 (5) [65]
iv, 3 µg/kg (2 min)	Buprenorphine	0.56	0.39	1.44	-	-	-	Oikkola et al. 1989 (6) [65]
iv, 3 µg/kg (2 min)	Buprenorphine	0.55	0.28	1.97	-	-	-	Oikkola et al. 1989 (7) [65]
iv, 3 µg/kg (2 min)	Buprenorphine	0.55	0.37	1.49	-	-	-	Oikkola et al. 1989 (8) [65]
iv, 3 µg/kg (2 min)	Buprenorphine	0.34	0.23	1.45	-	-	-	Oikkola et al. 1989 (9) [65]
iv, 3 µg/kg (2 min)	Buprenorphine	0.33	0.14	2.31	-	-	-	Oikkola et al. 1989 (10) [65]
<b>GMFE</b>		<b>1.54 (1.21–2.31)</b>		<b>1.54 (1.21–2.31)</b>		<b>9/10 with GMFE ≤ 2</b>		
		<b>41/45 with GMFE ≤ 2</b>		<b>41/45 with GMFE ≤ 2</b>		<b>1.45 (1.02–4.10)</b>		
		<b>16/18 with GMFE ≤ 2</b>		<b>16/18 with GMFE ≤ 2</b>		<b>16/18 with GMFE ≤ 2</b>		
<b>Buprenorphine iv preterms</b>								
iv, 3 µg/kg (30 min) 0.72 µg/kg/h (48 h)	Buprenorphine	95.54	67.34	1.39	2.74	3.02	0.91	Barrett et al. 1993 (1) [30]
iv, 3 µg/kg (30 min) 0.72 µg/kg/h (24 h)	Buprenorphine	26.99	31.77	0.85	2.15	2.80	0.77	Barrett et al. 1993 (2) [30]
iv, 3 µg/kg (30 min) 0.72 µg/kg/h (11 h)	Buprenorphine	18.81	4.71	3.99	2.99	0.73	4.10	Barrett et al. 1993 (3) [30]
<b>Overall GMFE</b>		<b>1.37 (1.00–3.99)</b>		<b>1.37 (1.00–3.99)</b>		<b>1.45 (1.02–4.10)</b>		
		<b>41/45 with GMFE ≤ 2</b>		<b>41/45 with GMFE ≤ 2</b>		<b>16/18 with GMFE ≤ 2</b>		

-: not calculated, DDI: drug-drug-interaction, GMFE: geometric mean fold error, iv: intravenous, m.d.: multiple dose, obs: observed, pred: predicted

Table S6: Predicted and observed AUC<sub>last</sub> and C<sub>max</sub> values of buprenorphine and norbuprenorphine plasma concentrations (continued)

Route	Compound	Pred [µg·h/ml]	Obs [µg·h/ml]	Pred/Obs	Pred [µg/ml]	Obs [µg/ml]	Pred/Obs	Pred [ng/ml]	Obs [ng/ml]	Reference
iv, 3 µg/kg (30 min)	Buprenorphine	120.02	95.53	1.26	2.76	2.29	1.21	2.29	1.21	Barrett et al. 1993 (4) [30]
iv, 3 µg/kg (30 min)	Buprenorphine	85.51	134.06	0.64	2.88	4.55	0.63	4.55	0.63	Barrett et al. 1993 (5) [30]
iv, 3 µg/kg (30 min)	Buprenorphine	66.15	28.34	2.33	4.64	3.20	1.45	3.20	1.45	Barrett et al. 1993 (6) [30]
iv, 3 µg/kg (30 min)	Buprenorphine	322.93	220.52	1.46	5.34	4.46	1.20	4.46	1.20	Barrett et al. 1993 (7) [30]
iv, 3 µg/kg (30 min)	Buprenorphine	99.31	230.04	0.43	2.05	4.17	0.49	4.17	0.49	Barrett et al. 1993 (8) [30]
iv, 3 µg/kg (30 min)	Buprenorphine	797.92	583.00	1.37	10.17	10.42	0.98	10.42	0.98	Barrett et al. 1993 (9) [30]
iv, 3 µg/kg (30 min)	Buprenorphine	132.68	99.25	1.34	2.74	2.50	1.10	2.50	1.10	Barrett et al. 1993 (10) [30]
iv, 3 µg/kg (30 min)	Buprenorphine	238.11	209.79	1.14	3.05	3.33	0.92	3.33	0.92	Barrett et al. 1993 (11) [30]
iv, 3 µg/kg (30 min)	Buprenorphine	485.01	528.79	0.92	4.47	7.59	0.59	7.59	0.59	Barrett et al. 1993 (12) [30]
<b>GMFE</b>		<b>1.57 (1.09–3.99)</b>		<b>9/12 with GMFE ≤ 2</b>		<b>1.44 (1.02–4.10)</b>		<b>10/12 with GMFE ≤ 2</b>		
<b>Overall GMFE</b>		<b>1.37 (1.00–3.99)</b>		<b>41/45 with GMFE ≤ 2</b>		<b>1.45 (1.02–4.10)</b>		<b>16/18 with GMFE ≤ 2</b>		

–: not calculated, **DDI**: drug-drug-interaction, **GMFE**: geometric mean fold error, **iv**: intravenous, **m.d.**: multiple dose, **obs**: observed, **pred**: predicted

## 4.6 Buprenorphine and Norbuprenorphine PBPK Model Sensitivity Analysis

A sensitivity analysis of the buprenorphine and norbuprenorphine PBPK models (adults and pediatrics) to single parameter changes (local sensitivity analysis) was performed. Sensitivities of the PBPK models were calculated as the relative changes of the predicted AUCs extrapolated to infinity ( $AUC_{inf}$ ) of buprenorphine and norbuprenorphine, respectively, to the relative variation of model input parameters in a steady-state scenario (1.4 mg (adults), 0.7 mg (children), 0.009 mg (preterm neonates), 168 hours long-term infusion, mimicking steady-state plasma concentrations of about 0.13 ng/ml, which were achieved with an administration of marketed transdermal buprenorphine patches [56]). Parameters, optimized as well as parameters fixed to literature values, were included into the analysis if they had significant impact in former models (e.g. glomerular filtration rate fraction, maximum reaction velocity, inhibition constants), if they might have a strong influence due to calculation methods used in the model (e.g. lipophilicity) and/or if they have been optimized. The analyses were performed using a relative perturbation of parameters of 10%. Model sensitivity to a model parameter was calculated as follows:

$$S = \frac{\Delta AUC_{inf}}{\Delta p} \cdot \frac{p}{AUC_{inf}} \quad (S18)$$

where  $S$  is the sensitivity of the  $AUC_{inf}$  to the examined model parameter,  $\Delta AUC_{inf}$  is the change of the  $AUC_{inf}$ ,  $AUC_{inf}$  is the simulated  $AUC_{inf}$  with the original parameter value,  $p$  is the original model parameter value and  $\Delta p$  is the variation of the model parameter value. A sensitivity value of +1.0 signifies that a 10% increase of the examined parameter causes a 10% increase of the simulated  $AUC_{inf}$ .

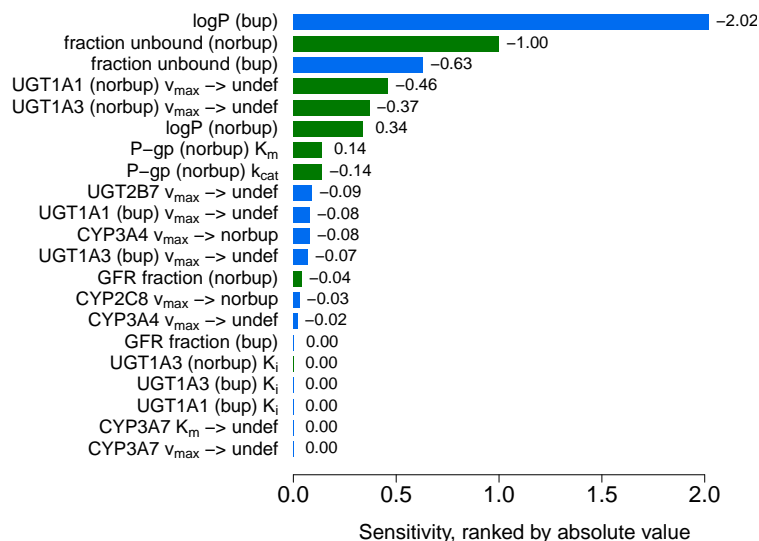


**Figure S9: Sensitivity analysis of the adult PBPK model for buprenorphine and norbuprenorphine.** Sensitivity of the model to single parameters, calculated as change of the simulated buprenorphine (blue) and norbuprenorphine (green)  $AUC_{inf}$  following a 168 hours long-term infusion, mimicking steady-state plasma concentrations of about 0.13 ng/ml, which were achieved with an administration of marketed transdermal buprenorphine patches in adults [56]. **bup**: buprenorphine, **GFR**: glomerular filtration rate,  **$k_{cat}$** : transport rate constant (turnover number),  **$K_i$** : concentration for half-maximal inhibition,  **$K_m$** : Michaelis-Menten constant, **norbup**: norbuprenorphine, **P-gp**: P-glycoprotein, **undef**: undefined metabolite,  **$v_{max}$** : maximum reaction velocity

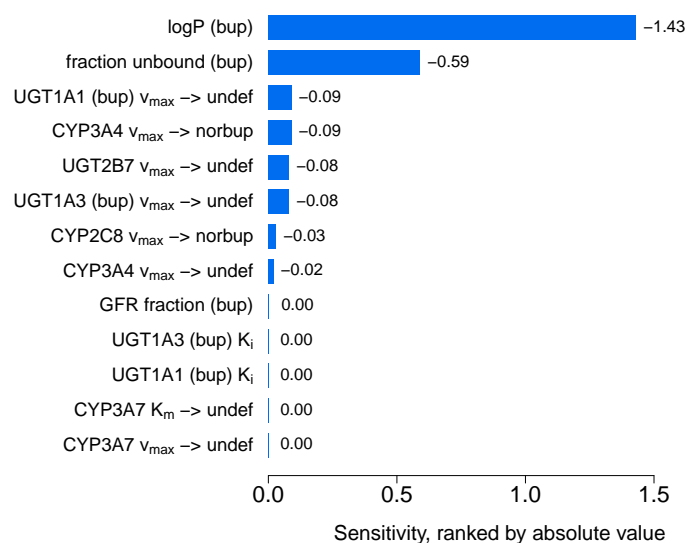


**Figure S10: Sensitivity analysis of the PBPK model in children for buprenorphine.** Sensitivity of the model to single parameters, calculated as change of the simulated buprenorphine (blue)  $AUC_{inf}$  following a 168 hours long-term infusion, mimicking steady-state plasma concentrations of about 0.13 ng/ml, which were achieved with an administration of marketed transdermal buprenorphine patches in adults [56]. **bup**: buprenorphine, **GFR**: glomerular filtration rate,  **$K_i$** : concentration for half-maximal inhibition,  **$K_m$** : Michaelis-Menten constant, **norbup**: norbuprenorphine, **undef**: undefined metabolite,  **$v_{max}$** : maximum reaction velocity

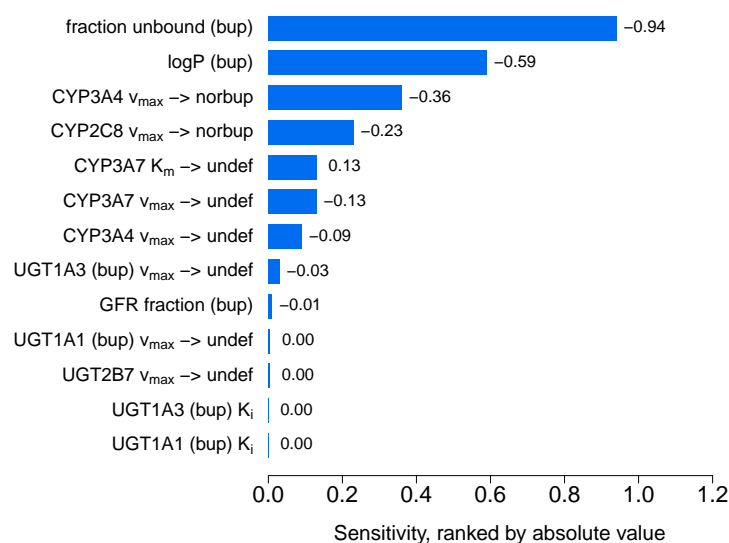


**Figure S11: Sensitivity analysis of the PBPK model in pediatrics for buprenorphine.** Sensitivity of the model to single parameters, calculated as change of the simulated buprenorphine  $AUC_{inf}$  following a 168 hours long-term infusion, mimicking steady-state plasma concentrations of about 0.13 ng/ml, which were achieved with an administration of marketed transdermal buprenorphine patches in adults [56]. **bup**: buprenorphine, **GFR**: glomerular filtration rate,  **$K_i$** : concentration for half-maximal inhibition,  **$K_m$** : Michaelis-Menten constant, **norbup**: norbuprenorphine, **undef**: undefined metabolite,  **$v_{max}$** : maximum reaction velocity

## References

- [1] Maharaj AR, Barrett JS, Edginton AN (2013) A workflow example of PBPK modeling to support pediatric research and development: case study with lorazepam. *The AAPS journal* 15(2):455–64
- [2] Maharaj AR, Edginton AN (2014) Physiologically Based Pharmacokinetic Modeling and Simulation in Pediatric Drug Development. *CPT: Pharmacometrics & Systems Pharmacology* 3(11):1–13
- [3] Leong R, Vieira MLT, Zhao P, Mulugeta Y, Lee CS, Huang SM, Burckart GJ (2012) Regulatory experience with physiologically based pharmacokinetic modeling for pediatric drug trials. *Clinical pharmacology and therapeutics* 91(5):926–31
- [4] Ince I, Solodenko J, Frechen S, Dallmann A, Niederalt C, Schlender J, Burghaus R, Lippert J, Willmann S (2019) Predictive Pediatric Modeling and Simulation Using Ontogeny Information. *The Journal of Clinical Pharmacology* 59(S1):S95–S103
- [5] Picard N, Cresteil T, Djebli N, Marquet P (2005) In vitro metabolism study of buprenorphine: evidence for new metabolic pathways. *Drug metabolism and disposition: the biological fate of chemicals* 33(5):689–95
- [6] Chang Y, Moody DE (2009) Glucuronidation of buprenorphine and norbuprenorphine by human liver microsomes and UDP-glucuronosyltransferases. *Drug metabolism letters* 3(2):101–7
- [7] Brown SM, Campbell SD, Crafford A, Regina KJ, Holtzman MJ, Kharasch ED (2012) P-glycoprotein is a major determinant of norbuprenorphine brain exposure and antinociception. *The Journal of pharmacology and experimental therapeutics* 343(1):53–61
- [8] Oechsler S, Skopp G (2010) An in vitro approach to estimate putative inhibition of buprenorphine and norbuprenorphine glucuronidation. *International Journal of Legal Medicine* 124(3):187–194
- [9] Obach RS (1997) Nonspecific binding to microsomes: impact on scale-up of in vitro intrinsic clearance to hepatic clearance as assessed through examination of warfarin, imipramine, and propranolol. *Drug metabolism and disposition: the biological fate of chemicals* 25(12):1359–69
- [10] Moody DE, Slawson MH, Strain EC, Laycock JD, Spanbauer AC, Foltz RL (2002) A Liquid Chromatographic-Electrospray Ionization-Tandem Mass Spectrometric Method for Determination of Buprenorphine, Its Metabolite, norBuprenorphine, and a Coformulant, Naloxone, That Is Suitable for in Vivo and in Vitro Metabolism Studies. *Analytical Biochemistry* 306(1):31–39
- [11] Williams JA, Ring BJ, Cantrell VE, Jones DR, Eckstein J, Ruterbories K, Hamman MA, Hall SD, Wrighton SA (2002) Comparative Metabolic Capabilities of CYP3A4, CYP3A5, and CYP3A7. *Drug Metabolism and Disposition* 30(8):883–891
- [12] Niwa T, Okamoto A, Narita K, Toyota M, Kato K, Kobayashi K, Sasaki S (2020) Comparison of steroid hormone hydroxylation mediated by cytochrome P450 3A subfamilies. *Archives of Biochemistry and Biophysics* 682:108283
- [13] Hindmarsh A, Reynolds D, Serban R, Woodward C, Gardner DJ, Cohen S, Taylor A, Peles S, Banks L, Shumaker D (2018) *Open Systems Pharmacology Suite Manual, Version 7.4*
- [14] Rodrigues AD (1999) Integrated cytochrome P450 reaction phenotyping: attempting to bridge the gap between cDNA-expressed cytochromes P450 and native human liver microsomes. *Biochemical pharmacology* 57(5):465–80

- [15] Stevens JC, Hines RN, Gu C, Koukouritaki SB, Manro JR, Tandler PJ, Zaya MJ (2003) Developmental Expression of the Major Human Hepatic CYP3A Enzymes. *Journal of Pharmacology and Experimental Therapeutics* 307(2):573–582
- [16] Everhart E, Cheung P, Mendelson J, Upton R, Jones R (1999) The mass balance of buprenorphine in humans. *Clinical Pharmacology & Therapeutics* 65(2):152–152
- [17] Chiang CN, Hawks RL (2003) Pharmacokinetics of the combination tablet of buprenorphine and naloxone. *Drug and alcohol dependence* 70(2 Suppl):S39–47
- [18] Willmann S, Höhn K, Edginton A, Sevestre M, Solodenko J, Weiss W, Lippert J, Schmitt W (2007) Development of a physiology-based whole-body population model for assessing the influence of individual variability on the pharmacokinetics of drugs. *Journal of Pharmacokinetics and Pharmacodynamics* 34(3):401–431
- [19] Valentin J (2002) Basic anatomical and physiological data for use in radiological protection: reference values. *Annals of the ICRP* 32(3-4):1–277
- [20] National Center for Health Statistics (1997) Third National Health and Nutrition Examination Survey (NHANES III). Tech. rep., Hyattsville, MD 20782
- [21] Nishimura M, Yaguti H, Yoshitsugu H, Naito S, Satoh T (2003) Tissue distribution of mRNA expression of human cytochrome P450 isoforms assessed by high-sensitivity real-time reverse transcription PCR. *Journal of the Pharmaceutical Society of Japan* 123(5):369–75
- [22] Nishimura M, Naito S (2005) Tissue-specific mRNA Expression Profiles of Human ATP-binding Cassette and Solute Carrier Transporter Superfamilies. *Drug Metabolism and Pharmacokinetics* 20(6):452–477
- [23] Nishimura M, Naito S (2006) Tissue-Specific mRNA Expression Profiles of Human Phase I Metabolizing Enzymes Except for Cytochrome P450 and Phase II Metabolizing Enzymes. *Drug Metabolism and Pharmacokinetics* 21(5):357–374
- [24] Open Systems Pharmacology Suite Community (2018) PK-Sim<sup>®</sup> Ontogeny Database Documentation, Version 7.3. <https://github.com/Open-Systems-Pharmacology/OSPSuite.Documentation/blob/master/PK-SimOntogenyDatabaseVersion7.3.pdf>, accessed: 2020-03-25
- [25] Margailan G, Rouleau M, Klein K, Fallon JK, Caron P, Villeneuve L, Smith PC, Zanger UM, Guillemette C (2015) Multiplexed Targeted Quantitative Proteomics Predicts Hepatic Glucuronidation Potential. *Drug Metabolism and Disposition* 43(9):1331–1335
- [26] National Center for Biotechnology Information (NCBI) (2010) Expressed Sequence Tags (EST) from UniGene.
- [27] Hanke N, Frechen S, Moj D, Britz H, Eissing T, Wendl T, Lehr T (2018) PBPK Models for CYP3A4 and P-gp DDI Prediction: A Modeling Network of Rifampicin, Itraconazole, Clarithromycin, Midazolam, Alfentanil, and Digoxin. *CPT: Pharmacometrics and Systems Pharmacology* 7(10):647–659
- [28] Prasad B, Evers R, Gupta A, Hop CECA, Salphati L, Shukla S, Ambudkar SV, Unadkat JD (2014) Interindividual Variability in Hepatic Organic Anion-Transporting Polypeptides and P-Glycoprotein (ABCB1) Protein Expression: Quantification by Liquid Chromatography Tandem Mass Spectroscopy and Influence of Genotype, Age, and Sex. *Drug Metabolism and Disposition* 42(1):78–88

- [29] McCarver DG, Hines RN (2002) The ontogeny of human drug-metabolizing enzymes: phase II conjugation enzymes and regulatory mechanisms. *The Journal of pharmacology and experimental therapeutics* 300(2):361–6
- [30] Barrett D, Simpson J, Rutter N, Kurihara-Bergstrom T, Shaw P, Davis S (1993) The pharmacokinetics and physiological effects of buprenorphine infusion in premature neonates. *British Journal of Clinical Pharmacology* 36(3):215–219
- [31] Kajosaari LI, Laitila J, Neuvonen PJ, Backman JT (2005) Metabolism of repaglinide by CYP2C8 and CYP3A4 in vitro: effect of fibrates and rifampicin. *Basic & clinical pharmacology & toxicology* 97(4):249–56
- [32] Rajaonarison J, Lacarelle B, Catalin J, Placidi M, Rahmani R (1992) 3'-azido-3'-deoxythymidine drug interactions. Screening for inhibitors in human liver microsomes. *Drug Metab Dispos* 20(4):578–584
- [33] Chiou WJ, de Morais SM, Kikuchi R, Voorman RL, Li X, Bow DAJ (2014) In vitro OATP1B1 and OATP1B3 inhibition is associated with observations of benign clinical unconjugated hyperbilirubinemia. *Xenobiotica* 44(3):276–282
- [34] Soars MG, Petullo DM, Eckstein JA, Kasper SC, Wrighton SA (2004) An assessment of udp-glucuronosyltransferase induction using primary human hepatocytes. *Drug metabolism and disposition: the biological fate of chemicals* 32(1):140–8
- [35] Trottier J, El Husseini D, Perreault M, Pâquet S, Caron P, Bourassa S, Verreault M, Inaba TT, Poirier GG, Bélanger A, Guillemette C, Trauner M, Barbier O (2010) The Human UGT1A3 Enzyme Conjugates Norursodeoxycholic Acid into a C 23 -ester Glucuronide in the Liver. *Journal of Biological Chemistry* 285(2):1113–1121
- [36] Templeton IE, Houston JB, Galetin A (2011) Predictive Utility of In Vitro Rifampin Induction Data Generated in Fresh and Cryopreserved Human Hepatocytes, Fa2N-4, and HepaRG Cells. *Drug Metabolism and Disposition* 39(10):1921–1929
- [37] Reitman ML, Chu X, Cai X, Yabut J, Venkatasubramanian R, Zajic S, Stone JA, Ding Y, Witter R, Gibson C, Roupe K, Evers R, Wagner JA, Stoch A (2011) Rifampin's Acute Inhibitory and Chronic Inductive Drug Interactions: Experimental and Model-Based Approaches to Drug-Drug Interaction Trial Design. *Clinical Pharmacology & Therapeutics* 89(2):234–242
- [38] Greiner B, Eichelbaum M, Fritz P, Kreichgauer HP, von Richter O, Zundler J, Kroemer HK (1999) The role of intestinal P-glycoprotein in the interaction of digoxin and rifampin. *Journal of Clinical Investigation* 104(2):147–153
- [39] Buckley DB, Wiegand CM, Prentiss PL, Fahmi OA (2013) Time-course of cytochrome P450 (CYP450) induction in cultured human hepatocytes: Evaluation of activity and mRNA expression profiles for six inducible CYP450 enzymes. *ISSX*.
- [40] Wishart DS, Knox C, Guo AC, Shrivastava S, Hassanali M, Stothard P, Chang Z, Woolsey J (2006) DrugBank: a comprehensive resource for in silico drug discovery and exploration. *Nucleic acids research* 34(Database issue):D668–72
- [41] Merck Research Laboratories (2006) The Merck Index 14th edition: Rifampin. Merck & Co., Inc., Whitehouse Station, NJ, USA
- [42] Boman G, Ringberger VA (1974) Binding of rifampicin by human plasma proteins. *European journal of clinical pharmacology* 7(5):369–73

- [43] Baneyx G, Parrott N, Meille C, Iliadis A, Lavé T (2014) Physiologically based pharmacokinetic modeling of CYP3A4 induction by rifampicin in human: influence of time between substrate and inducer administration. *European journal of pharmaceutical sciences : official journal of the European Federation for Pharmaceutical Sciences* 56:1–15
- [44] Loos U, Musch E, Jensen JC, Mikus G, Schwabe HK, Eichelbaum M (1985) Pharmacokinetics of oral and intravenous rifampicin during chronic administration. *Klinische Wochenschrift* 63(23):1205–11
- [45] Tirona RG, Leake BF, Wolkoff AW, Kim RB (2003) Human organic anion transporting polypeptide-C (SLC21A6) is a major determinant of rifampin-mediated pregnane X receptor activation. *The Journal of pharmacology and experimental therapeutics* 304(1):223–8
- [46] Nakajima A, Fukami T, Kobayashi Y, Watanabe A, Nakajima M, Yokoi T (2011) Human arylacetamide deacetylase is responsible for deacetylation of rifamycins: rifampicin, rifabutin, and rifapentine. *Biochemical pharmacology* 82(11):1747–56
- [47] Collett A, Tanianis-Hughes J, Hallifax D, Warhurst G (2004) Predicting P-glycoprotein effects on oral absorption: correlation of transport in Caco-2 with drug pharmacokinetics in wild-type and *mdr1a*(-/-) mice in vivo. *Pharmaceutical research* 21(5):819–26
- [48] Shou M, Hayashi M, Pan Y, Xu Y, Morrissey K, Xu L, Skiles GL (2008) Modeling, prediction, and in vitro in vivo correlation of CYP3A4 induction. *Drug metabolism and disposition: the biological fate of chemicals* 36(11):2355–70
- [49] Hirano M, Maeda K, Shitara Y, Sugiyama Y (2006) Drug-drug interaction between pitavastatin and various drugs via OATP1B1. *Drug metabolism and disposition: the biological fate of chemicals* 34(7):1229–36
- [50] Annaert P, Ye ZW, Stieger B, Augustijns P (2010) Interaction of HIV protease inhibitors with OATP1B1, 1B3, and 2B1. *Xenobiotica; the fate of foreign compounds in biological systems* 40(3):163–76
- [51] Rodgers T, Leahy D, Rowland M (2005) Physiologically based pharmacokinetic modeling 1: Predicting the tissue distribution of moderate-to-strong bases. *Journal of Pharmaceutical Sciences* 94(6):1259–1276
- [52] Rodgers T, Rowland M (2006) Physiologically based pharmacokinetic modelling 2: Predicting the tissue distribution of acids, very weak bases, neutrals and zwitterions. *Journal of Pharmaceutical Sciences* 95(6):1238 – 1257
- [53] Hagelberg NM, Fihlman M, Hemmilä T, Backman JT, Laitila J, Neuvonen PJ, Laine K, Olkkola KT, Saari TI (2016) Rifampicin decreases exposure to sublingual buprenorphine in healthy subjects. *Pharmacology Research & Perspectives* 4(6):e00271
- [54] Tod M, Jullien V, Pons G (2008) Facilitation of Drug Evaluation in Children by Population Methods and Modelling†. *Clinical Pharmacokinetics* 47(4):231–243
- [55] Mahmood I, Tegenge MA (2019) A Comparative Study Between Allometric Scaling and Physiologically Based Pharmacokinetic Modeling for the Prediction of Drug Clearance From Neonates to Adolescents. *The Journal of Clinical Pharmacology* 59(2):189–197
- [56] Kapil RP, Cipriano A, Friedman K, Michels G, Shet MS, Colucci SV, Apseloff G, Kitzmiller J, Harris SC (2013) Once-Weekly Transdermal Buprenorphine Application Results in Sustained and Consistent Steady-State Plasma Levels. *Journal of Pain and Symptom Management* 46(1):65–75

- [57] Edginton AN, Schmitt W, Voith B, Willmann S (2006) A Mechanistic Approach for the Scaling of Clearance in Children. *Clinical Pharmacokinetics* 45(7):683–704
- [58] Bai SA, Xiang Q, Finn A (2016) Evaluation of the Pharmacokinetics of Single- and Multiple-dose Buprenorphine Buccal Film in Healthy Volunteers. *Clinical Therapeutics* 38(2):358–369
- [59] Bartlett AJ, Lloyd-Jones JG, Rance MJ, Flockhart IR, Dockray GJ, Bennett MR, Moore RA (1980) The radioimmunoassay of buprenorphine. *European Journal of Clinical Pharmacology* 18(4):339–345
- [60] Bullingham RE, McQuay HJ, Moore A, Bennett MR (1980) Buprenorphine kinetics. *Clinical pharmacology and therapeutics* 28(5):667–72
- [61] Bullingham RE, McQuay HJ, Porter EJ, Allen MC, Moore RA (1982) Sublingual buprenorphine used postoperatively: ten hour plasma drug concentration analysis. *British journal of clinical pharmacology* 13(5):665–73
- [62] Mendelson J, Upton RA, Everhart ET, Jacob III P, Jones RT (1997) Bioavailability of Sublingual Buprenorphine. *The Journal of Clinical Pharmacology* 37(1):31–37
- [63] Kuhlman JJ, Lalani S, Maglulo J, Levine B, Darwin WD, Johnson RE, Cone EJ (1996) Human Pharmacokinetics of Intravenous, Sublingual, and Buccal Buprenorphine. *Journal of Analytical Toxicology* 20(6):369–378
- [64] Huestis M, Cone E, Pirnay S, Umbricht A, Preston K (2013) Intravenous buprenorphine and norbuprenorphine pharmacokinetics in humans. *Drug and Alcohol Dependence* 131(3):258–262
- [65] Olkkola K, Maunuksela E, Korpela R (1989) Pharmacokinetics of intravenous buprenorphine in children. *British Journal of Clinical Pharmacology* 28(2):202–204

A.2 SUPPLEMENTARY DOCUMENT TO PUBLICATION II – PBPK MODELING  
OF FENTANYL IN ADULT AND PEDIATRIC PATIENTS

## Pharmaceutics

# Supplementary Materials: PBPK Modeling Providing Insights into Fentanyl Pharmacokinetics in Adults and Pediatric Patients

Lukas Kovar, Andreas Weber, Michael Zemlin, Yvonne Kohl, Robert Bals, Bernd Meibohm,  
Dominik Selzer and Thorsten Lehr

## Contents

<b>1</b>	<b>PBPK Model Building</b>	<b>2</b>
1.1	PBPK Model Building – General . . . . .	2
1.2	Clearance in Neonates with Increased Intraabdominal Pressure . . . . .	3
1.3	System-dependent Parameters and Virtual Populations . . . . .	4
<b>2</b>	<b>Drug-Drug-Interaction (DDI) Modeling</b>	<b>6</b>
2.1	DDI Modeling – General . . . . .	6
2.2	Mathematical Implementation of DDIs . . . . .	6
2.2.1	Competitive Inhibition . . . . .	6
2.2.2	Mechanism-Based Inhibition (MBI) . . . . .	6
<b>3</b>	<b>PBPK Model Evaluation</b>	<b>8</b>
3.1	Adult PBPK Model Evaluation . . . . .	9
3.2	Pediatric PBPK Model Evaluation . . . . .	17
3.3	Quantitative PBPK Model Evaluation . . . . .	21
3.4	Mean Relative Deviation (MRD) Values of Fentanyl and Norfentanyl Plasma Concentration Predictions . . . . .	21
3.5	Geometric Mean Fold Error (GMFE) of $AUC_{last}$ Predictions . . . . .	23
3.6	Fentanyl and Norfentanyl PBPK Model Sensitivity Analysis . . . . .	24
	<b>References</b>	<b>26</b>

## 1 PBPK Model Building

### 1.1 PBPK Model Building – General

For *a priori* physiologically-based pharmacokinetic (PBPK) predictions in pediatrics, a common workflow is to first model and evaluate the PBPK model with published pharmacokinetics (PK) data in adults. Subsequently, the model is extrapolated to pediatric populations [1–5]. While the general model building process is depicted in the methods section of the main manuscript, this section provides additional model information.

The fentanyl PBPK model includes the metabolic pathway of fentanyl to the inactive metabolite norfentanyl via Cytochrome P450 (CYP) 3A4 and CYP3A7 [6], an unspecific hepatic clearance metabolizing fentanyl to other non-specified metabolites, distribution and excretion via P-glycoprotein (P-gp), as well as renal excretion through glomerular filtration [7–9]. The involvement of CYP3A7 in the metabolic elimination of fentanyl is still unclear [6, 10]. As CYP3A4 and CYP3A7 share a similar substrate spectrum [5, 11] and since CYP3A7 is the major fetal form of CYP3A [11], this CYP enzyme might be important for PK predictions of fentanyl in pediatric populations. Hence, CYP3A7 was incorporated in the model. Unfortunately,  $K_m$  and  $V_{max}$  values for the metabolism of fentanyl via CYP3A7 have not been published in the literature. Yet, a study by Williams and colleagues provided information on the relative metabolic capabilities of CYP3A4 and CYP3A7 to metabolize various molecules (n=15) and compared respective  $K_m$  [ $\mu\text{mol/L}$ ] and  $V_{max}$  [ $\text{nmol/min/nmol P450}$ ] values [11]. The dataset was further expanded with the  $K_m$  and  $V_{max}$  values from three more molecules [12]. On average,  $K_m$  values for CYP3A7 were 5.1 times higher in comparison to the corresponding  $K_m$  values of CYP3A4 for the investigated substances, while  $V_{max}$  values appeared to be 75% lower. Subsequently, these factors were utilized and multiplied with the  $K_m$  and  $k_{cat}$  values for the metabolism of fentanyl through CYP3A4 (117  $\mu\text{mol/L}$  and 20.6 1/min) in order to obtain the model input parameters for CYP3A7. This resulted in a  $K_m$  value of 596  $\mu\text{mol/L}$  and a  $k_{cat}$  value of 5.22 1/min.

In addition, various *in vitro* and animal studies as well as a DDI study with quinidine suggest that fentanyl is a substrate of P-gp [13–16]. As a consequence, fentanyl was implemented to be a substrate of the transport protein P-gp in the developed PBPK model. In contrast, there were no information, which state that norfentanyl is a substrate of P-gp. As a result, norfentanyl was not implemented as a substrate of the transport protein P-gp. Since norfentanyl is predominantly eliminated via urine, a renal clearance was implemented [8]. Parameter optimization yielded a glomerular filtration rate fraction of 4.3 indicating tubular secretion in the PBPK model.

**Table S1:** Tissue-plasma partition coefficients of the final fentanyl PBPK model.

Organ	Fentanyl <sup>a</sup>				Norfentanyl <sup>b</sup>
	Adults	Neonates	Infants	Children	Adults
Bone	1.43	1.46	1.39	1.27	2.11
Brain	1.55	1.97	1.90	1.73	28.53
Fat	2.15	1.82	2.05	2.09	1.37
Gonads	4.07	3.51	3.31	3.04	11.77
Heart	3.68	3.13	2.95	2.72	21.02
Kidney	7.77	6.26	5.88	5.43	16.76
Large Intestine	4.40	4.09	3.87	3.55	8.15
Liver Pericentral	7.13	5.83	5.47	5.05	19.23
Liver Periportal	7.13	5.83	5.47	5.05	19.23
Lung	6.19	5.11	4.81	4.43	9.27
Muscle	4.21	3.77	3.58	3.28	2.81
Pancreas	3.38	3.34	3.18	2.91	4.31
Saliva	0.21	0.33	0.32	0.29	0.82
Skin	3.10	3.33	3.19	2.90	6.70
Small Intestine	4.40	4.09	3.87	3.55	8.15
Spleen	4.94	4.01	3.76	3.47	6.86
Stomach	4.40	4.09	3.87	3.55	8.15

Partition coefficients between intracellular space and plasma.

Mean ages of the adult, child, infant, and neonate population were 32 years, 2.7 years, 6.5 months, and 0.4 days, respectively, adapted from [8, 17, 18]

<sup>a</sup> Estimated via Rodgers and Rowland [19–21]

<sup>b</sup> Estimated via Schmitt [22]

## 1.2 Clearance in Neonates with Increased Intraabdominal Pressure

In the gathered pediatric clinical trial data, several of the neonates showed a significantly reduced fentanyl clearance [18, 23, 24]. It was hypothesized that this might partly be due to an increased intra-abdominal pressure resulting in a decreased hepatic clearance [18, 23, 24]. The plasma concentration-time profiles of four of these patients were depicted in the study by Gauntlett et al. and Koehntop et al., respectively [23, 24]. The profiles were digitized and used as an internal training dataset. In order to account for the reduced elimination, a factor was estimated for each patient and multiplied with the catalytic rate constant values for CYP3A4 and CYP3A7 as well as with the unspecific hepatic clearance. The resulting factors are shown in Table S2. The arithmetic mean of these factors was then used to adapt the clearance of the remaining 6 patients with proposed increased intraabdominal pressure. If no information on intraabdominal pressure was available in a study, the clearance was adapted for all patients with abdominal surgery [23].

**Table S2:** Estimated factors for clearance adjustment in pediatric patients who had abdominal surgery.

Study ID	Estimated Factor	Study Reference
Gauntlett et al. (1)	0.168	[23]
Gauntlett et al. (2)	0.148	[23]
Koentrop et al. (1)	0.089	[24]
Koentrop et al. (2)	0.259	[24]
<b>Arithmetic mean</b>	<b>0.166</b>	

### 1.3 System-dependent Parameters and Virtual Populations

The demographic characteristics of the study populations (see Tables 1–2 in the main manuscript) were used to create virtual individuals with the respective system-dependent physiological parameters such as blood flow rates and organ compositions in PK-Sim<sup>®</sup>. The applied algorithms for the generation of these virtual individuals have been previously reported [25]. If no information on the patient demographics were available, a 30-year-old male was assumed with body weight, height and BMI values according to the PK-Sim<sup>®</sup> database.

As Stader and colleagues pointed out, for most anatomical, physiological, and biological parameters, a sample size of at least 100 individuals is recommended [26]. For system parameters with high variability, such as enzyme and transporter abundance, a virtual population containing 500 individuals might be more appropriate [26]. Simulations with  $n=100$  and  $n=500$  for various dosing regimens (i.e. including iv bolus, short infusions and long-term infusions) were tested resulting in negligibly small differences in simulated plasma concentration-time profiles. Thus, predictions with virtual populations were simulated with 100 individuals.

Virtual individuals were generated for virtual populations according to the respective population demographics (see Tables 1–2 in the main manuscript) for each study separately. Demographics of virtual individuals (i.e. age, height, weight and corresponding organ volumes, tissue compositions, blood flow rates, etc.) were varied by an implemented algorithm in PK-Sim<sup>®</sup> within the limits of the ICRP (International Commission on Radiological Protection) and NHANES (National Health and Nutrition Examination Survey) databases, respectively [27, 28]. If no age range was reported in the clinical trial with adult patients, virtual populations were created with individuals 20 to 50 years of age and without specific weight or height restrictions as implemented in PK-Sim<sup>®</sup>. Tissue expression distributions of enzymes and proteins were used according to the PK-Sim<sup>®</sup> expression database [29–31].

Furthermore, expression variability of the implemented enzymes (i.e. CYP3A4 and CYP3A7) and of the transport protein P-gp was implemented. System-dependent parameters, such as information on reference concentrations and the respective variabilities of enzymes and transporters are shown in Table S3.

**Table S3:** System-dependent parameters and expression of relevant enzymes and transporters.

Enzyme / Transporter	Mean reference concentration [ $\mu\text{mol/L}$ ] <sup>a</sup>	GSD of the reference concentration in adults <sup>b</sup>	Relative expression in different organs <sup>c</sup>	Ontogeny function	Half-life liver [hours]	Half-life Intestine [hours]
<b>Enzymes</b>						
CYP3A4	4.32 [32]	1.18 (liver)[33] 1.45 (intestine)[33]	RT-PCR [29]	[33]	36	23
CYP3A7	7.98 [34]	1.25 [33]	RT-PCR [29]	[33]	36	23
<b>Transporters</b>						
P-gp	1.00 <sup>d</sup>	1.70, 1.84, 1.78, 1.60 [35] <sup>e</sup>	RT-PCR [30] <sup>f</sup>	[36] <sup>g</sup>	36	23
<b>Processes</b>						
Unspecific hepatic clearance of fentanyl	-	1.40 <sup>h</sup>	-	-	-	-

**CYP:** cytochrome P450, **GSD:** Geometric standard deviation, **P-gp:** P-glycoprotein, **RT-PCR:** reverse transcription polymerase chain reaction

<sup>a</sup> [ $\mu\text{mol protein/L}$ ] in the tissue of the highest expression

<sup>b</sup> for information on geometric standard deviation in pediatrics, please refer to [33]

<sup>c</sup> PK-Sim<sup>®</sup> expression database profile

<sup>d</sup> reference concentration was set to 1.0  $\mu\text{mol/L}$  and  $k_{\text{cat}}$  optimized according to [37]

<sup>e</sup> geometric standard deviations for neonates, infants, children and adults, respectively, according to [36]

<sup>f</sup> with the relative expression in intestinal mucosa increased by factor 3.57 according to [38]

<sup>g</sup> since no specific ontogeny function for P-gp is implemented in PK-Sim<sup>®</sup>, the ontogeny function from Prasad et al. was used [36]

<sup>h</sup> geometric standard deviation with coefficient of variation (CV) of 35% assumed

## 2 Drug-Drug-Interaction (DDI) Modeling

### 2.1 DDI Modeling – General

Voriconazole is an inhibitor of two CYP enzymes, CYP3A4 and CYP2C9. While voriconazole inhibits CYP2C9 competitively, it acts as both a competitive and mechanism-based inhibitor in case of CYP3A4 [39]. For the assessment of the DDI with voriconazole a previously developed voriconazole PBPK model was used [39]. Voriconazole shows dose- and time-dependent nonlinear pharmacokinetics which was well captured in the simulations of the used voriconazole PBPK model [39]. The parameters of the model can be found in the respective publication [39].

The DDI simulations presented in the manuscript are pure predictions. The DDI study was not used for model input parameter estimation during fentanyl and norfentanyl PBPK model development. Interaction parameters necessary for DDI simulation were obtained from the published DDI perpetrator PBPK model. With that, the adult PBPK model could not only be evaluated by its predictive performance with the test dataset but also by prediction of a DDI study [7].

### 2.2 Mathematical Implementation of DDIs

#### 2.2.1 Competitive Inhibition

Competitive inhibition describes the competition of substrate and inhibitor for reversibly binding to the active site of an enzyme or transporter. The inhibition can be overcome by high substrate concentrations leading to a concentration-dependency of the inhibition. Hence, the maximum reaction velocity  $V_{max}$  is not affected during a competitive inhibition, while  $K_m$  is increased through the inhibition process yielding  $K_{m,app}$  (Equation S1). The reaction velocity ( $v$ ) for the substrate during concomitant administration with a competitive inhibitor is described by Equation S2 [33]:

$$K_{m,app} = K_m \cdot \left( 1 + \frac{[I]}{K_i} \right) \quad (S1)$$

$$v = \frac{V_{max} \cdot [S]}{K_{m,app} + [S]} \quad (S2)$$

with  $K_{m,app}$  = Michaelis-Menten constant in the presence of inhibitor,  $K_m$  = Michaelis-Menten constant,  $[I]$  = free inhibitor concentration,  $K_i$  = dissociation constant of the inhibitor-enzyme/transporter complex,  $v$  = reaction velocity,  $V_{max}$  = maximum reaction velocity,  $[S]$  = free substrate concentration.

#### 2.2.2 Mechanism-Based Inhibition (MBI)

While competitive inhibition is a reversible mechanism, mechanism-based inhibition (MBI) is an irreversible type of inhibition. *De novo* synthesis of the inactivated protein and clearance of the mechanism-based inactivator is required for the enzyme or transporter to return to baseline activity (time-dependency). During an MBI the protein degradation rate constant ( $k_{deg}$ ) is increased yielding  $k_{deg,app}$  (Equation S3), while the synthesis ( $R_{syn}$ ) is not affected by the inhibition process. The protein turnover during MBI is described by Equation S4. In addition, as mechanism-based inactivators are also competitive inhibitors, the  $K_m$  in the Michaelis-Menten reaction velocity equation is substituted by  $K_{m,app}$  as in Equation S5 [33]:

$$k_{deg,app} = k_{deg} + \left( \frac{k_{inact} \cdot [I]}{K_I + [I]} \right) \quad (S3)$$

$$\frac{dE(t)}{dt} = R_{syn} - k_{deg,app} \cdot E(t) \quad (S4)$$

$$v = \frac{V_{max} \cdot [S]}{K_{m,app} + [S]} = \frac{k_{cat} \cdot E(t) \cdot [S]}{K_{m,app} + [S]} \quad (S5)$$

with  $k_{deg,app}$  = enzyme or transporter degradation rate constant in the presence of mechanism-based inactivator,  $k_{deg}$  = enzyme or transporter degradation rate constant,  $k_{inact}$  = maximum inactivation rate constant,  $[I]$  = free inactivator concentration,  $K_I$  = concentration for half-maximal inactivation,  $E(t)$  = enzyme or transporter concentration,  $R_{syn}$  = rate of enzyme or transporter synthesis,  $v$  = reaction velocity,  $V_{max}$  = maximum reaction velocity,  $[S]$  = free substrate concentration,  $K_{m,app}$  = Michaelis-Menten constant in the presence of inactivator,  $k_{cat}$  = catalytic rate constant.

Hereby,  $k_{deg}$  can be computed from the half-lives ( $t_{1/2}$ ) of the specific enzyme, which are depicted in Table S2, with  $k_{deg} = \ln(2)/t_{1/2}$ . Moreover,  $R_{syn}$  is calculated by  $R_{syn} = E_{0,Enzyme} \cdot k_{deg}$ , with  $E_{0,Enzyme}$  being the amount of this enzyme in the tissue of interest before mechanism-based inhibition.

### 3 PBPK Model Evaluation

The descriptive and predictive performance of the developed adult and pediatric PBPK models is comprehensively depicted in this section. Semilogarithmic and linear plots of plasma concentration-time profiles (population predictions) are compared to the profiles observed for both adult and pediatric PBPK models in Figures S1, S2, S5 and S6. Additionally, plots of population predictions of fractions of fentanyl excreted unchanged in urine (linear plots) are compared to measured values in Figure S2. Moreover, goodness-of-fit plots comparing predicted to observed plasma concentrations are shown in Figures S3 and S7.

Predicted compared to observed area under the plasma concentration-time curves from the first to the last data point ( $AUC_{last}$ ) values are depicted in Figures S4 and S8.

The mean relative deviation (MRD) values as well as the predicted and observed  $AUC_{last}$  values including the geometric mean fold errors (GMFE) are listed in Tables S4 and S5. Local sensitivity analyses were performed with the PBPK model for adult, child, infant, full-term neonate and preterm neonate subpopulations. Detailed descriptions and the results of the sensitivity analyses are shown in Section 3.6.

### 3.1 Adult PBPK Model Evaluation

In this section, semilogarithmic and linear plots of plasma concentration-time profiles, linear plots of fractions of fentanyl dose excreted unchanged in urine (Figures S1 and S2), a goodness-of-fit plot of predicted compared to observed plasma concentrations (Figure S3) and a goodness-of-fit plot of predicted compared to observed  $AUC_{last}$  values (Figure S4) after intravenous administration of fentanyl in adults are shown.

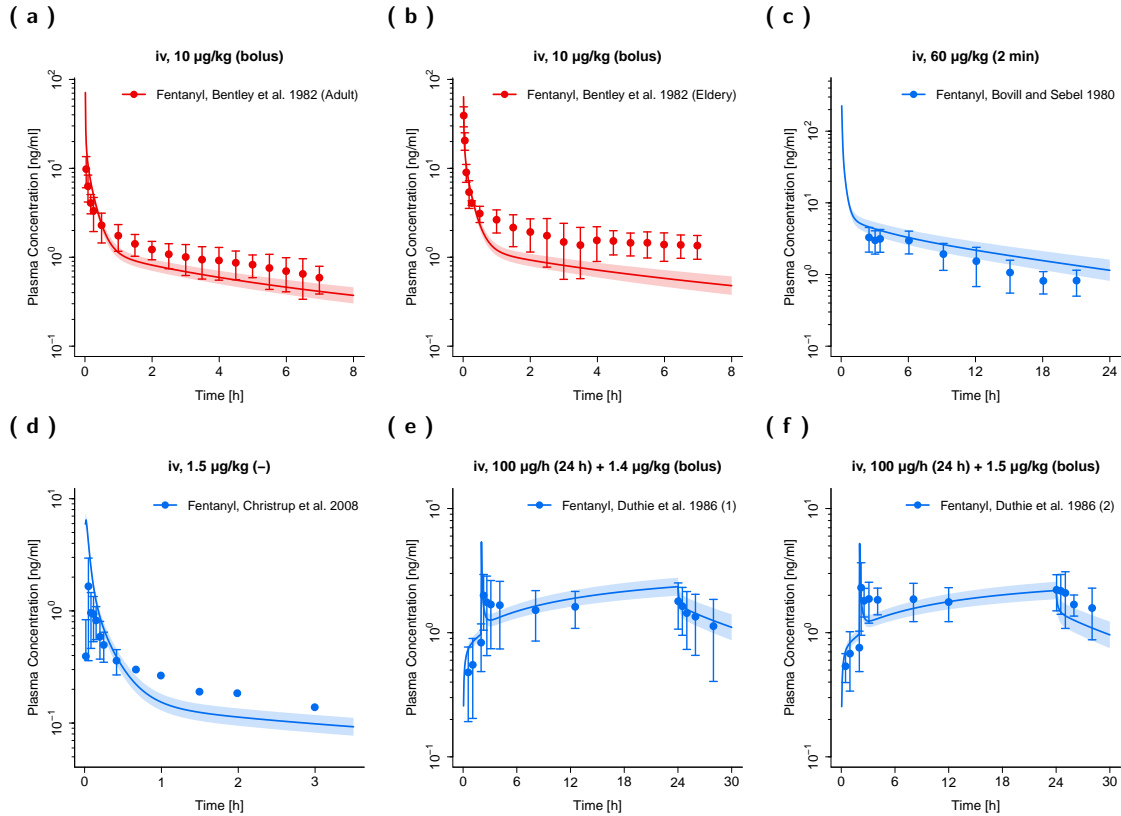


**Figure S1: Fentanyl (blue: venous blood, darkblue: venous blood from central venous catheters, red: arterial blood) and norfentanyl (green: venous blood) plasma concentration-time profiles (semilogarithmic) after intravenous administration of fentanyl in adults.** Observed data are shown as circles, if available  $\pm$  standard deviation (SD). Population simulation ( $n=100$ ) geometric means are shown as lines; the shaded areas represent the predicted population geometric SD. References with numbers in parentheses link to a specific observed dataset ID described in the study table (Table 1 in the main manuscript). Predicted and observed  $AUC_{last}$  values are compared in Table S5. **DDI**, drug-drug-interaction; **iv**, intravenous.

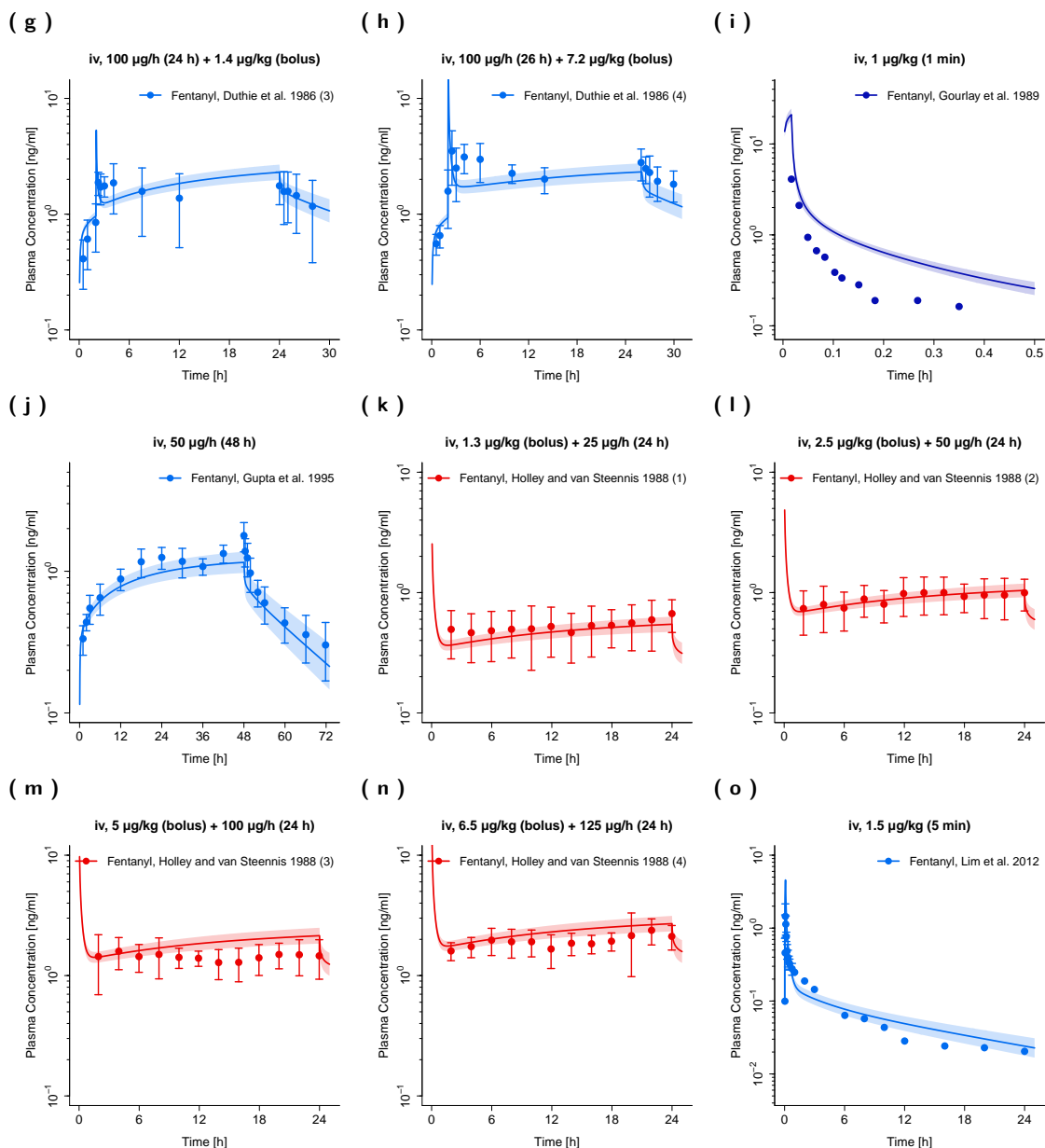


**Figure S1: Fentanyl (blue: venous blood, darkblue: venous blood from central venous catheters, red: arterial blood) and norfentanyl (green: venous blood) plasma concentration-time profiles (semilogarithmic) after intravenous administration of fentanyl in adults.** Observed data are shown as circles, if available  $\pm$  standard deviation (SD). Population simulation ( $n=100$ ) geometric means are shown as lines; the shaded areas represent the predicted population geometric SD. References with numbers in parentheses link to a specific observed dataset ID described in the study table (Table 1 in the main manuscript). Predicted and observed  $AUC_{last}$  values are compared in Table S5. DDI, drug-drug-interaction; iv, intravenous.(continued)

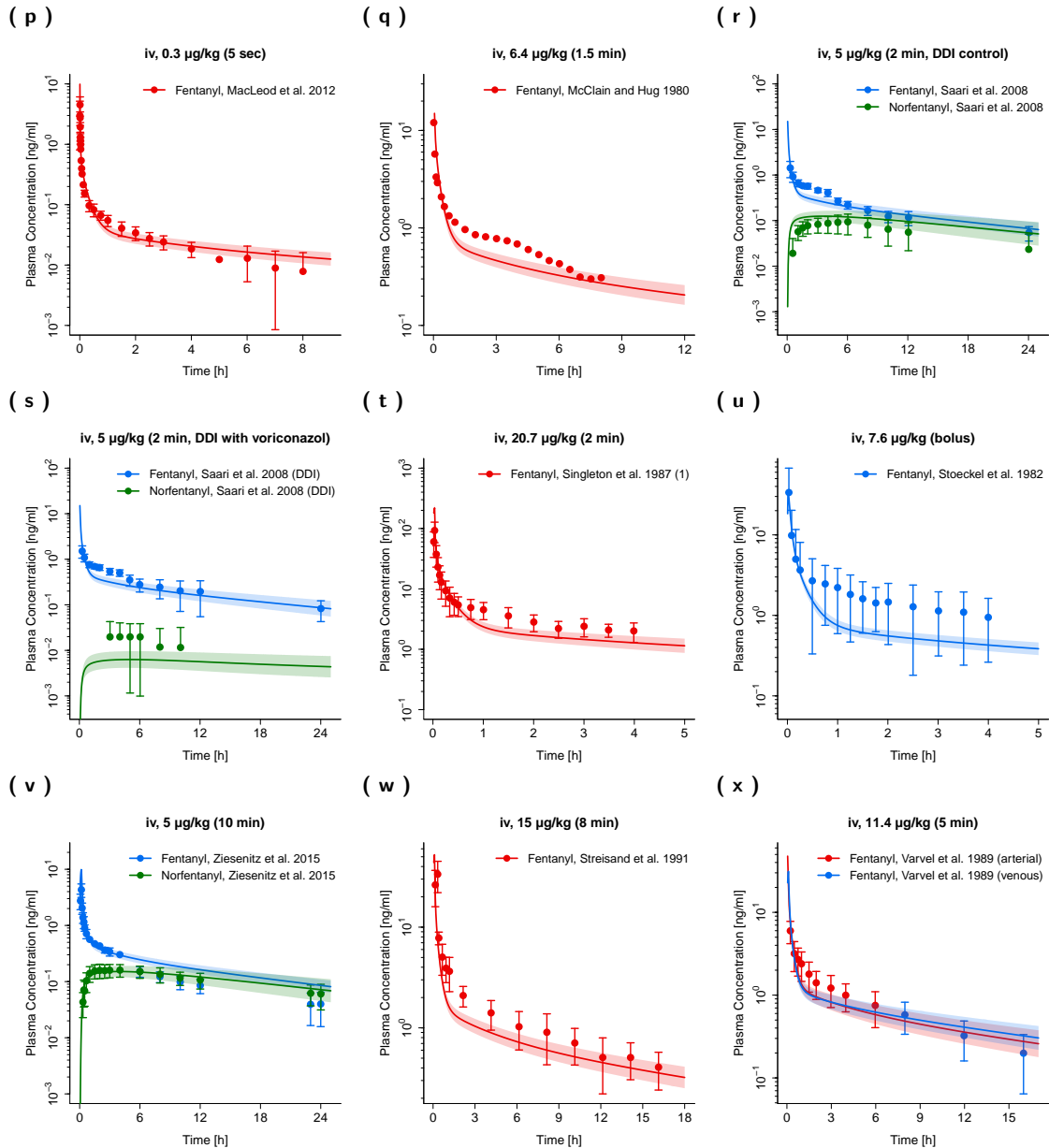


**Figure S1: Fentanyl (blue: venous blood, darkblue: venous blood from central venous catheters, red: arterial blood) and norfentanyl (green: venous blood) plasma concentration-time profiles (semilogarithmic) after intravenous administration of fentanyl in adults.** Observed data are shown as circles, if available  $\pm$  standard deviation (SD). Population simulation ( $n=100$ ) geometric means are shown as lines; the shaded areas represent the predicted population geometric SD. References with numbers in parentheses link to a specific observed dataset ID described in the study table (Table 1 in the main manuscript). Predicted and observed  $AUC_{last}$  values are compared in Table S5. DDI, drug-drug-interaction; iv, intravenous.(continued)

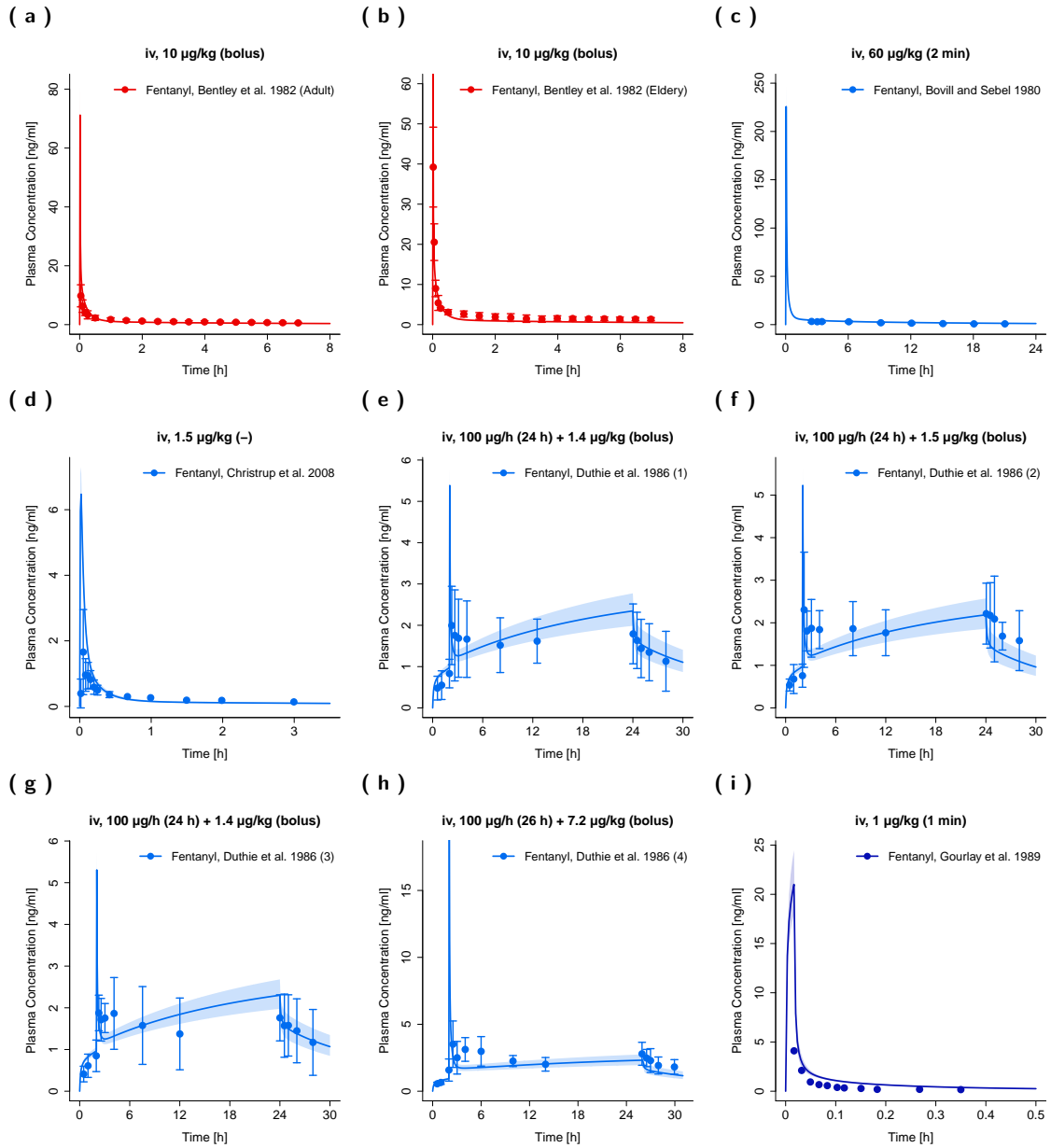


**Figure S2: Fentanyl (blue: venous blood, darkblue: venous blood from central venous catheter, red: arterial blood) and norfentanyl (green: venous blood) plasma concentration-time profiles (linear) as well as fraction of fentanyl dose excreted unchanged in urine (yellow) after intravenous administration of fentanyl in adults.** Observed data are shown as circles, if available  $\pm$  standard deviation (SD). Population simulation ( $n=100$ ) geometric means are shown as lines; the shaded areas represent the predicted population geometric SD. References with numbers in parentheses link to a specific observed dataset ID described in the study table (Table 1 in the main manuscript). Predicted and observed  $AUC_{last}$  values are compared in Table S5. DDI, drug-drug-interaction; iv, intravenous.

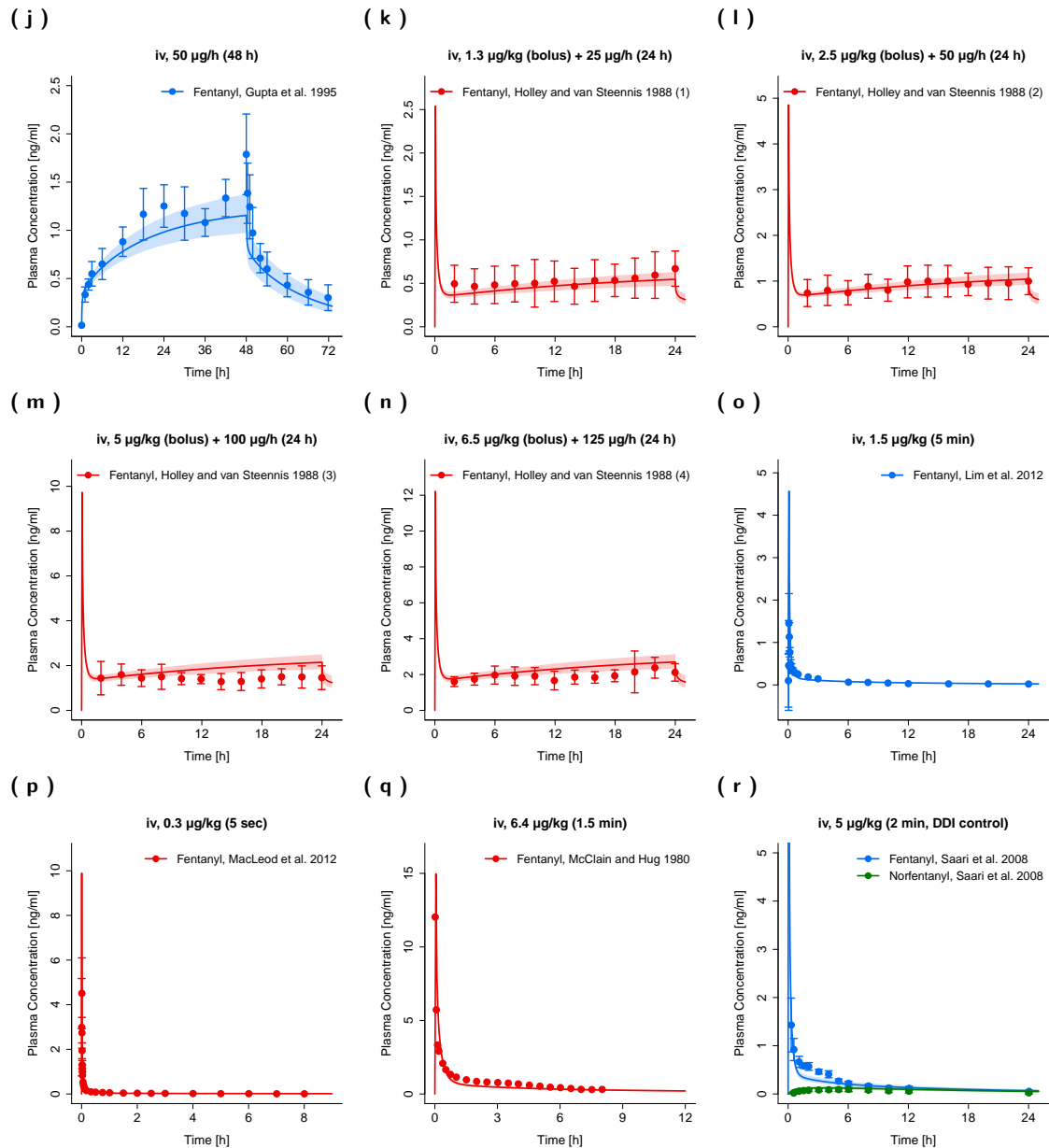


**Figure S2: Fentanyl (blue: venous blood, darkblue: venous blood from central venous catheter, red: arterial blood) and norfentanyl (green: venous blood) plasma concentration-time profiles (linear) as well as fraction of fentanyl dose excreted unchanged in urine (yellow) after intravenous administration of fentanyl in adults.** Observed data are shown as circles, if available  $\pm$  standard deviation (SD). Population simulation ( $n=100$ ) geometric means are shown as lines; the shaded areas represent the predicted population geometric SD. References with numbers in parentheses link to a specific observed dataset ID described in the study table (Table 1 in the main manuscript). Predicted and observed  $AUC_{last}$  values are compared in Table S5. DDI, drug-drug-interaction; iv, intravenous.(continued)

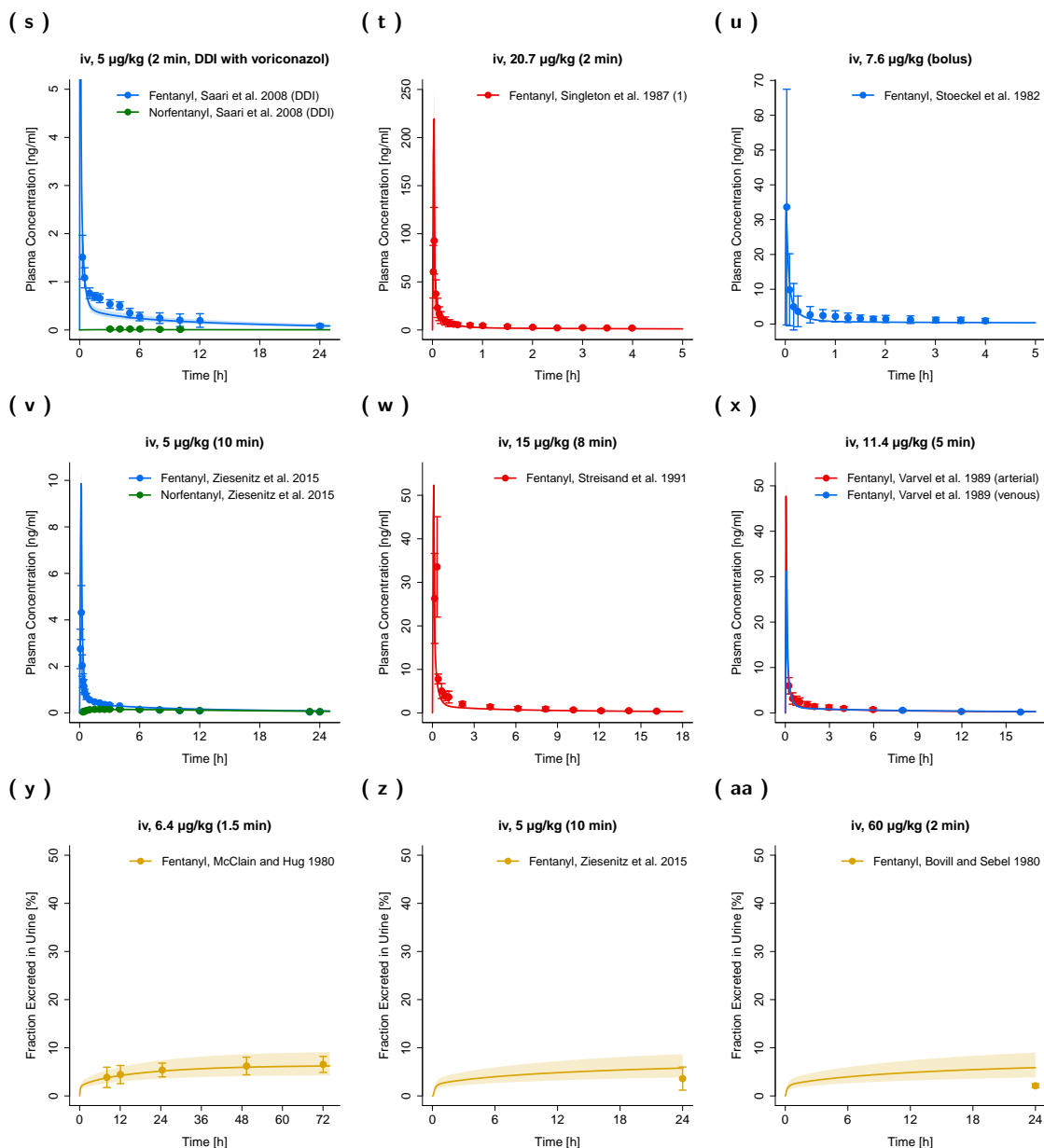


**Figure S2: Fentanyl (blue: venous blood, darkblue: venous blood from central venous catheter, red: arterial blood) and norfentanyl (green: venous blood) plasma concentration-time profiles (linear) as well as fraction of fentanyl dose excreted unchanged in urine (yellow) after intravenous administration of fentanyl in adults.** Observed data are shown as circles, if available  $\pm$  standard deviation (SD). Population simulation ( $n=100$ ) geometric means are shown as lines; the shaded areas represent the predicted population geometric SD. References with numbers in parentheses link to a specific observed dataset ID described in the study table (Table 1 in the main manuscript). Predicted and observed  $\text{AUC}_{\text{last}}$  values are compared in Table S5. DDI, drug-drug-interaction; iv, intravenous.(continued)

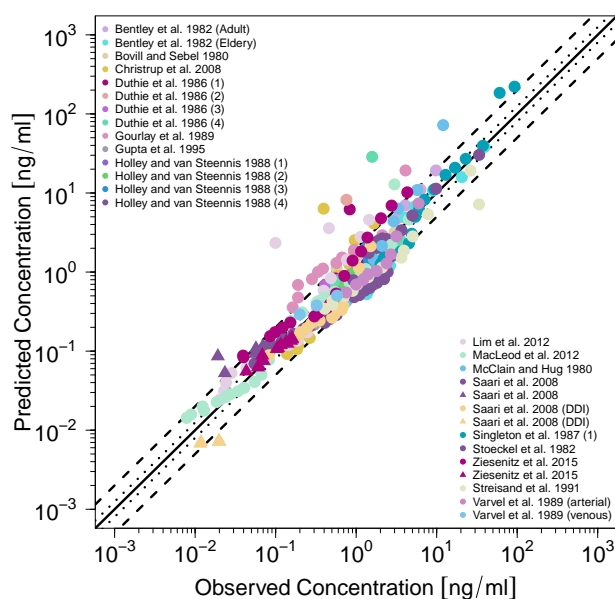
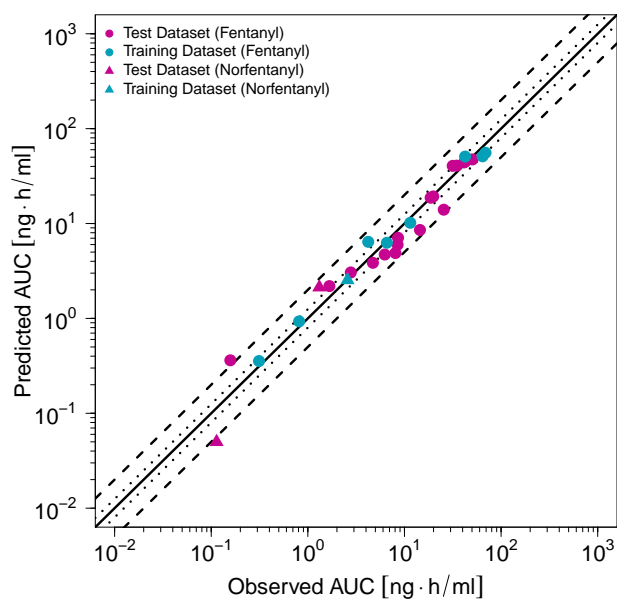


**Figure S3: Predicted versus observed plasma concentrations of fentanyl and norfentanyl after intravenous administration of fentanyl in adults.** Each symbol represents a single plasma concentration (circles: fentanyl, triangles: norfentanyl). The black solid line marks the line of identity. Black dotted lines indicate 1.25-fold, black dashed lines indicate 2-fold deviation.

(a) AUC - Test vs. Training



(b) AUC - Arterial vs. Venous Blood

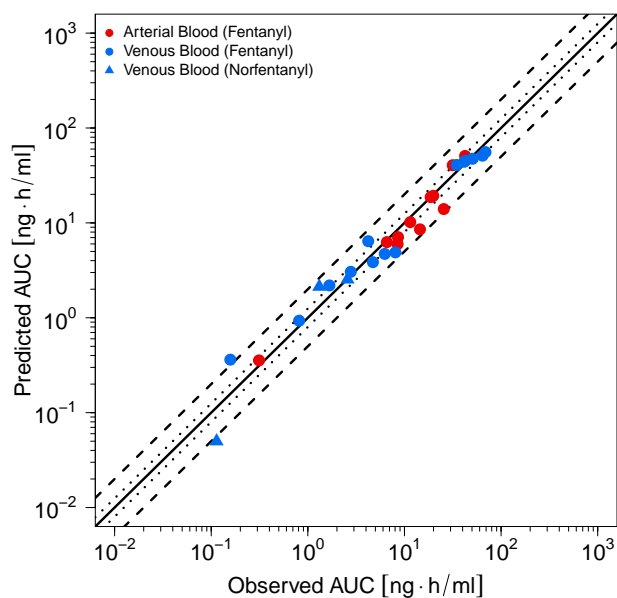


**Figure S4: Predicted versus observed fentanyl and norfentanyl AUC values after intravenous administration of fentanyl in adults grouped by test and training dataset (a) and by arterial and venous blood samples (b).** Each symbol represents the  $AUC_{last}$  of a different plasma profile. The black solid lines mark the lines of identity. Black dotted lines indicate 1.25-fold, black dashed lines indicate 2-fold deviation. **AUC**, area under the plasma concentration-time curve from the first to the last data point.

### 3.2 Pediatric PBPK Model Evaluation

In this section, semilogarithmic and linear plots of plasma concentration-time profiles (Figures S5 and S6), a goodness-of-fit plot of predicted compared to observed plasma concentrations (Figure S7) and a goodness-of-fit plot of predicted compared to observed  $AUC_{last}$  values (Figure S8) after intravenous administration of fentanyl in pediatrics are shown.

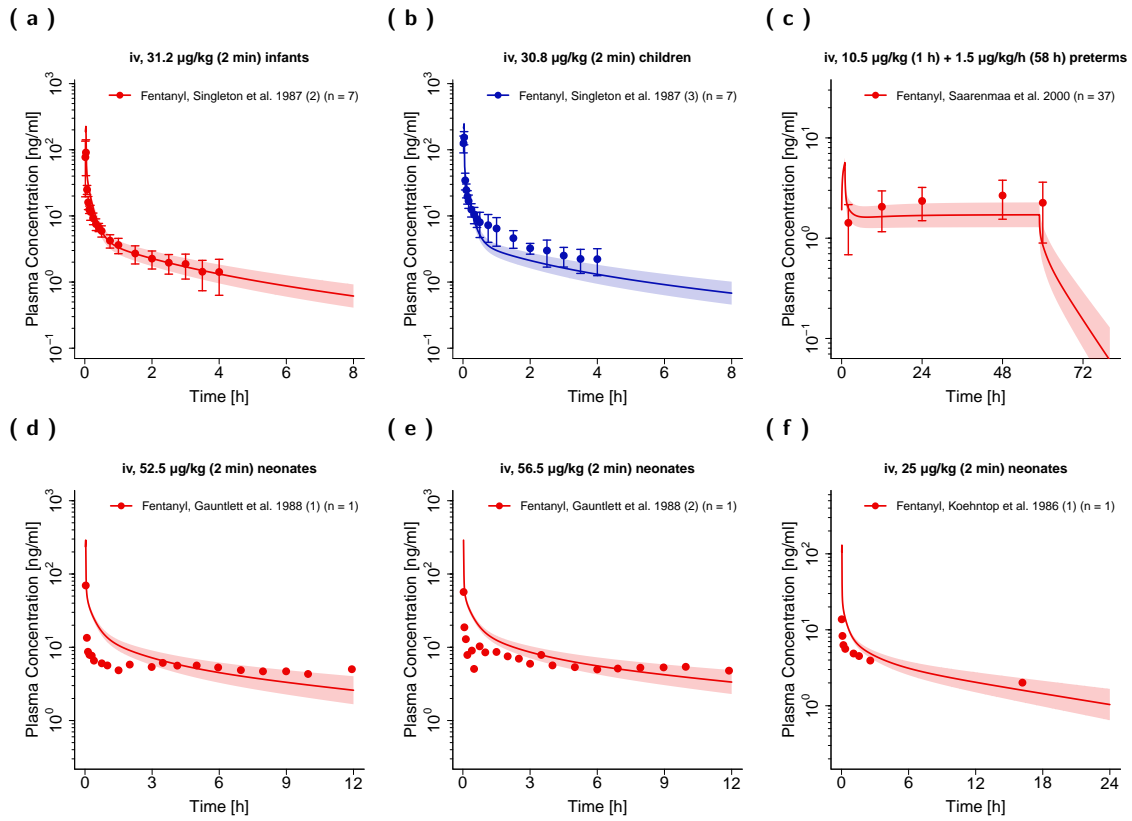


**Figure S5: Fentanyl (darkblue: venous blood from central venous catheter, red: arterial blood) plasma concentration-time profiles (semilogarithmic) after intravenous administration of fentanyl in pediatrics.** Observed data are shown as circles, if available  $\pm$  standard deviation (SD). Population simulation ( $n=100$ ) geometric means are shown as lines; the shaded areas represent the predicted population geometric SD. References with numbers in parentheses link to a specific observed dataset ID described in the study table (Table 2 in the main manuscript). Predicted and observed  $AUC_{last}$  are compared in Table S5. iv, intravenous.

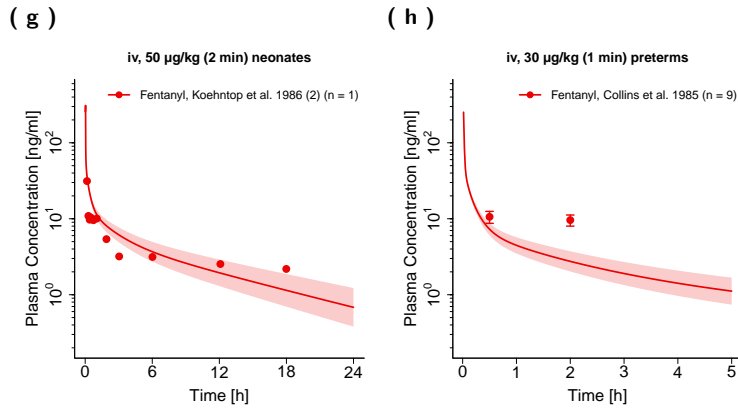


**Figure S5: Fentanyl (darkblue: venous blood from central venous catheter, red: arterial blood) plasma concentration-time profiles (semilogarithmic) after intravenous administration of fentanyl in pediatrics.** Observed data are shown as circles, if available  $\pm$  standard deviation (SD). Population simulation (n=100) geometric means are shown as lines; the shaded areas represent the predicted population geometric SD. References with numbers in parentheses link to a specific observed dataset ID described in the study table (Table 2 in the main manuscript). Predicted and observed  $AUC_{last}$  are compared in Table S5. iv, intravenous.(continued)

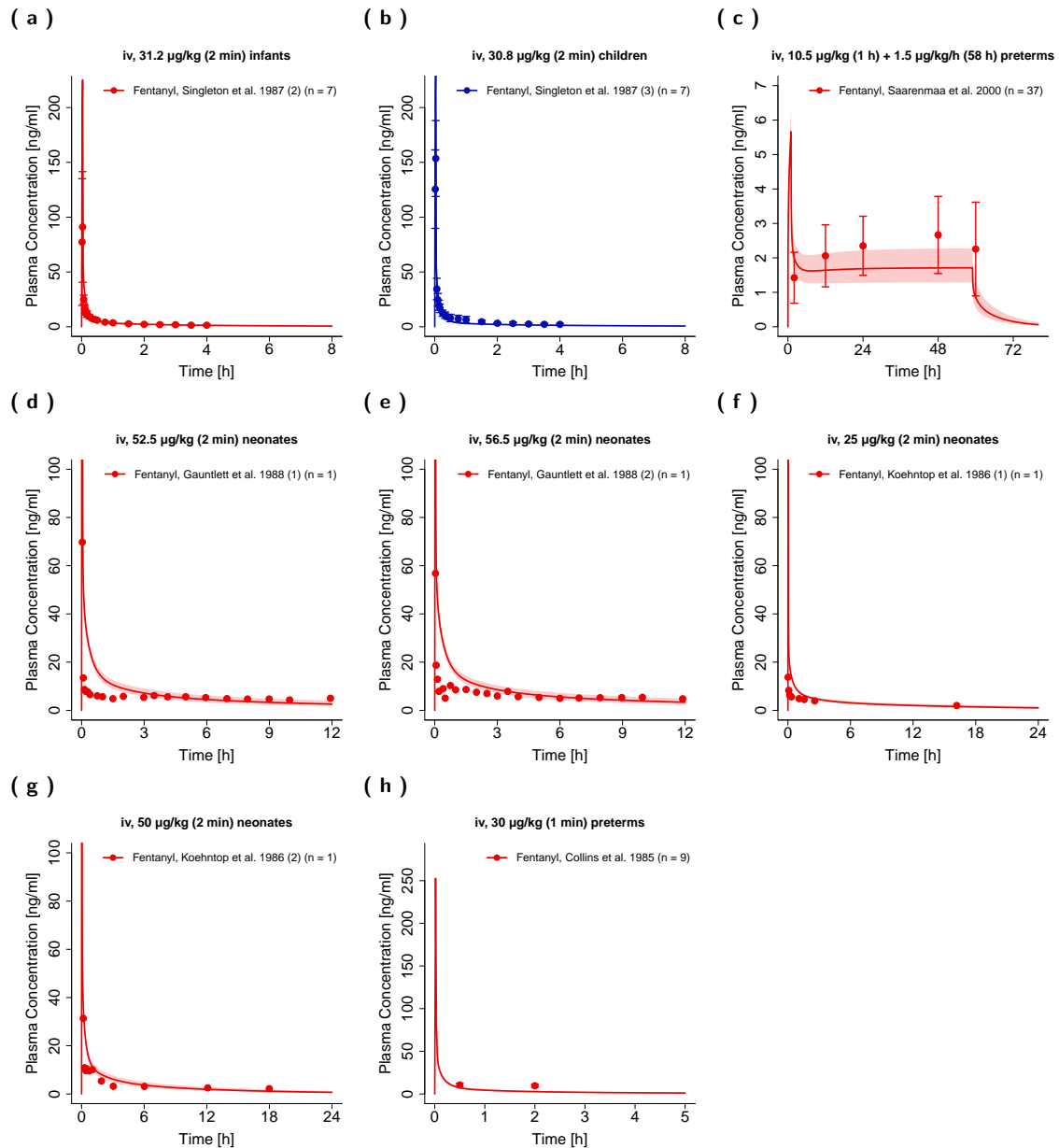


**Figure S6: Fentanyl (darkblue: venous blood from central venous catheter, red: arterial blood) plasma concentration-time profiles (linear) after intravenous administration of fentanyl in pediatrics.** Observed data are shown as circles, if available  $\pm$  standard deviation (SD). Population simulation (n=100) geometric means are shown as lines; the shaded areas represent the predicted population geometric SD. References with numbers in parentheses link to a specific observed dataset ID described in the study table (Table 2 in the main manuscript). Predicted and observed  $\text{AUC}_{\text{last}}$  values are compared in Table S5. iv, intravenous.

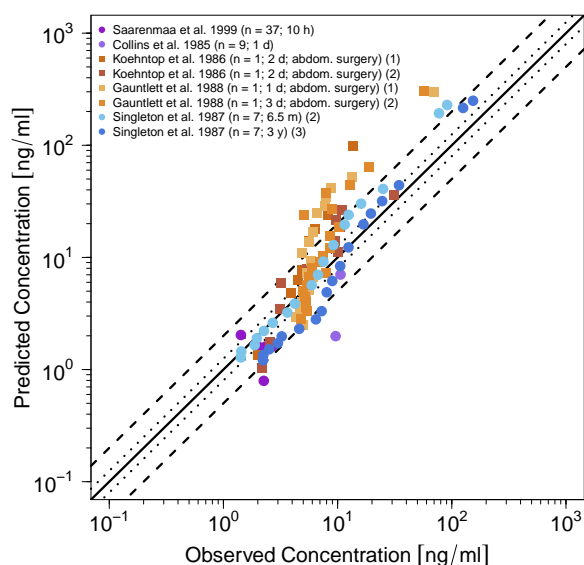


**Figure S7: Predicted versus observed plasma concentrations of fentanyl for the pediatric PBPK model.** Squares depict values for individual patients with adjusted clearances due to increased intraabdominal pressure, circles depict values for study populations without adjustment of clearances. Here, each symbol represents a single concentration. The black solid line marks the line of identity. Black dotted lines indicate 1.25-fold, black dashed lines indicate 2-fold deviation. **abdom**, abdominal.

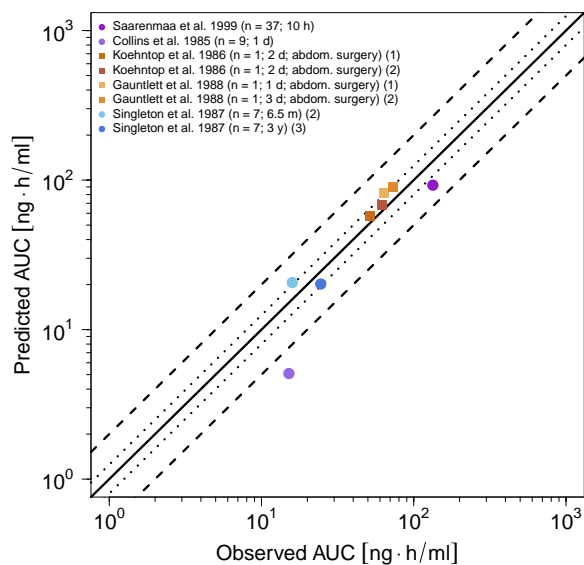


**Figure S8: Predicted versus observed AUC of fentanyl for the pediatric PBPK model.** Squares depict values for individual patients with adjusted clearances due to increased intraabdominal pressure, circles depict values for study populations without adjustment of clearances. Here, each symbol represents the AUC of a single concentration-time profile. The black solid line marks the line of identity. Black dotted lines indicate 1.25-fold, black dashed lines indicate 2-fold deviation. **abdom**, abdominal; **AUC**, area under the plasma concentration-time curve from the first to the last data point.

### 3.3 Quantitative PBPK Model Evaluation

Two quantitative performance measures, the mean relative deviations (MRD) of the predicted plasma concentrations for all observed and the respective predicted plasma concentrations and the geometric mean fold errors (GMFE) of the predicted versus observed  $AUC_{last}$  values, were calculated according to Equation S6 and Equation S7, respectively.  $C_{max}$  values were not calculated as  $C_{max}$  values of a substance administered as intravenous bolus injection or as short-term infusions are very sensitive to the timing of blood sampling.

$$MRD = 10^x \text{ with } x = \sqrt{\frac{1}{n} \sum_{i=1}^n (\log_{10} \hat{c}_i - \log_{10} c_i)^2} \quad (S6)$$

Here,  $c_i$  is the  $i$ th observed plasma concentration,  $\hat{c}_i$  is the respective predicted plasma concentration and  $n$  equals the number of observed values. Calculated MRD values for all studies are given in Table S4.

$$GMFE = 10^x \text{ with } x = \frac{1}{n} \sum_{i=1}^n \left| \log_{10} \left( \frac{A\hat{U}C_i}{AUC_i} \right) \right| \quad (S7)$$

Here,  $AUC_i$  is the  $i$ th observed  $AUC_{last}$  value,  $A\hat{U}C_i$  is the predicted  $AUC_{last}$  value and  $n$  equals the number of studies. The calculated GMFE values are shown in Table S5.

### 3.4 Mean Relative Deviation (MRD) Values of Fentanyl and Norfentanyl Plasma Concentration Predictions

**Table S4:** Mean relative deviation (MRD) values of fentanyl and norfentanyl plasma concentration predictions.

Study ID	Compound	Blood Sample	Dose [ $\mu\text{g}/\text{kg}$ ] <sup>a</sup>	Dose [ $\mu\text{g}/\text{h}$ ] <sup>b</sup>	Administration	MRD	Reference
<b>Fentanyl iv adults</b>							
Bentley et al. 1982 (Adult)	Fentanyl	arterial	10.0		iv (bolus)	1.61	[40]
Bentley et al. 1982 (Eldery)	Fentanyl	arterial	10.0		iv (bolus)	1.94	[40]
Bovill and Sebel 1980	Fentanyl	venous	60.0		iv (2 min)	1.41	[41]
Christrup et al. 2008	Fentanyl	venous	1.5		iv (-)	2.56	[42]
Duthie et al. 1986 (1)	Fentanyl	venous	1.4	100.0	iv (24 h + bolus)	1.79	[43]
Duthie et al. 1986 (2)	Fentanyl	venous	1.5	100.0	iv (24 h + bolus)	2.00	[43]
Duthie et al. 1986 (3)	Fentanyl	venous	1.4	100.0	iv (24 h + bolus)	1.30	[43]
Duthie et al. 1986 (4)	Fentanyl	venous	7.2	100.0	iv (26 h + bolus)	2.37	[43]
Gourlay et al. 1989	Fentanyl	venous <sup>c</sup>	1		iv (1 min)	2.71	[44]
Gupta et al. 1995	Fentanyl	venous <sup>d</sup>		50.0	iv (48 h)	1.34	[45]
Holley and van Steennis 1988 (1)	Fentanyl	arterial	1.3	25.0	iv (loading dose + 24 h)	1.17	[46]
Holley and van Steennis 1988 (2)	Fentanyl	arterial	2.5	50.0	iv (loading dose + 24 h)	1.07	[46]
Holley and van Steennis 1988 (3)	Fentanyl	arterial	5.0	100.0	iv (loading dose + 24 h)	1.33	[46]
Holley and van Steennis 1988 (4)	Fentanyl	arterial	6.5	125.0	iv (loading dose + 24 h)	1.22	[46]
Lim et al. 2012	Fentanyl	venous	1.5		iv (5 min)	2.62	[47]
MacLeod et al. 2012	Fentanyl	arterial	0.3		iv (5 sec)	1.49	[48]
McClain and Hug 1980	Fentanyl	arterial	6.4		iv (1.5 min)	1.77	[9]
Saari et al. 2008	Fentanyl	venous	5.0		iv (2 min)	1.49	[7]
Saari et al. 2008	Norfentanyl	venous	5.0		iv (2 min)	1.87	[7]
Saari et al. 2008 (DDI)	Fentanyl	venous	5.0		iv (2 min)	1.51	[7]
Saari et al. 2008 (DDI)	Norfentanyl	venous	5.0		iv (2 min)	2.40	[7]
Singleton et al. 1987 (1)	Fentanyl	arterial	20.7		iv (2 min)	1.65	[17]
Stoeckel et al. 1982	Fentanyl	venous	7.6		iv (bolus)	2.00	[49]
Streisand et al. 1991	Fentanyl	arterial	15.0		iv (8 min)	1.87	[50]
Varvel et al. 1989	Fentanyl	arterial	11.4		iv (5 min)	1.51	[51]
Varvel et al. 1989	Fentanyl	venous	11.4		iv (5 min)	1.29	[51]

<sup>a</sup> dose of bolus injection or short-infusion

<sup>b</sup> dose of long-term infusion

<sup>c</sup> venous blood samples from a central venous catheter

<sup>d</sup> sample information was not specified, venous blood samples were assumed

**DDI:** drug-drug-interaction, **iv:** intravenous, **MRD:** mean relative deviation

**Table S4:** Mean relative deviation (MRD) values of fentanyl and norfentanyl plasma concentration predictions. (*continued*)

Study ID	Compound	Blood Sample	Dose [ $\mu\text{g}/\text{kg}$ ] <sup>a</sup>	Dose [ $\mu\text{g}/\text{h}$ ] <sup>b</sup>	Administration	MRD	Reference
Ziesenitz et al. 2015	Fentanyl	venous	5.0		iv (10 min)	1.72	[8]
Ziesenitz et al. 2015	Norfentanyl	venous	5.0		iv (10 min)	1.12	[8]
<b>MRD</b>						<b>1.77 (1.07–2.71)</b>	
						<b>22/28 with MRD <math>\leq</math> 2</b>	
<b>Fentanyl iv children</b>							
Collins et al. 1985	Fentanyl	arterial	30.0		iv (1 min)	3.16	[52]
Gauntlett et al. 1988 (1)	Fentanyl	arterial	52.5		iv (2 min)	2.43	[23]
Gauntlett et al. 1988 (2)	Fentanyl	arterial	56.5		iv (2 min)	2.25	[23]
Koehntop et al. 1986 (1)	Fentanyl	arterial	25.0		iv (1–3 min)	2.62	[24]
Koehntop et al. 1986 (2)	Fentanyl	arterial	50.0		iv (1–3 min)	1.71	[24]
Saarenmaa et al. 2000	Fentanyl	arterial	10.5	1.5	iv (1 h + 58 h)	1.79	[18]
Singleton et al. 1987 (2)	Fentanyl	arterial	31.2		iv (2 min)	1.53	[17]
Singleton et al. 1987 (3)	Fentanyl	venous	30.8		iv (2 min)	1.64	[17]
<b>MRD</b>						<b>2.04 (1.53–3.16)</b>	
						<b>4/8 with MRD <math>\leq</math> 2</b>	

<sup>a</sup> dose of bolus injection or short-infusion<sup>b</sup> dose of long-term infusion<sup>c</sup> venous blood samples from a central venous catheter<sup>d</sup> sample information was not specified, venous blood samples were assumed

DDI: drug-drug-interaction, iv: intravenous, MRD: mean relative deviation

3.5 Geometric Mean Fold Error (GMFE) of AUC<sub>last</sub> PredictionsTable S5: Predicted and observed AUC<sub>last</sub> values of fentanyl and norfentanyl plasma concentrations.

Study ID	Compound	Blood Sample	Dose [ $\mu\text{g}/\text{kg}$ ] <sup>a</sup>	Dose [ $\mu\text{g}/\text{h}$ ] <sup>b</sup>	Administration	AUC <sub>last</sub>			Reference
						Pred [ $\text{ng}/\text{h}/\text{ml}$ ]	Obs [ $\text{ng}/\text{h}/\text{ml}$ ]	Pred/Obs	
<b>Fentanyl iv adults</b>									
Bentley et al. 1982 (Adult)	Fentanyl	arterial	10.0		iv (bolus)	7.08	8.58	0.83	[40]
Bentley et al. 1982 (Elderly)	Fentanyl	arterial	10.0		iv (bolus)	8.55	14.47	0.59	[40]
Bovill and Sebel 1980	Fentanyl	venous	60.0		iv (2 min)	40.76	34.67	1.18	[41]
Christrup et al. 2008	Fentanyl	venous	1.5		iv (-)	0.93	0.81	1.15	[42]
Duthie et al. 1986 (1)	Fentanyl	venous	1.4	100.0	iv (24 h + bolus)	45.21	42.71	1.06	[43]
Duthie et al. 1986 (2)	Fentanyl	venous	1.5	100.0	iv (24 h + bolus)	47.42	50.60	0.94	[43]
Duthie et al. 1986 (3)	Fentanyl	venous	1.4	100.0	iv (24 h + bolus)	44.10	41.61	1.06	[43]
Duthie et al. 1986 (4)	Fentanyl	venous	7.2	100.0	iv (26 h + bolus)	55.72	69.00	0.81	[43]
Gourlay et al. 1989	Fentanyl	venous <sup>c</sup>	1		iv (1 min)	0.36	0.16	2.30	[44]
Gupta et al. 1995	Fentanyl	venous <sup>d</sup>		50.0	iv (48 h)	51.12	64.32	0.79	[45]
Holley and van Steennis 1988 (1)	Fentanyl	arterial	1.3	25.0	iv (loading dose + 24 h)	10.18	11.48	0.89	[46]
Holley and van Steennis 1988 (2)	Fentanyl	arterial	2.5	50.0	iv (loading dose + 24 h)	19.31	19.87	0.97	[46]
Holley and van Steennis 1988 (3)	Fentanyl	arterial	5.0	100.0	iv (loading dose + 24 h)	40.55	31.57	1.28	[46]
Holley and van Steennis 1988 (4)	Fentanyl	arterial	6.5	125.0	iv (loading dose + 24 h)	50.81	42.43	1.20	[46]
Lim et al. 2012	Fentanyl	venous	1.5	2.19	iv (5 min)	1.67	1.31	1.27	[47]
MacLeod et al. 2012	Fentanyl	arterial	0.3	0.36	iv (5 sec)	0.36	0.31	1.14	[48]
McClain and Hug 1980	Fentanyl	arterial	6.4	6.27	iv (1.5 min)	6.27	6.58	0.95	[9]
Saari et al. 2008	Fentanyl	venous	5.0	4.71	iv (2 min)	3.86	4.71	0.82	[7]
Saari et al. 2008	Norfentanyl	venous	5.0	2.13	iv (2 min)	2.13	1.31	1.62	[7]
Saari et al. 2008 (DDI)	Fentanyl	venous	5.0	4.71	iv (2 min)	4.71	6.25	0.75	[7]
Saari et al. 2008 (DDI)	Norfentanyl	venous	5.0	0.05	iv (2 min)	0.05	0.11	0.44	[7]
Singleton et al. 1987 (1)	Fentanyl	arterial	20.7	18.70	iv (2 min)	18.70	18.66	1.00	[17]
Stoekel et al. 1982	Fentanyl	venous	7.6	4.89	iv (bolus)	4.89	8.06	0.61	[49]
Straisand et al. 1991	Fentanyl	arterial	15.0	13.99	iv (8 min)	13.99	25.51	0.55	[50]
Varvel et al. 1989	Fentanyl	arterial	11.4	5.99	iv (5 min)	5.99	8.49	0.71	[51]
Varvel et al. 1989	Fentanyl	venous	11.4	3.05	iv (5 min)	3.05	2.78	1.10	[51]
Ziesenitz et al. 2015	Fentanyl	venous	5.0	6.41	iv (10 min)	6.41	4.22	1.52	[8]
Ziesenitz et al. 2015	Norfentanyl	venous	5.0	2.54	iv (10 min)	2.54	2.57	0.99	[8]
<b>GMFE</b>						<b>1.30 (1.00–2.30)</b>			
<b>Fentanyl iv children</b>						<b>26/28 with GMFE <math>\leq</math> 2</b>			
Collins et al. 1985	Fentanyl	arterial	30.0		iv (1 min)	5.09	15.14	0.34	[52]
Gauntlett et al. 1988 (1)	Fentanyl	arterial	52.5		iv (2 min)	81.92	63.85	1.28	[23]
Gauntlett et al. 1988 (2)	Fentanyl	arterial	56.5		iv (2 min)	90.19	72.67	1.24	[23]
Kochtop et al. 1986 (1)	Fentanyl	arterial	25.0		iv (1–3 min)	57.43	51.80	1.11	[24]
Kochtop et al. 1986 (2)	Fentanyl	arterial	50.0		iv (1–3 min)	68.19	61.67	1.11	[24]
Saarenmaa et al. 2000	Fentanyl	arterial	10.5	1.5	iv (1 h + 58 h)	92.50	133.53	0.69	[18]
Singleton et al. 1987 (2)	Fentanyl	arterial	31.2		iv (2 min)	20.65	15.93	1.30	[17]
Singleton et al. 1987 (3)	Fentanyl	venous <sup>a</sup>	30.8		iv (2 min)	20.18	24.51	0.82	[17]
<b>GMFE</b>						<b>1.38 (1.11–2.98)</b>			
<b>7/8 with GMFE <math>\leq</math> 2</b>									

<sup>a</sup> dose of bolus injection or short-infusion<sup>b</sup> dose of long-term infusion<sup>c</sup> venous blood samples from a central venous catheter<sup>d</sup> sample information was not specified, venous blood samples were assumed

DDI: drug-drug-interaction, GMFE: geometric mean fold error, iv: intravenous, Obs: observed, Pred: predicted

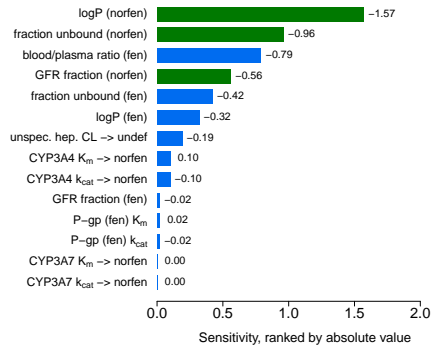
### 3.6 Fentanyl and Norfentanyl PBPK Model Sensitivity Analysis

A sensitivity analysis of the developed PBPK models (adults and pediatrics) to single parameter changes was performed (local sensitivity analysis). It needs to be noted, that sensitivity to parameters regarding the metabolite norfentanyl was not investigated for the pediatric models as norfentanyl plasma concentration measurements were only available in clinical studies with adults. In case of full-term neonates, sensitivity was examined for model parameters (1) with metabolic clearance adaptation due to increased intraabdominal pressure (see Section 1.2) and (2) without metabolic clearance adaptation. Sensitivities of the PBPK models were calculated as the relative changes of the predicted area under the plasma concentration-time curve extrapolated to infinity ( $AUC_{inf}$ ) of fentanyl and norfentanyl, respectively, to the relative variation of model input parameters in a short infusion scenario (20.7  $\mu\text{g}/\text{kg}$  fentanyl administered over two minutes [17]). Parameters, optimized as well as parameters fixed to literature values, were included into the analysis if they had significant impact in former models (e.g. glomerular filtration rate fraction), if they could have a decisive influence due to calculation methods used in the model (e.g. lipophilicity) and/or if they have been optimized. The analyses were performed using a relative perturbation of parameters of 10%. Model sensitivity to a parameter was calculated as follows:

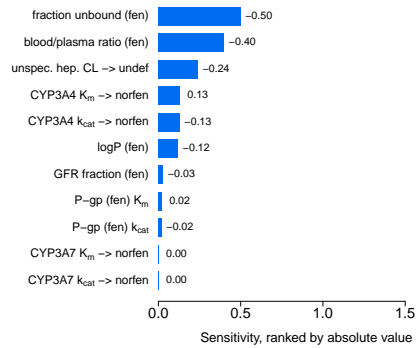
$$S = \frac{\Delta AUC_{inf}}{\Delta p} \cdot \frac{p}{AUC_{inf}} \quad (\text{S8})$$

where  $S$  is the sensitivity of the  $AUC_{inf}$  to the examined model parameter,  $\Delta AUC_{inf}$  is the change of the  $AUC_{inf}$ ,  $AUC_{inf}$  is the simulated  $AUC_{inf}$  with the original parameter value,  $p$  is the original model parameter value and  $\Delta p$  is the change of the model parameter value. A sensitivity value of +1.0 signifies that a 10% increase of the examined parameter causes a 10% increase of the simulated  $AUC_{inf}$ .

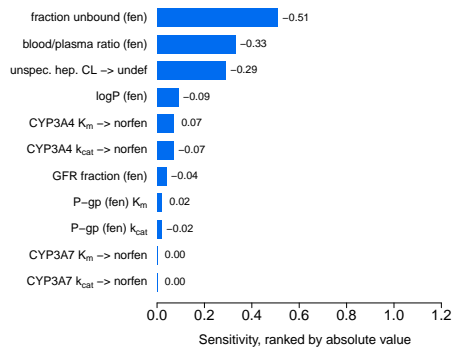
( a ) Adults



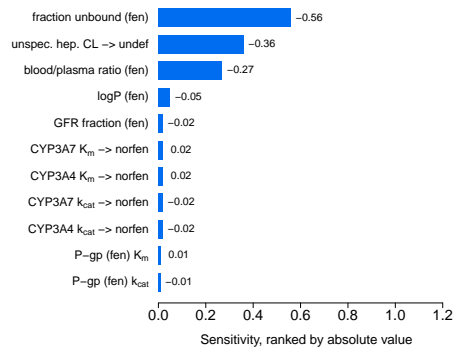
( b ) Children



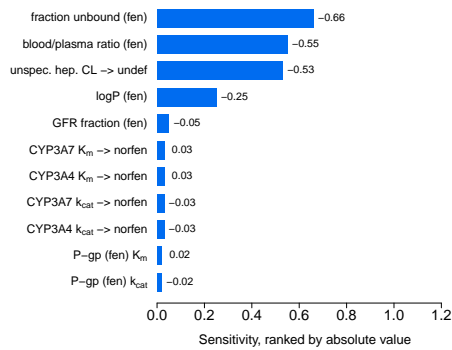
( c ) Infants



( d ) Full-term Neonates



( e ) Full-term Neonates  
(Intraabdominal Pressure)



( f ) Preterm Neonates

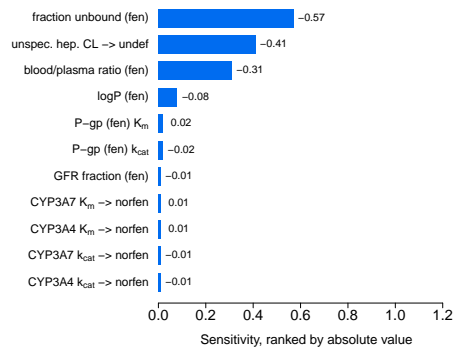


**Figure S9: Sensitivity analyses of the fentanyl PBPK model in different populations.** Sensitivity of the model to single parameters, calculated as change of the simulated  $AUC_{inf}$  of fentanyl and norfentanyl, respectively, following a short infusion scenario (20.7  $\mu\text{g}/\text{kg}$  of fentanyl administered over two minutes [17]).  $AUC_{inf}$ : area under the plasma concentration-time curve extrapolated to infinity, **CYP**: Cytochrome P450, **fen**: fentanyl, **GFR**: glomerular filtration rate,  $k_{cat}$ : catalytic rate constant,  $K_m$ : Michaelis-Menten constant, **norfen**: norfentanyl, **P-gp**: P-glycoprotein, **undef**: undefined metabolite, **unspec. hep. CL**: unspecific hepatic clearance.

## References

- [1] Maharaj AR, Barrett JS, Edginton AN (2013) A workflow example of PBPK modeling to support pediatric research and development: case study with lorazepam. *The AAPS journal* 15(2):455–64
- [2] Maharaj AR, Edginton AN (2014) Physiologically Based Pharmacokinetic Modeling and Simulation in Pediatric Drug Development. *CPT: Pharmacometrics & Systems Pharmacology* 3(11):1–13
- [3] Leong R, Vieira MLT, Zhao P, Mulugeta Y, Lee CS, Huang SM, Burckart GJ (2012) Regulatory experience with physiologically based pharmacokinetic modeling for pediatric drug trials. *Clinical pharmacology and therapeutics* 91(5):926–31
- [4] Ince I, Solodenko J, Frechen S, Dallmann A, Niederalte C, Schlender J, Burghaus R, Lippert J, Willmann S (2019) Predictive Pediatric Modeling and Simulation Using Ontogeny Information. *The Journal of Clinical Pharmacology* 59(S1):S95–S103
- [5] Kovar L, Schräpel C, Selzer D, Kohl Y, Bals R, Schwab M, Lehr T (2020) Physiologically-Based Pharmacokinetic (PBPK) Modeling of Buprenorphine in Adults, Children and Preterm Neonates. *Pharmaceutics* 12(6):578
- [6] Feierman DE, Lasker JM (1996) Metabolism of fentanyl, a synthetic opioid analgesic, by human liver microsomes. Role of CYP3A4. *Drug metabolism and disposition: the biological fate of chemicals* 24(9):932–9
- [7] Saari TI, Laine K, Neuvonen M, Neuvonen PJ, Olkkola KT (2008) Effect of voriconazole and fluconazole on the pharmacokinetics of intravenous fentanyl. *European Journal of Clinical Pharmacology* 64(1):25–30
- [8] Ziesenitz VC, König SK, Mahlke NS, Skopp G, Haefeli WE, Mikus G (2015) Pharmacokinetic interaction of intravenous fentanyl with ketoconazole. *Journal of Clinical Pharmacology* 55(6):708–717
- [9] McClain DA, Hug CC (1980) Intravenous fentanyl kinetics. *Clinical Pharmacology and Therapeutics* 28(1):106–114
- [10] Lötsch J, Walter C, Parnham MJ, Oertel BG, Geisslinger G (2013) Pharmacokinetics of Non-Intravenous Formulations of Fentanyl. *Clinical Pharmacokinetics* 52(1):23–36
- [11] Williams JA, Ring BJ, Cantrell VE, Jones DR, Eckstein J, Ruterbories K, Hamman MA, Hall SD, Wrighton SA (2002) Comparative Metabolic Capabilities of CYP3A4, CYP3A5, and CYP3A7. *Drug Metabolism and Disposition* 30(8):883–891
- [12] Niwa T, Okamoto A, Narita K, Toyota M, Kato K, Kobayashi K, Sasaki S (2020) Comparison of steroid hormone hydroxylation mediated by cytochrome P450 3A subfamilies. *Archives of Biochemistry and Biophysics* 682:108283
- [13] Yu C, Yuan M, Yang H, Zhuang X, Li H (2018) P-glycoprotein on blood-brain barrier plays a vital role in fentanyl brain exposure and respiratory toxicity in rats. *Toxicological Sciences* 164(1):353–362
- [14] Henthorn TK, Liu Y, Mahapatro M, Ng KY (1999) Active transport of fentanyl by the blood-brain barrier. *Journal of Pharmacology and Experimental Therapeutics* 289(2):1084–1089
- [15] Thompson SJ, Koszdin K, Bernards CM (2000) Opiate-induced analgesia is increased and prolonged in mice lacking P-glycoprotein. *Anesthesiology* 92(5):1392–1399

- [16] Kharasch ED, Hoffer C, Altuntas TG, Whittington D (2004) Quinidine as a Probe for the Role of P-Glycoprotein in the Intestinal Absorption and Clinical Effects of Fentanyl. *Journal of Clinical Pharmacology* 44(3):224–233
- [17] Singleton Ma, Rosen JI, Fisher DM (1987) Plasma concentrations of fentanyl in infants, children and adults. *Canadian Journal of Anaesthesia* 34(2):152–155
- [18] Saarenmaa E, Neuvonen PJ, Fellman V (2000) Gestational age and birth weight effects on plasma clearance of fentanyl in newborn infants. *Journal of Pediatrics* 136(6):0767–0770
- [19] Rodgers T, Rowland M (2006) Physiologically-based Pharmacokinetic Modeling 2: Predicting the tissue distribution of acids, very weak bases, neutrals and zwitterions. *Journal of Pharmaceutical Sciences* 95:1238–1257
- [20] Rodgers T, Leahy D, Rowland M (2005) Physiologically based pharmacokinetic modeling 1: Predicting the tissue distribution of moderate-to-strong bases. *Journal of Pharmaceutical Sciences* 94:1259–1276
- [21] Rodgers T, Rowland M (2007) Mechanistic approaches to volume of distribution predictions: understanding the processes. *Pharmaceutical research* 24(5):918–33
- [22] Schmitt W (2008) General approach for the calculation of tissue to plasma partition coefficients. *Toxicology in vitro : an international journal published in association with BIBRA* 22(2):457–67
- [23] Gauntlett IS, Fisher DM, Hertzka RE, Kuhis E, Spellman MJ, Rudolph C (1988) Pharmacokinetics of Fentanyl in Neonatal Humans and Lambs. *Anesthesiology* 69(5):683–687
- [24] Koehntop DE, Rodman JH, Brundage DM, Hegland MG, Buckley JJ (1986) Pharmacokinetics of fentanyl in neonates. *Anesthesia and Analgesia* 65(3):227–232
- [25] Willmann S, Höhn K, Edginton A, Sevestre M, Solodenko J, Weiss W, Lippert J, Schmitt W (2007) Development of a physiology-based whole-body population model for assessing the influence of individual variability on the pharmacokinetics of drugs. *Journal of Pharmacokinetics and Pharmacodynamics* 34(3):401–431
- [26] Stader F, Penny MA, Siccardi M, Marzolini C (2019) A Comprehensive Framework for Physiologically-Based Pharmacokinetic Modeling in Matlab. *CPT: Pharmacometrics & Systems Pharmacology* 8(7):psp4.12399
- [27] Valentin J (2002) Basic anatomical and physiological data for use in radiological protection: reference values. *Annals of the ICRP* 32(3-4):1–277
- [28] National Center for Health Statistics (1997) Third National Health and Nutrition Examination Survey (NHANES III). Tech. rep., Hyattsville, MD 20782
- [29] Nishimura M, Yaguti H, Yoshitsugu H, Naito S, Satoh T (2003) Tissue distribution of mRNA expression of human cytochrome P450 isoforms assessed by high-sensitivity real-time reverse transcription PCR. *Journal of the Pharmaceutical Society of Japan* 123(5):369–75
- [30] Nishimura M, Naito S (2005) Tissue-specific mRNA Expression Profiles of Human ATP-binding Cassette and Solute Carrier Transporter Superfamilies. *Drug Metabolism and Pharmacokinetics* 20(6):452–477
- [31] Nishimura M, Naito S (2006) Tissue-Specific mRNA Expression Profiles of Human Phase I Metabolizing Enzymes Except for Cytochrome P450 and Phase II Metabolizing Enzymes. *Drug Metabolism and Pharmacokinetics* 21(5):357–374

- [32] Rodrigues AD (1999) Integrated cytochrome P450 reaction phenotyping: attempting to bridge the gap between cDNA-expressed cytochromes P450 and native human liver microsomes. *Biochemical pharmacology* 57(5):465–80
- [33] Open Systems Pharmacology Suite Community (2018) PK-Sim<sup>®</sup> Ontogeny Database Documentation, Version 7.3. <https://github.com/Open-Systems-Pharmacology/OSPSuite.Documentation/blob/master/PK-SimOntogenyDatabaseVersion7.3.pdf>, accessed: 2020-03-25
- [34] Stevens JC, Hines RN, Gu C, Koukouritaki SB, Manro JR, Tandler PJ, Zaya MJ (2003) Developmental Expression of the Major Human Hepatic CYP3A Enzymes. *Journal of Pharmacology and Experimental Therapeutics* 307(2):573–582
- [35] Prasad B, Evers R, Gupta A, Hop CECA, Salphati L, Shukla S, Ambudkar SV, Unadkat JD (2014) Interindividual Variability in Hepatic Organic Anion-Transporting Polypeptides and P-Glycoprotein (ABCB1) Protein Expression: Quantification by Liquid Chromatography Tandem Mass Spectroscopy and Influence of Genotype, Age, and Sex. *Drug Metabolism and Disposition* 42(1):78–88
- [36] Prasad B, Gaedigk A, Vrana M, Gaedigk R, Leeder J, Salphati L, Chu X, Xiao G, Hop C, Evers R, Gan L, Unadkat J (2016) Ontogeny of Hepatic Drug Transporters as Quantified by LC-MS/MS Proteomics. *Clinical Pharmacology & Therapeutics* 100(4):362–370
- [37] Meyer M, Schneckener S, Ludewig B, Kuepfer L, Lippert J (2012) Using Expression Data for Quantification of Active Processes in PBPK Modeling. *Drug Metabolism and Disposition* 40(5):892–901
- [38] Hanke N, Frechen S, Moj D, Britz H, Eissing T, Wendl T, Lehr T (2018) PBPK Models for CYP3A4 and P-gp DDI Prediction: A Modeling Network of Rifampicin, Itraconazole, Clarithromycin, Midazolam, Alfentanil, and Digoxin. *CPT: Pharmacometrics and Systems Pharmacology* 7(10):647–659
- [39] Li X, Frechen S, Moj D, Lehr T, Taubert M, hsuan Hsin C, Mikus G, Neuvonen PJ, Olkkola KT, Saari TI, Fuhr U (2019) A Physiologically Based Pharmacokinetic Model of Voriconazole Integrating Time-Dependent Inhibition of CYP3A4, Genetic Polymorphisms of CYP2C19 and Predictions of Drug–Drug Interactions. *Clinical Pharmacokinetics* (0123456789)
- [40] Bentley JB, Borel JD, Nenad RE, Gillespie TJ (1982) Age and Fentanyl Pharmacokinetics. *Anesthesia & Analgesia* 61(12):968–971
- [41] Bovill JG, Sebel PS (1980) Pharmacokinetics of high-dose fentanyl: A study in patients undergoing cardiac surgery. *British Journal of Anaesthesia* 52(8):795–801
- [42] Christrup L, Foster D, Popper L, Troen T, Upton R (2008) Pharmacokinetics, efficacy, and tolerability of fentanyl following intranasal versus intravenous administration in adults undergoing third-molar extraction: A randomized, double-blind, double-dummy, two-way, crossover study. *Clinical Therapeutics* 30(3):469–481
- [43] Duthie D, McLaren A, Nimmo W (1986) Pharmacokinetics Of Fentanyl During Constant Rate I.V. Infusion For The Relief Of Pain After Surgery. *British Journal of Anaesthesia* 58(9):950–956
- [44] Gourlay GK, Kowalski SR, Plummer JL, Cherry DA, Gaukroger P, Cousins MJ (1989) The transdermal administration of fentanyl in the treatment of postoperative pain: pharmacokinetics and pharmacodynamic effects. *Pain* 37(2):193–202

- [45] Gupta SK, Southam MA, Hwang SS (1995) Evaluation of Diurnal Variation in Fentanyl Clearance. *The Journal of Clinical Pharmacology* 35(2):159–162
- [46] Holley FO, Van Steennis C (1988) Postoperative analgesia with fentanyl: Pharmacokinetics and pharmacodynamics of constant-rate I.V. and transdermal delivery. *British Journal of Anaesthesia* 60(6):608–613
- [47] Lim CBS, Schug SA, Sunderland VB, Paech MJ, Liu Y (2012) A Phase I Pharmacokinetic and Bioavailability Study of a Sublingual Fentanyl Wafer in Healthy Volunteers. *Anesthesia & Analgesia* 115(3):1
- [48] MacLeod DB, Habib AS, Ikeda K, Spyker DA, Cassella JV, Ho KY, Gan TJ (2012) Inhaled Fentanyl Aerosol in Healthy Volunteers. *Anesthesia & Analgesia* 115(5):1071–1077
- [49] Stoeckel H, Schüttler J, Magnussen H, Hengstmann J (1982) Plasma Fentanyl Concentrations And The Occurrence Of Respiratory Depression In Volunteers. *British Journal of Anaesthesia* 54(10):1087–1095
- [50] Streisand JB, Varvel JR, Stanski DR, Maire LL, Ashburn MA, Hague BI, Tarver SD, Stanley TH (1991) Absorption and Bioavailability of Oral Transmucosal Fentanyl Citrate. *Anesthesiology* 75(2):223–229
- [51] Varvel JR, Shafer SL, Hwang SS, Coen PA, Stanski DR (1989) Absorption Characteristics of Transdermally Administered Fentanyl. *Anesthesiology* 70(6):928–934
- [52] Collins C, Koren G, Crean P, Klein J, Roy WL, MacLeod SM (1985) Fentanyl pharmacokinetics and hemodynamic effects in preterm infants during ligation of patent ductus arteriosus. *Anesthesia and Analgesia* 64(11):1078–1080

A.3 SUPPLEMENTARY DOCUMENT TO PUBLICATION III – PBPK MODELING  
OF NICOTINE BRAIN TISSUE CONCENTRATIONS

**Clinical Pharmacokinetics****Comprehensive parent-metabolite PBPK/PD modeling insights into nicotine replacement therapy strategies****Electronic Supplementary Material**

Lukas Kovar<sup>1</sup>, Dominik Selzer<sup>1</sup>, Hannah Britz<sup>1</sup>, Neal Benowitz<sup>2</sup>, Gideon St.Helen<sup>2</sup>, Yvonne Kohl<sup>3</sup>, Robert Bals<sup>4</sup> and Thorsten Lehr<sup>1</sup>

<sup>1</sup> Clinical Pharmacy, Saarland University, Saarbrücken, Germany

<sup>2</sup> Department of Medicine, University of California, San Francisco, CA, USA

<sup>3</sup> Fraunhofer Institute for Biomedical Engineering IBMT, Sulzbach, Germany

<sup>4</sup> Department of Internal Medicine V, Saarland University, Homburg, Germany

**Running Heading**

A PBPK/PD model of nicotine including brain concentration patterns during smoking and smoking cessation strategies.

**Funding**

This project has received funding from the German Federal Ministry of Education and Research (BMBF), 031L0153, «Alternativmethoden zum Tierversuch» and 03XP0196, «NanoCare4.0 – Anwendungssichere Materialinnovationen». Data used for model development were collected in part with the support of grants DA039264 and DA012393 from the National Institute on Drug Abuse, U.S.A.

**Conflict of Interest**

Neal Benowitz has been a consultant to Pfizer and Achieve Life Sciences, companies that market or are developing smoking cessation medications. He has also been a paid witness in litigation against tobacco companies. No potential conflicts of interest were disclosed by the other authors (Lukas Kovar, Dominik Selzer, Hannah Britz, Gideon St.Helen, Yvonne Kohl, Robert Bals and Thorsten Lehr).

**Corresponding Author**

Prof. Dr. Thorsten Lehr

Clinical Pharmacy, Saarland University, Campus C2 2, 66123 Saarbrücken.

Phone: +49 681 302 70255

Fax: +49 681 302 70258

Email: [thorsten.lehr@mx.uni-saarland.de](mailto:thorsten.lehr@mx.uni-saarland.de)

## Contents

<b>1</b>	<b>PBPK/PD model development</b>	<b>3</b>
<b>2</b>	<b>PBPK/PD model building</b>	<b>3</b>
2.1	General PBPK model building . . . . .	3
2.2	Nicotine gum PBPK model building . . . . .	4
2.3	Transdermal patch PBPK model building . . . . .	5
2.4	Pulmonary PBPK model building . . . . .	5
2.5	PBPK/PD model building . . . . .	6
2.6	Clinical study data . . . . .	8
2.6.1	Clinical study data of nicotine . . . . .	8
2.6.2	Clinical study data of cotinine . . . . .	10
2.6.3	PD clinical study data . . . . .	11
2.7	Drug-dependent parameters . . . . .	12
2.8	Formulation-dependent parameters . . . . .	14
2.9	Parameters of the final PD heart rate model . . . . .	16
2.10	System-dependent parameters and virtual populations . . . . .	17
<b>3</b>	<b>PBPK/PD model evaluation</b>	<b>18</b>
3.1	Intravenous administration of nicotine . . . . .	19
3.2	Intravenous administration of cotinine . . . . .	26
3.3	Oral administration of nicotine (including nicotine gums) . . . . .	31
3.4	Transdermal administration of nicotine (nicotine patches) . . . . .	39
3.5	Pulmonary administration of nicotine (combustible cigarettes with estimated pulmonary nicotine exposure and e-cigarettes) . . . . .	45
3.6	Pulmonary administration of nicotine (combustible cigarettes with machine smoked nicotine yields) . . . . .	51
3.7	Brain tissue concentration simulations . . . . .	57
3.8	Quantitative PBPK model evaluation . . . . .	58
3.8.1	Mean relative deviations (MRD) . . . . .	58
3.8.2	Geometric mean fold errors (GMFE) . . . . .	61
3.9	$AUC_{last}$ and $C_{max}$ goodness of fit plots . . . . .	64
3.10	Nicotine and cotinine PBPK model sensitivity analysis . . . . .	65
3.11	Heart rate population predictions after nicotine intake . . . . .	67
3.12	Heart rate simulations . . . . .	69
	<b>References</b>	<b>70</b>

## 1 PBPK/PD model development

In this study, a physiologically based pharmacokinetic/pharmacodynamic (PBPK/PD) parent-metabolite model of nicotine and cotinine was developed. 90 reported observed plasma concentration-time profiles after intravenous (iv), oral, transdermal and pulmonary administration, a brain tissue concentration-time profile and 11 heart rate profiles were digitized from 34 clinical studies and split into an internal training and an external test dataset.

The training dataset was selected in a way to inform all the physiological processes implemented in the model. Hence, for cotinine PBPK model building three plasma profiles of cotinine administered intravenously were used which covered a broad dosing range and included information on urinary excretion of cotinine. For the nicotine PBPK model building plasma profiles of nonsmokers and smokers after intravenous administration were included in the training dataset with a broad dosing range including studies with cotinine metabolite data, information on fraction of nicotine excreted unchanged to urine and fraction of nicotine metabolized to cotinine. Moreover, a study with plasma concentrations of cytochrome P450 (CYP) 2A6 poor metabolizer (PM) and a study with brain tissue concentrations after nicotine intake were included in the training dataset in order to inform model input parameters for CYP2B6 and brain transporters.

For the PD heart rate model, three studies with intravenous administration were used for model training which covered the largest timeframe of heart rate measurements and the highest nicotine plasma concentrations.

A tabular overview of all clinical studies and the division into test and training datasets are shown in Tables S2.6.1 to S2.6.3.

## 2 PBPK/PD model building

### 2.1 General PBPK model building

Drug-specific model input parameters for nicotine and cotinine were obtained from published *in vitro* and human pharmacokinetic (PK) data (see Table S2.7.1). Cotinine and nicotine model input parameters which could not be adequately informed from literature were estimated using the *parameter identification* function in PK-Sim<sup>®</sup>.

Parameter estimation was performed by

1. fitting the cotinine model to
  - cotinine observed intravenous data
  - published fractions of cotinine dose excreted unchanged to urine
2. fitting the nicotine model to
  - nicotine and cotinine observed intravenous data
  - nicotine and cotinine observed oral data
  - nicotine brain tissue concentrations after pulmonary nicotine intake
  - published fractions of nicotine dose excreted unchanged to urine
  - published fraction of nicotine dose metabolized to cotinine [1]

of the training dataset with the Monte Carlo algorithm.

For the simulation of different studies, the reported mean values for age, weight, height and ethnic and genetic background of each study protocol were used to create representative virtual individuals. If no information on these demographics was available, a standard 30-year-old male European was assumed with weight and height values according to the PK-Sim<sup>®</sup> database. Distribution and elimination processes including CYP enzymes and transporters were implemented according to literature [1–3]. The nicotine model incorporates (1) metabolism of nicotine to its major metabolite cotinine via two CYP enzymes, (2) unspecific metabolic hepatic clearance (responsible for the remaining hepatic metabolism of nicotine including metabolism via UGT2B10 (uridine 5'-diphosphoglucuronosyltransferase 2B10) and FMO3 (flavin-containing monooxygenase 3)) and (3) influx and efflux transport of nicotine over the blood-brain-barrier (BBB). For cotinine, an unspecific metabolic hepatic clearance was implemented in the model. Additionally, renal excretion through glomerular filtration was implemented as an elimination pathway for both compounds, as they are subject to glomerular filtration under physiological conditions [2, 4].

To model the metabolic clearance of nicotine to cotinine, which accounts for about three quarters of nicotine elimination, nicotine metabolism via CYP2A6 and CYP2B6 was implemented in accordance with literature [1, 2]. Nicotine is primarily metabolized via CYP2A6. However, in CYP2A6-PM that lack CYP2A6 metabolism, and thus cotinine production diminishes, CYP2B6 is responsible for a modest nicotine conversion to cotinine [2]. A PM plasma-concentration time profile was included in the training dataset to estimate CYP2B6 metabolism in the model [5]. Relative CYP enzyme expression in different organs of the body was implemented using PK-Sim<sup>®</sup> expression database reverse transcription-polymerase chain reaction profile (CYP2A6) [6] and protein tissue data from the ProteomicsDB database (CYP2B6) [7].

The Michaelis-Menten constant ( $K_m$ ) value for CYP2A6 was fitted with bounds obtained from literature [8–11]. According to published data, nicotine clearance in smokers is about 15 % lower compared to nonsmokers [12]. To account for this difference, the catalytic rate constant ( $k_{cat}$ ) of CYP2A6 was estimated separately for the smoker subpopulation leading to a lower  $k_{cat}$  in comparison to the non-smoker subpopulation. Since PM show no CYP2A6 activity,  $k_{cat}$  for PM was set to 0 [5]. Moreover, since nicotine is metabolized not solely to cotinine, an unspecific first-order hepatic clearance was implemented and was fitted during parameter optimization.

As published literature suggests, influx and efflux of nicotine over the BBB play an important role for nicotine brain tissue concentration kinetics [3]. Hence, an influx and an efflux transporter with nicotine specific transport and Michaelis-Menten kinetics were added to the BBB in PK-Sim<sup>®</sup>. The  $k_{cat}$  value for the BBB nicotine influx transporter and  $K_m$  and  $k_{cat}$  values for the BBB efflux transporter were fitted to nicotine brain tissue concentrations from literature [13], the  $K_m$  value for the BBB influx transporter was obtained from literature [3]. Subsequently, this implementation yielded to a reasonable description of experimental nicotine brain tissue concentrations (see Figures S3.5.1r and S3.5.2r). A summary of all drug-dependent PBPK model parameters is shown in Table S2.7.1.

## 2.2 Nicotine gum PBPK model building

To model and simulate nicotine gum consumption, nicotine was administered via the oral route in PK-Sim<sup>®</sup>. The corresponding nicotine release from the gum was implemented according to an empirical release function (PK-Sim<sup>®</sup> table release) based on published *in vitro* release profile data of Nicorette<sup>®</sup> chewing gum [14]. Although bucal absorption was neglected, predictions of plasma concentration-time profiles showed very promising results (see Figures S3.3.1j to S3.3.1t and Figures S3.3.2j to S3.3.2t).

### 2.3 Transdermal patch PBPK model building

The modeling and simulation of the administration of nicotine via transdermal therapeutic systems (TTS) was implemented via a two-compartment skin model. Here, the skin is divided into the lipophilic *stratum corneum* (SC) and hydrophilic deeper skin layers (DSL) which are composed of the *viable Epidermis* and *Dermis*. As shown before, a two-compartment skin model is typically a sufficiently accurate description for the transport of various compounds if the storage capacity and/or the permeability of the SC and DSL compartments should be taken into account [15–17].

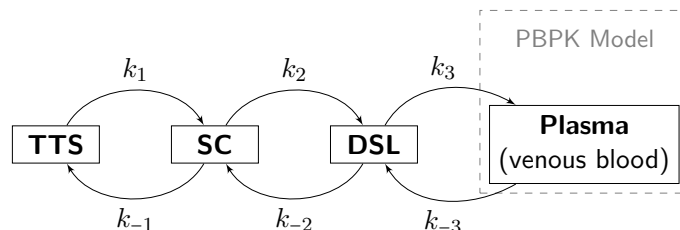


Figure S2.3.1: Schematic depiction of the nicotine transdermal absorption model.

Since detailed information about TTS composition is typically scarce it was assumed that the transdermal patch could be described as a homogenous matrix system. A schematic representation of the transdermal absorption model is depicted in Figure S2.3.1. Diffusion is considered the main driving force of substance transport through the skin. Thus, the mass flux between the compartments was modeled via first-order kinetics (Equations S1 to S3). The transdermal model was implemented in MoBi<sup>®</sup> and subsequently connected to the PBPK model.

$$\frac{dm_{TTS}}{dt} = k_{-1} \cdot m_{SC} - k_1 \cdot m_{TTS} \quad (S1)$$

$$\frac{dm_{SC}}{dt} = k_1 \cdot m_{TTS} - k_{-1} \cdot m_{SC} + k_{-2} \cdot m_{DSL} - k_2 \cdot m_{SC} \quad (S2)$$

$$\frac{dm_{DSL}}{dt} = k_2 \cdot m_{SC} - k_{-2} \cdot m_{DSL} + k_{-3} \cdot m_{Plasma} - k_3 \cdot m_{DSL} \quad (S3)$$

Simulations for plasma concentration-time profiles after TTS application of nicotine are shown in Figure S3.4.1 and Figure S3.4.2. Estimated transfer parameters are summarized in Table S2.8.3.

### 2.4 Pulmonary PBPK model building

Inhalation of combustible cigarettes and electronic cigarettes (e-cigarettes) was modeled as zero-order pulmonary administration kinetics since overall specific activity in mainstream smoke was shown to be constant from puff to puff in a radioisotopically labelled tobacco constituents study [18]. The rate of nicotine delivery equals the nicotine dose administered divided by the number of puffs and the puff duration. If the number of puffs and the puff duration were not provided, the delivery rate was set equal to the nicotine dose administered divided by the smoking period. The intracellular subcompartment of the lung was selected as target compartment in PK-Sim<sup>®</sup>.

Studies on inhalation of combustible cigarettes typically state nicotine doses derived from machine smoked yields of the investigated brand or type of cigarette. However, machine smoked yields of combustible cigarettes are typically not equivalent to human nicotine uptake for the products under investigation since they do not adequately represent human smoking behavior leading to a false

representation of the actual amount of nicotine reaching systemic circulation [19]. To overcome this issue two sets of simulations were performed:

- The application of combustible cigarettes was simulated with the stated cigarette nicotine yield provided by the study protocol (Figure S3.6.1 and Figure S3.6.2).
- The actual pulmonary nicotine exposure with combustible cigarettes was estimated (Table S2.8.2) while fixing all other model parameters (Figure S3.5.1 and Figure S3.5.2). This was executed for all studies with combustible cigarettes where venous blood plasma concentrations were reported.

The mean deviation of estimated pulmonary nicotine exposure to machine smoked nicotine yields was 31 % (see Table S2.8.2). For simulation of plasma concentration-time profiles for e-cigarettes, nicotine doses as stated in the respective study were used. For combustible cigarettes and e-cigarettes, 100 % of the administered dose was assumed to reach the lung compartment since bioavailability of nicotine after smoking is reported to be very high [2].

## 2.5 PBPK/PD model building

A PD model was added to the PBPK model to be able to describe the positive chronotropic effect of nicotine [20, 21] based on its PK. Direct-effect  $E_{max}$  models implemented as relative (proportional to heart rate baseline) and absolute effect with and without tolerance development were used to describe the effect. The model, which best described heart rate including drug effect, was the direct-effect  $E_{max}$  model with absolute effect including a tolerance development based on a recently published heart rate tolerance model [22]. This model had been developed to characterize the decrease in heart rate by the selective S1P<sub>1</sub> receptor modulator ponesimod.

Here, placebo data had been utilized to characterize heart rate changes during the course of the day due to circadian rhythm in the absence of a drug before the direct-effect  $I_{max}$  model with tolerance development was added. However, in contrast to the drug ponesimod, nicotine does not decrease but increases heart rate via activation of nicotine receptors. Therefore, the  $I_{max}$  effect was changed to an  $E_{max}$  effect and the PD model for heart rate ( $HR$ ) was defined as

$$circ = amp \cdot \cos\left(\frac{2\pi}{24} \cdot (t - shift)\right) \quad (S4)$$

$$E = \frac{E_{max} \cdot c^h}{EC_{50}^h + c^h} \quad (S5)$$

$$tol = 1 + \frac{A_{tol}^\gamma}{tol_{50}^\gamma} \quad (S6)$$

$$\frac{dA_{tol}}{dt} = tol_{in} \cdot c - tol_{out} \cdot A_{tol} \quad (S7)$$

$$\alpha_{total} = \frac{E}{tol} \quad (S8)$$

$$HR = HR_{baseline}(1 + circ) + \alpha_{total} \quad (S9)$$

where  $circ$  is a circadian function with a 24-h period,  $t$  is the time,  $amp$  denotes the daily heart rate variation as percentage of the estimated baseline heart rate ( $HR_{baseline}$ ) and  $shift$  represents the time from dosing until time of the maximum daily heart rate.  $tol_{in}$  and  $tol_{out}$  are first-order rate constants describing appearance and disappearance of tolerance in a tolerance compartment ( $A_{tol}$ ),  $c$  is the concentration of nicotine in the peripheral venous blood plasma,  $E_{max}$  the maximum positive

chronotropic effect of nicotine without tolerance,  $h$  the hill coefficient and  $EC_{50}$  the concentration required to achieve half of the maximum drug effect.  $tol_{50}$  and  $\gamma$  represent scaling parameters describing the relationship between the tolerance compartment and the overall tolerance ( $tol$ ) influencing the drug effect and leading to a total effect  $\alpha_{total}$ .

The tolerance compartment was implemented to describe the extent of acute tolerance development of the system and its subsequent reduction of the drug effect on heart rate following the administration of nicotine. The appearance of tolerance was set to depend on the concentration of nicotine which has been shown in the literature [23]. To obtain values for the PD model input parameters, optimization was performed by fitting the PD model to heart rate data of the training dataset using the *parameter identification* function with the Monte Carlo algorithm in MoBi<sup>®</sup> while fixing the parameters of the PK model. The circadian amplitude ( $amp$ ) was provided by the published tolerance model [22]. Circadian shift time for each study was fitted if no dosing information with regards to daytime was available. Otherwise, the circadian shift was calculated using the time of dosing and the time for maximum heart rate. Time of peak heart rate was gathered from the published tolerance model and set to 5:42 PM – a value that is in good agreement with data published before [24, 25]. For studies which lack data on absolute heart rate values, published mean heart rate data was added to heart rate changes from baseline [26]. Figure 1 in the main manuscript shows a structural overview of the developed PBPK/PD model. The parameter set for the PD model is summarized in Table S2.9.1 and simulated heart rate profiles after the administration of nicotine in comparison to observed data is depicted in Figure S3.11.1.

## 2.6 Clinical study data

### 2.6.1 Clinical study data of nicotine used for PBPK model building and evaluation

Table S2.6.1: Clinical study data of nicotine used for PBPK model building and evaluation.

Study	Route	Dose		Subjects					Weight [kg]	Cotinine metabolite	
		Dataset	[mg]	[µg/kg]	N	Smokers [%]	Females [%]	Age [y]			
Andersson and Arner 2001 [27]	iv (30 min, s.d.)	e		15.0	11	0.0	0.0		(20–32)	-	no
Benowitz and Jacob 1993 (1) [12]	iv (30 min, s.d.)	i		15.0	11	0.0	18.2	34.0	(22–58)	-	yes
Benowitz and Jacob 1993 (2) [12]	iv (30 min, s.d.)	i		15.0	11	100.0	18.2	33.0	(22–51)	-	yes
Benowitz and Jacob 1993 (3) [12]	iv (30 min, s.d.)	e		60.0	11	100.0	18.2	33.0	(22–51)	-	yes
Benowitz and Jacob 1994a (1) <sup>a</sup> [1]	iv (30 min, s.d.)	e	4.2	60.0	20	100.0	50.0	36.0	(23–51)	70.5 (53.0–100.4)	yes
Benowitz et al. 1991a (1) [28]	iv (24 h, s.d.)	i	19.8		14	100.0	0.0	39.0	(27–64)	72.8 (56.2–103.9)	yes
Benowitz et al. 1994b [29]	iv (24 h, s.d.)	i		288.0	12	100.0	0.0	34.0	(20–55)	76.4 (60.0–96.9)	yes
Feyerabend et al. 1985 (1) [30]	iv (1 min, s.d.)	i	1.8	25.0	5	100.0	0.0		(24–41)	69.3	no
Gourlay and Benowitz 1997 (1) [31]	iv (30 min, s.d.)	e	5.1	60.0	12	100.0	0.0		38.0	-	yes
Molander et al. 2001 (young) [32]	iv (10 min, s.d.)	e	28.0	20	100.0	100.0	50.0		(22–43)	-	yes
Molander et al. 2001 (elderly) [32]	iv (10 min, s.d.)	e	28.0	20	100.0	100.0	60.0		(65–76)	-	yes
Porchet et al. 1988 (1) <sup>b</sup> [23]	iv (30 min, m.d.)	e	75.0	8	100.0	0.0	0.0	36.0	(22–43)	-	no
Porchet et al. 1988 (2) <sup>c</sup> [23]	iv (30 min, m.d.)	e	75.0	8	100.0	0.0	0.0	36.0	(22–43)	-	no
Porchet et al. 1988 (3) <sup>d</sup> [23]	iv (30 min, m.d.)	e	75.0	8	100.0	0.0	0.0	36.0	(22–43)	-	no
Zevin et al. 1997 (1) <sup>e</sup> [33]	iv (30 min, s.d.)	i	15.0	12	0.0	0.0	50.0	33.0	(18–47)	73.0	no
Zevin et al. 1997 (2) <sup>f</sup> [33]	iv (30 min, s.d.)	e	15.0	12	0.0	0.0	50.0	33.0	(18–47)	73.0	no
Benowitz et al. 1991b (1) [34]	po (cap, s.d.)	i	3.0		7	100.0	0.0		(24–48)	77.1 (68.1–89.9)	no
Benowitz et al. 1991b (2) [34]	po (cap, s.d.)	e	4.0		2	100.0	0.0		(24–48)	-	no
Benowitz et al. 1991b (3) [34]	po (cap, s.d.)	e	6.0		1	100.0	0.0		(24–48)	-	no
Benowitz et al. 2010 [35]	po (*, q.i.d., 5 days)	e	0.05		12	0.0	0.0	50.0	(20–61)	-	yes
Green et al. 1999 (1) [36]	po (cap, s.d.)	i	6.0		12	0.0	0.0	41.7	(21–33)	73.0 (57.0–96.0)	yes
Green et al. 1999 (2) [36]	po (cap, s.d.)	e	15.0	12	0.0	0.0	41.7	28.0	(21–33)	73.0 (57.0–96.0)	yes
Jarvis et al. 1988 [37]	po (cap, 7 times/day, 5 days)	e	4.0	1	0.0	0.0	-		(27–54)	-	yes
Xu et al. 2002 (NM) [5]	po (cap, s.d.)	i	4.0	6	7.1	64.3			-	-	yes
Xu et al. 2002 (PM) [5]	po (cap, s.d.)	i	4.0	3	7.1	64.3			-	-	yes
Benowitz et al. 1988 (1) [21]	gum (s.d.)	e	4.0	10	100.0	0.0	0.0		(24–61)	-	no
Choi et al. 2003 (1) [38]	gum (s.d.)	e	2.0	25	100.0	100.0	52.0		33.7	-	no
Choi et al. 2003 (2) [38]	gum (13 gums, m.d.)	e	2.0	24	100.0	100.0	53.8		29.0	-	no
Choi et al. 2003 (3) [38]	gum (s.d.)	e	4.0	20	100.0	100.0	50.0		31.0	-	no
Choi et al. 2003 (4) [38]	gum (13 gums, m.d.)	e	4.0	26	100.0	100.0	53.8		29.0	-	no
Dautzenberg et al. 2007 [39]	gum (12 gums, m.d.)	e	2.0	24	100.0	0	0		-	-	no
Du 2018 (1) [40]	gum (s.d.)	e	2.0	62	100.0	47.6			26.8 (19–51)	-	no
Du 2018 (2) [40]	gum (s.d.)	e	4.0	73	100.0	47.6			26.8 (19–51)	-	no
Hansson et al. 2017 (1) [41]	gum (s.d.)	e	2.0	42	100.0	43.2			28.4 (19–49)	-	no
Hansson et al. 2017 (2) [41]	gum (s.d.)	e	4.0	40	100.0	43.2			28.4 (19–49)	-	no

values for age and weight are given as mean (range)

<sup>a</sup> not given; **cap**, capsule; **cigs**<sup>+</sup>, cigarettes; **combust**<sup>+</sup>, combustible; **e**, external test dataset; **e-cigs**, e-cigarettes; **i**, internal training dataset; **iv**, intravenous;

**m.d.**, multiple dose; **N**, number of individuals studied; **NM**, normal metabolizer; **po**, oral; **q.i.d.**, four times daily; **q.d.**, once daily; **s.d.**, single dose

<sup>a</sup> fraction of nicotine dose metabolized to cotinine depicted <sup>b</sup> two nicotine iv infusions 90 minutes separated <sup>c</sup> two nicotine iv infusions 150 minutes separated <sup>d</sup> two nicotine iv infusions 240 minutes separated

<sup>e</sup> nicotine iv and placebo po administered concurrently <sup>f</sup> nicotine iv and cotinine po administered concurrently <sup>g</sup> loading dose of the nicotine patch <sup>h</sup> six patches over seven days with no patch on day two



## 2.6.2 Clinical study data of cotinine used for PBPK model building and evaluation

Table S2.6.2: Clinical study data of cotinine used for PBPK model building and evaluation.

Study	Route	Dataset	Dose		Subjects				Weight [kg]
			[mg]	[µg/kg]	N	Smokers [%]	Females [%]	Age [y]	
Benowitz and Jacob 1994a (2) [1]	iv (30 min, s.d.)	e	4.4	60.0	6	0.0	50.0	37.0 (27-39)	73.2 (58-94)
De Schepper et al. 1987 (1) [4]	iv (30 min, s.d.)	i	5.0		4	0.0	0.0	(22-24)	(64-73)
De Schepper et al. 1987 (2) [4]	iv (30 min, s.d.)	i	10.0		4	0.0	0.0	(22-24)	(64-73)
De Schepper et al. 1987 (3) [4]	iv (30 min, s.d.)	i	20.0		3	0.0	0.0	(22-24)	(64-73)
Curvall et al. 1990 (1) [52]	iv (1.5-3 min, s.d.)	e	5.0		7	0.0	22.2	31.6 (23-56)	72.2 (55-85)
Curvall et al. 1990 (2) [52]	iv (1.5-3 min, s.d.)	e	10.0		9	0.0	22.2	31.6 (23-56)	72.2 (55-85)
Curvall et al. 1990 (3) [52]	iv (1.5-3 min, s.d.)	e	20.0		9	0.0	22.2	31.6 (23-56)	72.2 (55-85)
Zevin et al. 1997 (3) [33]	iv (30 min, s.d.)	e		15.0	12	0.0	50.0	33.0 (18-47)	73.0
Zevin et al. 1997 (4) [33]	iv (30 min, s.d.)	e		15.0	12	0.0	50.0	33.0 (18-47)	73.0

values for age and weight are given as mean (range)

e, external test dataset; i, internal training dataset; iv, intravenous; N, number of individuals studied; s.d., single dose

2.6.3 Clinical study data used for PD model building and evaluation

Table S2.6.3: Clinical study data of nicotine used for PD model building and evaluation.

Study	Route	Dataset	Dose			Subjects			
			[mg]	[µg/kg]	N	Smokers [%]	Females [%]	Age [y]	Weight [kg]
Andersson and Amer 2001 [27]	iv (30 min, s.d.)	e		15.0	11	0.0	0.0	(20–32)	-
Porchet et al. 1988 (1) <sup>a</sup> [23]	iv (30 min, m.d.)	i		75.0	8	100.0	0.0	36.0 (22–43)	-
Porchet et al. 1988 (2) <sup>b</sup> [23]	iv (30 min, m.d.)	i		75.0	8	100.0	0.0	36.0 (22–43)	-
Porchet et al. 1988 (3) <sup>c</sup> [23]	iv (30 min, m.d.)	i		75.0	8	100.0	0.0	36.0 (22–43)	-
Benowitz et al. 1988 (1) [21]	gum (s.d.)	e	4.0		10	100.0	0.0	(24–61)	-
Benowitz et al. 1988 (2) [21]	inhalation (combust. cigs., s.d.)	e	1.5		10	100.0	0.0	(24–61)	-
Gilbert et al. 1989 (1) [53]	inhalation (combust. cigs., s.d.)	e	0.1		40	50.0	50.0	28.8 (25–35)	-
Gilbert et al. 1989 (2) [53]	inhalation (combust. cigs., s.d.)	e	0.8		40	50.0	50.0	28.8 (25–35)	-
Gourlay and Benowitz 1997 (2) [31]	inhalation (combust. cigs., s.d.)	e	1.9		6	100.0	0.0	38.0	85.0
Mendelson et al. 2008 [48]	inhalation (3 combust. cigs., m.d.)	e	0.8		12	100.0	0.0	25.7	-
St. Helen et al. 2016 [50]	inhalation (e-cigs., s.d.)	e	1.2		13	100.0	46.1	38.4 (19–58)	-
Heart rate simulation (4 cigs.)	inhalation (4 cigs., m.d.)	-	1.4		100	100.0	0.0	30.0 (20–40)	80.4 (70.4 - 90.4)
Heart rate simulation (16 cigs.)	inhalation (16 cigs., m.d.)	-	1.4		100	100.0	0.0	30.0 (20–40)	80.4 (70.4 - 90.4)
Heart rate simulation (16 gums)	gum (16 gums, m.d.)	-	2.0		100	100.0	0.0	30.0 (20–40)	80.4 (70.4 - 90.4)
Heart rate simulation (transdermal)	transdermal (24 h, s.d.)	-	52.5 <sup>d</sup>		100	100.0	0.0	30.0 (20–40)	80.4 (70.4 - 90.4)

values for age and weight are given as mean (range)

-, not given; **cigs.**, cigarettes; **combust.**, combustible; **e**, external test dataset; **i**, internal training dataset; **iv**, intravenous; **m.d.**, multiple dose; **N**, number of individuals studied; **s.d.**, single dose

<sup>a</sup> two nicotine iv infusions 90 minutes separated

<sup>b</sup> two nicotine iv infusions 150 minutes separated

<sup>c</sup> two nicotine iv infusions 240 minutes separated

<sup>d</sup> loading dose of the nicotine patch

## 2.7 Drug-dependent parameters of the final parent-metabolite nicotine-cotinine PBPK model

Table S2.7.1: Drug-dependent parameters of the final nicotine-cotinine PBPK model.

Parameter	Nicotine Model			Cotinine Model			Description
	Unit	Value	Reference	Value	Reference	Value	
MW	g/mol	162.2	[54] <sup>a</sup>	176.2	[54] <sup>b</sup>		Molecular weight
pK <sub>a1</sub>		8.1 (basic)	[55]	4.5 (basic)	[56]		Acid dissociation constant 1
pK <sub>a2</sub>		3.3 (basic)	[55]				Acid dissociation constant 2
logP		1.6*	1.2, 1.4 [55, 57]	-0.1*	0.21 [54] <sup>b</sup>		Lipophilicity
Solubility (pH)	mg/mL	93.3 (7.0)	[54] <sup>a</sup>	117.0 (7.0)	[54] <sup>b</sup>		Solubility
f <sub>u</sub>	%	95.1	80.0-95.1 [58]	97.4	[59]		Fraction unbound (plasma)
CYP2A6 K <sub>M</sub>	μmol/L	29.4*	11.0, 32.0, 33.0, 144.0 [8-11]				CYP2A6 Michaelis-Menten constant
CYP2A6-NM k <sub>cat</sub> (nonsmokers)	1/min	12.0*	n.a.				CYP2A6-NM catalytic rate constant for nonsmokers
CYP2A6-NM k <sub>cat</sub> (smokers)	1/min	10.5*	n.a.				CYP2A6-NM catalytic rate constant for smokers
CYP2A6-PM k <sub>cat</sub>	1/min	0.0	[5]				CYP2A6-PM catalytic rate constant
CYP2B6 K <sub>M</sub>	μmol/L	820.0	[60]				CYP2B6 Michaelis-Menten constant
CYP2B6 k <sub>cat</sub>	1/min	16.0*	n.a.				CYP2B6 catalytic rate constant
BBB-transporter <sub>in</sub> K <sub>M</sub>	μmol/L	92.4	[3]				BBB-transporter <sub>in</sub> Michaelis-Menten constant
BBB-transporter <sub>in</sub> k <sub>cat</sub>	1/s	5.3E+03*	n.a.				BBB-transporter <sub>in</sub> catalytic rate constant
BBB-transporter <sub>out</sub> K <sub>M</sub>	μmol/L	7.0E-05*	n.a.				BBB-transporter <sub>out</sub> Michaelis-Menten constant
BBB-transporter <sub>out</sub> k <sub>cat</sub>	1/s	0.4*	n.a.				BBB-transporter <sub>out</sub> catalytic rate constant
Cell permeabilities		calculated	PK-Sim <sup>®</sup> Standard [61]	calculated	PK-Sim <sup>®</sup> Standard [61]		Permeation across cell membranes
Partition coefficients		calculated <sup>c</sup>	Rodgers and Rowland [62-64]	calculated <sup>c</sup>	PK-Sim <sup>®</sup> Standard [61]		Organ-plasma partition coefficients
GFR fraction		1.0		6.0E-02*			Fraction of GFR used for passive elimination by the kidney
Unspecific hepatic clearance	1/min	0.3*	n.a.	2.0E-02*	n.a.		Elimination from plasma (first order process in the liver)

BBB, blood-brain-barrier; CYP, cytochrome P450; GFR, glomerular filtration rate; n.a., not available; NM, normal metabolizer; PM, poor metabolizer

\* model input parameter estimated

<sup>a</sup> DrugBank entry for nicotine. <https://www.drugbank.ca/drugs/DB00184>. Accessed 21 Oct 2019

<sup>b</sup> DrugBank entry for cotinine. <https://www.drugbank.ca/metabolites/DBMET00519>. Accessed 21 Oct 2019

<sup>c</sup> for details see Table S2.7.2

**Table S2.7.2:** Tissue-plasma partition coefficients of the final nicotine-cotinine PBPK model.

Tissue	Nicotine <sup>a</sup>	Cotinine <sup>b</sup>
Bone	1.27	0.70
Brain	1.89	0.88
Fat	0.74	0.74
Gonads	3.27	0.82
Heart	2.24	0.81
Kidney	4.15	0.82
Stomach	2.90	0.84
Small intestine	2.90	0.84
Large intestine	2.90	0.84
Liver periportal	3.96	0.81
Liver pericentral	3.96	0.81
Lung	3.25	0.83
Muscle	3.05	0.83
Pancreas	2.46	0.77
Skin	2.10	0.72
Spleen	2.86	0.80

Partition coefficients between intracellular space and plasma

<sup>a</sup> Estimated via Rodgers and Rowland [62–64]

<sup>b</sup> Estimated via PK-Sim<sup>®</sup> Standard [61]

## 2.8 Formulation-dependent parameters of the final nicotine-cotinine PBPK model

**Table S2.8.1:** Formulation-dependent parameters of the final nicotine-cotinine PBPK model for oral application of nicotine.

Study	Dissolution			Tablet time delay factor	Description
	$t_{lag}$ [min]	50 % dissolved [min]	Shape		
Benowitz et al. 1991b (1) [34]	10.5	22.0	1.9	0.2	capsule
Benowitz et al. 1991b (2) [34]	10.5	22.0	1.9	0.2	capsule
Benowitz et al. 1991b (3) [34]	10.5	22.0	1.9	0.2	capsule
Benowitz et al. 2010 [35]	-	-	-	-	oral solution
Green et al. 1999 (1) [36]	167.4	346.9	0.5	0.7	capsule
Green et al. 1999 (2) [36]	167.4	346.9	0.5	0.7	capsule
Jarvis et al. 1988 [37]	-	-	-	-	oral solution
Xu et al. 2002 (NM) [5]	5	59.6	1.8	0.2	capsule
Xu et al. 2002 (PM) [5]	5	59.6	1.8	0.2	capsule
Benowitz et al. 1988 (1) [21]	-	-	-	-	gum <sup>a</sup>
Choi et al. 2003 (1) [38]	-	-	-	-	gum <sup>a</sup>
Choi et al. 2003 (2) [38]	-	-	-	-	gum <sup>a</sup>
Choi et al. 2003 (3) [38]	-	-	-	-	gum <sup>a</sup>
Choi et al. 2003 (4) [38]	-	-	-	-	gum <sup>a</sup>
Du 2018 (1) [40]	-	-	-	-	gum <sup>a</sup>
Du 2018 (2) [40]	-	-	-	-	gum <sup>a</sup>
Dautzenberg et al. 2007 [39]	-	-	-	-	gum <sup>a</sup>
Hansson et al. 2017 (1) [41]	-	-	-	-	gum <sup>a</sup>
Hansson et al. 2017 (2) [41]	-	-	-	-	gum <sup>a</sup>
Hansson et al. 2017 (3) [41]	-	-	-	-	gum <sup>a</sup>
Brain tissue concentration simulation (gum, 2 mg)	-	-	-	-	gum <sup>a</sup>
Brain tissue concentration simulation (gum, 4 mg)	-	-	-	-	gum <sup>a</sup>
Heart rate simulation (gum, 2 mg)	-	-	-	-	gum <sup>a</sup>

NM, normal metabolizer; PM, poor metabolizer

<sup>a</sup> Release kinetics profile used from Morjaria et al. (PK-Sim<sup>®</sup> table release) [14]

**Table S2.8.2:** Reported machine smoked nicotine yield and estimated human pulmonary nicotine exposure of combustible cigarettes for studies under investigation.

Study	Exposure [mg]	
	Machine smoked nicotine yield	Estimated yield
Benowitz et al. 1982 (1) [46]	0.4	0.4
Fearon et al. 2017 (Study 2) [47]	0.5	0.7
Feyerabend et al. 1985 (3) [30]	0.8	1.1
Mendelson et al. 2008 [48]	0.8	1.2
Fearon et al. 2017 (Study 1) [47]	1.0	1.3
Benowitz et al. 1982 (2) [46]	1.2	1.4
Feyerabend et al. 1985 (4) [30]	1.3	1.5
Feyerabend et al. 1985 (2) [30]	1.3	2.0
Russell et al. 1983 [49]	1.4	2.2
Benowitz et al. 1988 (2) [21]	1.5	1.6
Gourlay and Benowitz 1997 (2) [31]	1.9	2.2
Feyerabend et al. 1985 (5) [30]	2.4	1.5
Benowitz et al. 1982 (3) [46]	2.5	1.8
St. Helen et al. 2019 (2)	-	2.4

-, not given

**Table S2.8.3:** Drug product-dependent and system-dependent parameters of the transdermal nicotine PBPK model.

Study	Loading dose [mg]	TTS/SC		SC/DSL		DSL/Plasma	
		$k_1$ [ $\frac{1}{\text{min}}$ ]	$k_{-1}$ [ $\frac{1}{\text{min}}$ ]	$k_2$ [ $\frac{1}{\text{min}}$ ]	$k_{-2}$ [ $\frac{1}{\text{min}}$ ]	$k_3$ [ $\frac{1}{\text{min}}$ ]	$k_{-3}$ [ $\frac{1}{\text{min}}$ ]
Bannon et al. 1989 (1) [42]	15.00	8.63E-04	2.79E-03	1.93E+01	3.39E+00	9.63E-03	4.72E-03
Bannon et al. 1989 (2) [42]	30.00	8.63E-04	2.79E-03	1.93E+01	3.39E+00	9.63E-03	4.72E-03
Bannon et al. 1989 (3) (m.d.) [42]	30.00	8.63E-04	2.79E-03	1.93E+01	3.39E+00	9.63E-03	4.72E-03
Bannon et al. 1989 (4) [42]	60.00	8.63E-04	2.79E-03	1.93E+01	3.39E+00	9.63E-03	4.72E-03
Benowitz et al. 1991a (2) [28]	52.50	2.24E-04	8.35E-02	8.27E-01	1.18E-04	8.10E-03	1.64E-05
Fant et al. 2000 [43] (Upjohn, m.d.)	24.90	3.69E-01	4.60E+00	2.98E-02	8.57E-01	5.42E-01	1.85E+00
Fant et al. 2000 [43] (Novartis, m.d.)	52.50	1.11E-03	8.29E-03	5.00E-03	1.68E-02	3.46E+01	7.61E-01
Fant et al. 2000 [43] (Alza, m.d.)	114.00	1.57E-01	1.35E+01	2.24E+00	1.63E-01	3.60E-02	6.26E+01
Gupta et al. 1993 (1) [44]	105.05	9.83E-01	2.40E+01	1.17E-01	9.93E-01	8.24E-01	4.00E+01
Gupta et al. 1993 (2) (m.d.) [44]	105.05	9.83E-01	2.40E+01	1.17E-01	9.93E-01	8.24E-01	4.00E+01
Brain tissue concentration simulation (transdermal)	52.50	1.11E-03	8.29E-03	5.00E-03	1.68E-02	3.46E+01	7.61E-01
Heart rate simulation (transdermal)	52.50	1.11E-03	8.29E-03	5.00E-03	1.68E-02	3.46E+01	7.61E-01

$k_1$ , first order rate constant for nicotine transport from nicotine patch into *stratum corneum*

$k_{-1}$ , first order rate constant for nicotine transport from *stratum corneum* back into nicotine patch

$k_2$ , first order rate constant for nicotine transport from *stratum corneum* into deeper skin layers

$k_{-2}$ , first order rate constant for nicotine transport from deeper skin layers back into *stratum corneum*

$k_3$ , first order rate constant for nicotine transport from deeper skin layers into plasma

$k_{-3}$ , first order rate constant for nicotine transport from plasma back into deeper skin layers

DSL, deeper skin layers; m.d., multiple dose; SC, stratum corneum; TTS, transdermal therapeutic system

## 2.9 Parameters of the final PD heart rate model

**Table S2.9.1:** Drug-dependent and system-dependent parameters of the final PD model.

Parameter	Unit	Value	Reference	Standard deviation	Description <sup>a</sup>
$E_{\max}$	bpm	111.6	n.a.		Maximum possible heart rate elevation without tolerance
$EC_{50}$	ng/mL	33.7	n.a.		Concentration at half-maximum elevation
$h$		1.3	n.a.		Hill coefficient
$tol_{in}$	1/h	15.3	n.a.		Tolerance appearance rate
$tol_{out}$	1/h	0.2	n.a.		Tolerance disappearance rate
$tol_{50}$	ng/mL	11.7	n.a.		Scaling parameter for tolerance
$\gamma$		0.4	n.a.		Nonlinearity parameter
amp	%	6.3 <sup>c</sup>	[22]		Circadian amplitude
$HR_{BL[27]}$	bpm	111.5	n.a.	10.0 [26]	Baseline heart rate for [27]
$HR_{BL[21](1)}$	bpm	65.2	n.a.	7.0 [26]	Baseline heart rate for [21] (1)
$HR_{BL[21](2)}$	bpm	64.7	n.a.	7.0 [26]	Baseline heart rate for [21] (2)
$HR_{BL[53](1)}$	bpm	73.6	n.a.	10.0 [26]	Baseline heart rate for [53] (1)
$HR_{BL[53](2)}$	bpm	78.5	n.a.	10.0 [26]	Baseline heart rate for [53] (2)
$HR_{BL[31]}$	bpm	81.6	n.a.	7.0 [26]	Baseline heart rate for [31]
$HR_{BL[48]}$	bpm	68.8	n.a.	10.0 [26]	Baseline heart rate for [48]
$HR_{BL[50]}$	bpm	72.2	n.a.	7.0 [26]	Baseline heart rate for [50]
$HR_{BL[23](1)}$	bpm	60.1	n.a.	7.0 [26]	Baseline heart rate for [23](1)
$HR_{BL[23](2)}$	bpm	60.1	n.a.	7.0 [26]	Baseline heart rate for [23](2)
$HR_{BL[23](3)}$	bpm	60.1	n.a.	7.0 [26]	Baseline heart rate for [23](3)
$HR_{BL}$ , HR simulations	bpm	78.0	[26]	7.0 [26]	Baseline heart rate for HR simulations
$shift_{BL[27]}$	h	9.7	[22, 27] <sup>b</sup>		Circadian time shift for [27]
$shift_{BL[21](1)}$	h	10.7	n.a.		Circadian time shift for [21] (1)
$shift_{BL[21](2)}$	h	10.7	n.a.		Circadian time shift for [21] (2)
$shift_{BL[53](1)}$	h	8.2	[22, 53] <sup>b</sup>		Circadian time shift for [53] (1)
$shift_{BL[53](2)}$	h	8.2	[22, 53] <sup>b</sup>		Circadian time shift for [53] (2)
$shift_{BL[31]}$	h	2.7	n.a.		Circadian time shift for [31]
$shift_{BL[48]}$	h	7.7	[22, 48] <sup>b</sup>		Circadian time shift for [48]
$shift_{BL[50]}$	h	8.2	[22, 50] <sup>b</sup>		Circadian time shift for [50]
$shift_{BL[23](1)}$	h	6.7	n.a.		Circadian time shift for [23] (1)
$shift_{BL[23](2)}$	h	6.7	n.a.		Circadian time shift for [23] (2)
$shift_{BL[23](3)}$	h	6.7	n.a.		Circadian time shift for [23] (3)

n.a., not available

<sup>a</sup> Descriptions carried over from [22]

<sup>b</sup> Computed

<sup>c</sup> amp was set to 0 for HR simulations in Section 3.12 for better comparability

## 2.10 System-dependent parameters and virtual populations

System-dependent parameters for the PBPK/PD model, including reference concentrations with geometric standard deviation, tissue expression as well as protein half-lives of all enzymes and transporters implemented in the model are summarized in Table S2.10.1.

**Table S2.10.1:** System-dependent parameters and expression of relevant enzymes, transporters and other ADME processes.

	Reference concentration		Relative expression	Half-life [h]	
	Mean [ $\mu\text{mol/L}$ ] <sup>a</sup>	GSD <sup>b</sup>		Liver	Intestine
<b>Enzymes</b>					
CYP2A6-NM	2.72 [65]	1.40	RT-PCR <sup>c</sup> [66]	26.0	23.0
CYP2A6-PM	2.72 [65]	1.40	RT-PCR <sup>c</sup> [66]	26.0	23.0
CYP2B6	1.56 [65]	1.40	ProteomicsDB <sup>d</sup> [7]	32.0	23.0
<b>Transporters</b>					
BBB-transporter <sub>in</sub>	1.00 <sup>e</sup> [6]	1.40		36.0	23.0
BBB-transporter <sub>out</sub>	1.00 <sup>e</sup> [6]	1.40		36.0	23.0
<b>Processes</b>					
Unspecific hepatic clearance of nicotine	-	1.40			
Unspecific hepatic clearance of cotinine	-	1.40			

**ADME**, absorption, distribution, metabolism and elimination; **CYP**, cytochrome P450; **GSD**, Geometric standard deviation; **NM**, normal metabolizer; **PM**, poor metabolizer; **RT-PCR**, reverse transcription polymerase chain reaction

<sup>a</sup> In the tissue of the highest expression

<sup>b</sup> Geometric standard deviation with coefficient of variation (CV) of 35 % assumed

<sup>c</sup> PK-Sim<sup>®</sup> expression database profile

<sup>d</sup> ProteomicsDB entry for CYP2B6. <https://www.proteomicsdb.org/proteomicsdb/#human/proteinDetails/P20813/expression>. Accessed 21 Oct 2019

<sup>e</sup> If no information available it was set to 1.0  $\mu\text{mol/L}$  and  $k_{\text{cat}}$  optimized according to [6]

Virtual populations of 100 individuals for each study were set up according to the population demographics of each respective simulated study. If no age range was specified, virtual populations were created with individuals 20 to 50 years of age and without specific body weight or height restrictions as implemented in PK-Sim<sup>®</sup>.

In the generated virtual populations demographics such as age, height, weight and corresponding organ volumes, tissue compositions, blood flow rates, etc. were varied by an implemented algorithm in PK-Sim<sup>®</sup> within the limits of the ICRP (International Commission on Radiological Protection) or Japanese databases [61, 67]. Furthermore, the reference concentrations of both the metabolizing enzymes CYP2A6 and CYP2B6 and the nicotine transporters in the BBB as well as unspecific hepatic clearance rates of nicotine and cotinine were set to be log-normally distributed with a relative standard deviation of 35 %. Heart rate was set to be normally distributed with variabilities according to Umetani et al. [26]. For details on study populations see Tables S2.6.1 to S2.6.3. Simulations were generated with the virtual populations with geometric mean  $\pm$  geometric standard deviation and plotted with the corresponding observed data (see Section 3).

### 3 PBPK/PD model evaluation

The descriptive (internal training dataset) and predictive (external test dataset) performance of the PBPK/PD model is comprehensively demonstrated: Linear and semilogarithmic plots of population predictions are compared to observed plasma concentration-time profiles, fractions excreted to urine, brain tissue concentrations (Sections 3.1 to 3.6) and heart rate profiles (Section 3.11). Moreover, goodness-of-fit plots comparing predicted to observed plasma concentrations are shown in Figures S3.1.3, S3.2.3, S3.3.3, S3.4.3, S3.5.3, S3.6.3 and S3.11.2.

Predicted compared to observed area under the concentration–time curves from the first to the last data point ( $AUC_{last}$ ) and maximum concentrations ( $C_{max}$ ) values of all studies are shown in Figure S3.9.1 and of each route of administration separately in Figures S3.1.4, S3.2.4, S3.3.4, S3.4.4, S3.5.4 and S3.6.4. The predicted and observed  $AUC_{last}$  and  $C_{max}$  values of all studies including the geometric mean fold error (GMFE) and the mean relative deviation (MRD) values of all studies are listed in Tables S3.8.1 and S3.8.2.

A local sensitivity analysis was performed with a simulation of the highest studied pulmonary dose in steady-state (30 times 2.5 mg over 15 hours). A detailed description and the results of the sensitivity analysis can be found in Section 3.10.

### 3.1 Intravenous administration of nicotine

In this section, linear and semilogarithmic plots of plasma concentration-time profiles, linear plots of fractions of nicotine dose excreted unchanged to urine (Figs. S3.1.1 and S3.1.2), goodness-of-fit plots of predicted compared to observed plasma concentrations (Fig. S3.1.3) and goodness-of-fit plots of predicted compared to observed  $AUC_{last}$  and  $C_{max}$  values (Fig. S3.1.4) after intravenous administration of nicotine are shown.

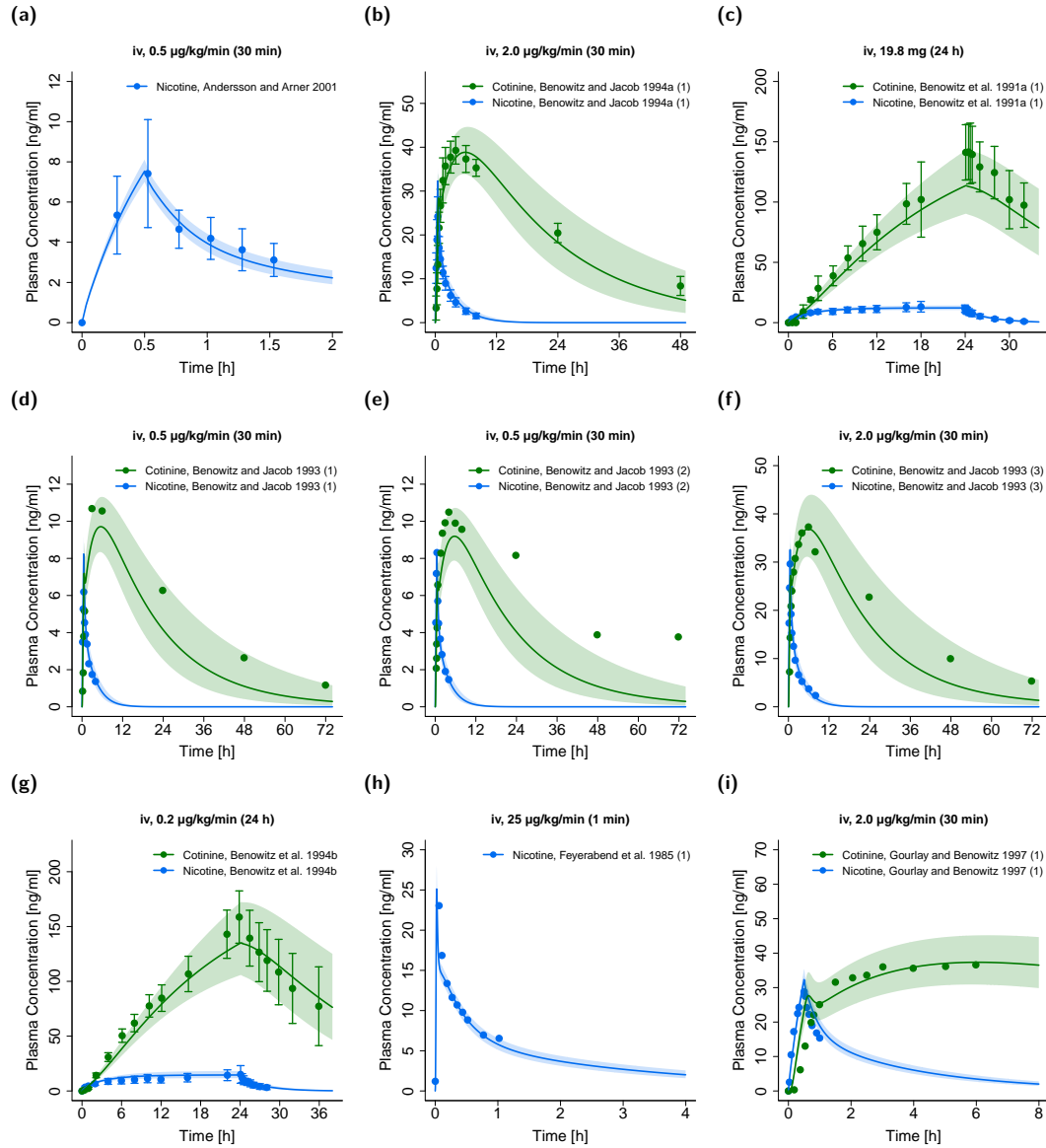


**Figure S3.1.1:** Nicotine (●, ●) and cotinine metabolite (●, ●) plasma concentration-time profiles (linear) and nicotine fraction excreted unchanged to urine (●) after intravenous administration of nicotine. Observed data are shown as circles, if available  $\pm$  standard deviation (SD). Population simulation ( $n=100$ ) geometric means are shown as lines; the shaded areas represent the predicted population geometric SD. References with numbers in parentheses link to a specific observed dataset described in the study table with detailed information about dosing regimens (Table S2.6.1). Predicted and observed  $AUC_{last}$  and  $C_{max}$  values are compared in Table S3.8.2. iv, intravenous; m.d., multiple dose.

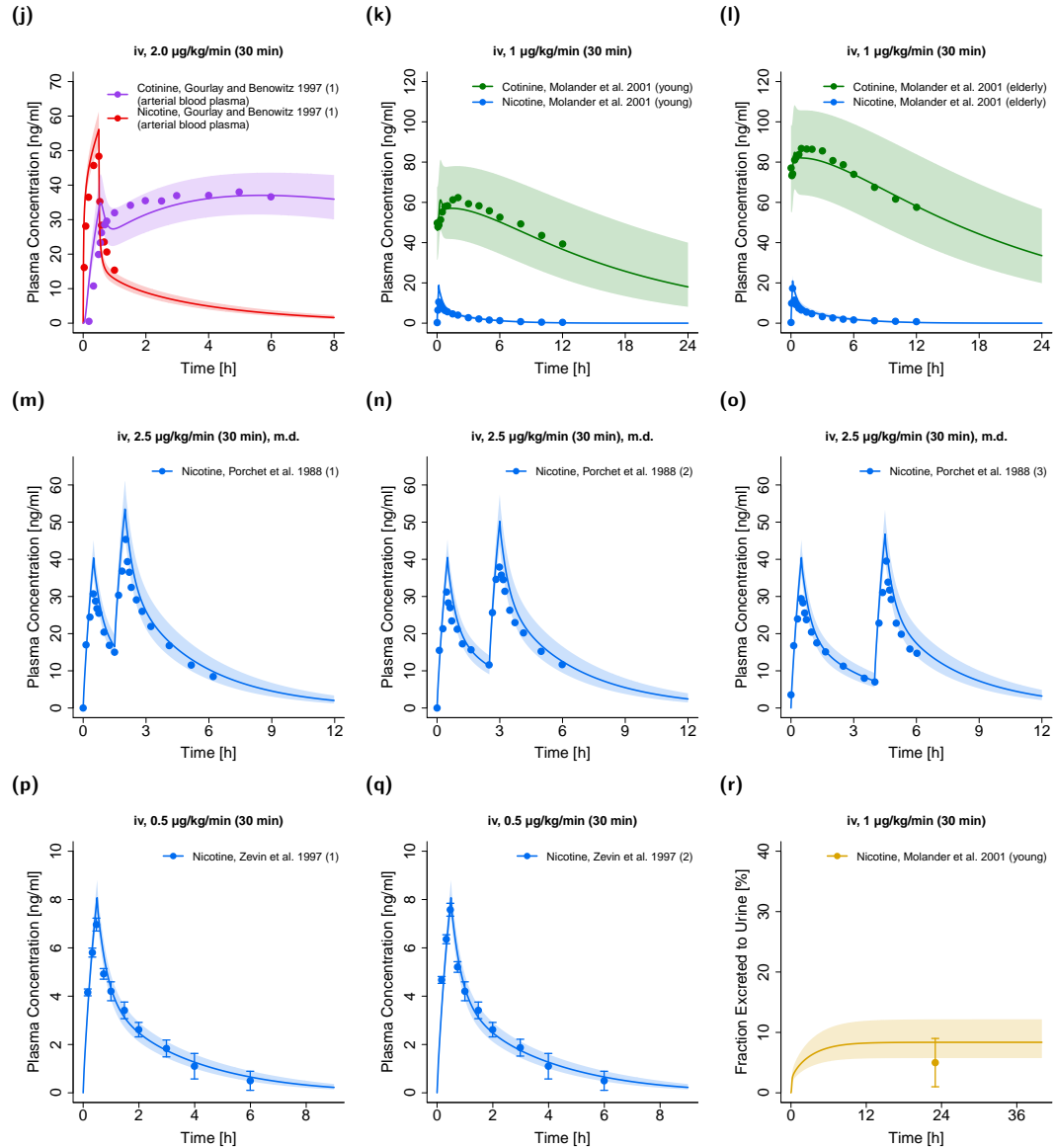


**Figure S3.1.1: Nicotine (●, ●) and cotinine metabolite (●, ●) plasma concentration-time profiles (linear) and nicotine fraction excreted unchanged to urine (●) after intravenous administration of nicotine.** Observed data are shown as circles, if available ± standard deviation (SD). Population simulation (n=100) geometric means are shown as lines; the shaded areas represent the predicted population geometric SD. References with numbers in parentheses link to a specific observed dataset described in the study table with detailed information about dosing regimens (Table S2.6.1). Predicted and observed  $AUC_{last}$  and  $C_{max}$  values are compared in Table S3.8.2. iv, intravenous; m.d., multiple dose. (continued)

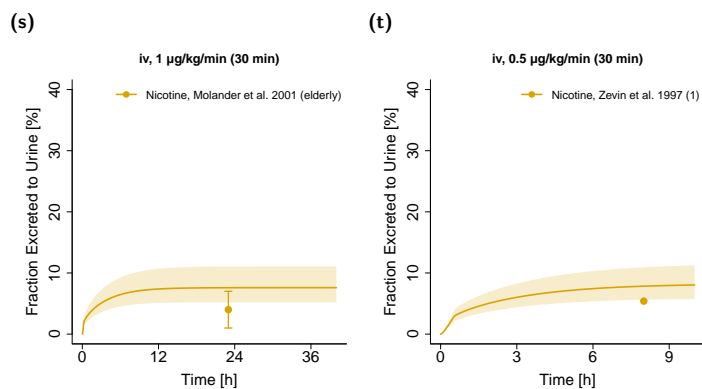


**Figure S3.1.1: Nicotine (●, ●) and cotinine metabolite (●, ●) plasma concentration-time profiles (linear) and nicotine fraction excreted unchanged to urine (●) after intravenous administration of nicotine.** Observed data are shown as circles, if available  $\pm$  standard deviation (SD). Population simulation ( $n=100$ ) geometric means are shown as lines; the shaded areas represent the predicted population geometric SD. References with numbers in parentheses link to a specific observed dataset described in the study table with detailed information about dosing regimens (Table S2.6.1). Predicted and observed  $AUC_{last}$  and  $C_{max}$  values are compared in Table S3.8.2. **iv**, intravenous; **m.d.**, multiple dose. (continued)

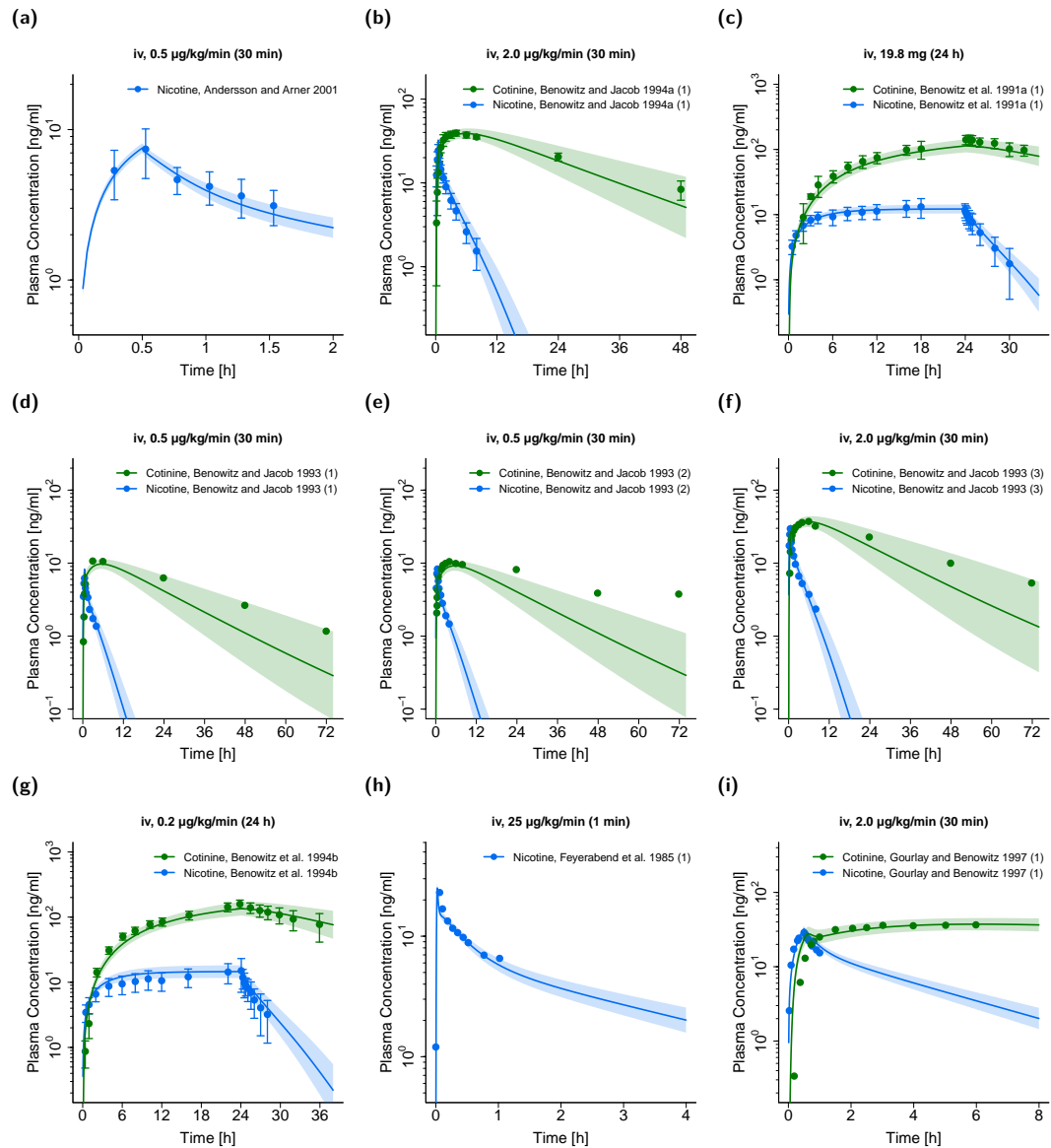


**Figure S3.1.2:** Nicotine (●, ●) and cotinine metabolite (●, ●) plasma concentration-time profiles (semilogarithmic) after intravenous administration of nicotine. Observed data are shown as circles, if available  $\pm$  standard deviation (SD). Population simulation ( $n=100$ ) geometric means are shown as lines; the shaded areas represent the predicted population geometric SD. References with numbers in parentheses link to a specific observed dataset described in the study table with detailed information about dosing regimens (Table S2.6.1). Predicted and observed  $\text{AUC}_{\text{last}}$  and  $C_{\text{max}}$  values are compared in Table S3.8.2. iv, intravenous; m.d., multiple dose.

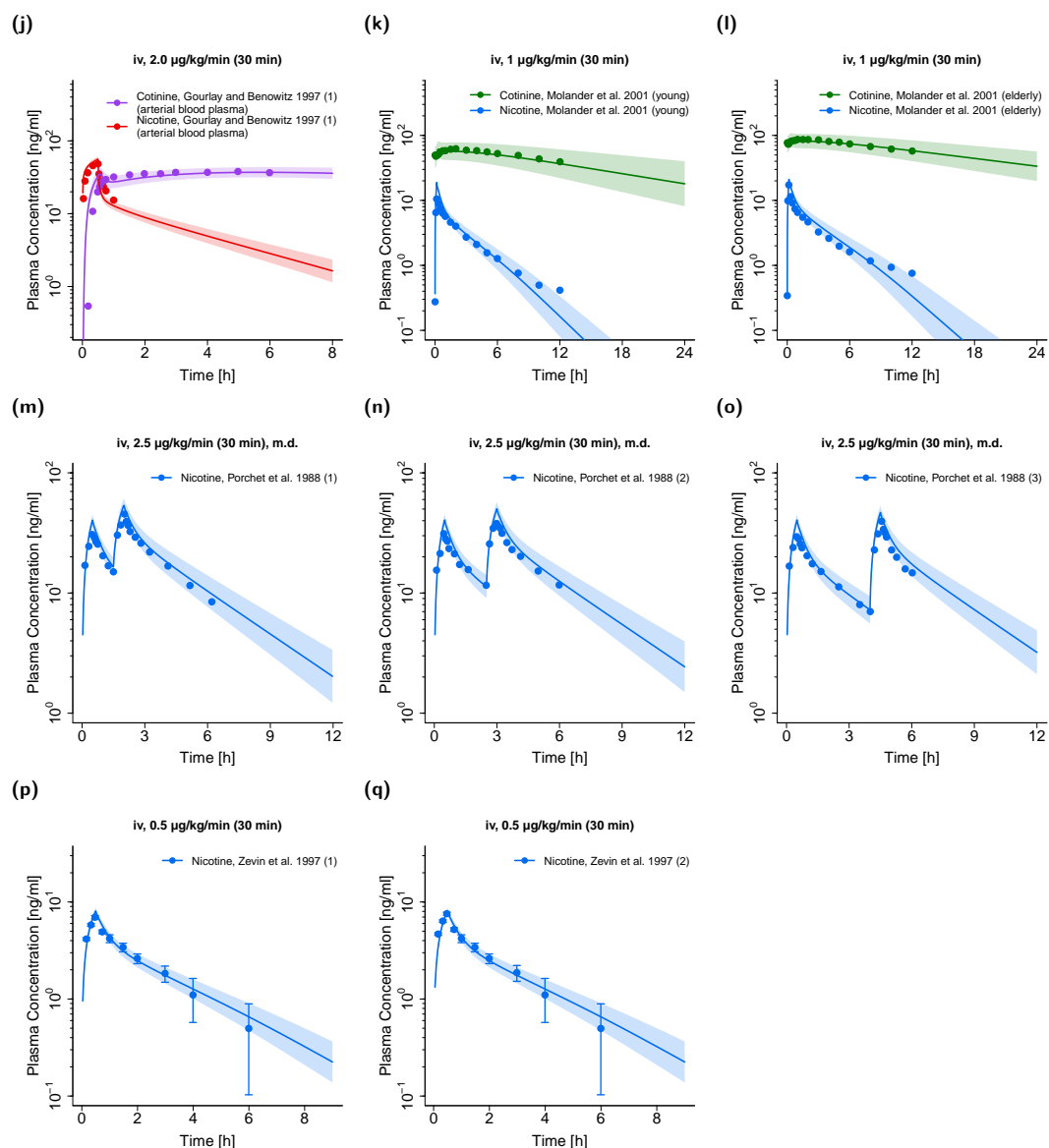
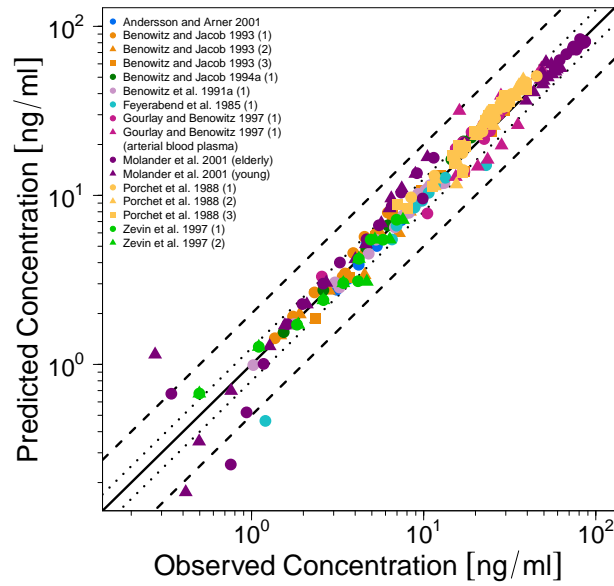


**Figure S3.1.2: Nicotine (●, ●) and cotinine metabolite (●, ●) plasma concentration-time profiles (semilogarithmic) after intravenous administration of nicotine.** Observed data are shown as circles, if available  $\pm$  standard deviation (SD). Population simulation ( $n=100$ ) geometric means are shown as lines; the shaded areas represent the predicted population geometric SD. References with numbers in parentheses link to a specific observed dataset described in the study table with detailed information about dosing regimens (Table S2.6.1). Predicted and observed  $AUC_{last}$  and  $C_{max}$  values are compared in Table S3.8.2. **iv**, intravenous; **m.d.**, multiple dose. (continued)

(a) Nicotine



(b) Cotinine metabolite

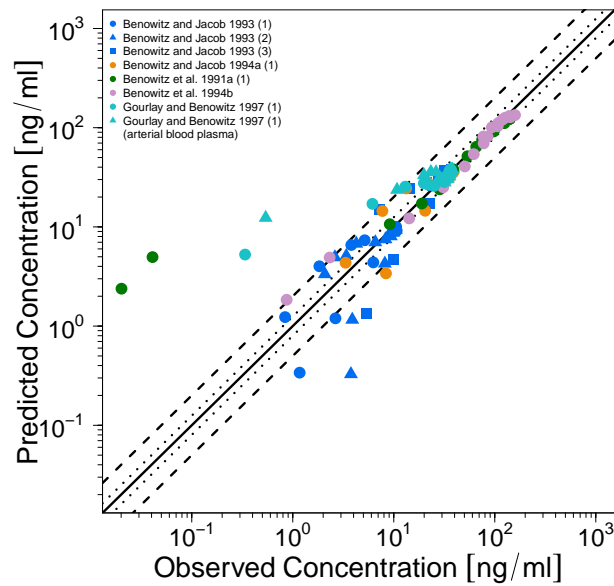
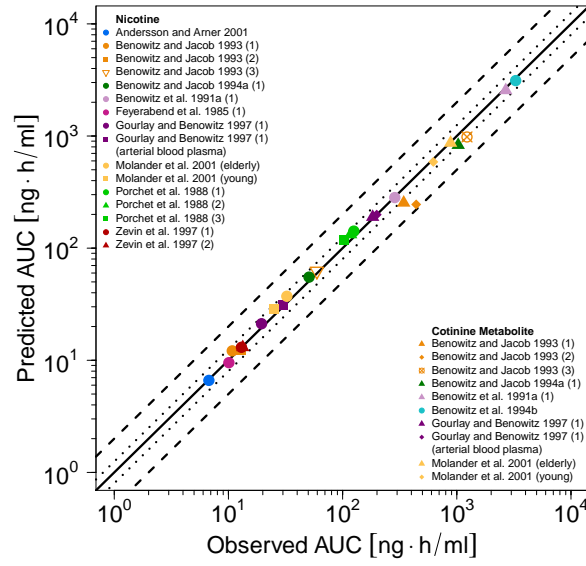
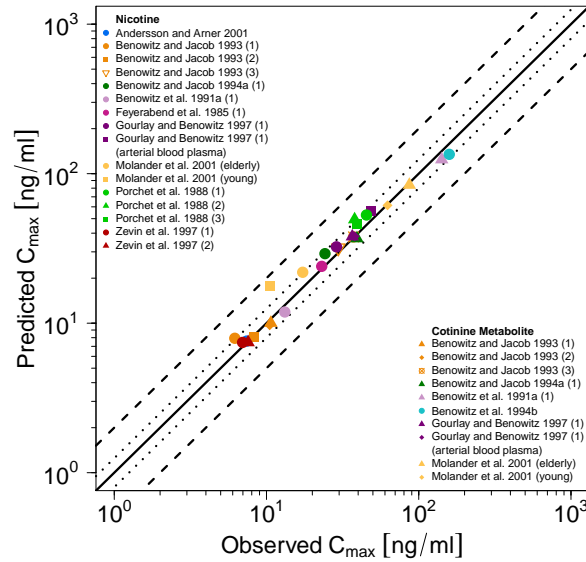


Figure S3.1.3: Predicted versus observed plasma concentrations ((a) nicotine, (b) cotinine metabolite) after intravenous administration of nicotine. The black solid (—) lines mark the lines of identity. Black dotted lines (.....) indicate 1.25-fold, black dashed lines (- -) indicate 2-fold deviation.

(a) AUC



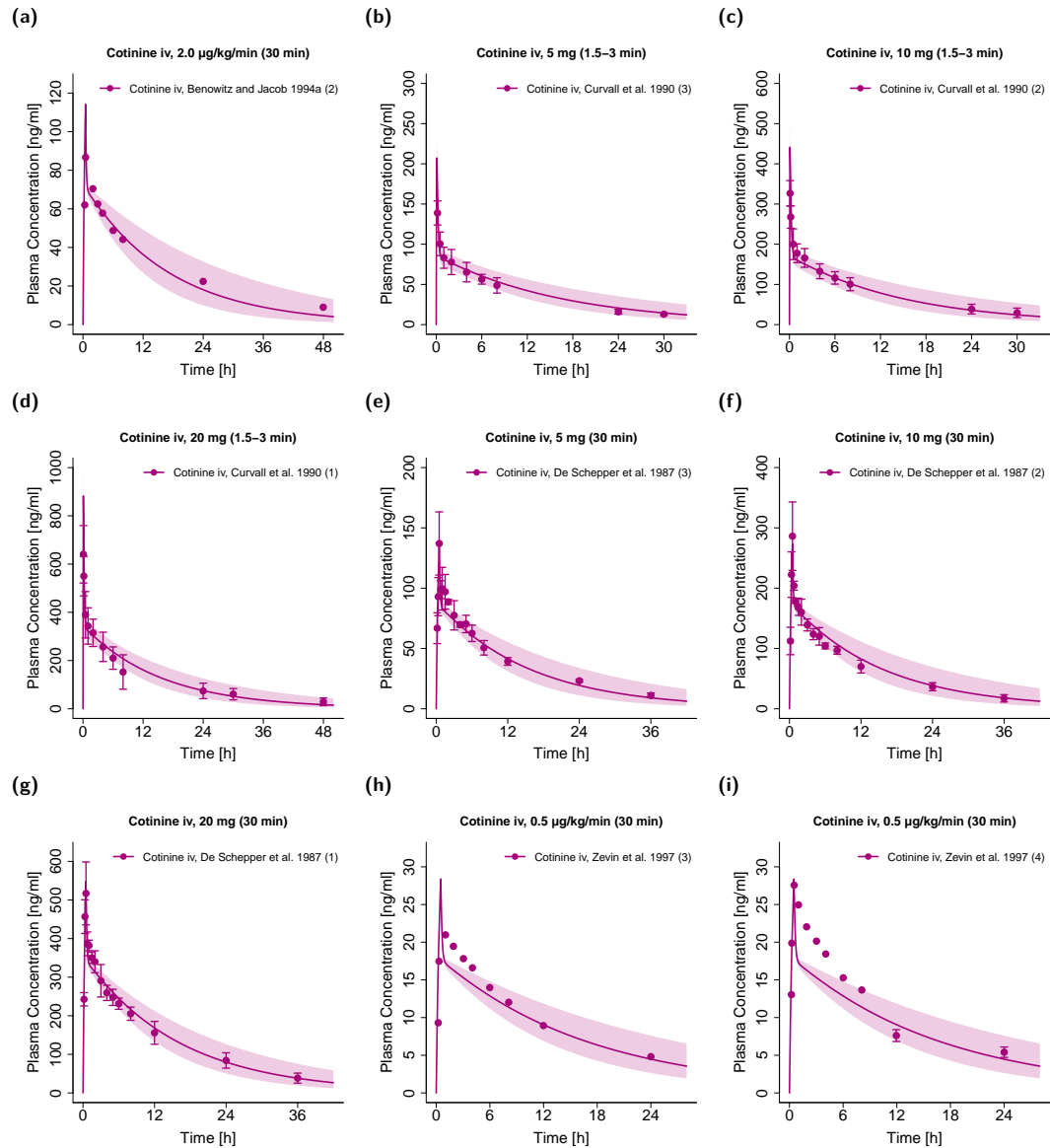
(b) C<sub>max</sub>



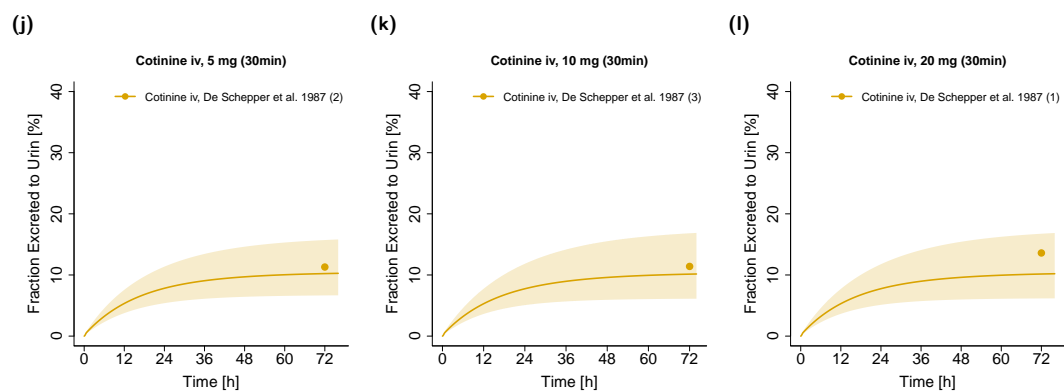
**Figure S3.1.4: Predicted versus observed nicotine and cotinine metabolite AUC (a) and C<sub>max</sub> (b) values after intravenous administration of nicotine.** Each symbol represents the AUC<sub>last</sub> or C<sub>max</sub> of a different plasma profile. The black solid (—) lines mark the lines of identity. Black dotted lines (····) indicate 1.25-fold, black dashed lines (---) indicate 2-fold deviation. **AUC**, area under the plasma concentration–time curve from the first to the last data point; **C<sub>max</sub>**, maximum plasma concentration.

### 3.2 Intravenous administration of cotinine

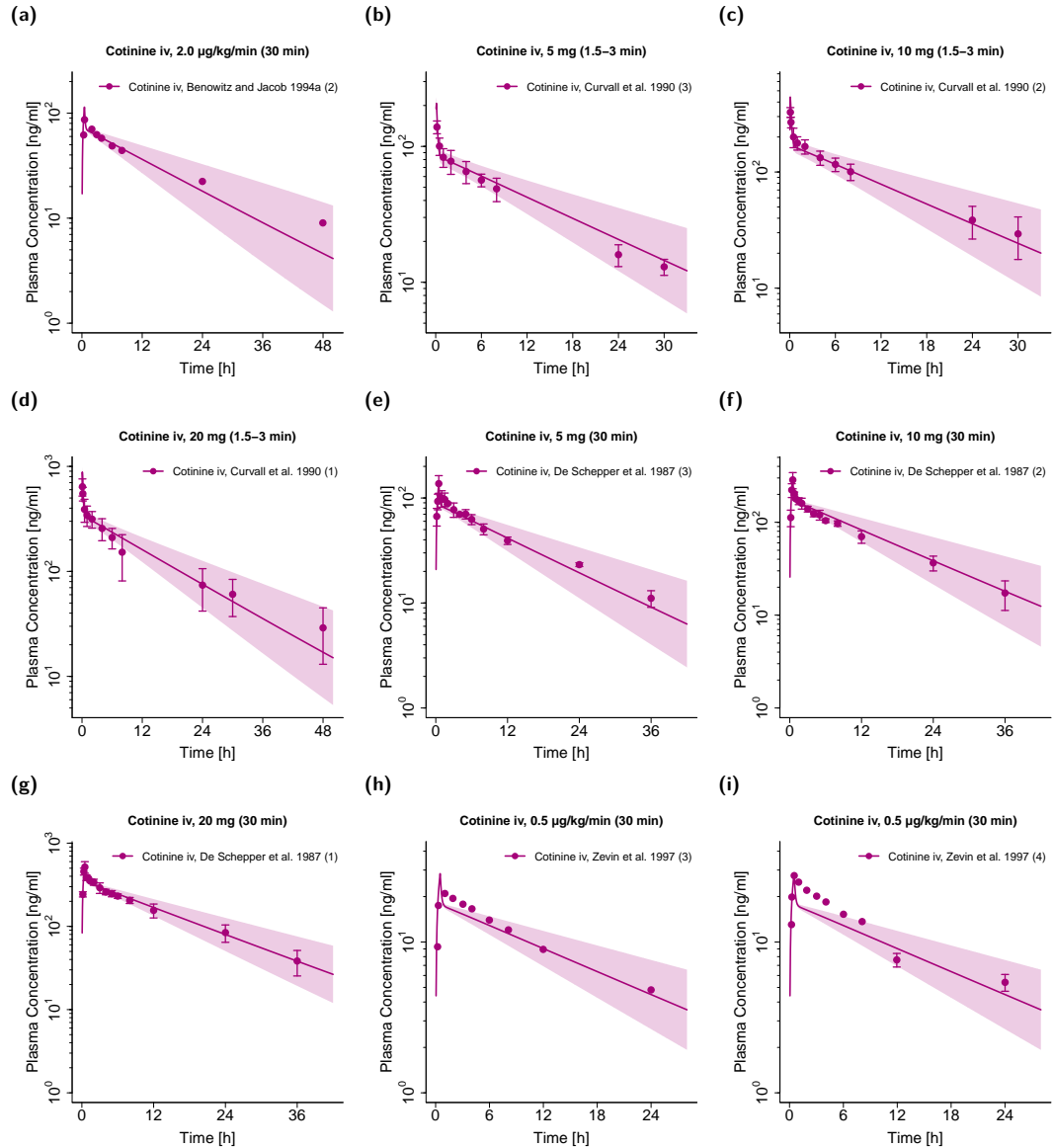
In this section, linear and semilogarithmic plots of plasma concentration-time profiles, linear plots of fractions of cotinine dose excreted unchanged to urine (Figs. S3.2.1 and S3.2.2), a goodness-of-fit plot of predicted compared to observed plasma concentrations (Fig. S3.2.3) and goodness-of-fit plots of predicted compared to observed  $AUC_{last}$  and  $C_{max}$  values (Fig. S3.2.4) after intravenous administration of cotinine are shown.



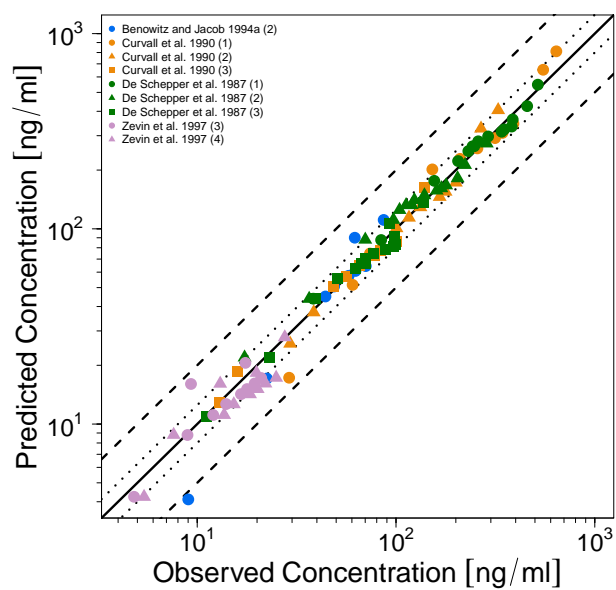
**Figure S3.2.1: Cotinine plasma concentration-time profiles (linear) and cotinine fraction excreted unchanged to urine after intravenous administration of cotinine.** Observed data are shown as circles ( $\bullet$ ,  $\bullet$ ), if available  $\pm$  standard deviation (SD). Population simulation ( $n=100$ ) geometric means are shown as lines ( $-$ ,  $-$ ); the shaded areas represent the predicted population geometric SD. References with numbers in parentheses link to a specific observed dataset described in the study table (Table S2.6.2). Predicted and observed  $AUC_{last}$  and  $C_{max}$  values are compared in Table S3.8.2. iv, intravenous.



**Figure S3.2.1: Cotinine plasma concentration-time profiles (linear) and cotinine fraction excreted unchanged to urine after intravenous administration of cotinine.** Observed data are shown as circles ( $\bullet$ ,  $\bullet$ ), if available  $\pm$  standard deviation (SD). Population simulation ( $n=100$ ) geometric means are shown as lines ( $-$ ,  $-$ ); the shaded areas represent the predicted population geometric SD. References with numbers in parentheses link to a specific observed dataset described in the study table (Table S2.6.2). Predicted and observed  $AUC_{last}$  and  $C_{max}$  values are compared in Table S3.8.2. iv, intravenous. (continued)

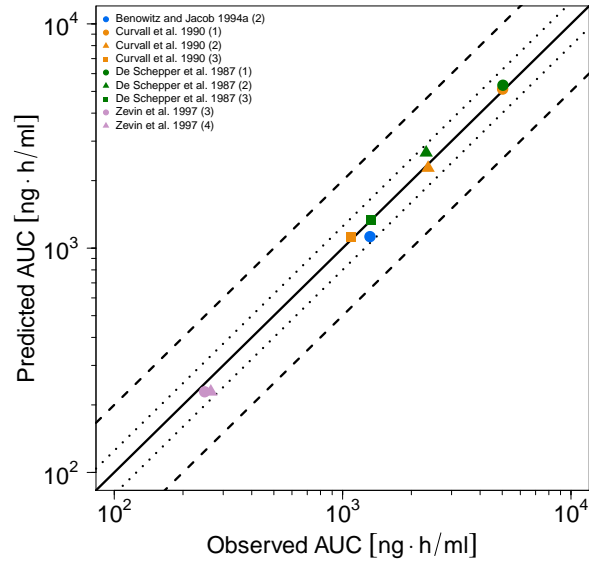
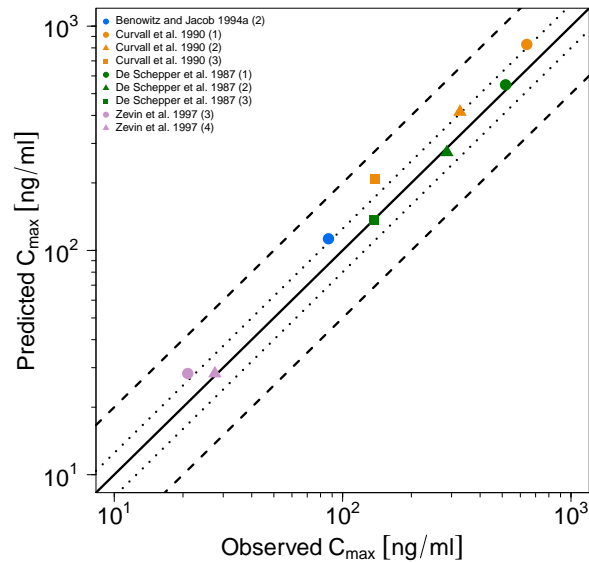


**Figure S3.2.2: Cotinine plasma concentration-time profiles (semilogarithmic) after intravenous administration of cotinine.** Observed data are shown as circles (●), if available  $\pm$  standard deviation (SD). Population simulation ( $n=100$ ) geometric means are shown as lines (—); the shaded areas represent the predicted population geometric SD. References with numbers in parentheses link to a specific observed dataset described in the study table (Table S2.6.2). Predicted and observed  $AUC_{last}$  and  $C_{max}$  values are compared in Table S3.8.2. iv, intravenous.



**Figure S3.2.3: Predicted versus observed plasma concentrations after intravenous administration of cotinine.** The black solid (—) line marks the line of identity. Black dotted lines (⋯) indicate 1.25-fold, black dashed lines (--) indicate 2-fold deviation.

(a) AUC

(b) C<sub>max</sub>

**Figure S3.2.4: Predicted versus observed cotinine AUC (a) and C<sub>max</sub> (b) values after intravenous administration of cotinine.** Each symbol represents the AUC<sub>last</sub> or C<sub>max</sub> of a different plasma profile. The black solid (—) lines mark the lines of identity. Black dotted lines (····) indicate 1.25-fold, black dashed lines (--) indicate 2-fold deviation. **AUC**, area under the plasma concentration–time curve from the first to the last data point; **C<sub>max</sub>**, maximum plasma concentration.

### 3.3 Oral administration of nicotine (including nicotine gums)

In this section, linear and semilogarithmic plots of plasma concentration-time profiles (Figs. S3.3.1 and S3.3.2), goodness-of-fit plots of predicted compared to observed plasma concentrations (Fig. S3.3.3) and goodness-of-fit plots of predicted compared to observed  $AUC_{last}$  and  $C_{max}$  values (Fig. S3.3.4) after oral administration of nicotine including nicotine gums are shown.

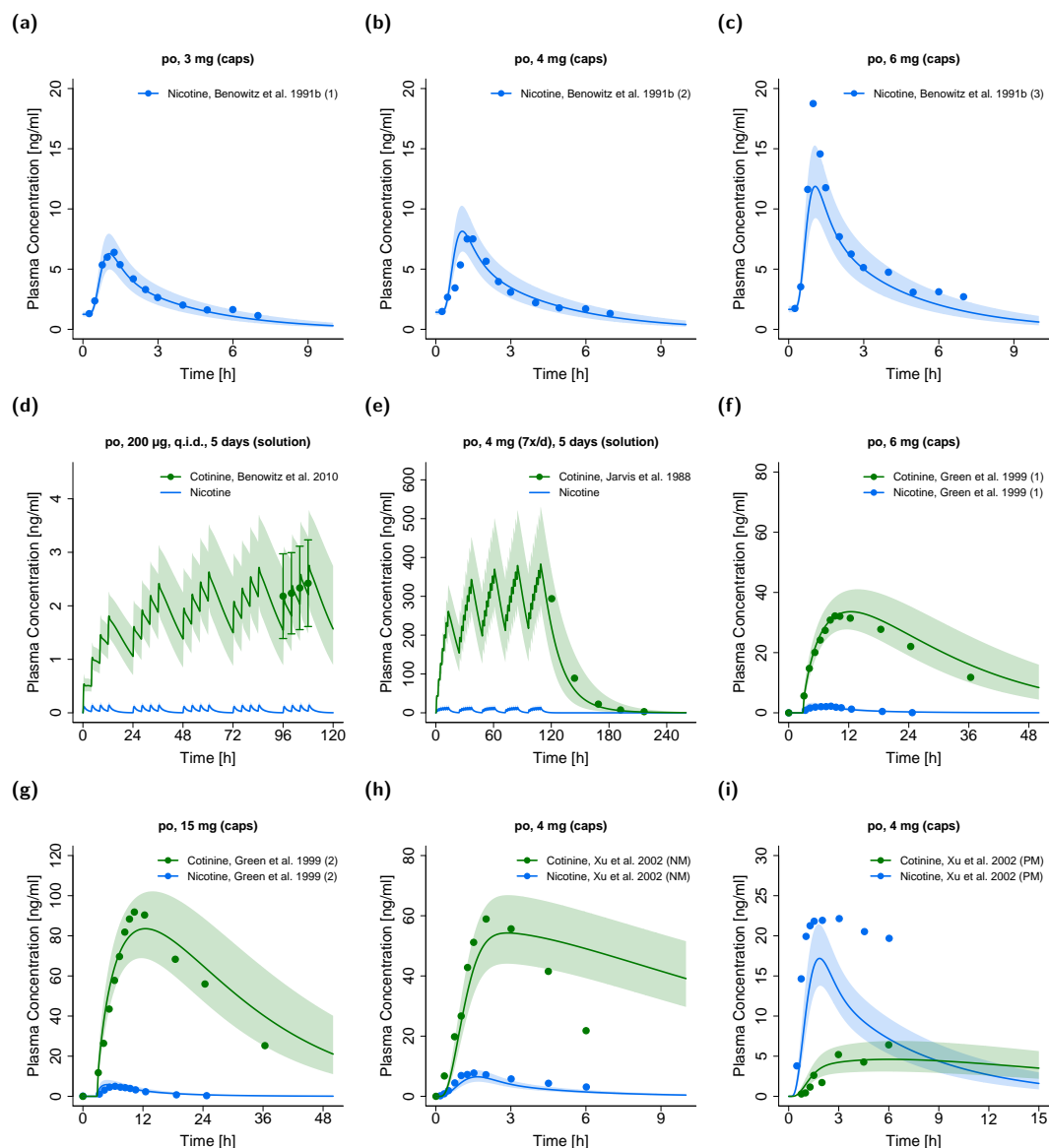


**Figure S3.3.1: Nicotine and cotinine metabolite plasma concentration-time profiles (linear) after oral administration of nicotine.** Observed data are shown as circles ( $\bullet$ ,  $\bullet$ ), if available  $\pm$  standard deviation (SD). Population simulation ( $n=100$ ) geometric means are shown as lines ( $-$ ,  $-$ ); the shaded areas represent the predicted population geometric SD. References with numbers in parentheses link to a specific observed dataset described in the study table with detailed information about dosing regimens (Table S2.6.1). Predicted and observed  $AUC_{last}$  and  $C_{max}$  values are compared in Table S3.8.2. **m.d.**, multiple dose; **NM**, Normal Metabolizer; **PM**, Poor Metabolizer; **po**, oral; **q.i.d.**, four times daily.

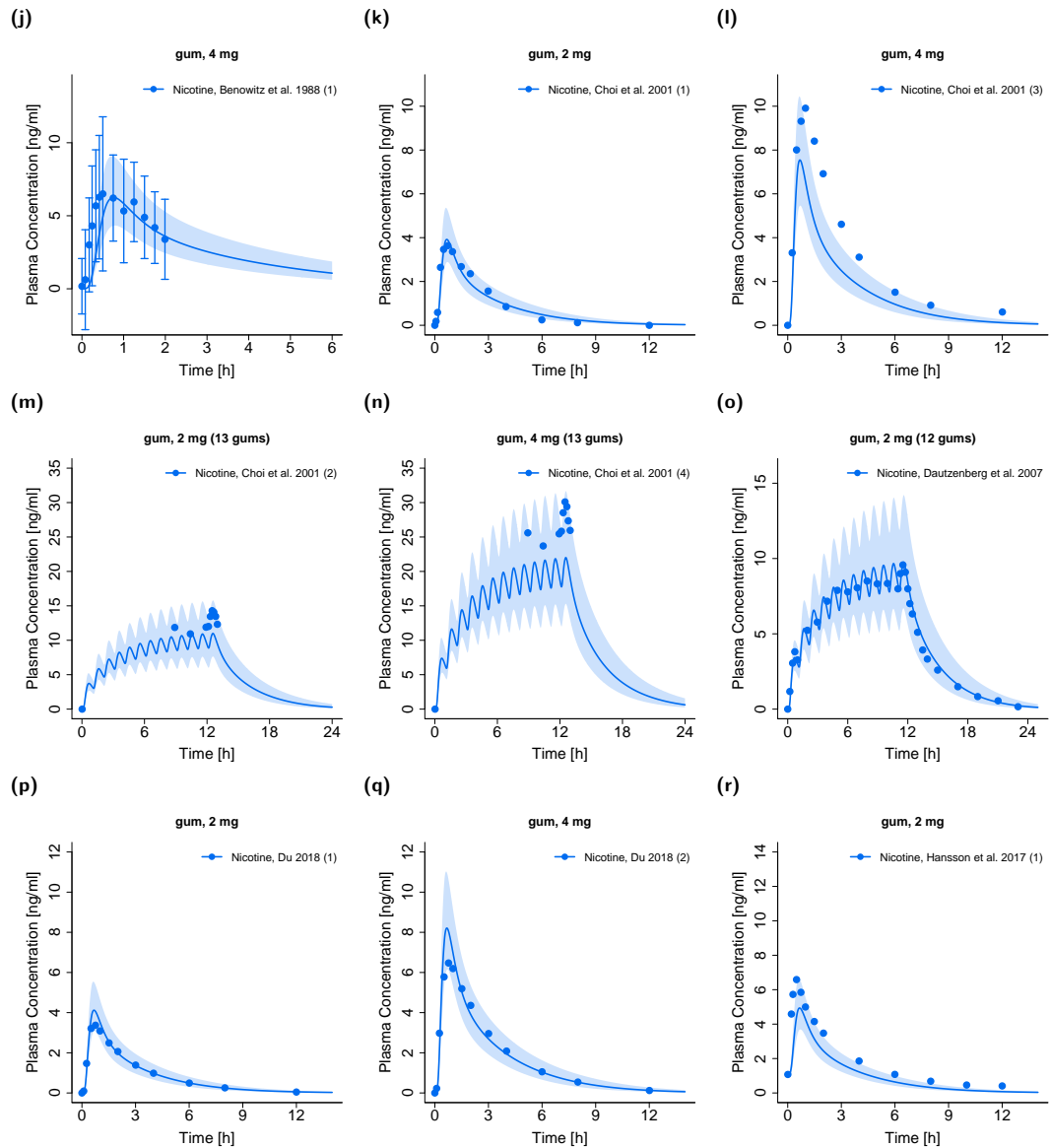


**Figure S3.3.1: Nicotine and cotinine metabolite plasma concentration-time profiles (linear) after oral administration of nicotine.** Observed data are shown as circles ( $\bullet$ ,  $\bullet$ ), if available  $\pm$  standard deviation (SD). Population simulation ( $n=100$ ) geometric means are shown as lines ( $-$ ,  $-$ ); the shaded areas represent the predicted population geometric SD. References with numbers in parentheses link to a specific observed dataset described in the study table with detailed information about dosing regimens (Table S2.6.1). Predicted and observed  $AUC_{last}$  and  $C_{max}$  values are compared in Table S3.8.2. **m.d.**, multiple dose; **NM**, Normal Metabolizer; **PM**, Poor Metabolizer; **po**, oral; **q.i.d.**, four times daily. (continued)

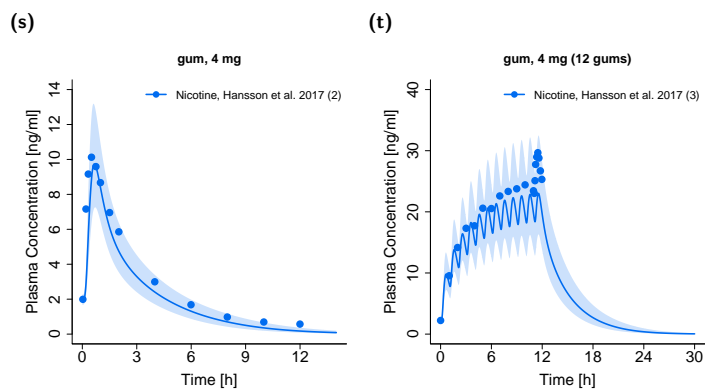


**Figure S3.3.1: Nicotine and cotinine metabolite plasma concentration-time profiles (linear) after oral administration of nicotine.** Observed data are shown as circles ( $\bullet$ ,  $\bullet$ ), if available  $\pm$  standard deviation (SD). Population simulation ( $n=100$ ) geometric means are shown as lines ( $-$ ,  $-$ ); the shaded areas represent the predicted population geometric SD. References with numbers in parentheses link to a specific observed dataset described in the study table with detailed information about dosing regimens (Table S2.6.1). Predicted and observed  $AUC_{last}$  and  $C_{max}$  values are compared in Table S3.8.2. **m.d.**, multiple dose; **NM**, Normal Metabolizer; **PM**, Poor Metabolizer; **po**, oral; **q.i.d.**, four times daily. (continued)

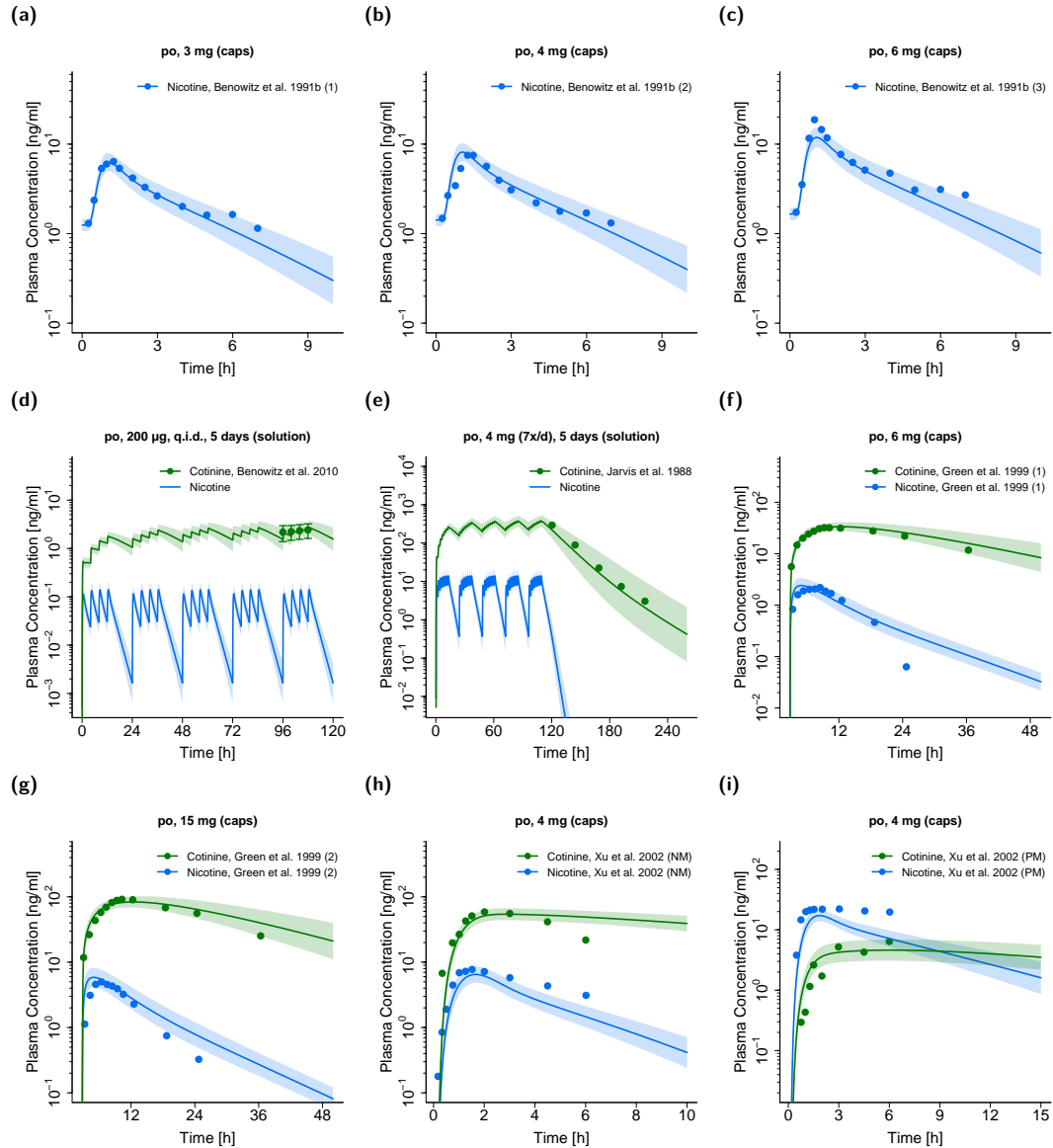


**Figure S3.3.2: Nicotine and cotinine metabolite plasma concentration-time profiles (semilogarithmic) after oral administration of nicotine.** Observed data are shown as circles ( $\bullet$ ,  $\bullet$ ), if available  $\pm$  standard deviation (SD). Population simulation ( $n=100$ ) geometric means are shown as lines ( $-$ ,  $-$ ); the shaded areas represent the predicted population geometric SD. References with numbers in parentheses link to a specific observed dataset described in the study table with detailed information about dosing regimens (Table S2.6.1). Predicted and observed  $AUC_{last}$  and  $C_{max}$  values are compared in Table S3.8.2. **m.d.**, multiple dose; **NM**, Normal Metabolizer; **PM**, Poor Metabolizer; **po**, oral; **q.i.d.**, four times daily.

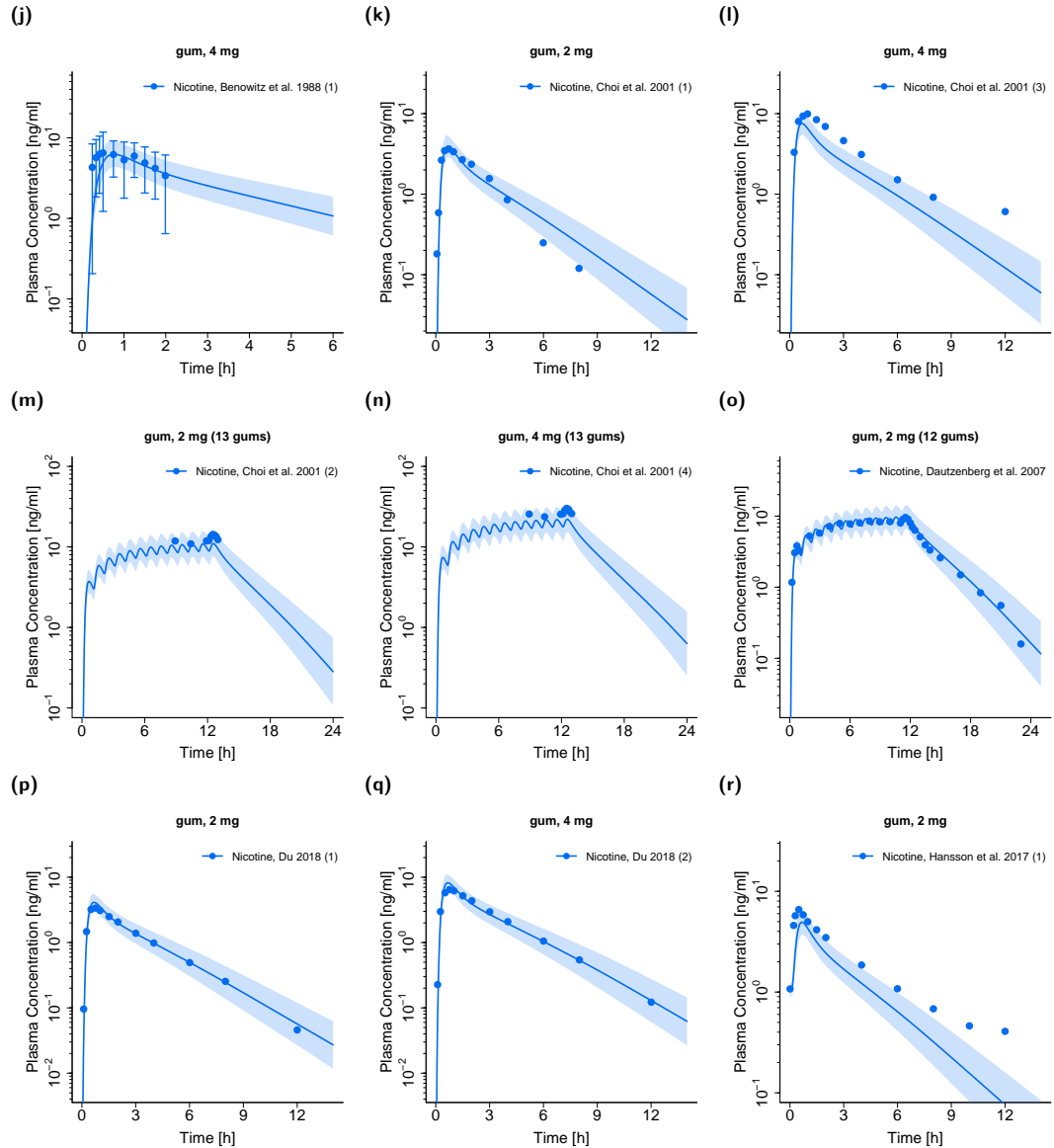


**Figure S3.3.2: Nicotine and cotinine metabolite plasma concentration-time profiles (semilogarithmic) after oral administration of nicotine.** Observed data are shown as circles (●, ●), if available ± standard deviation (SD). Population simulation (n=100) geometric means are shown as lines (—, —); the shaded areas represent the predicted population geometric SD. References with numbers in parentheses link to a specific observed dataset described in the study table with detailed information about dosing regimens (Table S2.6.1). Predicted and observed  $AUC_{last}$  and  $C_{max}$  values are compared in Table S3.8.2. **m.d.**, multiple dose; **NM**, Normal Metabolizer; **PM**, Poor Metabolizer; **po**, oral; **q.i.d.**, four times daily. (continued)

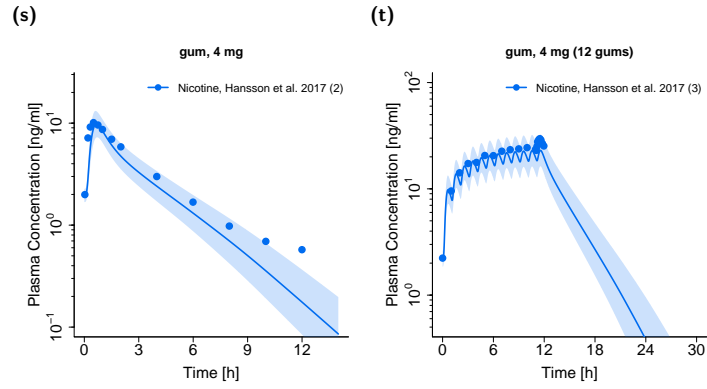
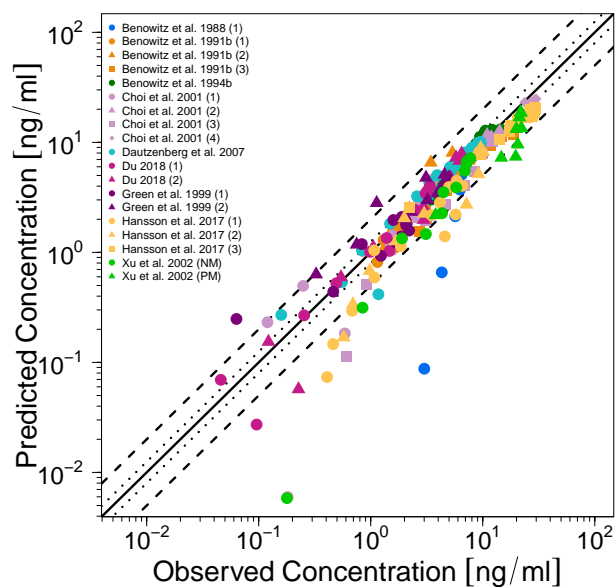


**Figure S3.3.2: Nicotine and cotinine metabolite plasma concentration-time profiles (semilogarithmic) after oral administration of nicotine.** Observed data are shown as circles ( $\bullet$ ,  $\bullet$ ), if available  $\pm$  standard deviation (SD). Population simulation ( $n=100$ ) geometric means are shown as lines ( $-$ ,  $-$ ); the shaded areas represent the predicted population geometric SD. References with numbers in parentheses link to a specific observed dataset described in the study table with detailed information about dosing regimens (Table S2.6.1). Predicted and observed  $AUC_{last}$  and  $C_{max}$  values are compared in Table S3.8.2. **m.d.**, multiple dose; **NM**, Normal Metabolizer; **PM**, Poor Metabolizer; **po**, oral; **q.i.d.**, four times daily. (continued)

## (a) Nicotine



## (b) Cotinine metabolite

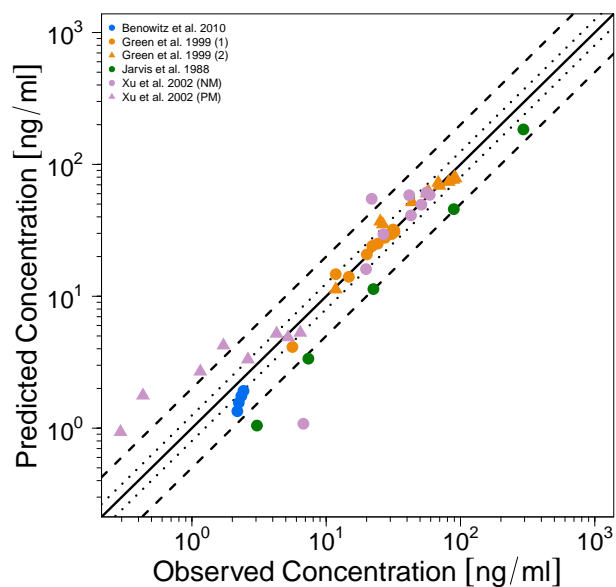
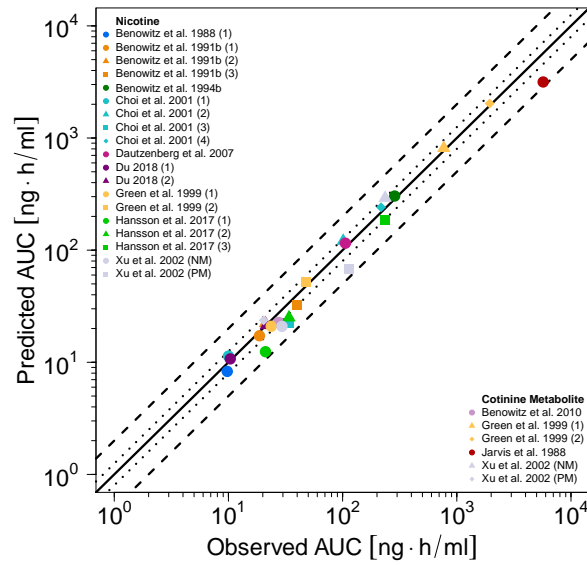
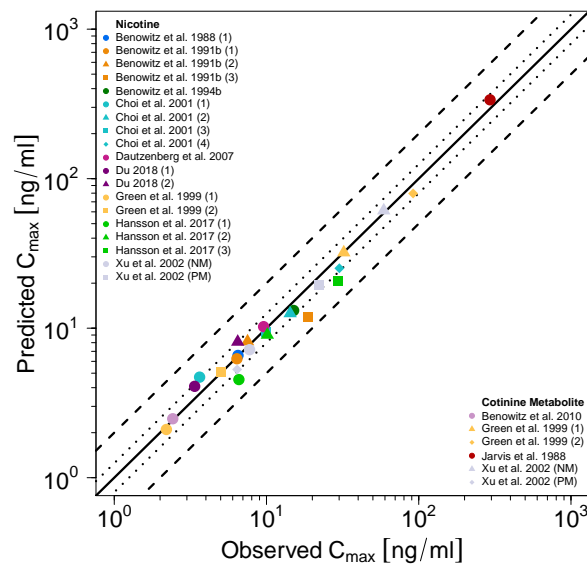


Figure S3.3.3: Predicted versus observed plasma concentrations ((a) nicotine, (b) cotinine metabolite) after oral administration of nicotine (including nicotine gums). The black solid (—) lines mark the lines of identity. Black dotted lines (.....) indicate 1.25-fold, black dashed lines (---) indicate 2-fold deviation.

(a) AUC

(b)  $C_{\max}$ 

**Figure S3.3.4: Predicted versus observed nicotine and cotinine metabolite AUC (a) and  $C_{\max}$  (b) values after oral administration of nicotine.** Each symbol represents the  $AUC_{\text{last}}$  or  $C_{\max}$  of a different plasma profile. The black solid (—) lines mark the lines of identity. Black dotted lines (.....) indicate 1.25-fold, black dashed lines (---) indicate 2-fold deviation. **AUC**, area under the plasma concentration–time curve from the first to the last data point;  **$C_{\max}$** , maximum plasma concentration.

### 3.4 Transdermal administration of nicotine (nicotine patches)

In this section, linear and semilogarithmic plots of plasma concentration-time profiles (Figs. S3.4.1 and S3.4.2), goodness-of-fit plots of predicted compared to observed plasma concentrations (Fig. S3.4.3) and goodness-of-fit plots of predicted compared to observed  $AUC_{last}$  and  $C_{max}$  values (Fig. S3.4.4) after transdermal administration of nicotine with nicotine patches are shown.

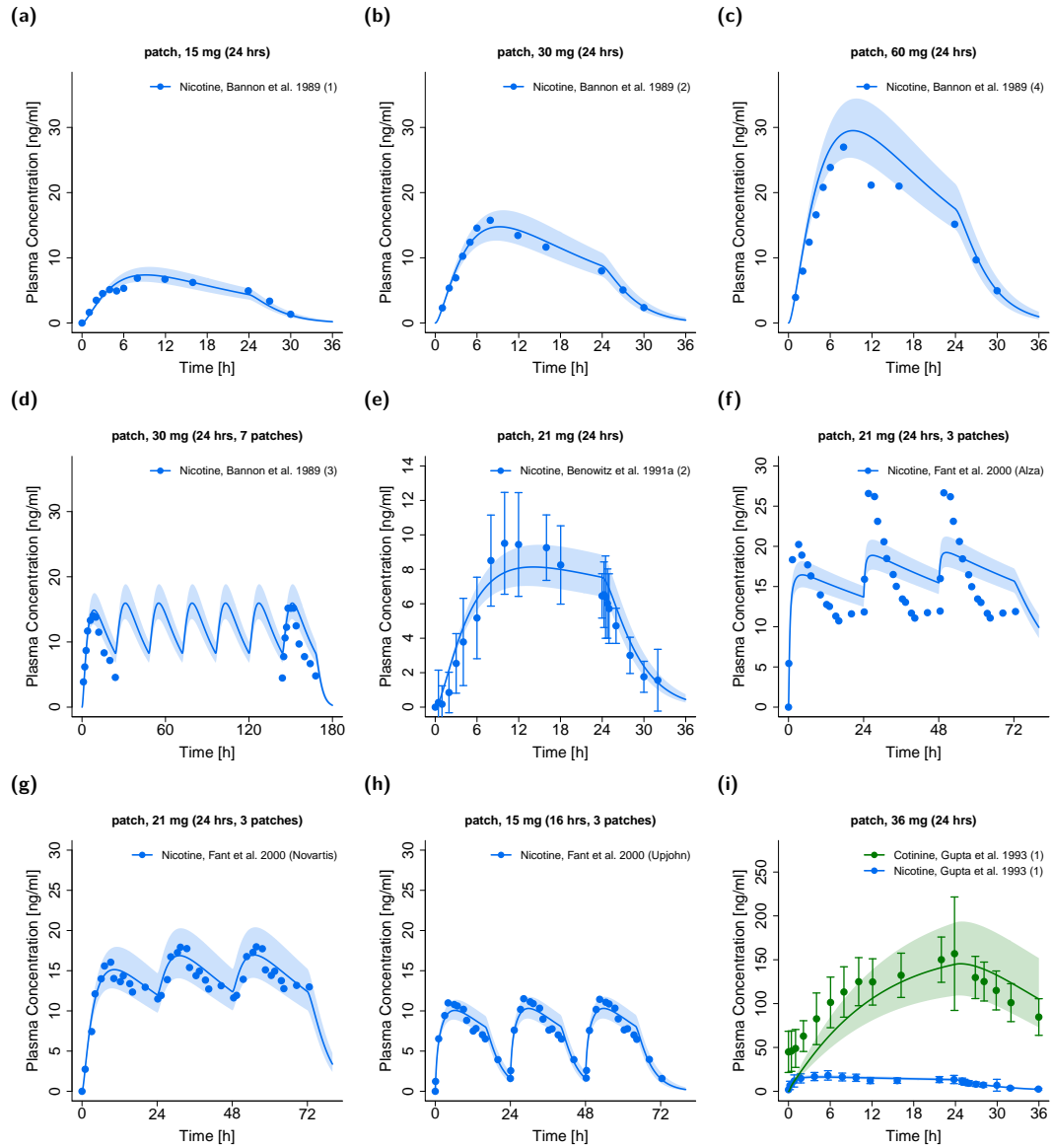


**Figure S3.4.1: Nicotine and cotinine metabolite plasma concentration-time profiles (linear) after transdermal administration of nicotine (nicotine patch).** Observed data are shown as circles (•, ●), if available  $\pm$  standard deviation (SD). Population simulation ( $n=100$ ) geometric means are shown as lines (—, —); the shaded areas represent the predicted population geometric SD. References with numbers in parentheses link to a specific observed dataset described in the study table with detailed information about dosing regimens (Table S2.6.1). Predicted and observed  $AUC_{last}$  and  $C_{max}$  values are compared in Table S3.8.2. **patch**, transdermal therapeutic system (nicotine patch).

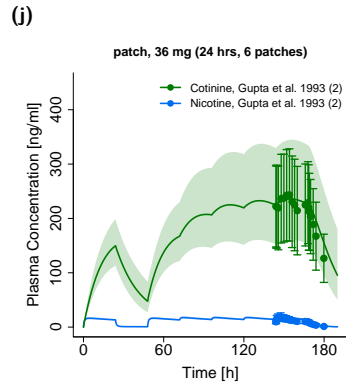


**Figure S3.4.1: Nicotine and cotinine metabolite plasma concentration-time profiles (linear) after transdermal administration of nicotine (nicotine patch).** Observed data are shown as circles (•, ●), if available  $\pm$  standard deviation (SD). Population simulation (n=100) geometric means are shown as lines (—, —); the shaded areas represent the predicted population geometric SD. References with numbers in parentheses link to a specific observed dataset described in the study table with detailed information about dosing regimens (Table S2.6.1). Predicted and observed  $AUC_{last}$  and  $C_{max}$  values are compared in Table S3.8.2. **patch**, transdermal therapeutic system (nicotine patch). (continued)

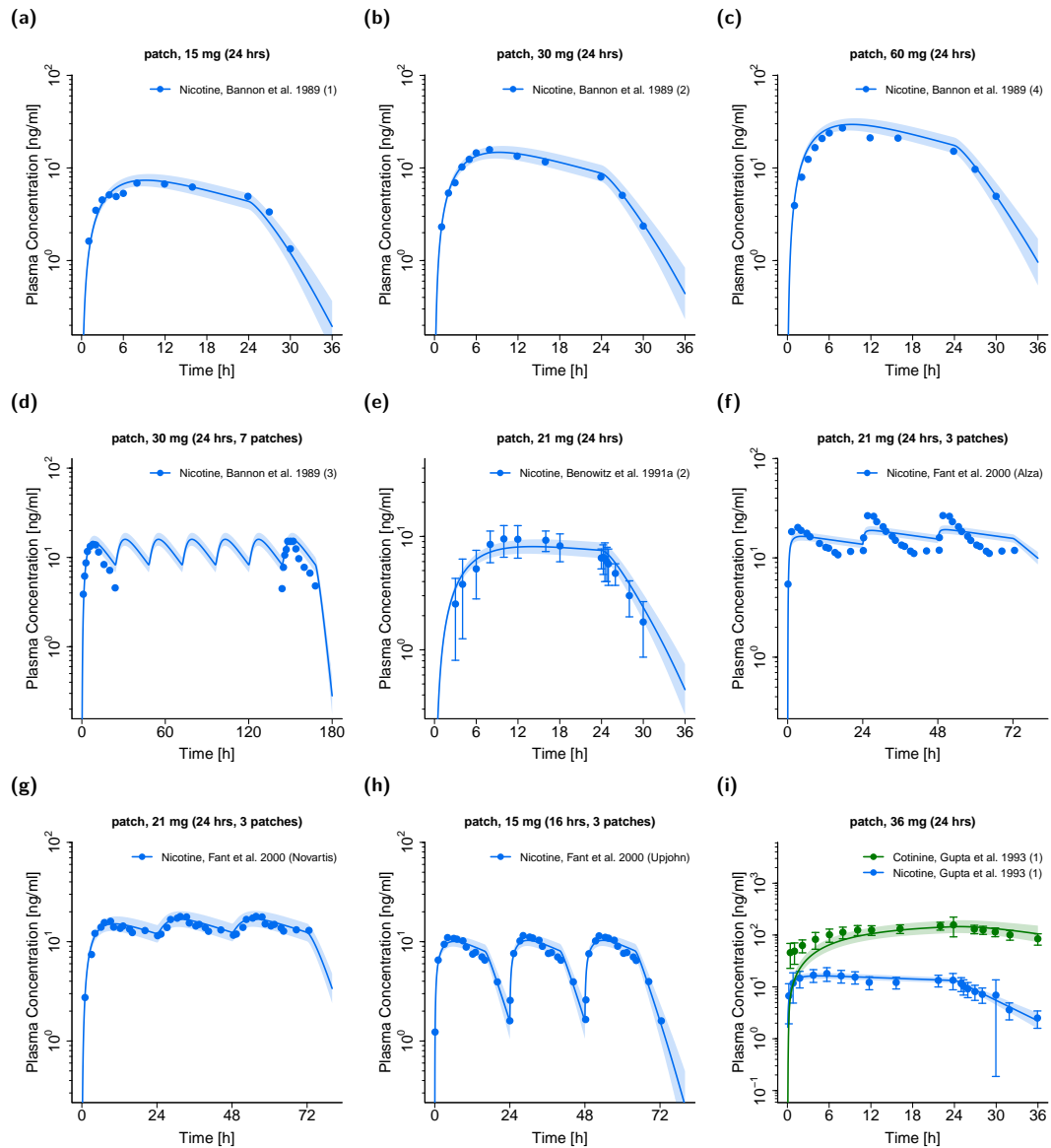


**Figure S3.4.2: Nicotine and cotinine metabolite plasma concentration-time profiles (semilogarithmic) after transdermal administration of nicotine (nicotine patch).** Observed data are shown as circles ( $\bullet$ ,  $\bullet$ ), if available  $\pm$  standard deviation (SD). Population simulation ( $n=100$ ) geometric means are shown as lines ( $-$ ,  $-$ ); the shaded areas represent the predicted population geometric SD. References with numbers in parentheses link to a specific observed dataset described in the study table with detailed information about dosing regimens (Table S2.6.1). Predicted and observed  $AUC_{last}$  and  $C_{max}$  values are compared in Table S3.8.2. **patch**, transdermal therapeutic system (nicotine patch).

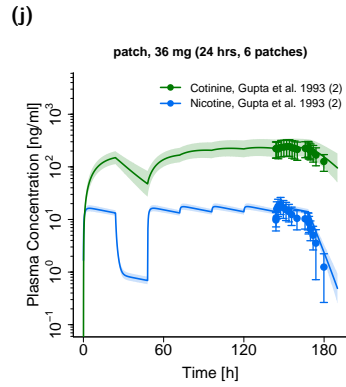
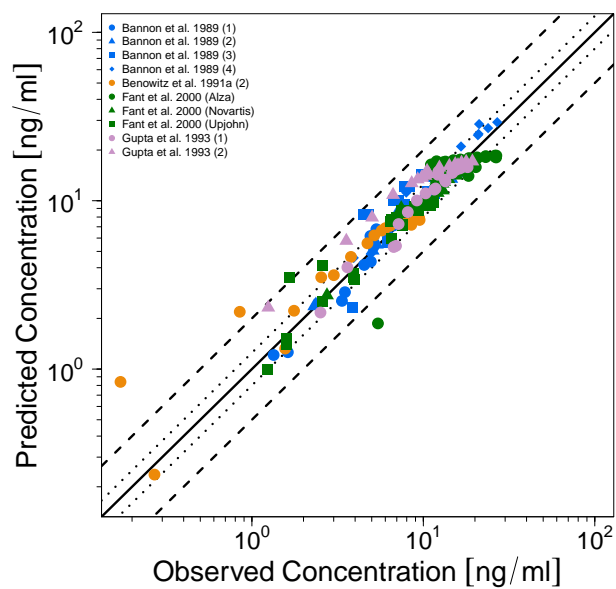


**Figure S3.4.2: Nicotine and cotinine metabolite plasma concentration-time profiles (semilogarithmic) after transdermal administration of nicotine (nicotine patch).** Observed data are shown as circles (●, ●), if available  $\pm$  standard deviation (SD). Population simulation (n=100) geometric means are shown as lines (—, —); the shaded areas represent the predicted population geometric SD. References with numbers in parentheses link to a specific observed dataset described in the study table with detailed information about dosing regimens (Table S2.6.1). Predicted and observed  $AUC_{last}$  and  $C_{max}$  values are compared in Table S3.8.2. **patch**, transdermal therapeutic system (nicotine patch). (continued)

## (a) Nicotine



## (b) Cotinine metabolite

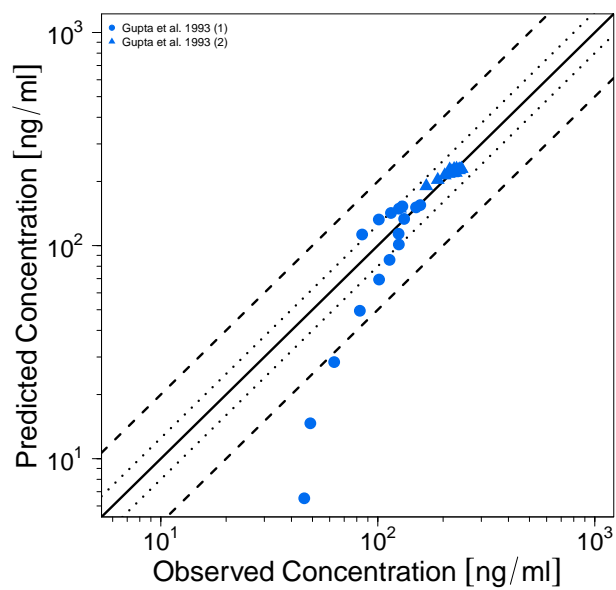
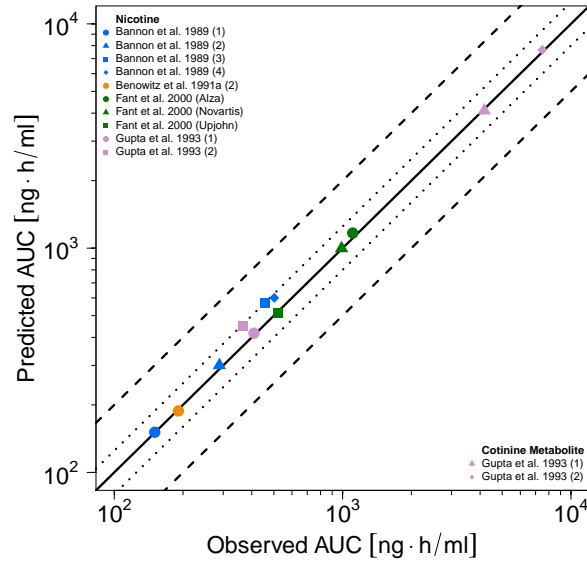
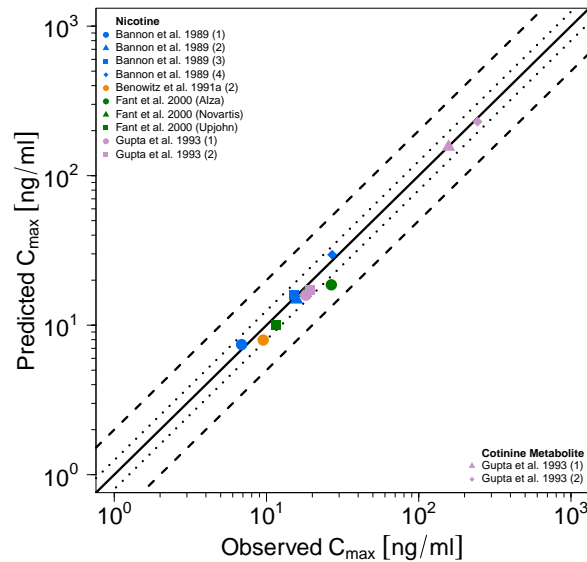


Figure S3.4.3: Predicted versus observed plasma concentrations ((a) nicotine, (b) cotinine metabolite) after transdermal administration of nicotine (nicotine patches). The black solid (—) lines mark the lines of identity. Black dotted lines (.....) indicate 1.25-fold, black dashed lines (---) indicate 2-fold deviation.

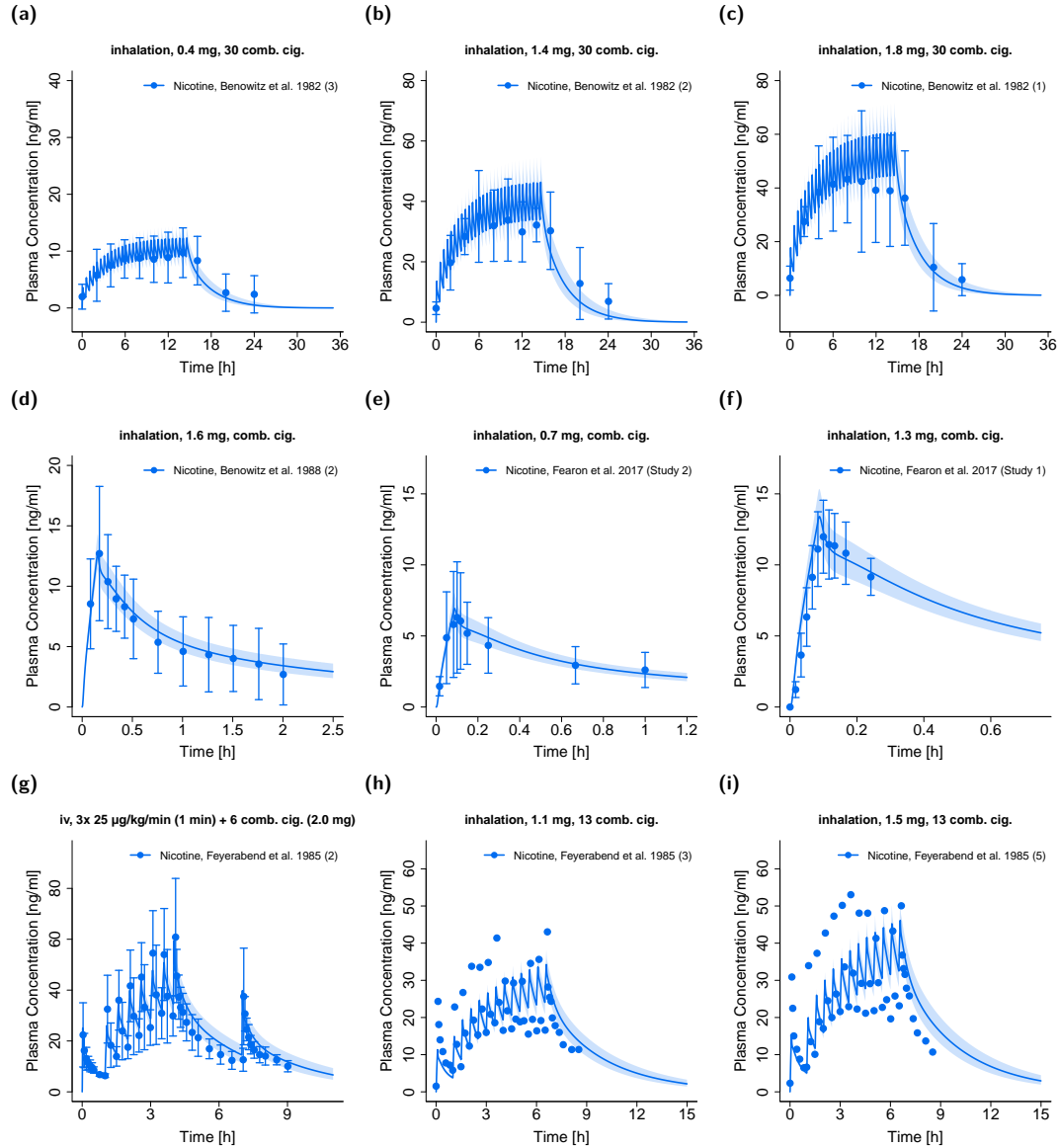
(a) AUC

(b)  $C_{\max}$ 

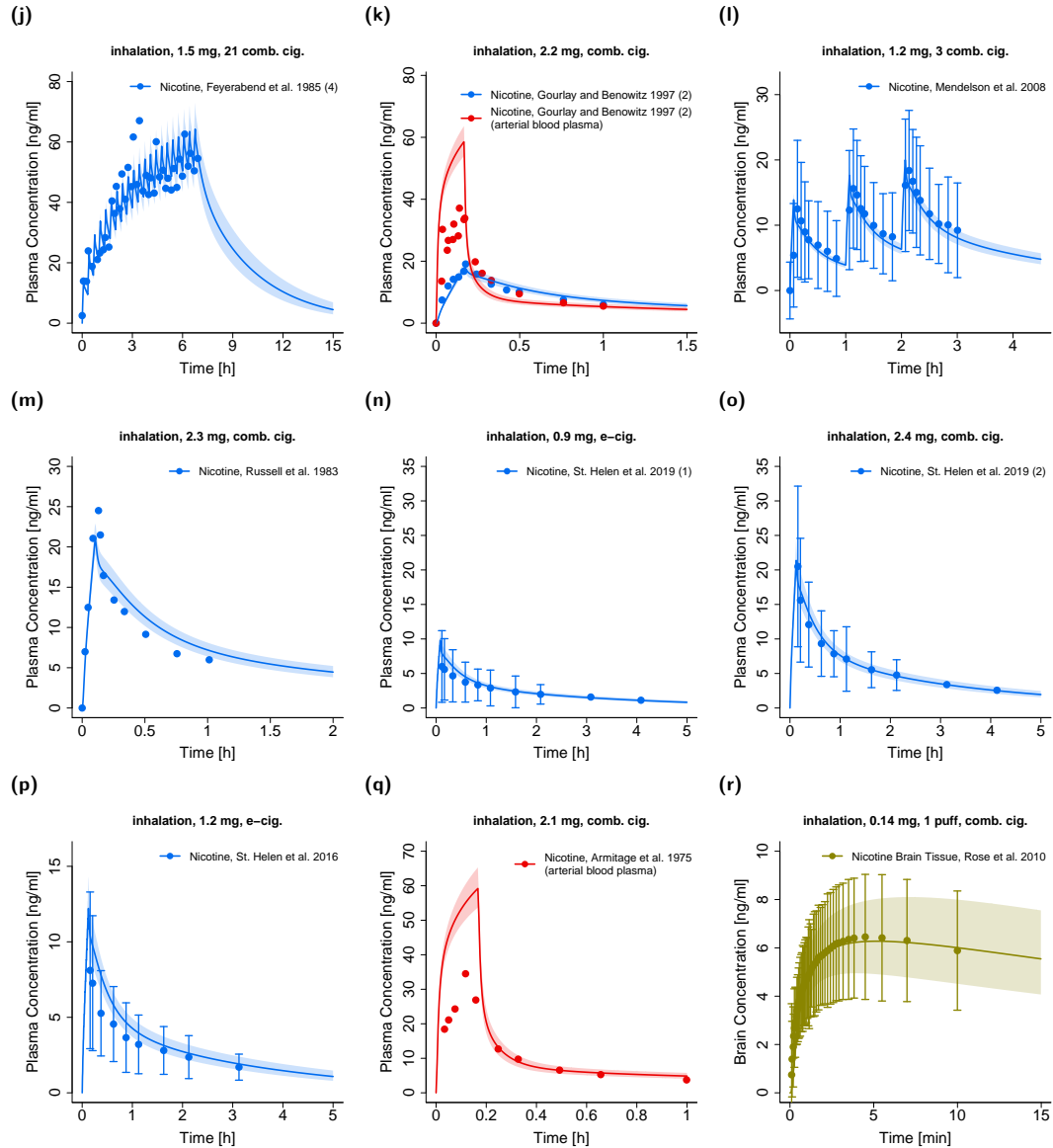
**Figure S3.4.4: Predicted versus observed nicotine and cotinine metabolite AUC (a) and  $C_{\max}$  (b) values after transdermal administration of nicotine (nicotine patches).** Each symbol represents the  $AUC_{\text{last}}$  or  $C_{\max}$  of a different plasma profile. The black solid (—) lines mark the lines of identity. Black dotted lines (.....) indicate 1.25-fold, black dashed lines (- -) indicate 2-fold deviation. **AUC**, area under the plasma concentration–time curve from the first to the last data point;  **$C_{\max}$** , maximum plasma concentration.

### 3.5 Pulmonary administration of nicotine (combustible cigarettes with estimated pulmonary nicotine exposure and e-cigarettes)

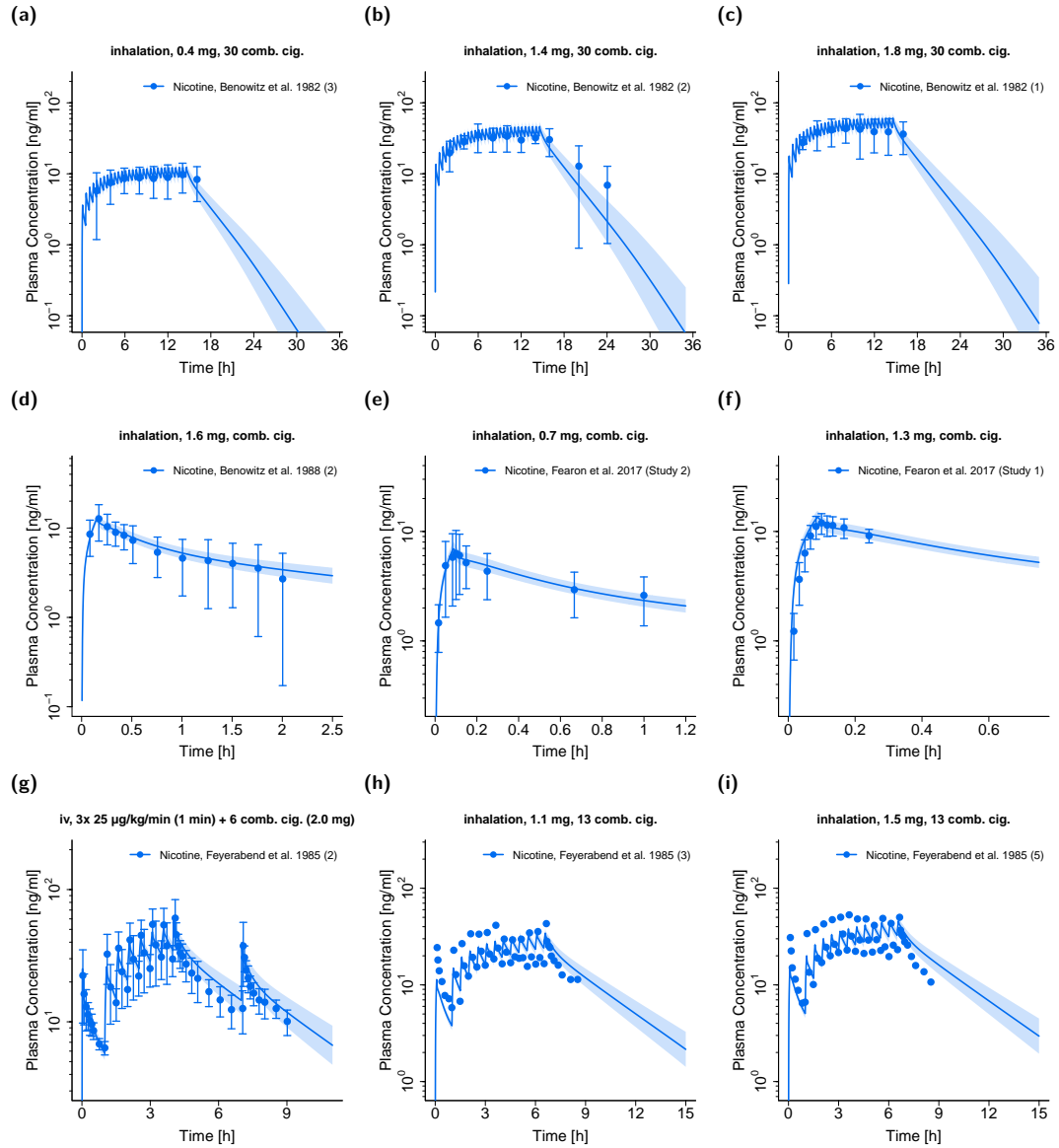
In this section, linear and semilogarithmic plots of plasma and brain tissue concentration-time profiles (Figs. S3.5.1 and S3.5.2), goodness-of-fit plots of predicted compared to observed plasma concentrations (Fig. S3.5.3) and predicted versus observed  $AUC_{last}$  and  $C_{max}$  values (Fig. S3.5.4) after administration of combustible cigarettes (with estimated pulmonary nicotine exposure) and e-cigarettes are shown.



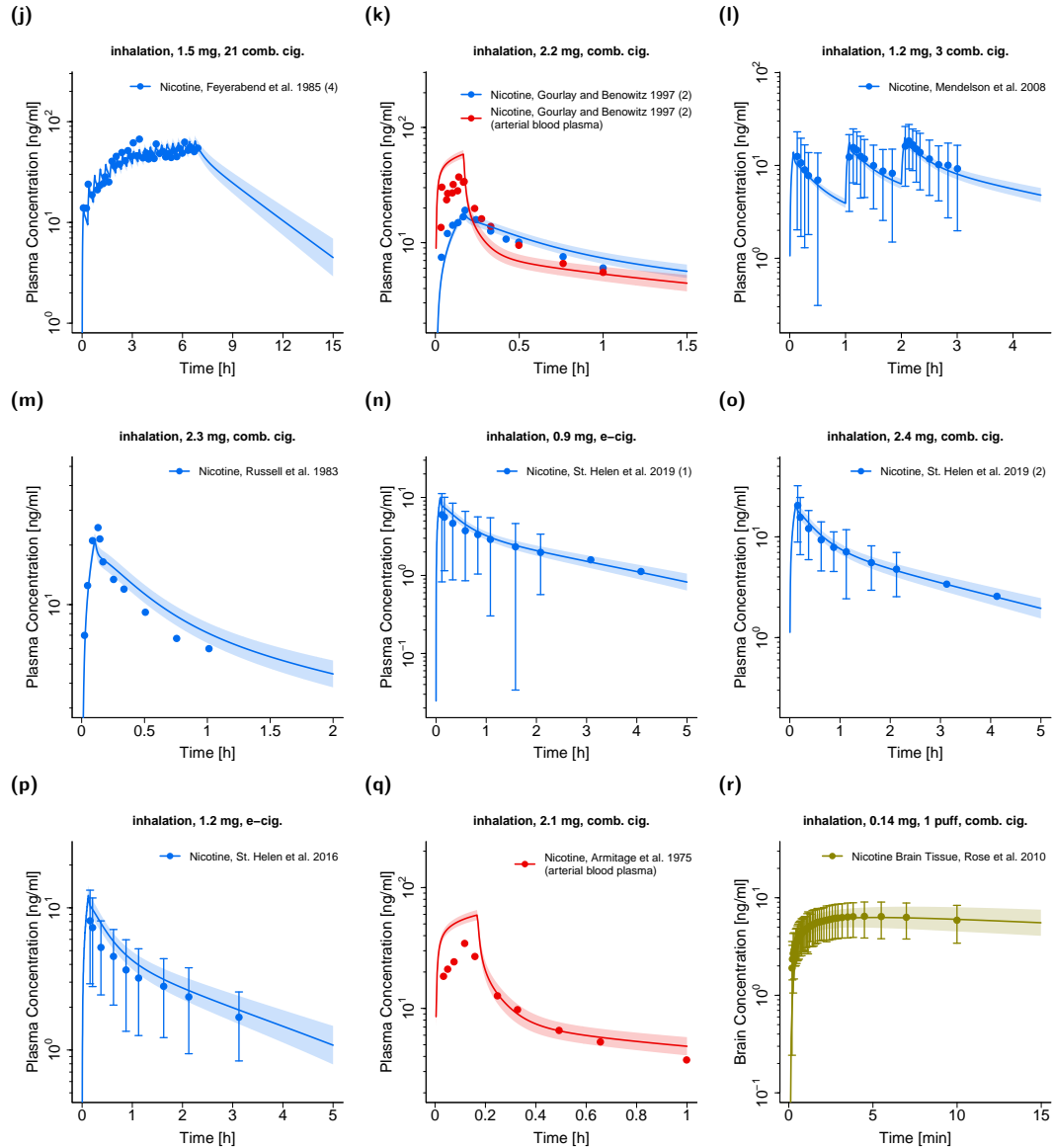
**Figure S3.5.1: Nicotine plasma (●, ●) and brain tissue (●) concentration-time profiles (linear) after inhalation (combustible cigarettes and e-cigarettes).** Observed data are shown as circles, if available  $\pm$  standard deviation (SD). Population simulation ( $n=100$ ) geometric means are shown as lines; the shaded areas represent the predicted population geometric SD. For venous blood plasma simulations (–) estimated pulmonary nicotine exposures for combustible cigarettes were used (see Table S2.8.2). References with numbers in parentheses link to a specific observed dataset described in the study table (Table S2.6.1). Predicted and observed  $AUC_{last}$  and  $C_{max}$  values are compared in Table S3.8.2. **comb. cig.**, combustible cigarette; **e-cig.**, e-cigarette; **iv**, intravenous.



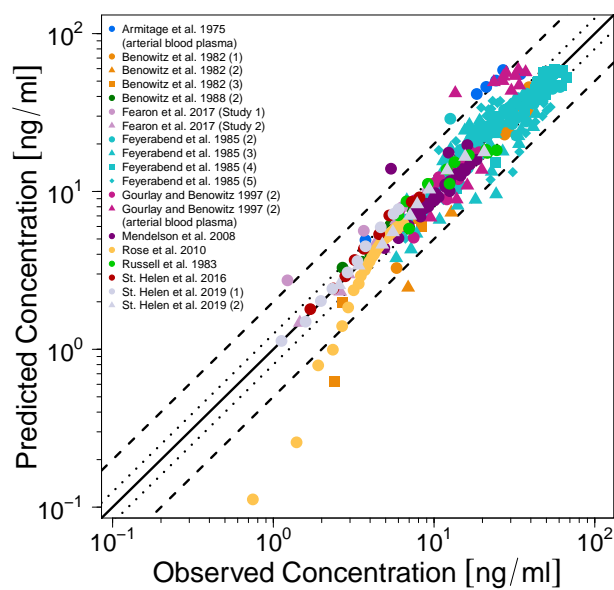
**Figure S3.5.1: Nicotine plasma (●, ●) and brain tissue (●) concentration-time profiles (linear) after inhalation (combustible cigarettes and e-cigarettes).** Observed data are shown as circles, if available  $\pm$  standard deviation (SD). Population simulation ( $n=100$ ) geometric means are shown as lines; the shaded areas represent the predicted population geometric SD. For venous blood plasma simulations (–) estimated pulmonary nicotine exposures for combustible cigarettes were used (see Table S2.8.2). References with numbers in parentheses link to a specific observed dataset described in the study table (Table S2.6.1). Predicted and observed  $AUC_{last}$  and  $C_{max}$  values are compared in Table S3.8.2. **comb. cig.**, combustible cigarette; **e-cig.**, e-cigarette; **iv**, intravenous. (continued)



**Figure S3.5.2: Nicotine plasma (●, ●) and brain tissue (●) concentration-time profiles (semilogarithmic) after inhalation (combustible cigarettes and e-cigarettes).** Observed data are shown as circles, if available  $\pm$  standard deviation (SD). Population simulation ( $n=100$ ) geometric means are shown as lines; the shaded areas represent the predicted population geometric SD. For venous blood plasma simulations (–) estimated pulmonary nicotine exposures for combustible cigarettes were used (see Table S2.8.2). References with numbers in parentheses link to a specific observed dataset described in the study table (Table S2.6.1). Predicted and observed  $AUC_{last}$  and  $C_{max}$  values are compared in Table S3.8.2. **comb. cig.**, combustible cigarette; **e-cig.**, e-cigarette; **iv**, intravenous.

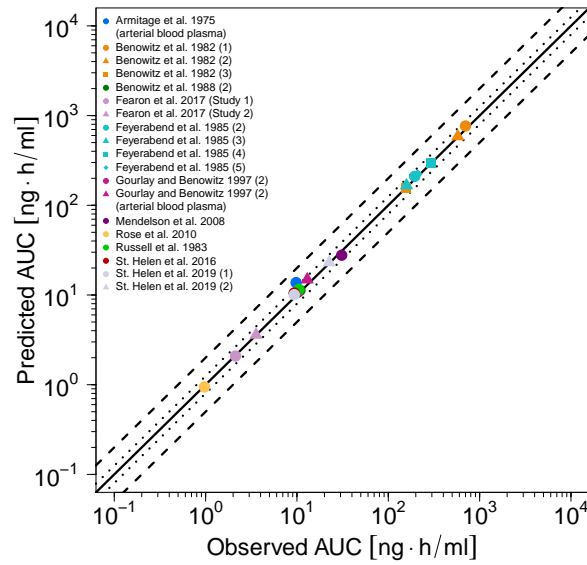
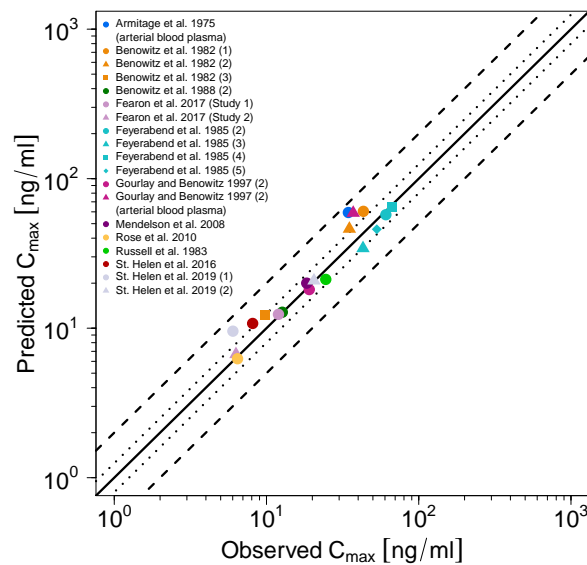


**Figure S3.5.2: Nicotine plasma (•, ●) and brain tissue (●) concentration-time profiles (semilogarithmic) after inhalation (combustible cigarettes and e-cigarettes).** Observed data are shown as circles, if available  $\pm$  standard deviation (SD). Population simulation ( $n=100$ ) geometric means are shown as lines; the shaded areas represent the predicted population geometric SD. For venous blood plasma simulations (–) estimated pulmonary nicotine exposures for combustible cigarettes were used (see Table S2.8.2). References with numbers in parentheses link to a specific observed dataset described in the study table (Table S2.6.1). Predicted and observed  $AUC_{last}$  and  $C_{max}$  values are compared in Table S3.8.2. **comb. cig.**, combustible cigarette; **e-cig.**, e-cigarette; **iv**, intravenous. (continued)



**Figure S3.5.3: Predicted versus observed nicotine concentrations after pulmonary administration of combustible cigarettes (with estimated pulmonary nicotine exposure) and e-cigarettes.** The black solid (—) line marks the line of identity. Black dotted lines (.....) indicate 1.25-fold, black dashed lines (- -) indicate 2-fold deviation.

(a) AUC

(b)  $C_{\max}$ 

**Figure S3.5.4: Predicted versus observed nicotine AUC (a) and  $C_{\max}$  (b) values after pulmonary administration of combustible cigarettes (with estimated pulmonary nicotine exposure) and e-cigarettes.** Each symbol represents the  $AUC_{\text{last}}$  or  $C_{\max}$  of a different profile. The black solid (—) lines mark the lines of identity. Black dotted lines (⋯) indicate 1.25-fold, black dashed lines (--) indicate 2-fold deviation. **AUC**, area under the concentration–time curve from the first to the last data point;  **$C_{\max}$** , maximum concentration.

### 3.6 Pulmonary administration of nicotine (combustible cigarettes with machine smoked nicotine yields)

In this section, linear and semilogarithmic plots of plasma concentration-time profiles (Figs. S3.6.1 and S3.6.2), goodness-of-fit plots of predicted compared to observed plasma concentrations (Fig. S3.6.3) and goodness-of-fit plots of predicted compared to observed  $AUC_{last}$  and  $C_{max}$  values (Fig. S3.6.4) after administration of combustible cigarettes (with machine smoked nicotine yields) are shown.

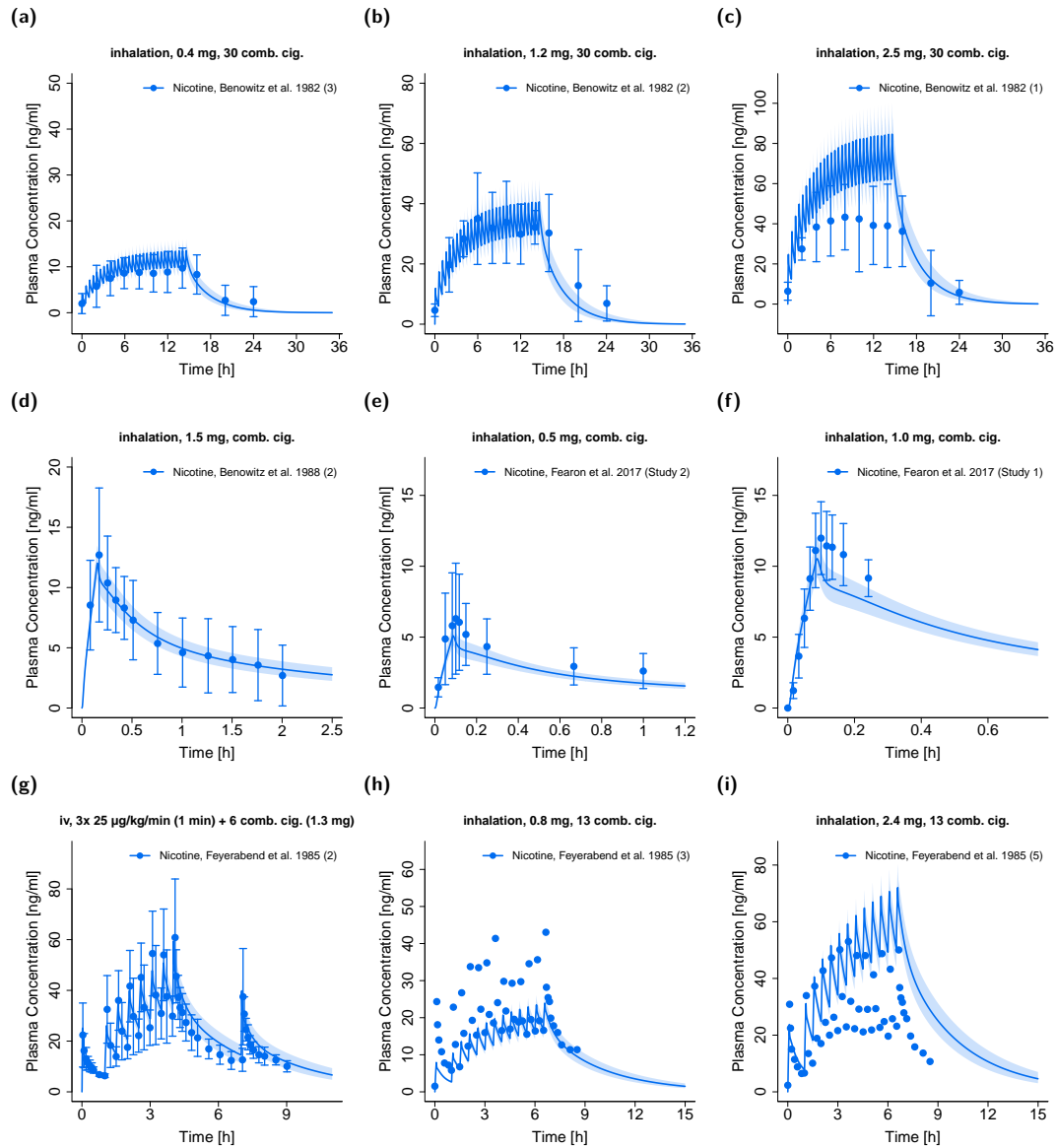


**Figure S3.6.1: Nicotine plasma (•, •) concentration-time profiles (linear) after inhalation (combustible cigarettes with machine smoked nicotine yields).** Observed data are shown as circles, if available  $\pm$  standard deviation (SD). Population simulation ( $n=100$ ) geometric means are shown as lines; the shaded areas represent the predicted population geometric SD. Machine smoked nicotine yields from the respective studies were used for nicotine doses (see Table S2.8.2). References with numbers in parentheses link to a specific observed dataset described in the study table (Table S2.6.1). **comb. cig.**, combustible cigarette; **iv**, intravenous.

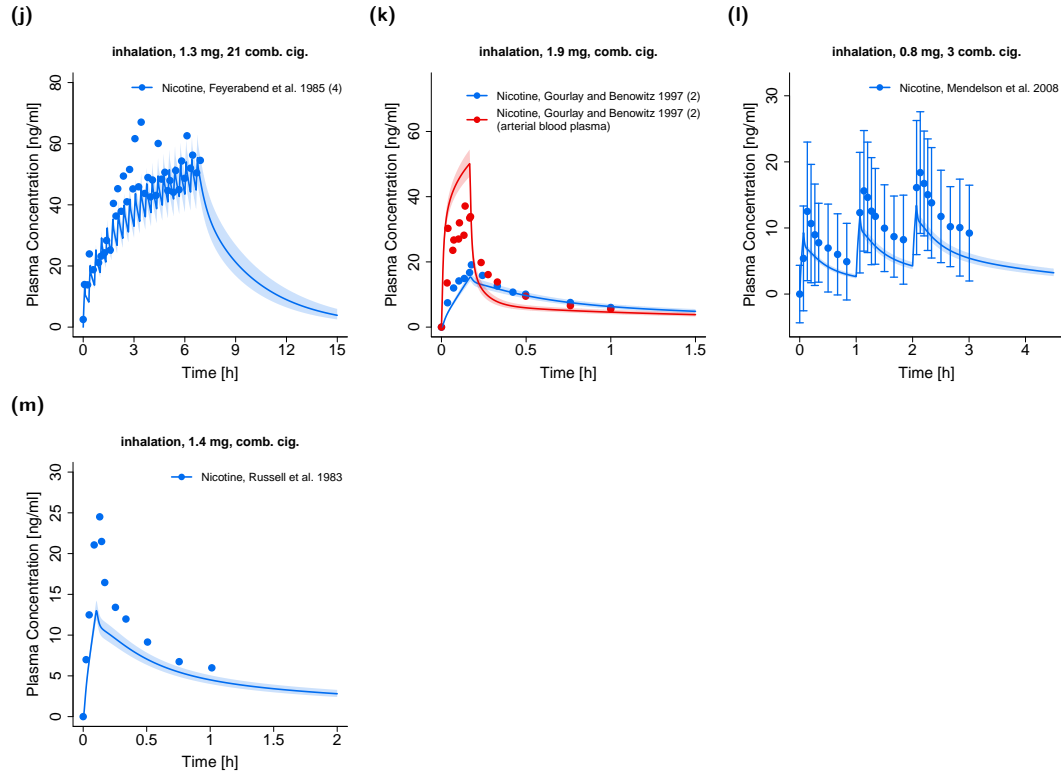


**Figure S3.6.1: Nicotine plasma (•, •) concentration-time profiles (linear) after inhalation (combustible cigarettes with machine smoked nicotine yields).** Observed data are shown as circles, if available  $\pm$  standard deviation (SD). Population simulation ( $n=100$ ) geometric means are shown as lines; the shaded areas represent the predicted population geometric SD. Machine smoked nicotine yields from the respective studies were used for nicotine doses (see Table S2.8.2). References with numbers in parentheses link to a specific observed dataset described in the study table (Table S2.6.1). **comb. cig.**, combustible cigarette; **iv**, intravenous. (continued)

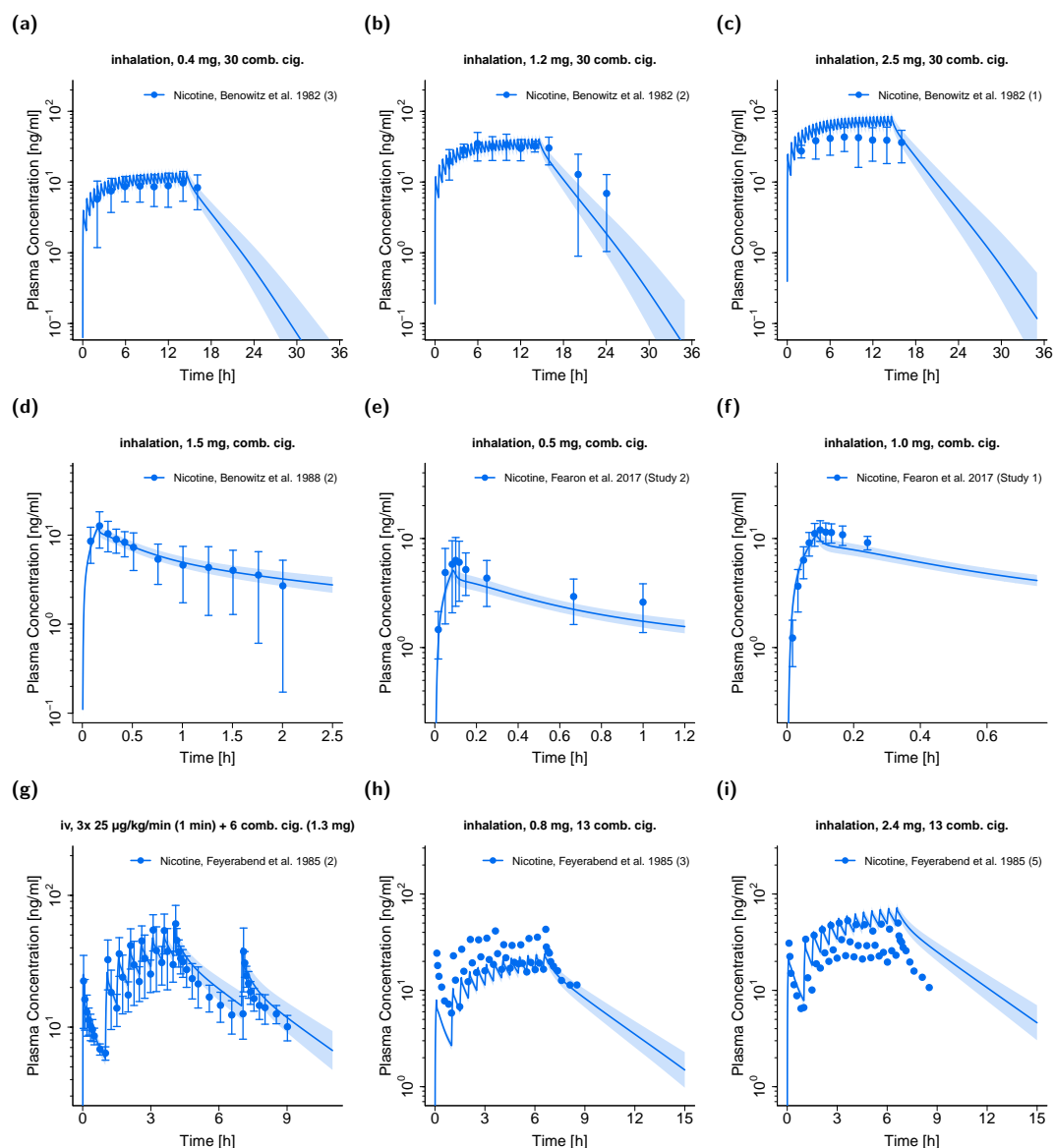


**Figure S3.6.2: Nicotine plasma (●, ●) concentration-time profiles (semilogarithmic) after inhalation (combustible cigarettes with machine smoked nicotine yields).** Observed data are shown as circles, if available  $\pm$  standard deviation (SD). Population simulation ( $n=100$ ) geometric means are shown as lines; the shaded areas represent the predicted population geometric SD. Machine smoked nicotine yields from the respective studies were used for nicotine doses (see Table S2.8.2). References with numbers in parentheses link to a specific observed dataset described in the study table (Table S2.6.1). **comb. cig.**, combustible cigarette; **iv**, intravenous.

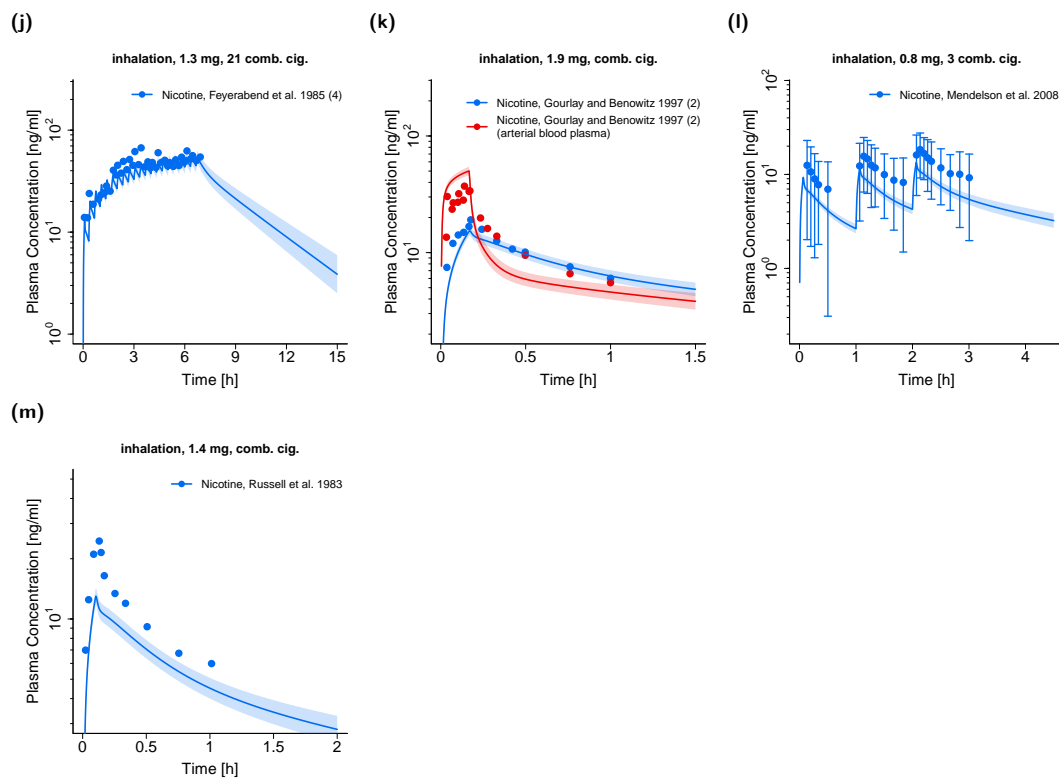


**Figure S3.6.2: Nicotine plasma (•, •) concentration-time profiles (semilogarithmic) after inhalation (combustible cigarettes with machine smoked nicotine yields).** Observed data are shown as circles, if available  $\pm$  standard deviation (SD). Population simulation ( $n=100$ ) geometric means are shown as lines; the shaded areas represent the predicted population geometric SD. Machine smoked nicotine yields from the respective studies were used for nicotine doses (see Table S2.8.2). References with numbers in parentheses link to a specific observed dataset described in the study table (Table S2.6.1). **comb. cig.**, combustible cigarette; **iv**, intravenous. (continued)

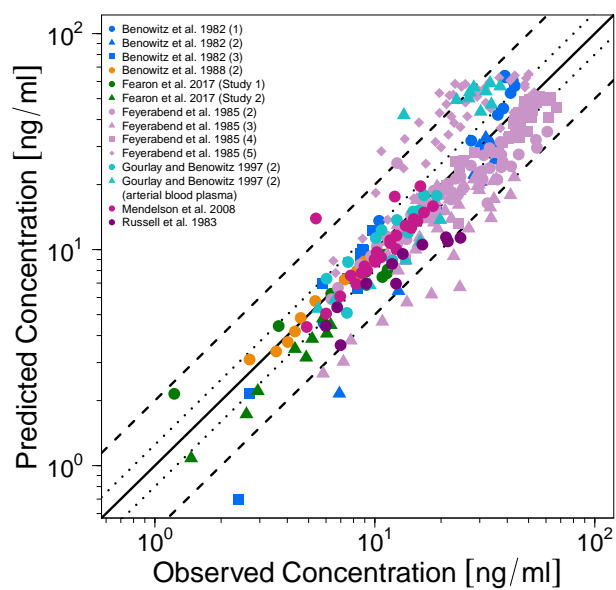
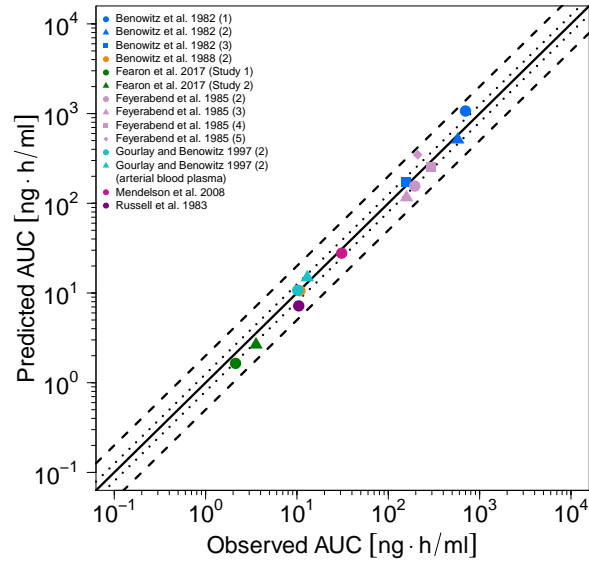
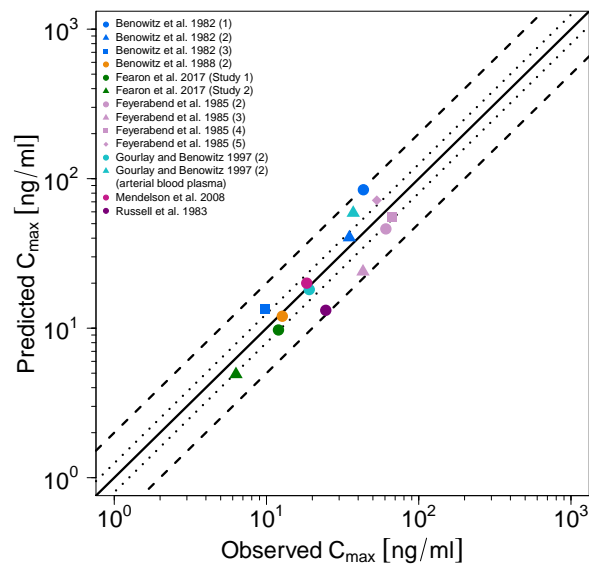


Figure S3.6.3: Predicted versus observed nicotine plasma concentrations after pulmonary administration of combustible cigarettes with machine smoked nicotine yields. The black solid (—) line marks the line of identity. Black dotted lines (.....) indicate 1.25-fold, black dashed lines (---) indicate 2-fold deviation.

(a) AUC

(b) C<sub>max</sub>

**Figure S3.6.4: Predicted versus observed nicotine AUC<sub>last</sub> (a) and C<sub>max</sub> (b) values after pulmonary administration of combustible cigarettes with machine smoked nicotine yields.** Each symbol represents the AUC<sub>last</sub> or C<sub>max</sub> of a different plasma profile. The black solid (—) lines mark the lines of identity. Black dotted lines (····) indicate 1.25-fold, black dashed lines (--) indicate 2-fold deviation. **AUC**, area under the plasma concentration–time curve from the first to the last data point; **C<sub>max</sub>**, maximum plasma concentration.

## 3.7 Brain tissue concentration simulations

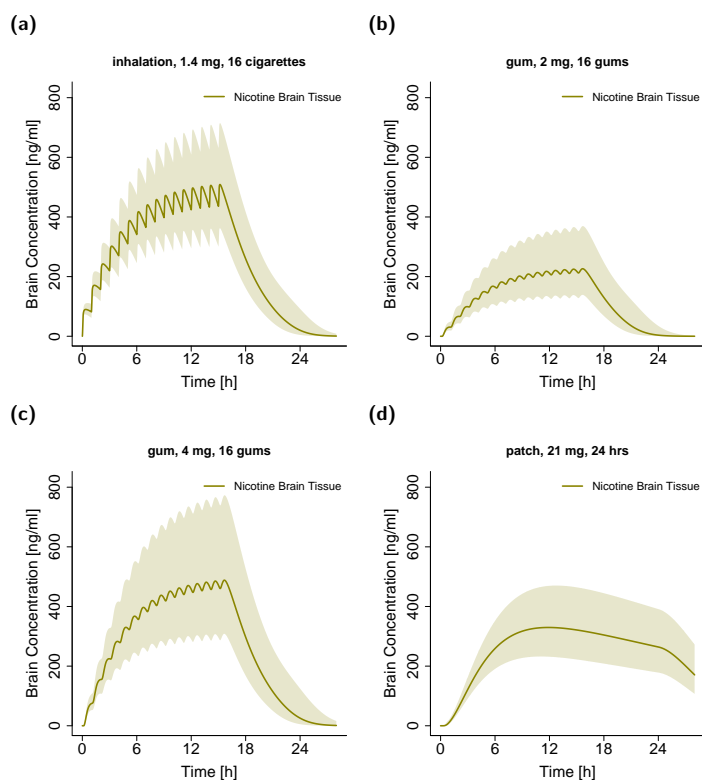


Figure S3.7.1: Simulations of **nicotine brain tissue** concentration-time profiles after pulmonary (16 hours), oral (2 mg and 4 mg gums, 16 hours) and transdermal (patch, 24 hours) nicotine administration. Population simulation (n=100) geometric means are shown as lines (-); the shaded areas represent the predicted population geometric SD. Detailed information about dosing regimens, study populations and model input parameters is given in Tables S2.6.1, S2.8.1 and S2.8.3. **patch**, transdermal therapeutic system (nicotine patch).

### 3.8 Quantitative PBPK model evaluation

As quantitative performance measures, mean relative deviations (MRD) of the predicted plasma concentrations for all observed and the corresponding predicted plasma concentrations and the geometric mean fold errors (GMFE) of the  $AUC_{last}$  and  $C_{max}$  were calculated according to Equation S10 and Equation S11, respectively.

$$MRD = 10^x \text{ with } x = \sqrt{\frac{1}{n} \sum_{i=1}^n (\log_{10} \hat{c}_i - \log_{10} c_i)^2} \quad (S10)$$

Here,  $c_i$  is the  $i$ th observed plasma concentration,  $\hat{c}_i$  is the respective predicted plasma concentration and  $n$  equals the number of observed values. Overall MRD values of  $\leq 2$  were considered as reasonable predictions [68]. MRD values for all studies are given in Table S3.8.1.

The GMFE was calculated for all observed  $AUC_{last}$  and  $C_{max}$  values according to Equation S11.

$$GMFE = 10^x \text{ with } x = \frac{1}{n} \sum_{i=1}^n \left| \log_{10} \left( \frac{\hat{a}_i}{a_i} \right) \right| \quad (S11)$$

Here,  $a_i$  is the  $i$ th observed  $AUC_{last}$  or  $C_{max}$  value, respectively,  $\hat{a}_i$  is the predicted  $AUC_{last}$  or  $C_{max}$  value, respectively, and  $n$  equals the number of studies. The calculated GMFE values are shown in Table S3.8.2.

#### 3.8.1 Mean relative deviation (MRD) values of nicotine and cotinine concentration predictions

**Table S3.8.1:** Mean relative deviation (MRD) values of nicotine and cotinine plasma concentration predictions.

Route	Dose	MRD	Reference
<b>Nicotine</b>			
iv (1 min, s.d.)	25.0 µg/kg	1.41	Feyerabend et al. 1985 (1) [30]
iv (10 min, s.d.)	28.0 µg/kg	1.62	Molander et al. 2001 (young) [32]
iv (10 min, s.d.)	28.0 µg/kg	1.50	Molander et al. 2001 (elderly) [32]
iv (24 h, s.d.)	19.8 mg	1.06	Benowitz et al. 1991a (1) [28]
iv (24 h, s.d.)	288.0 µg/kg	1.12	Benowitz et al. 1994b [29]
iv (30 min, m.d.)	75.0 µg/kg	1.16	Porchet et al. 1988 (1) [23]
iv (30 min, m.d.)	75.0 µg/kg	1.19	Porchet et al. 1988 (2) [23]
iv (30 min, m.d.)	75.0 µg/kg	1.19	Porchet et al. 1988 (3) [23]
iv (30 min, s.d.)	15.0 µg/kg	1.09	Andersson and Arner 2001 [27]
iv (30 min, s.d.)	60.0 µg/kg	1.11	Benowitz and Jacob 1994a (1) [1]
iv (30 min, s.d.)	15.0 µg/kg	1.15	Benowitz and Jacob 1993 (1) [12]
iv (30 min, s.d.)	15.0 µg/kg	1.13	Benowitz and Jacob 1993 (2) [12]
iv (30 min, s.d.)	60.0 µg/kg	1.16	Benowitz and Jacob 1993 (3) [12]
iv (30 min, s.d.)	60.0 µg/kg	1.20	Gourlay and Benowitz 1997 (1) [31]
iv (30 min, s.d.)	60.0 µg/kg	1.40	Gourlay and Benowitz 1997 (1) (arterial blood plasma) [31]
iv (30 min, s.d.)	15.0 µg/kg	1.17	Zevin et al. 1997 (1) [33]
iv (30 min, s.d.)	15.0 µg/kg	1.20	Zevin et al. 1997 (2) [33]
iv and inhalation (1 min, m.d. plus 6 combustible cigarettes)	1.8; 2.0 mg	1.21	Feyerabend et al. 1985 (2) [30]
po (cap, s.d.)	4.0 mg	1.17	Benowitz et al. 1991b (2) [34]
po (cap, s.d.)	3.0 mg	1.26	Benowitz et al. 1991b (1) [34]
po (cap, s.d.)	6.0 mg	1.31	Benowitz et al. 1991b (3) [34]
po (cap, s.d.)	6.0 mg	1.60	Green et al. 1999 (1) [36]
po (cap, s.d.)	15.0 mg	1.48	Green et al. 1999 (2) [36]
po (cap, s.d.)	4.0 mg	3.10	Xu et al. 2002 (NM) [5]
po (cap, s.d.)	4.0 mg	1.75	Xu et al. 2002 (PM) [5]

Overall MRD: 1.52 (80/91 with MRD  $\leq 2$ )

-, not given; **cap**, capsule; **iv**, intravenous; **m.d.**, multiple dose; **MRD**, mean relative deviation;

**NM**, normal metabolizer; **PM**, poor metabolizer; **po**, oral; **q.d.**, once daily; **q.i.d.**, four times daily; **s.d.**, single dose;

<sup>a</sup> cotinine metabolite

Table S3.8.1: Mean relative deviation (MRD) values of nicotine and cotinine plasma concentration predictions. (continued)

Route	Dose	MRD	Reference
gum (m.d., 12 gums)	2.0 mg	1.28	Dautzenberg et al. 2007 [39]
gum (m.d., 12 gums)	4.0 mg	1.37	Hansson et al. 2017 (3) [41]
gum (m.d., 13 gums)	4.0 mg	1.89	Choi et al. 2001 (3) [38]
gum (m.d., 13 gums)	2.0 mg	1.15	Choi et al. 2001 (2) [38]
gum (s.d.)	4.0 mg	3.51	Benowitz et al. 1988 (1) [21]
gum (s.d.)	2.0 mg	2.96	Choi et al. 2001 (1) [38]
gum (s.d.)	4.0 mg	1.21	Choi et al. 2001 (4) [38]
gum (s.d.)	2.0 mg	1.50	Du 2018 (1) [40]
gum (s.d.)	4.0 mg	1.55	Du 2018 (2) [40]
gum (s.d.)	2.0 mg	2.26	Hansson et al. 2017 (1) [41]
gum (s.d.)	4.0 mg	1.72	Hansson et al. 2017 (2) [41]
inhalation (13 combustible cigarettes, m.d.)	1.1 mg	1.40	Feyerabend et al. 1985 (3) [30]
inhalation (13 combustible cigarettes, m.d.)	1.5 mg	1.39	Feyerabend et al. 1985 (5) [30]
inhalation (21 combustible cigarettes, m.d.)	1.5 mg	1.15	Feyerabend et al. 1985 (4) [30]
inhalation (3 combustible cigarettes, m.d.)	1.2 mg	1.27	Mendelson et al. 2008 [48]
inhalation (30 combustible cigarettes, m.d.)	1.8 mg	1.58	Benowitz et al. 1982 (3) [46]
inhalation (30 combustible cigarettes, m.d.)	1.4 mg	1.48	Benowitz et al. 1982 (2) [46]
inhalation (30 combustible cigarettes, m.d.)	0.4 mg	1.25	Benowitz et al. 1982 (1) [46]
inhalation (combustible cigarettes, s.d.)	2.2 mg	1.19	Gourlay and Benowitz 1997 (2) [31]
inhalation (combustible cigarettes, s.d.)	2.2 mg	1.73	Gourlay and Benowitz 1997 (2) (arterial blood plasma) [31]
inhalation (combustible cigarettes, s.d.)	1.6 mg	1.09	Benowitz et al. 1988 (2) [21]
inhalation (combustible cigarettes, s.d.)	0.7 mg	1.08	Fearon et al. 2017 (Study 2) [47]
inhalation (combustible cigarettes, s.d.)	1.3 mg	1.36	Fearon et al. 2017 (Study 1) [47]
inhalation (combustible cigarettes, s.d.)	2.2 mg	1.20	Russell et al. 1983 [49]
inhalation (combustible cigarettes, s.d.)	2.4 mg	1.08	St. Helen et al. 2019 (2) [51]
inhalation (combustible cigarettes, s.d.)	2.1 mg	1.69	Armitage et al. 1975 (arterial blood plasma) [45]
inhalation (combustible cigarettes, s.d.)	0.14 mg	1.57	Rose et al. 2010 [13]
inhalation (e-cigarettes, s.d.)	0.9 mg	1.17	St. Helen et al. 2019 (1) [51]
inhalation (e-cigarettes, s.d.)	1.2 mg	1.16	St. Helen et al. 2016 [50]
transdermal (16 h, m.d.)	15.0 mg	1.08	Fant et al. 2000 (Novartis) [43]
transdermal (24 h, m.d.)	21.0 mg	1.34	Fant et al. 2000 (Alza) [43]
transdermal (24 h, m.d.)	21.0 mg	1.19	Fant et al. 2000 (Upjohn) [43]
transdermal (24 h, m.d., 7 days)	30.0 mg	1.36	Bannon et al. 1989 (3) [42]
transdermal (24 h, q.d., 7 days)	36.0 mg	1.40	Gupta et al. 1993 (2) [44]
transdermal (24 h, s.d.)	52.5 mg	1.56	Benowitz et al. 1991a (2) [28]
transdermal (24 h, s.d.)	15 mg	1.18	Bannon et al. 1989 (1) [42]
transdermal (24 h, s.d.)	30 mg	1.07	Bannon et al. 1989 (2) [42]
transdermal (24 h, s.d.)	60 mg	1.22	Bannon et al. 1989 (4) [42]
transdermal (24 h, s.d.)	36 mg	1.12	Gupta et al. 1993 (1) [44]
<b>Nicotine MRD</b>		<b>1.44</b>	<b>(60/64 with MRD ≤ 2)</b>
<b>Cotinine</b>			
iv (1.5-3 min, s.d.)	20.0 mg	1.10	Curvall et al. 1990 (3) [52]
iv (1.5-3 min, s.d.)	10.0 mg	1.14	Curvall et al. 1990 (2) [52]
iv (1.5-3 min, s.d.)	5.0 mg	1.24	Curvall et al. 1990 (1) [52]
iv (10 min, s.d.) <sup>a</sup>	28.0 µg/kg	1.08	Molander et al. 2001 (young) [32]
iv (10 min, s.d.) <sup>a</sup>	28.0 µg/kg	1.04	Molander et al. 2001 (elderly) [32]
iv (24 h, s.d.) <sup>a</sup>	19.8 mg	4.74	Benowitz et al. 1991a (1) [28]
iv (24 h, s.d.) <sup>a</sup>	288.0 µg/kg	1.32	Benowitz et al. 1994b [29]
iv (30 min, s.d.) <sup>a</sup>	60.0 µg/kg	1.46	Benowitz and Jacob 1994a (1) [1]
iv (30 min, s.d.)	60.0 µg/kg	1.37	Benowitz and Jacob 1994a (2) [1]
iv (30 min, s.d.) <sup>a</sup>	15.0 µg/kg	1.87	Benowitz and Jacob 1993 (1) [12]
iv (30 min, s.d.) <sup>a</sup>	60.0 µg/kg	2.22	Benowitz and Jacob 1993 (2) [12]
iv (30 min, s.d.) <sup>a</sup>	60.0 µg/kg	1.68	Benowitz and Jacob 1993 (3) [12]
iv (30 min, s.d.) <sup>a</sup>	60.0 µg/kg	2.32	Gourlay and Benowitz 1997 (1) [31]
iv (30 min, s.d.) <sup>a</sup>	60.0 µg/kg	2.36	Gourlay and Benowitz 1997 (1) (arterial blood plasma) [31]
iv (30 min, s.d.)	15.0 µg/kg	1.25	Zevin et al. 1997 (3) [33]
iv (30 min, s.d.)	15.0 µg/kg	1.26	Zevin et al. 1997 (4) [33]
iv (30 min, s.d.)	20.0 mg	1.10	De Schepper et al. 1987 (3) [4]
iv (30 min, s.d.)	10.0 mg	1.14	De Schepper et al. 1987 (2) [4]
<b>Overall MRD: 1.52 (80/91 with MRD ≤ 2)</b>			

-, not given; **cap**, capsule; **iv**, intravenous; **m.d.**, multiple dose; **MRD**, mean relative deviation;

**NM**, normal metabolizer; **PM**, poor metabolizer; **po**, oral; **q.d.**, once daily; **q.i.d.**, four times daily; **s.d.**, single dose;

<sup>a</sup> cotinine metabolite

**Table S3.8.1:** Mean relative deviation (MRD) values of nicotine and cotinine plasma concentration predictions. (*continued*)

Route	Dose	MRD	Reference
iv (30 min, s.d.)	5.0 mg	1.09	De Schepper et al. 1987 (1) [4]
po (-, q.i.d., 5 days) <sup>a</sup>	0.05 mg	1.42	Benowitz et al. 2010 [35]
po (cap, 7 times/day, 5 days) <sup>a</sup>	4.0 mg	2.14	Jarvis et al. 1988 [37]
po (cap, s.d.) <sup>a</sup>	6.0 mg	1.12	Green et al. 1999 (1) [36]
po (cap, s.d.) <sup>a</sup>	15.0 mg	1.18	Green et al. 1999 (2) [36]
po (cap, s.d.) <sup>a</sup>	4.0 mg	2.01	Xu et al. 2002 (NM) [5]
po (cap, s.d.) <sup>a</sup>	4.0 mg	2.20	Xu et al. 2002 (PM) [5]
transdermal (24 h, q.d., 7 days) <sup>a</sup>	36.0 mg	1.06	Gupta et al. 1993 (2) [44]
transdermal (24 h, s.d.) <sup>a</sup>	36.0 mg	1.91	Gupta et al. 1993 (1) [44]
<b>Cotinine MRD</b>		<b>1.77</b>	<b>(20/27 with MRD ≤ 2)</b>
<b>Overall MRD: 1.52 (80/91 with MRD ≤ 2)</b>			
-, not given; <b>cap</b> , capsule; <b>iv</b> , intravenous; <b>m.d.</b> , multiple dose; <b>MRD</b> , mean relative deviation;			
<b>NM</b> , normal metabolizer; <b>PM</b> , poor metabolizer; <b>po</b> , oral; <b>q.d.</b> , once daily; <b>q.i.d.</b> , four times daily; <b>s.d.</b> , single dose;			
<sup>a</sup> cotinine metabolite			

## 3.8.2 Geometric mean fold error (GMFE) for nicotine and cotinine concentration-time profiles

Table S3.8.2: Predicted and observed  $AUC_{last}$  and  $C_{max}$  values of nicotine, cotinine metabolite and cotinine after intravenous administration

Route	Dose	$AUC_{last}$			$C_{max}$			Reference
		Pred	Obs	Pred/Obs	Pred	Obs	Pred/Obs	
<b>Nicotine</b>								
iv (1 min, s.d.)	25.0 µg/kg	9.52	10.09	0.94	24.01	23.05	1.04	Feyerabend et al. 1985 (1) [30]
iv (10 min, s.d.)	28.0 µg/kg	28.70	24.92	1.15	17.63	10.51	1.68	Molander et al. 2001 (young) [32]
iv (10 min, s.d.)	28.0 µg/kg	37.25	32.47	1.15	21.91	17.29	1.27	Molander et al. 2001 (elderly) [32]
iv (24 h, s.d.)	19.8 mg	282.59	286.29	0.99	11.88	13.19	0.90	Benowitz et al. 1991a (1) [28]
iv (24 h, s.d.)	288.0 µg/kg	304.03	285.59	1.06	13.14	15.07	0.87	Benowitz et al. 1994b [29]
iv (30 min, m.d.)	75.0 µg/kg	141.94	125.34	1.13	52.92	45.36	1.17	Porchet et al. 1988 (1) [23]
iv (30 min, m.d.)	75.0 µg/kg	132.54	117.64	1.13	49.40	37.91	1.30	Porchet et al. 1988 (2) [23]
iv (30 min, m.d.)	75.0 µg/kg	117.40	103.33	1.14	45.99	39.51	1.16	Porchet et al. 1988 (3) [23]
iv (30 min, s.d.)	15.0 µg/kg	6.62	6.74	0.98	7.59	7.42	1.02	Andersson and Arner 2001 [27]
iv (30 min, s.d.)	60.0 µg/kg	55.19	50.80	1.09	29.18	24.22	1.20	Benowitz and Jacob 1994a (1) [1]
iv (30 min, s.d.)	15.0 µg/kg	12.14	10.80	1.12	7.93	6.19	1.28	Benowitz and Jacob 1993 (1) [12]
iv (30 min, s.d.)	15.0 µg/kg	12.40	12.87	0.96	8.02	8.31	0.97	Benowitz and Jacob 1993 (2) [12]
iv (30 min, s.d.)	60.0 µg/kg	62.36	59.51	1.05	31.87	29.62	1.08	Benowitz and Jacob 1993 (3) [12]
iv (30 min, s.d.)	60.0 µg/kg	21.19	19.50	1.09	32.42	28.81	1.12	Gourlay and Benowitz 1997 (1) [31]
iv (30 min, s.d.)	60.0 µg/kg	30.85	29.86	1.03	56.34	48.36	1.17	Gourlay and Benowitz 1997 (1) (arterial blood plasma) [31]
iv (30 min, s.d.)	15.0 µg/kg	13.06	13.00	1.00	7.44	6.96	1.07	Zevin et al. 1997 (1) [33]
iv (30 min, s.d.)	15.0 µg/kg	13.06	13.35	0.98	7.44	7.58	0.98	Zevin et al. 1997 (2) [33]
iv and inhalation (1 min, m.d. plus 6 combustible cigarettes)	1.8; 2.0 mg	210.37	194.84	1.08	57.41	60.83	0.94	Feyerabend et al. 1985 (2) [30]
po (cap, s.d.)	4.0 mg	17.24	18.70	0.92	6.24	6.39	0.98	Benowitz et al. 1991b (2) [34]
po (cap, s.d.)	3.0 mg	22.28	21.08	1.06	8.14	7.51	1.08	Benowitz et al. 1991b (1) [34]
po (cap, s.d.)	6.0 mg	32.16	39.65	0.81	11.88	18.75	0.63	Benowitz et al. 1991b (3) [34]
po (cap, s.d.)	6.0 mg	20.96	23.69	0.88	2.10	2.20	0.96	Green et al. 1999 (1) [36]
po (cap, s.d.)	15.0 mg	52.25	47.69	1.10	5.10	5.00	1.02	Green et al. 1999 (2) [36]
po (cap, s.d.)	4.0 mg	20.91	29.45	0.71	7.18	7.74	0.93	Xu et al. 2002 (NM) [5]
po (cap, s.d.)	4.0 mg	67.38	112.77	0.60	19.30	22.15	0.87	Xu et al. 2002 (PM) [5]
gum (m.d., 12 gums)	2.0 mg	115.38	105.77	1.09	10.24	9.58	1.07	Dautzenberg et al. 2007 [39]
gum (m.d., 12 gums)	4.0 mg	185.20	232.74	0.80	20.65	29.68	0.70	Hansson et al. 2017 (3) [41]
gum (m.d., 13 gums)	4.0 mg	22.63	34.08	0.66	9.40	9.91	0.95	Choi et al. 2001 (3) [38]
gum (m.d., 13 gums)	2.0 mg	120.80	101.20	1.19	12.56	14.30	0.88	Choi et al. 2001 (2) [38]
gum (s.d.)	4.0 mg	8.30	9.76	0.85	6.57	6.50	1.01	Benowitz et al. 1988 (1) [21]
gum (s.d.)	2.0 mg	11.36	10.01	1.13	4.71	3.64	1.29	Choi et al. 2001 (1) [38]
gum (s.d.)	4.0 mg	241.18	217.14	1.11	25.16	30.10	0.84	Choi et al. 2001 (4) [38]
gum (s.d.)	2.0 mg	10.73	10.37	1.03	4.08	3.37	1.21	Du 2018 (1) [40]
gum (s.d.)	4.0 mg	21.40	21.48	1.00	8.10	6.47	1.25	Du 2018 (2) [40]

Total GMFE ( $AUC_{last}$ ): 1.12 (1.00–1.80)Total GMFE ( $C_{max}$ ): 1.15 (1.00–1.72)-, not given; AUC, area under the concentration-time curve from the first to the last data point; cap, capsule;  $C_{max}$ , maximum concentration; GMFE, geometric mean fold error;

iv, intravenous; m.d., multiple dose; NM, normal metabolizer; obs, observed; PM, poor metabolizer; po, oral; pred, predicted; q.i.d., four times daily; s.d., single dose;

<sup>a</sup> cotinine metabolite

Table S3.8.2: Predicted and observed AUC<sub>last</sub> and C<sub>max</sub> values of nicotine, cotinine after intravenous administration and cotinine metabolite (continued)

Route	Dose	AUC <sub>last</sub>			C <sub>max</sub>			Reference
		Pred	Obs	Pred/Obs	Pred	Obs	Pred/Obs	
gum (s.d.)	2.0 mg	12.43	21.11	0.59	4.53	6.59	0.69	Hansson et al. 2017 (1) [41]
gum (s.d.)	4.0 mg	25.07	33.92	0.74	9.02	10.13	0.89	Hansson et al. 2017 (2) [41]
inhalation (13 combustible cigarettes, m.d.)	1.1 mg	166.34	158.34	1.05	34.22	43.04	0.80	Feyerabend et al. 1985 (3) [30]
inhalation (13 combustible cigarettes, m.d.)	1.5 mg	222.82	209.81	1.06	45.87	53.04	0.86	Feyerabend et al. 1985 (5) [30]
inhalation (21 combustible cigarettes, m.d.)	1.5 mg	292.69	291.80	1.00	64.21	67.05	0.96	Feyerabend et al. 1985 (4) [30]
inhalation (3 combustible cigarettes, m.d.)	1.2 mg	27.80	30.89	0.90	20.01	18.38	1.09	Mendelson et al. 2008 [48]
inhalation (30 combustible cigarettes, m.d.)	1.8 mg	155.80	156.44	1.00	12.26	9.72	1.26	Benowitz et al. 1982 (3) [46]
inhalation (30 combustible cigarettes, m.d.)	1.4 mg	585.29	576.54	1.02	46.16	35.03	1.32	Benowitz et al. 1982 (2) [46]
inhalation (30 combustible cigarettes, m.d.)	0.4 mg	766.59	700.24	1.09	60.49	43.29	1.40	Benowitz et al. 1982 (1) [46]
inhalation (combustible cigarettes, s.d.)	2.2 mg	10.73	10.20	1.05	18.12	19.10	0.95	Gourlay and Benowitz 1997 (2) [31]
inhalation (combustible cigarettes, s.d.)	2.2 mg	14.87	12.97	1.15	58.99	37.13	1.59	Gourlay and Benowitz 1997 (2) (arterial blood plasma) [31]
inhalation (combustible cigarettes, s.d.)	1.6 mg	11.27	10.79	1.04	12.79	12.70	1.01	Benowitz et al. 1988 (2) [21]
inhalation (combustible cigarettes, s.d.)	0.7 mg	3.60	3.57	1.01	6.69	6.30	1.06	Fearon et al. 2017 (Study 2) [47]
inhalation (combustible cigarettes, s.d.)	1.3 mg	2.09	2.13	0.98	12.38	11.98	1.03	Fearon et al. 2017 (Study 1) [47]
inhalation (combustible cigarettes, s.d.)	2.2 mg	11.53	10.46	1.10	21.21	24.51	0.87	Russell et al. 1983 [49]
inhalation (combustible cigarettes, s.d.)	2.4 mg	23.06	22.58	1.02	20.80	20.50	1.01	St. Helen et al. 2019 (2) [51]
inhalation (combustible cigarettes, s.d.)	2.1 mg	13.76	9.79	1.41	59.41	34.50	1.72	Armitage et al. 1975 (arterial blood plasma) [45]
inhalation (combustible cigarettes, s.d.)	0.14 mg	0.94	0.97	0.97	6.25	6.45	0.97	Rose et al. 2010 [13]
inhalation (e-cigarettes, s.d.)	0.9 mg	10.10	9.34	1.08	9.55	6.02	1.59	St. Helen et al. 2019 (1) [51]
inhalation (e-cigarettes, s.d.)	1.2 mg	10.52	9.33	1.13	10.76	8.11	1.33	St. Helen et al. 2016 [50]
transdermal (16 h, m.d.)	15.0 mg	997.83	989.51	1.01	16.41	17.97	0.91	Fant et al. 2000 (Novartis) [43]
transdermal (24 h, m.d.)	21.0 mg	1168.23	1107.57	1.05	18.62	26.65	0.70	Fant et al. 2000 (Alza) [43]
transdermal (24 h, m.d.)	21.0 mg	516.08	521.19	0.99	9.96	11.52	0.86	Fant et al. 2000 (Upjohn) [43]
transdermal (24 h, q.d., 7 days)	30.0 mg	568.18	457.57	1.24	15.98	15.19	1.05	Bannon et al. 1989 (3) [42]
transdermal (24 h, s.d.)	36.0 mg	451.81	366.48	1.23	17.16	19.33	0.89	Gupta et al. 1993 (2) [44]
transdermal (24 h, s.d.)	52.5 mg	188.12	190.92	0.99	7.96	9.51	0.84	Benowitz et al. 1991a (2) [28]
transdermal (24 h, s.d.)	15.0 mg	151.09	150.41	1.00	7.42	6.86	1.08	Bannon et al. 1989 (1) [42]
transdermal (24 h, s.d.)	30.0 mg	300.41	288.76	1.04	14.81	15.76	0.94	Bannon et al. 1989 (2) [42]
transdermal (24 h, s.d.)	60.0 mg	600.29	501.96	1.20	29.60	26.98	1.10	Bannon et al. 1989 (4) [42]
transdermal (24 h, s.d.)	36.0 mg	417.71	409.07	1.02	15.87	18.12	0.88	Gupta et al. 1993 (1) [44]
<b>Nicotine GMFE</b>		<b>1.11 (1.00–1.70)</b>			<b>1.17 (1.01–1.72)</b>			
<b>Cotinine</b>								
iv (1.5–3 min, s.d.)	20.0 mg	1123.80	1091.34	1.03	207.30	138.84	1.49	Curvall et al. 1990 (3) [52]
iv (1.5–3 min, s.d.)	10.0 mg	2278.15	2367.41	0.96	414.59	326.58	1.27	Curvall et al. 1990 (2) [52]
iv (1.5–3 min, s.d.)	5.0 mg	5120.26	5019.92	1.02	829.19	640.50	1.29	Curvall et al. 1990 (1) [52]
iv (10 min, s.d.) <sup>a</sup>	28.0 µg/kg	587.72	622.84	0.94	61.40	62.36	0.98	Molander et al. 2001 (young) [32]
iv (10 min, s.d.) <sup>a</sup>	28.0 µg/kg	868.09	882.38	0.98	84.08	86.76	0.97	Molander et al. 2001 (elderly) [32]
<b>Total GMFE (AUC<sub>last</sub>): 1.12 (1.00–1.80)</b>		<b>1.11 (1.00–1.70)</b>			<b>1.17 (1.01–1.72)</b>			
<b>Total GMFE (C<sub>max</sub>) : 1.15 (1.00–1.72)</b>								

<sup>a</sup>, not given; AUC, area under the concentration–time curve from the first to the last data point; cap, capsule; C<sub>max</sub>, maximum concentration; GMFE, geometric mean fold error;

iv, intravenous; m.d., multiple dose; NM, normal metabolizer; obs, observed; PM, poor metabolizer; po, oral; pred, predicted; q.d., four times daily; s.d., single dose;

<sup>a</sup> cotinine metabolite

Table S3.8.2: Predicted and observed  $AUC_{last}$  and  $C_{max}$  values of nicotine, cotinine after intravenous administration and cotinine metabolite (continued)

Route	Dose	$AUC_{last}$			$C_{max}$			Reference
		Pred	Obs	Pred/Obs	Pred	Obs	Pred/Obs	
iv (24 h, s.d.) <sup>a</sup>	19.8 mg	2556.29	2683.54	0.95	124.38	141.56	0.88	Benowitz et al. 1991a (1) [28]
iv (24 h, s.d.) <sup>a</sup>	288.0 µg/kg	3121.84	3278.14	0.95	134.73	158.64	0.85	Benowitz et al. 1994b [29]
iv (30 min, s.d.) <sup>a</sup>	60.0 µg/kg	830.69	1028.67	0.81	36.88	39.28	0.94	Benowitz and Jacob 1994a (1) [1]
iv (30 min, s.d.) <sup>a</sup>	60.0 µg/kg	1125.82	1317.41	0.85	112.74	86.71	1.30	Benowitz and Jacob 1994a (2) [1]
iv (30 min, s.d.) <sup>a</sup>	15.0 µg/kg	253.91	342.80	0.74	10.03	10.69	0.94	Benowitz and Jacob 1993 (1) [12]
iv (30 min, s.d.) <sup>a</sup>	60.0 µg/kg	245.43	440.95	0.56	9.68	10.49	0.92	Benowitz and Jacob 1993 (2) [12]
iv (30 min, s.d.) <sup>a</sup>	60.0 µg/kg	981.12	1228.36	0.80	37.76	37.29	1.01	Benowitz and Jacob 1993 (3) [12]
iv (30 min, s.d.) <sup>a</sup>	60.0 µg/kg	189.53	183.33	1.03	37.97	36.61	1.04	Gourlay and Benowitz 1997 (1) [31]
iv (30 min, s.d.) <sup>a</sup>	60.0 µg/kg	198.99	198.82	1.00	38.10	38.01	1.00	Gourlay and Benowitz 1997 (1) (arterial blood plasma) [31]
iv (30 min, s.d.)	15.0 µg/kg	228.90	248.78	0.92	28.26	20.98	1.35	Zevin et al. 1997 (3) [33]
iv (30 min, s.d.)	15.0 µg/kg	228.93	264.75	0.86	28.26	27.57	1.03	Zevin et al. 1997 (4) [33]
iv (30 min, s.d.)	20.0 mg	1332.21	1329.89	1.00	136.93	137.05	1.00	De Schepper et al. 1987 (3) [4]
iv (30 min, s.d.)	10.0 mg	2664.42	2322.18	1.15	273.85	286.25	0.96	De Schepper et al. 1987 (2) [4]
iv (30 min, s.d.)	5.0 mg	5328.83	5034.70	1.06	547.70	517.04	1.06	De Schepper et al. 1987 (1) [4]
po (-, q.i.d., 5 days) <sup>a</sup>	0.05 mg	22.68	27.48	0.83	2.48	2.42	1.02	Benowitz et al. 2010 [35]
po (cap, 7 times/day, 5 days) <sup>a</sup>	4.0 mg	3161.91	5705.77	0.55	336.93	294.00	1.15	Jarvis et al. 1988 [37]
po (cap, s.d.) <sup>a</sup>	6.0 mg	813.08	769.41	1.06	32.07	32.19	1.00	Green et al. 1999 (1) [36]
po (cap, s.d.) <sup>a</sup>	15.0 mg	2030.27	1942.74	1.05	79.60	91.85	0.87	Green et al. 1999 (2) [36]
po (cap, s.d.) <sup>a</sup>	4.0 mg	291.79	235.60	1.24	61.21	58.91	1.04	Xu et al. 2002 (NM) [5]
po (cap, s.d.) <sup>a</sup>	4.0 mg	23.67	20.36	1.16	5.29	6.42	0.83	Xu et al. 2002 (PM) [5]
transdermal (24 h, q.d., 7 days) <sup>a</sup>	36.0 mg	7638.70	7499.03	1.02	228.97	243.25	0.94	Gupta et al. 1993 (2) [44]
transdermal (24 h, s.d.) <sup>a</sup>	36.0 mg	4106.03	4172.18	0.98	155.78	156.90	0.99	Gupta et al. 1993 (1) [44]
<b>Cotinine GMFE</b>			<b>1.14 (1.00–1.80)</b>			<b>1.11 (1.00–1.49)</b>		
<b>Total GMFE (<math>AUC_{last}</math>):</b>			<b>1.12 (1.00–1.80)</b>					
<b>Total GMFE (<math>C_{max}</math>):</b>			<b>1.15 (1.00–1.72)</b>					

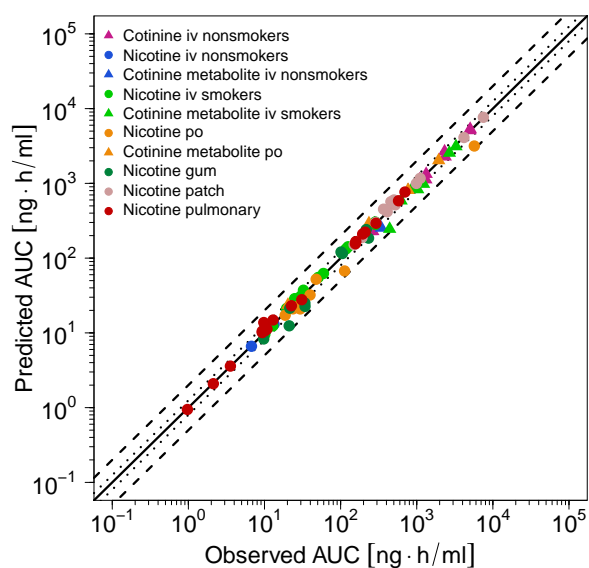
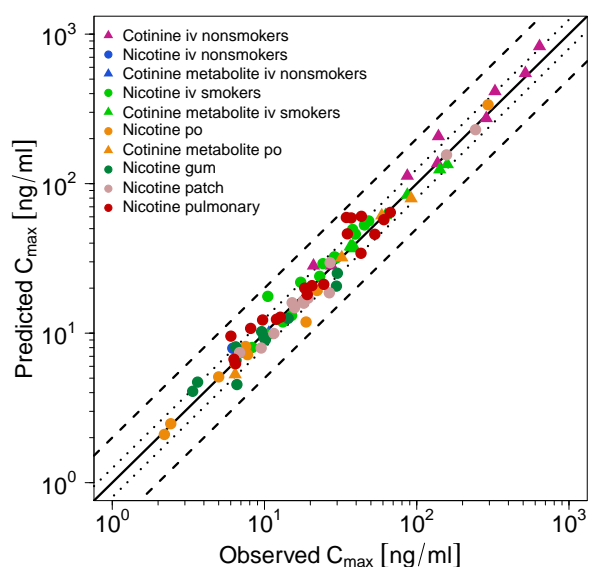
<sup>a</sup>, not given;  $AUC$ , area under the concentration–time curve from the first to the last data point; **cap**, capsule;  **$C_{max}$** , maximum concentration; **GMFE**, geometric mean fold error;

iv, intravenous; m.d., multiple dose; NM, normal metabolizer; obs, observed; PM, poor metabolizer; po, oral; pred, predicted; q.d., once daily; q.i.d., four times daily; s.d., single dose;

<sup>a</sup> cotinine metabolite

3.9  $AUC_{last}$  and  $C_{max}$  goodness of fit plots

(a) AUC

(b)  $C_{max}$ 

**Figure S3.9.1: Predicted versus observed nicotine and cotinine  $AUC_{last}$  (a) and  $C_{max}$  (b) values.** Each symbol represents the  $AUC_{last}$  or  $C_{max}$  of a different plasma profile (circles: nicotine, triangles: cotinine metabolite and cotinine iv). The black solid (—) lines mark the lines of identity. Black dotted lines (.....) indicate 1.25-fold, black dashed lines (---) indicate 2-fold deviation. **AUC**, area under the concentration–time curve from the first to the last data point;  **$C_{max}$** , maximum concentration; **iv**, intravenous; **patch**, transdermal therapeutic system (nicotine patch); **po**, oral.

### 3.10 Nicotine and cotinine PBPK model sensitivity analysis

A sensitivity analysis of the final nicotine and cotinine PBPK model to single parameter changes (local sensitivity analysis) was performed. Sensitivity of the PBPK model was measured as the relative change of the AUC from the last applied dose in a steady-state scenario extrapolated to infinity ( $AUC_{inf}$ ) of the largest applied pulmonary dose of nicotine in the clinical studies used for the PBPK model development (30 times 2.5 mg during 15 hours). Parameters, optimized as well as parameters fixed to literature values, were included into the analysis if they had significant impact in former models (e.g. glomerular filtration rate fraction) or if they might have a strong influence due to calculation methods used in the model (e.g. fraction unbound) and/or if they have been optimized. Model sensitivity to a model parameter was calculated as the ratio of the relative change of the simulated  $AUC_{inf}$  of nicotine and cotinine metabolite, respectively, to the relative variation of the parameter around the value used in the final model according to Equation S12.

$$S = \frac{\Delta AUC_{inf}}{\Delta p} \cdot \frac{p}{AUC_{inf}} \quad (S12)$$

where  $S$  is the sensitivity of the  $AUC_{inf}$  to the examined model parameter,  $\Delta AUC_{inf}$  is the change of the  $AUC_{inf}$ ,  $AUC_{inf}$  is the simulated  $AUC_{inf}$  with the original parameter value,  $p$  is the original model parameter value and  $\Delta p$  is the variation of the model parameter value. A sensitivity value of +1.0 signifies that a 10 % increase of the examined parameter causes a 10 % increase of the simulated  $AUC_{inf}$ . The analysis was performed using a relative perturbation of parameters of 10 %.

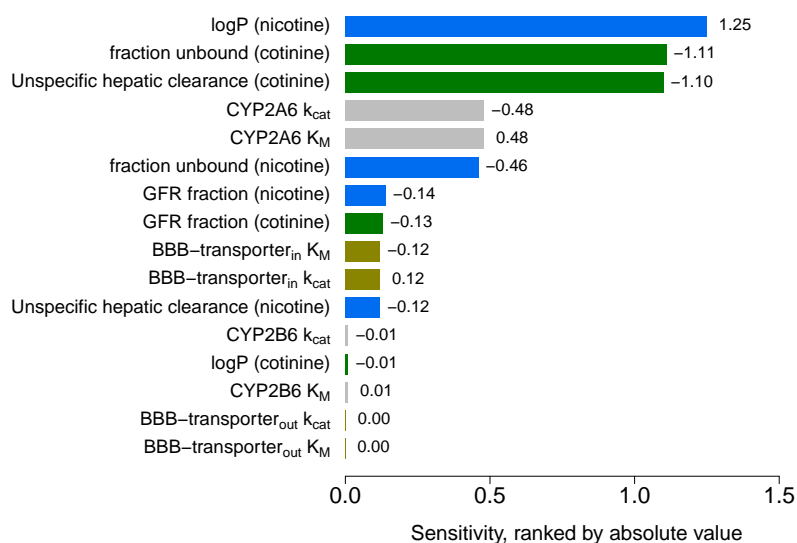


**Figure S3.10.1: Nicotine and cotinine PBPK model local sensitivity analysis.** Sensitivity of the model to single parameters, measured as change of the simulated area under the plasma concentration-time curve of nicotine and cotinine metabolite, respectively, from the last applied dose in a steady-state scenario (30 times 2.5 mg over 15 hours) extrapolated to infinity ( $AUC_{inf}$ ). A sensitivity value of +1.0 signifies that a 10 % increase of the examined parameter causes a 10 % increase of the simulated  $AUC_{inf}$ .

The results of the local sensitivity analysis (see Figure S3.10.1) reveal that, among the tested parameters, lipophilicity of nicotine and fraction unbound and unspecific hepatic clearance of cotinine have the biggest impact on the tested nicotine and cotinine  $AUC_{inf}$ . The analysis underlines the model's

sensitivity to changes in the lipophilicity of nicotine, which plays a key role in many calculation methods (e.g. partition coefficients) in the PBPK model. The fact that the unspecific hepatic clearance of cotinine represents the major route of elimination for cotinine in the model explains the high sensitivity of the model to this parameter. Additionally, the high sensitivity to the fraction unbound of cotinine is to be expected, as the fraction unbound determines the concentrations available for all pharmacokinetic processes. Values for the fractions unbound used in the model have been obtained from literature [58, 59] and were not subject to any fitting endeavours.

### 3.11 Heart rate population predictions after nicotine intake compared to observed data

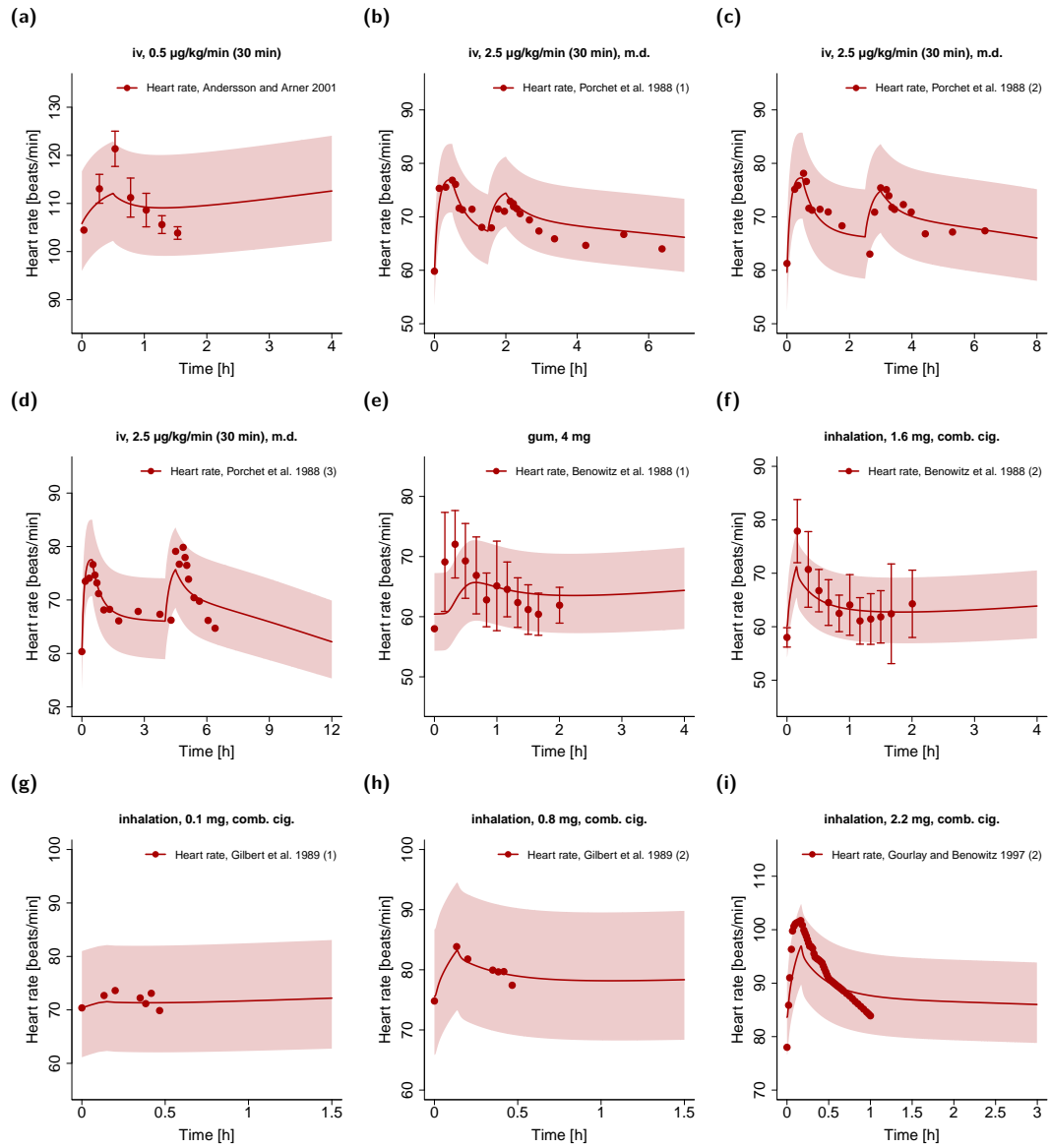


**Figure S3.11.1: Heart rate profiles after intravenous, oral and pulmonary administration of nicotine.** Observed data are shown as circles (●), if available ± standard deviation (SD). Population simulation (n=100) geometric means are shown as lines (—); the shaded areas represent the predicted population geometric SD. References with numbers in parentheses link to a specific observed dataset described in the study table with detailed information about dosing regimens (Tables S2.6.3 and S2.8.2). **comb. cig.**, combustible cigarette; **e-cig.**, e-cigarette; **iv**, intravenous; **m.d.**, multiple dose.

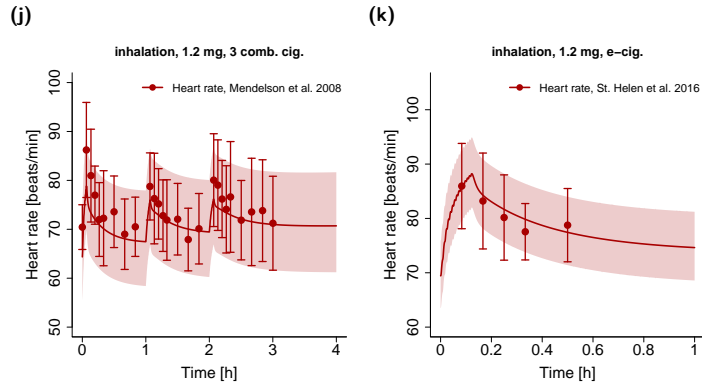


**Figure S3.11.1: Heart rate profiles after intravenous, oral and pulmonary administration of nicotine.** Observed data are shown as circles (●), if available ± standard deviation (SD). Population simulation (n=100) geometric means are shown as lines (—); the shaded areas represent the predicted population geometric SD. References with numbers in parentheses link to a specific observed dataset described in the study table with detailed information about dosing regimens (Tables S2.6.3 and S2.8.2). **comb. cig.**, combustible cigarette; **e-cig.**, e-cigarette; **iv**, intravenous; **m.d.**, multiple dose.(continued)

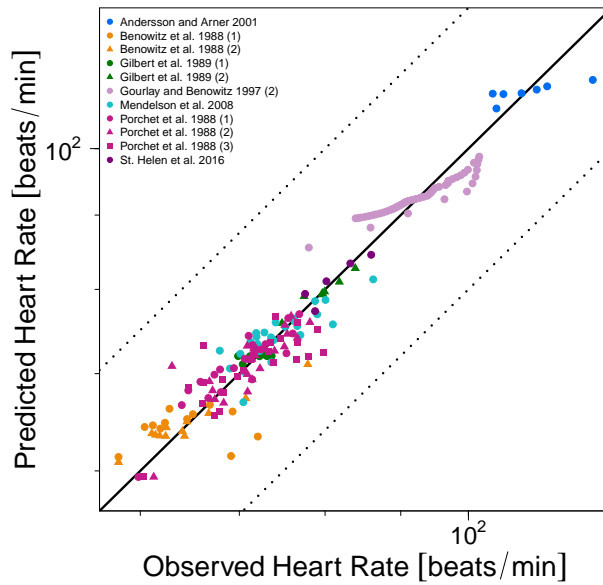


**Figure S3.11.2: Predicted versus observed heart rates after nicotine intake.** The black solid (—) line marks the line of identity, black dotted lines (.....) indicate 1.25-fold deviation.

## 3.12 Heart rate simulations

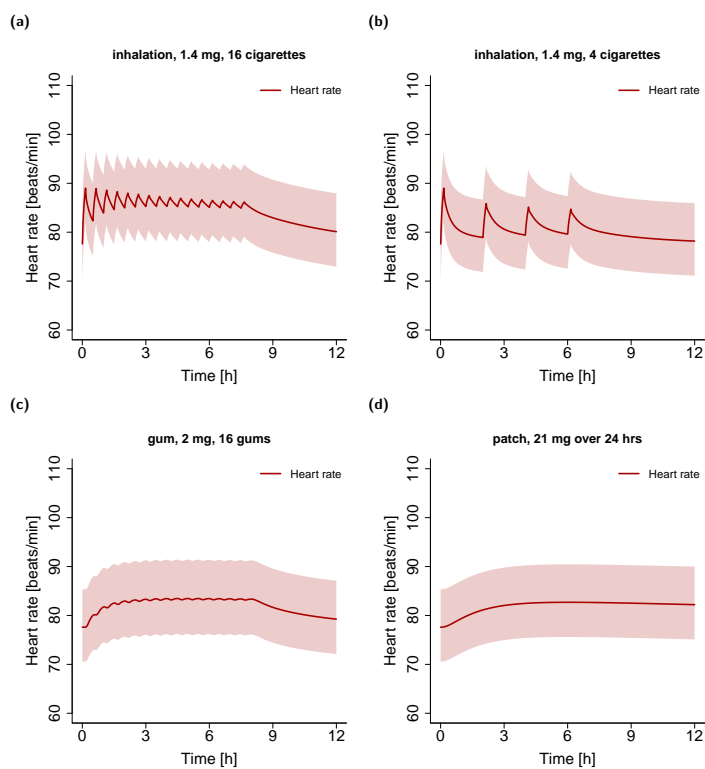


**Figure S3.12.1:** Simulations of heart rate profiles after pulmonary (16 cigarettes and 4 cigarettes, respectively), oral (16 gums) and transdermal (1 patch) nicotine administration. Population simulation geometric means are shown as lines (—); the shaded areas represent the predicted population geometric SD. Detailed information about dosing regimens, study populations and model input parameters is given in Tables S2.6.3, S2.8.1 and S2.8.3. **patch**, transdermal therapeutic system (nicotine patch).

## References

- [1] Benowitz NL, Jacob P (1994) Metabolism of nicotine to cotinine studied by a dual stable isotope method. *Clinical Pharmacology & Therapeutics* 56(5):483–493
- [2] Hukkanen J, Jacob P, Benowitz NL (2005) Metabolism and disposition kinetics of nicotine. *Pharmacological reviews* 57(1):79–115
- [3] Tega Y, Yamazaki Y, Akanuma Si, Kubo Y, Hosoya Ki (2018) Impact of Nicotine Transport across the Blood-Brain Barrier: Carrier-Mediated Transport of Nicotine and Interaction with Central Nervous System Drugs. *Biological & pharmaceutical bulletin* 41(9):1330–1336
- [4] De Schepper PJ, Van Hecken A, Daenens P, Van Rossum JM (1987) Kinetics of cotinine after oral and intravenous administration to man. *European Journal of Clinical Pharmacology* 31(5):583–588
- [5] Xu C, Rao YS, Xu B, Hoffmann E, Jones J, Sellers EM, Tyndale RF (2002) An in vivo pilot study characterizing the new CYP2A6\*7, \*8, and \*10 alleles. *Biochemical and biophysical research communications* 290(1):318–324
- [6] Meyer M, Schneckener S, Ludewig B, Kuepfer L, Lippert J (2012) Using Expression Data for Quantification of Active Processes in PBPK Modeling. *Drug Metab Dispos* 40(5):892–901
- [7] Schmidt T, Samaras P, Frejno M, Gessulat S, Barnert M, Kienegger H, Krcmar H, Schlegl J, Ehrlich HC, Aiche S, Kuster B, Wilhelm M (2018) ProteomicsDB. *Nucleic acids research* 46(D1):D1271–D1281
- [8] Yamazaki H, Inoue K, Hashimoto M, Shimada T (1999) Roles of CYP2A6 and CYP2B6 in nicotine C-oxidation by human liver microsomes. *Archives of Toxicology* 73(2):65–70
- [9] Fukami T, Nakajima M, Yoshida R, Tsuchiya Y, Fujiki Y, Katoh M, McLeod HL, Yokoi T (2004) A novel polymorphism of human CYP2A6 gene CYP2A6\*17 has an amino acid substitution (V365M) that decreases enzymatic activity in vitro and in vivo. *Clinical Pharmacology and Therapeutics* 76(6):519–527
- [10] Hosono H, Kumondai M, Maekawa M, Yamaguchi H, Mano N, Oda A, Hirasawa N, Hiratsuka M (2017) Functional Characterization of 34 CYP2A6 Allelic Variants by Assessment of Nicotine C -Oxidation and Coumarin 7-Hydroxylation Activities. *Drug Metabolism and Disposition* 45(3):279–285
- [11] Murphy SE, Raulinaitis V, Brown KM (2005) Nicotine 5'-oxidation and methyl oxidation by P450 2A enzymes. *Drug Metabolism and Disposition* 33(8):1166–1173
- [12] Benowitz NL, Jacob P (1993) Nicotine and cotinine elimination pharmacokinetics in smokers and nonsmokers. *Clinical pharmacology and therapeutics* 53(3):316–323
- [13] Rose JE, Mukhin AG, Lokitz SJ, Turkington TG, Herskovic J, Behm FM, Garg S, Garg PK (2010) Kinetics of brain nicotine accumulation in dependent and nondependent smokers assessed with PET and cigarettes containing 11C-nicotine. *Proceedings of the National Academy of Sciences of the United States of America* 107(11):5190–5195
- [14] Morjaria Y, Irwin WJ, Barnett PX, Chan RS, Conway BR (2004) In vitro release of nicotine from chewing gum formulations. *Dissolution Technologies* 11(2):12–15

- [15] Davies M, Pendlington RU, Page L, Roper CS, Sanders DJ, Bourner C, Pease CK, MacKay C (2011) Determining Epidermal Disposition Kinetics for Use in an Integrated Nonanimal Approach to Skin Sensitization Risk Assessment. *Toxicological Sciences* 119(2):308–318
- [16] McCarley KD, Bunge AL (2001) Pharmacokinetic models of dermal absorption. *Journal of Pharmaceutical Sciences* 90(11):1699–1719
- [17] Selzer D, Hahn T, Naegel A, Heisig M, Kostka K, Lehr C, Neumann D, Schaefer U, Wittum G (2013) Finite dose skin mass balance including the lateral part: Comparison between experiment, pharmacokinetic modeling and diffusion models. *Journal of Controlled Release* 165(2):119–128
- [18] Houseman TH (1973) Studies of Cigarette Smoke Transfer Using Radioisotopically Labelled Tobacco Constituents Part II: The Transference of Radioisotopically Labelled Nicotine to Cigarette Smoke. *Beitrage zur Tabakforschung International/ Contributions to Tobacco Research* 7(3):142–147
- [19] Hammond D, Fong GT, Cummings KM, O'Connor RJ, Giovino GA, McNeill A (2006) Cigarette yields and human exposure: A comparison of alternative testing regimens. *Cancer Epidemiology Biomarkers and Prevention* 15(8):1495–1501
- [20] Simon DL, Iglauer A (1960) The acute effect of chewing tobacco and smoking in habitual users\*. *Annals of the New York Academy of Sciences* 90(1):119–132
- [21] Benowitz NL, Porchet H, Sheiner L, Jacob P (1988) Nicotine absorption and cardiovascular effects with smokeless tobacco use: comparison with cigarettes and nicotine gum. *Clinical pharmacology and therapeutics* 44(1):23–28
- [22] Lott D, Lehr T, Dingemans J, Krause A (2018) Modeling Tolerance Development for the Effect on Heart Rate of the Selective S1P1 Receptor Modulator Ponesimod. *Clinical pharmacology and therapeutics* 103(6):1083–1092
- [23] Porchet HC, Benowitz NL, Sheiner LB (1988) Pharmacodynamic model of tolerance: application to nicotine. *The Journal of pharmacology and experimental therapeutics* 244(1):231–236
- [24] Gill A, Hoogwerf BJ, Burger J, Bruce S, Macconell L, Yan P, Braun D, Giaconia J, Malone J (2010) Vascular Effect of exenatide on heart rate and blood pressure in subjects with type 2 diabetes randomized pilot study. *Cardiovascular Diabetology* 9:1–7
- [25] Vandewalle G, Middleton B, Rajaratnam SMW, Stone BM, Thorleifsdottir B, Arendt J, Dijk DJ (2007) Robust circadian rhythm in heart rate and its variability: influence of exogenous melatonin and photoperiod. *Journal of Sleep Research* 16(2):148–155
- [26] Umetani K, Singer DH, McCraty R, Atkinson M (1998) Twenty-four hour time domain heart rate variability and heart rate: Relations to age and gender over nine decades. *Journal of the American College of Cardiology* 31(3):593–601
- [27] Andersson K, Arner P (2001) Systemic nicotine stimulates human adipose tissue lipolysis through local cholinergic and catecholaminergic receptors. *International Journal of Obesity* 25(8):1225–1232
- [28] Benowitz NL, Chan K, Denaro CP, Jacob P (1991) Stable isotope method for studying transdermal drug absorption: the nicotine patch. *Clinical pharmacology and therapeutics* 50(3):286–293
- [29] Benowitz NL, Jacob P, Fong I, Gupta S (1994) Nicotine metabolic profile in man: comparison of cigarette smoking and transdermal nicotine. *The Journal of pharmacology and experimental therapeutics* 268(1):296–303

- [30] Feyerabend C, Ings RM, Russel MA (1985) Nicotine pharmacokinetics and its application to intake from smoking. *British journal of clinical pharmacology* 19(2):239–247
- [31] Gourlay SG, Benowitz NL (1997) Arteriovenous differences in plasma concentration of nicotine and catecholamines and related cardiovascular effects after smoking, nicotine nasal spray, and intravenous nicotine. *Clinical Pharmacology and Therapeutics* 62(4):453–463
- [32] Molander L, Hansson A, Lunell E (2001) Pharmacokinetics of nicotine in healthy elderly people. *Clinical Pharmacology and Therapeutics* 69(1):57–65
- [33] Zevin S, Jacob P, Benowitz N (1997) Cotinine effects on nicotine metabolism. *Clinical Pharmacology and Therapeutics* 61(6):649–654
- [34] Benowitz NL, Jacob P, Denaro C, Jenkins R (1991) Stable isotope studies of nicotine kinetics and bioavailability. *Clinical pharmacology and therapeutics* 49(3):270–277
- [35] Benowitz NL, Dains KM, Dempsey D, Yu L, Jacob P (2010) Estimation of nicotine dose after low-level exposure using plasma and urine nicotine metabolites. *Cancer Epidemiology and Prevention Biomarkers* 19(5):1160–1166,
- [36] Green JT, Evans BK, Rhodes J, Thomas GA, Ranshaw C, Feyerabend C, Russell MA (1999) An oral formulation of nicotine for release and absorption in the colon: its development and pharmacokinetics. *British journal of clinical pharmacology* 48(4):485–493
- [37] Jarvis MJ, Russell MAH, Benowitz NL, Feyerabend C (1988) Elimination of cotinine from body fluids: Implications for noninvasive measurement of tobacco smoke exposure. *American Journal of Public Health* 78(6):696–698
- [38] Choi JH, Dresler CM, Norton MR, Strahs KR (2003) Pharmacokinetics of a nicotine polacrilex lozenge. *Nicotine & Tobacco Research* 5(5):635–644,
- [39] Dautzenberg B, Nides M, Kienzler JL, Callens A (2007) Pharmacokinetics, safety and efficacy from randomized controlled trials of 1 and 2 mg nicotine bitartrate lozenges (Nicotinell). *BMC clinical pharmacology* 7:11
- [40] Du D (2018) A Single-Dose, Crossover-Design Bioequivalence Study Comparing Two Nicotine Gum Formulations in Healthy Subjects. *Advances in therapy* 35(8):1169–1180
- [41] Hansson A, Rasmussen T, Kraiczi H (2017) Single-Dose and Multiple-Dose Pharmacokinetics of Nicotine 6 mg Gum. *Nicotine & Tobacco Research* 19(4):477–483
- [42] Bannon YB, Corish J, Corrigan OI, Devane JG, Kavanagh M, Mulligan S (1989) Transdermal delivery of nicotine in normal human volunteers: a single dose and multiple dose study. *European journal of clinical pharmacology* 37(3):285–290
- [43] Fant RV, Henningfield JE, Shiffman S, Strahs KR, Reitberg DP (2000) A pharmacokinetic crossover study to compare the absorption characteristics of three transdermal nicotine patches. *Pharmacology, biochemistry, and behavior* 67(3):479–482
- [44] Gupta SK, Benowitz NL, Jacob P, Rolf CN, Gorsline J (1993) Bioavailability and absorption kinetics of nicotine following application of a transdermal system. *British journal of clinical pharmacology* 36(3):221–227
- [45] Armitage AK, Dollery CT, George CF, Houseman TH, Lewis PJ, Turner DM (1975) Absorption and metabolism of nicotine from cigarettes. *British medical journal* 4(5992):313–316

- [46] Benowitz NL, Kuyt F, Jacob P (1982) Circadian blood nicotine concentrations during cigarette smoking. *Clinical pharmacology and therapeutics* 32(6):758–764
- [47] Fearon IM, Eldridge A, Gale N, Shepperd CJ, McEwan M, Camacho OM, Nides M, McAdam K, Proctor CJ (2017) E-cigarette Nicotine Delivery: Data and Learnings from Pharmacokinetic Studies. *American journal of health behavior* 41(1):16–32
- [48] Mendelson JH, Goletiani N, Sholar MB, Siegel AJ, Mello NK (2008) Effects of smoking successive low- and high-nicotine cigarettes on hypothalamic-pituitary-adrenal axis hormones and mood in men. *Neuropsychopharmacology* 33(4):749–760
- [49] Russell MA, Jarvis MJ, Feyerabend C, Fernö O (1983) Nasal nicotine solution: a potential aid to giving up smoking? *British medical journal (Clinical research ed)* 286(6366):683–684
- [50] St Helen G, Havel C, Dempsey DA, Jacob III P, Benowitz NL (2016) Nicotine delivery, retention and pharmacokinetics from various electronic cigarettes. *Addiction* 111(3):535–544,
- [51] St Helen G, Nardone N, Addo N, Dempsey D, Havel C, Jacob P, Benowitz N (in press 2019) Differences in nicotine intake and effects from electronic and combustible cigarettes among dual users. *Addiction*
- [52] Curvall M, Elwin CE, Kazemi-Vala E, Warholm C, Enzell CR (1990) The pharmacokinetics of cotinine in plasma and saliva from non-smoking healthy volunteers. *European Journal of Clinical Pharmacology* 38(3):281–287
- [53] Gilbert DG, Robinson JH, Chamberlin CL, Spielberger CD (1989) Effects of smoking/nicotine on anxiety, heart rate, and lateralization of EEG during a stressful movie. *Psychophysiology* 26(3):311–320
- [54] Wishart DS, Knox C, Guo AC, Shrivastava S, Hassanali M, Stothard P, Chang Z, Woolsey J (2006) DrugBank: a comprehensive resource for in silico drug discovery and exploration. *Nucleic Acids Research* 34(Supplement 1):D668–D672,
- [55] Nielsen HM, Rassing MR (2002) Nicotine permeability across the buccal TR146 cell culture model and porcine buccal mucosa in vitro: Effect of pH and concentration. *European Journal of Pharmaceutical Sciences* 16(3):151–157
- [56] Alharbi O, Xu Y, Goodacre R (2014) Simultaneous multiplexed quantification of nicotine and its metabolites using surface enhanced Raman scattering. *Analyst* 139(19):4820–4827
- [57] Zissimos AM, Abraham MH, Barker MC, Box KJ, Tam KY (2002) Calculation of Abraham descriptors from solvent–water partition coefficients in four different systems; evaluation of different methods of calculation. *Journal of the Chemical Society, Perkin Transactions 2* pp 470–477
- [58] Svensson CK (1987) Clinical Pharmacokinetics of Nicotine. *Clinical Pharmacokinetics* 12(1):30–40
- [59] Benowitz NL, Kuyt F, Jacob P, Jones RT, Osman AL (1983) Cotinine disposition and effects. *Clinical pharmacology and therapeutics* 34(5):604–611
- [60] Dicke KE, Skrlin SM, Murphy SE (2005) Nicotine and 4-(methylnitrosamino)-1-(3-pyridyl)-butanone metabolism by cytochrome P450 2B6. *Drug metabolism and disposition: the biological fate of chemicals* 33(12):1760–1764
- [61] Open Systems Pharmacology Suite Community (2018) Open Systems Pharmacology Suite Manual

- [62] Rodgers T, Rowland M (2006) Physiologically based pharmacokinetic modelling 2: Predicting the tissue distribution of acids, very weak bases, neutrals and zwitterions. *Journal of Pharmaceutical Sciences* 95(6):1238 – 1257
- [63] Rodgers T, Leahy D, Rowland M (2005) Physiologically based pharmacokinetic modeling 1: Predicting the tissue distribution of moderate-to-strong bases. *Journal of Pharmaceutical Sciences* 94(6):1259 – 1276
- [64] Rodgers T, Rowland M (2007) Mechanistic approaches to volume of distribution predictions: understanding the processes. *Pharmaceutical research* 24(5):918–933
- [65] Rodrigues AD (1999) Integrated cytochrome P450 reaction phenotyping: attempting to bridge the gap between cDNA-expressed cytochromes P450 and native human liver microsomes. *Biochemical pharmacology* 57(5):465–480
- [66] Nishimura M, Yaguti H, Yoshitsugu H, Naito S, Satoh T (2003) Tissue distribution of mRNA expression of human cytochrome P450 isoforms assessed by high-sensitivity real-time reverse transcription PCR. *Yakugaku zasshi : Journal of the Pharmaceutical Society of Japan* 123(5):369–75
- [67] Valentin J (2002) Basic anatomical and physiological data for use in radiological protection: reference values. *Annals of the ICRP* 32(3-4):1–277
- [68] Edginton AN, Schmitt W, Willmann S (2006) Development and evaluation of a generic physiologically based pharmacokinetic model for children. *Clinical pharmacokinetics* 45(10):1013–1034

PUBLICATION HISTORY

---

## B.1 RESEARCH ARTICLES

**In Vitro–In Silico Modeling of Caffeine and Diclofenac Permeation in Static and Fluidic Systems with a 16HBE Lung Cell Barrier.**

Lukas Kovar, Lena Wien, Dominik Selzer, Yvonne Kohl, Robert Bals and Thorsten Lehr.

*Pharmaceutics* 2022;15(2):250. DOI: 10.3390/ph15020250.

**External Model Performance Evaluation of Twelve Infliximab Population Pharmacokinetic Models in Patients with Inflammatory Bowel Disease.**

Christina Schräpel, Lukas Kovar, Dominik Selzer, Ute Hofmann, Florian Tran, Walter Reinisch, Matthias Schwab and Thorsten Lehr.

*Pharmaceutics* 2021;13(9):1368. DOI: 10.3390/pharmaceutics13091368.

**Influence of Physicochemical Characteristics and Stability of Gold and Silver Nanoparticles on Biological Effects and Translocation across an Intestinal Barrier—A Case Study from In Vitro to In Silico.**

Yvonne Kohl, Michelle Hesler, Roland Drexel, Lukas Kovar, Stephan Dähnhardt-Pfeiffer, Dominik Selzer, Sylvia Wagner, Thorsten Lehr, Hagen von Briesen and Florian Meier.

*Nanomaterials* 2021;11(6):1358. DOI: 10.3390/nano11061358.

**Physiologically-Based Pharmacokinetic (PBPK) Modeling Providing Insights into Fentanyl Pharmacokinetics in Adults and Pediatric Patients.**

Lukas Kovar, Andreas Weber, Michael Zemlin, Yvonne Kohl, Robert Bals, Bernd Meibohm, Dominik Selzer and Thorsten Lehr.

*Pharmaceutics* 2020;12(10):908. DOI: 10.3390/pharmaceutics12100908.

**Physiologically-Based Pharmacokinetic (PBPK) Modeling of Buprenorphine in Adults, Children and Preterm Neonates.**

Lukas Kovar, Christina Schräpel, Dominik Selzer, Yvonne Kohl, Robert Bals, Matthias Schwab and Thorsten Lehr.

*Pharmaceutics* 2020;12(6):578. DOI: 10.3390/pharmaceutics12060578.

**Comprehensive Parent-Metabolite PBPK/PD Modeling Insights into Nicotine Replacement Therapy Strategies.**

Lukas Kovar, Dominik Selzer, Hannah Britz, Neal Benowitz, Gideon St. Helen, Yvonne Kohl, Robert Bals and Thorsten Lehr.

*Clin Pharmacokinet* 2020;59(9):1119-1134. DOI: 10.1007/s40262-020-00880-4.

## B.2 REVIEW ARTICLES

**A Scoping Review of the Evidence Behind CYP2D6 Inhibitor Classifications.**  
Emily J. Cicali, D. Max Smith, Benjamin Q. Duong, Lukas G. Kovar, Larisa H. Cavallari and Julie A. Johnson.  
*Clin Pharmacol Ther* 2020;108(1):116-125. DOI: 10.1002/cpt.1768.

## B.3 CONFERENCE ABSTRACTS

**Physiologically Based Pharmacokinetic (PBPK) Modeling of Buprenorphine, Fentanyl and Nicotine Providing Insights into Brain Tissue Disposition, Drug-Drug Interactions and Pediatric Plasma Concentrations.**  
Lukas Kovar, Dominik Selzer and Thorsten Lehr.  
In: International PhD/Postdoc Meeting 2021 – Deutsche Pharmazeutische Gesellschaft (DPhG), digital (2021).

**Physiologically based pharmacokinetic (PBPK) modeling of (E)-clomiphene drug-drug-gene interactions with CYP2D6 and clarithromycin.**  
Christina Schräpel, Lukas Kovar, Simeon Rüdeshheim, Boian Ganchev, Patrick Kröner, Svitlana Igel, Reinhold Kerb, Thomas E. Mürdter, Matthias Schwab and Thorsten Lehr.  
In: PAGE Meeting, digital (2021).

**Predictive Model Performance of Population Pharmacokinetic (popPK) and Physiologically Based Pharmacokinetic (PBPK) Models for Infliximab Concentrations.**  
Christina Schräpel, Lukas Kovar, Ute Hofmann, Walter Reinisch, Matthias Schwab and Thorsten Lehr.  
In: e:Med Kick-off Meeting, digital (2020).

**A physiologically based pharmacokinetic/pharmacodynamic (PBPK/PD) parent-metabolite model of nicotine including its chronotropic effect and CYP2A6/CYP2B6 metabolism.**  
Lukas Kovar, Hannah Britz, Dominik Selzer, Neal L Benowitz, Yvonne Lydia Kohl, Robert Bals and Thorsten Lehr.  
In: Annual Meeting – Deutsche Pharmazeutische Gesellschaft (DPhG), Heidelberg (2019).

**Physiologically-based pharmacokinetic (PBPK) modelling of nicotine and its main metabolite cotinine in healthy volunteers and smokers.**  
Lukas Kovar, Hannah Britz, Yvonne Lydia Kohl, Robert Bals and Thorsten Lehr.  
In: PAGE Meeting, Stockholm (2019).

**Physiologically-based pharmacokinetic (PBPK) modelling of a CYP3A4/P-gp ddi network with ketoconazole, midazolam, alfentanil, repaglinide and digoxin.**  
Jan-Georg Wojtyniak, Hannah Britz, Fatima Zahra Marok, Denise Türk, Laura Fuhr, Lukas Kovar, Nina Hanke, Matthias Schwab and Thorsten Lehr.

In: PhD/Postdoc Meeting 2019 – Deutsche Pharmazeutische Gesellschaft (DPHG), Darmstadt (2019).

**Impact of Different P2Y<sub>12</sub> Inhibitors on Cardiovascular Outcomes in Diabetic versus Non-Diabetic Patients: Insights From Real-World Data.**

Mohamed H. Shahin, Lukas G. Kovar, D. Max Smith, Amanda R. Elsey, Kristin W. Weitzel, R. David Anderson, Rhonda M. Cooper-DeHoff, David R. Nelson, Julie A. Johnson and Larisa H. Cavallari.

*Circulation* 138.Suppl\_1 (2018): A12787-A12787.

B.4 ORAL PRESENTATIONS

**Diabetes as a Clinical Predictor of Variability in Response to Clopidogrel Treatment after Percutaneous Coronary Intervention (PCI).**

Lukas G. Kovar, Mohamed H. Shahin, D. Max Smith, Julie A. Johnson and Larisa H. Cavallari.

In: PK/PD Expert Meeting – Arbeitsgemeinschaft für angewandte Humanpharmakologie e.V., Friedrichroda (2019).

B.5 OTHERS

**Der „Teil-Lockdown“ und seine möglichen Szenarien.**

Lukas Kovar, Katharina Och, Quirin Werthner and Thorsten Lehr.

*DAZ* 2020;47:4572-4575.

**Pharmakometrie erklärt: Wie verändert sie die moderne Pharmazie?**

Lukas Kovar, Jan-Georg Wojtyniak, Christina Schräpel and Thorsten Lehr.

*PZ Prisma* 2020;26:217-230.

**Maßgeschneidert: Die Pharmakogenetik ebnet den Weg für erfolgreiche individualisierte Interventionen.**

Lukas Kovar, Stephan Schmidt and Hartmut Derendorf.

*DAZ* 2018;48:3000-3004.

